NASA Conference Publication 2077

Quiet, Powered-Lift Propulsion

A conference held at
Lewis Research Center
Cleveland, Ohio
November 14-15, 1978

NASA

NASA Conference Publication 2077

Quiet, Powered-Lift Propulsion

A conference held at
Lewis Research Center
Cleveland, Ohio
November 14-15, 1978

PREFACE

This publication contains the papers presented at the conference on Quiet Powered-Lift Propulsion held at the NASA Lewis Research Center, November 14 and 15, 1978.

The first day and a half of the conference was devoted to a review of the Quiet, Clean, Short-Haul Experimental Engine (QCSEE) program, which is nearing completion. The last half day included progress reports on other NASA and Air Force powered-lift technology programs.

The purpose of the conference was to provide representatives from government, industry, and universities with the latest results of programs exploring new propulsion technology for powered-lift aircraft systems. The broad application potential of some of the technology presented was an added incentive for conducting the conference.

Carl C. Ciepluch
NASA Lewis Research Center
Chairman

CONTENTS

vi

QCSEE PROGRAM BACKGROUND*

Carl Ciepluch
NASA Lewis Research Center

INTRODUCTION

The QCSEE (Quiet, Clean, Short-Haul Experimental Engine) program recently
reached a major milestone with the completion of the contracted part of the
program. Accordingly, an overall review of the program is presented as part of
this conference.

Before the QCSEE program details are presented in the papers that follow,
it is of interest to review events that led to this program. Included in this
review are the reasons for initiating the program, the studies that preceded
and helped to define the program, and the technology efforts that provided the
technical base necessary to reduce program risk. In addition to this back-
ground information, the technical objectives and overall schedule of the pro-
gram are presented.

QCSEE PROGRAM GENESIS

During the early 1970's a major government study entitled the Civil Avia-
tion Research and Development Policy Study was undertaken to determine the
benefits, appropriate areas, and appropriate levels of government-supported
aeronautical research and development. This study indicated that the two major
problems affecting the viability and growth of the air transportation industry
were aircraft noise and airport congestion. Since aircraft engine exhaust pol-
lution was just emerging as an environmental concern at the time of this study,
it was included as a major problem area.

Aircraft noise impedes air traffic growth because of (1) the problems
noise creates in siting new airports and expanding existing ones and (2) the
flight restrictions noise creates for aircraft operations at night. This air-
craft noise problem is still with us.

A new short-haul air transportation system was considered to be promising
for relieving air traffic density. This new short-haul system would be sepa-
rated, as much as possible from the long-haul system, thus helping to relieve
the traffic problems at large airports. This short-haul system would operate
out of existing close-in small airports or on special out of-the-way short run-
ways at large airports. Therefore, since these aircraft would be required to
operate from relatively short runways, the use of a powered-lift type of air-
craft would be required. Powered-lift aircraft employ some of the engine
thrust to help lift the aircraft so shorter field length operations are possi-
ble. This subject is discussed in more detail later in this paper. Finally,

*For Early Domestic Dissemination.

in order for the short-haul transportation system to be seriously considered for implementation, it must be economical.

The QCSEE program was initiated, therefore, to develop a suitable propulsion technology base for future powered-lift short-haul aircraft. The technology advancement was to emphasize the areas of low noise, low exhaust emissions, and high performance. Although the QCSEE program was generally focused toward powered-lift short-haul aircraft, it was recognized that many of the advanced technology elements in the program would have broader applications. These possible applications include, for example, conventional takeoff and landing and military subsonic aircraft.

SHORT-HAUL AIRCRAFT STUDIES

Prior to the QCSEE program, several powered-lift short-haul aircraft studies were undertaken. These studies were performed under contract by the Lockheed Company and Douglas Aircraft Company (refs. 1 to 9). The objective of these studies was to evaluate the overall viability of a new short-haul aircraft system. This included determining whether this short-haul system would be compatible with the existing air transportation system. Also studied were the prospects for achieving stringent aircraft noise goals and whether the short-haul system would be economically practical. Additional study objectives were to determine promising powered-lift aircraft configurations and to identify critical technology needs.

Overall study results were generally favorable in regard to the viability of the short-haul transportation system, and these studies identified propulsion as a key area for technology advancement.

The three different methods studied for obtaining powered lift are illustrated in figure 1. The externally blown flap concept is the simplest. The engines are mounted under the wing, and to obtain the vertical thrust component for added aircraft lift the engine exhaust is deflected downward by wing flaps. The upper surface blown flap concept has the engines mounted over the wing. The vertical thrust vector is again obtained by deflecting the engine exhaust downward with wing flaps. This concept has an acoustical advantage because the aircraft wing shields ground observers from the aft engine noise. In the augmentor wing approach to powered lift, the engine fan air is ducted to and introduced into a flap-ejector configuration at the wing trailing edge. The ejector action results in augmentation of the wing lift as well as the fan flow thrust. This augmentation thrust reduces the size of the engine that is needed. There are, however, several advantages to this approach. One disadvantage is the complexity which results from using the flap-ejector and another is the considerable amount of piping and valving required. The second is a potentially higher noise aircraft. The higher noise results from the higher fan pressure ratio engine that is needed to keep fan flow duct sizes reasonable. The studies showed that the externally blown flap and upper surface blown flap powered-lift concepts were preferred. Consequently, the QCSEE program began propulsion technology development for both of these concepts.

2

Another factor that emerged from the studies was the need for low pressure ratio fans if the noise goal was to be met. This is illustrated in figure 2 where aircraft noise in EPNdB is plotted against fan pressure ratio. The data shown in figure 2 are representative of the externally blown flap type of powered-lift aircraft. The figure shows that to meet the stringent 95 EPNdB study noise goal at a 152-meter (500-ft) sideline distance a fan pressure ratio in the vicinity of 1.25 is required. This fan pressure ratio is significantly lower than those used in most aircraft engines. Low fan pressure ratios result in high bypass ratio turbofan engines, which characteristically have low fan and core engine exhaust velocities. These lower exhaust velocities reduce the jet-flap interaction noise that is a major noise source for powered-lift aircraft.

The aircraft studies also investigated the effect of aircraft runway length on the economics of powered-lift aircraft. Figure 3 shows typical results. Again, data for the externally blown flap type of aircraft are shown. A significant reduction in direct operating cost can be seen as runway length is increased from 600 to 900 meters (2000 to 3000 ft). The direct operating cost reduction is about 15 percent, but the rate of decrease diminishes in the vicinity of 900-meter (3000-ft) runways.

A 600-meter- (2000-ft-) runway aircraft was the minimum runway length considered because the vast majority of airports that can handle commercial flights have at least 600-meter (2000-ft) runways. Above a 900-meter (3000-ft) runway length a conventional aircraft with an advanced mechanical flap system becomes competitive from a direct operating cost standpoint. It, therefore, appears that future powered-lift aircraft will probably be designed for about a 900-meter (3000-ft) runway length capability. However, in the QCSEE program the more challenging 600-meter (2000-ft) runway length requirement was kept as the goal.

ENGINE STUDIES

In parallel with the short-haul aircraft studies, several engine companies conducted engine studies. The companies involved were General Electric and Allison (refs. 10 to 13). The objectives for the engine studies were to (1) perform a parametric study of the engine cycle to determine the engine cycles that best meet the study objectives, (2) perform preliminary design and installation evaluation of the most promising propulsion systems, and (3) determine advanced technology needs and alternative technology development programs.

These studies identified the variable pitch fan, which is used primarily for obtaining reverse thrust, as an attractive feature for short-haul aircraft engines. The advantage is illustrated in figure 4. The figure shows that for aircraft noise levels around 95 EPNdB the variable pitch fan with lightweight composite blades has a significant operating cost advantage over the conventional fixed pitch fan with metal blades. The advantage of the variable pitch fan results from the lighter fan blades and a significantly lower thrust re-

3

versing system weight. In the fixed pitch fan engine the conventional target type of thrust reverser employed becomes very large and heavy at the required low fan pressure ratios.

There are other significant engine study results. Because of the low aircraft noise goal, a low fan pressure ratio and correspondingly low fan tip are required. It was found that using speed reduction gears between the turbine drive and the fan improved the direct operating cost by about 1 percent. This improvement resulted because the gears (1) reduce the number of turbine stages and accordingly the overall weight of the engine and (2) improve the cruise specific fuel consumption. Although speed reduction gears raise concerns of reliability and maintenance costs in turbine engines, developing this technology further appears worthwhile.

Turbofan engines designed for low fan pressure ratio operation tend to suffer a high thrust lapse (or decrease) between takeoff and cruise conditions. One way to increase cruise thrust is to use a variable area fan exhaust nozzle to raise the fan pressure ratio at cruise within the limits of acceptable stall margin. The studies indicate that the improved cruise thrust performance was worth the added complexity of a variable area fan nozzle.

Because of the importance of low engine exhaust velocity to low jet-flap interaction noise, particularly in the case of externally blown flap configurations, exhaust velocity decayer nozzles were examined in the engine studies to determine if they were economically attractive. Although the decayer nozzles were effective in reducing exhaust velocity and thus jet-flap interaction noise, they were found to be quite heavy and to introduce internal pressure losses. These disadvantages combined to produce a significant operating cost penalty. The net effect was that the decayer nozzle was not attractive for this application.

QCSEE TECHNOLOGY BASE EXPANSION

During the aircraft and engine studies it became evident that there were several areas where the technology base was insufficient to begin an experimental QCSEE type engine program without significant risk. Accordingly, a component technology program was initiated in those key areas. These areas are described in the following sections.

Low Pressure Ratio Fans

Low pressure ratio fans, which were discussed previously, are important to low engine noise. Aerodynamic and acoustic characteristics of low pressure ratio fans were investigated at both small- and large-scale sizes. Figure 5 is a photograph of one of a series of 1.83-meter- (6-ft-) diameter fans that was investigated at Lewis Research Center. This fan has a relatively low design pressure ratio of 1.2.

Variable Pitch Fans

Technology development was also undertaken in the variable pitch fan area. Again both small- and large-scale fans were investigated. Work was conducted both under contract and in-house. Figure 6 is a photograph of the Q-FAN/T55 engine that was tested here at Lewis. The variable pitch fan which develops a pressure ratio of about 1.2 was designed and built by the Hamilton Standard Company. The engine and model fans provided valuable data on variable pitch fan aerodynamics in forward and reverse thrust, acoustics, and the mechanics of blade pitch change.

Lightweight Fan Blades

Another technology development area was lightweight fan blades. These blades are very important to the successful development of variable pitch fans. One key problem area for these blades has been satisfactory foreign-object-damage (FOD) resistance. Figure 7 shows a photograph of two of the composite material blades built to investigate improved FOD resistance. The construction details of these blades are described in subsequent papers in the QCSEE program review. The blade on the left is mounted on a blade retention system which is used for support during FOD tests in a whirl rig.

Powered-Lift Acoustics

Powered-lift acoustics technology development was undertaken because of the importance this noise source has in powered-lift aircraft noise. Acoustic research was conducted on scale models of the three previously described powered-lift concepts - namely, externally blown flap, upper surface blown flap, and augmentor wing. Figure 8 shows an example. In this experimental setup, laboratory compressed air was used to simulate engine exhaust. Large-scale tests, such as in figure 9, were also conducted at Lewis. In this photograph, a TF34 engine is being used in an acoustic experiment on an EBF powered-lift configuration.

QCSEE TECHNICAL GOALS

The previously discussed short-haul aircraft and engine studies and the component technology program formed the basis for establishing the program goals (see table I). Because of the importance of low noise to any future aircraft and particularly short-haul aircraft, very stringent goals were established. The takeoff and approach aircraft noise level was set at 95 EPNdB. A reverse thrust noise level of 100 PNdB was also established. And finally, a 95-EPNdB noise contour (or footprint) area of 1.29 square kilometers (1/2 sq mile) was required. These noise goals represent aircraft noise levels which are significantly below existing FAA regulations. This subject is discussed in more detail later in the papers on acoustics.

The goal for exhaust pollutants was to meet the EPA 1979 emission levels. Achieving these emission levels is a very challenging task.

The installed thrust level goals for the two experimental engines in the program are as indicated. In the QCSEE program, the engine used in an externally blown flap type aircraft is referred to as the under-the-wing (UTW) engine and that used for an upper surface blown flap type aircraft as the over-the-wing (OTW) engine. These thrust levels are a result of the desire to be in the 88 960-newton (20 000-lb) thrust class of engine and the use of an existing advanced technology engine core. The reverse thrust goal was set at 35 percent of the forward takeoff thrust.

A relatively challenging goal was also set for the engine thrust to weight ratios. The thrust to weight ratio goals required extensive use of lightweight materials, and this is the most significant item in the QCSEE program related to improved aircraft perfromance and economics.

Finally, improved engine thrust response characteristics were required. The approach to takeoff thrust transient was to be accomplished in 1 second, and the transient to reverse thrust in 1.5 seconds. This improved thrust response was found to be necessary for the powered-lift short runway operation type of aircraft.

QCSEE SCHEDULE

Major program milestones are shown in table II. The program began at the beginning of 1974. The contracted effort, for which the General Electric Co. was the prime contractor, included the design, fabrication, and testing of the two experimental engines - namely, the UTW and OTW engines. The contracted work was completed in the summer of 1978. The two engines are now at Lewis for further testing. The engine testing will include powered-lift and engine acoustics and possibly additional engine controls experiments. The engine experiments at Lewis will be completed by the end of 1979.

REFERENCES

1. Higgins, T. P.; Stout, E G.; and Sweet, H. S.: Study of Quiet Turbofan STOL Aircraft for Short-Haul Transportation. NASA CR-2355, 1973.

2. Renshaw, J. H.: Quiet Turbofan STOL Aircraft for Short-Haul Transportation, Volume 1. (Lockheed-California Co.; NASA Contract NAS2-6995.) NASA CR-114612, 1973.

3. Renshaw, J. H.: Quiet Turbofan STOL Aircraft for Short-Haul Transportation, Volume 2. (Lockheed-California Co.; NASA Contract NAS2-6995.) NASA CR-114613, 1973.

4. Study of Quiet Turbofan STOL Aircraft for Short-Haul Transportation, Volume 1, Summary. NASA CR-2353, 1974.

5. Study of Quiet Turbofan STOL Aircraft for Short-Haul Transportation, Volume 2, Aircraft. (MDC-J4371-Vol. 2, Douglas Aircraft Co., Inc.; NASA Contract NAS2-6994.) NASA CR-114607, 1973.

6. Study of Quiet Turbofan STOL Aircraft for Short-Haul Transportation, Volume 3, Airports. (MDC-J4371-Vol. 3, Douglas Aircraft Co., Inc.; NASA Contract NAS2-6994.) NASA CR-114608, 1973.

7. Study of Quiet Turbofan STOL Aircraft for Short-Haul Transportation, Volume 4, Markets. (MDC-J4371-Vol. 4, Douglas Aircraft Co., Inc.; NASA Contract NAS2-6994.) NASA CR-114609, 1973.

8. Study of Quiet Turbofan STOL Aircraft for Short-Haul Transportation, Volume 5, Economics. (MDC-J4371-Vol. 5, Douglas Aircraft Co., Inc.; NASA Contract NAS2-6994.) NASA CR-114610, 1973.

9. Study of Quiet Turbofan STOL Aircraft for Short-Haul Transporation, Volume 6, Systems Analysis. (MDC-J4371-Vol. 6, Douglas Aircraft Co., Inc.; NASA Contract NAS2-6994.) NASA CR-114611, 1973.

10. Neitzel, R. E.; Lee, R.; and Chamay, A. J.: QCSEE Task 2: Engine and Installation Preliminary Design. (General Electric Co.; NASA Contract NAS3-16726.) NASA CR-134738, 1973.

11. Helms, H. E.: Quiet Clean STOL Experimental Engine Study Program, Task 1, Parametric Propulsion Systems Studies. (EDR-7543, Detroit Diesel Allison; NASA Contract NAS3-16727.) NASA CR-135015, 1972.

12. Helms, H. E.: Quiet Clean STOL Experimental Engine Study Program, Task 2, Preliminary Design Studies, Part A. (EDR-7610-Pt. A, Detroit Diesel Allison; NASA Contract NAS3-16727.) NASA CR-153053, 1972.

13. Helms, H. E.: Quiet Clean STOL Experimental Engine Study Program, Task 2, Preliminary Design Studies, Part B. (EDR-7610-Pt. B, Detroit Diesel Allison; NASA Contract NAS3-16727.) NASA CR-143051, 1972.

TABLE I. - QCSEE TECHNICAL GOALS

[FOUR-ENGINE, 400 320-N (90 000-lb) THRUST AIRCRAFT.]

NOISE*
    APPROACH, EPNdB 95
    TAKEOFF, EPNdB 95
    REVERSE, PNdB 100
    95 EPNdB CONTOUR AREA, sq km (sq mile) 1.29 (0.5)
POLLUTION . . . . EPA 1979 EMISSION LEVELS
INSTALLED THRUST
    FORWARD, UTW, N (lb) **77 395 (17 400)
    FORWARD, OTW, N (lb) **90 294 (**20 300)
    REVERSE, % 35
INSTALLED THRUST/WEIGHT
    UTW 4.3
    OTW 4.7
THRUST RESPONSE
    APPROACH TO TAKEOFF, sec 1.0
    APPROACH TO REVERSE, sec 1.5

*SIDELINE, 152 m (500 ft).
**WITH CONIC NOZZLES.

TABLE II. - QCSEE PROGRAM SCHEDULE

QCSEE PROGRAM SCHEDULE

MILESTONES	1974	1975	1976	1977	1978	1979
CONTRACT - GENERAL ELECTRIC						
ENGINE/NACELLE DESIGN						
PRELIMINARY	▬					
UTW DETAIL	▬					
OTW DETAIL		▬				
FABRICATION						
UTW B.P.* NACELLE		▬▬▬				
OTW B.P. NACELLE		▬▬▬▬				
UTW COMP NACELLE		▬▬▬▬▬				
TESTS						
UTW B.P. NACELLE			▬			
OTW B.P. NACELLE				▬		
UTW COMP** NACELLE				▬ ▪		
NASA LEWIS TESTS						
OTW B.P. NACELLE					▬▬▭	
UTW COMP NACELLE						▭▭

*BOILERPLATE.
**COMPOSITE.

CS-78-3284

8

POWERED-LIFT AIRCRAFT CONCEPTS

EXTERNALLY
BLOWN FLAP

UPPER SURFACE
BLOWN FLAP

AUGMENTOR WING
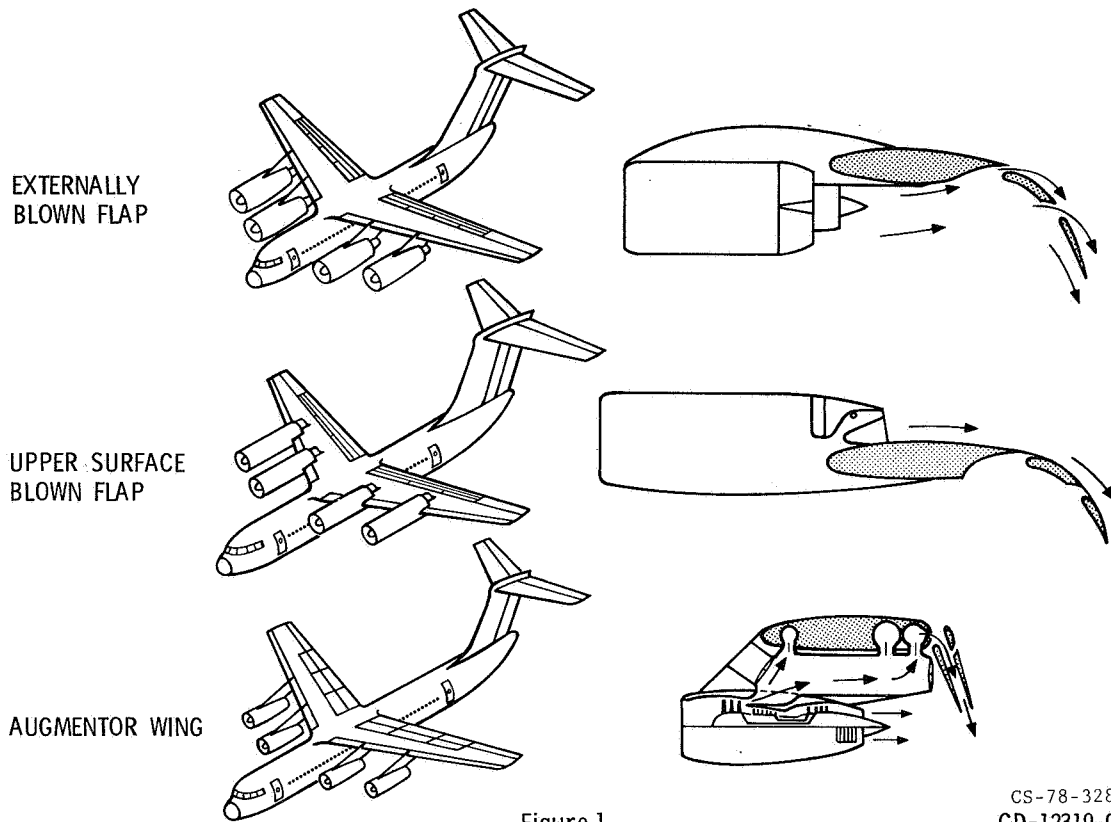
CS-78-3285
CD-12319-02

Figure 1

EFFECT OF FAN PRESSURE RATIO ON NOISE

AIRCRAFT NOISE
(4 ENGINE),
152 m (500 ft)
SIDELINE,
EPNdB

FULLY SUPPRESSED ENGINES
EXTERNALLY BLOWN FLAP CONFIGURATION

GOAL

FAN PRESSURE RATIO

CS-78-3282

Figure 2

9
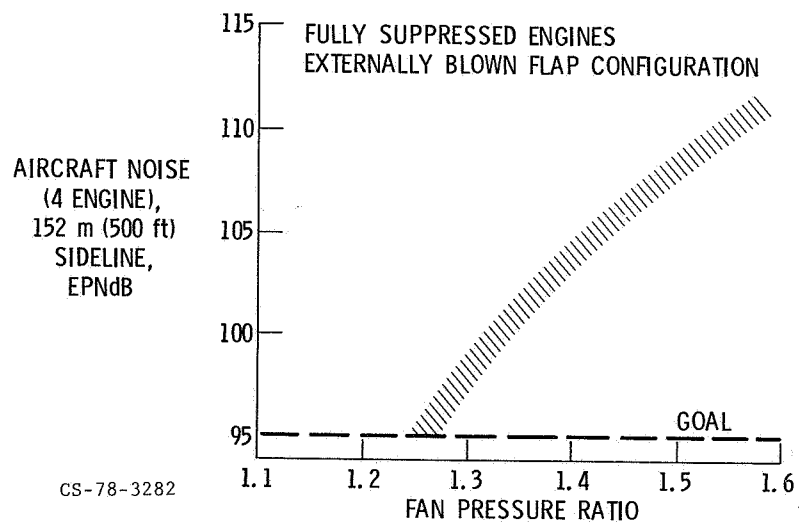
TYPICAL EFFECT OF RUNWAY LENGTH ON OPERATING COST

POWERED LIFT CONFIGURATIONS

CS-78-3283
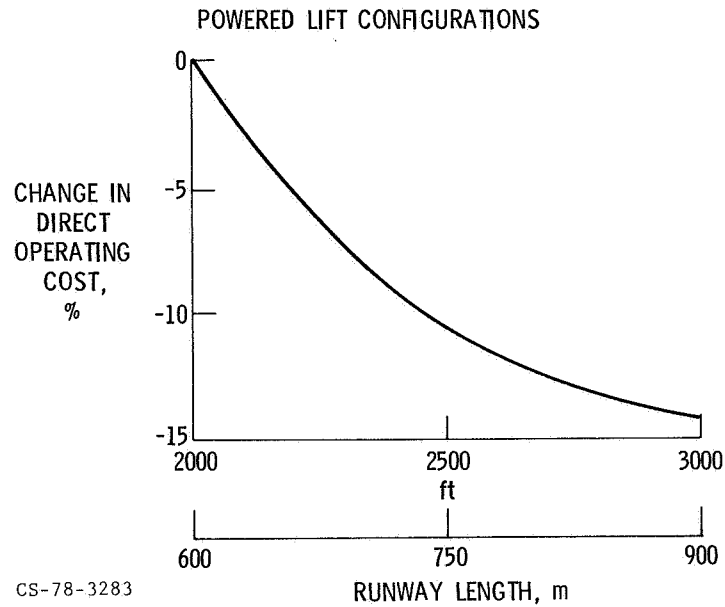
Figure 3

ADVANTAGE OF VARIABLE PITCH FANS

EXTERNALLY BLOWN FLAP AIRCRAFT
600 m (2000 ft) RUNWAY

CS-78-3281 AIRCRAFT NOISE, 152 m (500 ft) SIDELINE, EPNdB

Figure 4

10
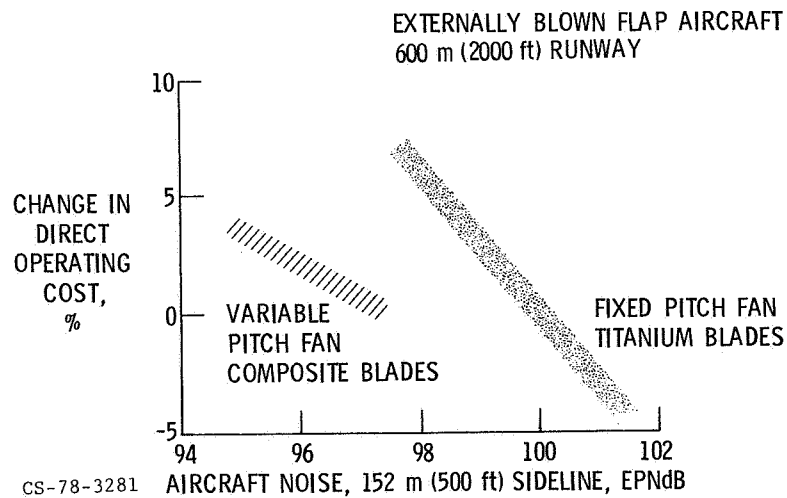
LARGE SCALE LOW PRESSURE RATIO FAN
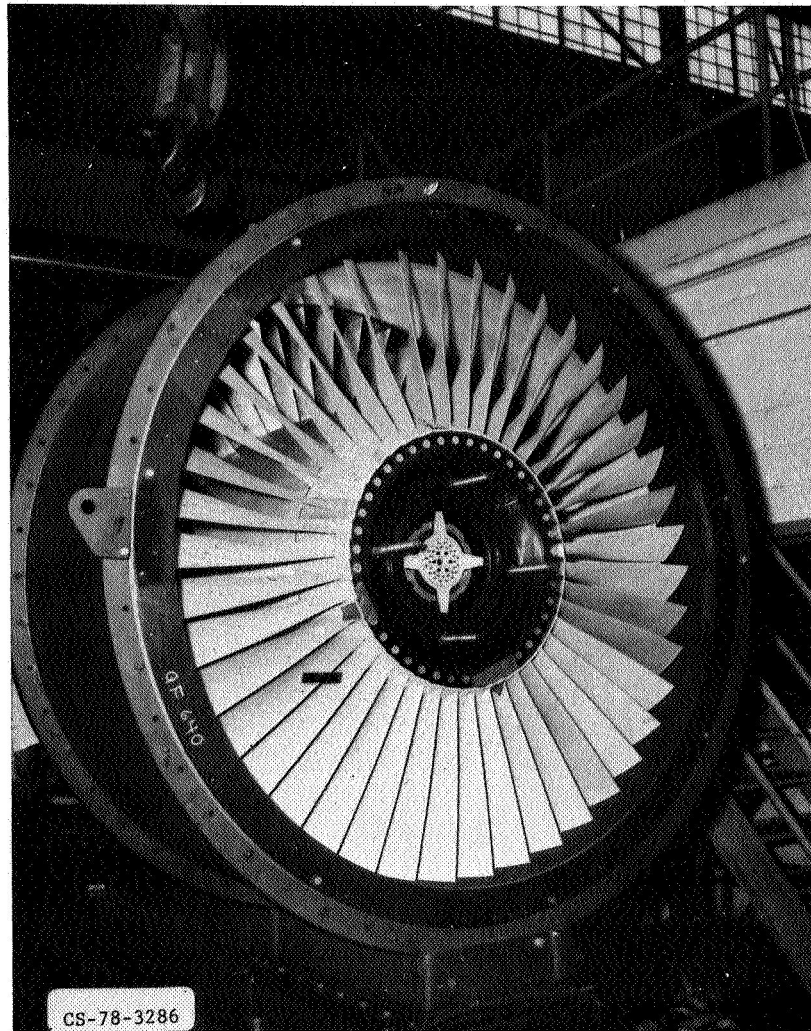

Figure 5

Q-FAN/T55 VARIABLE PITCH ENGINE
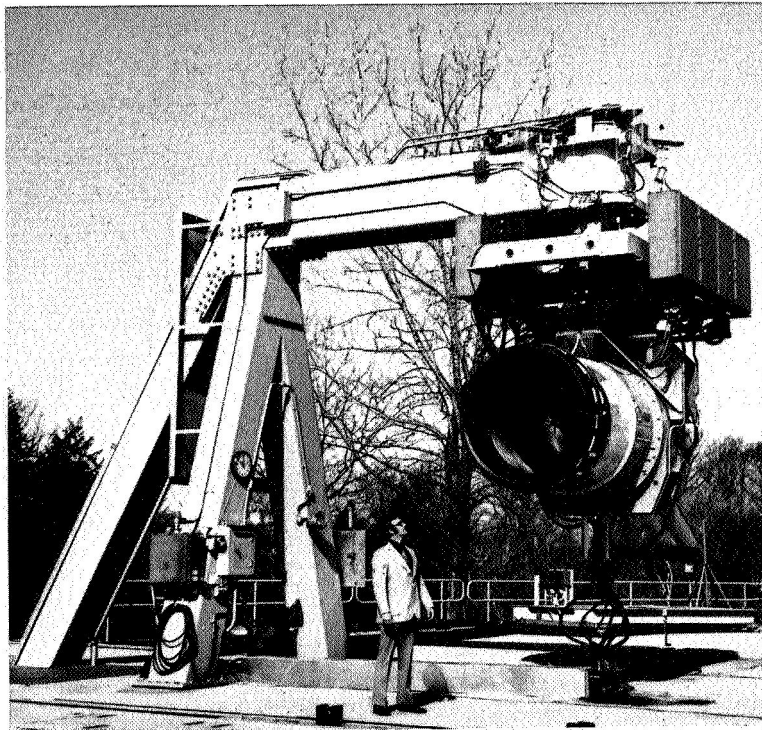
Figure 6
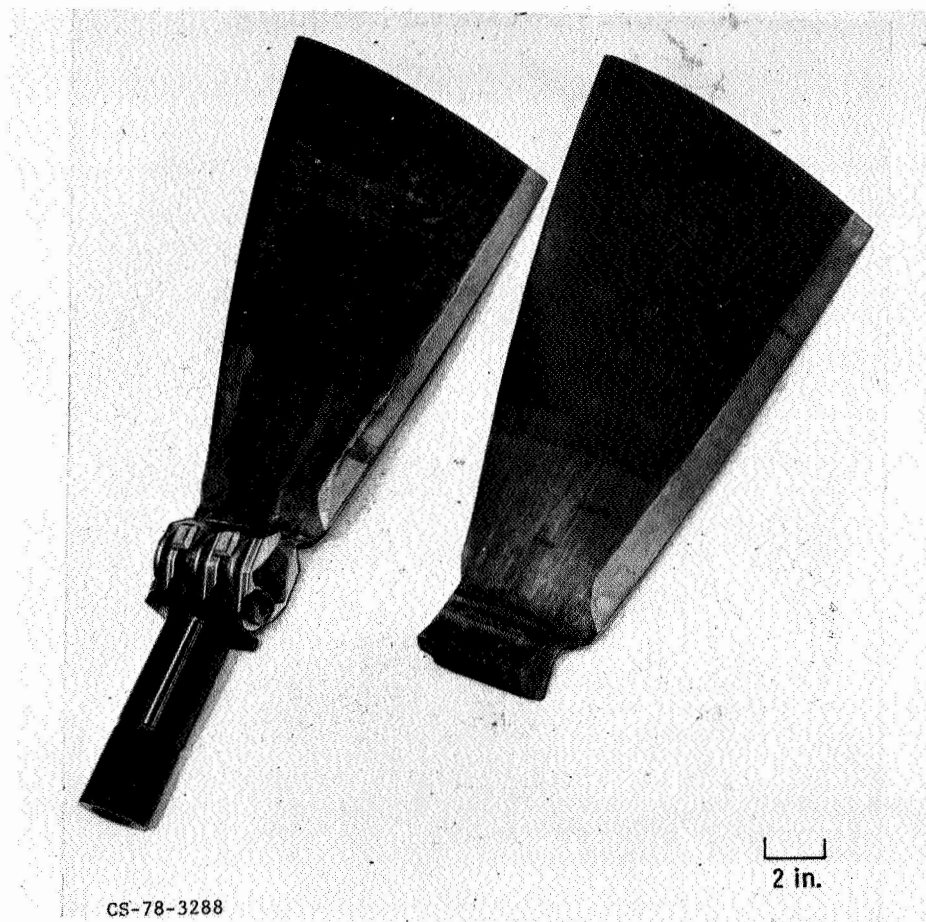
COMPOSITE FAN BLADES FOR FOREIGN-OBJECT-DAMAGE TESTING

CS-78-3288

2 in.

Figure 7

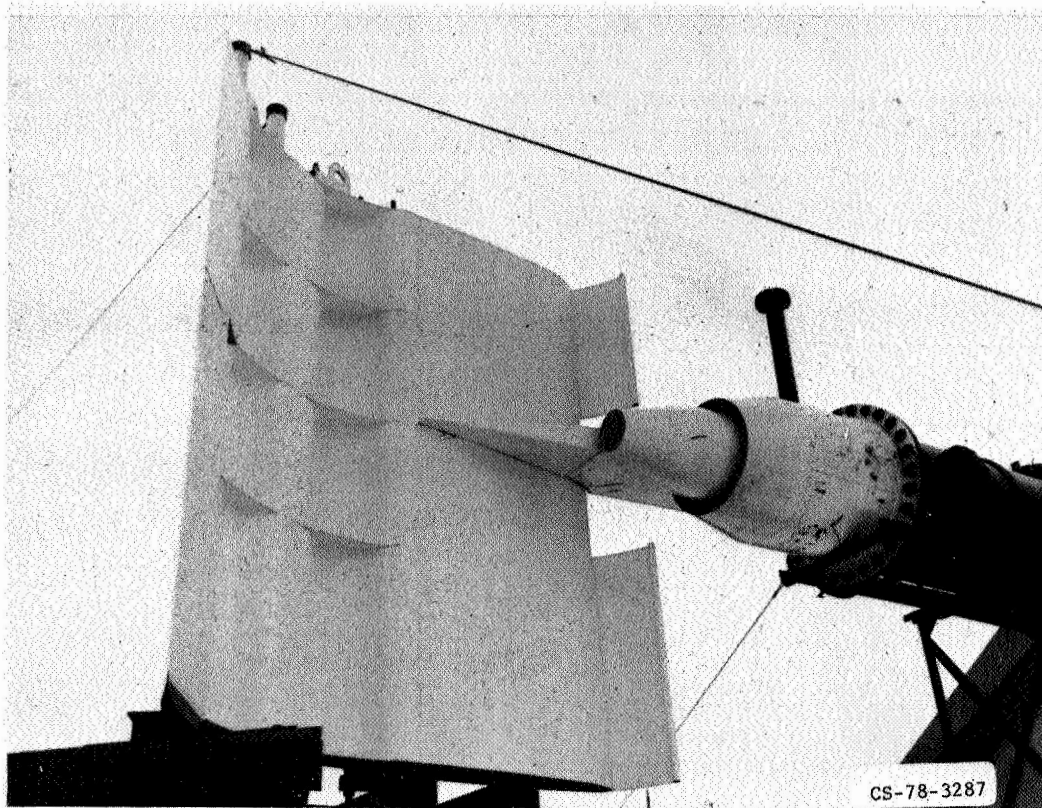# SCALE-MODEL POWERED-LIFT ACOUSTIC TEST

CS-78-3287

Figure 8

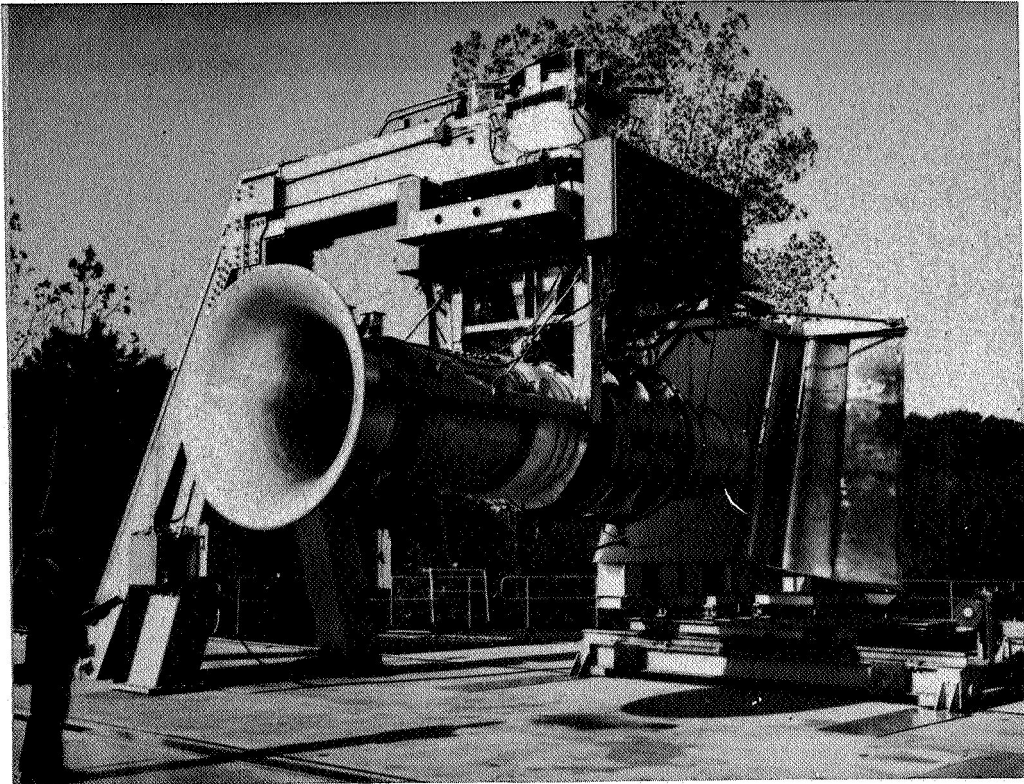# LARGE SCALE POWERED-LIFT ACOUSTIC TEST

Figure 9

QCSEE DESCRIPTION*

A.P. Adamson
General Electric Company
Cincinnati, Ohio

INTRODUCTION

This paper will set the stage for those that follow by presenting an overview of the design approach, engines, and program. The major thrust of the QCSEE Program has been concerned with the environmental needs of the short-haul transport. As discussed in the previous paper, techniques were needed to reduce noise and emissions without seriously compromising the economics of the aircraft system. This paper describes the design approach used to meet the overall program objectives, describes the experimental engines and summarizes the test programs conducted with the UTW and OTW propulsion systems.

PROGRAM OBJECTIVES

The major program objective was to provide the technology needed for a future short-haul transport. As you will see, the engines incorporated an unusual number of advanced technology features to meet the following design objectives:

  o   Reduced noise levels

  o   Reduced atmospheric pollution

  o   High installed thrust to weight ratio

  o   Attractive SFC

  o   Powered lift

  o   Rapid thrust response

  o   Reverse Thrust

  o   Integration of aircraft/propulsion

The noise objective of 95 EPNdB represents about 15 dB less than FAR36 requirements at the same sideline distance. The pollution objective was to

meet the difficult EPA 1979 standards for NO_x, carbon monoxide, and un-burned hydrocarbon emissions. In addition to these challenging environmental goals, economics placed special emphasis on the need for a high thrust-to-weight ratio and low specific fuel consumption. Other requirements result from the unique operating mode of a short-haul aircraft.

DESIGN APPROACH

The approach that was taken to meet the above design objective was as follows:

o	Noise	- Low tip speed fan
		Low jet velocity
		High throat Mach no. inlet
		Integrated acoustic treatment
o	Pollution	- Double annular combustor
o	Thrust/Weight	- Extensive use of composites
		Main reduction gear
		Integrated nacelle structure/fan frame
o	SFC	- High bypass ratio
		Variable fan nozzle
o	Powered Lift	- Variable pitch fan (UTW)
		Target reverser (OTW)
o	Integration	- Digital electric control interface
		Top mounted accessories

Jet flap interaction noise is a major contributor to the total noise signature of the aircraft. The maximum allowable engine noise and exhaust velocity are seriously limited by the jet-flap system. The under-the-wing installation results in direct impingement of the exhaust jet on the wing flap, while the over-the-wing installation provides some noise shielding for the sideline observer. As shown in figure 1, jet velocities were selected for each of the engines to keep this noise source about 3 dB below the total system noise for a balanced acoustic design. A very low jet

velocity (and very low fan pressure ratio) was required for the UTW engine. A somewhat higher fan pressure ratio was selected for the OTW engine. The low noise goal also dictated a low tip speed fan having reduced blade passing frequency as well as careful selection of the numbers of fan blades and vanes, and adequate spacing between them.

ENGINE SYSTEMS

Forward radiated noise was reduced by the use of a high throat Mach number inlet shown in the drawing of the UTW propulsion system (fig. 2). Further suppression was added as needed by structural acoustic panels and by an acoustic splitter in the fan discharge duct.

Both QCSEE engines incorporated the YF101 core, to take advantage of its advanced state of development. The combustor used in this core was already smoke-free but it did not meet the pollution objectives. A new double annular combustor was conceived to fit into the same envelope and to reduce emissions. This design was a spin-off from the NASA Lewis Experimental Clean Combustor Program.

The need for a high thrust-to-weight ratio was addressed by the extensive use of graphite and Kevlar in the fan blades, frame, and nacelle. This permitted the nacelle wall to be made integral with the engine, combining two structures into one. For example, the outer casing of the fan frame functions as the engine outer flowpath as well as a portion of the external nacelle.

Short-haul aircraft tend to require fairly high thrust-lapse rates so that the engines can operate near the bottom of their SFC bucket at moderate altitude cruise. Low pressure ratio fans inherently have this characteristic. The best fan efficiency for low pressure ratio fans occurs with relatively low fan tip speeds so a reduction gear was required. A variable area fan exhaust nozzle was necessary to keep the fan pressure ratio from dropping too low at cruise with detrimental effects on SFC and to provide sufficient altitude thrust. Though high lapse rate is needed for STOL aircraft, the very low pressure ratio fans used for low noise have an even higher lapse rate than desired and need all the help they can get at altitude.

Another characteristic needed to achieve low SFC levels is a high cycle pressure ratio. Selection of the YF101 core was made for reasons of program cost and risk and its appropriately advance technology level. The use of a low pressure ratio fan with this core resulted in a lower than desired overall cycle pressure ratio. A more optimum cycle could have been produced by adding booster stages to the fan or by a higher pressure ratio core, but this technology is already well in hand and was not considered to be worth the added program cost.

19

The short take-off requirement implies a short landing and an effective thrust reverser. The low pressure ratio UTW fan lends itself to a reverse pitch fan which can provide reverse thrust without heavy variable geometry nacelle components.

A digital control was required to permit optimum coordinated control of the variable pitch fan, the variable nozzle, and the core engine with acceptable pilot work load. Numerous other functions were also provided such as maintenance of safety limits and condition monitoring functions. Top mounted accessories were used on the UTW engine to permit lower weight, better maintainability, and low drag.

The OTW engine is shown in figure 3. It required a "D" shaped exhaust nozzle to turn the flow downward and spread it over the wing and flap. Area control was provided by variable side doors. Since this engine has a fixed pitch fan, thrust reversal is provided by pivoting the roof of the nozzle to form a target reverser blocker.

System studies which were conducted by McDonnell-Douglas and by Boeing helped direct the engine design activity including control interface definitions. Baseline UTW and OTW aircraft designs were established to identify propulsion and installation requirements. Economic studies were conducted to assess the payoff of the new engine technologies. American Airlines contributed requirements for the aircraft and an operational scenario for the short route structure. They also consulted on maintenance features, mechanical design, and reliability.

Figure 4 shows the baseline airplane projected by Douglas using the UTW engine. It would employ four QCSEE engines mounted under the wing and is based on the Douglas YC-15 technology. The major characteristics are listed on the figure.

Figure 5 shows the baseline airplane projected by Boeing using the OTW engine. It is somewhat larger, taking advantage of the greater thrust of four OTW engines, and is based on technology developed for the YC-14. The two aircraft were shown to be very competitive for short-haul operation.

These studies reached the conclusion that the 2000 foot runway requirement was too stringent, and that 3000 feet was more realistic based on projected airport availability. Another significant result was recognition that in both installations, the engines would be mounted so high that a work stand would be required for all maintenance operations, regardless of accessory location. This fact permitted the engine and aircraft accessories to be mounted in the pylon area reducing the nacelle drag for both installations, and allowing shorter, more direct service lines from the wing.

Details of the UTW engine can be seen in figure 6. The inlet, the fan blades, the fan frame, the fan outer duct, and the fan variable nozzle are all made of graphite or Kevlar with epoxy binder. The fan inner duct

is made of graphite with NASA Lewis developed PMR polyimide resin for higher temperature operation.

Acoustic treatment is used in the inlet, the fan frame, the core inlet duct, the fan exhaust duct and splitter, and the core exhaust nozzle. The latter includes a two level acoustic absorber for high and low frequencies.

The two stage F101 power turbine drives the fan through the reduction gear.

The fan nozzle is shown in the cruise position It opens part way for take-off and approach and further for reverse where it functions as an inlet.

Recognizing the critical nature of the blade pitch control system, many concepts were studied and two variable pitch systems were built and tested. A cam/harmonic drive design was supplied by Hamilton Standard, and a ball spline system by General Electric. The main reduction gear was designed and developed by Curtiss-Wright.

The major design parameters of the UTW engine are listed in table I. Note the low fan tip speed, which, used in conjunction with a 2.5 reduction gear ratio, permitted the use of a two-stage low pressure turbine. The low fan pressure ratio resulted in a very low jet velocity, meeting the acoustic requirement discussed earlier. Note the high bypass ratio made possible by the energetic core and the low pressure ratio fan.

Shown in figure 7 is a cross-section of the OTW engine. All nacelle components were of boilerplate construction for reasons of cost and to allow the evaluation of interchangeable acoustic panels. The fan uses fixed-pitch titanium blades of a geometry that would allow substitution of composite materials. The "D" shaped exhaust nozzle was tested in an inverted position, so that in the reverse thrust mode, the exhaust would be directed downward, away from the test facility and instrumentation lines.

Major design parameters of the OTW engine are listed on table II. The tip diameter and airflow were identical to those of the UTW engine to permit the same inlets and fan frames to be used. A somewhat higher fan tip speed was used to achieve the higher allowable exhaust velocity and fan pressure ratio with resultant higher overall pressure ratio and lower bypass ratio. Hub pressure rise was higher than outer panel pressure rise to permit better supercharging.

An electronic control system was desired for both engines to provide a digital interface with an aircraft on-board computer. The control accepts a command for percent-rated-thrust. Several safety limits were automatically maintained including a calculated maximum temperature. Numerous provisions in the control are included to reduce the pilot work load. Inlet Mach number is automatically maintained via nozzle, blade angle, and

speed variations to 0.8 or the maximum value consistent with other requirements. Rapid thrust response is achieved via automatic blade and nozzle area variations with minimum required fan and core speed variations. In the OTW engine, fuel flow and compressor stator vane angles are automatically adjusted to provide maximum rate of thrust change with minimum required core speed change.

Automatic restructuring of the control computer is provided via Kahlman filtering techniques to permit operation with failed sensors.

Forty items of condition monitoring information are provided to the aircraft computer by a digital data bus. The control is engine mounted, cooled by fan inlet induced airflow, and designed to be comaptible with the engine environment.

Figure 8 shows the UTW engine test installation, with the composite nacelle. Note the wide open exhaust nozzle flaps consistent with reverse flow. The entire engine structure visible is graphite or Kevlar.

The highlights of the UTW test program are listed in table III. One hundred fifty three hours of testing were completed on this engine. The initial test series included boilerplate nacelle components and the Hamilton Standard variable pitch actuation system. The second series contained the composite nacelle and the General Electric variable pitch system. Performance and acoustic measurements in forward and reverse thrust were completed in several different acoustic configurations.

Figure 9 shows the OTW engine test installation with the boilerplate inverted "D" nozzle. Note the variable side doors, the boilerplate inlet, and the transition section forward of the reverser.

Highlights of the OTW test program are listed in table IV. Fifty eight hours of testing were completed, all with boilerplate nacelle components. Test results will be described in the papers that follow.

Both engines were delivered to NASA following completion of tests at the General Electric Peebles, Ohio test site. Further testing is in process here at Lewis with a simulated wing and flap section to secure more complete acoustic data, including the effect of jet flap interaction on the total noise signature.

TABLE I. - UTW DESIGN PARAMETERS

Total Airflow, kg/s (lb/sec) ———————————— 405.5 (894))

Fan Tip Diameter, cm (in.) ———————————— 180.3 (71)

Fan Tip Speed, m/s (ft/sec) ———————————— 289.6 (950)

Bypass Ratio ———————————————————— 11.8

Fan Pressure Ratio ———————————————— 1.27

Overall Pressure Ratio ———————————————— 13.7

Jet Velocity (Core), m/s (ft/sec) ——————————— 244.7 (803)

Jet Velocity (Bypass), m/s ———————————— 204.2 (670)

Gear Ratio ———————————————————— 2.5

TABLE II. - OTW DESIGN PARAMETERS

Total Airflow, kg/s (lb/sec) ———————————— 405.5 (894)

Fan Tip Diameter, cm (in.) ———————————— 180.3 (71)

Fan Tip Speed, m/s (ft/sec) ———————————— 350.5 (1150)

Bypass Ratio ———————————————————— 10.2

Fan Pressure Ratio ———————————————— 1.34

Overall Pressure Ratio ———————————————— 17.0

Jet Velocity (Core), m/s (ft/sec) ————— ⎫
                                        ⎬ Mixed 239.9 (787)
Jet Velocity (Bypass) ————— ⎭

Gear Ratio ———————————————————— 2.1

TABLE III. - UTW TEST HISTORY

Boilerplate Nacelle, Cam-Harmonic Pitch Actuation

47 Hours (9/2/76 — 12/17/76)

- Mechanical and Controls Checkout
- Aero Performance Mapping — Bellmouth Inlet
- Performance Ratings — High Mach Inlet
- Reverse Thrust Test (Incomplete)

Composite Nacelle, Ball Spline Pitch Actuation

106 Hours (9/8/77 — 4/27/78, 7/13/78 — 7/21/78)

- Mechanical and Performance Checkout
- Acoustic Baseline — Bellmouth/Hardwall
- Suppressed Acoustic Test — High Mach Inlet, Treatment
- Reverse Thrust Performance and Acoustics
- Acoustic Technology and Control Tests

TABLE IV. - OTW TEST HISTORY

Boilerplate Nacelle

58 Hours (4/6/77 — 6/9/77)

- Mechanical and Controls Checkout
- Aero Performance Mapping — Bellmouth Inlet
- Performance Ratings — High Mach Inlet
- Reverse Thrust Performance
- Acoustic Baseline — Bellmouth, Hardwall
- Suppressed Acoustics — High Mach Inlet, Treatment
- Transient Thrust Response

24

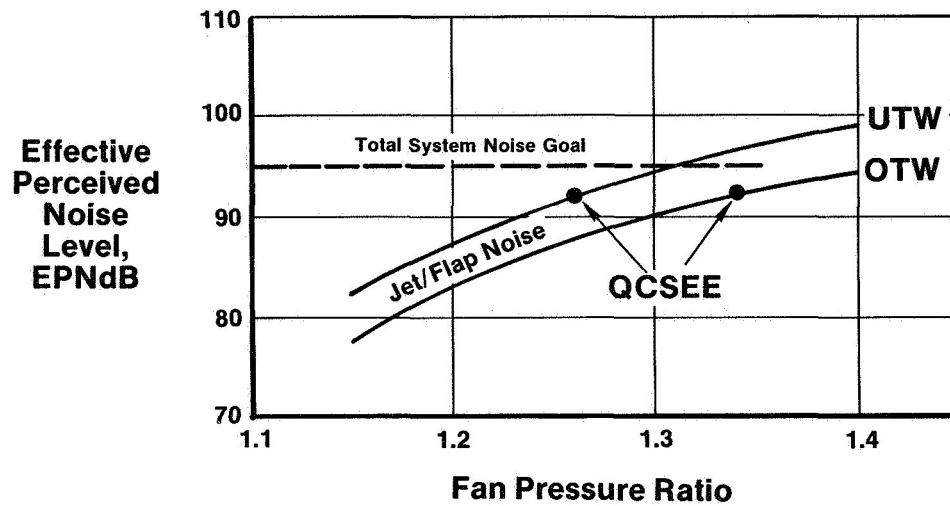# Effect of Jet Flap Noise on Fan Pressure Ratio Selection
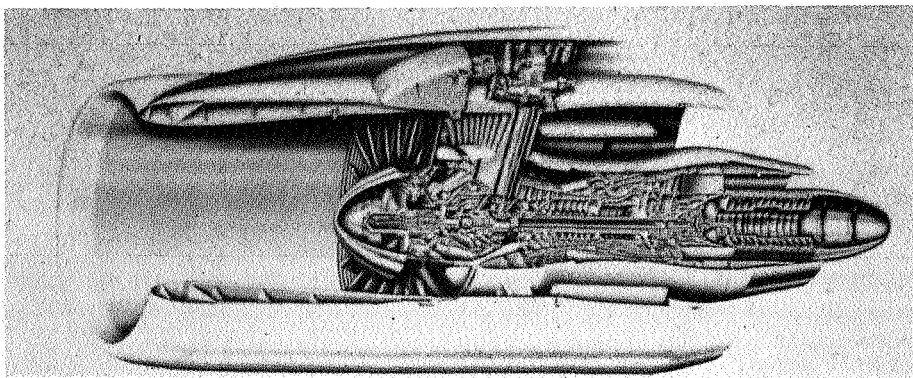

Figure 1

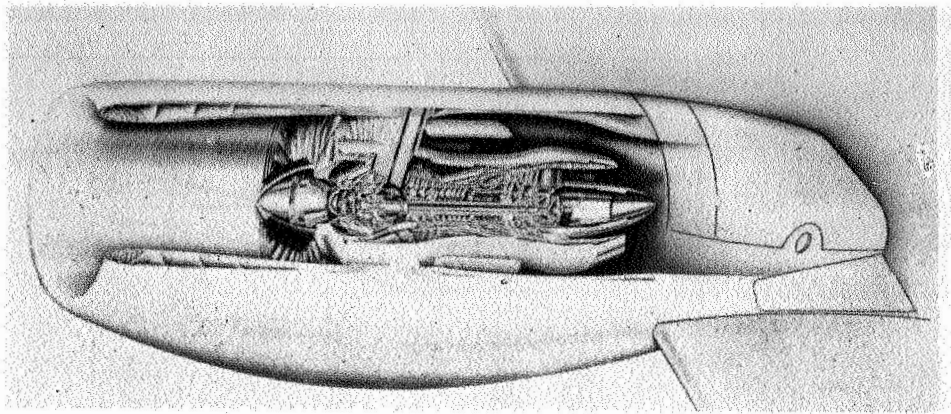# UTW Propulsion System

Figure 2

25

OTW Propulsion System

Figure 3

Baseline UTW Aircraft

70,620 kg (155,700 lb) TOGW
926 km (500 n.mi.) Range
162 Passengers
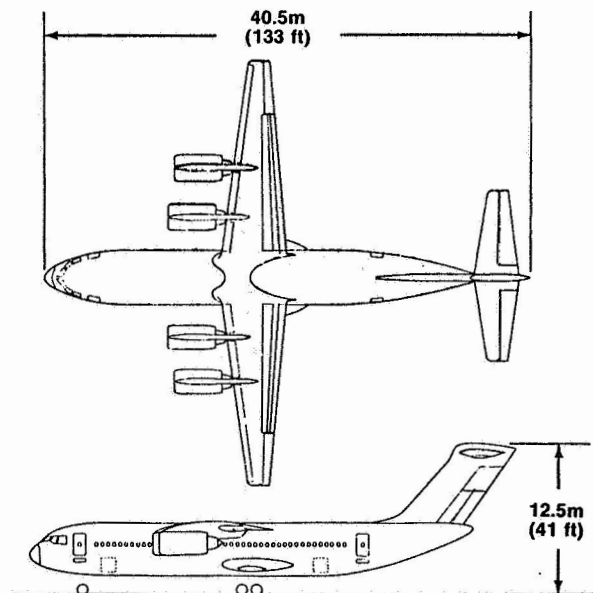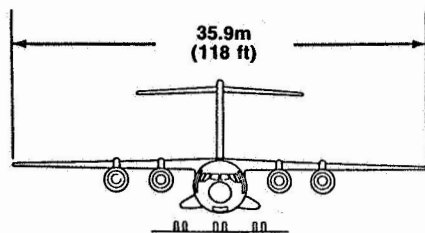**914.4 m (3000 ft) Runway**
4 Engines @ 81,400N (18,300 lb) Thrust

40.5m (133 ft)

35.9m (118 ft)

12.5m (41 ft)

Figure 4

Baseline OTW Aircraft

90,040 kb (198,500 lb) TOGW
926 km (500 n.mi.) Range
197 Passengers
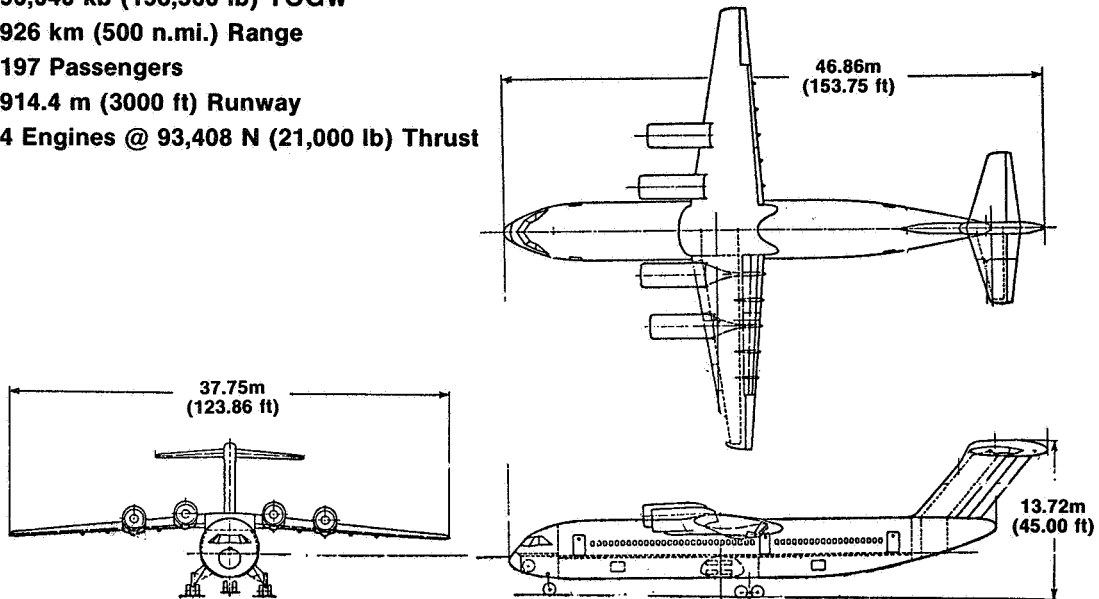**914.4 m (3000 ft) Runway**
4 Engines @ 93,408 N (21,000 lb) Thrust

46.86m
(153.75 ft)

37.75m
(123.86 ft)

13.72m
(45.00 ft)

Figure 5

UTW Cross-Section

Digital Control

F101 Core & LPT

High Throat Mach No. Inlet

Main Reduction Gear

Composite Fan Duct

Acoustic Splitter

Variable Area Composite Fan Nozzle

Variable Pitch Composite Blades

Composite Fan Frame

Composite Core Cowl
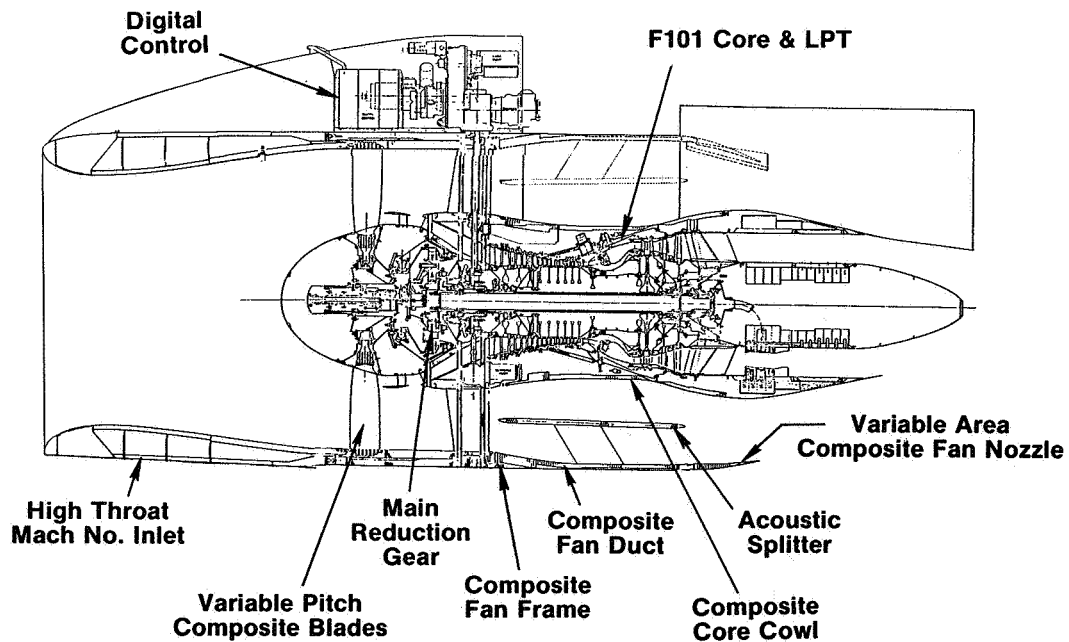
Figure 6

OTW Cross-Section

Full Authority Digital Control

F101 Core & LPT

Fixed Pitch Titanium Blades

Main Reduction Gear

Composite Fan Frame

"D" Shaped Exhaust Nozzle/Thrust Reverser
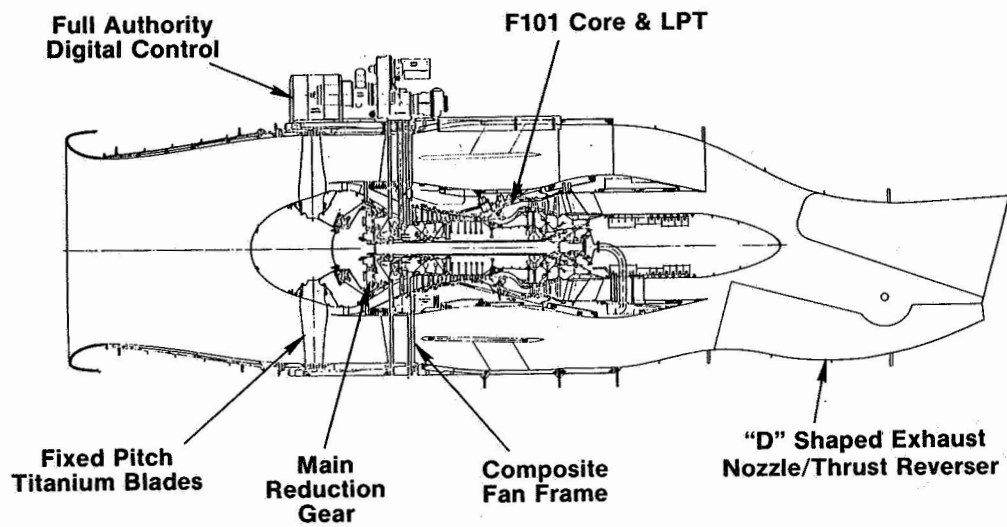
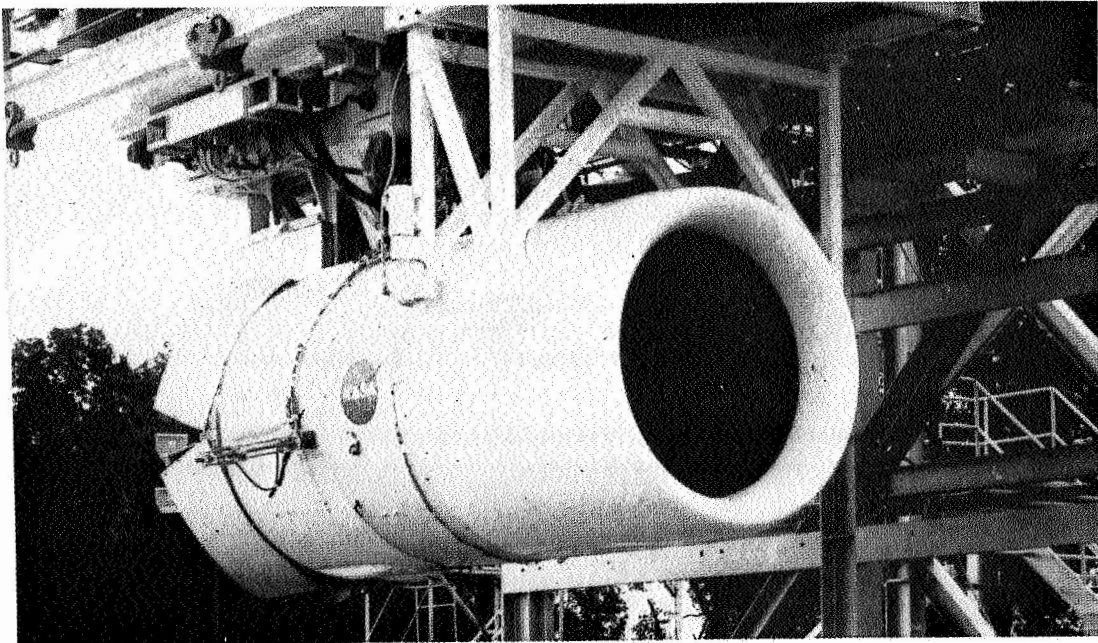Figure 7

QCSEE UTW Engine

Figure 8

OTW Propulsion System
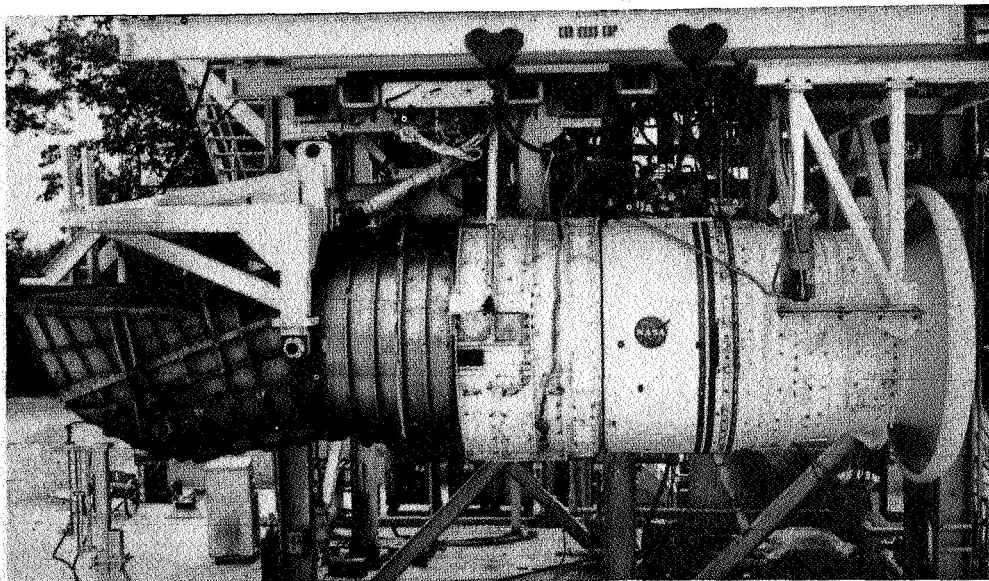# Test Installation

Figure 9

QCSEE FAN AERODYNAMIC DESIGN AND PERFORMANCE*

C.C. Koch
General Electric Company
Cincinnati, Ohio

INTRODUCTION

Two different fans were designed for the QCSEE program, each tailored to a particular engine cycle and operational requirements. The reversible - pitch fan for the Under-the-Wing engine is described in the first section of this paper. Its aerodynamic design, scale model test results and engine performance test results are presented. The design of the fixed-pitch fan for the Over-the-Wing engine is described in the second section, along with its performance measured during engine tests.

UTW FAN AERODYNAMICS

Aerodynamic Design - A cross section of the fan for the UTW engine is shown in figure 1. One of the notable features of this fan was the low aspect ratio, unshrouded, composite rotor. The low tip speed rotor blades were attached to a variable pitch mechanism and were fully reversible through either flat pitch or stall pitch. The flowpath over the rotor tip was made to be a portion of a sphere to avoid changes in tip clearance as the rotor pitch was varied. Circumferential groove casing treatment was used over the rotor tip to increase stall margin at cruise with little or no efficiency penalty.

Another notable feature of the design was the unusual arrangement of the fan stators. The inner stator vane was placed under a ring-shaped island closely coupled to the fan rotor which served as the primary splitter dividing the bypass flow from the flow to the core engine. An annular slot was left open aft of this assembly, and a second flow splitter was provided at the rear of the slot for use during reverse operation. The split stator arrangement was chosen over more conventional alternatives, such as a full span stator, because it reduced the length required from fan rotor to core compressor inlet, and because it allowed the rotor hub's full loading potential to be used without incurring high stator hub Mach numbers or loadings. The close coupled splitter and inner stator arrangement by itself would have been unsatisfactory for reverse operation, because flow drawn backwards through the bypass stream outlet guide vanes and entering the core engine would have impinged upon the highly-cambered inner stators at incidence angles of perhaps minus 70°. The annular slot was thus provided to allow air to be drawn directly into the core engine in reverse operation, significantly improving the pressure recovery of the core flow.

31

The bypass stream outlet guide vanes served as structural elements in the fan frame. The pylon nose was integrated into the vane/frame, and circumferentially varying airfoil geometry was used to guide the flow smoothly around the pylon. A wide spacing between the fan rotor and the bypass vane/frame was used to reduce noise.

Key operating points for the UTW fan are indicated on the portion of the predicted performance map shown in figure 2. The takeoff point was selected to be on a low operating line, at a bypass stream pressure ratio of 1.27, to keep jet velocity low for reduced noise. The engine inlet was sized at this point to have a high throat Mach number of 0.79 to reduce forward radiated fan noise. The maximum cruise point pressure ratio of 1.38 was on a higher operating line, reached by closing the variable exhaust nozzle, to increase thrust at altitude. The corrected airflow at cruise was limited to the takeoff value because inlet losses would have become unacceptable if the inlet throat Mach number were increased. The fan's aerodynamic design point was chosen to be on an intermediate operating line.

Some advantages of the variable pitch rotor for forward mode operation are shown in figure 3. The dashed speedlines indicate how fan flow at a given speed could be varied by changing rotor pitch. At the takeoff condition it was estimated that the fan speed required to achieve the objective flow and pressure ratio could be reduced approximately 3% by opening the rotor pitch by 2°. This potentially could result in a worthwhile reduction in noise. At cruise, the speed could be increased several percent by closing the rotor pitch 2°. This both increased fan stall margin and also reduced the low pressure turbine's loading thereby increasing its efficiency. Variable pitch could thus allow the trends of fan efficiency versus speed and pitch angle and of turbine efficiency versus speed and loading to be exploited to seek a minimum level of fuel consumption at cruise.

A summary of fan aerodynamic design parameters is given in table I. The low tip speed of 306 m/s (1005 ft/sec) and the high bypass ratio of 11.3 are notable features. Also notable is the low solidity of the fan rotor; the solidity was less than 1.0 across the full span of the blade to permit the rotor to be reversed.

A photograph of the full scale UTW fan rotor is shown in figure 4. The black color of the blades is a result of the graphite-epoxy material used; the metal strip on the leading edge is for erosion resistance. The low aspect ratio and low solidity of the blades are apparent in this photo. Part of the variable pitch mechanism can be seen in the hub of the fan.

A section through the bypass vane/frame is shown in figure 5. Each of the 33 low aspect ratio vanes was a structural member made of composite material. The pylon extended forward to the leading edge of the vane row and contained the accessory drive shaft. The leading edge of the pylon nose was given a cambered airfoil shape to properly align it with the approaching flow. Five different types of airfoils, each with its own unique camber and stagger, were used to divert the flow smoothly around the pylon. Two of the five types of airfoils are shown. A non-standard vane spacing was even used

to the left side, or suction, surface of the pylon's nose to help reduce a local high back pressure region so as to avoid potential performance losses or noise sources.

The generation of reverse thrust by changing the rotor pitch is illustrated in the next series of figures. A top view of the rotor at its nominal design pitch angle in forward mode operation is shown in figure 6 for reference. Airflow approaches the rotor axially, as there are no inlet guide vanes to impart swirl. Hub, pitchline and tip blade sections are shown to illustrate the twist required to keep the blade aligned with the relative flow direction.

As shown in figure 7, when the blade is reversed through flat pitch, the blade is closed some 70°-90°. During closure, the normal forward flow drops smoothly to zero, and then reverse flow is gradually established. In reverse, flow is drawn backward through the bypass vane/frame, and the absolute flow vector is given swirl opposite to the direction of rotor rotation. The twist of the blade is in the wrong sense in revese mode; flow through the hub is blocked off by the rotor, and only the tip section pumps air out the inlet duct. It can also be seen that the blade's camber is in the wrong sense when the blade is reversed through flat pitch, since the flow is deflected away from the axial direction rather than toward axial. In order to pump the air despite the reverse camber, the blade must operate at a high incidence angle. It is thus expected that the pumping ability and the efficiency of the fan will be relatively low when reversed through flat pitch.

Blade orientation when reversed through stall is shown in figure 8. In this case the blade is opened 95°-105°. Initially a stall takes place, and after further opening, normal airflow ceases and reverse flow becomes established. The trailing edge of the rotor becomes the effective leading edge during reverse through stall pitch operation. Although the rotor's twist is still in the wrong sense, and the flow is still blocked at the hub, the camber is now in the proper direction for a compressor blade. It is thus expected that pumping and efficiency will be highest when the rotor is reversed through stall.

Scale Model Test Results - A 50.8 cm (20-inch) diameter model, having a 0.282 linear scale factor, of the UTW fan was built for aero performance and acoustic testing. A photo of the scale model fan is shown in figure 9. Adjustable metal blades were used for the test rig. These could be fixed at any pitch angle, but could not be varied while running. Tests were conducted in both forward and reverse modes of operation at several pitch angles in each mode.

A performance map for the bypass portion of the fan flow in forward mode operation at the nominal design rotor pitch angle is shown in figure 10. The design pressure ratio, flow and efficiency are indicated by the target symbols, and the objective stall line is shown dotted. Performance maps similar to the one shown were also obtained at 5° open and 5° closed rotor pitch angle settings. Tests results indicated that stall margin goals and the design point efficiency goal of 86.5% had been met. At 100% speed the design flow was achieved at low operating lines, but flow and pressure ratio were

below objectives on an operating line through the design point. Analysis indicated that the rotor blade tip sections lacked circulation capacity at higher loadings. A redesign to increase rotor camber would have increased the pumping of the fan on the design operating line, but because of the low solidity this might have reduced efficiency by opening the throat areas. For this reason, and because of a tight manufacturing schedule, it was decided that the blades to be built for the full scale engine would not be re-designed.

The 95% speed lines obtained at the three pitch angles are shown in figure 11. This is the fan speed at which takeoff thrust was to be obtained in the experimental engine, and the objective takeoff flow, pressure ratio and efficiency are indicated in the figure by solid symbols. Despite the fan's lower-than-design pumping capacity, the flexibility of the variable rotor pitch feature enabled the fan to meet the very important engine system takeoff flow and pressure ratio goals simply by opening the rotor 3° from nominal instead of 2° as originally estimated.

Fan hub performance measured during scale model tests at 100% design corrected speed for the three rotor pitch angles is shown in figure 12. Design hub pressure ratio was nearly achieved at design flow with the nominal design pitch angle. The 78% hub efficiency goal was met at the design operating line, and was exceeded by a substantial margin at higher operating lines.

Reverse mode test results from the fan scale model program are shown in figure 13. Fan pressure ratio from the OGV exit to the engine inlet throat is plotted versus rotor corrected flow for five different reverse pitch angle settings: closed through flat pitch by 73° and 78°, and opened through stall pitch by 95°, 100° and 105°. The data points for a given pitch angle represent different speeds. Only a single operating line could be evaluated at each pitch angle, since the engine inlet (which serves as the exhaust nozzle in reverse mode operation) was a fixed geometry device. The various combinations of flow and pressure ratio needed to achieve the reverse thrust objective of 35% of takeoff thrust are indicated by the heavy dark band. Although the reverse thrust goal could not be met when reversing through flat pitch because of speed limits or high rotor stresses, the reverse thrust ojective was met for all three of the reverse through stall pitch angles tested.

Engine Test Results - Full scale fan performance was evaluated during tests of the UTW experimental engine. The engine, shown during build-up in figure 14, was fully instrumented for performance testing, and data were re-corded in both forward and reverse modes of operation. Since all tests were conducted at sea-level static inlet conditions, emphasis was placed on deter-mining performance on lower operating lines near the takeoff power setting.

Fan bypass stream performance in the forward mode of operation is shown in figure 15. All data points are at the objective takeoff corrected speed, 95% of the aero design value, and are at three different rotor pitch angle settings. The solid speed lines in the background indicate performance mea-sured during scale model tests. The full scale fan's performance on the engine was very close to that expected as a result of the scale model tests;

the efficiency appeared to be slightly better than in the scale model, espe-
cially with the rotor closed 5°. Full scale fan tests confirmed that the
takeoff flow and pressure ratio goals could be met at 95% speed with
approximately a 3° open rotor pitch angle setting. Similar good agreement
with the scale model test results was obtained over the entire range of
speeds and pitch angles that could be evaluated in the engine.

Full scale fan hub performance at 95% corrected speed for the same three
pitch angle is shown in figure 16. In the engine tests, fan hub data were
recorded at the inlet of the core engine rather than behind the fan's inner
stator, and thus stator exit total pressure was reduced by an estimated 1.5%
transition duct pressure loss. At the low pressure ratio of the fan hub at
the takeoff condition, this duct loss reduced the efficiency by approximately
seven points. The fan hub turbomachinery efficiency at takeoff pressure
ratio was actually about 80% rather than being in the low 70's as shown in
figure 16 for the overall hub compression. As shown in the figure, the fan
hub performance in the engine was better than in the scale model tests, par-
ticularly at closed rotor pitch angles, and the core engine supercharging
goal was exceeded.

A limited amount of reverse through stall pitch testing was conducted on
the engine with the aero performance instrumentation installed. These engine
test results are shown in figure 17 plotted as overall pressure ratio from
atmospheric engine inlet to fan rotor exit versus total engine flow corrected
by engine inlet conditions. The upper family of curves indicates reverse
mode performance predicted from the scale model tests, while the symbols
indicate engine test data. Although flow at a given speed and pitch angle
was within a few percent of the scale model level, the engine's fan overall
pressure ratio was noticeably lower than expected. Since the inlet pressure
was taken as atmospheric for the data in figure 17, higher flow induction
losses in the exhaust duct would have contributed to the low apparent fan
pressure ratio. Limited traverse data taken in the engine's aft duct during
reverse operation indicated that pressure recovery was 1-2% lower than mea-
sured in the fan scale model tests, and the recovery could well have been
even lower than the traverse data indicated. The apparent low fan operating
line could also be the result of the effective discharge area being larger in
the engine than in the scale model. The blockage due to fan exit pressure
rakes was less in the engine than in the scale model, but this difference
alone was not sufficient to fully account for the low operating line. A
final possibility is that some other factor may have affected the size of
the stagnant flow region along the centerline of the engine inlet, thus
altering the fan's effective discharge area. Possible causes of this effect
include differences in the ratio of core engine flow to fan flow and differ-
ences in fan rotor hub platform shapes. Although insufficient data were re-
corded during engine tests to resolve this question, it is an area that de-
serves further testing and analysis since it directly affects the ability to
predict the reverse mode performance of this type of fan.

Although the fan's pumping in reverse mode was less than expected, the
engine system was able to produce 27% of takeoff thrust in reverse, compared
to the goal of 35%. While less than the goal, this level of reverse thrust
is believed to be sufficient for many applications.

35

UTW Fan Performance Summary - Principal performance results of the UTW fan tests are as follows:

In the scale model test program -

o   The engine bypass efficiency goal of 86.5% was met, but flow and pressure ratio were low by about 5% at the design operating line.

o   Engine takeoff flow and pressure ratio goals were met at 95% speed, provided the rotor pitch angle was opened 1° more than originally predicted.

In the engine test program -

o   Engine data in forward mode agreed well with scale model perfor-
ı   mance through 95% speed on the takeoff operating line, and hub efficiency in particular was 1-3 points higher.

o   Engine reverse thrust was less than expected from scale model tests, but 27% of takeoff thrust was achieved versus a goal of 35%.

OTW FAN AERODYNAMICS

Aerodynamic Design - A cross section of the fan for the OTW engine is shown in figure 18. Compared to the UTW fan, the OTW fan had a conventional fixed pitch rotor and had a higher tip speed, a higher pressure ratio and a higher rotor solidity. It also had low aspect ratio unshrouded rotor blades that were designed to be fabricated from composite materials, although tita-nium blades were used in the QCSEE OTW experimental engine. A flow splitter and inner stator were close-coupled behind the rotor, and the composite by-pass vane/frame was identical in its aero design to that used in the UTW engine.

A portion of the predicted OTW fan performance map is shown in figure 19. The aero design point bypass pressure ratio was 1.36. This point was selected to be midway between the lower, takeoff, operating line and the higher, cruise, operating line. A variable exhaust nozzle enabled the fan operating line to be adjusted to meet flight conditions. Maximum cruise and takeoff again occurred at the same flow because of inlet throat Mach number limits.

A summary of OTW fan aerodynamic design parameters is listed in table II. The fan's tip speed of 1175 ft/sec, while higher than in the UTW engine, was still a relatively low value. Of those features listed the aerodynamic design feature of greatest significance in the OTW fan was the effort to achieve a high hub pressure ratio. The design radial profile of total pres-sure ratio at the fan rotor exit is shown in figure 20. The average hub

pressure ratio was 1.43, higher than the 1.36 average value in the bypass stream. The tip speed was set 17% higher than in the UTW fan, and a higher rotor hub solidity (made possible by use of a fixed pitch rotor was used to aid in achieving the high core supercharging.

A photograph of the rotor for the OTW fan is shown in figure 21. The low aspect ratio (2.1) of the 28 unshrouded titanium blades is evident in this view.

Engine Test Results - Fan performance was evaluated during tests of the Over-the-Wing Engine. There was no scale model component test conducted for the OTW fan. A photograph of the OTW engine during build-up is shown in figure 22. A full complement of fan performance instrumentation was installed during the engine tests.

Fan bypass stream performance data from the engine tests are shown in figure 23. At 100% design corrected speed the fan exceeded its flow and pressure ratio goals by '2-3%. The 86.5% bypass stream efficiency goal for the experimental engine was met or exceeded along an operating line through the design point. Peak fan efficiency was on a lower operating line than the lowest tested, possibly near the takeoff operating line, so the exact level of peak efficiency at high speed was not determined. No stall testing was attempted during the engine performance runs, and no fan stalls were encountered. It was thus not possible to determine if the fan was able to meet its stall margin objectives, although 10% stall margin was demonstrated at 95% corrected speed.

Fan hub performance results are shown in figure 24. These were based on measurements recorded at core engine inlet, so the design objective pressure ratio and efficiency on this performance map (indicated by the target symbols) have been lowered consistent with an estimated 1.5% transition duct pressure loss. Hub performance results were quite encouraging in that the high level of core supercharging was achieved at 100% speed. Efficiencies at the design operating line were approximately equal to the goal (78% for the turbomachinery alone) and were significantly higher than the goal at higher operating lines.

OTW Fan Performance Summary - Principal performance results of the OTW fan tests are as follows:

o   Fan bypass pressure ratio and flow exceeded design goals by 2-3%, and the engine's bypass efficiency goal of 86.5% was met at the design operating condition.

o   The high design hub pressure ratio was exceeded, and the design hub efficiency goal of 78% was' met at the design operating line. Peak hub efficiency was quite high.

37

CONCLUSIONS

Both the OTW and UTW fans performed satisfactorily during sea-level static engine tests, and most of the fan aero performance goals established for the experimental engine programs were met. Some further development of the UTW fan would be required for it to meet its altitude cruise performance goals, and the reduced pumping of this fan during engine reverse mode tests needs to be understood and improved. Important advances in fan aero technology were demonstrated during the QCSEE program, and these advanced fan features can be used with confidence in future turbofan engines for short-haul aircraft.

TABLE I. – UTW FAN AERO DESIGN FEATURES

Tip Speed	306 m/s (1005 ft/sec)
Radius Ratio	0.44
Specific Flow	199 kg/sec-m^2 (40.8 lbm/sec-ft^2)
Bypass Pressure Ratio	1.34
Core Pressure Ratio	1.23
Bypass Ratio	11.3
Inlet Tip Relative Mach No.	1.13
Rotor Tip Solidity	0.95
Rotor Hub Solidity	0.98
Rotor Aspect Ratio	2.1
Number of Blades	18
Number of OGV's/Inner Stators	33/96

TABLE II. – OTW FAN AERO DESIGN FEATURES

Tip Speed	358 m/s (1175 ft/sec)
Radius Ratio	0.42
Specific Flow	194 kg/sec-m2 (39.8 lbm/sec-ft2)
Bypass Pressure Ratio	1.36
Core Pressure Ratio	1.43
Bypass Ratio	9.9
Inlet Tip Relative Mach No.	1.22
Rotor Tip Solidity	1.30
Rotor Hub Solidity	2.23
Rotor Aspect Ratio	2.1
Number of Rotor Blades	28
Number of OGV's/Inner Stators	33/156

39

UTW Fan Cross-Section
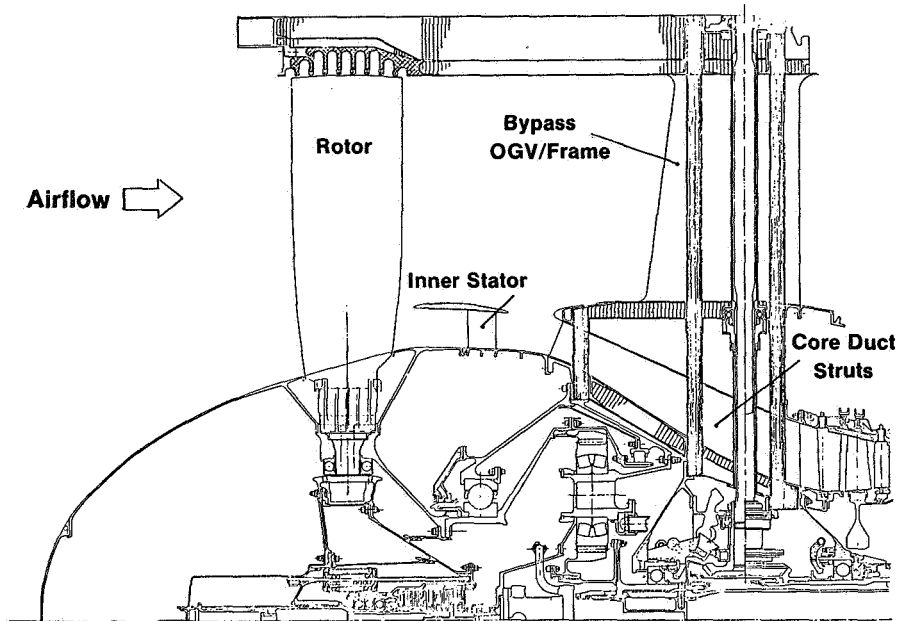
Figure 1

UTW Variable-Pitch Fan Design Map

Figure 2

40
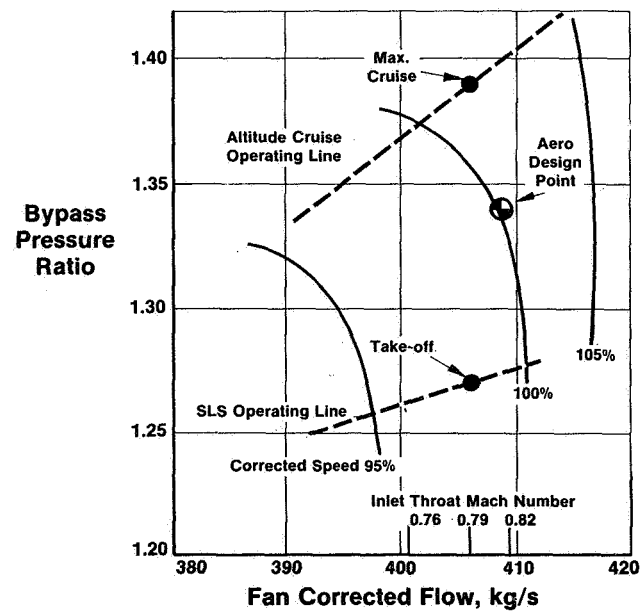
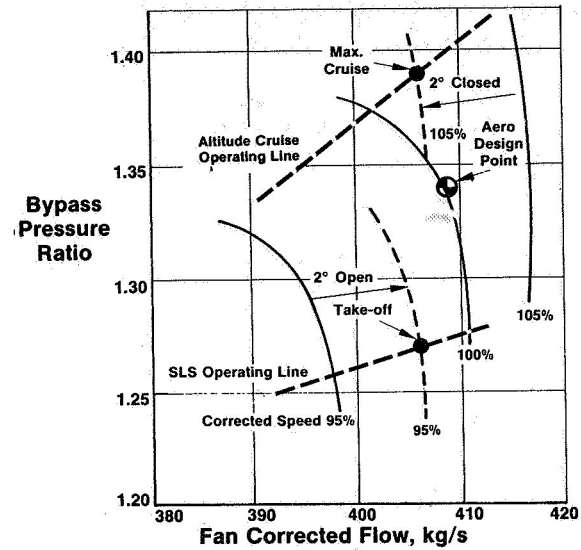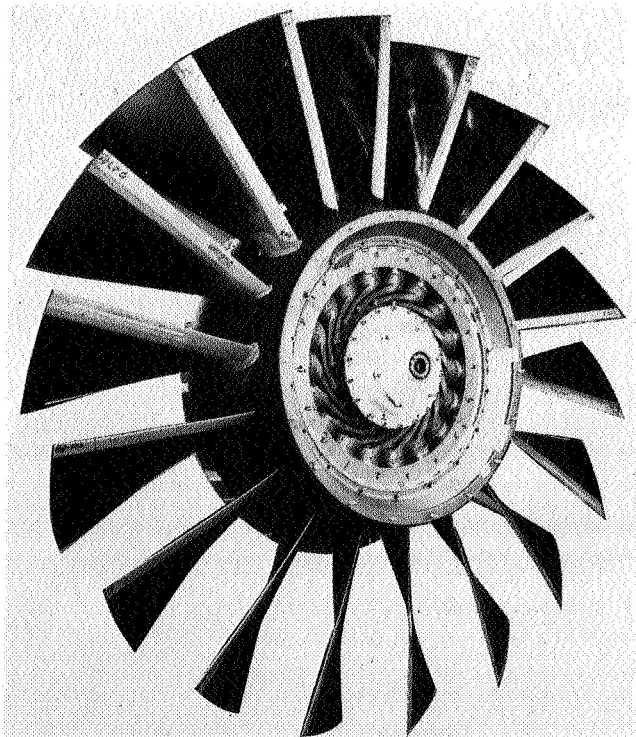# UTW Variable-Pitch Fan Design Map

Figure 3

UTW Fan Rotor

Figure 4

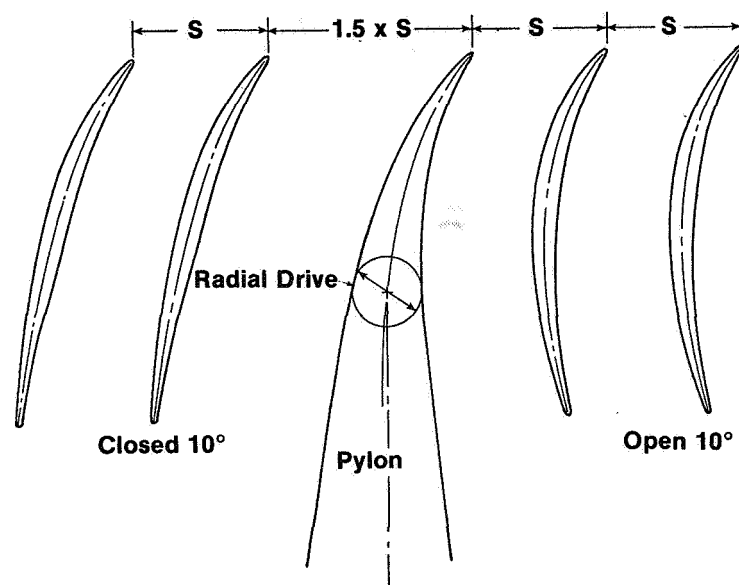# Fan Bypass OGV Design

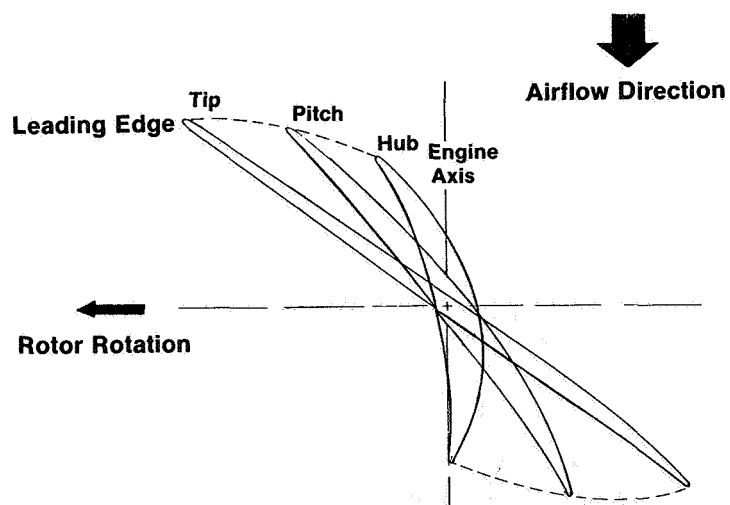

Figure 5

UTW Fan Rotor Blade
Forward Mode Operation

Figure 6

UTW Fan Rotor Blade
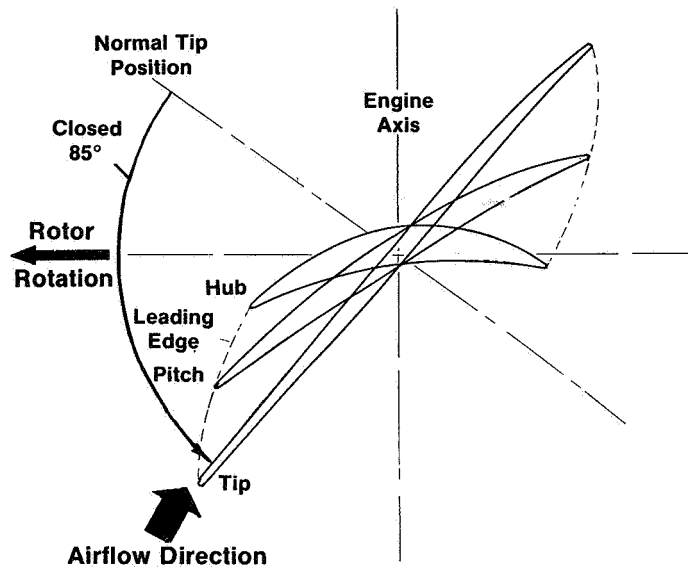# Reverse Through Flat Pitch Operation

Figure 7
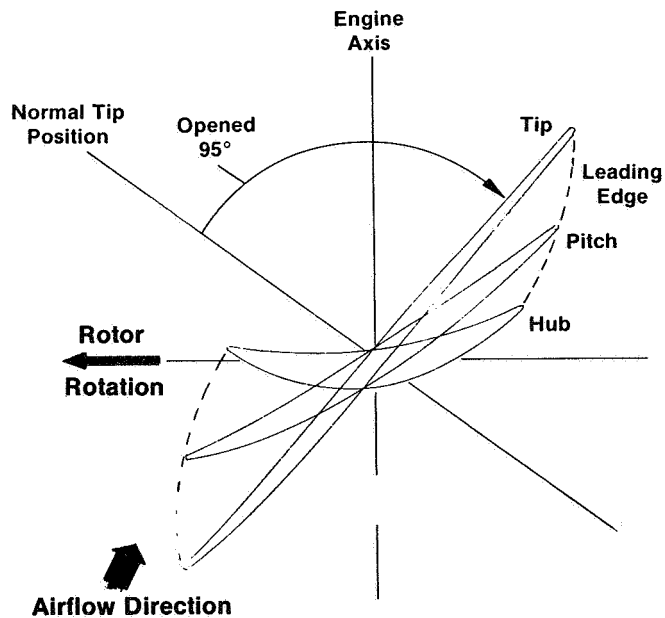
UTW Fan Rotor Blade
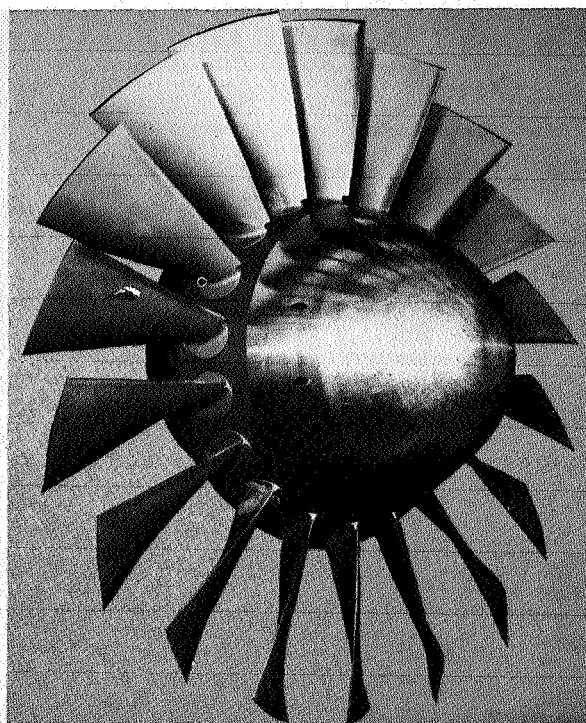# Reverse Through Stall Operation

Figure 8

43

Figure 9

UTW Fan Scale Model
Bypass Performance

Nominal Rotor Pitch Angle

Figure 10

44
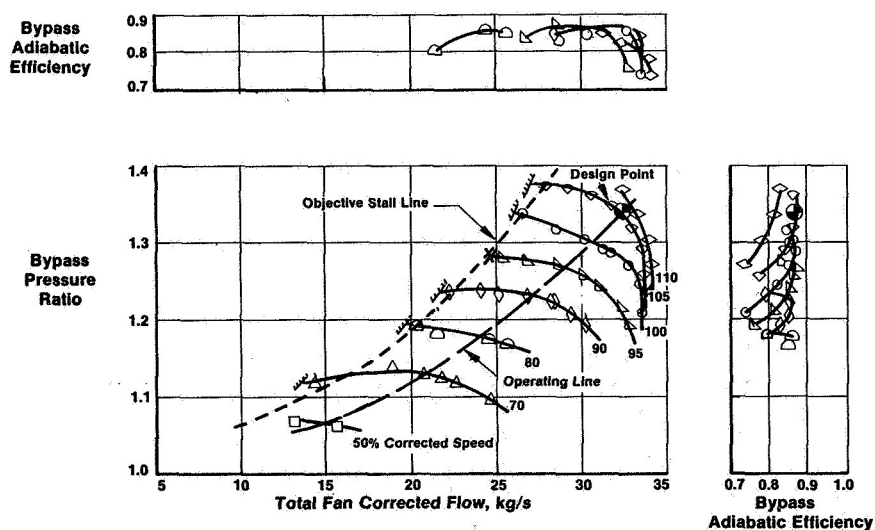
UTW Fan Take-off Operation
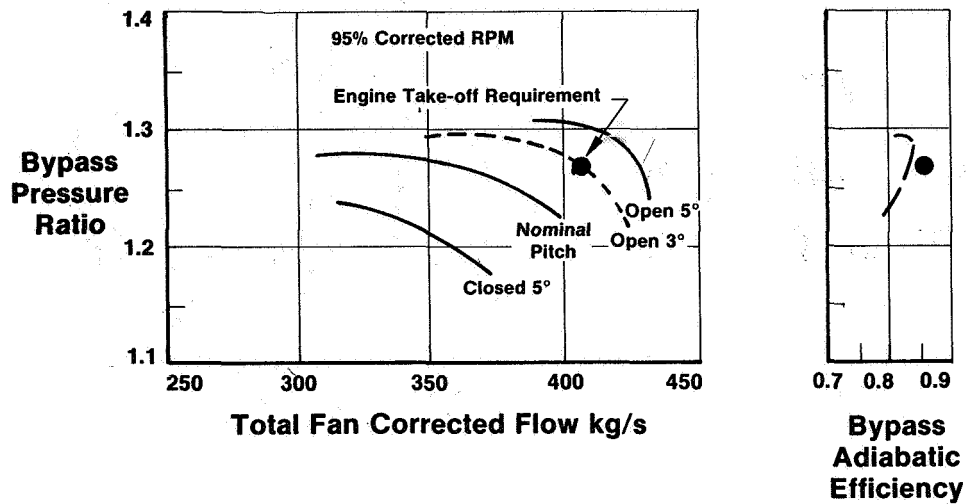
Scaled From Scale Model Data

Bypass Pressure Ratio

95% Corrected RPM

Engine Take-off Requirement

Open 5°

Nominal Pitch —Open 3°

Closed 5°

Total Fan Corrected Flow kg/s

Bypass Adiabatic Efficiency

0.7 0.8 0.9

Figure 11

UTW Fan Scale Model

Hub Performance
100% Corrected Speed

Hub Pressure Ratio

Design Point

Open 5°

Nominal Pitch

Operating Line

Closed 5°

Total Fan Corrected Flow, kg/s

Hub Adiabatic Efficiency
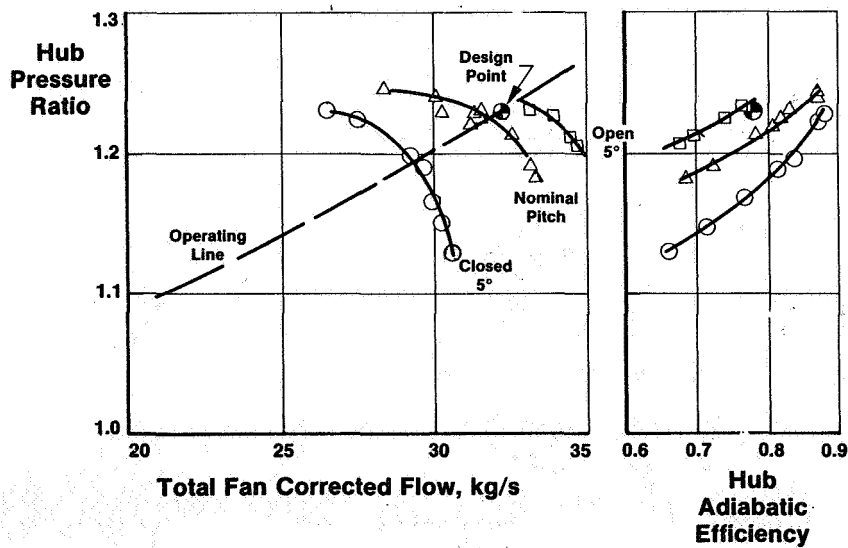
0.6 0.7 0.8 0.9

Figure 12

45

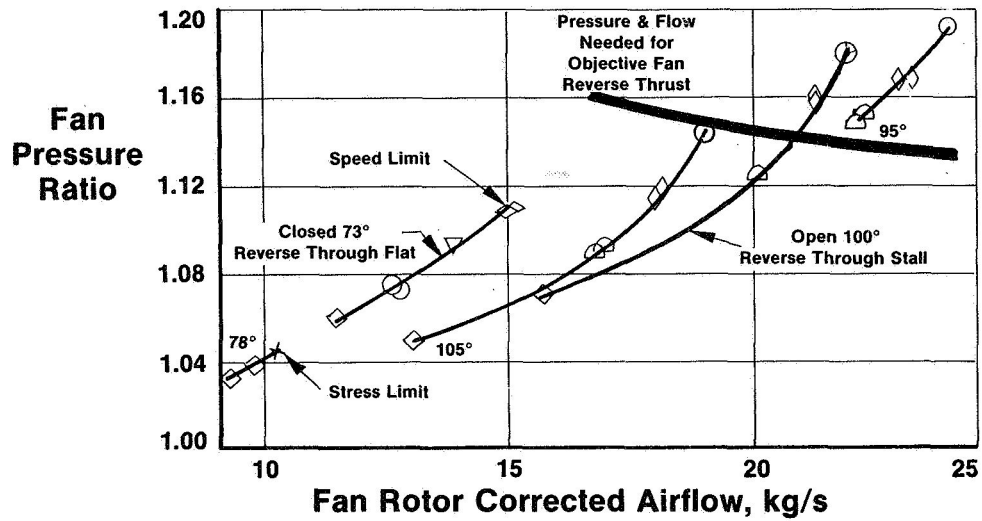# UTW Fan Scale Model Reverse Mode Performance

Figure 13

UTW Fan

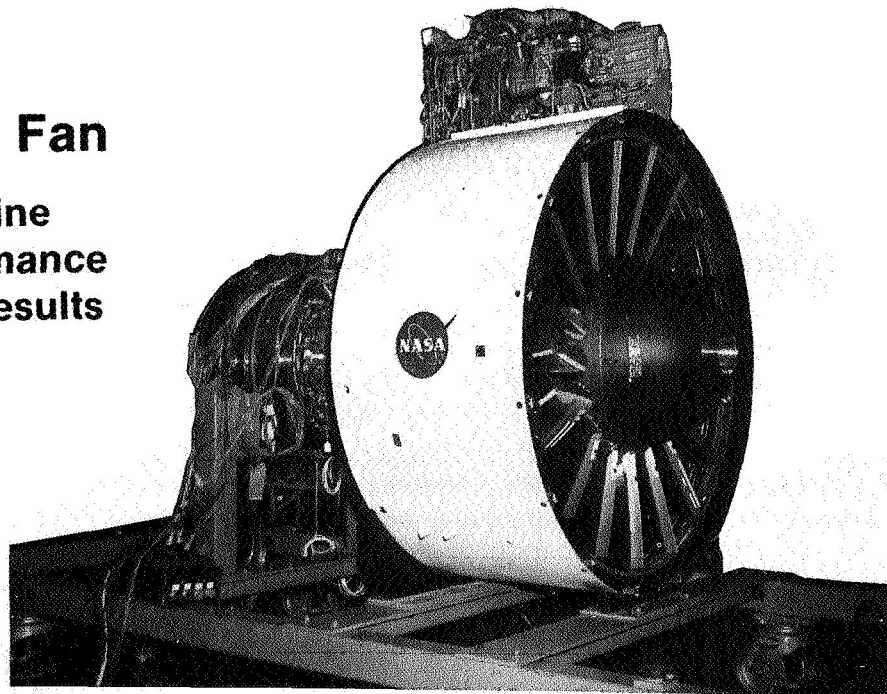### Engine Performance Test Results

Figure 14

46

UTW Engine
Fan Bypass Performance at 95% Speed
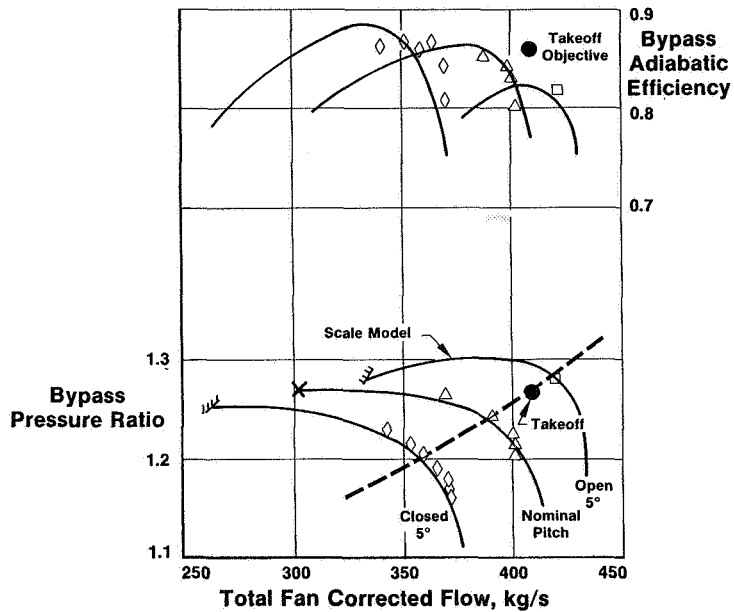
Figure 15

UTW Engine
Fan Hub Performance at 95% Speed
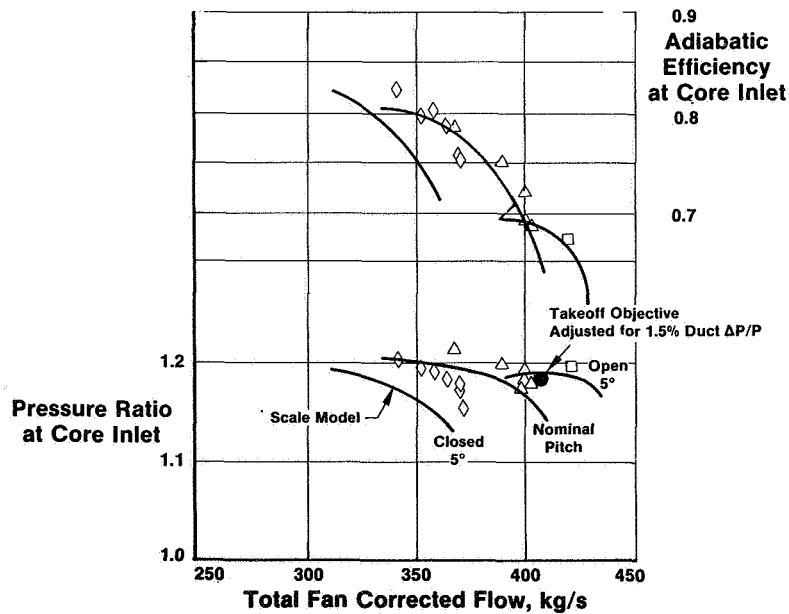

Figure 16

47

UTW Engine
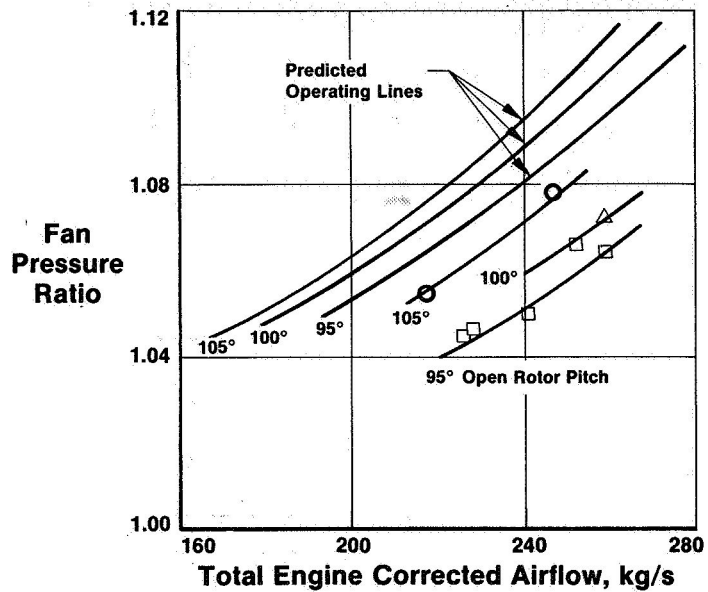# Fan Reverse Performance
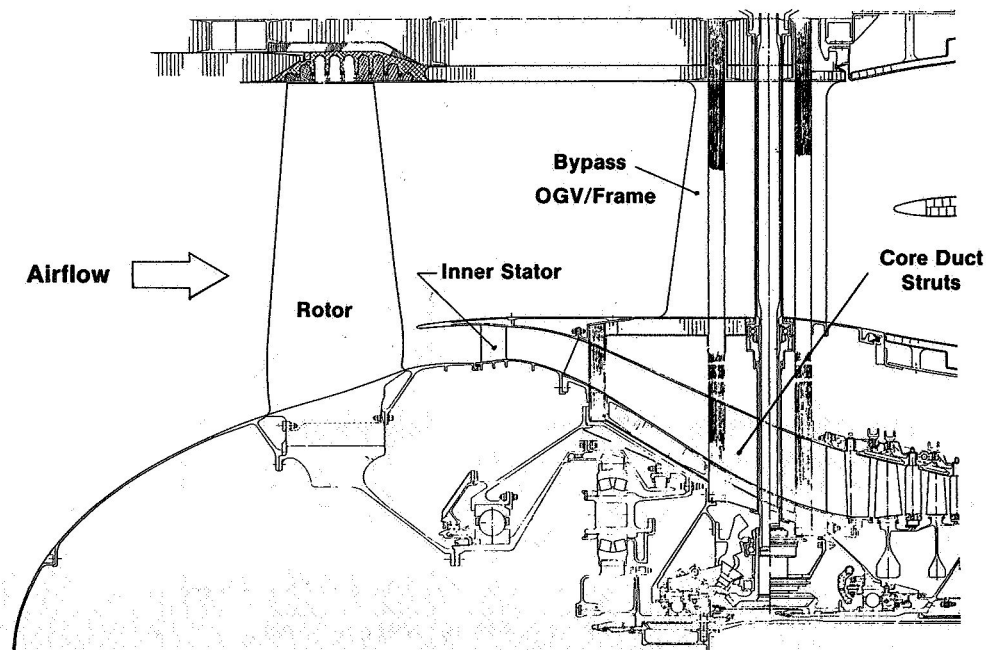

Figure 17

OTW Fan Cross-Section

Figure 18

48

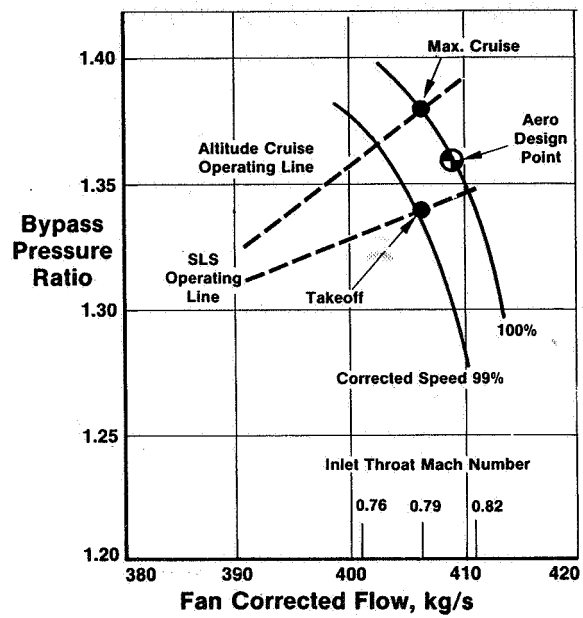# OTW Fan Design Map

Figure 19

Rotor Design Total-Pressure Ratio Radial Profile
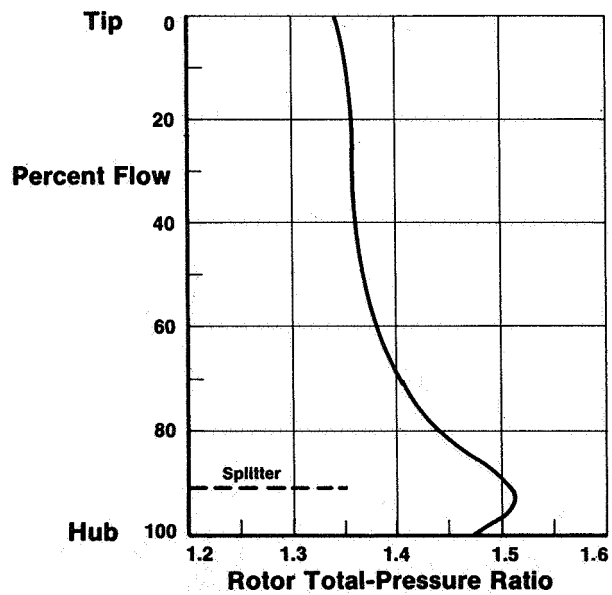

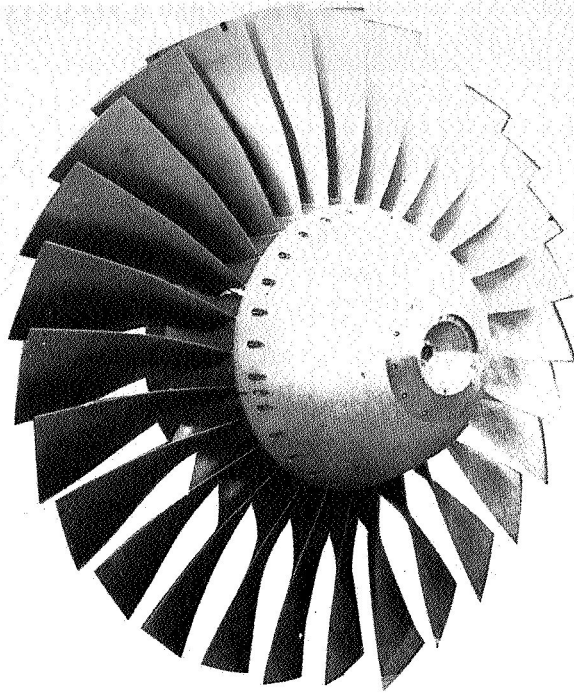Figure 20

**OTW
Fan
Rotor**

Figure 21

OTW Fan

**Engine
Performance
Test Results**
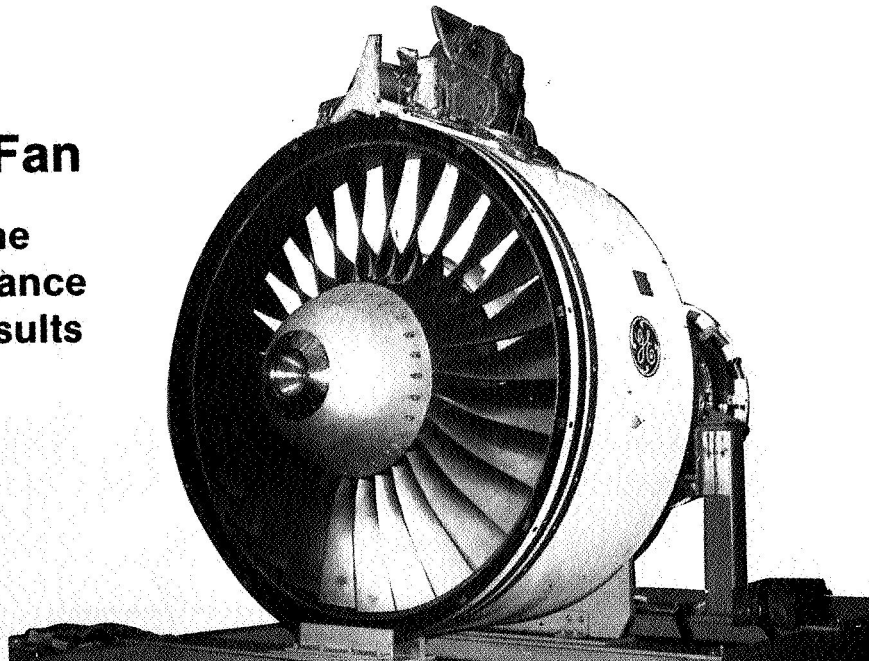
Figure 22

OTW Fan Bypass Performance
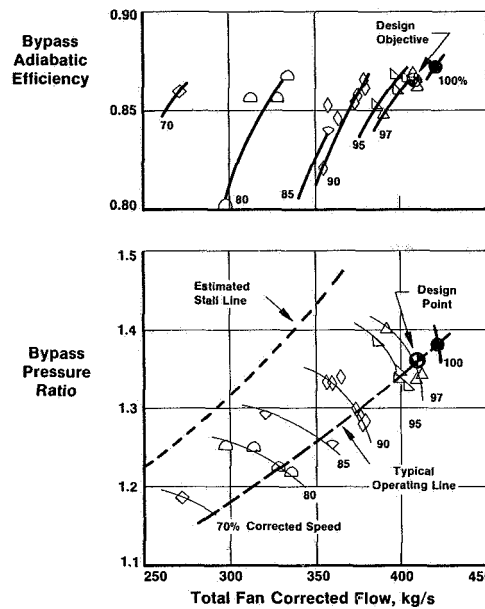
Figure 23

OTW Fan Hub Performance

Figure 24

51
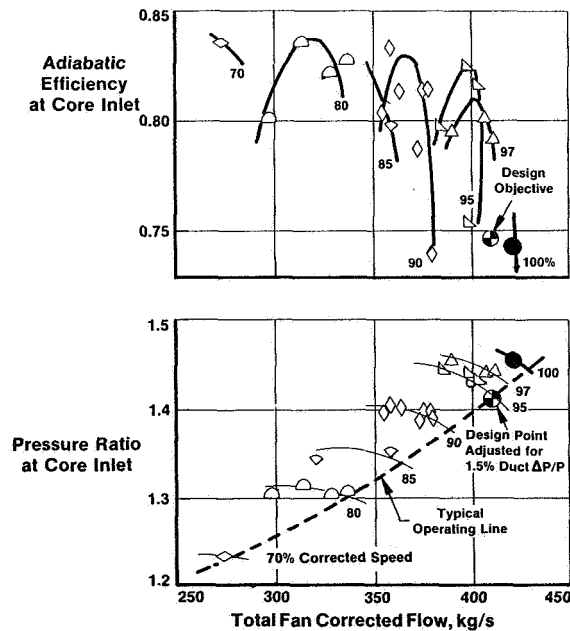
QCSEE CAM/HARMONIC PITCH ACTUATION SYSTEM[*]

R.M. Levintan
Hamilton Standard
Windsor Locks, Connecticut

INTRODUCTION

This paper covers the program that was conducted to design, fabricate and test a pitch change actuation system for the under-the-wing QCSEE engine. The term "Cam/Harmonic" will become clearer to you as the details of the system are described. As you will see, the concept embodies a number of significant technology advancements that have not been embodied in previous variable pitch systems. The work was performed under a cost-shared, sub-contract to G.E. and culminated with deliverty of the actuation system for incorporation into the initial build of the under-the-wing engine. The paragraphs that follow will cover the design requirements for this system, alternate concepts studied, a description of the selected design, and results of whirl rig testing of the system prior to engine operation.

DESIGN REQUIREMENTS

The design criteria for the actuation system were established consistent with the demands of commercial service. The mission cycles, major component life and bearing life values used for the design reflected this philosophy as follows.

o   48,000 Missions

o   36,000 Hours Major Components
    9,000 Hours Bearings and Expendables

o   Actuation Rate 135°/sec

o   Feedback Accuracy ±1/4°

o   Net Blade Twisting Moment - Function of Blade Angle

No compromise in design criteria or weight were accommodated for the fact that the system was to be used in a short test life, experimental engine. The only deviation from this approach was in selection of such readily available items such as hydraulic motors, servo valves, etc.

The high rate of pitch change capability designed into the system reflected the need to accomplish very rapid reverse thrust dictated by STOL aircraft operation. In addition, rapid thrust response would be possible for go-around operation. The feedback accuracy is important to obtain control system accuracy.

The actuation system is required to overcome the twisting moment loads inherently present in a variable pitch system; these loads vary as a function of blade angle as shown in figure 1. The twisting moment values shown were used in the design and were provided by G.E. The centrifugal moment curve is sinusoidal and it is a function of the mass distribution of the blade about the pitch change axis and the centrifugal field. The aerodynamic twisting moment is the torque generated by the center of pressure about the pitch change axis. The sum of these two torques is the net value. The frictional moment of the blade retention bearing due to centifugal pull was also supplied by G.E. as a constant maximum value. The zero degree setting is the static, takeoff setting.

The large range of blade angle travel was initially established so that reversing of the fan could be accomplished both through stall, that is in the open pitch direction,as well as in the closed pitch direction. Model and full scale engine testing conducted while the design was in process showed that much higher levels of reverse thrust could be achieved by the through "stall" approach. As a result, the closed pitch method was never implemented in the hardware phase.

ALTERNATE CONCEPTS STUDIED

Prior to initiation of the contracted effort, an in-depth study was conducted to select an optimum concept.

Ten designs of various mechanical and hydraulic arrangements were studied; and a comparative assessment was made using weight plus six other criteria such as reliability and development risk. The matrix was reduced to six choices for more in-depth evaluation and the matrix of criteria was increased to ten factors. The selected cam/harmonic system scored heavily in the following areas.

o   Weight

o   Reliability

o   Simplicity

o   Accessibility of Controls

DESCRIPTION OF SELECTED SYSTEM

The key elements of the mechanism are depicted on the block diagram and schematic shown in figures 2 and 3.

The input from the G.E. supplied digital control system is a blade angle position command to the electro-hydraulic servo valve; the servo meters flow from a remote hydraulic source to power a hydraulic motor, the output of which drives a high speed flexible shaft.

The output position of the hydraulic motor provides a feedback signal from an LVDT to the digital control. Although the remainder of the system is open loop, it does provide a high degree of positioning accuracy. A differential gear transfers the torque of the flex shaft from the stationary reference to the rotating fan. This torque is then increased, with a corresponding speed decrease, by the harmonic drive which produces a very high speed reduction. The output of the harmonic drive is transmitted to the blade through the cam which rotates the trunnion arm. The combination of the trunnion arm and the contour of the cam track provides the desired output torque-versus-blade angle characteristic. The no-back is a simple locking device which fixes blade angle in the absence of any input motion on the flex shaft.

The key design features of the system are more apparent in figure 4.

The beta regulator which comprises the servo valve, hydraulic motor and feedback signal is packaged as a unit and mounted remotely from the fan for ease of replacement; since the control portion of actuation systems have historically been the major contributor to unscheduled removals. In addition, the remote mounting is a less hostile environment as compared to a location inside the fan in this area which would be in close proximity to the gear box.

The overall gear ratio between the hydraulic motor and the fan blade is 1000:1. Of this, 200:1 is provided by the harmonic drive. This high reduction is provided in a very small envelope and for a minimum weight. The principle of its operation will be explained in a moment.

The QCSEE fan has a large disk as well as a higher RPM than previous variable pitch systems resulting in a significant weight penalty of oil that would be required to fill the disk, in addition there would be an increased potential leakage due to a high centrifugal induced oil pressure. As a result of these considerations, dry lubrication was used for the cam track and roller. The G.E. designed retention used greased packaged bearings. As a consequence, the interior of the rotor is accessible for visual inspection.

The no-back is a coil-spring device which as noted earlier locks the system when there is no input motion from the Beta regulator. The system is self energizing in that a very low magnitude of back-drive torque will lock it. Similarly, it is released by extremely low levels of input drive torque.

Such features as the low torque, high speed drive between the Beta regulator and the harmonic drive, elimination of oil in the disk and the lightweight no-back made this concept the lighest of the ten systems that were evaluated.

Lubrication for the flex shaft, no back; differential gear and harmonic drive is provided for by a low oil flow from the Beta regulator through the flexible drive housing. This flow is centrifuged into these components and returns to the gear box scavenge area. A benefit of this configuration is the elimination of high pressure hydraulic transfer across the compressor inlet or through the gear box, thereby, improving safety and reliability.

Another maintenance feature is the ability to replace the flexible shaft from the Beta regulator end, without disturbing the fan assembly.

I've indicated that the harmonic drive is one of the key elements in achieving a lightweight design. Its operating principle is illustrated by figure 5.

Rotation of the input wave generator which you can see has three lobes, causes a distortion of the thin flex spline member. The passage of two lobes past a given point on the output lobe causes the output circular spline to advance one tooth.

Since there are three lobes, the output motion per revolution of the wave generator is three teeth as indicated, which combined with the number of teeth used, 600, provides a 200:1 ratio.

Because the teeth are quite small, a key design parameter is ratcheting capacity, that is the ability to resist "skipping" or "slipping." Under the combination of load induced deflection and thermal effects the harmonic drive was tested as a component prior to initiation of the whirl rig test.

This device has been used in such applications as the duct tilting mechanism on the Bell X-22 VTOL aircraft and on the wheel drive system for the lunar rover.

The harmonic drive components are shown in figure 6; the wave generator and circular spline are designed for high radial stiffness to minimize radial deflection under load. The flex spline is, of course, designed to continually deform during its operating lifetime.

The cam, shown in figure 7, provides contoured tracks for the 18 cam follower arms and bearings. The cam contour coupled with the variation in the effective moment arm provides the variable torque ratio required to match the loads-versus-blade angle requirements shown earlier. This hollow structure is made of a hardened steel; its diameter is dictated by the envelope required to locate the grooves on a spherical surface as well as by the structural requirements of the groove walls.

WHIRL RIG TEST

A 60-hour whirl test using an electric motor drive was performed on the system prior to engine test. A disk and 18 counterweights were supplied for this purpose by G.E. The counterweights provide twisting moment loads by virtue of their mass distribution when operating in a centrifugal field.

The whirl rig test was conducted using the entire actuation system including the Beta regulator assembly.

The objectives of the program were designed to prove acceptable performance and durability characteristics prior to engine test by demonstrating actuation rates and position accuracy, and by limited endurance operation.

Figure 8 is a photograph of the test rig. The rotor assembly is shown in the background; the 18 blade counterweights and cam arms are also visible. The housing in the foreground was used to mount the flexible drive shaft and the Beta regulator. The drive shaft was configured exactly as it would be in the engine even though the fan in this test was being driven from the front; this method was used for ease of testing.

The test program consisted of functional, structural and endurance testing. Test results produced an average pitch change rate of 116°/sec with a maximum rate of 135°/sec. Although this was less than the 135°/sec average value specified, it was judged to be a satisfactory level of performance. Perhaps more important was the demonstration of blade travel from positive thrust to full reverse thrust through stall of approximately one second. The required blade positioning accuracy of ±¼° was attained, and although not a requirement, a hysterisis of 1½° was demonstrated as was the ability to provide a minimum step change of ½° in blade angle.

The most important result of the testing was demonstrating compliance with the load capability of the system as measured against the levels specified by G.E. which were presented earlier. The no-back was demonstrated to hold the fan blade in a locked position under the maximum load or overspeed condition. A total of 550 simulated mission cycles were accomplished; each cycle consisted of sixteen blade angle/RPM combination including one reverse cycle.

The results of the testing were in an overall sense positive, with very little "fix" and retest required. Moreover, the system was judged to have satisfied specification requirements; it was therefore subsequently assembled into the QCSEE under-the-wing engine.

UTW Fan Blade Twisting Moment
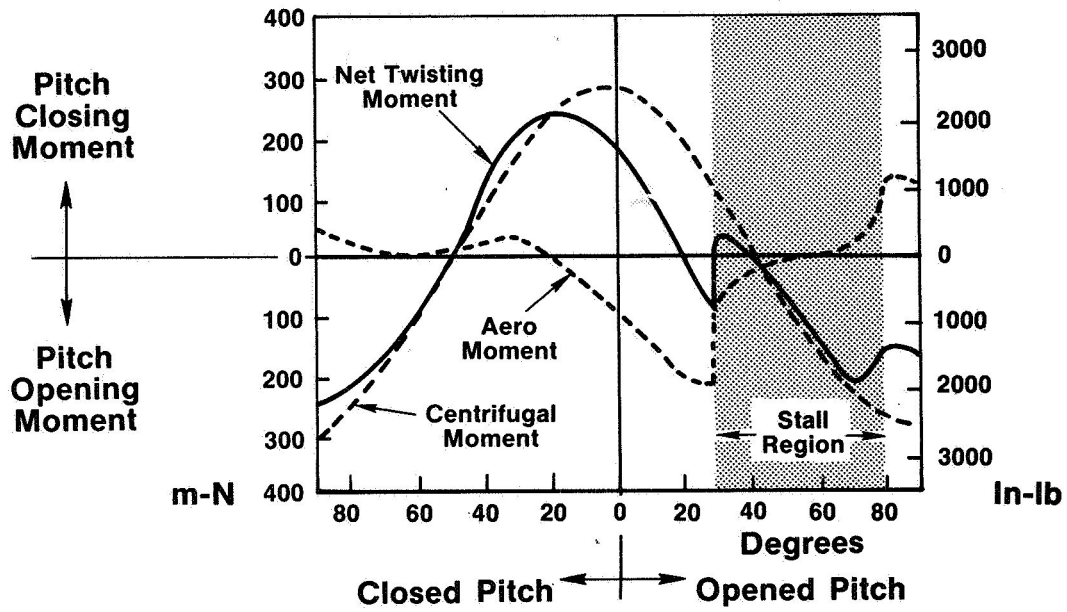
Figure 1

Pitch Change Mechanism

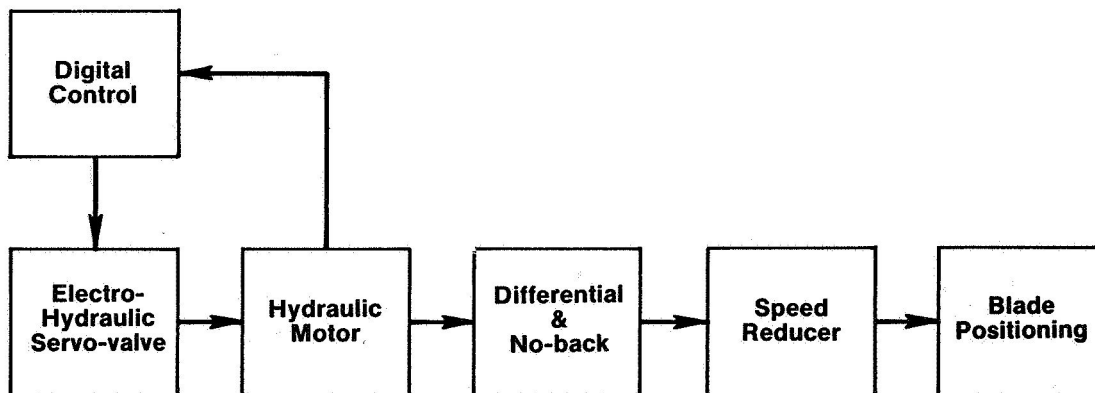Figure 2

Schematic
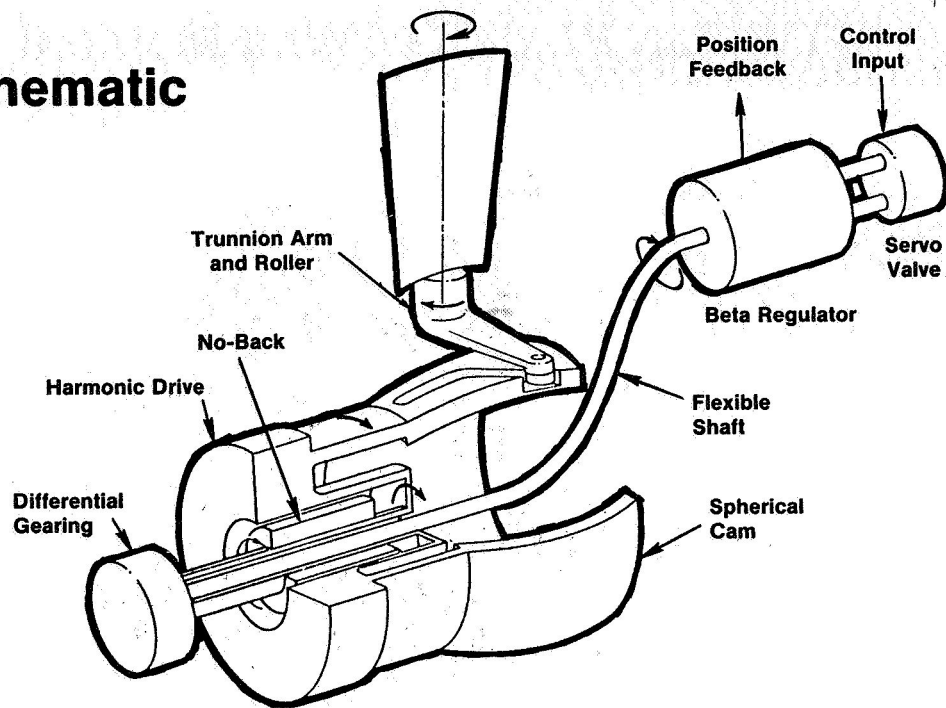

Figure 3

Cam/Harmonic Variable Pitch Actuator System
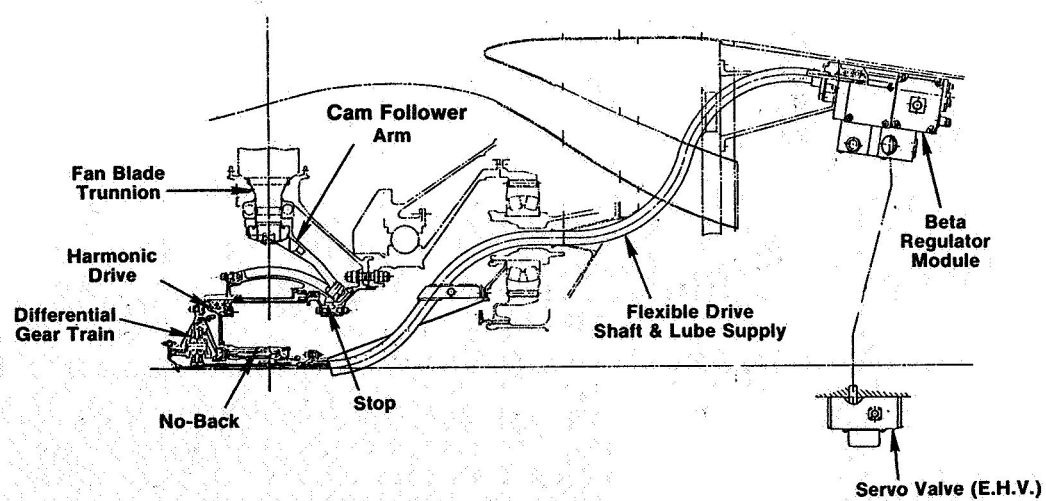
Figure 4

Harmonic Drive

Flex Spline
(600 Teeth)

Output Motion
Per Input Revolution
(200:1 Speed Ratio)

Input
Wave Generator
(3 Lobed)

Output
Circular Spline
(603 Teeth)

Figure 5

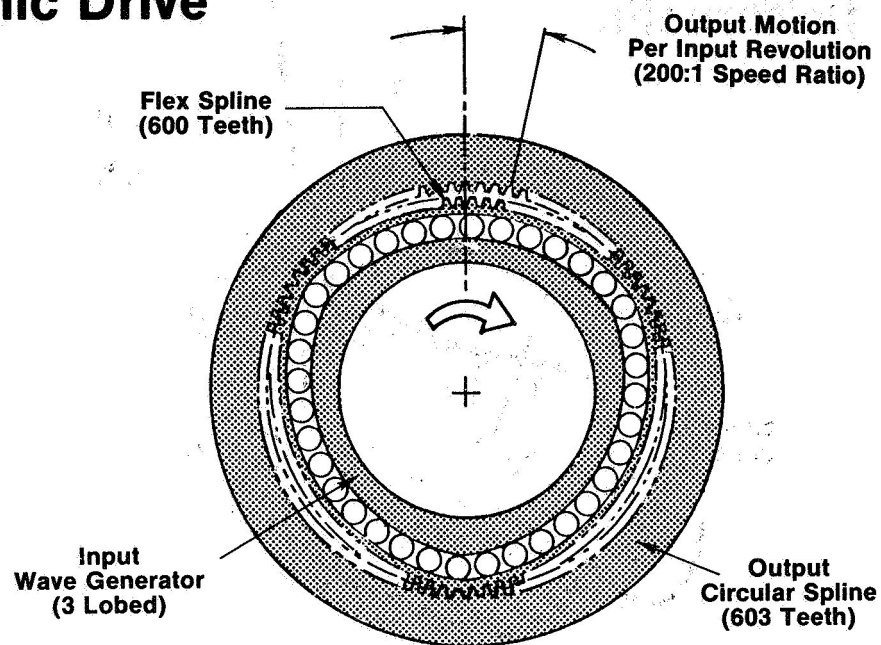# Harmonic Drive

Wave
Generator
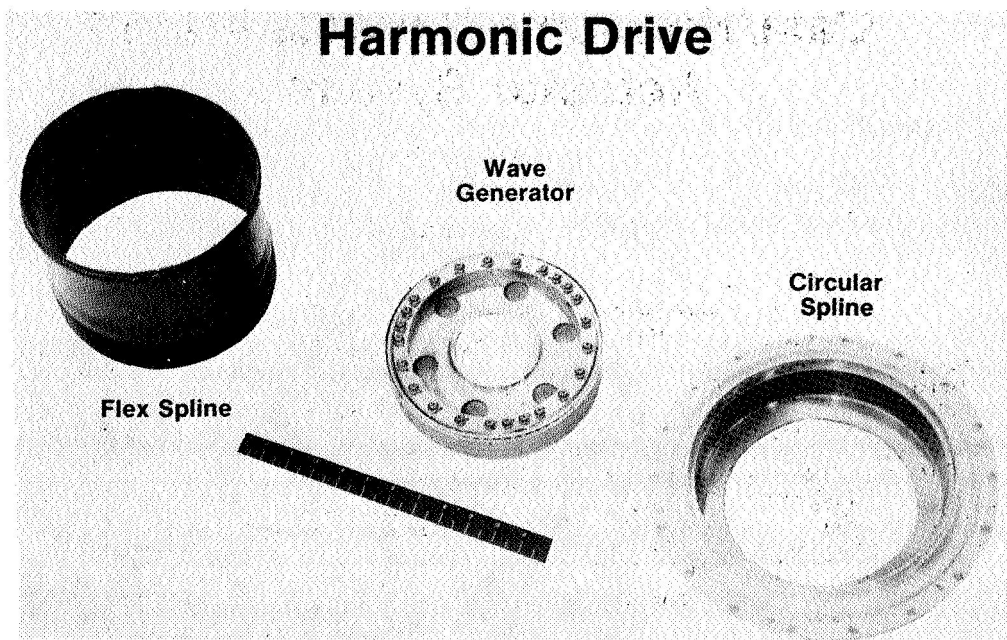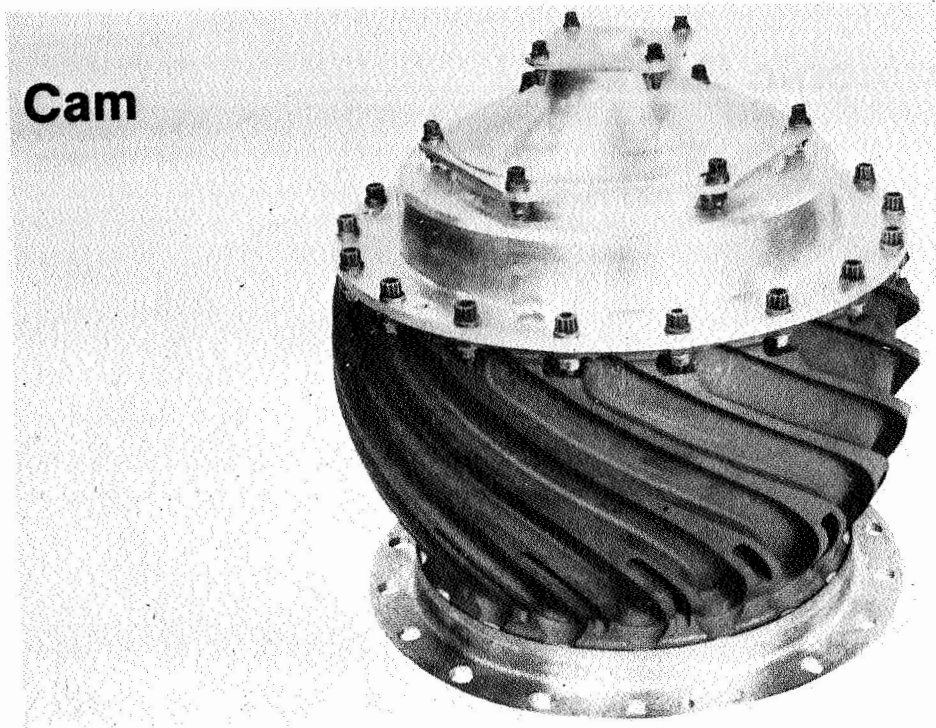
Circular
Spline

Flex Spline

Figure 6

Cam

Figure 7

Actuator in Whirl Rig
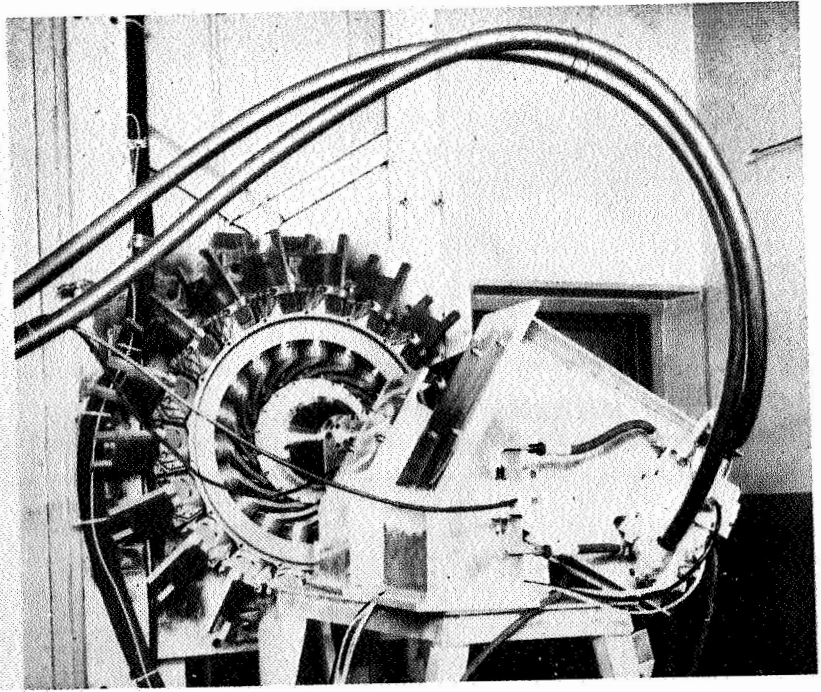
Figure 8

QCSEE BALL SPLINE PITCH ACTUATION SYSTEM*

R.H. Griswald
General Electric Company
Cincinnati, Ohio

INTRODUCTION

In the late 1974, General Electric launched a program to design, build and test a Variable Pitch Fan Actuation System for the QCSEE UTW engine. Reliability, maintainability, production costs and weight were evaluated for a number of candidate designs. This paper covers the selection of the ball spline system and a description of how it operates. Whirligig and engine test results are also discussed.

SYSTEM SELECTION

Using technology demonstrated on previous variable and reverse-pitch fan rigs, a second generation ball spline actuator was studied. Several alternate concepts were also evaluated, including worm gearing, "mini" gearboxes, individual screwjacks and a single planetary gearbox were all designed to the same conditions as the ball spline. The ball spline with two output ring gears was selected because it was the least complex and was extremely rugged. Its reduced parts count carried with it the promise of a lightweight, highly reliable design.

DESCRIPTIONS OF SELECTED SYSTEM

The actuator system as shown in figure 1, is made up of a ball screw, ball spline and two ring gears. The ring gears collect and synchronize the individual pinions that are attached to each of the 18 blade trunnions. As the input drive shaft is rotated, the two ring gears move in opposite directions. This imparts two equal reactions to each pinion, thus minimizing gear loads and providing a redundant load path.

The pitch change mechanism is shown schematically in figure 2 and as a block diagram in figure 3. It is made up of blade positioning, speed reducer, differential and noback, and is driven by a piston type hydraulic motor that is controlled by the servovalve. The servovalve is operated by the digital control, while the control, in turn, receives its position intelligence from the feedback. Motor output drives through the differential gearing and noback. The noback accommodates input movement in either direction of rotation

---

but prevents fan blade torque from backdriving the system. A stage of reduction gearing is required to match the output of the motor with the blade positioning mechanism.

This cross section, figure 4, shows the details of the system including:

o Hydraulic motor

o Feedback

o Gearing

o Noback

o Thrust bearings

o Ball screw

o Ball spline

o Torsion stops

o Ring gears

o Pinions

In order to actuate the fan blades, large axial forces must be generated in the load-path formed by the ball screw, thrust bearings and inner member of the ball spline. The key to minimizing actuator weight was in keeping this closed-loop-load-path short and on a small radius.

Key design features include the motor and feedback located near the actuator for crisp blade movement and accurate positioning. Redundant ring gears reduce steady state loads and improve reliability. The ball spline and ball screw are rugged proven designs. The differential gearing and noback are packaged together in order to simplify actuator assembly.

The ball spline and ball screw shown in figure 5 are the heart of the actuator assembly. Recirculating tracks of balls are lubricated by engine oil and transmit the required forces smoothly and efficiently. Ball tracks are hardened steel to assure long life. The drive package provides the input force and position intelligence for the actuation system. Two motion feedback transducers are mechanically coupled to the motor output shaft by gears and a spring loaded thread arrangement.

RIG TESTING

An actuator whirl rig test was run at General Electric using the breadboard digital control. Test objectives were:

o Proof test prior to engine running

o Demonstrate actuation rates and propulsion accuracy

o Demonstrate endurance during limited testing

64

o   Investigate compatibility with digital control

Figure 6 shows the GE system mounted in the whirl rig. This view is aft looking forward with respect to the engine. Clearly visible is the drive package and the simulated fan blades.

Testing of the GE system was completed in less than two weeks. Demonstrated average actuation rate was 125° per second. The system was compatible with the breadboard digital control, and blade positioning accuracy was demonstrated within 1/4° in forward thrust. A system hysteresis of 3° was uncovered when actuated back and forth at zero speed, but it did not compromise testing and no effort was made to reduce the value. Clearances in the actuator assembly, that exceed design predictions, appear to be responsible for this observed hysteresis.

Noback holding above maximum fan speed was demonstrated, and fifty mission cycles were run.

ENGINE TESTING

Both the Hamilton Standard Cam/Harmonic and the General Electric Ball Spline Systems were engine tested. Figure 7 shows the fan rotor with the Cam/Harmonic system installed. Clearly visible are the nested lever arms and the spherical cam that drives the blades in unison as the cam rotates with respect to the fan disk.

The cam/harmonic system completed 47 hours of engine testing. It accurately positioned the fan blades at lower speeds, but could not move the blades against the load when operating above 85% fan speed. Since this system handled the simulated blades during whirl rig testing, it was concluded that actual blade torques exceeded design estimates.

The ball spline system completed 106 hours of engine testing. Motor torque was increased 16% prior to engine test and the system crisply actuated the blades at all speed. There was an indicated 1.3° system hysteresis, based on airflow measurements, when the direction of blade movement was reversed while operating near nominal. This was again attributed to excessive actuator clearances and presented no operational problems.

CONCLUSIONS

It was concluded that both systems demonstrated concept feasibility during whirl rig and engine testing. Either system could be developed for operational use.

65

GE Ball Spline Actuator System

Blade Trunnion (18)

Pinion Gear (18)

Ring Gears(2)

Ball Spline

Fan Spinner

Input Drive Shaft

Ball Screw

Figure 1

Pitch Change Mechanism

Digital Control

Servo Valve

Blade Positioning Mechanism

Position Feedback

Speed Reducer Differential No-back
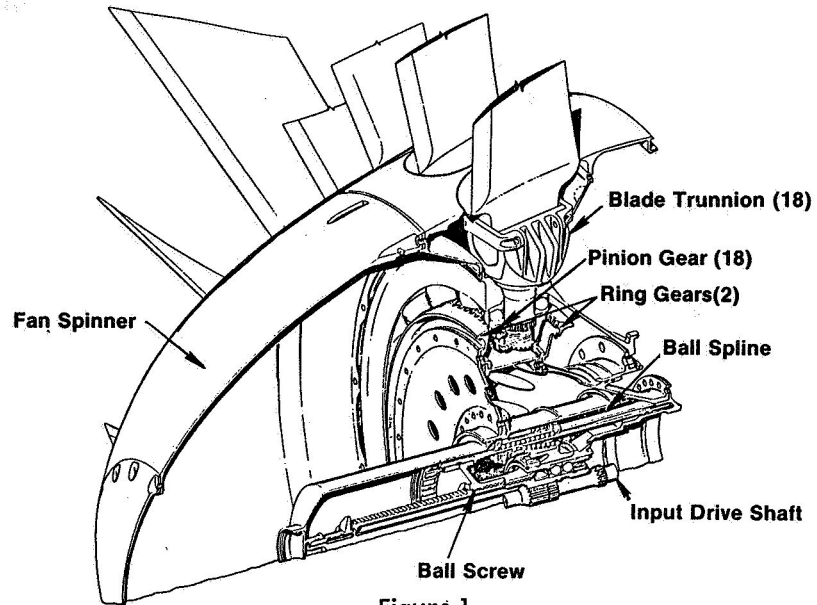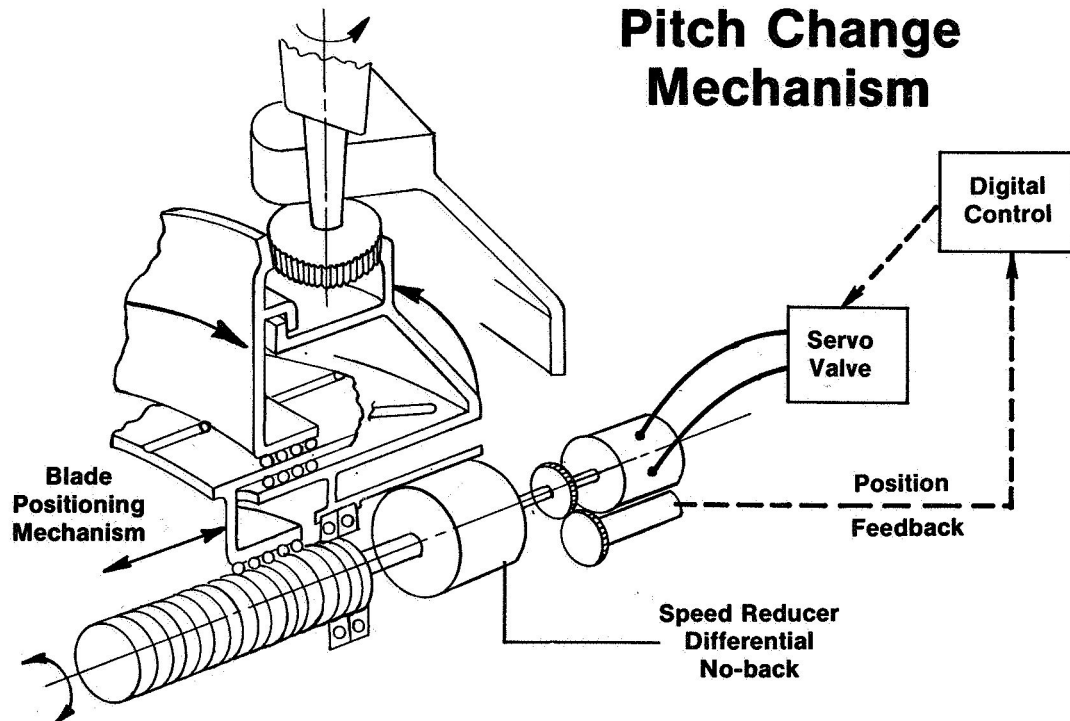
Figure 2

Pitch Change Mechanism
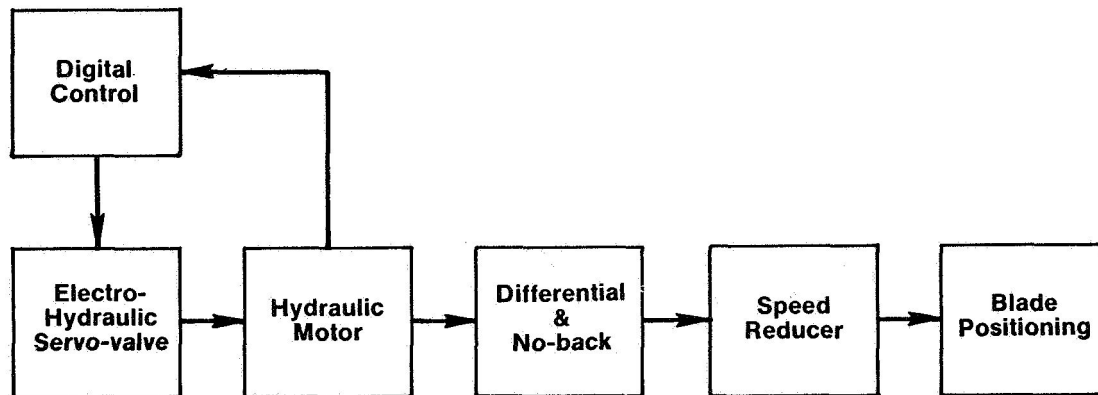
Figure 3

Ball Spline Actuation System

Figure 4

Pitch Actuation Components
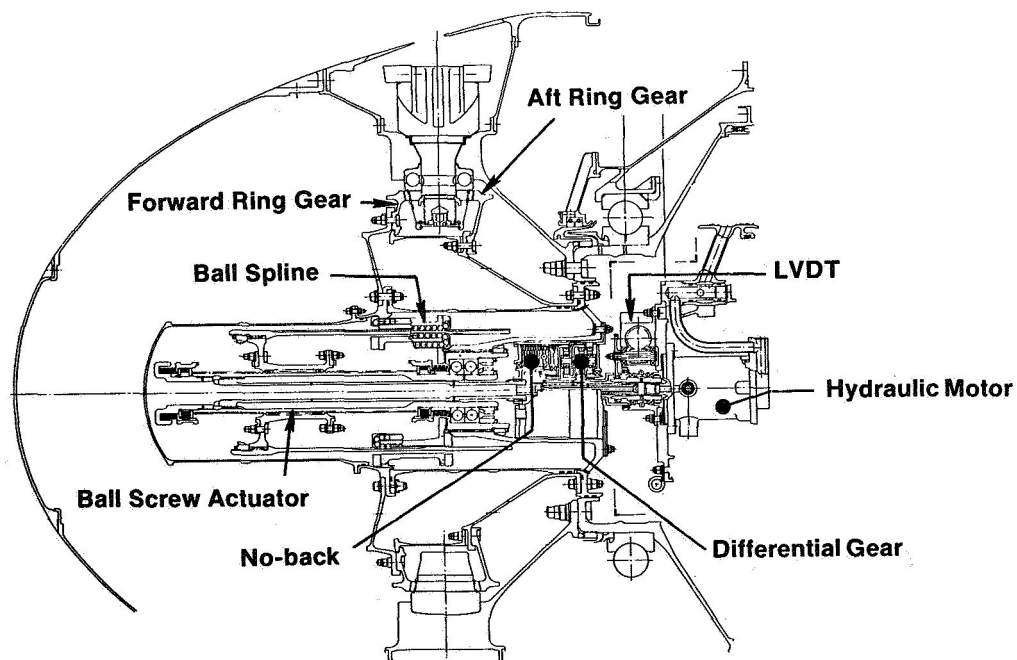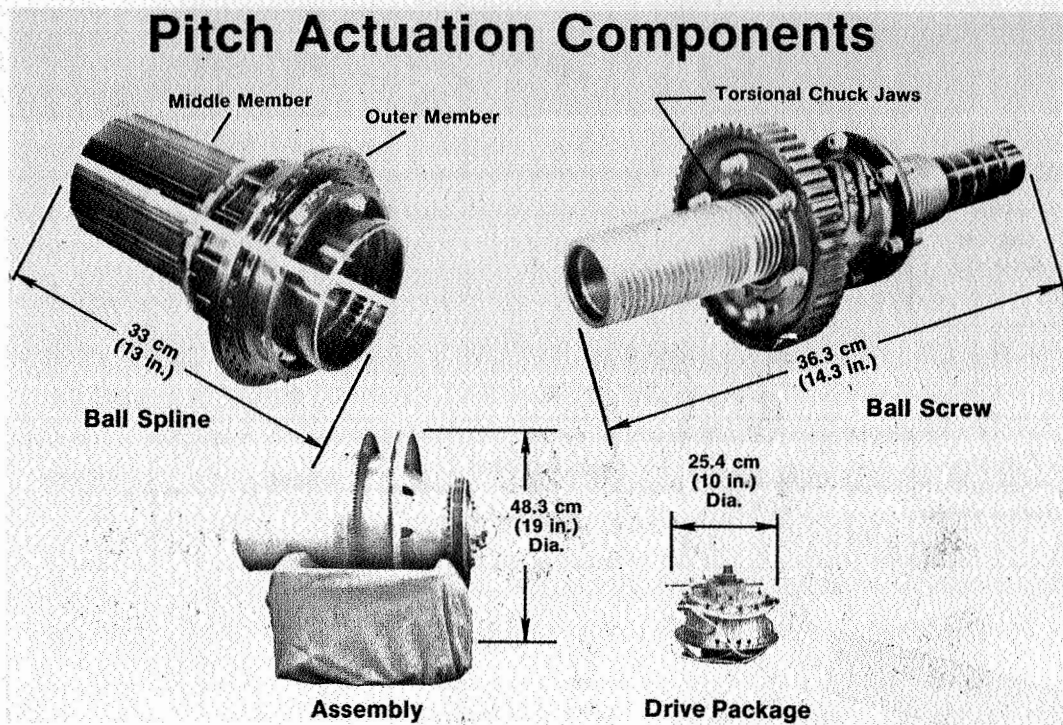
Figure 5

Whirl Rig Test Setup

Figure 6

Engine Test Results
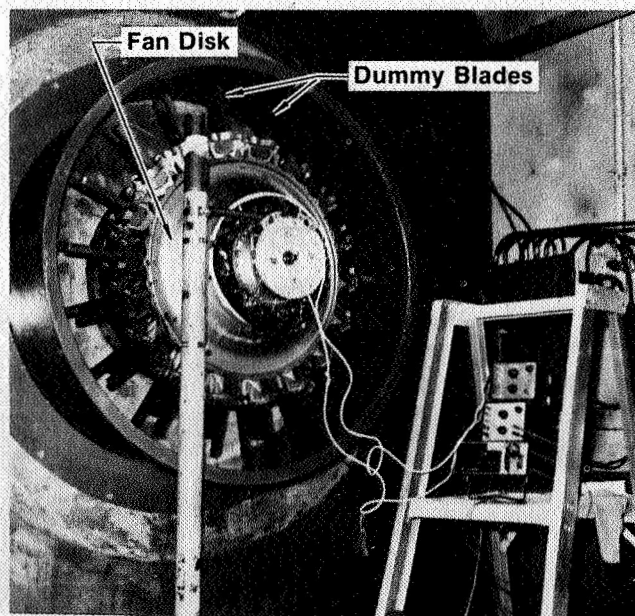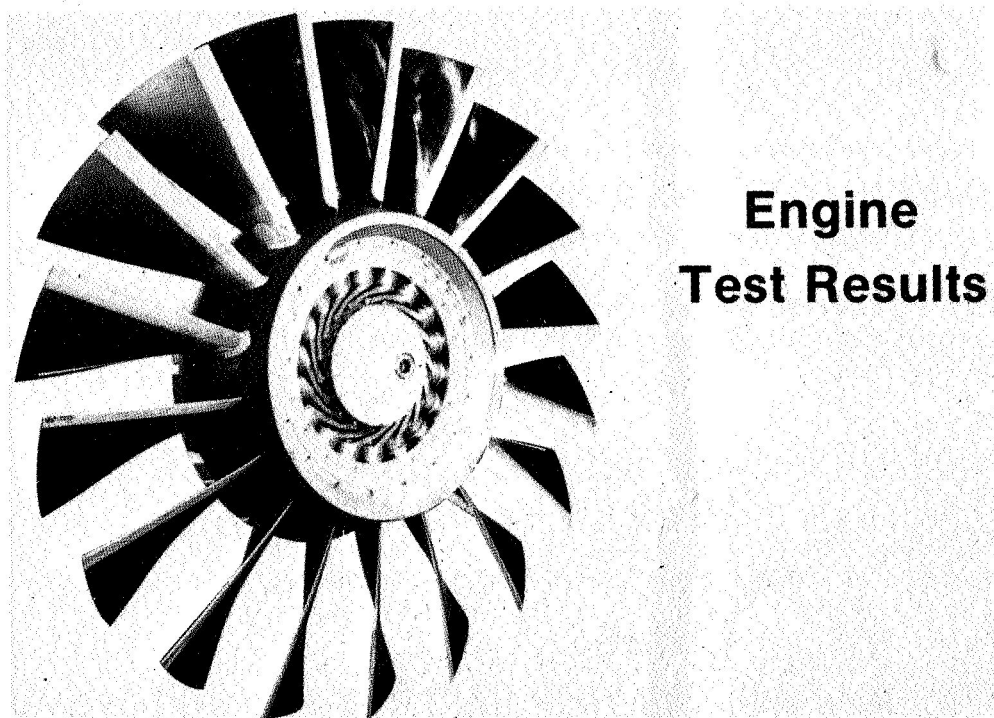
Figure 7

QCSEE MAIN REDUCTION GEAR*

O.W. Misel
Curtiss-Wright Corporation
Wood-Ridge, N.J.

INTRODUCTION

The NASA/GE Quiet Clean Short-haul Experimental Engine (QCSEE) concept is based on a light weight high speed power turbine driving a slower speed quiet fan. To accomplish this objective required a compatible compact, light-weight, high power capability main reduction gear. Two reduction gears designed, manufactured and rig tested by Curtiss-Wright under sub-contract to General Electric have given trouble free performance throughout the engine demonstration program.

This paper reviews the phases of the QCSEE Main Reduction Gears development program from the initial design requirements through engine test and conclusions. Each of these phases will be discussed in some detail.

DESIGN REQUIREMENTS

The QCSEE UTW Main Reduction Gear is shown in figure 1. One point of interest is that the maximum diameter of the gear is only 63.5 cm (25 in.) which was the maximum permissible to be compatible with the required engine housing air flow paths.

The under-the-wing (UTW) and over-the-wing (OTW) engine concepts were based on using the same core engine, but differing fan performance characteristics dictated different reduction ratios and power ratings. The main reduction gear feasibility design studies were directed toward approximately 2.5:1 ratio and 9321 kw (12,500 hp) at 3197 rpm fan speed for the UTW engine and approximately 2.1:1 ratio and 11,282 kw (15,130 hp) at 3782 rpm fan speed for the OTW engine.

The specified operating life objectives included 36,000 hours with a minimum of 6000 hours time between overhauls.(TBO).

Since light weight and minimum complexity were prime requirements for the engines a single lubrication system for the turbine, accessory drive and the main reduction gear using either MIL-L-7808 or MIL-L-23699 lubricant was specified. This also meant that special attention to gear design factors such as tooth spacing accuracy, involute profile modification, surface finish, gear misalignment and contact stress, was required to insure against scoring for these high performance gears.

Since both the UTW and OTW reduction gears were to be used on the same basic engine, identical interfaces between the reduction gears and the engine were specified. These interface points included:

o   Power turbine coupling to input gear

o   Gear support attachment to engine housing

o   Power output gear to fan shaft

o   Lubrication supply connection

The capability of the reduction gear unit to be installed and removed as an assembled module was another consideration.

Since "Quiet" is the "Q" in QCSEE, a low noise level for the reduction gear was an important objective. Considerations for a quiet gear started in the design phase.

DESIGN APPROACH

A number of years ago, Curtiss-Wright developed a 9000 hp turboprop military engine which included a two-stage epicyclic reduction gear. That reduction gear shown in figure 2 had an overall reduction ratio of 7.0:1 which included a 2.67:1 reduction in the primary stage. During an early conceptual phase of the QCSEE program use of the original YT-49 primary stage gear was considered. However, as the engine design studies progressed, the need for higher power capability and a different ratio were indicated, but the YT-49 reduction gear technology was still applicable. Features of the YT-49 gear utilized in the QCSEE main reduction gears include the fixed carrier star configuration, flexibility in the sun and ring gears and supports, straight spur gears and double row spherical roller bearings with the outer race integral with the star gear.

A schematic cross section of a QCSEE fixed carrier epicyclic star system reduction is shown in figure 3.

The major components of this epicyclic star gear system are:

o   Fixed star gear support

o   Diaphragm type sun gear coupling

o   Sun gear

o   Star gears

o   Ring gear

o   Lubrication system components

72

These gear sets were to be installed within the engine housing with the star carrier supported by the engine frame, the input gear supported by the power turbine shaft and output gear supported by the fan shaft.

The power input to the reduction gear is through the sun gear. With the fixed star gear carrier or support, the star gears serve as idler gears providing multiple power paths between the input sun gear and the output ring gear. In this configuration the star gear bearings are subjected to only the tangential gear tooth loads and not to added centrifugal loads as would be in the case of a conventional planetary with the carrier rotating.

Lubrication of the gearing is provided from the engine system through a single connecting tube to an oil manifold attached to the star gear trunnion support. An annular passage distributes oil to the individual trunnions where radial passages in the trunnions and bearing inner races provide lubrication to the star gear bearings. Spray tubes on the forward side of the manifold provide lubrication and cooling to the sun and star gear teeth. The spray tubes, which are not shown in this figure, have a number of jets spaced to distribute oil across the faces of the gear teeth.

Flexibly mounted gears is one of the key features of Curtiss-Wright's approach to achieving load equalization between power paths and across the faces of the gear teeth. A double diaphragm type coupling is used between the turbine shaft and the sun gear. The sun gear also incorporates flexibility in the web. The objective here is to allow the sun gear to be positioned by the mesh contacts with the star gears and be subjected to minimum influence of any relative radial motion between the turbine shaft and the star gear support. With the accurate machining of the star gear bearing trunnion locations and the gears, a very high degree of load equalization with the individual star gears is achieved. A flexible section between the ring gear and the spline attachment to the fan shaft allows this gear also to be positioned by the mesh contacts with the star gears and be subjected to minimum influence of any relative radial motion between the fan shaft and the star support. A cylindrical roller bearing between the aft end of the fan shaft and the member to which the star gear support is attached also helps to maintain the relative position of the fan shaft to the star gears.

Mounting of the star gear on a double row spherical roller bearing allows the gear to operate in a plane defined by the loaded tooth contacts with the sun and ring gears, thus providing good load distribution across the face width. In the design of the gear rims and star gear trunnion supports, section modulii are selected that provide relatively close matching of gear and tooth deflections for the mating gear teeth at each mesh. Consequently, deviation of the plane of rotation for the star gear bearing outer race from the plane of the inner race is very small.

Design factors contributing to smooth operation and low gear noise are the use of a minimum gear contact ratio equal to 2 and numbers of gear teeth selected for hunting and non-factorizing. A minimum contact ratio of 2 means that there are never less than two teeth in each gear in contact at each mesh.

In designing for hunting and non-factorizing the number of teeth in each gear is selected such that no two teeth in the gear set enter engagement simultaneously and the same two teeth in mating gears repeat engagement only after engagement with all other teeth in the mating gear.

DESIGN SUMMARY

Engine and fan trade-off performance studies by General Electric resulted in changes in power requirements and speed for the UTW and OTW main reduction gears final designs as shown in table I. The UTW power increased approximately 4% and the fan speed decreased slightly to 3157 rpm. The OTW power increased approximately 12% and the fan speed increased to 3860 rpm. These requirements were accommodated within the originally specified envelope. The number of star gears shown, six for the UTW gear and eight for the OTW gear, are the maximum that can fit in the available space allowed by the reduction ratios.

The UTW pitch line velocity of 97.5 m/s (19,200 ft/min) is only slightly higher than in the YT-49 gear while that for the OTW unit is approximately 30% greater. Neither of these are considered excessive.

The star gear bearing 0.74×10^6 DN value (bearing bore, mm X outer race rpm) for the UTW gear compares favorably with the 0.72×10^6 DN value for the YT-49 reduction gear. The 0.90×10^6 DN value for the OTW star gear bearing is higher than any known previous experience for a double row spherical roller bearing.

Design oil flow rates shown are divided between the star gear bearings and the gears. Approximately 35% of the flow goes to the bearings and 65% goes to the gears through the spray tube jets. The flow split for each spray tube is approximately 50% to the sun gear and 50% to the star gear on the out of mesh side.

Materials selected for the QCSEE main reduction gears were carburized AMS 6265 for the sun gear, star gears and the coupling, nitrided AMS 6470 for the ring gear and AMS 6415 for the star gear carrier. Heat treat data for the gears are:

Sun and star gear teeth:

      Finished case depth - 0.635-0.889 mm (0.025-0.035 in.)

      Case hardness - R_c 60-63

      Core hardness - R_c 32-40

Star gear spherical raceway:

      Finished case depth - 1.524-1.778 mm (0.060-0.070 in.)

      Case hardness - R_c 60-63

Ring gear   -

        Nitride depth   - 0.51 mm (0.020 in.)

        Case hardness   - 15N91 min.

Maximum limits selected for the gear design stresses were approximately 24.1 kN/cm^2 (35,000 psi) bending and 93.1 kN/cm^2 (135,000 psi) contact. These are well below AGMA allowables and Curtiss-Wright operating experience.

The spherical roller bearings have CEVM M-50 steel inner races and rollers and AMS 4616 silicon bronze, silver plated cages.

HARDWARE FABRICATION

Two UTW gear sets and three OTW sets were manufactured. Two sets of each were required for the back-to-back rig test and one of each of these test gear sets were subsequently installed in the engines.

RIG TESTING

Primary objectives of the rig test program were to demonstrate satisfactory operation and to determine operating characteristics of each of the reduction gear designs prior to installation in the engine.

Testing was conducted with two essentially identical reduction gears installed in a back-to-back test rig and torque loaded to simulate engine operating conditions.

Figure 4 shows a schematic cross section of the upper half of the test rig in which some engine reduction gear cavity and oil scavenging characteristics are simulated. The reduction gears are mounted by the star gear support in each end of the rig. The sun gears are connected through engine type diaphragm couplings and the input drive shaft. The ring gears are supported and connected by simulating engine fan shafts. An engine type oil anti-churning and scavenging screen was installed in the test gear end of the rig. Oil is supplied to the gears through engine type oil inlet tubes.

Rotation of one gear assembly relative to the other introduces the torque into the gear system.

Figure 5 shows the drive end of the test rig and also the torque loading hydraulic cylinders which by the application of hydraulic pressure rotate one end of the rig relative to the other and apply the load to the gears.

75

Significant results of the rig test are shown on table II. The reason for the OTW unit not being operated to 100% speed at 100% torque was not the fault of the gear but rather an overestimate of the capability of an aged motoring dynamometer when planning the test program.

The reduction gear efficiencies were a little lower than had been expected but it is believed improvement could have been accomplished through some lubrication and scavenging development in the vicinity of the sun and star gears.

The engine hardware oil baffle screen was installed in the test gear end of the rig at the start of the test program to verify or predict the scavenging characteristics of the engine. The rig operation appeared to indicate marginal scavenging accompanied by oil churning. Several scavenging and baffle screen modifications were evaluated. The OTW gear with the higher pitch line velocity appeared to be the more critical.

Upon conclusion of the rig test programs, the test gears were thoroughly inspected and delivered to General Electric for installation in the engines.

ENGINE TEST RESULTS

Figure 6 shows the UTW reduction gear, including the fan pitch change mechanism support, installed in the engine but with the fan shaft and ring gear removed.

We are happy to note that there were no operational problems with either the UTW or OTW gear sets during the engine operation.

The indicated reduction gear efficiency of 97.7% in the engine was somewhat lower than that experienced in the rig tests but this is attributed at least in part to inaccuracies in the method of estimating the sources of heat rejected to the oil and oil flow distribution from several sources within the engines.

It is believed some development effort related to the placement of the oil supplied to the gears and the scavenging characteristics both within and surrounding the gear set can improve the efficiency to a value even better than that previously shown for the rig tests.

Another item of interest in the engine test was gear noise. The gear noise level even at meshing frequencies appeared to be below that of the rest of the engine and indiscernible.

The UTW reduction gear set was inspected at an interim point in the engine operation. All parts passed Magneflux satisfactorily and tooth wear patterns were uniform. Slight corrosion was apparent on the ring gear due to inadequate removal of fingerprints, and slight evidence of bearing skidding was noted. Upon completion of the UTW engine operation, the engine was delivered by GE to NASA without disassembly. The OTW engine was also delivered

by GE to NASA after completion of operation without disassembly or gear inspection. Subsequent engine operation has been conducted at NASA.

CONCLUSIONS

Some general conclusions can be drawn from the rig test and engine operations. Both reduction gears have given trouble free performance during the entire engine demonstration tests.

Total time on the UTW gear is approximately 202 hours:

Test rig	49 hrs.
Engine	153 hrs.

Total time on the OTW gear is approximately 135 hours:

Test rig	36 hrs.
Engine-GE	58 hrs.
Engine-NASA	41 hrs.

Although this is hardly sufficient operating experience on which to guarantee achievement of the 36,000 hours life and 6000 hours TBO objectives, we believe that the feasibility of a geared fan drive has been satisfactorily demonstrated and we are confident that with the benefit of a little development effort an acceptable reduction gear performance and life for operation engines can be achieved.

TABLE I. - DESIGN SUMMARY

	UTW	OTW
• Gear Ratio	2.465	2.062
• Power Transmitted, kW (HP)	9708 (13,019)	12,610 (16,910)
• Maximum Fan Speed, RPM	3157	3860
• Number of Star Gears	6	8
• Pitch Line Velocity, m/s (ft/min)	97.5 (19,200)	119.3 (23,450)
• Pressure Angle, Degrees	21	21
• Diametral Pitch	7.5321	7.1884
• Bearing dN	.74 x 10^6	.9 x 10^6
• Oil Flow, m³/s (GPM)	.0833 (22)	.0945 (25)
• Heat Rejection, kJ/s (BTU/min)	116 (6600)	190 (10,800)
• Maximum bearing Temp., K (°F)	417 (290°)	417 (290°)

TABLE II. - RIG TEST RESULTS

	UTW	OTW
• Demonstrated Speed/Torque, %	100/125 105/50	80/109* 95/50*
		*Limited by Drive Power
• Completed	48.8 hr	36 hr
• At Max Speed and Torque, 344K (160°F) Oil Inlet		
Oil ΔT =	294K (70°F)	321K (119°F)
Oil Flow =	80 kg/min (177 lb/min)	91 kg/min (200 lb/min)
η Mech =	98.9%	98.7%

• Developed Lube/Scavenging System Through Several Configurations

QCSEE UTW Main Reduction Gear
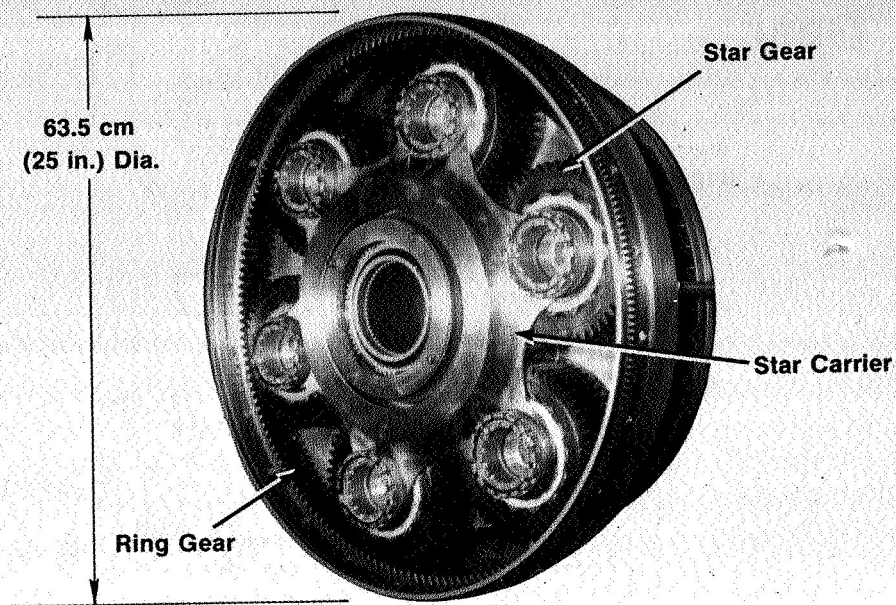
Figure 1

YT49-W-I Reduction Gear

Figure 2

79

Reduction Gear

Ring Gear

Fan Shaft

Star Gear

Sun Gear

Turbine Shaft
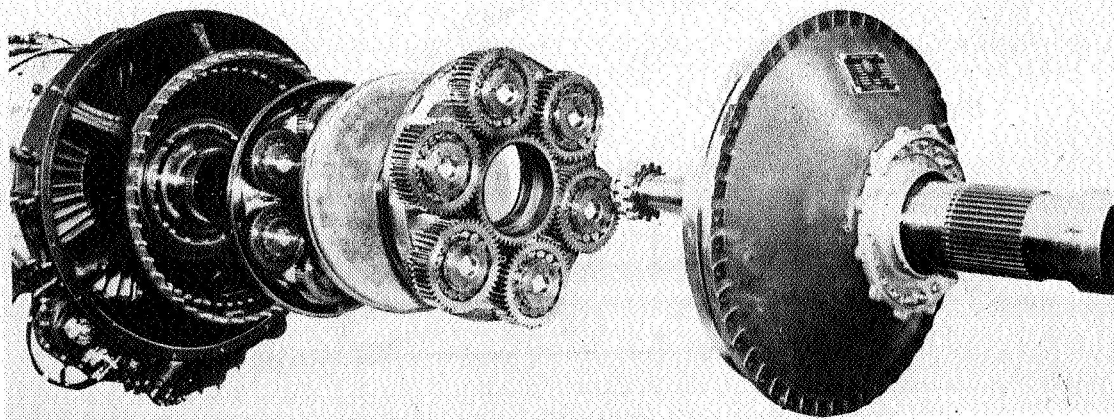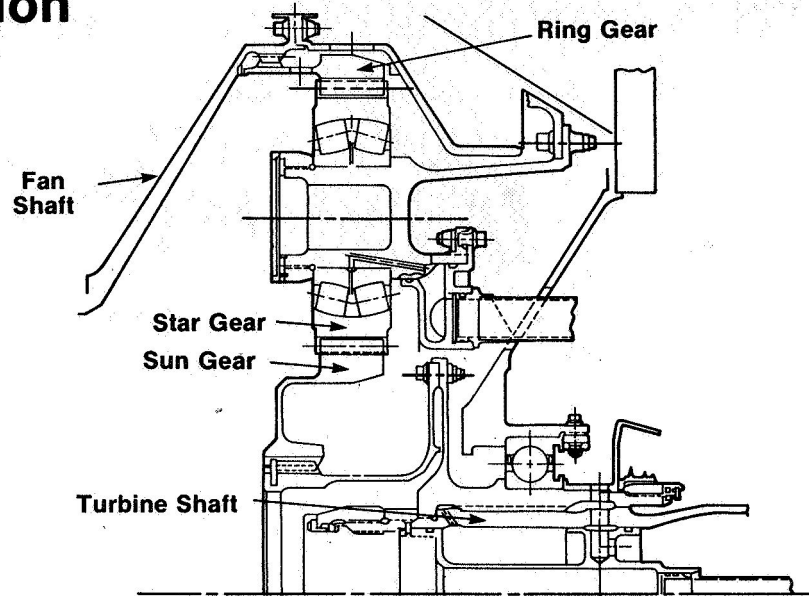
Figure 3

Main Reduction Gear Test Rig Schematic

Torque Plates

Slave Gear Set

Test Gear Set

Oil Inlet

Input Drive Shaft Oil Inlet

Figure 4

Main Reduction Gear Test Rig — Slave Unit (Drive) End
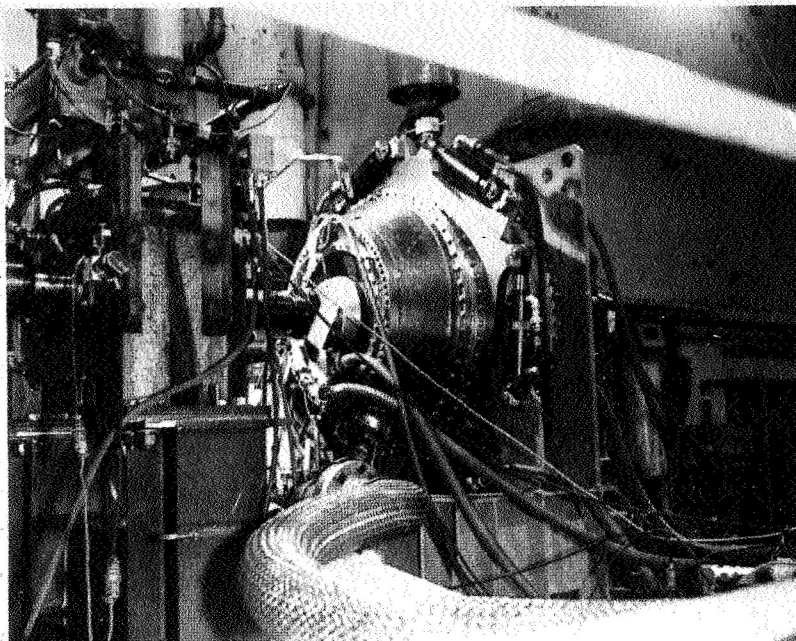
Figure 5

Engine Test Results
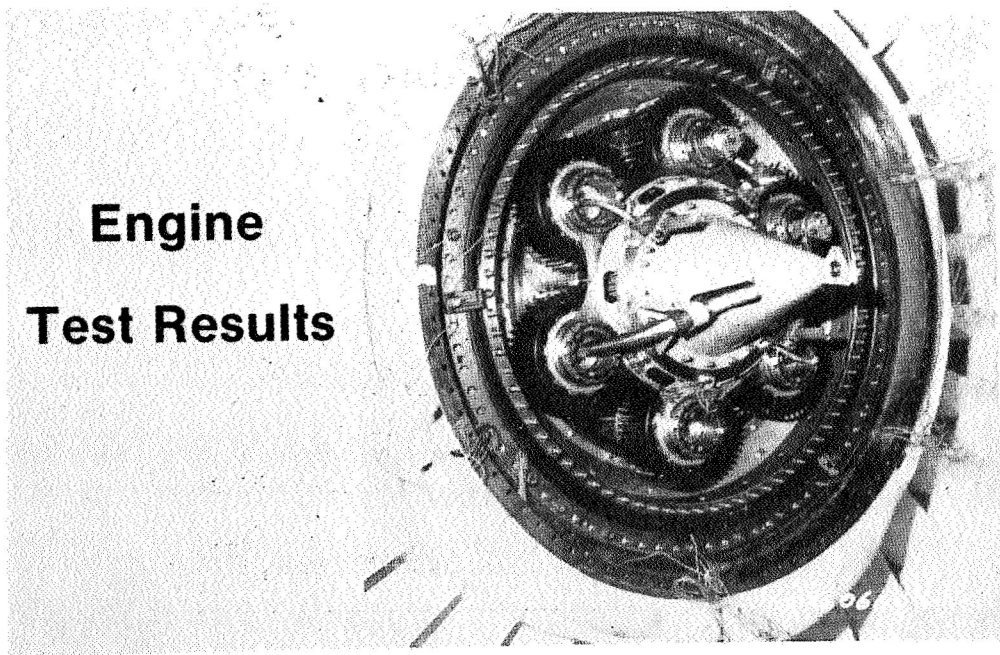
Figure 6

QCSEE COMPOSITE FRAME AND NACELLE*

C.L. Stotler
General Electric
Cincinnati, Ohio

INTRODUCTION

One of the major areas of new technology investigated under the QCSEE program was the application of advanced composite materials to major engine hardware. This paper discusses the applications as they pertain to the static components. The following paper will discuss their application to fan blades.

Two types of static structure were demonstrated during the program. The first of these was the fan frame which represents a structure requiring both high strength and stiffness. This is the main support point for the engine and will be discussed in some detail, covering the frame requirements, structural description, design, analysis, fabrication and testing. The second type of static structure that utilized advanced composite was the nacelle, which consisted of the inlet, outer cowl,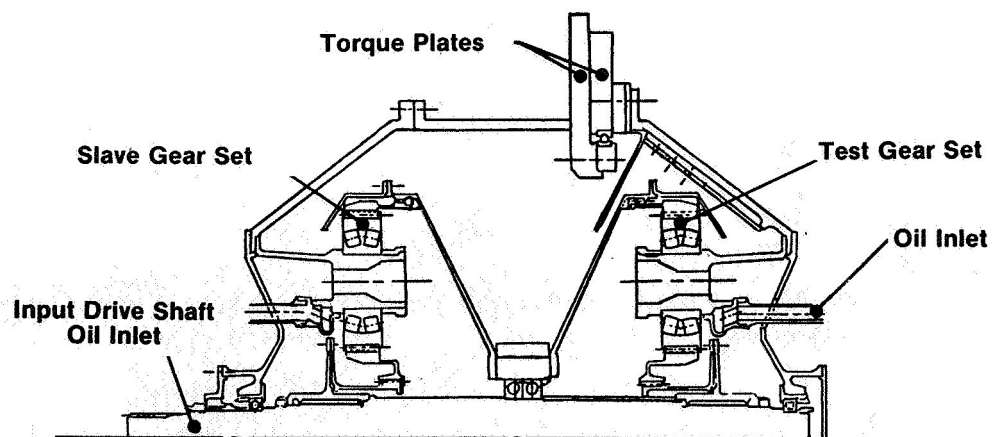 fan nozzle, and the inner cowl. For each of these areas, the design requirements will be discussed followed by a structural description, an outline of the basic analysis and a brief discussion of the fabrication techniques employed. The results of the engine testing will be summarized and some conclusions drawn.

COMPOSITE FAN FRAME

The graphite/epoxy fan frame, shown in figure 1, is the largest highly loaded advanced composite structure yet built for a turbofan engine. It is the first time the major structural support for such an engine was constructed utilizing advanced composite materials for virtually all of its components.

It has been estimated, based on two smaller composite frame programs conducted in 1972 through 1974, that this type of application could save from 25% to 35% in weight over an equivalent metal frame. These previous programs had generated sufficient technical confidence in the ability to undertake the design and fabrication of advanced composite frames without a back-up metal frame.

This program thus provided the somewhat unique opportunity to design a major composite engine structure from an original equipment point of view rather than a replacement component in an existing engine design. This permitted a much more integrated structure than is possible when constrained by the necessity of mating with existing hardware.

The QCSEE program included the design and testing of both an under-the-wing (UTW) and over-the-wing (OTW) propulsion system, thus requiring two advanced composite fan frames. The differences in these two frames were so minor as to have no effect on the basic frame structure. For simplicity then, all further discussion will pertain to the frame used in the UTW propulsion system.

DESIGN REQUIREMENTS

The QCSEE frame design was governed by the necessity for performing the following major structural and aerodynamic functions:

o   Provide the main engine forward attachment points for thrust, vertical and side loads.

o   Support the fan thrust bearing, variable-pitch system, reduction gear and compressor thrust bearing.

o   Support the inlet, aft outer and aft inner core cowls.

o   Support the core compressors at the forward casing flange.

o   Support the fan hub OGV's.

o   Provide the mounting position for the accessory gearbox and digital control.

STRUCTURAL DESCRIPTION

As can be seen in figure 2, the QCSEE integrated fan frame is a graphite/epoxy structure that incorporates the fan casing, fan bypass stator vanes and core frame into one all-bonded structure. It provides the primary support for the engine. Fan blade tip treatment and containment are provided by the grooved and Kevlar-filled structure integrated in the forward portion of the outer casing. Positioning of the fan and core engine bearing supports relative to the integral nacelle/outer casing is provided by 33 bypass vanes which also provide flow turning of the fan discharge. Due to the blockage caused by a pylon at the 12 o'clock position, the camber of these vanes are tailored differently depending on their circumferential position.

The hub of the frame is connected to the frame splitter through six equally spaced struts. The inner shell of the outer casing, the bypass duct and core duct surfaces of the frame splitter, and the pressure faces of the bypass vanes are perforated to provide acoustic suppression within the frame structure.

STRUCTURAL ANALYSIS

The frame was designed based on the load conditions shown in Table I.
The magnitudes of some of the more critical of these loads are shown in
figure 3. The basic structural concept used in the frame design is also
shown in this figure. The primary radial members of the frame consist of
three wheel-like structures. The forward wheel is a flat-spoked wheel,
comprised of a splitter ring, hub ring and six spokes. The middle and aft
wheels are flat-spoked wheels consisting of an outer casing ring, splitter
rings and 33 spokes connecting the outer casing ring to the splitter ring.
Shear panels of the proper aerodynamic shape are bonded to these wheels
to form the fan bypass stator vanes and the struts in the core flowpath.

The aft splitter ring contains the engine-mount attachment points.
These consist of a metal uniball at the 12 o'clock position which reacts
vertical and side load and two metal thrust brackets located 45° down on
either side of the uniball.

The internal and load distribution for the frame was determined using
a finite element computer program which represented the frame structure
as a combination of curved beams, straight beams, and plates, all capable
of having orthotropic material properties. A graphic comparison of the
analytical model to the actual hardware is shown in figure 4. In the core
region of the frame, the struts were modeled as three straight beams (repre-
senting the spokes of the wheels) connected to curved beams in the hub and
splitter region (rims of the wheels), all tied together by plates represent-
ing the flowpath and splitter walls. The fan flowpath area was represented
by radial beams representing the bypass vanes (wheel spokes and flowpath
panels were lumped together and appropriate section properties used for
these pseudo beams) tied to plates representing the outer casing forward to
the inlet. Appropriate structure was also included to represent the mount
structure and the compressor case back to the turbine frame.

A number of iterations were made on thickness and orientation of the
various elements of the model to arrive at an efficient structure which
would meet the design requirements. By these iterations it was possible to
take advantage of the ability to tailor composite materials to the specific
load requirements of the individual components. As can be seen in Table II,
a considerable amount of tailoring was possible.

Once the material configurations were selected, the computer model
was used to determine the final internal stresses in the frame components.
Several of the most critical of these are shown in Table III along with
the allowable stress for the specific lay-up pattern for the component.
The "Design Calculated Stress" for the "Critical Flight" conditions shown is
a conservative three times the actual calculated stress for that condition.
As can be seen in Table III, the stress allowable, as verified by material
properties tests, always exceeded the design calculated stress indicating
a safe design. The effect of different thermal coefficients where the
titanium bearing cones attached to the composite structure was also accounted
for as shown in Table IV.

Since one of the most critical areas of composite structures is the joining of the individually molded pieces, either by bonding or mechanical fastening, the critical joint areas of the frame were investigated by a series of individual subcomponent tests representing these areas. A total of 36 specimens representing 21 different areas of the frame were fabricated and tested to failure.

In all cases, the failing load of the subcomponent was in excess of the maximum design requirements of the area represented.

A summary of some of the more critical of these tests is shown in Table V and a typical failed subcomponent is shown in figure 5.

FABRICATION

Designing the frame was only the first part of the problem. It then remained to devise means for fabricating this large composite structure which, by its very nature required new frame fabrication concepts.

The fabrication of the QCSEE composite frame was a cyclic manufacturing process of bonding together numerous premolded graphite/epoxy parts and then machining the required interfaces in preparation for the next bonding cycle.

Since only two frames were to be fabricated, the fabrication process was designed to require a minimum amount of tooling, substituting hand benching and machining in its place. Although this is counter to the approach that would be employed in a production situation, it was felt that this would result in a lower overall cost in this case.

The frame was fabricated as two major sub-assemblies, the basic frame structure and the fan casing.

The basic frame sub-assembly required the pre-fabrication of the three wheels that provide the frame backbone. The forward wheel was cured out as one piece; however, the much larger mid and aft wheels were made up by adhesively bonding together a great many precured pieces in a steam heated press. The assembly of the pieces of such a wheel is shown in figure 6 and the completed wheel, just out of the press and prior to machining, can be seen in figure 7.

After these wheels were complete, the frame assembly was initiated by bonding the mid wheel to the aft wheel using pre-assembled honeycomb box structures to space the wheels axially at both the outer rings and the splitter rings. The forward wheel was then added in the same fashion. This assembled wheel structure is shown in figure 8.

To complete this sub-assembly, the pre-cured sump cone was bonded in placed as well as the pre-cured core strut skins and bypass vane skins. With the addition of appropriate reinforcing structure this completed the frame sub-assembly.

The outer casing subassembly was sequentially assembled on a male tool, which was cylindrical in shape, while the skins that went into this assembly were pre-cured in 120° segments in a female tool.

The first step was to pre-cure the fan flowpath skins. This was the surface requiring acoustic holes. These holes were laser drilled as shown in figure 9. This skin was put on the male tool and the tip treatment components bonded in place as shown in figure 10. A layer of aluminum honeycomb of the proper depth for the acoustic requirements was then bonded in place and a septem skin added to provide the back face of the acoustic panel. The containment system was installed at this time. Another layer of honeycomb was then added to obtain the proper casing depth. This completed the basic structure of the fan casing sub-assembly, seen in figure 11, since the outer skin would not be attached until the casing was assembled to the basic frame.

At this point, the two major sub-assemblies were mated (fig. 12), the fan casing outer diameter ground to the proper dimensions and the fan casing outer skin bonded in place. This completed the frame structure. All penetrations into the core were sealed, instrumentation and services installed and the frame painted. The completed frame is shown in figure 13 and 14.

TESTING

The fan frame was subjected to a series of static load tests to verify the overall structural adequacy. (All loads tests to verify the overall repeated structural adequacy.) All loads were applied to the frame through a simulated forward fan bearing cone and a simulated inlet. To simulate the proper boundary conditions on the frame, it was bolted to a simulated core engine. This assembly was then supported from the facility through the actual engine mount locations (fig. 15). In addition to determining the actual frame stiffnesses, the frame was tested to the loads imposed by the maximum operating thrust, thrust plus a 51.4 m/s (100 knot) cross wind and thrust plus the unbalance due to one blade out. The frame survived these tests with no damage and recorded stress levels were in good agreement with predictions.

The two composite fan frames built under this program were also, of course, used throughout the engine test phase of both the UTW and OTW engine. No structural problems resulted from these tests. Both the mount region and the bypass vanes were instrumented and monitored during engine testing. The indicated stress levels were very low but were in good agreement with the analysis for the conditions run.

The main problem encountered during engine operation was oil leakage from the sump where adequate sealing of all the penetrations for lines and

tubes could not be maintained. This problem was alleviated by filling the core struts and other selected areas with adhesive to provide an external seal. This was done on the test stand. Secondary FOD damage was also repairable on the stand.

CONCLUSIONS

Based on the information generated by the QCSEE program, the following conclusions have been reached as concern the use of graphite/epoxy for engine frames:

o   Composite construction shows promise for application to major engine frames. It has been shown that these frames can take advantage of some of the unique composite characteristics.

o   The static tests of the frame verified the analysis and engine tests were also in reasonable agreement.

o   As the frame was actually built, it was difficult to fabricate. The need for better part tooling and better assembly tooling was apparent. In the future it should be more efficient to use fewer individual pieces by more piece integration in the as molded condition.

o   The sump area was difficult to seal against oil leakage. The use of a metal sump liner would be desirable.

COMPOSITE NACELLE

The other major area of composite application to static structure in the QCSEE program was the flight type nacelle for the UTW engine. Virtually everything shown in figure 16, except for the test facility and some tubing, is constructed from advanced composite materials. In addition to the fan frame, which was discussed above, the inlet, outer cowl, and the fan nozzle can be seen. In addition, the inner cowl was also constructed of advanced composite material. These can be seen in the cut-away drawing shown in figure 17.

INLET

The inlet is of fairly conventional composite construction utilizing Kevlar/epoxy skins on aluminum honeycomb core. The inner barrel comprises the integral acoustic treatment with a 10% open area face sheet on the inner flowpath. The depth of the honeycomb core on the inner barrel varies as dictated by acoustic requirements. The porosity is molded into the face sheet as it is cured, just as is now the practice in making CF6 fiberglass sound

panels. The outer barrel is the primary load path. Both barrels are additionally supported by composite ring stiffeners. The leading edge was made from glass/epoxy for the QCSEE demonstrator engine but would be titanium for a flight engine due to anti-icing requirements. The critical inlet loads result from a 3g stall in combination with a dynamic landing. Typical stresses, deflections and margins of safety are shown in Table VI.

The inlet is attached to the fan casing by sixteen rotating latches. These points are the only critical local loads applied to the inlet. As such, a subcomponent test, see figure 18, was conducted of this area. The latch housing failure was within 1% of the rated latch capability. Analysis indicates that six consecutive latches would have to be open before failure would occur at maximum load.

OUTER COWL AND FAN NOZZLE

Both of these components were fabricated in the same manner, using the same materials. They are of full depth honeycomb sandwich construction with the outer skin being Kevlar/epoxy, the core being aluminum honeycomb flex core and the inner skin and structural rings graphite/epoxy. The only purpose for the inner skins being graphite was because of the 15% to 20% porosity required for acoustics. At that time, it was felt that this porosity could best be obtained by laser drilling and the initial attempts at laser drilling Kevlar/epoxy had not been as successful as laser drilling graphite/epoxy.

The pressure loading which designed these components is shown in figure 19. Typical stresses resulting from this loading are shown in Table VII along with the allowable stresses obtained from coupon testing. Several critical joint areas were also checked by subcomponent tests.

The fabrication of these components was reasonably straight forward, both being built-up on male tooling. The outer cowl is shown in Figure 20 as the outer surface of the honeycomb is being machined prior to bonding on the outer skin which is the last major operation. The nozzle actuator housing pans can be seen as well as the tunnels for routing the hydraulics and sync cables to the actuators. The completed outer cowl is shown in figure 21. The piano hinge which attaches cowl to the pylon can be seen. The external fairings for the actuators can also be noted.

The only difference in construction of the fan nozzle was in inclusion of spring loaded seals in the ends of the nozzle flaps which sealed the flaps against leakage in the forward flight nozzle position. These seals separated when the nozzle was in the reverse thrust position as shown in figure 22.

The most critical area in the outer cowl/fan nozzle system was the hinge ring in the back end of the outer cowl which supports the fan nozzle. This area was proof tested satisfactorily in the test shown in figure 23.

INNER COWL

The most ambitious application of composites to the QCSEE nacelle type hardware was in the area of the cowl where temperatures precluded the use of the familiar reinforced epoxy materials. Even with a typical heat shield installed, the operating temperature requirements were beyond epoxy capabilities as shown in figure 24.

Based on this information, it was decided to employ the NASA developed PMR 15 polyimide type resin system. This system not only met the temperature requirements but is relatively easy to process and produces low void content laminates. Woven graphite T300 cloth was chosen as the reinforcement because it provided the needed stiffness and was easier to fabricate with than tape. This is particularly true when using the PMR system because of its lack of tack compared to expoxies. This material could also be laser drilled to get the 15% to 25% porosity required for acoustic treatment in this component. The HRH 327 fiberglass/polyimide core was used because of temperature considerations.

Using these materials, a core cowl design was developed which resulted in a structure having typical ultimate calculated applied stresses shown in Table VIII. The allowable stresses in that table were the result of coupon tests. The completed core cowl is shown in figure 25. The steel aft ring that forms the slip joint with the outer side of the core nozzle can be seen as well as the hinges that attach the core cowl to the pylon. Each half of the core cowl was fabricated in two pieces due to the size of the laboratory autoclave. This would not be necessary in production. The split line can also be seen in the photograph. An interior view of the core is shown in figure 26. The flight weight core cowl would incorporate a standoff steel heat shield in the aft portion of the cowl. This heat shield was not built for the demonstrator engine, so a heat blanket was installed in its place and shop air dumped in in sufficient quantities to keep the core cowl temperatures to the levels they would be if the heat shield had been installed.

NACELLE TEST RESULTS

The nacelle components discussed above were run on the UTW engine with the following results:

o   No problems were encountered with the inlet.

o   No problems were encountered with the inner core cowl.

o   No problems were encountered with the outer cowl.

o   No problems were encountered with the fan nozzle when it was
     installed on the composite outer cowl, however, this nozzle
     was also used on the boilerplate outer cowl where the hinge

ring was bolted to the rear of the outer cowl rather than being bonded in. This hinge ring, due to a poorly designed bolted joint to the boilerplate outer cowl came off during reverse testing terminating the boilerplate nacelle tests.

o No environmental degradation was noted during engine operation.

CONCLUSIONS

Based on the information presented above, the following conclusions have been reached concerning the use of advanced composite materials in engine nacelle hardware.

o The program demonstrated the ability to design stiff, light, thin nacelle structures utilizing composite materials.

o Low temperature basic nacelle structures can be easily fabricated using state-of-the-art techniques.

o The PMR/graphite inner cowl provided a successful demonstration of a new high temperature composite system.

TABLE I. – FRAME LOADING CONDITIONS

- **Operating**
  - Flight and Landing
  - Gust Load Plus Crosswind and Max Thrust
  - Side Load — 4g Plus 1/3 of Gust Load

- **Emergency**
  - Seizure — Decelerating From Max. Speed to Zero In One Second
  - Crash — 9g Fwd, 2.25g Side, 4.5g Down,
    Max Thrust — 12g Fwd at Zero Thrust
  - Blade Out — Loss of Five Adjacent Composite Fan Blades at Max. RPM

TABLE II. – GEOMETRY OF COMPOSITE FRAME COMPONENTS

Material Type-AS Graphite/3501 Epoxy

Item	Layup Conf.			0° Datum
	0°	± 45°	90°	
Forward "Wheel"	50%	20%	30%	Radial
Middle "Wheel" and Aft	30%	20%	50%	Radial
Nacelle Panel	28.5%	57%	14.5%	Axial
Bypass Vane Panel	40%	40%	20%	Radial
Bypass Vane Spoke	80%	20%	0%	Radial
Bypass Vane Outer Ring	30%	20%	50%	Radial
Core Vane Panel	25%	50%	25%	Axial
	40%	40%	20%	Axial

92

TABLE III. – FRAME COMPONENT STRESSES

Load Condition	Location	Design Calculated Stress N/cm² (psi)	Stress Allowable N/cm² (psi)
5 Airfoils Out	Forward "Wheel" Hub Ring	37,230 (54,000)	42,750 (62,000)
5 Airfoils Out	Forward "Wheel" Spoke	53,570 (77,700)	65,500 (95,000)
Critical Flight	Bypass Vane Panel	40,920 (59,349)	57,230 (83,000)
5 Airfoils Out	Core Panel	8600 (12,471)	17,240 (25,000)
Critical Flight	Nacelle Panel	12,700 (18,417)	27,580 (40,000)

TABLE IV. – EFFECT OF DIFFERENT THERMAL COEFFICIENTS

Ring	α(RING — G/E) cm/cm/°K x 10⁻⁶ (in/in/°F x 10⁻⁶)	α(BRG — T 6-4) cm/cm/°K x 10⁻⁶ (in/in/°F x 10⁻⁶)	Thermal Stress N/cm² (psi)	Total Ring Stress Ncm² (psi)	Allowable Stress N/cm² (psi)
FWD HUB	4.5 (2.5)	8.46 (4.7)	2070 (3000)	39,300 (57,000)	42,700 (62,000)
MID HUB	2.34 (1.3)	8.46 (4.7)	4830 (7000)	25,500 (37,000)	60,000 (87,000)
AFT HUB	2.34 (1.3)	8.46 (4.7)	4830 (7000)	18,600 (27,000)	60,000 (87,000)

93

TABLE V. – SUBCOMPONENT TEST RESULTS

Type	Location	Required	Test
Core Strut/Ring	FWD	177,900 N (40,000 lb)	245,530 N (55,200 lb)
Core Strut/Ring	MID	214,000 N (48,100 lb)	298,000 N (67,000 lb)
Core Strut/Ring	AFT	20,000 N (4,500 lb)	105,000 N (23,700 lb)
Core Strut/Ring (Bending)	FWD	128,800 cmN (11,400 in.-lb)	165,000 cmN (14,600 in.-lb)
Core Ring (I.D. In Comp.)	FWD	18,080 cmN 1,600 in.-lb	427,140 cmN 37,800 in.-lb

TABLE VI. – INLET STRESSES AND DEFLECTIONS AT MAXIMUM LOAD CONDITION

3g Stall Plus Dynamic Landing

	Stress			
Type	Calculated N/cm² (psi)	Allowable N/cm² (psi)	Safety Factor	Deflection cm (in.)
Compression	1400 (2034)	12,377 (17,950)	7.8	0.058 (0.023)
Tension	1583 (2296)	27,097 (39,300)	16.1	
Shear	378 (584)	6033 (8750)	14.1	0.414 (0.163)
Burst	1806 (2620)	27,097 (39,300)	14.0	
Crush	3910 (5672)	12,377 (17,950)	2.2	

94

TABLE VII. – TYPICAL OUTER COWL STRESSES

Component	Mode	Calculated Stress/Load	Allowable Stress/Load
Outer Skin	Buckling	18,450 N/cm² (26,760 psi)	45,330 N/cm² (65,740 psi)
Forward Ring	Compression	165 N/cm² (240 psi)	910 N/cm² (1320 psi)
Aft Ring	Bending	23,277 N/cm² (33,760 psi)	77,221 N/cm² (112,000 psi)
Piano Hinge Fast.	Bearing	10,782 N (2,424 lb)	52,698 N (11,847 lb)

TABLE VIII. – TYPICAL CORE COWL STRESSES

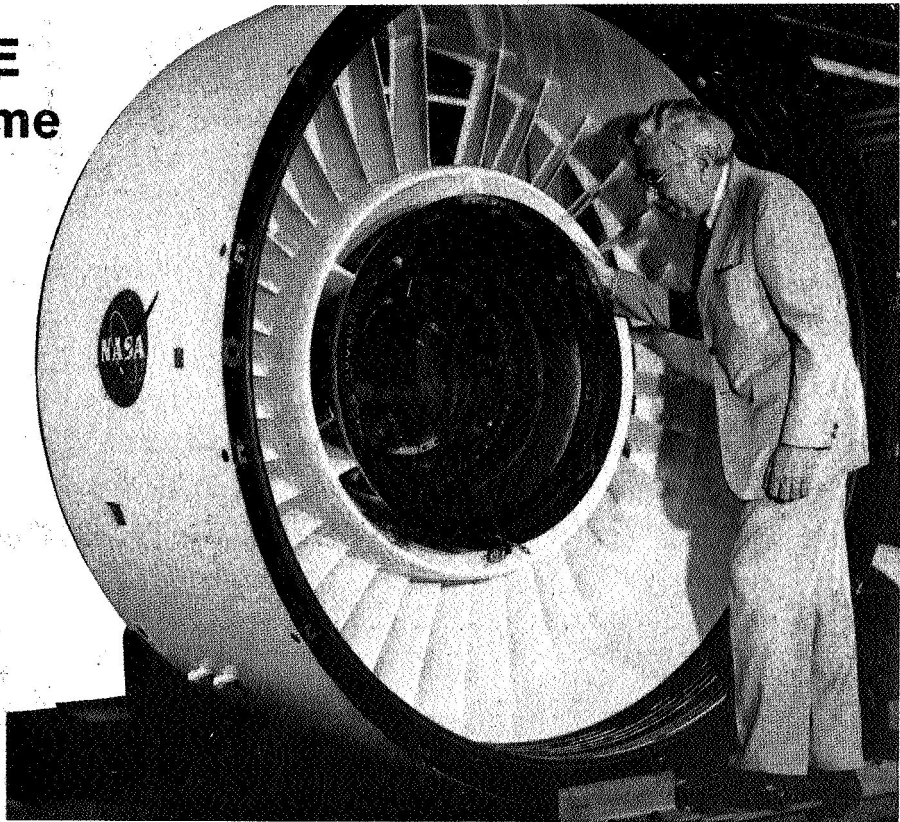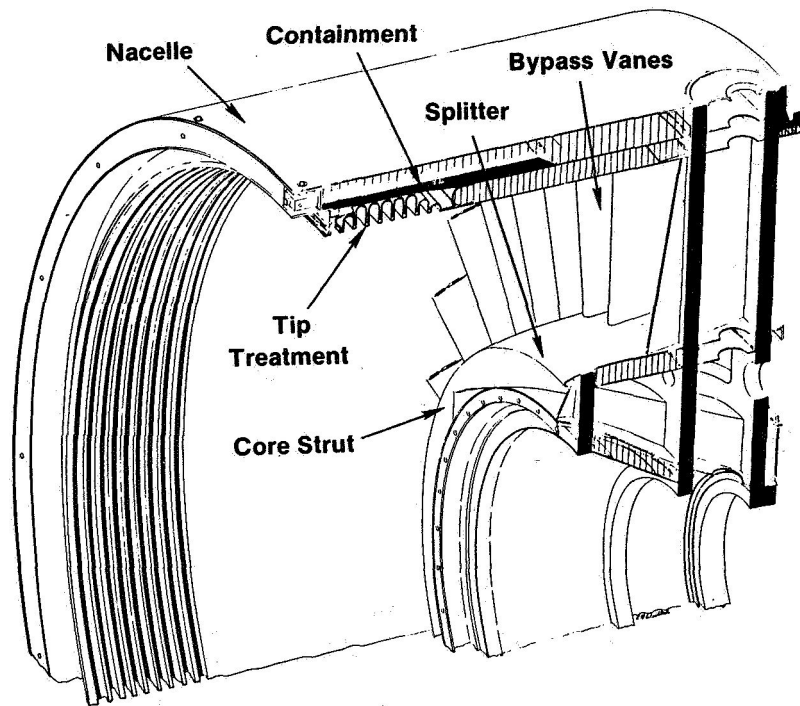| Load Condition	Component	Ultimate Calc. Stress N/cm² (psi)	Allowable Stress N/cm² (psi)
Forward Thrust	Outer Face Sheet Tension	8480 (12,300)	19,240 (27,900)
Reverse Thrust	Outer Face Sheet Compression	2290 (3324)	12,480 (18,100)
Forward Thrust	Inner Face Sheet Compression	11,420 (16,560)	29,990 (43,500)

QCSEE
Fan Frame

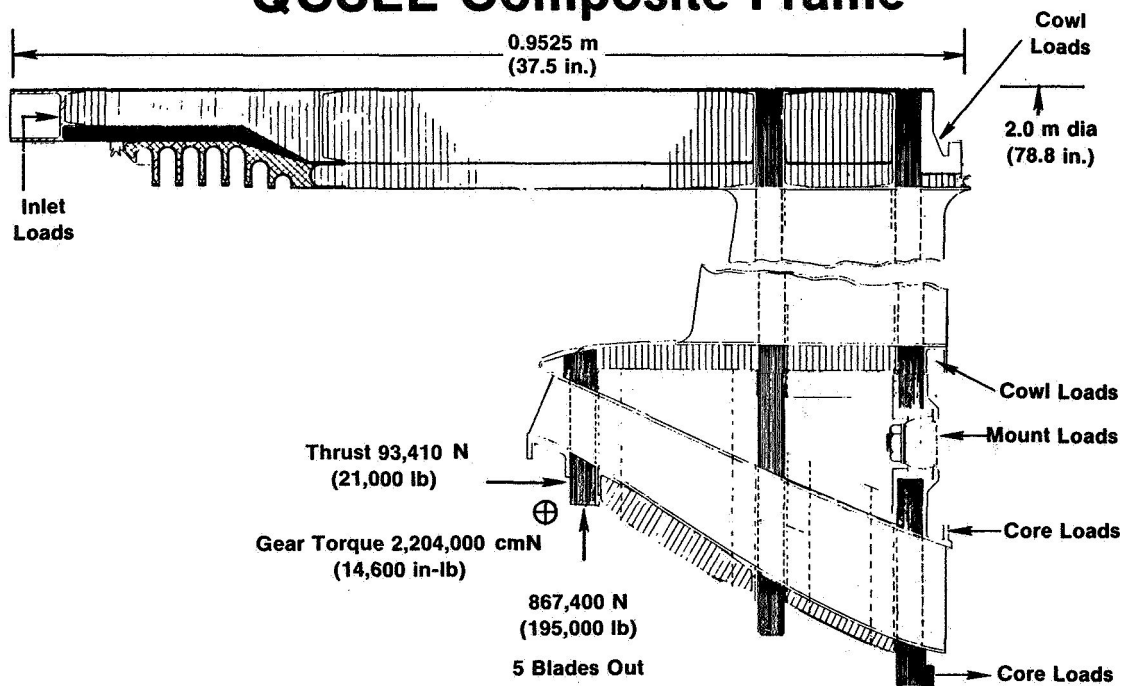Figure 1

Figure 2

QCSEE Composite Frame

0.9525 m
(37.5 in.)

Cowl
Loads

2.0 m dia
(78.8 in.)

Inlet
Loads

Cowl Loads

Mount Loads

Thrust 93,410 N
(21,000 lb)

Core Loads

Gear Torque 2,204,000 cmN
(14,600 in-lb)

867,400 N
(195,000 lb)

5 Blades Out

Core Loads

Figure 3

97

Analytical Model Comparison

Figure 4

Spoke Subcomponent Test

Tensile Failure
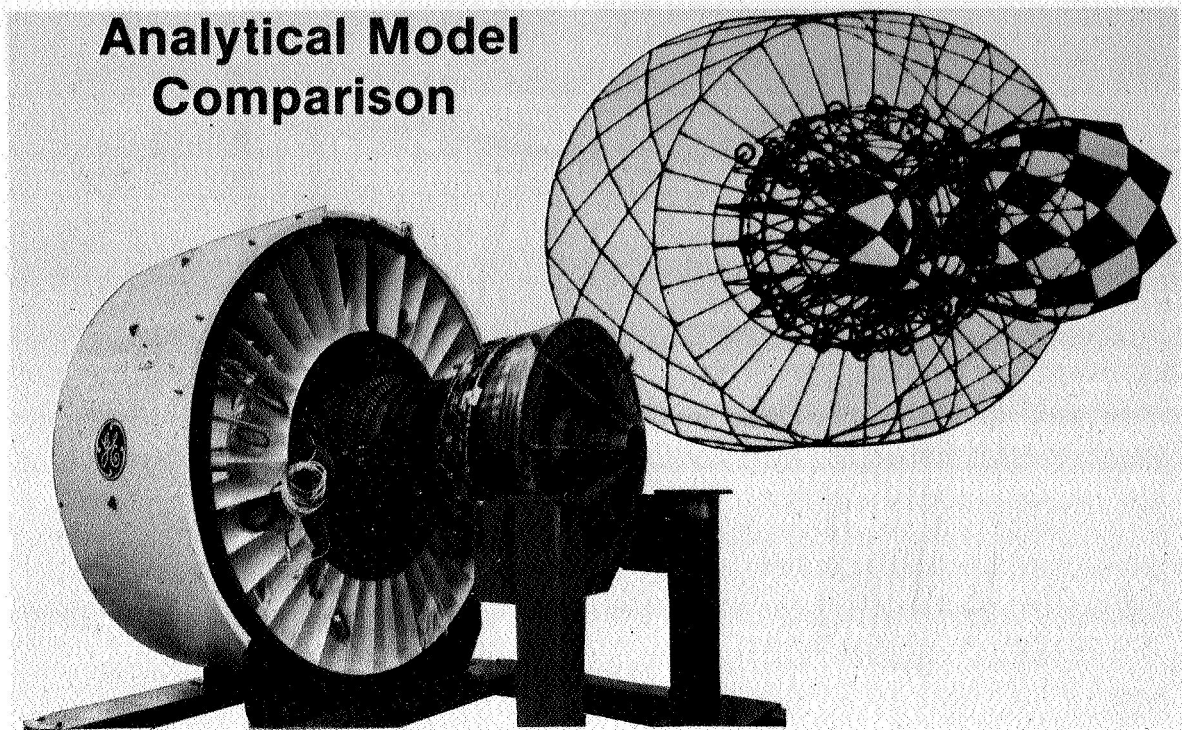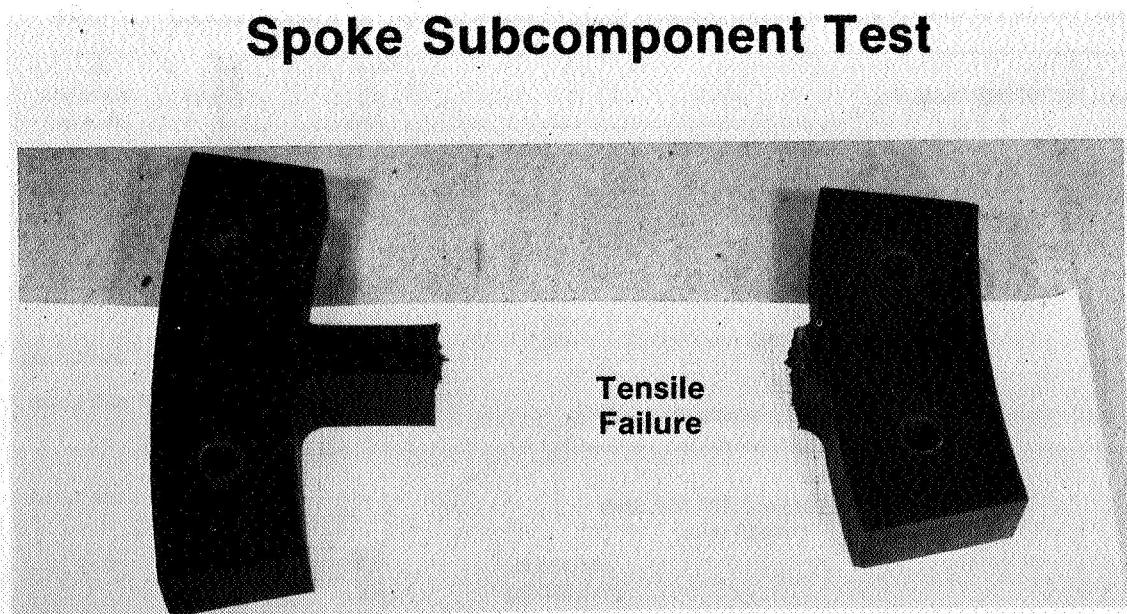
Figure 5

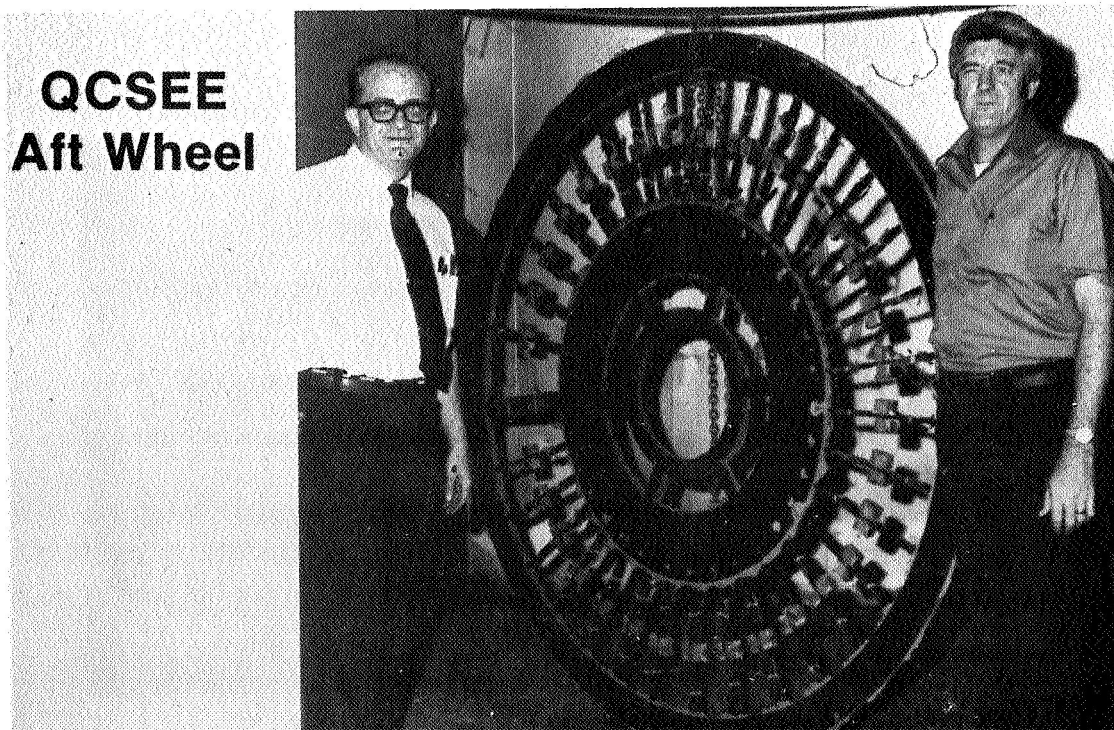# Assembly of Aft Wheel

Figure 6

Figure 7

99

Assembled Wheel Structure

Figure 8

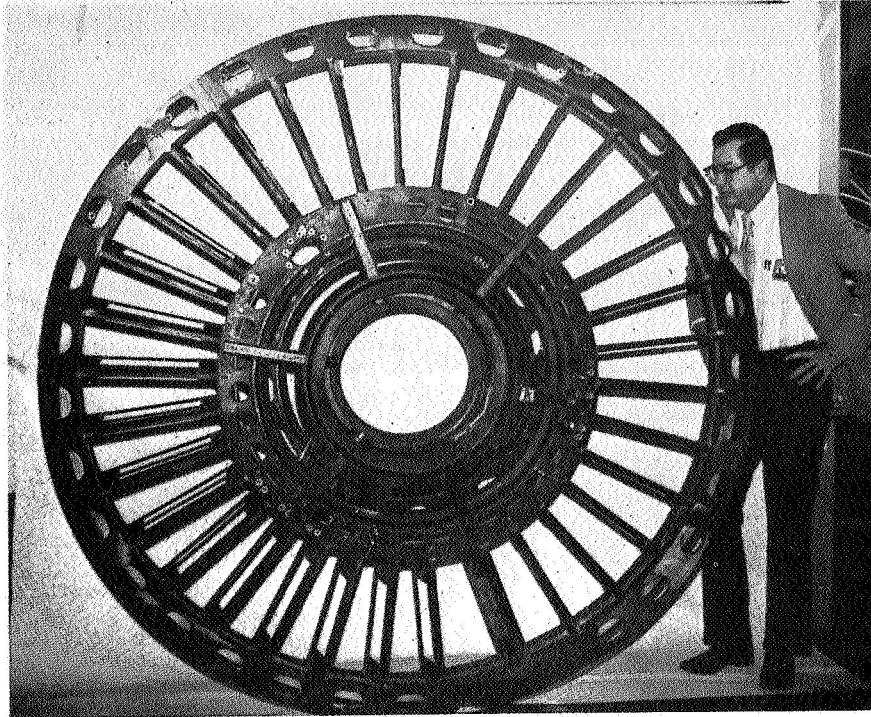# Laser Drilling of Acoustic Holes
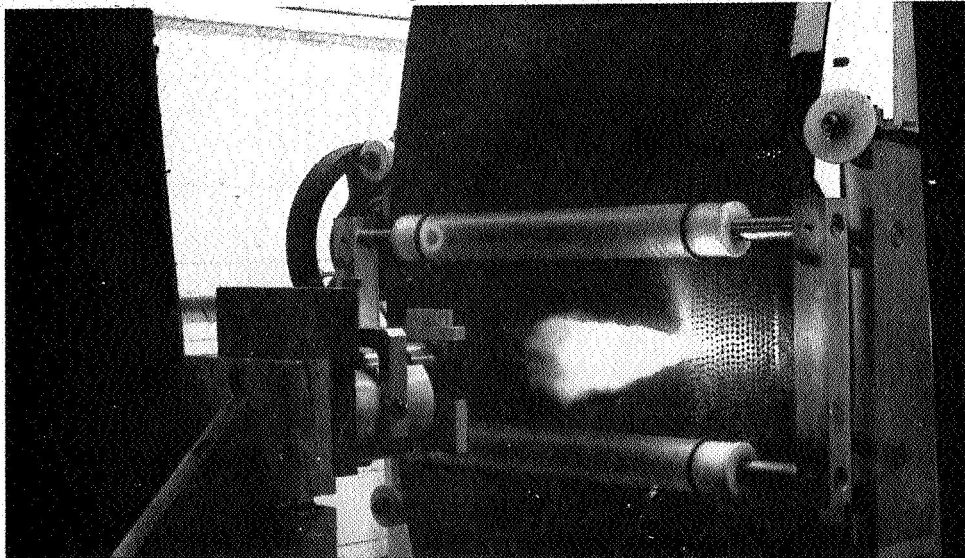
Figure 9

Fan Casing Fabrication
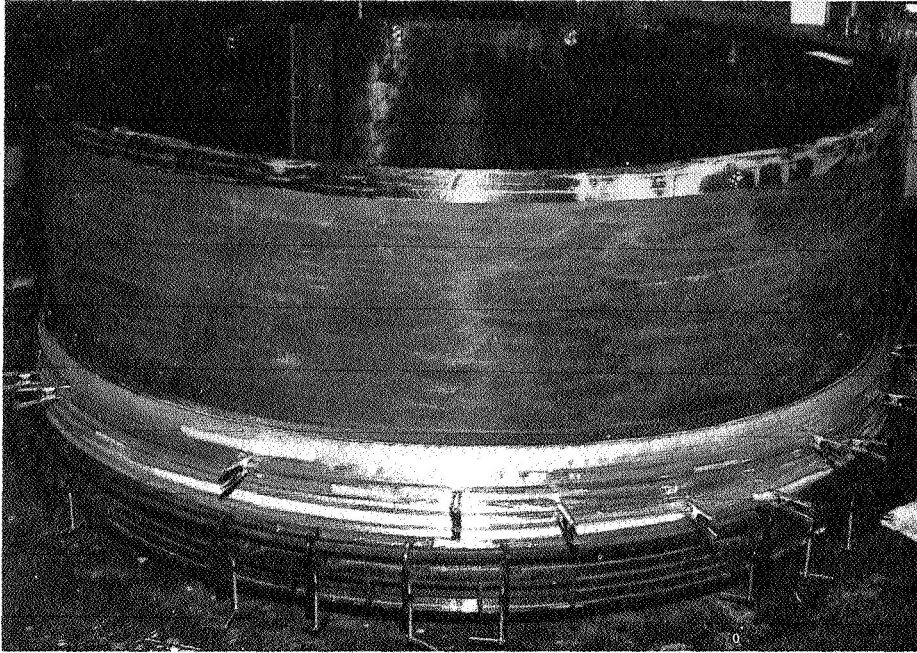
Figure 10

Fan Casing Sub-assembly
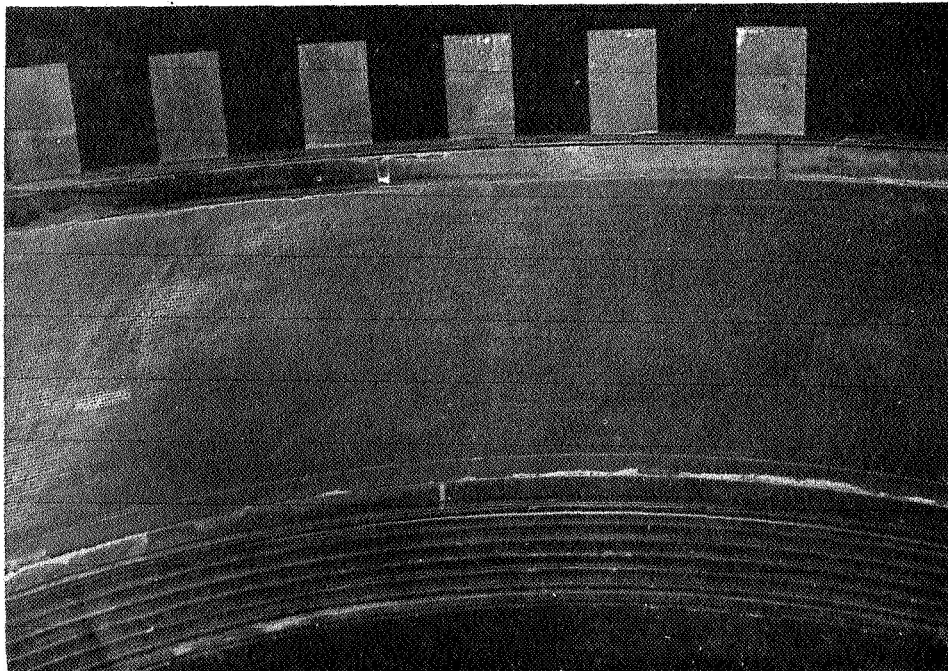
Figure 11

Assembling Fan Case to Frame
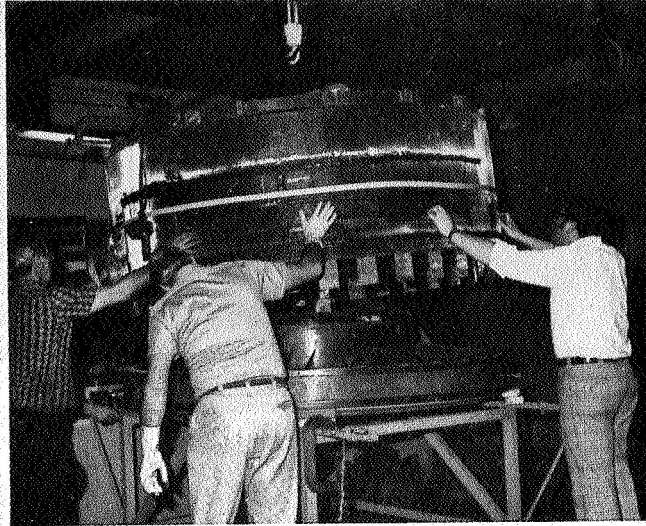
Figure 12

QCSEE Fan Frame
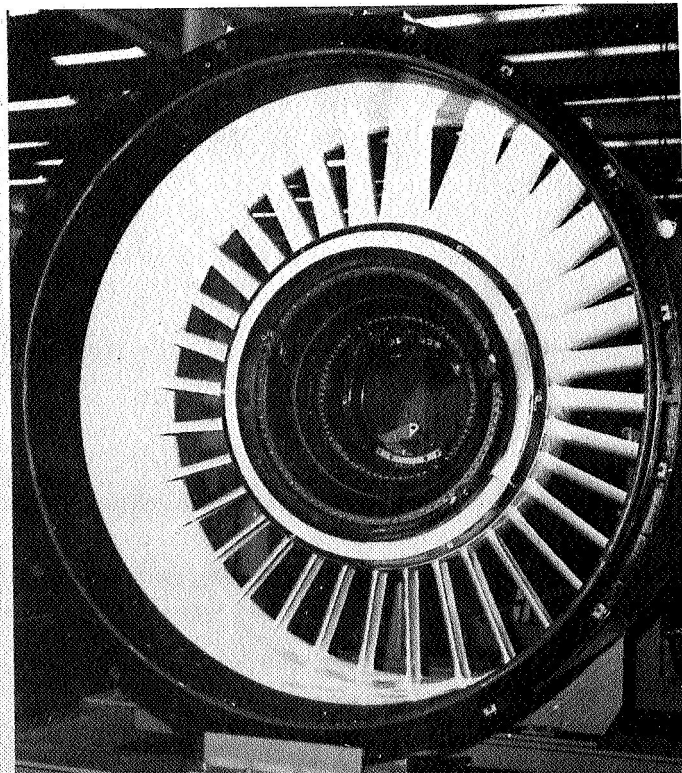
Figure 13

QCSEE
Fan Frame
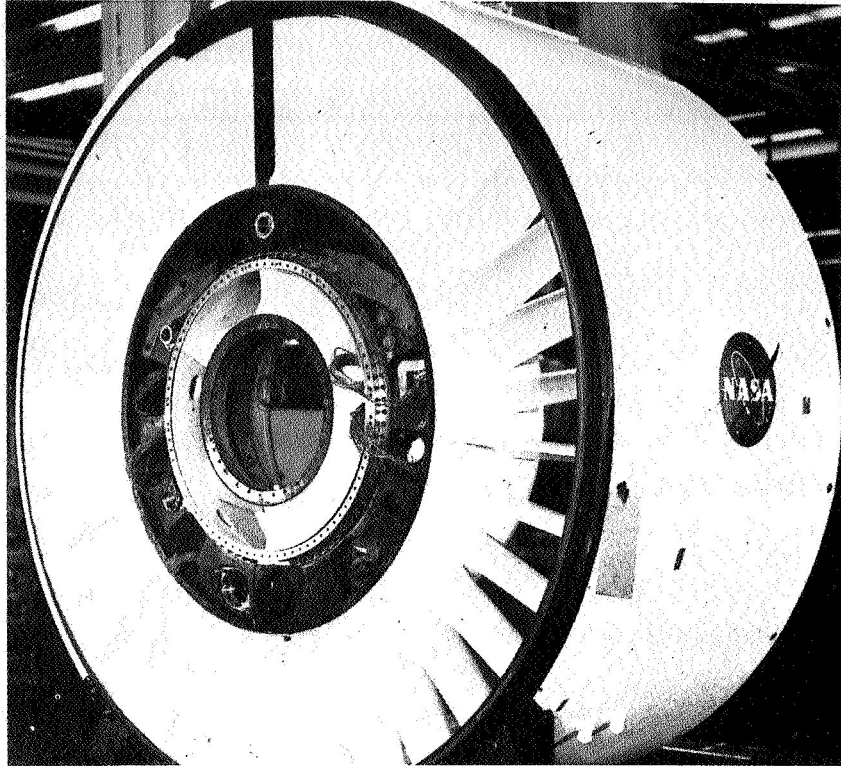
Figure 14

Static Test Set-up
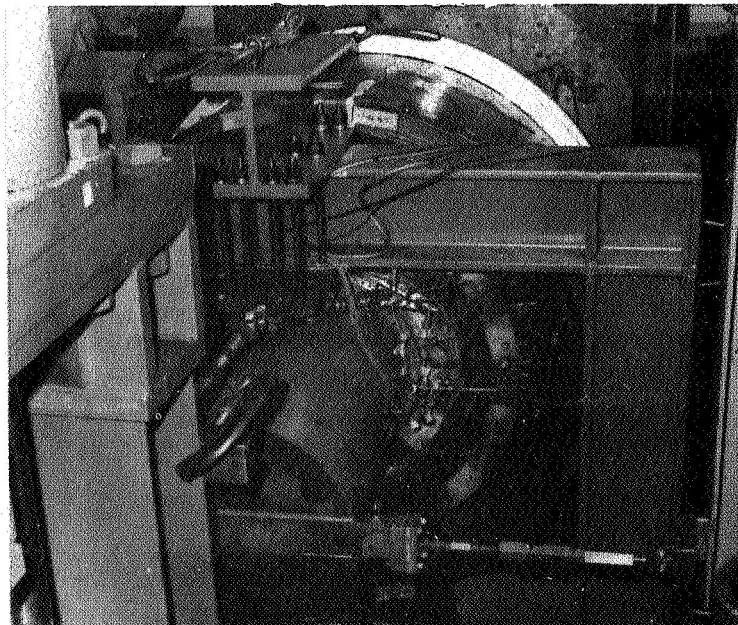
Figure 15

UTW Composite Nacelle
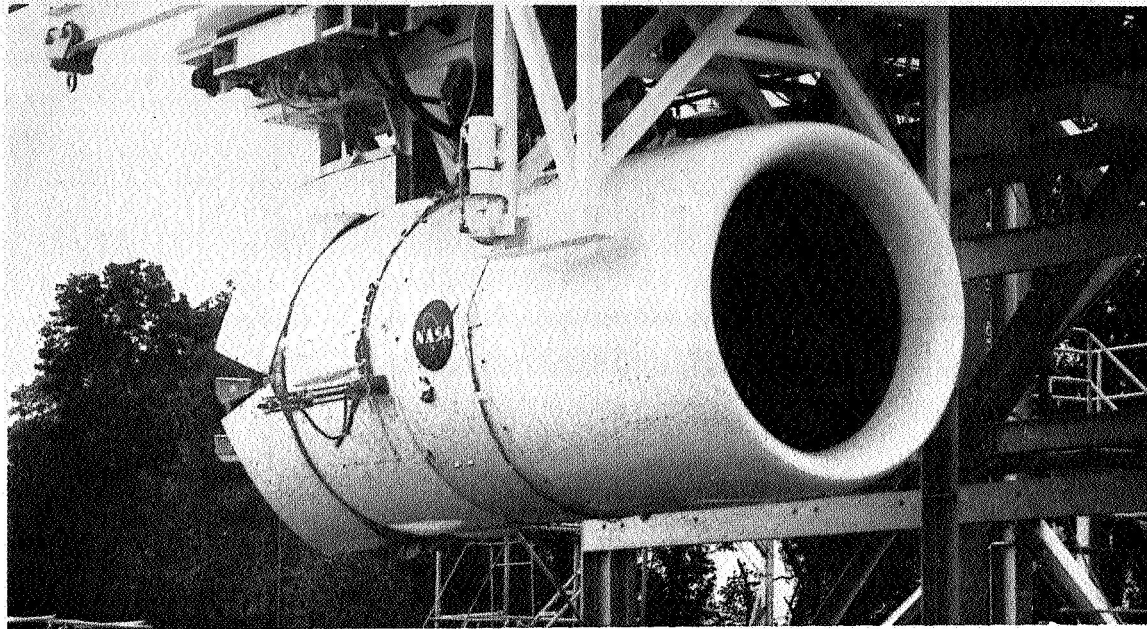
Figure 16

Composite Applications
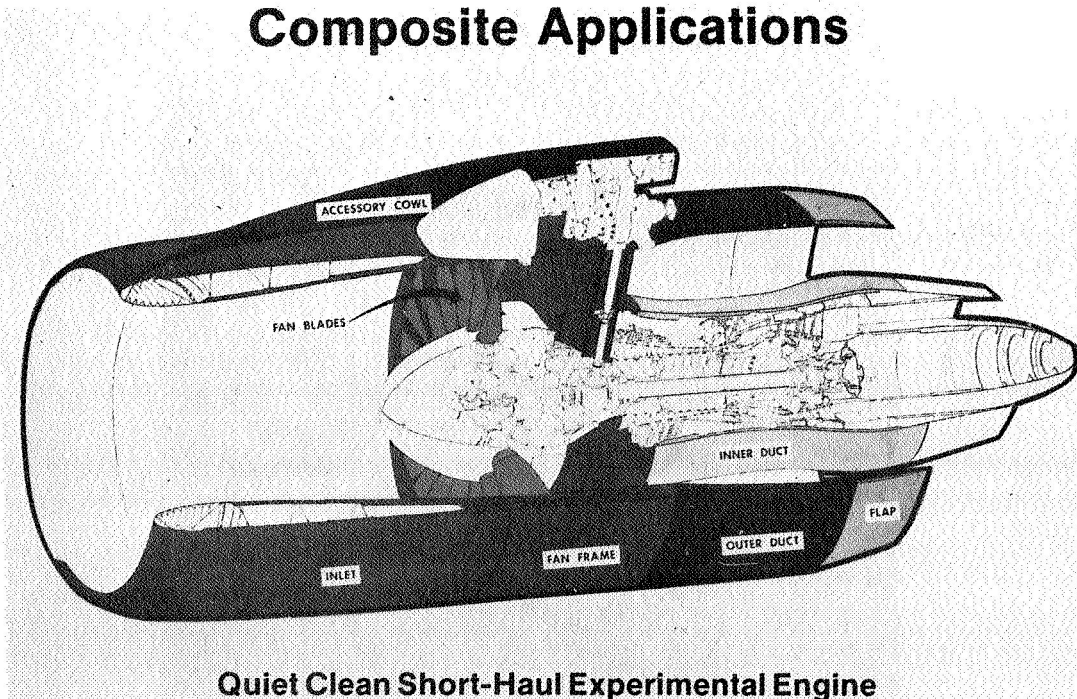
Quiet Clean Short-Haul Experimental Engine

Figure 17

Inlet-to-Frame Attachment Test
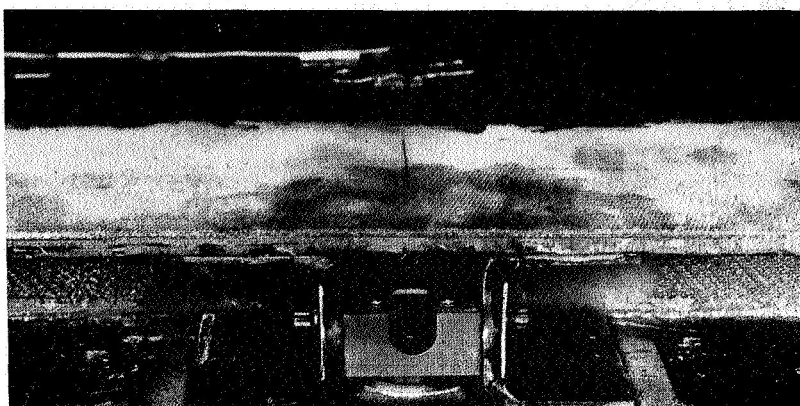
Figure 18

Differential Pressures

M = 0.92 at 6401 m (21,000 ft)

M = 0.227 at Sea Level

Differential Pressure, N/cm²

psi

Station Number
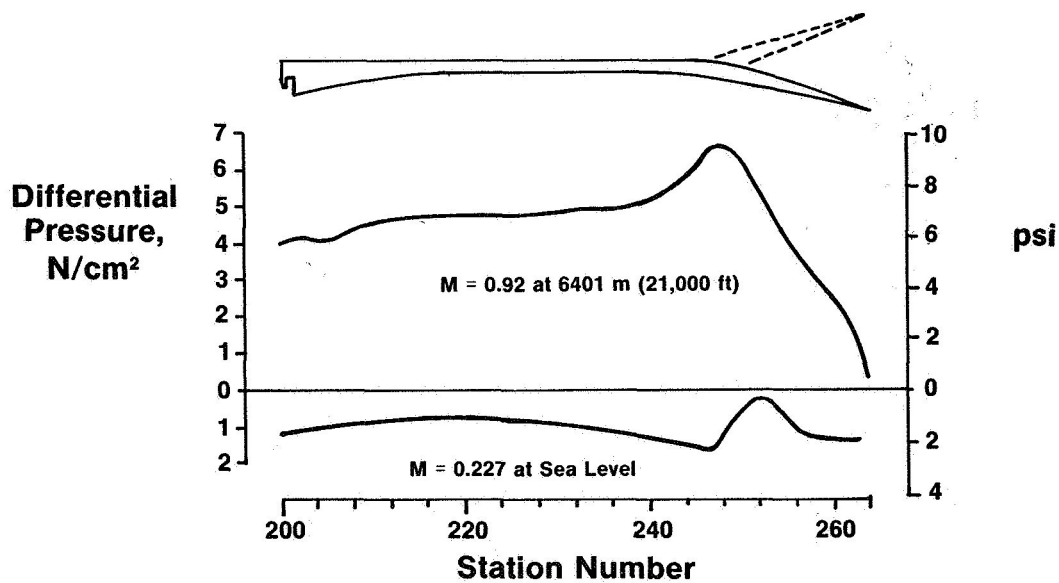
Figure 19

Outer Cowl Fabrication
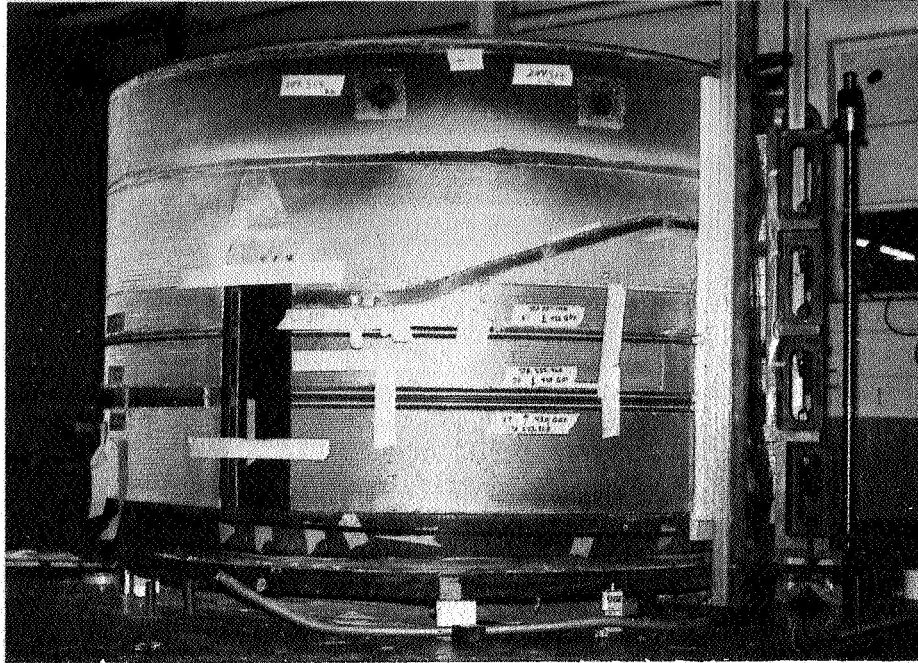
Figure 20

Completed Outer Cowl
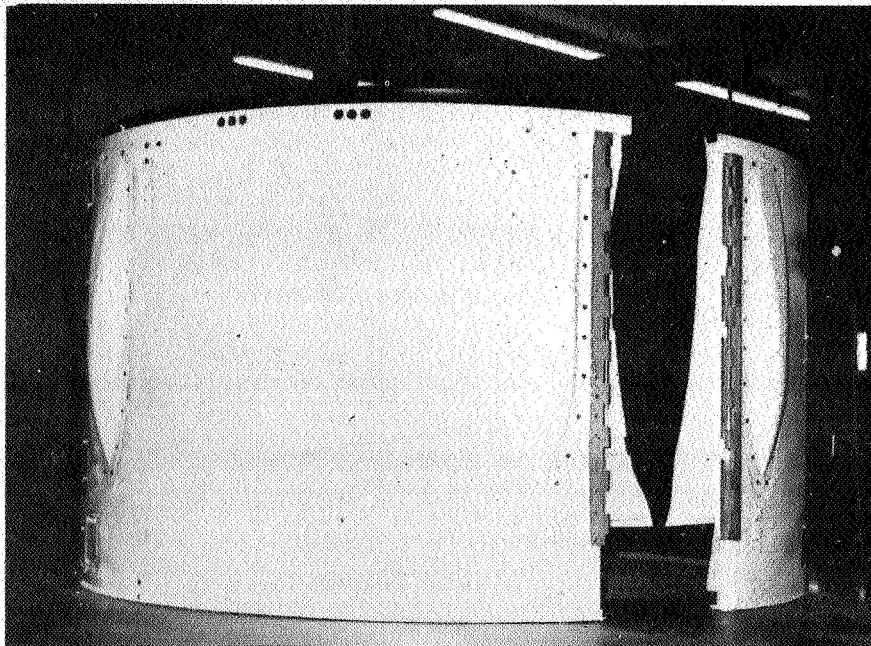
Figure 21

Fan Nozzle
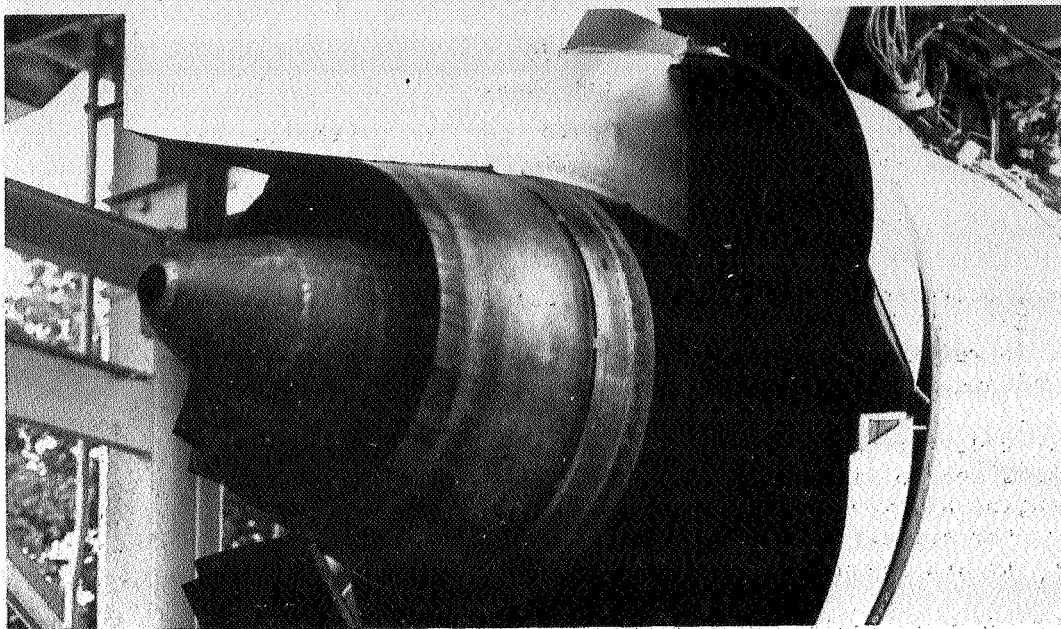
Figure 22

Static Load Test — Outer Cowl
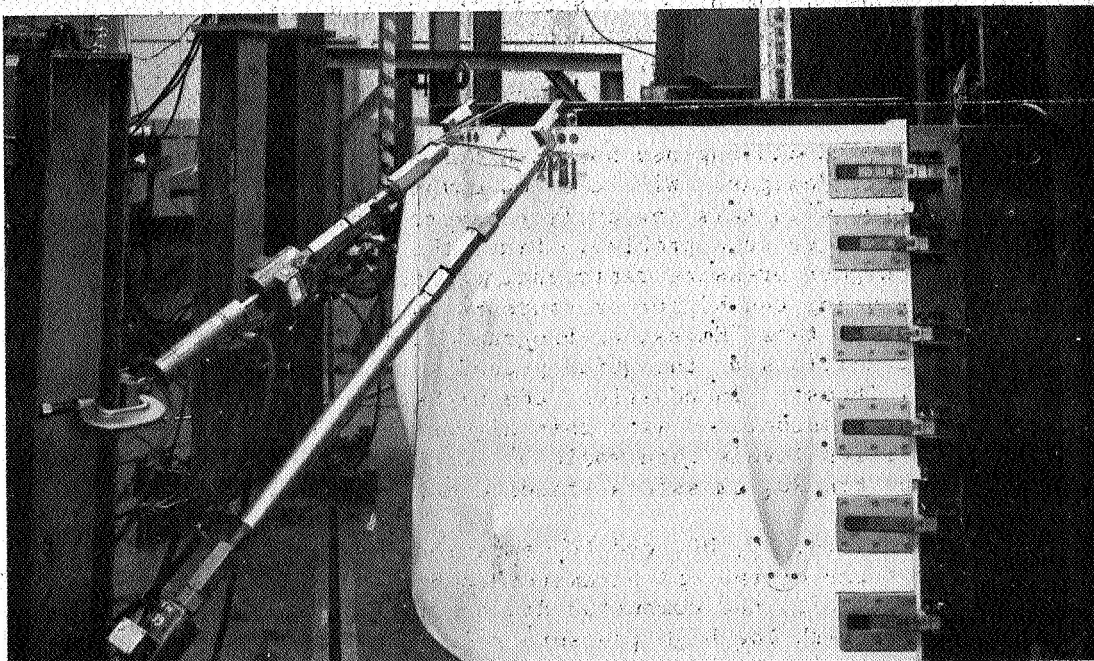
Figure 23

Inner Core Cowl Estimated Temperatures
Heat Shield Installed
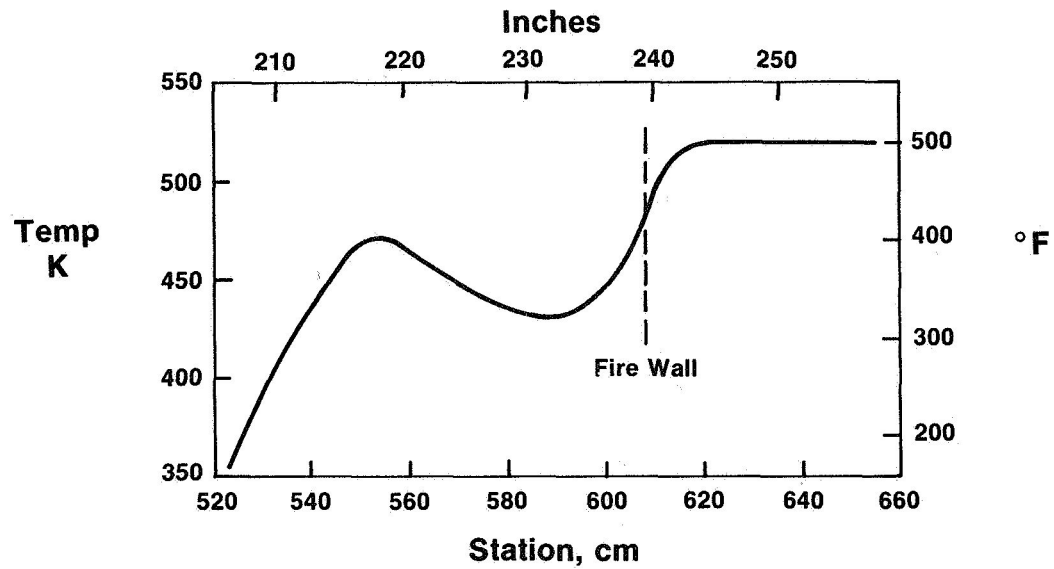
Figure 24

Completed Core Cowl
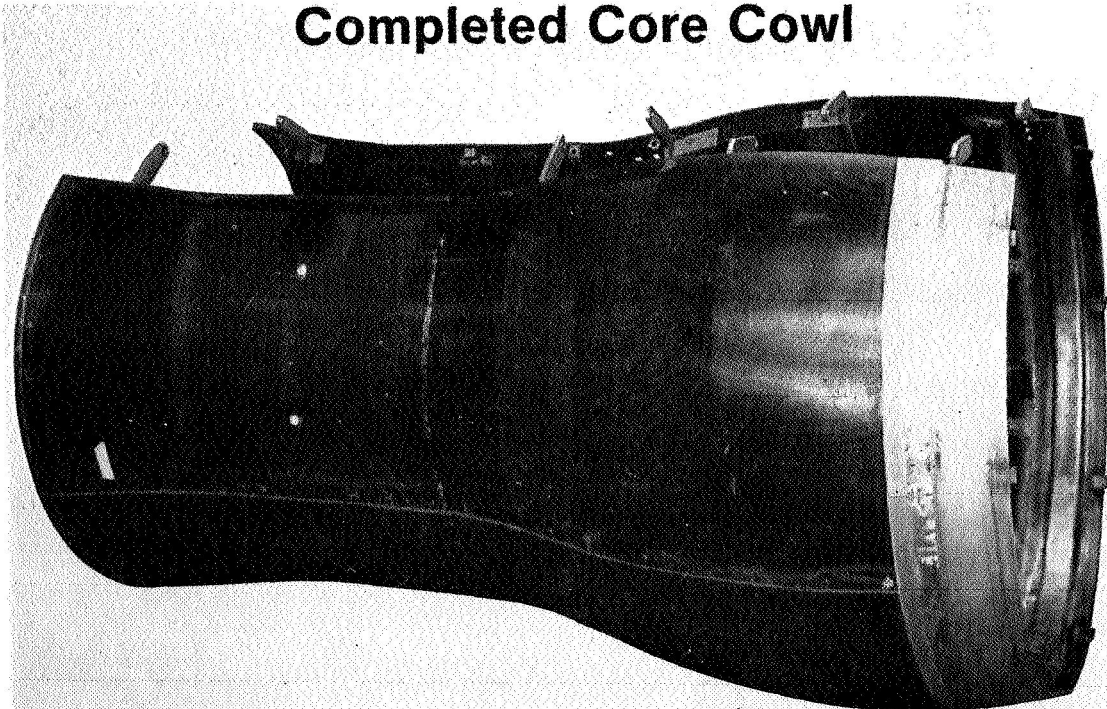
Figure 25

Core Cowl Interior View
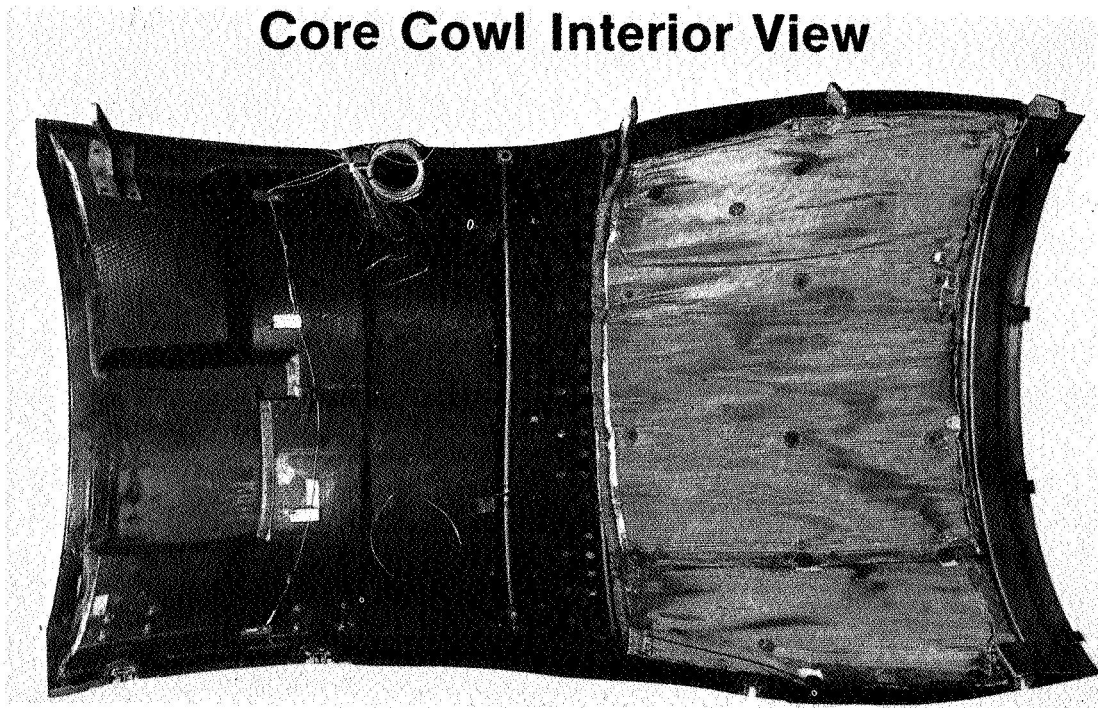
Figure 26

QCSEE COMPOSITE FAN BLADE DESIGN*

R.G. Stabrylla
General Electric Company
Cincinnati, Ohio

INTRODUCTION

This paper will cover the composite fan blades used in the Under the Wing experimental engine. The following subjects are included:

o   The background which led to the selection of composite materials for the fan blade application.

o   The blade aerodynamic and mechanical design requirements.

o   The blade mechanical and structural characteristics.

o   The blade performance in the UTW experimental engine.

o   The conclusion reached about the composite fan blades.

Although these blades did not meet all of the design goals originally set, they did perform acceptably in the engine.

DESIGN REQUIREMENTS

The mechanical design and materials selected for the UTW fan blades were dictated by the requirements associated with variable-pitch capability. The blades had to be capable of a very large angle of rotation over the whole engine speed range. To allow blade rotation the number of blades in the stage and their chord lengths had to be kept small so they could pass each other with no interference. To allow actuation of these blades at high rotor speeds with reasonable actuation forces, the blades had to be very light. To allow acceptable elastic stability with the blade geometry dictated by the variable-pitch-capability, the materials required very high specific stiffness and strength to density ratios. Composite materials, made up of graphite, S-glass, Kevlar and boron fibers in an epoxy matrix material have these characteristic properties.

Figure 1 indicates the effects of the VP requirement on fan blade geometry. On the left is a picture of the VP UTW fan, on the right is a picture of the OTW fan which did not have a VP requirement. Note the wide spaces between the UTW blades. This fan rotor has 18 blades whose root chord length is 14.7 cm (5.8 in.) compared to 28 blades with root chords of 20 cm (7.87 in.) used in the OTW rotor. Both blades were originally designed to use composite materials. The UTW blades weighed 43.3 kg (95.4 lb) while the composite OTW

111

blades weighed 55.3 kg (122 lb). The OTW blades used in the experimental engine were fabricated from titanium.

The aerodynamic design requirements for the UTW fan blades are shown in table I. Note that the airfoil solidity is less than 1.0 at all radial sections.

The mechanical design requirements of the fan blade fall into two major categories: variable pitch and structural integrity. Those requirements associated with variable pitch are uniquely the result of the need to be able to rotate the blades. For the UTW application, the blades had to be capable of rotation from the flat pitch to the stall pitch position which encompassed a blade rotation of over 170°. Obviously, to accomplish any rotation, shrouds could not be used. Finally, in order to be able to rotate the blades over the engine rotor full speed range with reasonable actuation forces, the blade weight had to be limited to less than 2.5 kg (5.5 lb) each. The actual blade weight was 2.4 kg (5.3 lb).

The design requirements associated with structural integrity are defined based on GE blade design practices and the engine's mission application. They encompass vibrational and steady state stresses, fatigue, FOD resistance, and maintainability considerations.

o   The design and materials selected for the blade are primarly dictated by the aeromechanical stability requirements. This is to avoid exciting blade natural frequencies by forcing functions due to aerodynamic flow.

o   Short-term steady state structural margin is defined as the capacity to operate the blade at 141% speed with no failure. (This represents a load factor of 2.) Thus, all blade stresses at this condition must be less than ultimate.

o   The blade must be capable of infinite high cycle fatigue life ($>10^6$ cycles) and have a low cycle capability of 48,000 engine starts. For aircraft use, the blades must pass the FAA certification test which defines bird strike tolerance limits. Finally, from an economic standpoint, the blade design must exhibit easy maintenance features such as replacement on-the-wing.

DESIGN DESCRIPTION

Figure 2 describes the design features of the composite blade. The airfoil and dovetail are fabricated from a number of 0.25 cm (0.010 in.) thick plies of composite pre-impregnated fibers which are cut out to various shapes and carefully layed up to satisfy the blade geometric requirements. These plies are of several different materials and are oriented in 0°, ±45° and 90° directions to give the blade the directional strengths and stiffnesses needed. These plies are laid up in a die and pressed in a carefully controlled time-temperature-pressure cycle. The leading edge is nickel plated

to improve the blade's erosion and FOD characteristics. The nickel is plated onto a stainless steel wire mesh which is bonded to the airfoil in a secondary operation. The remaining area of the airfoil is coated with a thin layer of polyurethane to reduce erosion due to dust, sand, and water. The platform, which forms part of the inner annulus flowpath, is round to allow blade rotation and still maintain a smooth inner flowpath for the air. The composite dovetail is bell-shaped and is encased in a 7075-T6 aluminum outsert. The outsert is cylindrical in shape and allows the blade to rotate during bird impacts thus reducing the stresses in the blade root. The purpose of this feature is to eliminate breaking the blade off at the root during foreign object impact.

Figure 3 shows half of the composite material plies that make up the blade. Four different materials are used in the blade. Note that the shape of each ply is different. Also shown are the proportions of the various materials used. The overall fiber volume fraction is 60%.

The platform is an integral part of the blade as shown in figure 4. It is put on the blade in a secondary operation. The round flowpath portion is made up of a number of graphite-epoxy plies bonded to the airfoil. The flowpath piece is supported by a lower face sheet also made up of graphite-epoxy. An aluminum honeycomb core is sandwiched between the flowpath and lower face sheets for stiffness. Finally, a leading edge strap of graphite-epoxy is put all-around the lower face sheet. The purpose of this strap is to hold the platform onto the blade in the event the shear bond fails. It is really a safety bandage.

The natural frequency characteristics of the blade/disk are shown on the Campbell diagram (fig. 5) as a function of fan speed. The blade was sized to satisfy aeroelastic stability criteria. This required the level of first torsional frequency shown. The second requirement was to have a good separation between the blade natural frequencies and all excitation lines at the 100% speed condition, which we do. The third goal was to have the first flex natural frequency above the 2/rev excitation line. This could not be done within the other design requirements, thus the first flex frequency was set to cross the 2/rev excitation line at about 67% speed which is a transient condition. During engine testing, it was found that stresses exceeded scope limits at the first flex 2/rev cross-over condition. The OTW blade also had a cross-over of its first flex with the 2/rev excitation line but because the longer blade hub chord length and the higher fatigue strength of titanium, the stresses were well below scope.

The Goodman diagram (fig. 6) was constructed using blade and specimen test data. The allowable curve is defined as 85% of test data. The test data was based on no delamination of specimens and blades for 10^6 cycles. Thus, this diagram represents a very conservative estimate relative to Goodman diagrams used for metals which are based on material fracture. For engine testing, the scope limits were set at 8.5 ksi to account for blade-to-blade variations, electronic errors, etc. Thus, during engine testing our scope limits were very conservative. During testing, scope limits were exceeded significantly a number of times, however, no delaminations have been found in the blades.

FOD RESISTANCE

The initial intent of the blade development effort was to develop a design that satisfied foreign object damage requirements. The FAA requirements for bird impacts are shown in table II. In addition, the more stringent GE goals are shown. GE's requirements are more demanding in the area of small birds. The rationale for the GE goals are based on experience with titanium blades and economics.

The FOD resistance of the preliminary blade design was evaluated in a whirligig impact facility (fig. 7). In these tests, the blades are rotated and a simulated RTV bird is injected into the path of the blade.

The results of one of the two tests performed is shown in figure 8. Blade serial number QP005 was impacted at simulated aircraft take off conditions with a 0.907 kg (2.0 lb) bird. The test conditions simulated an impact at the blade 80% span location for an aircraft forward velocity of 41.2 m/s (80 knots.) The bird to blade relative velocity was 275 m/s (904'/sec), the incidence angle was 33°, and the weight of the bird slice was 0.227 kg 1/2 lb). The blade did not break at the root. Keyhole rotation was noted in the movies. Post-test inspection of the blade showed it had lost 7% of its weight and approximately 90% of the airfoil was delaminated. Based on this result, it was concluded that the UTW composite fan blade design would not satisfy the FAA FOD requirements. Further, it was decided not to pursue the development of the FOD resistant design for the engine demonstration.

ENGINE TEST RESULTS

The blades performed acceptably during experimental engine test. The steady state stress levels were low and there were no indications of torsional instability. The only problems encountered were that the blade vibratory stress levels exceeded scope limits at the 2 per rev/first flex cross-over and high first flex vibratory stresses were also noted due to crosswind and tail wind test conditions at speeds above the 2/rev crossover. It should be pointed out that the scope limits defined for the composite blade were very conservative and no blade delamination occurred. Further, the titanium blades were also excited by crosswinds and tail winds.

In conclusion, the VP design required lightweight blades, the QCSEE composite blade is acceptable for experimental ground test only based on its lack of bird FOD resistance. Subsequent developments of other programs have identified candidate materials that could possibly solve this problem, however, none of this work has been completed to date. Some of these material candidates are:

o   Stitched or multidirectional weave polymerics

o   Superhybrid

o   Boron aluminum

o   Hollow titanium

o   Titanium matrix composites

In summary, the variable pitch fan imposed more stringent design requirements on the blade design which require use of lightweight designs.

TABLE I. – AERO DESIGN REQUIREMENTS

Aero Definition	UTW
Tip Speed	306 m/sec (1005 ft/sec)
Tip Diameter	180 cm (71 in.)
Radius Ratio	0.44
Number of Blades	18
Bypass Pressure Ratio	1.27 Takeoff
Aspect Ratio	2.11
Tip Chord	30.3 cm (11.91 in.)
Root Chord	14.8 cm (5.82 in.)
Solidity	
— Tip	0.95
— Root	0.98

TABLE II. – UTW COMPOSITE FAN BLADE
BIRD IMPACT DESIGN REQUIREMENTS

Bird Size kg (lbs)	Max No. Birds Ingested	FAA Requirement	GE Goals
.085 (.188)	16	Maintain 75% Engine Thrust	No Blade Damage
.68 (1.5)	8	Maintain 75% Engine Thrust	Maintain 75% Engine Thrust
1.8 (4)	1	Safe Shutdown	Safe Shutdown

Fan Rotors

UTW   OTW

Figure 1

Composite Fan Blade Features
UTW Engine

Local Transverse
Strengthening Plies

Polyurethane
Environmental
Protection
Coating

Boron Torsional
Stiffening Plies

Graphite/Kevlar
Centrifugal and
Flexural Load Plies

Nickle Plate
Leading Edge
FOD Protection

S-Glass
Flex Root Plies

Platform

Aluminum
Keyhole Outsert

Figure 2

117

Composite Fan Blade Ply Assembly

Airfoil Center

Airfoil Surface

Color	Material	% By Volume
	Type AS Graphite/PR288 Epoxy	36
	S-Glass/PR288 Epoxy	5
	Kevlar/PR288 Epoxy	37
	Boron/PR288 Epoxy	22

Figure 3

Composite Fan Blade Platform Construction

Upper Face Sheet (Hub Flowpath)

Honeycomb Core

Fan Blade Trailing Edge

Leading Edge Strap

Lower Face Sheet

Figure 4

Campbell Diagram Composite Fan Blade
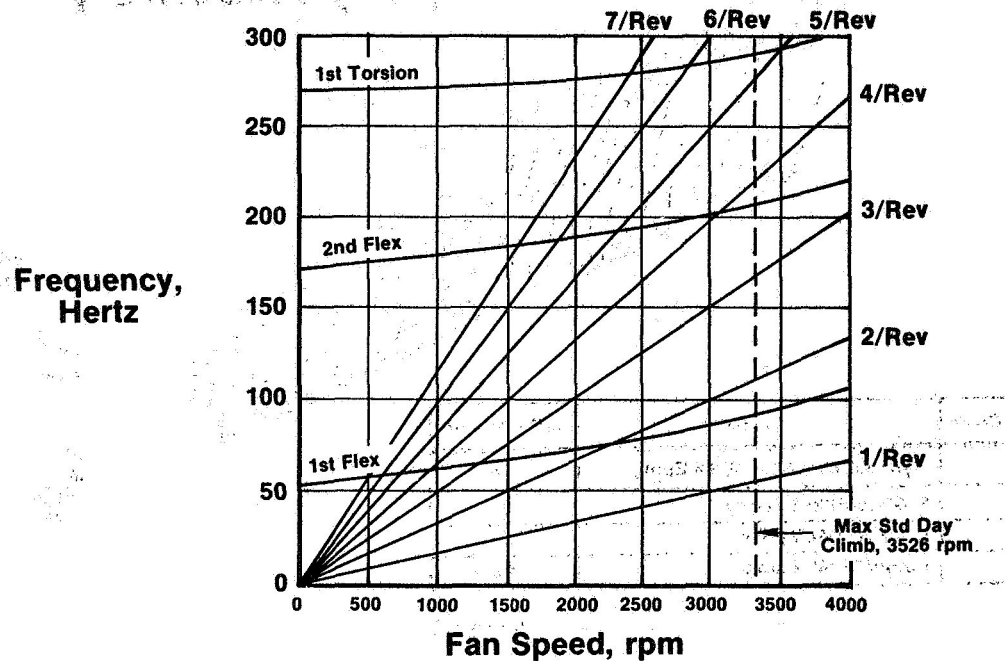
Figure 5

Goodman Diagram
Composite Fan Blade
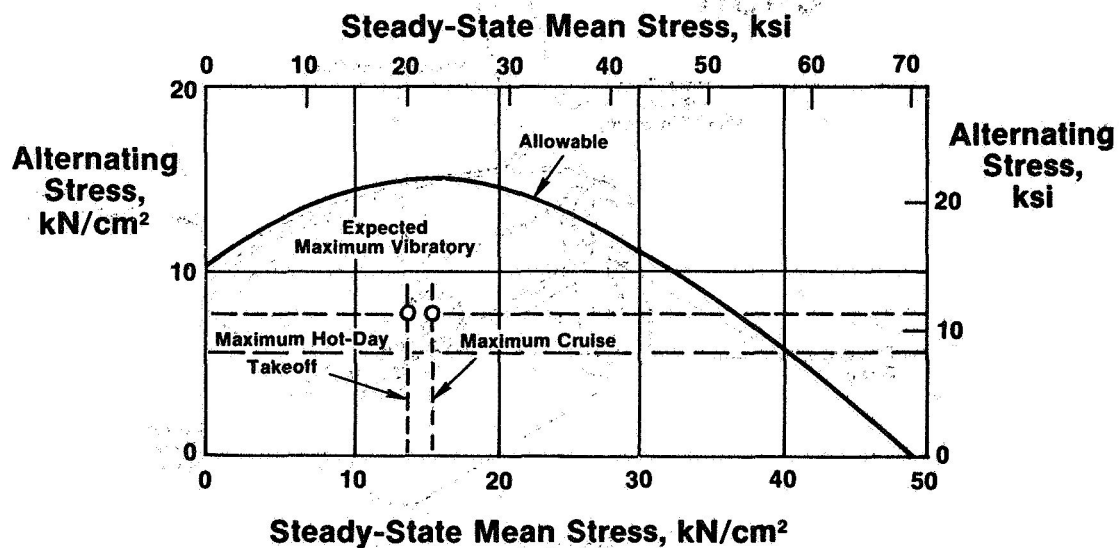
Figure 6

Whirligig Impact Test Facility
Composite Fan Blade
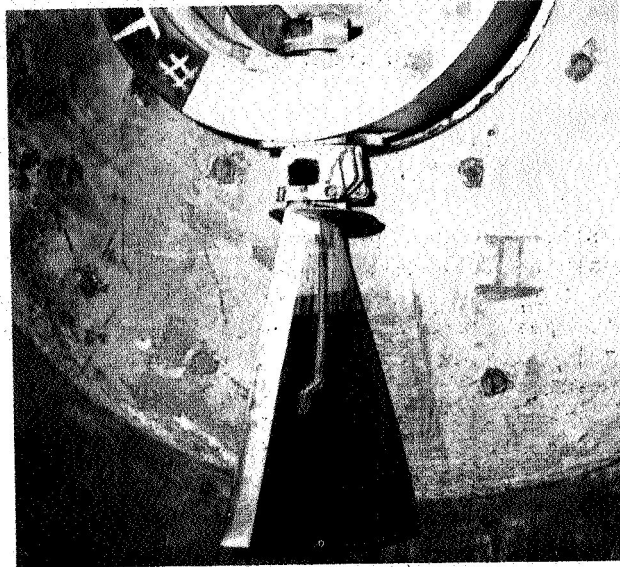
Figure 7

Bird Impact Test Results

Test Conditions
- Aircraft Takeoff
- 1.5 Pound Bird

Results
- 7% Weight Loss
- 90% Delamination
- No Root Failure

Figure 8

120

QCSEE COMBUSTOR EMISSIONS REDUCTIONS*

P.E. Sabla
General Electric Company
Cincinnati, Ohio

INTRODUCTION

This paper describes the design and development of the QCSEE low emissions combustor. Included is a discussion of the combustor requirements and the status of the current QCSEE conventional combustor design relative to the requirements. The design of an advanced combustor concept directed at meeting the very challenging emissions requirements for QCSEE is presented along with the key results obtained in development tests conducted with a prototype design of this advanced combustor concept. It was concluded at the completion of this program that this advanced combustor design would be suitable for the QCSEE application.

DESIGN REQUIREMENTS

In July 1973, the U.S. Environmental Protection Agency (EPA) issued standards to regulate and minimize the quantities of carbon monoxide (CO), hydrocarbons (HC), oxides of nitrogen (NO_x), and smoke emissions that may be discharged by aircraft when operating within or near airports. These standards were defined for several different categories and types of fixed-wing, commercial aircraft engines and are presented in terms of calculated parameters called the EPA Parameter (EPAP). This parameter is based on an EPA defined landing-takeoff cycle consisting of specific operating times at engine power settings for ground idle, takeoff, climbout, and approach. The CO and HC emissions are mostly generated at the lo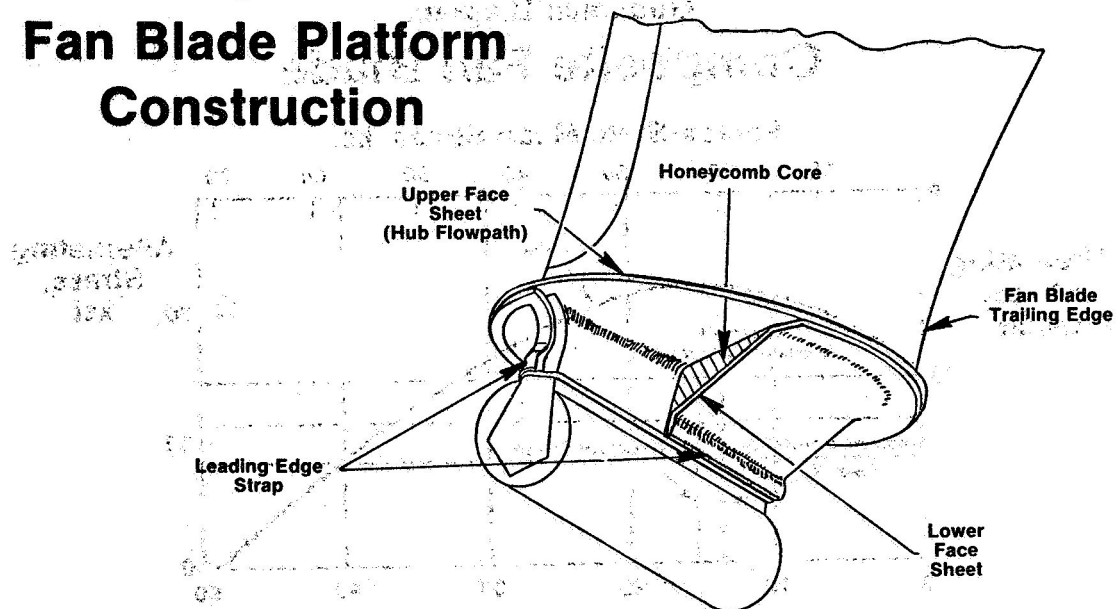w power ground idle conditions while the NO_x emissions are generated at the higher power settings including takeoff, climbout and approach.

The requirements for the QCSEE combustor were predicated on the basis that it meet the very stringent EPA standards for certified Class T2 subsonic engines. These standards, shown below, are presently scheduled to become effective in 1979:

QCSEE COMBUSTOR REQUIREMENTS

1979
EPA Stds.

CO	4.3	(lb./1000 lb.
HC	0.8	Thrust Per
NO_x	3.0	Hour-Cycle)
Smoke (SAE-SN)	22.0	

However, proposed amendments to these standards are currently being reviewed by the EPA. The promulgation of these revised standards could possibly result in relaxation of these requirements and the effectivity dates for Class T2 engines.

In addition to the combustor emissions requirements, the combustor must also be sized to fit within the dimensional envelope of the existing QCSEE core engine and meet performance requirements such as combustion efficiency, exhaust temperature distribution, and altitude ignition typically required for any modern advanced high bypass engine.

As shown in table I meeting the CO and HC emissions requirements in the QCSEE applications is particularly challenging, because of its more severe combustor inlet operating conditions at ground idle, compared to those of a current state-of-the-art engine such as the CF6-50. The CO and HC emissions of the QCSEE are strongly and adversely affected by these lower combustor inlet temperatures and pressures. In addition, these requirements must be met with a combustor sized to fit within the confines of the very short compact envelope of the F101 combustor casing. Figure 1 shows that most recent version of a single annular combustor configuration sized to fit the QCSEE and designed specifically for low emissions.

The QCSEE UTW and OTW engines both use the F101 core, resulting in low pressure ratio cycle designs. With the low combustor inlet temperatures and pressures associated with this low cycle pressure ratio, the NO_x emissions would not be expected to be a problem. Since the technology being developed was intended for higher pressure ratio engines, the development was carried out in a test rig using the higher pressure ratio cycle conditions listed in table II. The use of this "Emissions Program" cycle did result in improved combustor inlet conditions at the QCSEE ground idle power setting of 4.5% of Sea Level Takeoff Thrust. In addition, the higher combustor inlet temperatures and pressures associated with this higher pressure ratio cycle result in higher NO_x emission levels than would be expected with the original QCSEE cycles, making the EPA NO_x emissions standard more challenging.

Table III shows the CO, HC, and NO_x emission levels of the single annular combustor in terms of the EPA parameter compared to the program goals. As is shown in the table, the combustor did not meet the program goals for CO or NO_x emissions with the high pressure ratio cycle. Therefore, to meet the emissions goals in the short compact combustor envelope, a more advanced combustor concept was required.

122

APPROACH

The primary approach was to design and develop a double annular dome combustor, as shown in figure 2, based on technology developed previously in the NASA/GE Experimental Clean Combustor Program (ECCP). Figure 3 shows the much smaller size of a QCSEE double annular combustor compared to the CF6-50 size double annular combustor developed in the ECCP. The QCSEE double annular dome combustor uses many of the features of the CF6-50 double annular combustor, such as independently staged domes, counter rotating air-blast swirl cups, and pressure atomizing fuel nozzles. However, a substantial scale-down was needed particularly in its length and dome heights, compared to the ECCP design. The staged combustor concept permits operation of only the pilot stage dome, which is designed specifically to obtain low CO and HC emissions levels, at the low power operating conditions. At the high power operating condition both domes are operated with fuel staging selected to obtain low NO_x emission levels.

DEVELOPMENT PROGRAM

The development program was conducted using a sector combustor shown in figure 4. A disassembled view of this five swirl cup, ninety degree (90°) sector combustor is shown in figure 5. The tests were conducted in a rig designed to accept the sector combustor and duplicate exactly the flowpath of the F101 engine. Figure 6 shows a photograph of the test rig with the sector combustor installed. Although the major effort was focused on developing low CO and HC emissions at idle, the NO_x emissions levels of the QCSEE double annular combustor were also evaluated at simulated high power conditions; however, it was necessary to derate the pressure at higher power conditions and to adjust the measured NO_x emissions for the pressure difference.

TEST RESULTS

The number and types of combustor development tests conducted in the sector combustor program and the total number of test conditions at which data were acquired for each test category are shown below.

TEST SUMMARY

	Number of Test Configurations	Data Points
Emissions Development	32	310
Ignition Development	2	26
Combustor Performance	1	8
Fuel Spray Development	6	18

123

Figure 7 shows the four major categories of combustor configurations tested and the key design features of each. As shown in figure 8, the baseline configuration exceeded the emissions goals by a large margin. Significant improvements were obtained with modified geometry by increasing the pilot zone length in conjunction with cooling and dilution airflow modifications. Even further improvements in CO emissions were obtained by reducing the cup spacing in the pilot dome. This reduced cup spacing was obtained by relocating the pilot stage to the inner annulus. This configuration produced lower CO and HC emission levels than obtained on any of the previous configurations. These lower CO and HC emissions are believed to result from a reduction or elimination of the quenching regions between swirl cups. However, the very low CO and HC emission levels occurred at a fuel-air ratio below the QCSEE ground idle design fuel-air ratio. Therefore, to further reduce the CO emission levels at the QCSEE ground idle fuel-air ratio, an improved pilot stage swirl cup design with higher airflow capacity and improved atomization was developed as the final design.

Figure 9 shows the improved pilot swirl cup design and a similar design developed for the main stage. These design improvement features were incorporated with the previously developed design features to obtain the final configuration. Figure 10 shows the preferred sector combustor configuration and the key dimensions.

Table IV shows the emissions levels for the final double annular combustor configuration compared to those expected with the best single annular combustor. With this selected configuration, compliance with the program emissions goals, with a ground idle thrust of 4.5% takeoff thrust is projected.

The final configuration was also tested to investigate other important combustor performance characteristics. Figure 11 shows the altitude ignition results obtained with the final double annular combustor configuration.

These tests were conducted with the sector combustor subjected to combustor inlet conditions based on the altitude windmilling characteristics expected with QCSEE. The Jet A fuel temperatures were maintained at 244K to simulate in-flight conditions. As shown, excellent altitude relight results were obtained with successful ignition obtained in all regions tested within the flight envelope.

Although sector combustors are not generally conducive to accurate measurement of exhaust gas temperature pattern factors due to their limited circumferential size, data were acquired to examine trends. Because of the limited combustor airflow available for profile control and and the very short length of this combustor design, it is expected that additional tailoring of the combustor profile would be required before introduction into a production engine.

In conclusion, it was demonstrated in a prototype sector combustor test that a double annular dome combustor suitable for the QCSEE application can be developed which will satisfy the emissions goals of the Program at a ground idle thrust of 4.5%. Furthermore, the selected final configuration demonstrated excellent altitude relight performance for a combustor at this early stage of development. Other performance characteristics of this double annular design will require some further development before engine testing.

TABLE I. - QCSEE SINGLE ANNULAR COMBUSTOR

- **With 4% Ground Idle Thrust**
- **With Sectorized Burning at Idle**
- **High P/P QCSEE Cycle**
- **Jet A Fuel**

		Emissions Status	Goals
CO	**Pounds Per 1000 Pounds Thrust Per Hour Per Cycle**	7.2	4.3
HC		.6	.8
NOX		3.8	3.0

Conclusion:
Advanced Combustor Concept Required to Meet Emissions Goals

TABLE II. - EMISSIONS PROGRAM CYCLE SELECTION

	UTW Engine	OTW Engine	Emissions Program
Pressure Ratio	14	17	25
Pressure, N/cm² (psi)	143 (208)	172 (250)	245 (356)
Temperature, K(°R)	684 (1231)	726 (1307)	789 (1416)

126

TABLE III. − QCSEE COMBUSTOR DESIGN CHALLENGES

● **Meet 1979 CO/HC Emissions Standards with Low Ground Idle Combustor Inlet Operating Conditions**

	QCSEE	CF6-50
Combustor Inlet Temperature	415K (287 F)	429K (313 F)
Combustor Inlet Pressure	2.4 Atm. (36 psia)	2.9 Atm. (43 psia)
Engine Thrust at Idle (% Takeoff)	4.0	3.4

● **Meet Very Stringent NOX Emissions Goals**

TABLE IV. − EMISSION RESULTS FOR QCSEE DOUBLE ANNULAR
HIGH P/P QCSEE CYCLE

	Double Annular		Best Single Annular with Sector Burn at Idle		Goals	
	4.0%	4.5%	4.0%	4.5%		
CO	5.6	4.3	7.2	6.7	4.3	
HC	.32	.13	.57	.43	.8	lb/1000 lb Thrust Per Hour-Cycle
NOX	3.0*	3.0*	3.8	3.8	3.0	

* **Estimated Based on Sector Combustor Results at Simulated High Power Conditions**

127

QCSEE Single Annular Combustor
Low Emissions Design

21.1 cm
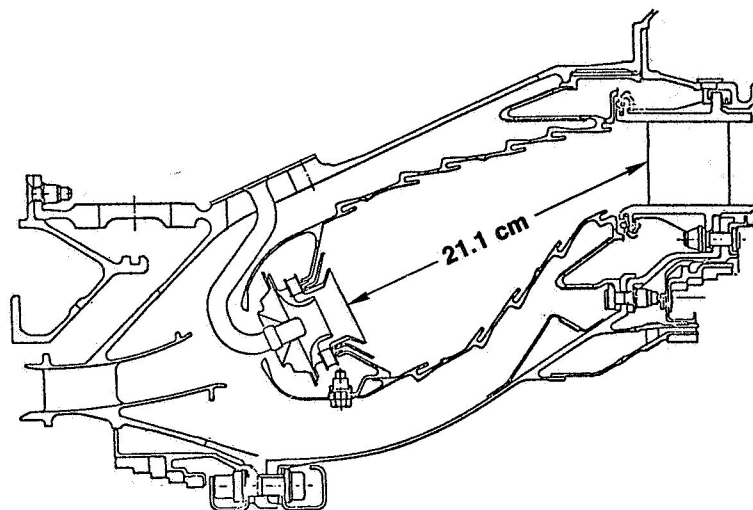
Figure 1

QCSEE Double-Annular Dome Combustor

Outer Liner
Dilution Holes

Outer Dome
Reverse Flow
Swirlers

Pilot
Stage

Main
Stage

Quick Quench
Inner Liner
Dilution Holes

Pressure Atomizing
Fuel Nozzles

Inner Dome
Reverse Flow
Swirlers
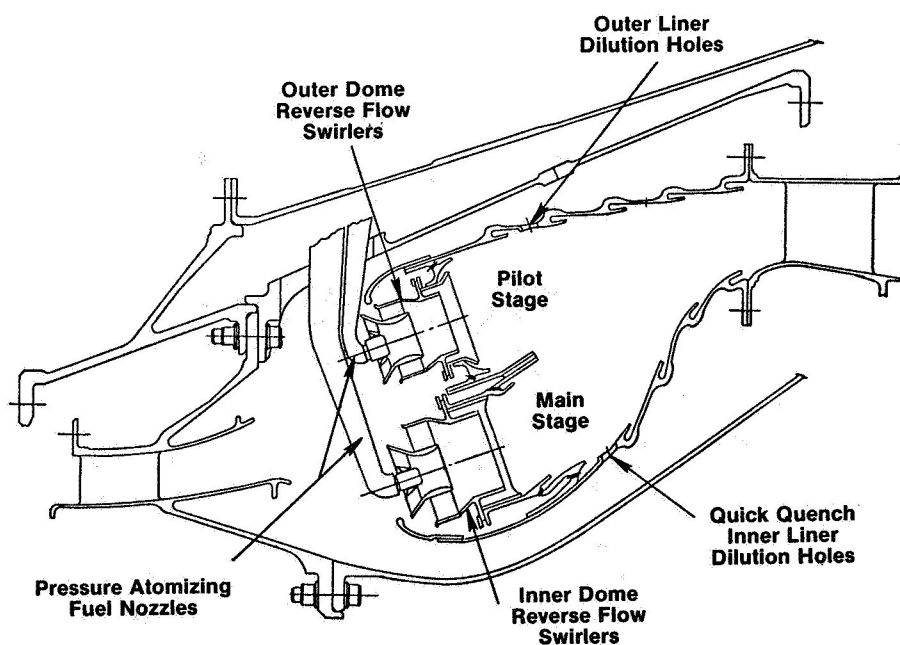
Figure 2

NASA QCSEE Double Annular Combustor

CF6-50

32.8 cm

17.7 cm

QCSEE
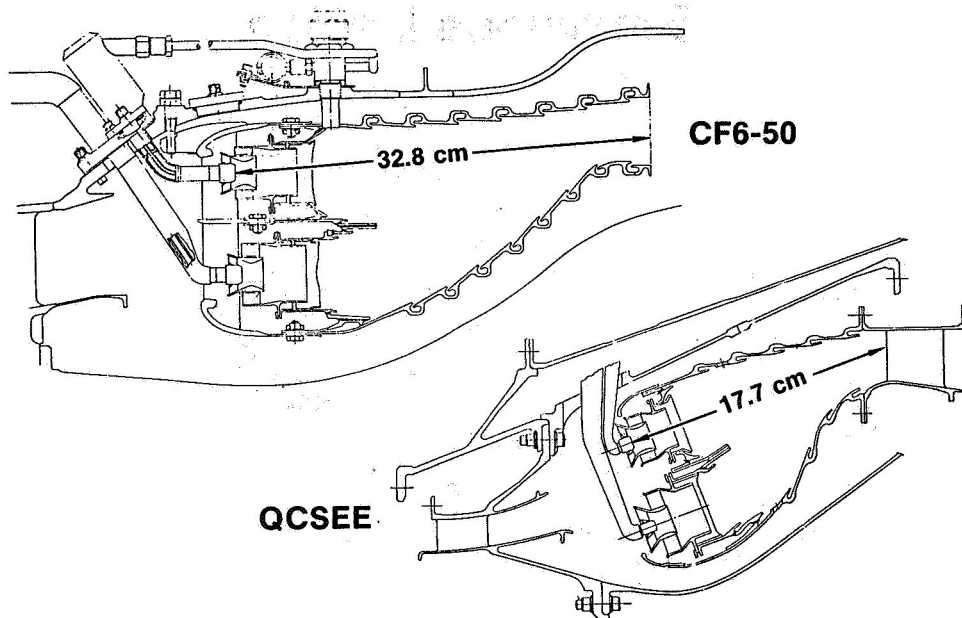
Figure 3

Double Annular Test Sector

Main

Pilot
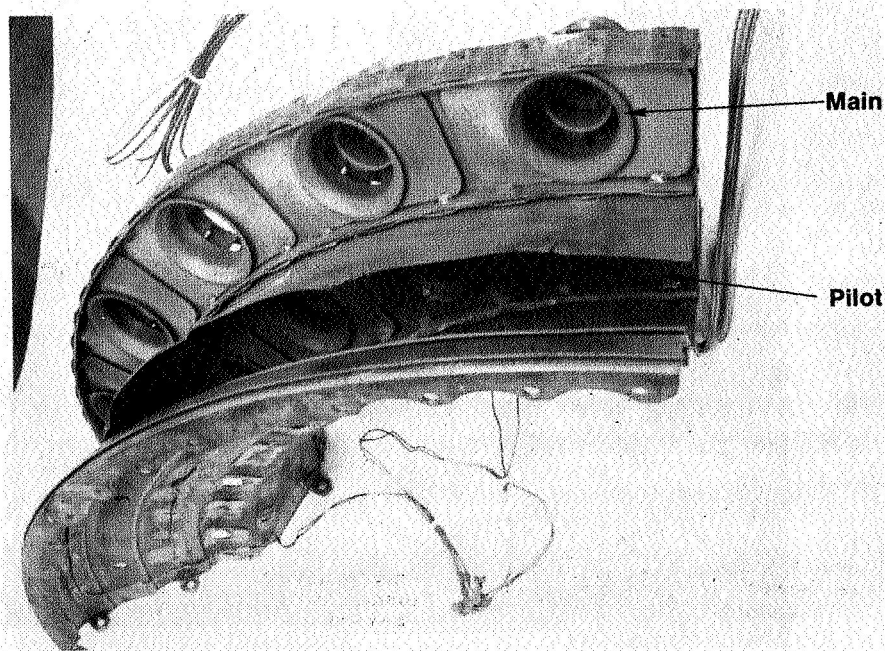
Figure 4

Double Annular Sector Prior to Assembly
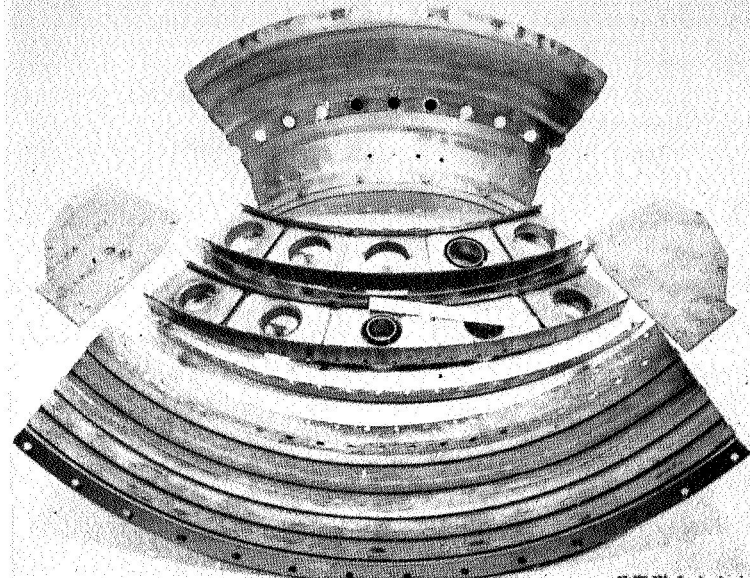
Figure 5

Double Annular Combustor Test Rig
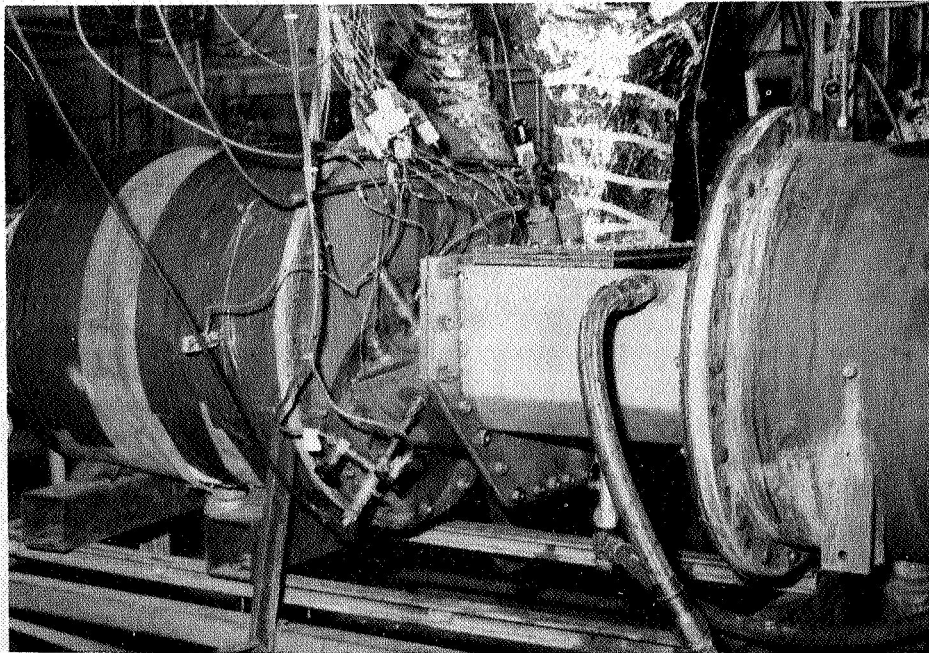
Figure 6

Key Development Test Results

Combustor Configurations

- **Baseline**

- **Modified Geometry**
  (Increased Combustion
  Zone Length)

PILOT

MAIN
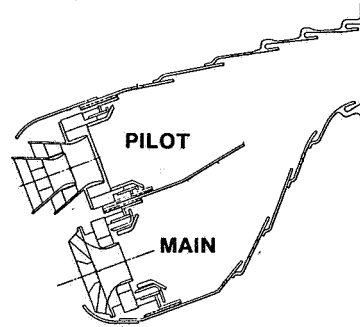
- **Inner Annular Pilot Dome**

- **Selected Final Design**
  (Radial Axial Air Blast Swirlers)

MAIN

PILOT
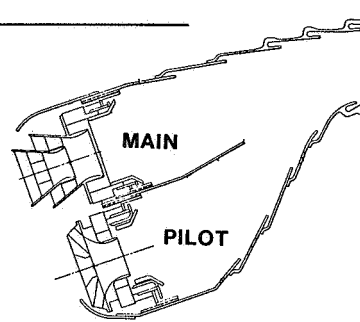
Figure 7

QCSEE Double Annular Combustor
Key Emissions Test Results

EIHC~gr/kg

HC

Baseline

- Jet A Fuel
- SLS Standard Day

Final Design

Goal

EICO~gr/kg

4.5% QCSEE Idle

CO

Baseline

Final Design

Goal

400   600   800

$T_3 \sim °K$

Figure 8

131
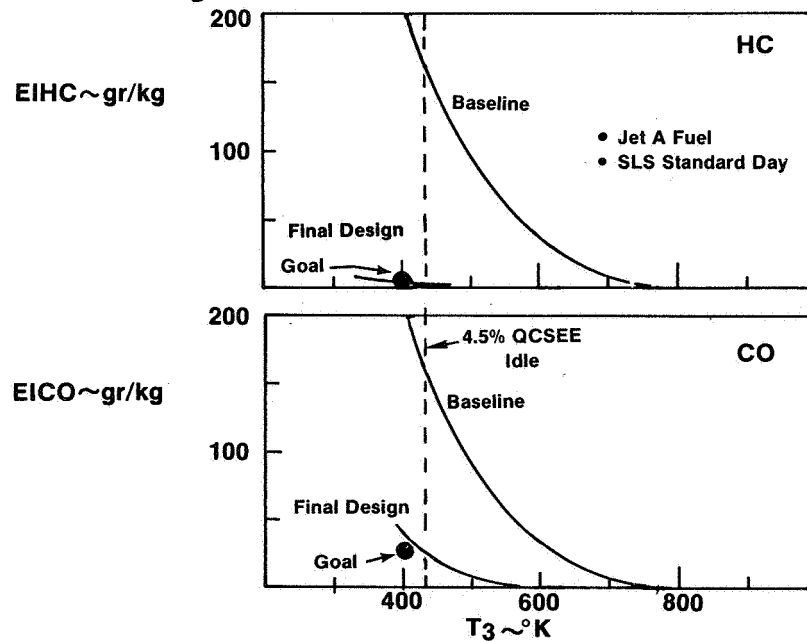
Final Design — Swirl Cups

Figure 9

Final Configuration

15.4 cm (6.07 in.)

6.35 (2.50)

MAIN

PILOT
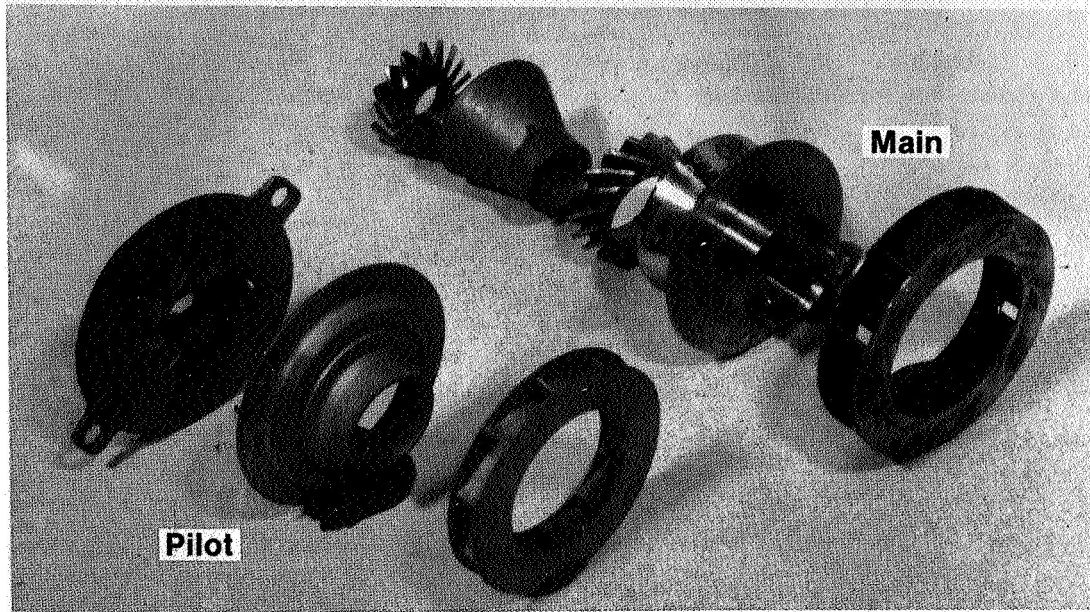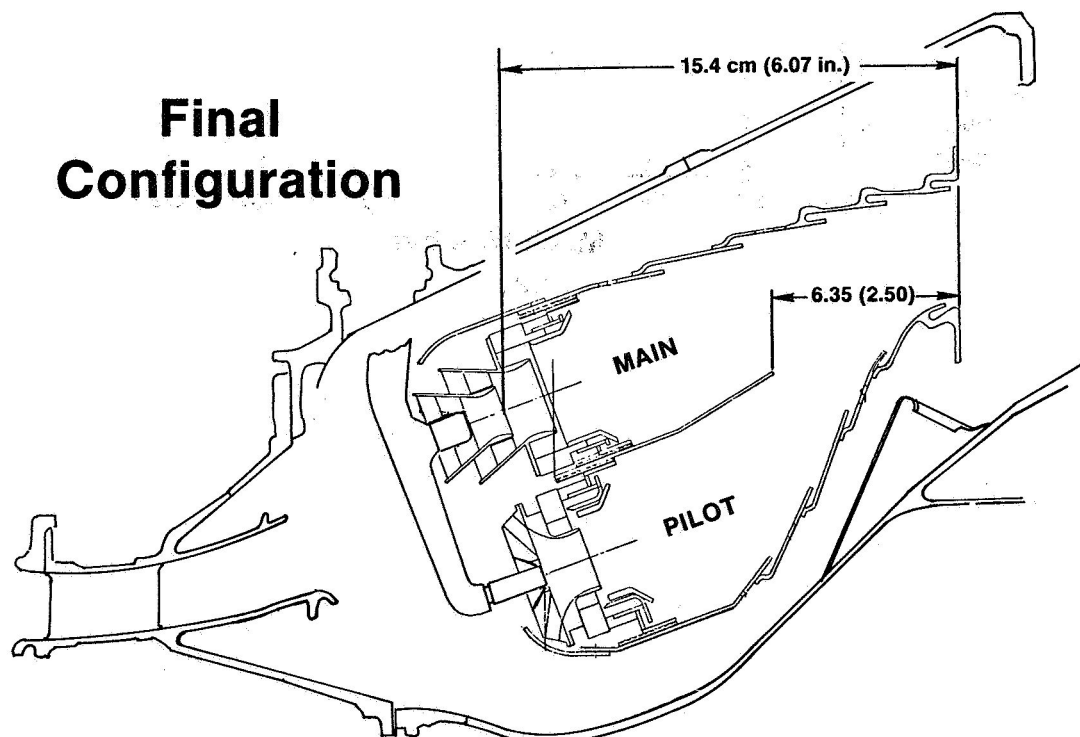
Figure 10

Altitude Ignition Results

- Cold Air
- Jet A Fuel (Cold)
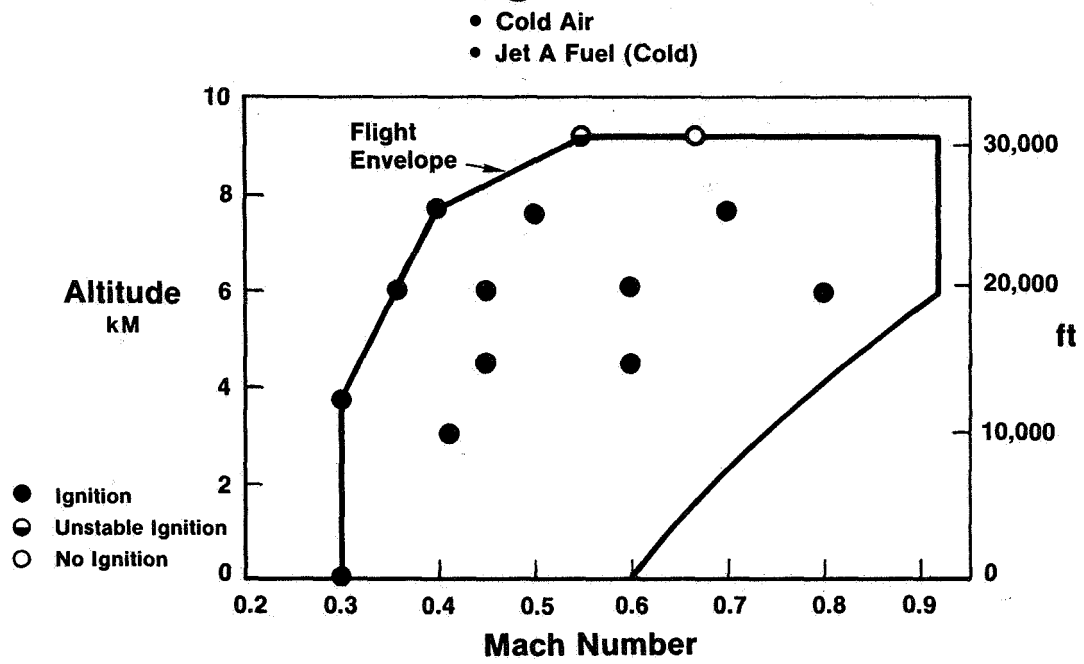
Figure 11

QCSEE CONTROL SYSTEM DESIGN AND ENGINE TEST RESULTS*

A.A. Saunders
General Electric Company
Cincinnati, Ohio

INTRODUCTION

A digital control was specified for the QCSEE propulsion system in anticipation that this technlogy would be required for an advanced short haul aircraft system. This anticipated need in conjunction with the general trend toward the use of digital computation in aircraft controls led to the requirement that the control be engine mounted for exposure to the vibratory and thermal environment.

This paper will present an overview of the propulsion control system requirements, the overall control system design, and the operational results achieved during the experimental engine test program. The Under-the-Wing (UTW) engine propulsion control will be presented first and the Over-the-Wing (OTW) engine propulsion control will be discussed next. As will be shown later, the propulsion system digital control performed satisfacorily throughout the engine test program. As a result of this development effort a digital control technology base has been established for the application of digital controls on many kinds of future aircraft propulsions systsems.

REQUIREMENTS

The control system design was based on a set of control system requirements which were developed from the needs of a short-haul aircraft system. The primary control system requirements are:

o   Set Percent Rated Thrust

o   Maintain Engine Safety Limits

o   Reduce Pilot Work Load

o   Control Inlet Mach Number

o   Provide Rapid Thrust Reponse

o   Facilitate Engine Condition Monitoring

o   Interface with Aircraft Digital Computer

---

*For Early Domestic Dissemination.

One of the primary functions of the propulsion control is to manipulate the engine variables to achieve the design thrust levels. The use of a digital control allowed the development of control system logic which related engine thrust to measurable engine parameters. These parameters were integrated and scheduled so that cockpit power level position (percent power setting) was directly related to percent of rated thrust. The thrust parameter selected for the UTW engine was propulsion system pressure ratio, compressor discharge static pressure divided by free stream total pressure (Ps3/PTO). The basic pressure ratio schedule was biased by engine inlet and aircraft operating conditions to achieve a relationship between rated thrust and cockpit power lever position over the flight envelope.

To achieve safe operation over the flight envelope the control system was designed to automatically maintain engine operation within normal physical limits. The control system incorporated logic to prevent engine overspeed or overtemperature. The specific mechanization of the limits will be discussed later.

Since operation of a short-haul aircraft into intercity airports could place heavy demands upon the pilot, it was required that system design should attempt to reduce pilot work load. To accommodate this objective the system was designed to automatically integrate the propulsion system variables, and engine safety limits.

One of the primary objectives of the QCSEE program was the development of noise reduction technology. Previous experiments had shown that operation with a high inlet throat Mach number would provide a substantial reduction in fan noise. To achieve this noise reduction benefit, it was necessary to provide automatic control of inlet throat Mach number at high power settings and demonstration of this capability was a UTW engine control requirement.

Studies by NASA prior to initiating the QCSEE program revealed that a short-haul aircraft would require rapid thrust response to achieve a safe go-around in the event of an an engine failure during landing approach. As a result of these studies, the propulsion system was required to provide rapid thrust response. The specific requirement was to achieve a thrust change from 62% to 95% in one second. This thrust response rate is approximately twice as fast as current engines.

Digital computers have the inherent capability to process, and transmit massive amounts of data rapidly. It was decided to utilize this capability and the QCSEE digital control was designed to collect and transmit 48 engine condition parameters. The parameters were such items as speeds, pressures, temperatures, and operating modes. The data was stored and displayed in the engine control room. With appropriate integration of the engine and aircraft digital controls a comprehensive condition monitoring system could be provided which would provide maintenance action information.

To be utilized effectively, a propulsion system digital control should have the capability to interface with an aircraft digital control system.

136

Through this interface, propulsion system commands from the aircraft and propulsion system operational data would be transmitted. Recognition of this need led to the requirement for a digital interface and transmission system between the experimental propulsion system and the engine control room.

Subsequent sections of this paper will provide detailed information on the manner by which requirements were implemented and demonstrated.

UTW SYSTEM DESCRIPTION

Figure 1 is a simplified schematic of the UTW propulsion control system. The UTW engine incorporated four manipulated variables: fan nozzle area, fan pitch angle, engine fuel flow, and core stator angle. The system to control these variables can be divided into three functional groups. These are: the system sensors, represented by the engine sensors and digital commands from the control room; the computer represented by the digital control and the system power represented by the system actuators. The digital control is the heart of the system; hence, it incorporates all of the control laws and logic to regulate the variables from engine idle to take-off thrust. The other major components in the system are: fuel pump, hydromechanical control and hydraulic pump.

In this control system, the fan nozzle and fan pitch actuators were manipulated solely by the digital control. Fuel flow was varied as programmed by the digital control, however, the hydromechanical control had the authority to override the digital control, and it also scheduled the core stator angle position. This mechanical override capability was incorporated for several reasons: development program cost, digital control memory size, and experimental engine safety. A secondary electromechanical power demand link which actuates the fuel stopcock and sets a core speed limit was also implemented for experimental engine safety.

The command and data link was a serial, time-multiplexed data transmission system consisting of digital serializers, optical isolaters, line drivers and line receivers. Data was transmitted and received at a one-megahertz rate. The command and data transmission process was regulated by the engine mounted digital control.

An engine-driven, accessory gearbox mounted, F101 engine fuel pump was utilized for fuel system pressurization and fuel delivery. The pump incorporates a fixed displacement vane element and a centrifugal boost element to charge the intake of the vane element. Rated pump speed is 6690 rpm; at this speed it has a capacity of 2.7×10^{-3} m³/sec. (42.8 gpm) with a pressure rise of 6.93×10^6 N/m² (1000 psi). The pump was designed and manufactured by Sperry-Vickers.

A modified F101 engine fuel control was used for fuel metering. This control uses a constant metering head and incorporates a servo operated

bypass valve to accommodate excess pump flow. The control incorporates hydromechanical devices for speed governing and for fuel and core stator scheduling, and provides a fuel system interface with the digital control. The control was designed and constructed by Woodward Governor Company.

The UTW engine incorporated an engine-driven, piston-type, pressure compensated hydraulic pump as a power supply for variable nozzle and variable fan pitch actuation. The pump supplies a constant pressure, variable-flow to the system servo valves, which are regulated by the digital control. The pump capability at 100% speed is 3.08×10^{-3} m^3/sec. (48.8 gpm) with a pressure rise of 2.36×10^7 N/m^2 (3350 psi). This relatively large flow capacity was required to provide rapid variable pitch actuation at low engine speeds. The pump was designed and manufactured by Abex Corporation.

Figure 2 shows a photograph of the engine mounted digital control. The package shown in the figure incorporates pressure transducers for sensing the pressures used in engine control, a separately powered analog control for limiting fan overspeed, and the digital control. The unit is powered by a variable-frequency, variable voltage engine driven alternator. Power dissipation is on the order of a 100 watts and is handled by air cooling. The cooling air source is free stream total pressure and the pressure sink is the fan inlet.

The digital control integrates electrical piece parts which consist of the following sub-assemblies: sensor excitation and signal conditioners, data acquisition, digital to analog converters, output signal conditioners, power supply regulators, and a special purpose digital computer. The digital computer is composed of five major sections: program memory, read/write memory, clock, central processor, and input/output unit. The computer has the capability to add, subtract, multiply, and divide and to branch upon command. The machine data word is twelve bits in length. The computer instruction set consists of 31 different instructions.

The program memory incorporates instructions which define the control laws and logic. The QCSEE-UTW control memory incorporated 3071 instructions to define the complete control strategy. Each instruction in the program memory is sequentially transmitted to the central processor for execution. The timing for instruction execution is controlled by the central processor. Execution time for the QCSEE UTW program was 7.46 milliseconds. Hence, the program was repeated 134 times per second.

The electrical components in the digital control consisted of a cominbination of discrete and medium scale integrated components. A type of logic called the low power Schottky TTL was selected for digital components. These devices were selected because they offered the best speed-power product. The digital control was designed and fabricated by the General Electric Company.

Figure 3 is a schematic of the UTW engine showing the control system sensors. All of these measured parameters, except core stator angle and

core inlet temperature, were collected by the digital control and used in the propulsion control logic. In addition, they were subsequently transmitted to the control room for display.

Fan inlet total temperatures and free stream total pressures were measured to evaluate flight conditions and were used for power control scheduling.

Inlet static pressure, along with free stream total pressure, were combined and used as a representation of inlet Mach number. The static pressure was measured at the 40% axial station in the inlet duct. This was done to eliminate pressure variations due to crosswinds. An empirical equation was used to convert the measured pressure ratio to average inlet throat Mach number.

Free stream total pressure was also used along with measured compressor discharge pressure to establish propulsion system pressure ratio, which is related to system thrust.

Fan pitch angle, fan nozzle area and core stator angle were meausred to allow for a loop closure in the control logic.

Fuel flow, compressor discharge temperature and pressure were measured for use in the computation of turbine inlet temperature.

Core inlet temperature, core speed and low pressure turbine speed were measured for use in physical speed limit, corrected speed limits, acceleration schedules and core stator schedule computations.

All of the sensors used in the system were current state-of-the-art type devices.

UTW OPERATING CHARACTERISTICS

One fundamental task performed in designing an automatic control system was to define the system control mode. This control mode definition process relates the engine cycle variables (speeds, pressures, temperatures, etc.) to the available manipulated variables (fuel flow, fan pitch, nozzle area) to achieve control of the vehicle and to obtain the desired operating characteristics. The objective of the analysis is to choose practical combinations of cycle parameters and manipulated variable which result in small variations in the engine cycle dependent variables (i.e., thrust, SFC, stall margin) at important operating conditions. The analysis process involves the comparison of potential control modes on the basis of accuracy, schedulability, stability, response and other performance considerations.

The QCSEE UTW engine incorporated three prime manipulated variables: fuel flow, fan pitch and fan nozzle area. During the mode selection

139

process these variables were paired with many combinations of engine cycle variables. The analysis resulted in selection of engine pressure ratio (Ps3/PTO), fan speed and inlet Mach number as controlled variables. These variables were paired with fuel flow, fan pitch and fan nozzle area.

As a result of this pairing of variables, selection of a percent power setting through movement of the power lever causes the following: engine fuel flow is varied to hold a schedule engine pressure ratio, fan pitch is varied to hold a scheduled fan speed and fan nozzle area is varied to hold a scheduled inlet Mach number. The above actions are implemented through the digital control. This variation of the manipulated variables is limited by both physical limits and cycle considerations. For example, maximum fan nozzle area was limited to 187 m^2 (2900 in.^{2}) because at this point the fan nozzle exit area became larger than the fan duct area, and nozzle variations no longer affected inlet Mach number. Fan pitch was limited to 10° closed from nominal due to actuator mechanical limits.

Figure 4 shows the relationship between fan nozzle area, inlet Mach number, and percent power demand at sea level conditions. Over the complete power setting range the digital control tries to position the fan nozzle to maintain an inlet Mach number of 0.79. However, in the lower percent power setting region (<70%) the nozzle is scheduled to the maximum area and inlet Mach number varies as a function of power setting. As the power demand is increased beyond approximately 70% the fan nozzle area begins to close to maintain a constant inlet Mach number.

Figure 5 shows the relationship between fan blade pitch angle, corrected speed and percent power setting at sea level standard conditions. In the lower power setting region fan speed varies with percent power setting because the fan pitch is closed to its minimum position. As the percent power setting is increased beyond approximately 55% the fan pitch begins to open toward the take-off position to hold fan speed constant at approximately 95%, which is the scheduled fan speed for take-off power. The fan speed is held constant at the higher power settings for transient response reasons which will be discussed later.

<center>UTW AUTOMATIC SAFETY LIMITS</center>

As noted earlier one of the primary control system functions is to prevent the engine from exceeding speed or temperature limits. To meet this requirement, limiting functions were incorporated in the hydromechanical and digital controls. The hydromechanical control incorporated a full range fly-ball governor on core speed, which would override the digital control input and reduce fuel flow if core speed attempted to exceed the scheduled value. The digital control memory incorporated fan speed and core speed limits which would cutback fuel flow if the speed limit was reached. The digital control unit also incorporated a separate analog control to cutoff fuel flow on the experimental engine if overspeed occurred in the low pressure turbine due to loss of load. Loss of load

could occur with a reduction gear failure or an extreme closure of the fan pitch at high power.

Turbine temperature was limited by a digital control function. The control memory incorporated an equation which calculated turbine inlet temperatures as a function of fuel flow, compressor discharge pressure and temperature. The control compared the calculated turbine inlet temperature with a limit and acted to cut back fuel flow to prevent operation beyond this limit. The digital control received fan case vibration signals from test facility instruments. The control program memory incorporated logic to automatically retard the experimental engine to idle power if vibration signals exceeded a safe level.

UTW TRANSIENT RESPONSE

As noted earlier the QCSEE engines were required to have rapid thrust response capability. The specific requirement was to achieve a thrust change from 62 to 95% thrust in one second. Figure 6 shows the results of a study using a transient model of the UTW engine. The QCSEE requirement is noted on the figure. The dashed line shows the response of a conventional turbofan in which fan speed and core speed are both varied with fuel flow. With a conventional system the required response could not be achieved due to compressor stall and turbine inlet temperature considerations.

The solid line on Figure 6 shows the predicted thrust repsonse with fan speed held constant through variation in the fan pitch angle. Holding fan speed constant results in the achievement of the required response since acceleration of the fan rotor is not required and changes in fan pitch angle results in rapid changes in fan air flow.

UTW CONTROL SYSTEM ENGINE TEST RESULTS

Several control system experiments were conducted during the overall engine test program. As noted earlier, the system is designed to hold the inlet throat Mach number constant at high power settings through variation of the fan nozzle area. Figure 7 shows the results of an inlet Mach number control experiment. This figure shows the results of a slow power increase. The control system inlet Mach number references has been set at a 0.75 level. As the power setting is increased, the fan nozzle automatically closes to maintain the inlet Mach Number essentially constant at the 0.75 level.

Figure 8 shows the results of a fan speed control experiment. As noted earlier, the digital control will automatically vary fan pitch angle to hold a constant fan speed. In this experiment the fan speed reference is set at a 2985 rpm level. As the power setting is increased

to demand a higher thrust level the fan pitch automatically opens to hold the fan speed essentially constant. Actual fan speed variation is approximately plus or minus one-half of one percent during the power advance. The fan pitch changes from approximately 2 degrees closed to 3 degrees open during the power change. The non-linearity in pitch angle change between 85 and 90 percent power demand is associated with an inter-action between the fan pitch and fan nozzle control systems. Between 85 and 90% power demand the fan nozzle has opened to the maximum open area and a relatively large pitch angle change is required to maintain fan speed. Above the 90 percent power setting the nozzle has closed and smaller changes in pitch angle are required to maintain control of fan speed.

Figure 9 shows the results of another experiment on inlet Mach number control. In this experiment, the engine power demand was held constant and the desired inlet Mach number reference was varied. As the inlet Mach number reference in the digital control was changed through an on-line adjustment the fan nozzle opened to hold the requested inlet Mach number level.

Recorded data was examined to determine the steady state stability of the control system when it was operated with the closed loop controls noted above. Throughout all of the closed loop operation, the steady state stability of the controlled variables (pressure ratio, inlet Mach number, fan speed) was excellent. Table I shows typical steady state stability results.

An important element in the engine control system is sensor accuracy. To evaluate this element, data measured by the engine control system sensors was compared to data measured with the experimental engine instrumentation. Table II shows the results of a comparison of digital control sensors and engine instrumentation.

UTW CONTROL SYSTEM SUMMARY

A multi-variable digital control system was designed and engine tested in QCSEE-UTW engine program. During the engine test program, accurate and stable control was achieved in all modes of operation. Closed loop control was demonstrated on an engine pressure ratio/fuel flow loop, inlet Mach number/fan nozzle area loop, and a fan speed/fan pitch loop. The digital communication link between the engine control and the engine control room was demonstrated and accurate steady state sensor performance was obtained.

DESIGN REQUIREMENTS - OTW

The control system requirments for the OTW engine were essentially the same as the UTW engine. However, the inlet Mach number control requirement

was eliminated, since the exhaust nozzle was manually varied and two new requirements were added. These new requirements were:

o   Failure indication and corrective action

o   Full authority digital control

The first of these requirements is associated with a concept which allows continued operation with failure of an engine control system sensor. The second requirement was added to allow further development of engine digital control system technology. The manner in which these requirements were implemented and demonstrated will be discussed in subsequent sections.

OTW CONTROL SYSTEM DESCRIPTION

Figure 10 is a simplified schematic of the OTW propulsion control system. The experimental engine incorporated two manipulated variables: engine fuel flow and core compressor stator angle. The system to control these variables can be divided into three functional groups. These are the system sensors, the digital control and the system actuators. The digital control is the heart of the system, it incorporates all of the control laws and logic to regulate the variables from engine start to maximum thrust. The digital control is identical to the UTW control except the control program memory has been revised to incorporate the OTW engine characteristics. The other major components in the system are the fuel pump, hydromechanical control and core stator actuators. These components are the same as on the UTW engine except for functional changes in the hydromechanical control. On the OTW engine, the hydromechanical functions associated with acceleration fuel and core stator scheduling were eliminated. These important functions were incorporated into the full authority digital control program memory.

OTW CONTROL SYSTEM SENSORS

Figure 11 is a schematic of the OTW engine and shows the control system sensors. The schematic is similar to the UTW system except for the following: the fan pitch and fan nozzle sensors have been eliminated, the core stator angle is sensed with an electrical transducer, and the core inlet temperature is calculated from fan inlet temperatures, fan speed and a fan efficiency function. This calculated value of core inlet temperature is used in a subsequent calculation by the digital control to establish corrected core speed.

143

OTW OPERATING CHARACTERISTICS

A control system analysis similar to the UTW engine effort was performed to select the controlled and manipulated variable pairs. Since the OTW experimental engine incorporated only one primary manipulated variable (fuel flow), the analysis process was less complicated. The analysis resulted in the pairing of corrected fan speed with engine fuel flow. Corrected fan speed was chosen because of its close correlation with turbofan thrust. Furthermore, the analysis resulted in the decision to schedule the core compressor stators with corrected core speed because this relationship provides good control of compressor stall margin. As a result of the above selection, movement of the percent power demand selector causes the digital control: to vary fuel flow to hold a scheduled corrected fan speed, and to schedule the core stator angle as a function of corrected core speed.

The digital control also incorporates the engine acceleration fuel schedule. This acceleration fuel limit is composed of two primary schedules The first schedule protects against compressor stall and the second protects against turbine overtemperature. Both functions are scheduled as a function of corrected core speed. The digital control memory incorporates logic to select the lower of the acceleration fuel limits which are computed from the two functions. Figure 12 depicts the OTW engine acceleration fuel schedule. The corrected core speed function is calculated from measured core speed, fan speed and fan inlet temperature. The corrected acceleration fuel limit is a function of fuel flow, compressor discharge pressure, fan speed and fan inlet temperature. The digital control logic compares the scheduled acceleration fuel limit with the real time calculated level of the acceleration fuel function and multiples the difference by compressor discharge pressure to establish the actual engine fuel flow limit.This calculation process is repeated approximately 80 times per second.

The OTW control system also incoporated engine limits for engine protection.

OTW TRANSIENT THRUST RESPONSE

As noted earlier the QCSEE engine was required to have rapid thrust response capability. The UTW and OTW requirements were the same. Figure 13 shows the results of a thrust response study using a transient model of the OTW engine. The thrust response requirement is noted on the figure. The dashed line on the figure shows the predicted response of a conventional turbofan in which fan speed and core speed are both varied with changes in engine fuel flow. With a conventional system, the required response could not be achieved due to the acceleration fuel schedule which is designed to prevent compressor stall and turbine overtemperature.

Since the required response could not be achieved using conventional methods a study was conducted to determine if the thrust response time could be improved by more effective use of the core stators. It was determined

that by setting the stators closed from the nominal schedule, the thrust response rate could be increased. When the core stators are, closed, the core speed increases to maintain sufficient power to hold the fan speed and maintain the thrust setting. Therefore, with closed core stators the core engine was not required to accelerate to achieve thrust response. The core stator closure was implemented by biasing the base stator schedule with the power demand signal, and by an operating mode signal. With a step increase in the power demand signal, the core stators would open rapidly to provide the power for fan acceleration to take-off speed. The solid line on Figure 13 shows the predicted thrust response of the OTW engine with the core stator reset function.

FAILURE INDICATION AND CORRECTIVE ACTION

One propulsion control technology objective in the QCSEE program was to reduce the impact of control system sensor failures. This concept was implemented by using the inherent capability of a digital computer to rapidly compare and act on a large amount of data.

The OTW digital control memory incorporated a non-linear model of the OTW engine cycle. This model was combined with a logic update scheme to form an extended Kalman filter which provided a calculated estimate of the engine sensor outputs. These calculated sensor values were compared with the measured sensor values. If the difference was small the engine model was updated to calculate new estimated sensor outputs. If an engine sensor fails, excessive error is detected and the engine sensor is automatically disconnected, and the engine continues to operate using the calculated value of the sensed output. The calculated value of a given sensor is based on the fact that sensed variables are interrelated through the engine model. Figure 14 is a schematic of the sensor failure indication and corrective action (FICA) concept. Figure 15 shows the results of dynamic simulator study on the OTW engine with the FICA concept incorporated. The data on the far left shows normal system operation with all sensors operating during a power chop and a power burst. The center set of data shows engine operation with a compressor discharge sensor failure. The data on the right shows operation with a fan speed sensor failure. Even with the failed sensors the dynamic simulation indicates that the engine should perform satisfactorily.

OTW CONTROL SYSTEM ENGINE TEST RESULTS

As noted earlier, the OTW digital control varied engine fuel flow to hold a scheduled corrected fan speed. Figure 16 shows typical engine test data. As noted on the figure scheduled and measured speed are nearly identical. Examination of recorded data also revealed excellent steady state fan speed stability.

145

A second primary function of the digital control was to schedule the compressor variable stators. Figure 17 shows the steady state schedule and typical data recorded during the engine test program. It should be noted that the corrected core speed is based on a calculated compressor inlet temperature.

One task of the propulsion control system is to prevent the engine from exceeding physical operating limits. One engine limit incorporated in the digital control memory was turbine inlet temperature. Turbine inlet temperature was calculated from fuel flow, compressor discharge pressure and compressor discharge temperature. The calculated value of turbine inlet temperature was compared to the limit and fuel flow was adjusted to prevent overtemperature. The OTW and UTW control incorporated this function. Figure 18 compares on-line turbine inlet temperature calculations by the digital control with post-test calculated values of turbine inlet temperature. The post-test data was calculated from cycle balance, using measured steady state engine data; whereas, the digital control data was continuously calculated from an emperical equation in the digital control program memory. At the higher temperature levels, where protection is required, the digital control data agrees with the post-test data within approximately one and one-half percent. Examination of recorded data showed that most of this error was associated with an error in fuel flow measurement. With further development of the fuel flow sensor an on-line, accurate calculated turbine inlet temperature could be implemented in a flight application.

During the engine test program the engine was operated on the calculated turbine temperature limit. The limit level could be varied through an on-line adjustment. Engine operation on the limit was stable.

During the engine start cycle, the control system schedules engine acceleration fuel flow to prevent compressor stall. As noted earlier the digital control incorporated the acceleration schedule in a series of poly-nominal equations. Figure 19 shows a typical start on the OTW engine with the full authority digital control. In this figure the engine is being motored at core speed of 4000 rpm at zero time on the air starter. At a time equal to approximately one second, the combustor ignitor is energized and the fuel stop cock is opened. An engine light is achieved at a time equal to approximately 2 seconds as indicated by the rise in turbine discharge temperature. Over the next 25 seconds the engine accelerates to idle speed. Through this period the digital control is calculating and implementing the acceleration fuel flow limit.

As noted earlier, the QCSEE engines were required to have rapid thrust response capability. Figure 20 shows the thrust response requirement and the results of one transient response experiment. The test results were obtained with a 25 degree core stator reset. As indicated on the figure the experimental engine met the thrust response requirement.

146

OTW CONTROL SYSTEM SUMMARY

A full authority engine mounted digital control was designed and tested on the QCSEE OTW engine. During the engine test program, the digital control functioned to provide reliable engine starting, it scheduled fan speed and core stator angle accurately, system stability was excellent from idle to full power, the calculated turbine inlet temperature concept was evaluated and the control system manipulated the engine variables to demonstrate the transient response requirement.

SUMMARY AND CONCLUSIONS

During the NASA/GE QCSEE program two engine mounted digital controls were designed, fabricated and tested on the two experimental engines. Throughout the engine test program of approximately 200 hours of operation, the digital controls scheduled the engine variables and maintained engine operation within all safety limits. Several experiments were performed during the engine test program to evaluate the control system capability with respect to control system requirements. Nearly all requirements were met satisfactorily. Table III compares primary control system requirements with engine test results. As a result of this successful development program, the digital control technology base has been expanded and will hasten the application of digital controls on future propulsion systems.

TABLE I. - STEADY STATE SYSTEM STABILITY

	Variation
• **Pressure Ratio**	$< \pm .05$
• **Mach Number**	$\pm .005$
• **Fan Speed**	± 20 **RPM**

TABLE II. - SENSOR ACCURACY
Engine Test Results

	% Variation
Fan Inlet Temperature	± 0.2
Compressor Discharge Temp.	-1.0
Compressor Discharge Pressure	$+0.4$
Fuel Flow	$+1.7$
Inlet Static Pressure	$+1.0$

TABLE III. - SUMMARY AND CONCLUSIONS

Requirements	Results	
	UTW	OTW
● Set Percent Rated Thrust	✔	✔
● Maintain Engine Safety Limits	✔	✔
● Reduce Pilot Workload	✔	✔
● Control Inlet Mach Number	✔	N/A
● Rapid Thrust Response	Partial	✔
● Failure Detection and Corrective Action	N/A	Partial
● Engine Condition Monitoring	✔	✔
● Interface with Aircraft Digital Computer	✔	✔

UTW — Control System Schematic

Figure 1

149
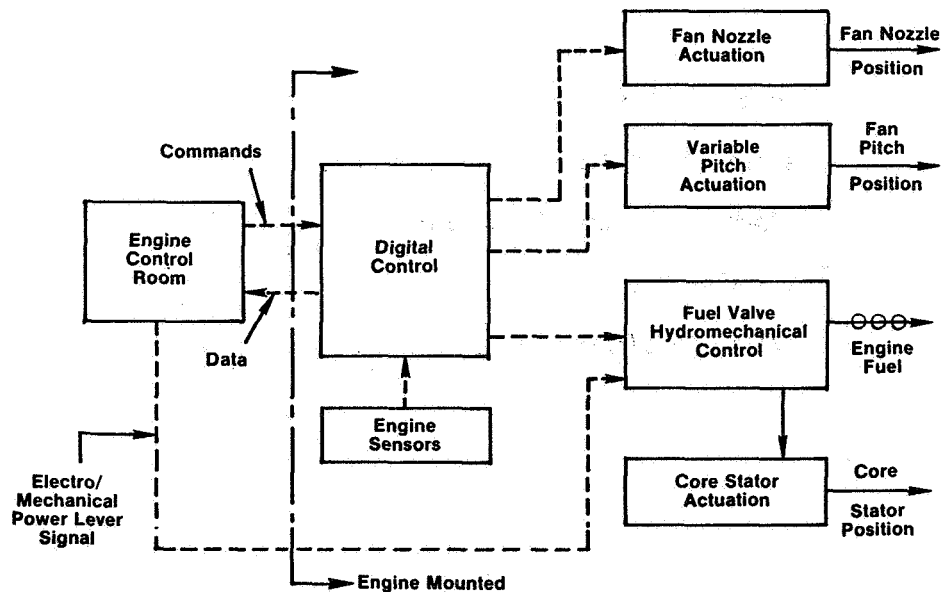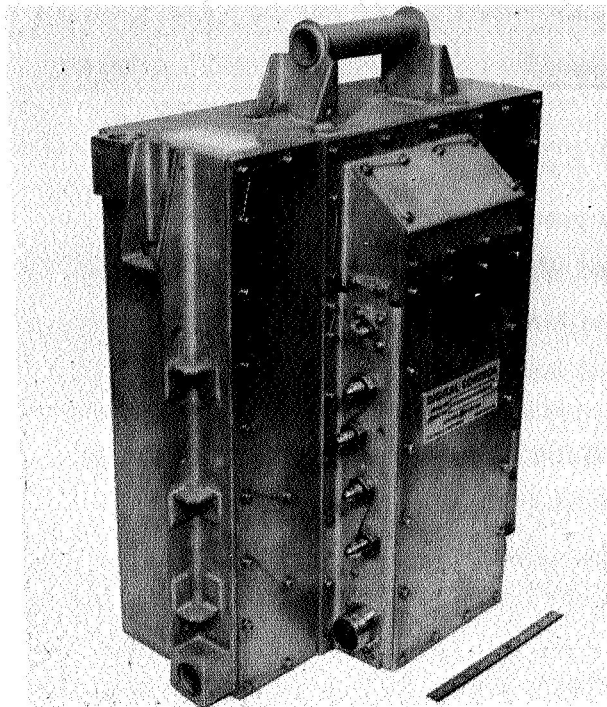
Figure 2

UTW — Control System Sensors

Fan Inlet Total Temperature

Free Stream Total Pressure

Compressor Discharge Total Temp. + Static Pressure

Fan Nozzle Area

Fan Pitch Angle

Core Inlet Total Temp.

Core Speed

Low Pressure Turbine Speed

Inlet Static Pressure

Core Stator Angle

Fuel Flow

Figure 3

UTW — Fan Nozzle Control Characteristics
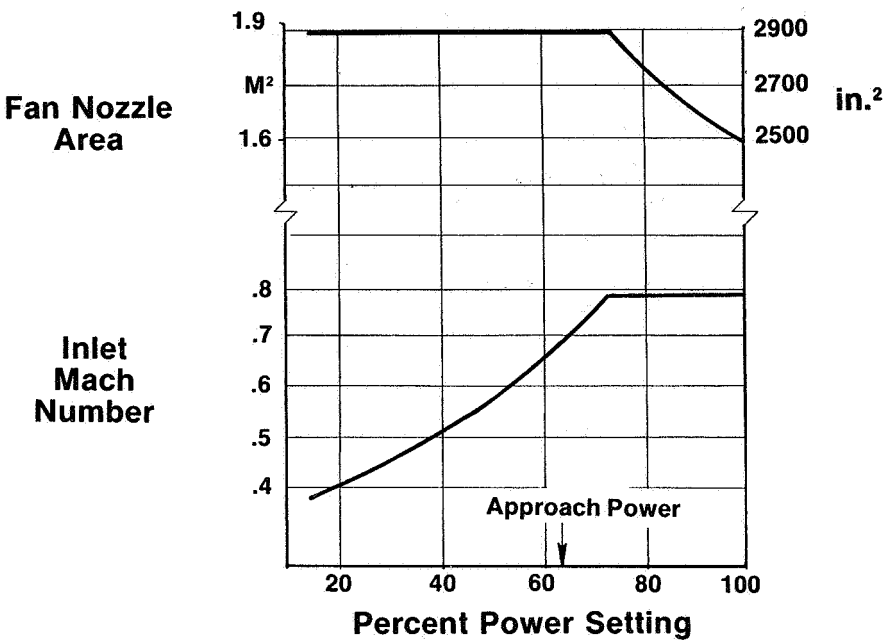
Figure 4

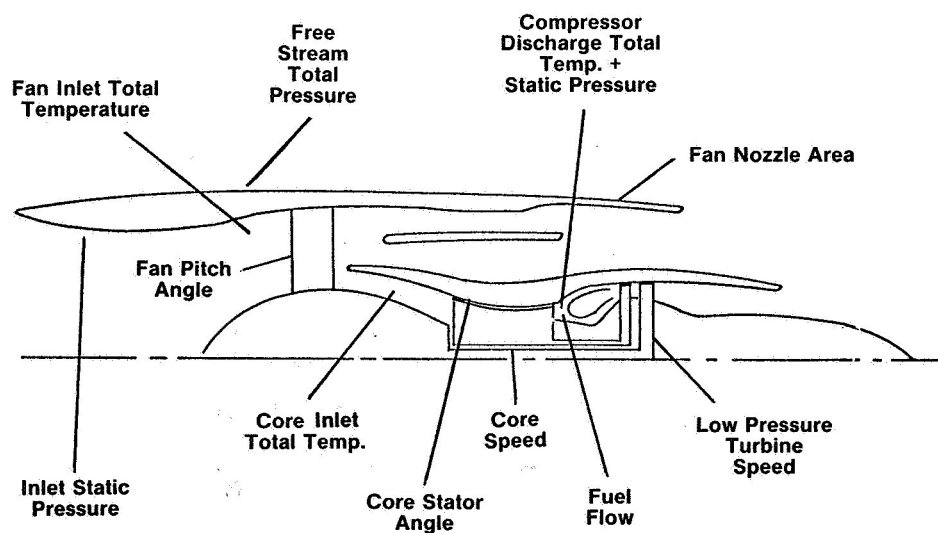# UTW — Fan Pitch Control Characteristic

Figure 5

151

UTW Engine
Predicted Transient Response

Time to 95%
Net Thrust,
Seconds

Conventional
Constant Fan Pitch
Configuration

Requirement

Constant Fan Speed Mode
(Selected)

Initial Net Thrust — %
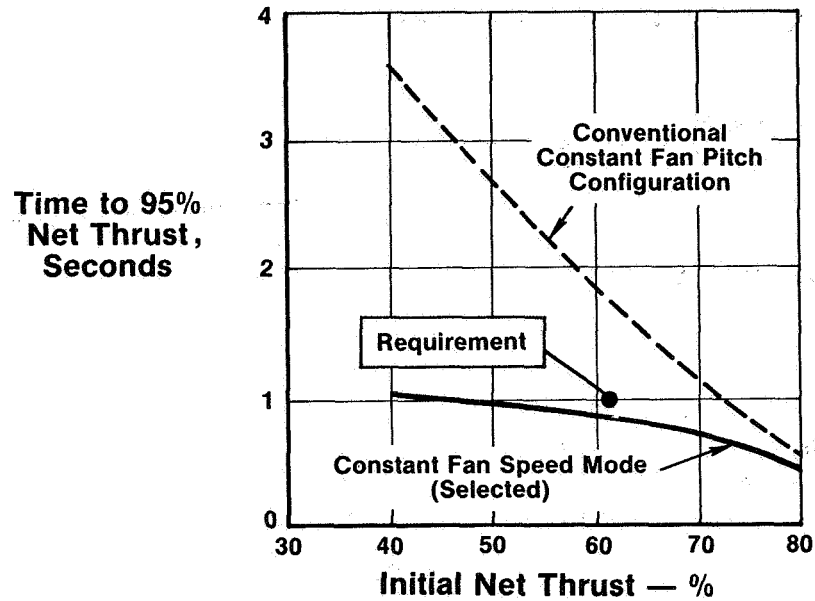
Figure 6

UTW Engine Test Results
Inlet Mach Number Control

Fan Nozzle
Area
m²

in.²

Inlet Mach
Number

Percent Power Setting

Figure 7

152
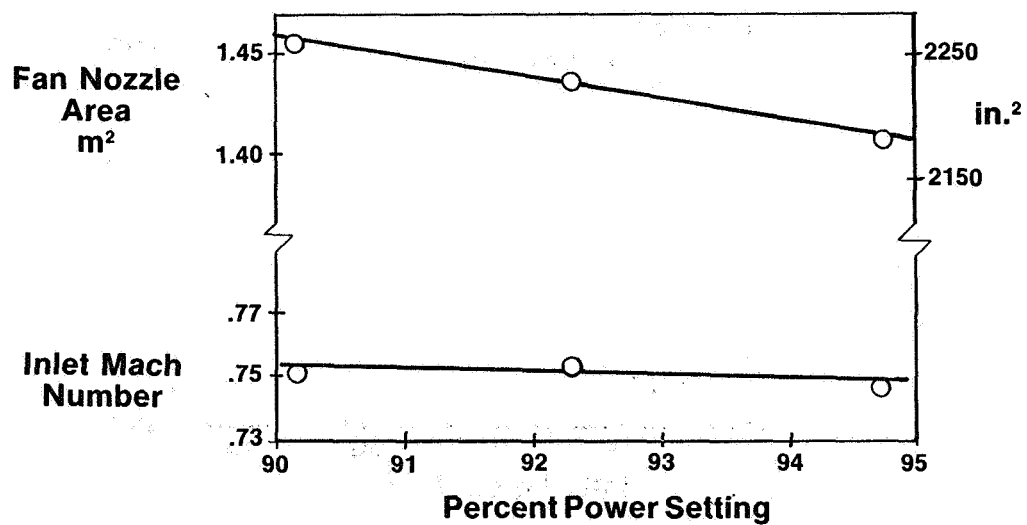
UTW Engine Test Results
Fan Speed Control
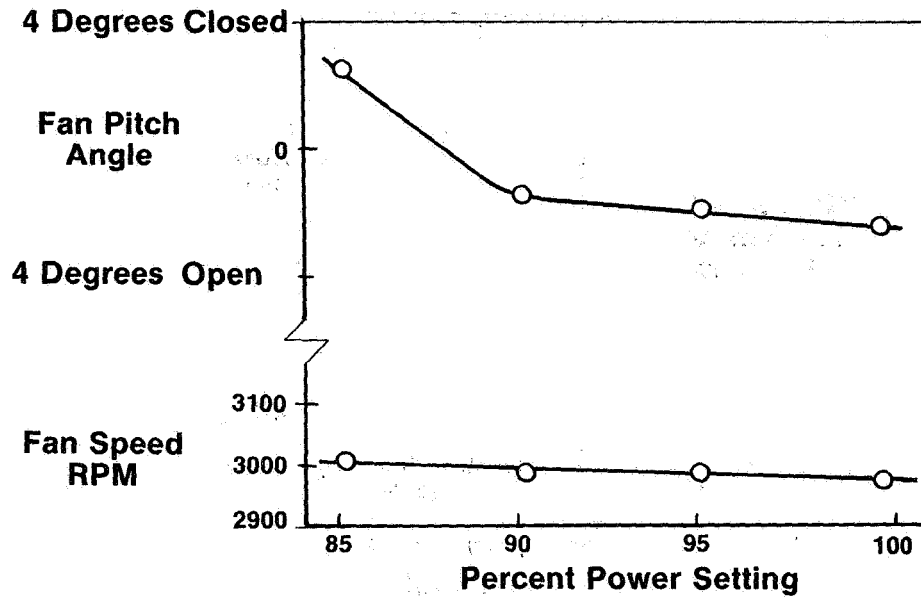
Figure 8

UTW Engine Test Results
Fan Exhaust Nozzle Tracking

Conditions:
Power Demand = 95%
Engine Pressure Ratio = 14.12

Figure 9

153
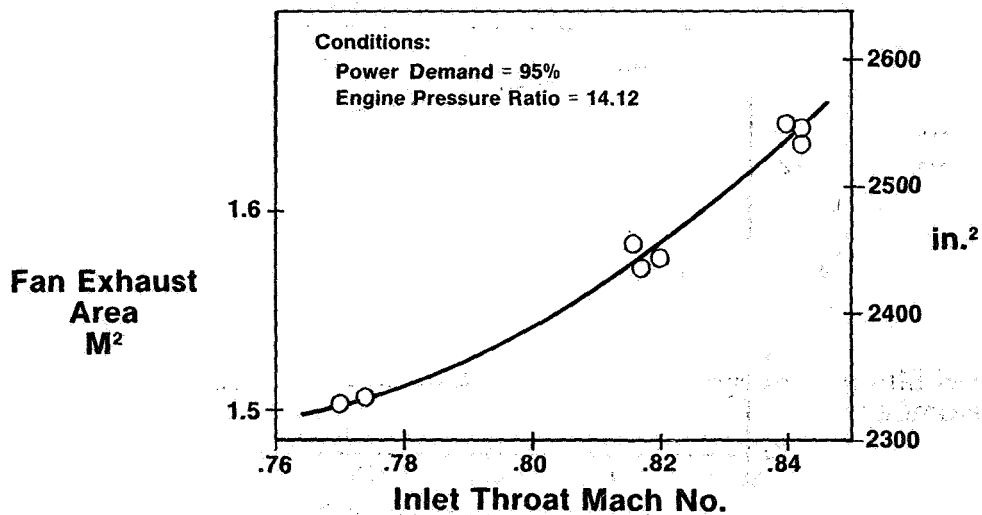
OTW — Control System Schematic
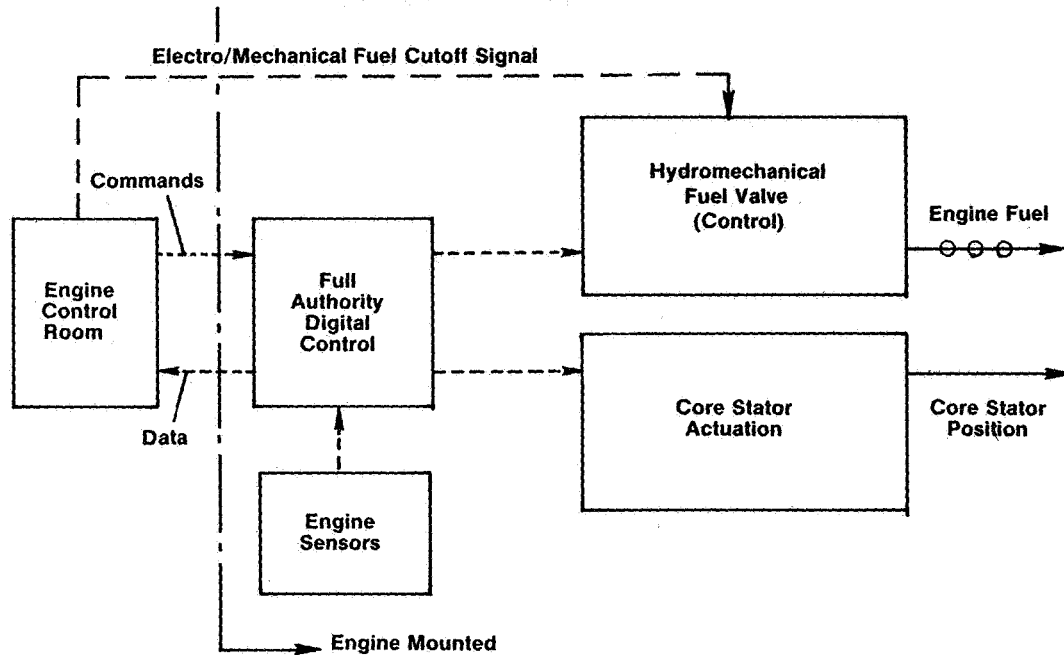
Figure 10

OTW — Control System Sensors
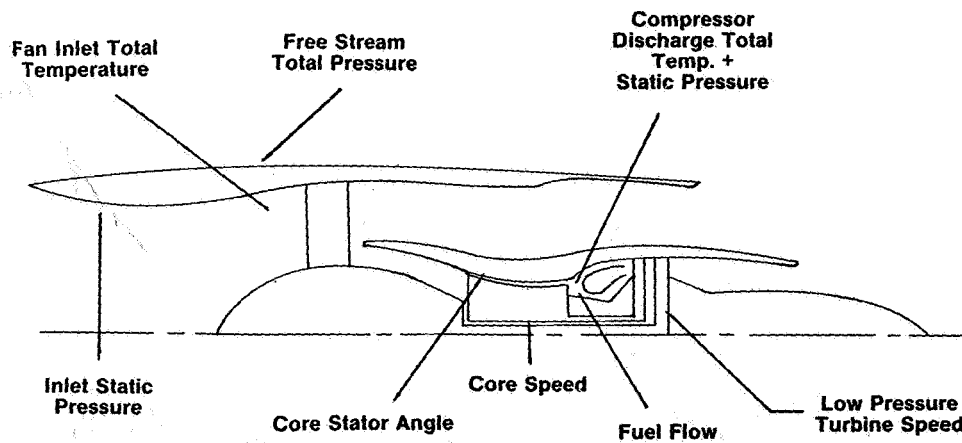
Figure 11

OTW — Acceleration Fuel Schedule
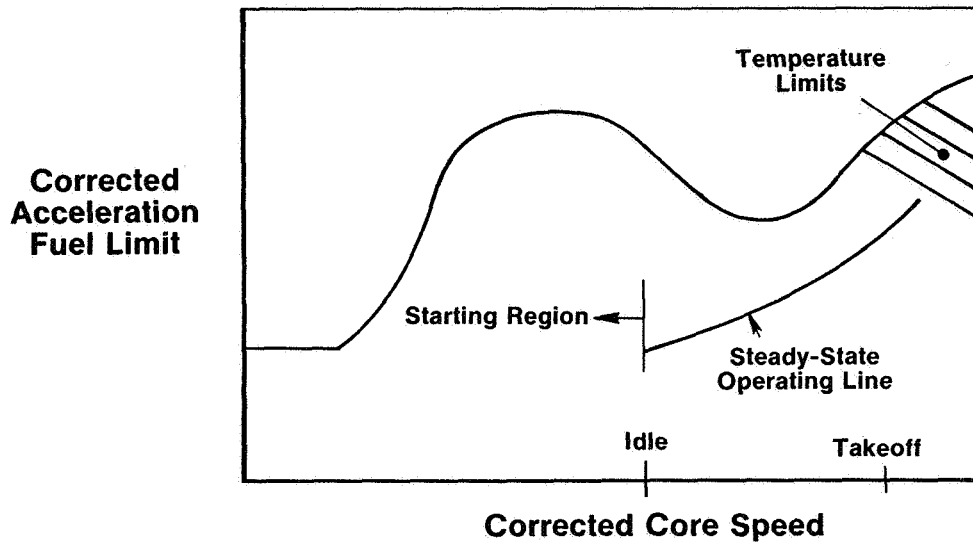
Figure 12

OTW Engine
Predicted Transient Response

Figure 13

155
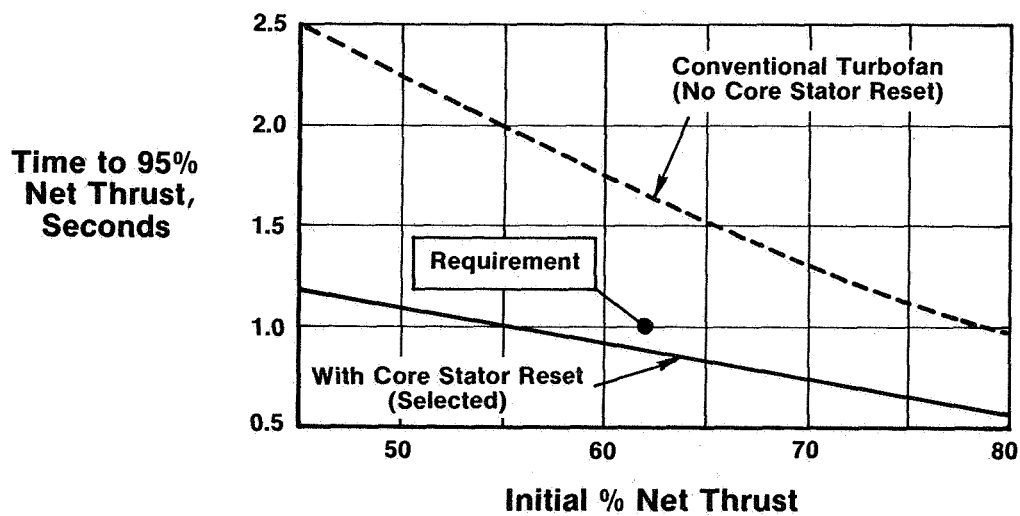
OTW — Failure Indication and Corrective Action
(FICA)
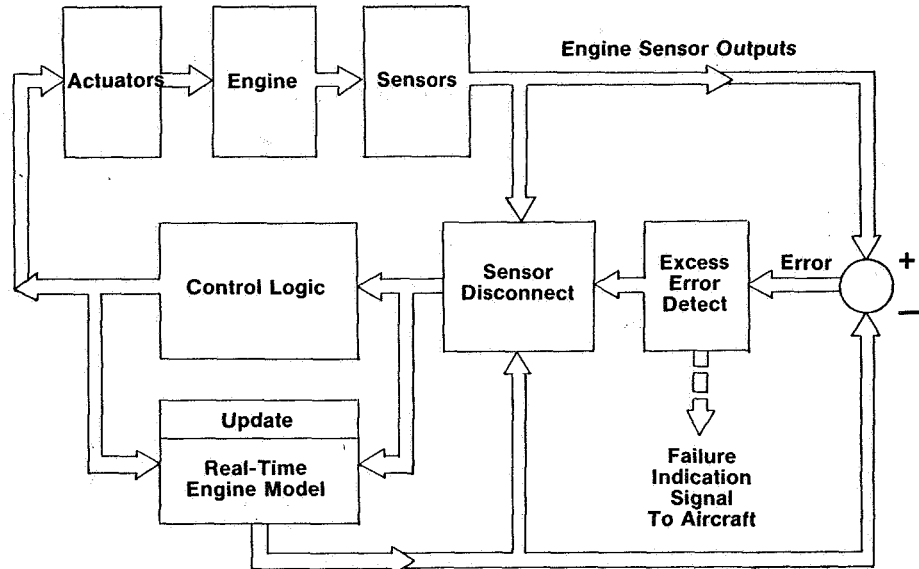
Figure 14

FICA Dynamic Simulation Results
Power Chop to 62% and Power Burst to 100%
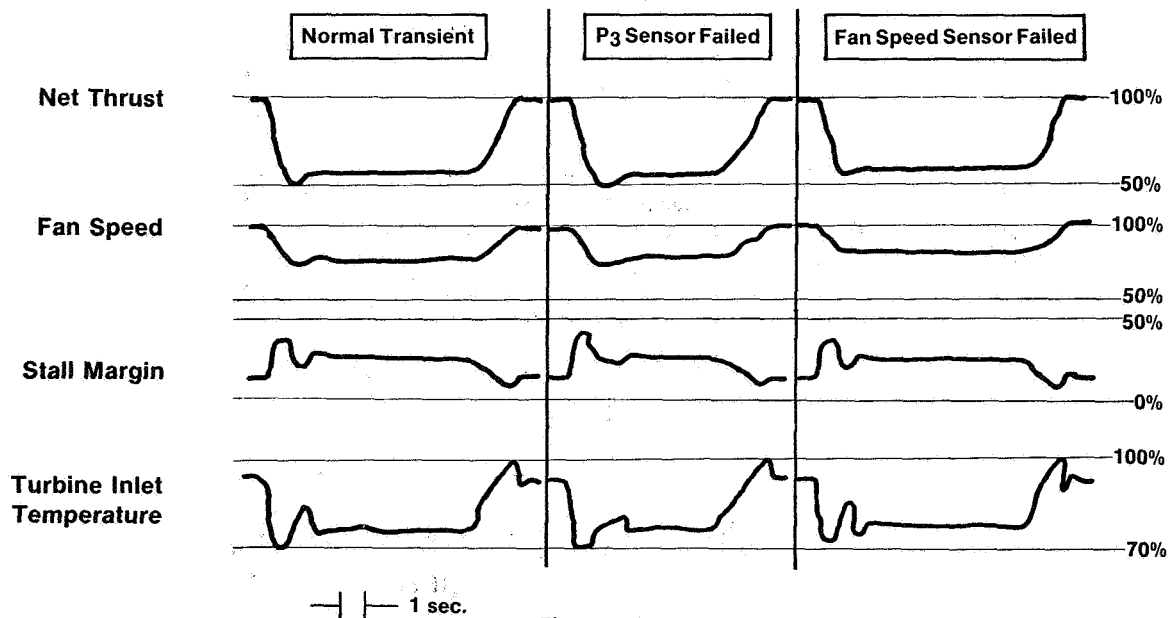
Figure 15

OTW Engine Test Results

Fan Speed Scheduling
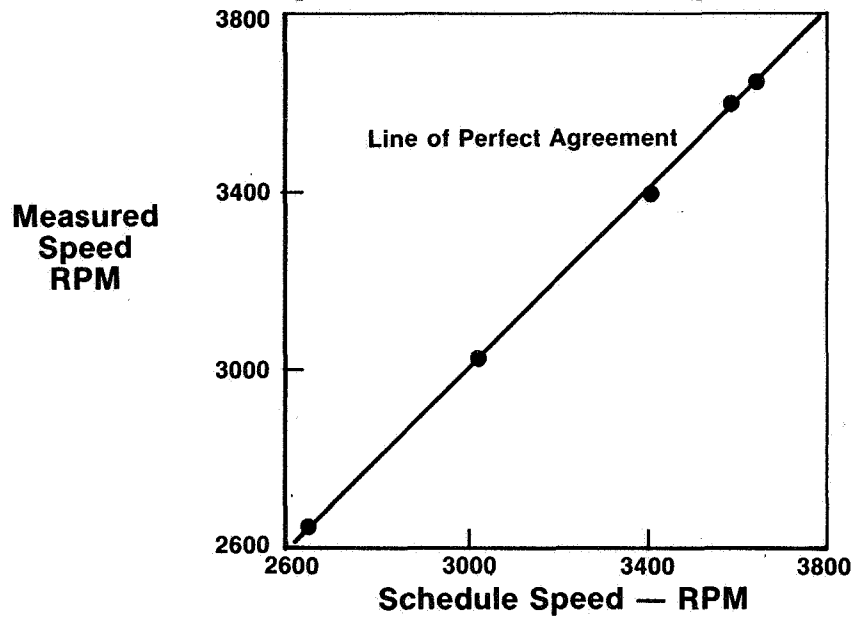
Figure 16

OTW Engine Test Results

Core Stator Control Performance
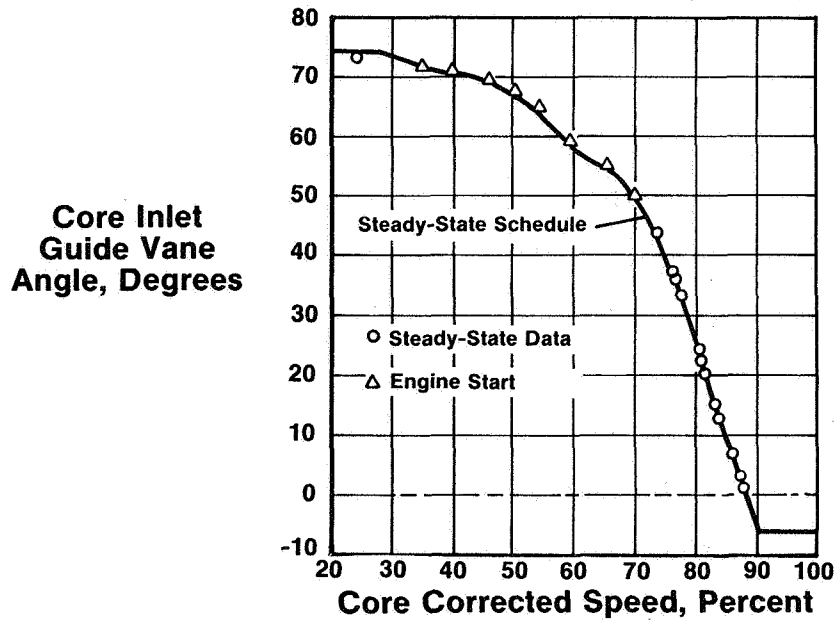
Figure 17

157

OTW Engine Test Results
Turbine Inlet Temperature Calculation Comparison

Digital Control, On Line Calculated Temperature, % of Max

△ Bellmouth Inlet
O Flight Inlet, Forward Mode
□ Flight Inlet, Reverse Mode

Line of Perfect Agreement

Post Test Calculated Cycle Average Temperature % of Max
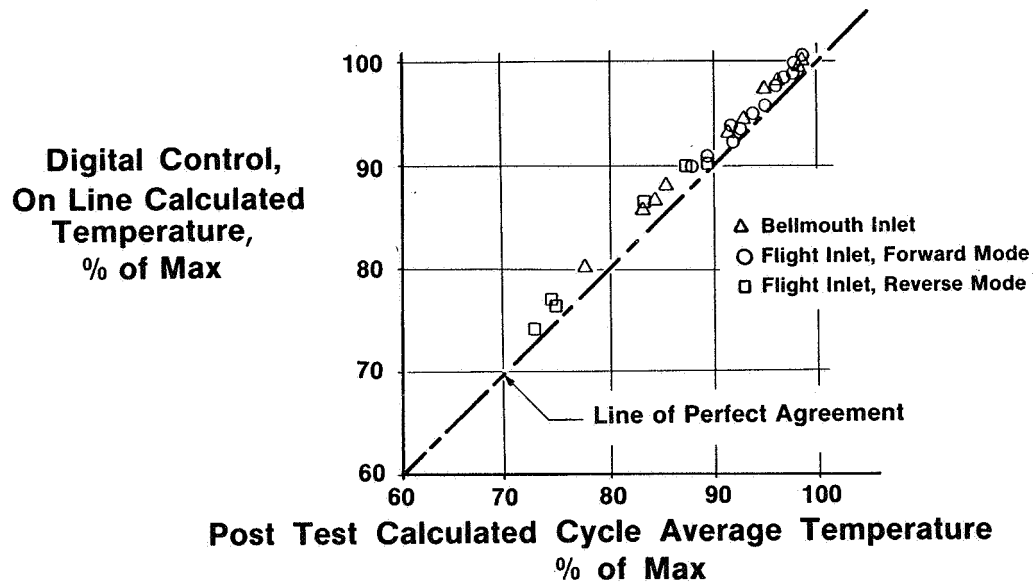
Figure 18

OTW Engine Test Results
Typical Engine Start

Fan Speed RPM

Open Stopcock

Fuel Flow Kg/hr

lb/hr

Turbine Discharge Temperature °C

Light

°F

25 secs

Core Speed RPM

Idle 10,200

Seconds

Figure 19

158

OTW Engine Test Results
Thrust Response

Percent
of
Maximum
Thrust

Figure 20

159

QCSEE UNDER-THE-WING NACELLE AERODYNAMICS*

John M. Abbott and Roger W. Luidens
NASA Lewis Research Center

INTRODUCTION

A substantial portion of the aerodynamic design of the nacelle for the QCSEE under-the-wing (UTW) engine evolved from model tests conducted jointly by the General Electric Co. and the NASA Lewis Research Center. This paper reviews the results of these tests and compares the results, where possible, with more recently acquired results of full-scale tests conducted by G.E. The nacelle components to be discussed herein are (1) the high-throat-Mach-number inlet and (2) the fan-exit nozzle when it is used as an inlet during reverse-thrust operation of the engine. Some comments will also be made concerning the expected cruise performance of the nacelle.

The installation of the UTW propulsion system on a conceptual short-haul aircraft is shown in figure 1. Note that the nacelles are large relative to the size of the aircraft, which fact points out the importance of designing the nacelles for low cruise drag. The nacelles are located on pylons forward of and below the wing leading edge so that the engine exhaust is properly positioned for blowing into the wing flaps to provide the powered lift. This location places the nacelle inlet in the high upwash field generated by the powered-lift system of wing and engine, and the inlet must be designed to operate efficiently in this flow environment.

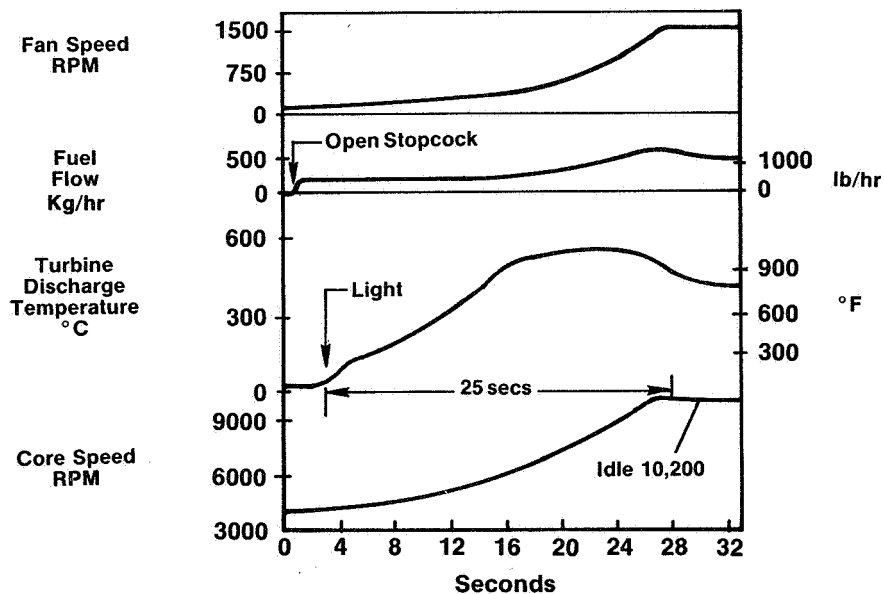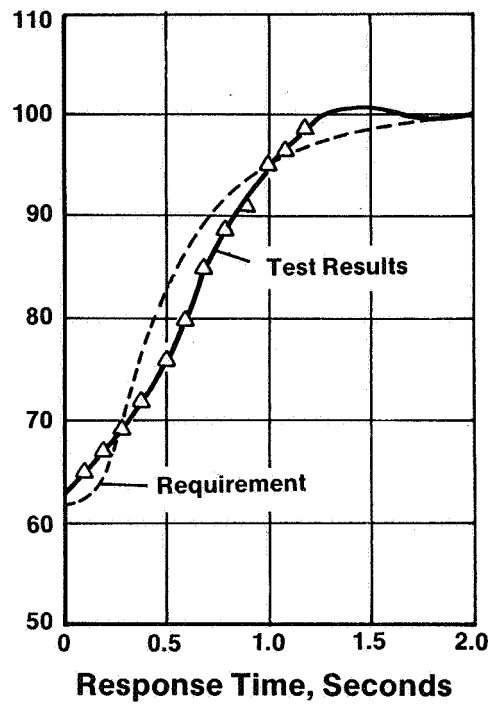A more detailed look at the UTW nacelle is shown in figure 2, which shows the high-throat-Mach-number inlet, and the multifunctional fan nozzle - multifunctional because it is used as a variable area convergent nozzle for forward thrust and, after it has flared out, as an inlet during reverse-thrust operation of the engine. Note that placing the accessories above the pylon reduces the projected frontal area (and hence drag) by allowing the accessories to fit within the silhouette of the pylon. In addition, this placement eliminates in the nacelle the characteristic lower bulge, which results in low static pressures leading to downward force and thus loss of aircraft lift. It also allows a tight integration of the fan cowl into the engine structure. This, in turn, permits thinner nacelle walls - approximately 10 centimeters (4 in.) all around, instead of the 25 centimeters (10 in.) on the top and sides and 50 centimeters (20 in.) on the bottom of the CF6-DC10 nacelle.

SYMBOLS

A_E exlet intake area

A_T exlet throat area

---

a	ellipse semimajor axis of internal lip
b	ellipse semiminor axis of internal lip
D_{FAN}	fan diameter
L	inlet length
$(M_{DD})_{DES}$	design drag divergence Mach number
M_{DUCT}	exlet duct Mach number
M_T	inlet throat Mach number
R_{FAN}	fan radius
R_{HL}	inlet highlight radius
R_{MAX}	inlet maximum radius
R_{THROAT}	inlet throat radius
V_0	free-stream velocity
α	inlet flow angle of attack
β	fan boattail angle
θ	exlet flare angle
θ_{MAX}	diffuser maximum wall angle
ψ	crosswind flow angle

INLET DESIGN REQUIREMENTS

The inlet design requirements are shown in figure 3. The design require-
ments are that the inlet provide low total-pressure distortion and high total-
pressure recovery while providing noise suppression by means of a high throat
Mach number. These requirements must be met at the flow conditions indicated
in the figure - those being at the static condition, which sets the design of
the top region of the inlet lip; in a 15-m/sec (30-knot), 90° crosswind, which
sets the design of the side of the inlet lip; and in a 41-m/sec (80-knot), 50°
upwash, which sets the design of the bottom region of the inlet lip. This last
condition exceeds that encountered by most conventional aircraft and is neces-
sitated by the location of the inlet in the high upwash flow field of the pro-
pulsive lift system. These three requirements could lead to an asymmetric in-
let lip design; however, as will be shown later, an asymmetric inlet was not
necessary - the QCSEE inlet is symmetric.

An additional requirement listed in the figure is low cruise drag. Be-
cause of the low QCSEE fan pressure ratio, the fan and, hence, the inlet diam-
eter are relatively large so that the inlet drag is a greater fraction of the
engine thrust. Designing for low cruise drag is thus of great importance.

162

INLET DESIGN

To determine an inlet design that would satisfy the design requirements under each of these flow conditions, an experimental test program was undertaken. Four different inlet geometries were designed with the aid of analytical flow prediction techniques. The inlet designs were tested at the 0.305-m (12-in.) size in the Lewis 9- by 15-foot low-speed wind tunnel to evaluate performance at static conditions in the 30 knot, 90° crosswind and in the 80 knot, 50° upwash. The results of this test program led to the selection of the aerodynamic design of the QCSEE inlet shown in figure 4. The design throat Mach number of the inlet was 0.79, having been determined by the need to provide high-throat-Mach-number noise suppression. This, then, sized the inlet throat radius, and enough diffuser length from throat to fan was provided to allow for the insertion of acoustical treatment needed for additional noise suppression. This resulted in a somewhat conservative diffuser design having a maximum wall angle of 8.7°. The model test program at Lewis established that an axisymmetric elliptical lip shape with an a/b of 2 and with a lip area contraction ratio of 1.46 would lead to an inlet design that would meet all of the low-speed design requirements. This lip, in turn, sized the inlet highlight radius or radius of the inlet at the leading edge.

The cruise design condition - a free-stream Mach number of 0.72 at engine design weight flow - determined the smallest maximum inlet radius R_{MAX} required for efficient turning of the inlet spillage flow at cruise. This inlet maximum radius, as determined by cruise design considerations, was also the minimum radius required to provide adequate structural soundness. Hence, the resulting inlet design was both aerodynamically and structurally efficient.

The overall dimensions of the inlet are such that the ratio of maximum inlet radius to fan radius, R_{MAX}/R_{FAN} is 1.1 and the ratio of inlet length to fan diameter L/D_{FAN} is 1. The inlet is relatively thin because of the high design throat Mach number and relatively long because of the need for acoustical treatment.

INLET PERFORMANCE

The QCSEE inlet aerodynamic performance is summarized in figures 5 to 7. Figure 5 shows the experimentally determined flow-separation angle bounds from the 0.305-m (12-in.) inlet tests. The data are shown in a plot of flow-separation angle against inlet throat Mach number at a free-stream velocity of 41 m/sec (80 knots). Below the data curve the flow is attached, and above the curve the flow is separated from the inlet lip, leading to high distortion and low recovery. Also shown in the figure is a possible QCSEE operating region. Note that at all inlet throat Mach numbers, from flight idle to takeoff, the inlet flow is attached up to the required flow angle of 50°. An estimated flow-separation bound for the full-scale, 1.80-m (71-in.) diameter inlet, also shown in the figure, is based on a boundary-layer-flow prediction program. As expected, with increasing scale and, hence, increasing Reynolds number, the

inlet flow remains attached to a higher flow angle, providing for a considerable margin between the QCSEE operating region and the separation bound.

Although the data are not shown, the inlet flow was attached up to a 90° flow angle over the throat Mach number operating range at a free-stream velocity of 15 m/sec (30 knots), thereby meeting the crosswind requirement.

Figure 6 shows the inlet total-pressure recovery for the QCSEE inlet at static conditions plotted against inlet throat Mach number. Two sets of data are shown: one for the 0.508-cm (20-in.) diameter inlet tested in the Lewis 9- by 15-foot tunnel and one for the full-scale inlet tested at G.E. Both inlets were fitted with flight lips and have acoustically treated diffuser walls.

One would normally expect the full-scale inlet to have a higher level of total-pressure recovery than the model inlet. The data, however, indicate a slightly higher recovery, at most 0.4 percent, results for the model. The difference between the two sets of data may be a result of inaccuracies in weight flow measurement and hence throat Mach number or differences between the two test installations. Regardless, this level of recovery seems acceptable at static conditions with a value of 0.988 for the full-scale inlet at the design throat Mach number of 0.79.

Figure 7 shows the effect of a free-stream velocity of 41 m/sec (80 knots) and the effect of the acoustically treated diffuser walls on the inlet total-pressure recovery. The data are shown for the 0.508-m (20-in.) model QCSEE inlet. The effect of free-stream velocity can be seen by comparing the solid curve and symbols (V_0 = 41 m/sec (80 knots)) with the dashed curve (V_0 = 0 or static condition). The slightly greater recovery for V_0 = 41 m/sec is a result of a reduction in local surface velocities over the inlet lip - the inlet cleanup effect. A similar improvement in performance with free-stream velocity would be expected with the full-scale inlet.

The inlet was tested at 41 m/sec (80 knots) with both hard and acoustically treated walls as indicated by the two different data symbols on the plot. As indicated the porous treated walls appear to have no effect at all on the inlet pressure recovery. A close examination of the boundary-layer profiles at the fan face, however, does show a greater total-pressure loss for the treated inlet, although not significant enough to affect the value of the overall area averaged recovery.

NACELLE CRUISE PERFORMANCE

The geometry of the UTW nacelle during cruise is shown in figure 8. The fan-exit nozzle is made up of four flaps, which are arranged to provide the 31-percent area decrease required in going from takeoff to cruise while maintaining an acceptable low boattail angle of 7° for cruise operation. From the nacelle cruise drag standpoint, the areas of most concern are the avoidance of drag divergence on the inlet external lip and of flow separation from the fan boattail at the cruise Mach number. The QCSEE nacelle has never actually been tested at cruise conditions; however, its drag rise characteristics may be

inferred from some other nacelle cruise testing done in the Lewis 8- by 6-foot transonic wind tunnel. Results of these tests are shown in figure 9.

The data in figure 9 are presented as a plot of pressure-drag coefficient versus free-stream Mach number for inlet pressure drag alone and for inlet and fan boattail pressure drag combined. The Lewis nacelle's inlet design drag-divergence Mach number was 0.8, and its fan boattail angle, β, was 16°. As the data curves indicate, drag divergence was encountered just about as expected, near a free-stream Mach number of 0.8. Now, the QCSEE inlet was designed for that same drag divergence Mach number, using the same cruise design charts as the Lewis inlet. Because the Lewis inlet encountered drag rise at about the predicted free-stream Mach number and because the QCSEE inlet was designed according to the same techniques, it is expected that the QCSEE inlet will not encounter drag rise until a free-stream Mach number of 0.8, which is sufficiently above the design cruise Mach number of 0.72. Also, the fan boattail angle for QCSEE is 7°, which is considerably lower than the 16° value for the Lewis nacelle. The low values of drag coefficient for the Lewis inlet and boattail combined, indicate that a 16° boattail angle provides acceptable cruise performance; hence, the more conservative 7° QCSEE boattail angle should also provide for efficient cruise performance.

REVERSE-THRUST PERFORMANCE

The final topic to be discussed is the performance of the nacelle when the UTW engine is operating in reverse thrust. The UTW fan is, of course, variable pitch, and reverse thrust is attained by changing the fan blade pitch to reverse the direction of the fan airflow and, hence, reverse the thrust. In this mode, the fan exit is now actually being used as an inlet and is referred to as the fan exlet (fig. 10).

Along with the actual engine geometry in reverse thrust, the geometry of a model used to develop the exlet data base is also shown in figure 10. An important difference between the engine exlet and the model exlet should be noted. At the time the model exlet tests were conducted, certain details of the exlet design were not known and were not incorporated into the model exlet design. In particular, note the gap between the exlet flaps and the nacelle body when the flaps are extended. These gaps do not appear at all in the model configuration.

Figure 11 shows the results of the model test program on a plot of total-pressure recovery versus exlet flare angle. Data are shown at static conditions and at a free-stream velocity of 41 m/sec (80 knots) for a duct Mach number of 0.4. The variation of the exlet contraction ratio A_E/A_T (from 1.4 to 2.8) and the presence or absence of the acoustic splitter account for the data bands. The narrowness of these bands indicates the relative insensitivity to contraction ratio and the splitter. Because the model results indicated that a flare angle of about 30° provides the highest pressure recovery, an angle of 29° was thus selected for the engine exlet. The figure also shows a data point obtained during the engine static test. The total-pressure recovery

is considerably lower than that expected from the model tests, 0.95 as opposed to 0.99. This value of 0.95 was determined from rake traverse data and from estimations of other losses that were not accounted for in the rake traverse data. These additional losses are due to all the gaps that open up with the flaps extended, the splitter support-strut wakes, the junctions between support struts, splitter, and nacelle, and the pylon boundary layer. None of these losses were present during the model tests.

The performance of the QCSEE engine in reverse thrust is shown in figure 12 where the QCSEE reverse-thrust levels are compared with those for QCSEE 0.508-m (20-in.) model tests and Q-fan, T55 tests - another variable-pitch engine capable of running in reverse thrust. The data are shown in a plot of reverse thrust in percent of takeoff thrust against fan speed. The QCSEE reverse-thrust goal was 35 percent of takeoff thrust, and the data from the QCSEE model and the T55 tests suggested this goal would be met. However, as the two QCSEE engine data points indicate, the goal was not reached and instead only 27 percent of takeoff thrust was realized. One possible explanation, although probably not the only explanation, for this low level of reverse thrust is the low level of engine exlet total-pressure recovery associated with the full-scale segmented exlet (indicated in fig. 11). The relatively high reverse-thrust levels of the QCSEE model and T55 engine tests were attained with bellmouth type exits on the fan ducts with correspondingly high total-pressure recoveries.

SUMMARY

This paper has presented results which show that for the UTW QCSEE engine, it was possible to design a nacelle with an inlet having high upwash angle capability, high pressure recovery, and expected low cruise drag while supplying the required level of noise suppression. An area which requires further work is the nacelle exlet, which when reconfigured to reduce total-pressure losses, should contribute to the attainment of the required level of reverse thrust.

BIBLIOGRAPHY

Abbott, John M.; Diedrich, James H.; and Williams, Robert C.: Low-Speed Aerodynamic Performance of 50.8-Centimeter-Diameter Noise-Suppressing Inlets for the Quiet, Clean, Short-Haul Experimental Engine (QCSEE). NASA TP-1178, 1978.

Albers, James A.; Stockman, Norbert O.; and Hirn, John J.: Aerodynamic Analysis of Several High Throat Mach Number Inlets for the Quiet, Clean, Short-Haul Experimental Engine. NASA TM X-3183, 1975.

Dietrich, Donald A.; Keith, Theo G.; and Kelm, Gary G.: Aerodynamic Performance of Flared Fan Nozzles Used as Inlets. NASA TM X-3367, 1976.

Jakubowski, A. K.; and Luidens, R. W.: Internal Cowl-Separation at High Incidence Angles. AIAA Paper 75-64, Jan. 1975.

Luidens, Roger W.: Inlet Technology for Powered-Lift Aircraft. Powered-Lift Aerodynamics and Acoustics. NASA SP-406, 1976, pp. 369-385.

Miller, Brent A.; Dastoli, Benjamin J.; and Wesoky, Howard L.: Effect of Entry-Lip Design on Aerodynamics and Acoustics of High Throat Mach Number Inlets for the Quiet, Clean, Short-Haul Experimental Engine. NASA TM X-3222, 1975.

Steffen, Fred W.: Cruise Performance of an Isolated 1.15 Pressure Ratio Turbofan Propulsion System Simulator at Mach Numbers From 0.6 to 0.85. NASA TM X-3064, 1974.

Vier, W. F.: Quiet, Clean, Short-Haul Experimental Engine (QCSEE) Test Results From a 14-cm Inlet for a Variable Pitch Fan Thrust Reverser. (R76AEG387, General Electric Co.; NASA Contract NAS3-18021.) NASA CR-134867, 1975.

CONCEPTUAL UTW SHORT-HAUL AIRCRAFT

POWERED LIFT OPERATION

CS-73093
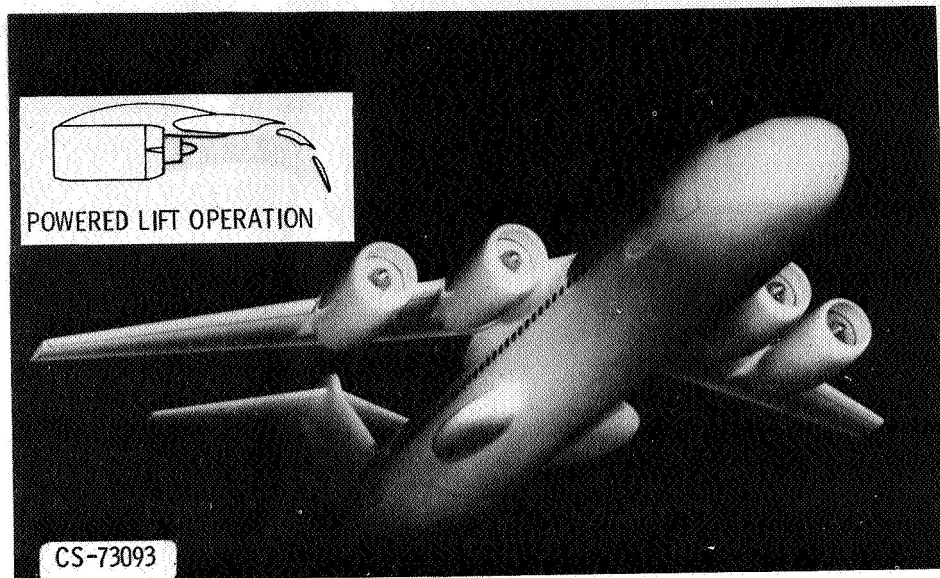
Figure 1

QCSEE UTW PROPULSION SYSTEM

UPPER PYLON ACCESSORIES
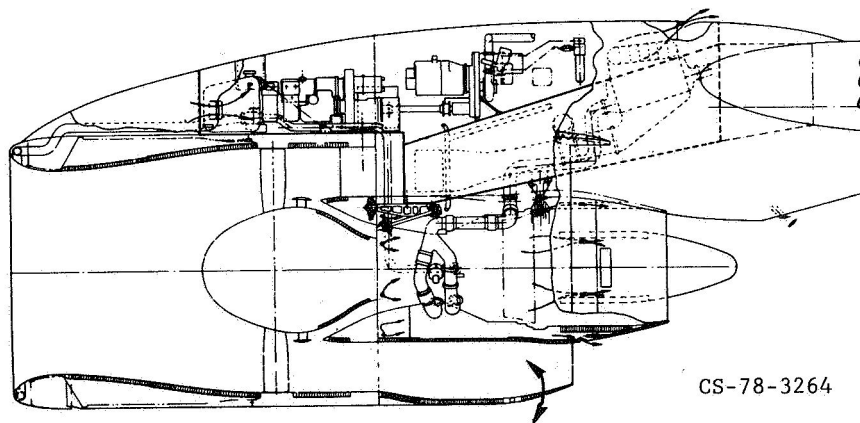
CS-78-3264

Figure 2

INLET REQUIREMENTS

DESIGN REQUIREMENTS:

   LOW DISTORTION
   HIGH PRESSURE RECOVERY
   NOISE SUPPRESSION
   LOW CRUISE DRAG

FLOW CONDITIONS:

STATIC

CROSSWIND:
$V_0 = 15$ m/sec (30 KNOTS),
$\psi = 90^0$

UPWASH:
$V_0 = 41$ m/sec (80 KNOTS),
$\alpha = 50^0$

CS-78-3273

Figure 3

INLET DESIGN

L

a

b

θ_{MAX}

R_{MAX}

R_{HL}
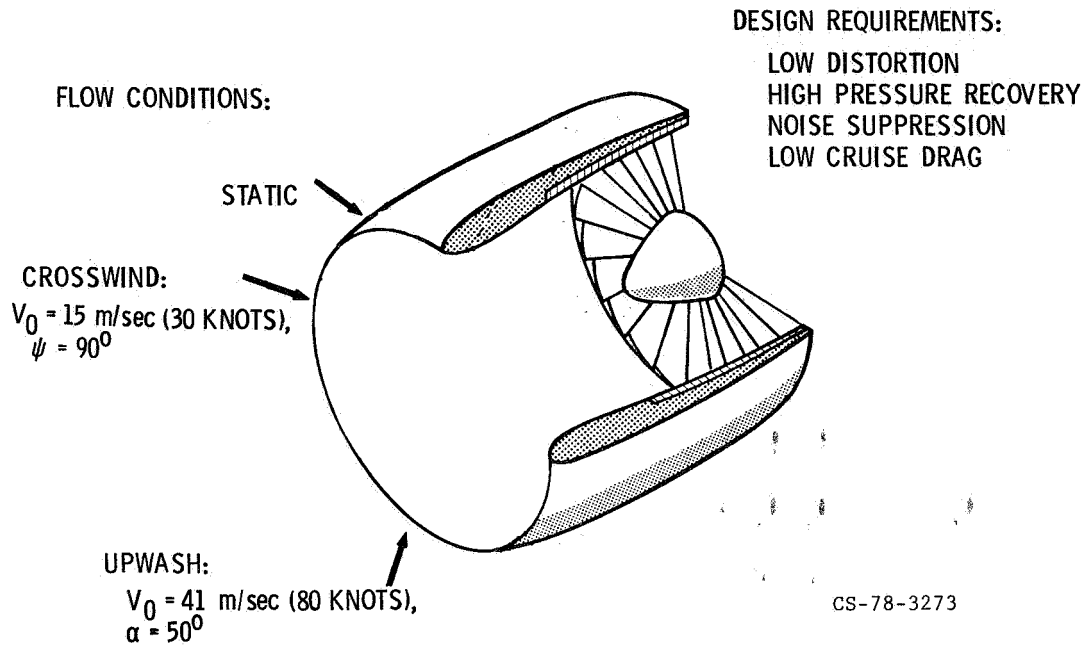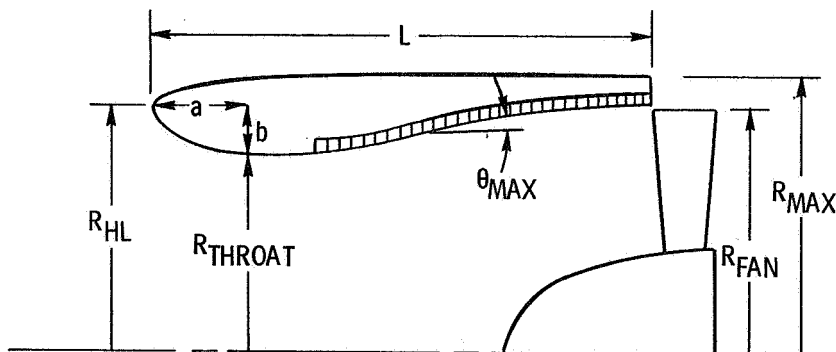
R_{THROAT}

R_{FAN}

$M_T = 0.79$

$\left(\dfrac{R_{HL}}{R_{THROAT}}\right)^2 = 1.46$

$\theta_{MAX} = 8.7^0$

$\dfrac{R_{MAX}}{R_{FAN}} = 1.10$

$\dfrac{a}{b} = 2.0$

$\dfrac{L}{D_{FAN}} = 1.0$

CS-78-3271

Figure 4

169

INLET SEPARATION BOUNDS

V_0 = 41 m/sec (80 KNOTS)

FLOW-
SEPARATION
ANGLE,
deg

—o— 0.305 m (12 in.) DIAM (MODEL)
— — — 1.80 m (71 in.) DIAM (ESTIMATED)

SEPARATED

ATTACHED

TAKEOFF (NOISE SUPPRESSION)

QCSEE OPERATING REGION

FLT IDLE

THROAT MACH NO.
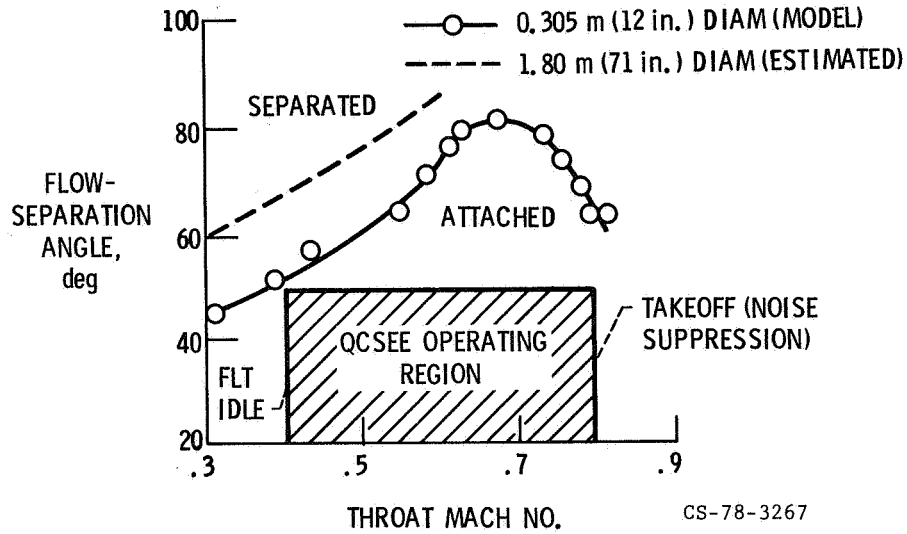
CS-78-3267

Figure 5

COMPARISON OF MODEL AND FULL SCALE RESULTS

V_0 = 0

O   1.80 m (71 in.) DIAM (TREATED)
□   0.508 m (20 in.) DIAM (TREATED)

TOTAL-
PRESSURE
RECOVERY

THROAT MACH NO.

CS-78-3504
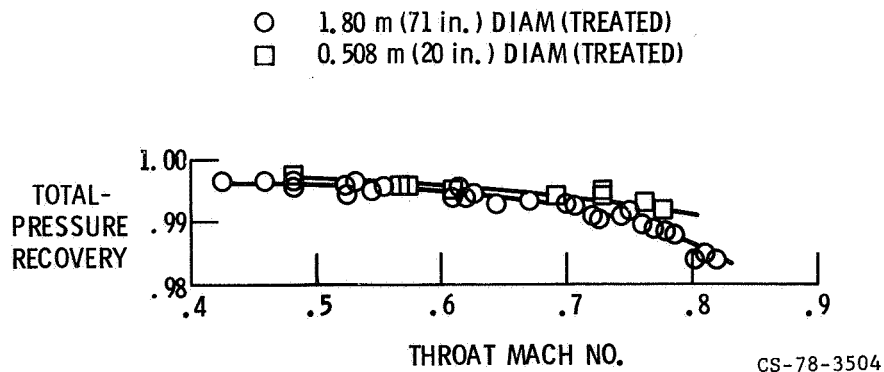
Figure 6

EFFECT OF FORWARD VELOCITY AND ACOUSTIC TREATMENT

0.508 m (20 in.) DIAM INLETS
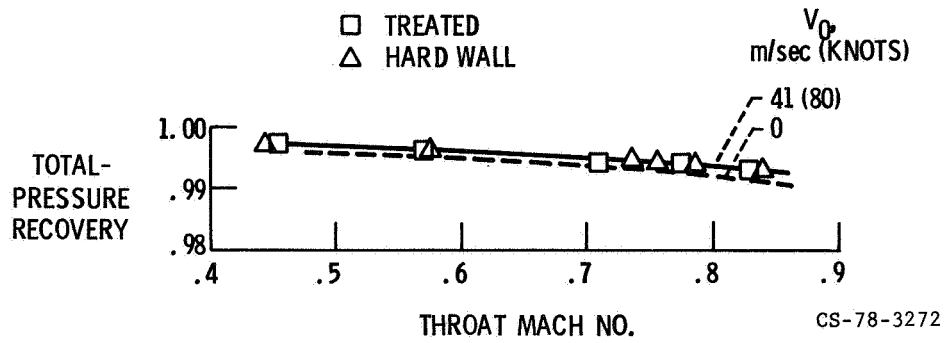
Figure 7

NACELLE GEOMETRY AT CRUISE

Figure 8

171

CRUISE DRAG

NACELLE	$(M_{DD})_{DES}$	β, deg
● LEWIS	0.8	16
NO DATA QCSEE	.8	7

PRESSURE-DRAG COEFF

QCSEE CRUISE MACH NO.

INLET + FAN BOATTAIL

INLET

FREE-STREAM MACH NO.
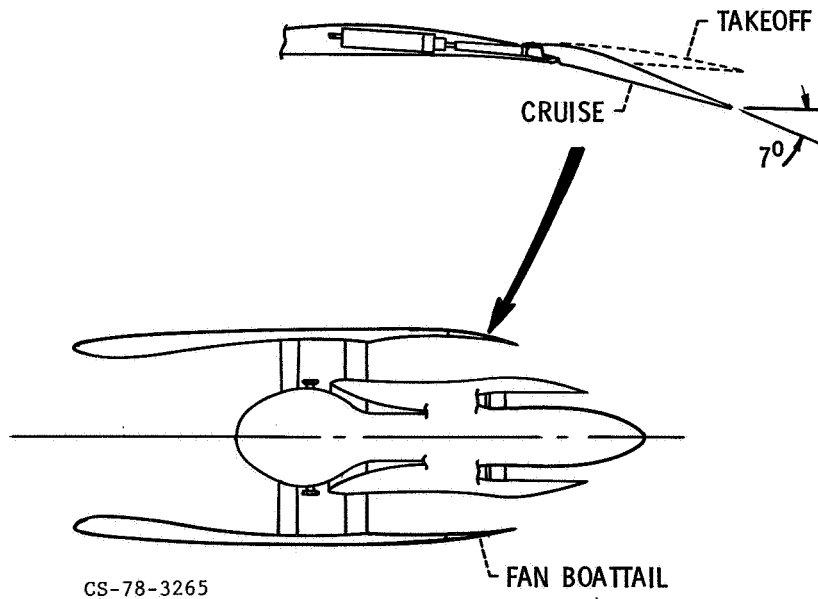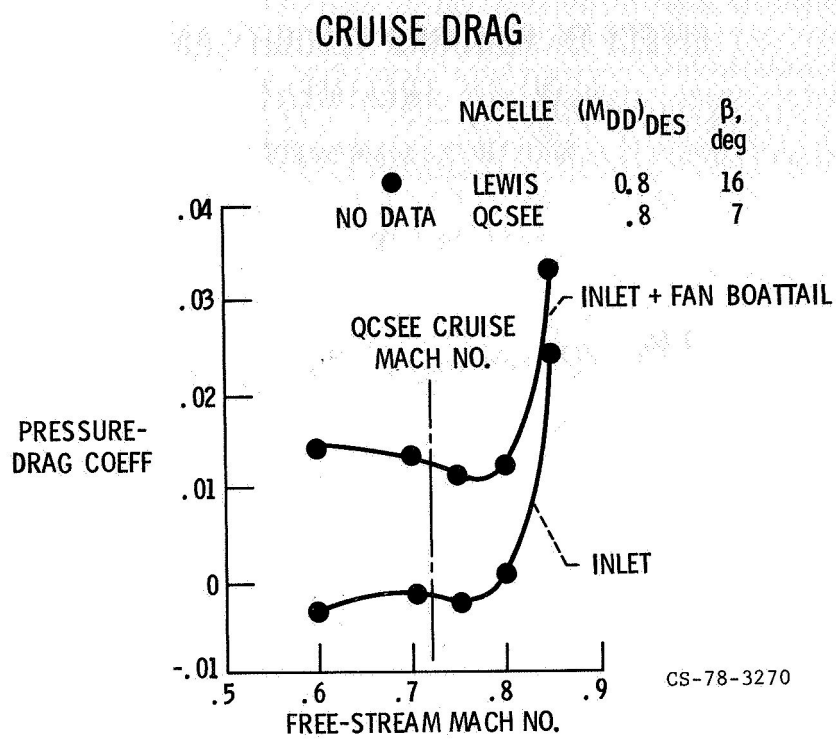
CS-78-3270

Figure 9

NACELLE GEOMETRY FOR REVERSE THRUST

ENGINE

MODEL

CS-78-3269

Figure 10

172

EXLET PRESSURE RECOVERY

$$\frac{A_E}{A_T} = 1.4 \text{ TO } 2.8$$

$$M_{DUCT} = 0.4$$

FREE-STREAM VELOCITY, m/sec (KNOTS)

MODEL

0

41 (80)

ENGINE $V_0 = 0$

TOTAL-PRESSURE RECOVERY

1.00
.98
.96
.94
.92
.90

FLARE ANGLE, θ, deg

0 10 20 30 40 50 60
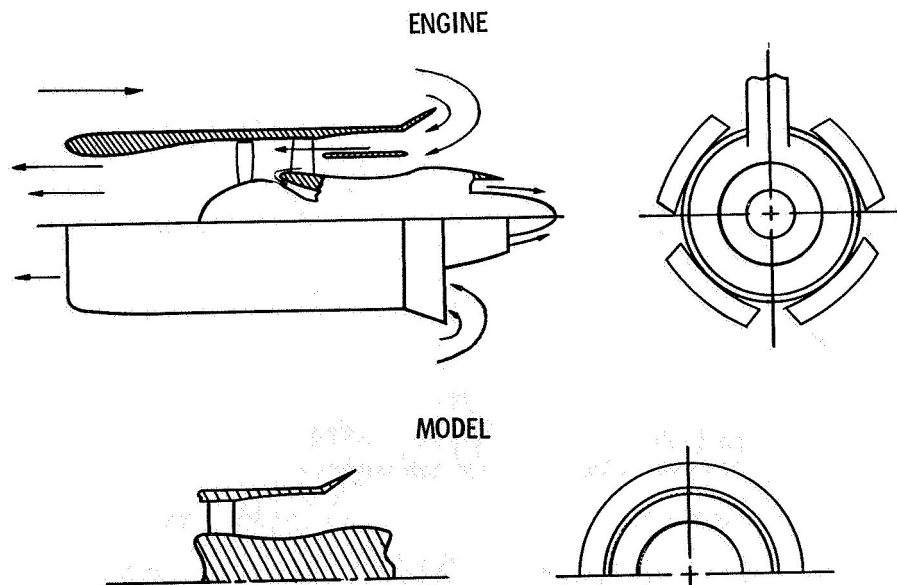
CS-78-3266
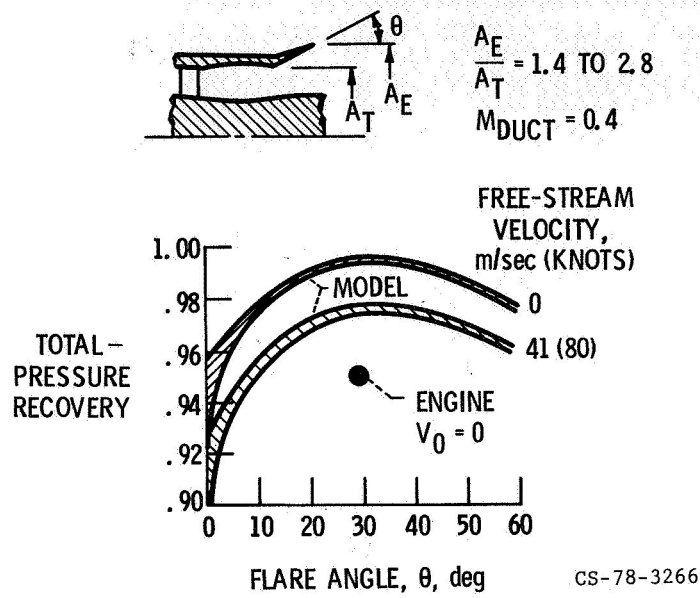
Figure 11

STATIC REVERSE THRUST THROUGH STALL PITCH

TEST	EXIT
Q-FAN T-55	BELL
QCSEE MODEL	BELL
QCSEE ENGINE	SEGM'T EXLET

REVERSE THRUST, % OF TAKEOFF THRUST

50
40
30
20
10

GOAL

FAN RPM, % DESIGN

50 60 70 80 90 100 110

CS-78-3268

Figure 12

173

QCSEE OVER-THE-WING NOZZLE AND THRUST REVERSER AERODYNAMICS[*]

Howard L. Wesoky
NASA Lewis Research Center

SUMMARY

The design objectives for the nozzle and thrust reverser of the QCSEE over-the-wing (OTW) propulsion system have been achieved. The nozzle provides high jet turning angles and efficiencies for flap angles up to 60°. Nozzle area variation between takeoff and cruise operation is provided by side doors. A top-mounted target-type thrust reverser provides the objective reverse thrust, but results in a back pressure effect which reduces the effective exit area. Further development would be required to obtain a nozzle and reverser for a flight propulsion system.

INTRODUCTION

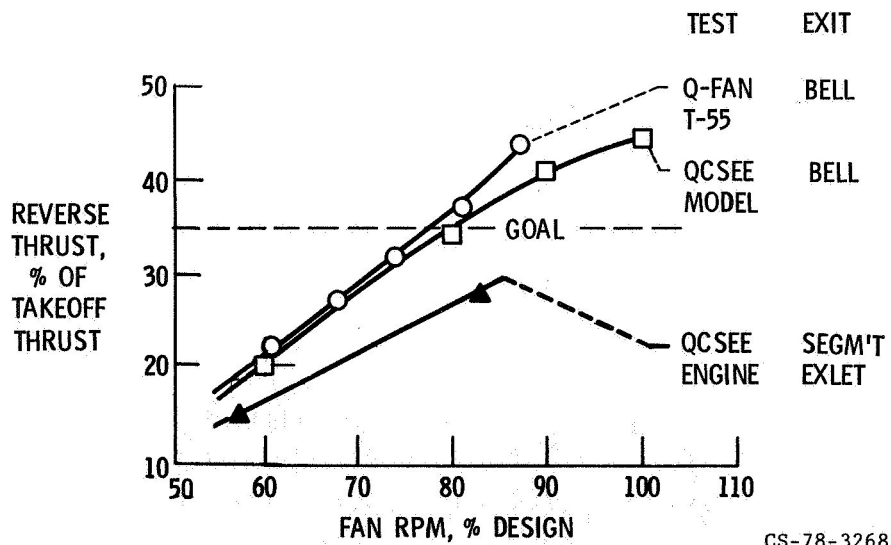This paper presents the results of the QCSEE over-the-wing (OTW) nozzle and thrust reverser development program and compares the available experimental engine test results with model data from the development program. The General Electric Company (GE) was the prime contractor for the design development, but considerable help and guidance were obtained from the NASA Langley Research Center and the Boeing Company, the two most prominent early proponents of upper surface blowing as a source of powered lift.

SYMBOLS

A_{cruise} nozzle physical exhaust area with side doors closed

A_{eff} nozzle effective exhaust area

ΔA_{eff} difference in nozzle effective exhaust area between configurations with side doors open and closed

C_{D-T} drag coefficient, net drag minus thrust force/qS

ΔC_{D} interference drag, total aircraft drag with propulsion effects minus aircraft clean-wing drag and isolated nacelle drag

C_{d} discharge coefficient, measured airflow/ideal airflow for A_{cruise}

---

[*]For Early Domestic Dissemination.

ΔC_d difference in discharge coefficient between configurations with nozzle side doors open and closed

C_L lift coefficient, lift force/qS

C_M momentum coefficient, actual gross thrust/qS

C_V velocity coefficient, actual gross thrust/ideal gross thrust

D_{TH} equivalent throat diameter of exhaust duct for thrust reverser (fig. 16)

H_B thrust reverser blocker height (fig. 16)

L thrust reverser lip length (fig. 16)

M_0 aircraft cruise Mach number

P_7 nozzle entrance total pressure

P_0 ambient static pressure

q dynamic pressure

S wing area

X_B thrust reverser blocker axial spacing (fig. 16)

X_p thrust reverser pivot axial spacing (fig. 16)

α aircraft angle of attack

β thrust reverser lip angle (fig. 16)

γ aircraft glide scope, flight path angle to horizon

δ_j nozzle exhaust flow angle

θ thrust reverser blocker angle (fig. 16)

φ thrust reverser side skirt angle (fig. 16)

DESIGN PROBLEM

    Design objectives for the OTW nozzle are shown in figure 1. An important point to note about the nozzle is that it was to be representative of current aircraft installation technology, but not tailored to a specific aircraft design. In particular, although the flow lines were to be representative of a 0.72 cruise Mach number, the scope of this project did not allow a detailed consideration of cruise drag by GE. However, some cruise drag information was

obtained in a general technology program related to the QCSEE Project, and this is discussed later in this paper.

For purposes of demonstrating the experimental engine, the two most significant nozzle design objectives are items 3 and 4 in figure 1. To demonstrate the installed acoustic characteristics of the OTW propulsion system with representative aerodynamic performance, it is necessary that the exhaust jet be attached to a simulated wing upper surface for all flap positions. A large nozzle exhaust area variation between takeoff and cruise conditions is a requirement of the very-high-bypass, quiet-engine cycle and mission.

The jet turning objective was satisfied in part by using the D-shape exhaust for the nozzle indicated in figure 1. The side doors shown provided the needed area variation and also helped the jet turning. Further details of this exhaust system are given later in this paper.

A requirement for the OTW nozzle design was that it include a thrust reverser with the performance requirements indicated in figure 2. Preliminary studies indicated a need for reverse thrust equivalent to 35 percent of takeoff static thrust. Because the approach and landing speed of a STOL aircraft is so low, the reverser must operate at very low aircraft speeds without the reversed airflow being reingested, a phenomenon which could cause the engine to surge or exceed a temperature limit.

Before the performance details are discussed, it is interesting to compare (fig. 3) the QCSEE OTW nozzle with the nozzle of the CF6 engine used on the YC-14, the prototype Air Force STOL transport, which is discussed in another paper (ref. 1). Because the design objectives for the YC-14 and QCSEE OTW nozzle installations are similar, it would seem that the technology developed for the YC-14 could be directly applied to the QCSEE design. However, when the QCSEE nozzle design was complete, the only important feature which remained the same as for the YC-14 was the crown line (i.e., top of the nacelle) boattail angle. Significantly unique performance characteristics were discovered for the QCSEE nozzle and reverser in all three major operational regimes: low flight speed with powered lift, cruise flight speed, and reverse thrust.

The high bypass ratio and low fan pressure ratio of QCSEE result in a large exit area requirement relative to the YC-14, as indicated in the figure by the ratio of cruise exit area to nacelle cross-sectional area and the ratio of takeoff exit area to cruise area. In turn, the large area requirement results in a smaller width-height ratio for the QCSEE nozzle.

Although the large doors on both sides of the QCSEE nozzle increase its effective aspect ratio, in the original design, this alone was insufficient to produce the thin, wide jet necessary to satisfy the 60° jet turning requirement. In static jet turning tests (ref. 2) with an early version of the QCSEE nozzle and a wing and flap, the jet was well attached to the flap, but was very thick with vortex rollup of the edges. The relatively low jet turning angle resulting from this effect was improved by increasing the boattail angle along the width of the nozzle; the increased angle, in turn, thinned the jet and caused it to spread along the wing span. Extension of the high boattail angle

to the edges of the D-nozzle causes abrupt shoulders in the QCSEE nacelle rela-
tive to the well-rounded YC-14 nacelle. This shape results in a possible
cruise drag problem, because vortices apparently form at the shoulders and
cause external flow separation from the aft nozzle.

Reverse thrust performance of the QCSEE is also affected by the large exit
area requirement in the following manner. The blocker or target used to re-
verse the exhaust jet results in a back pressure effect which reduces the ef-
fective area of the exhaust. Because the YC-14 installation has a larger area
convergence between the fan and the nozzle exit (as indicated by the area ra-
tios in fig. 3), this installation can more easily include the large geometric
area required to balance the reduction in flow coefficient caused by the
blocker.

DEVELOPMENT PROGRAM

The design of the QCSEE OTW nozzle and thrust reverser was based on a
model test program conducted by GE and NASA (refs. 2 to 4) at the Langley Re-
search Center. Approximately 1/12 scale models were used in parametric inves-
tigations, as indicated in figure 4. Tandem, tip-turbine-driven fan engine
simulators were used to represent the QCSEE OTW propulsion system. Axial and
normal force components were measured with both isolated nacelle models and
with sections of a wing and flap installed. The same engine simulation and
force balance were used to test thrust reverser models.

Primary objectives of the model test program were to demonstrate the 60°
of jet turning required with a 60° flap setting and to demonstrate a reverse
thrust level equivalent to 35 percent of takeoff thrust. Nozzle velocity and
discharge coefficients were also measured, but the number of pressure and tem-
perature instruments was limited by facility capability and was less than nor-
mally considered satisfactory for highly accurate definition of the coeffi-
cients. However, the accuracy is considered adequate for establishing trends
such as the effects of side door angle and installed performance with a wing
and flap.

NOZZLE PERFORMANCE

Static and Low Speed Model Test Results

Figure 5 is a schematic representation of the flow path which resulted
from the nozzle tests. Also shown are the areas of the nacelle used for the
side area control doors and for the thrust reverser blocker. Obviously, devel-
opment of such a highly three-dimensional flow path required a large amount of
cut-and-try experimentation, with the Langley and Boeing data base used as a
guide.

Also shown in the figure is the uninstalled (i.e., isolated) model nozzle
performance (ref. 3) at a pressure ratio of 1.25, about midway between the

QCSEE takeoff and landing values. A 25° door opening produced an effective area increase of about 20 percent, slightly less than the design objective, but considered adequate by the engine designers at a later stage of propulsion system development. A wider opening of the side doors produced very little increase in the effective area. The exhaust flow angle for the uninstalled nozzle was 12.2° for the takeoff configuration and 7.8° for the cruise configuration. In this and later figures, takeoff refers to the nozzle configuration with the side doors open 25°, while cruise refers to the configuration with the doors closed. It should be noted that the internal roof angle of the nozzle is 23.5° at the crown line, 5° less than the boattail angle, to provide structural integrity.

Model installed jet turning. - Jet static turning performance for a model QCSEE OTW nozzle installed on a wing with a 60° flap is shown in figure 6, along with other Boeing and NASA data from a paper by Wimpress (ref. 5). The polar coordinate data presentation, often called a spider plot for obvious reasons, shows both turning angle and efficiency. Turning angle is determined by a vector summation of normal and axial force components, while efficiency is defined by the ratio of the resultant force to the nozzle thrust measured without a wing and flap. The QCSEE model turning angle (ref. 2) was about 60°, 4° to 5° higher than the YC-14 turning angle with a similar flap having a 60° chord line angle. The efficiencies for both installations were nearly 90 percent, toward the high end of the data band which includes results for various flap angles and nozzle configurations. These results for the QCSEE OTW nozzle were considered to meet the design requirement and were very encouraging based on the comparison with the data base.

The turning performance of the nozzle at simulated flight conditions was confirmed by wind tunnel tests (ref. 2) on the single engine semispan model shown in figure 7. Although a semispan model of a four-engine aircraft would properly have two engines, only one engine was mounted on the model at a position midway between the positions normally occupied by two engines. This was done because the purpose of the wind tunnel tests was primarily to evaluate the effect of forward speed on the turning characteristics of the D-nozzle, and previous experience had shown that interference effects between two adjacent jets would not reduce the turning performance of either jet. Tufts attached to the upper surface of the wing and flap showed that the jet spreading under forward flight conditions was nearly identical with that observed under static conditions. The tufts showed good flow attachment and confirmed that the static flow attachment characteristics are retained with the wind on. Measurements of longitudinal aerodynamic characteristics of this model with the QCSEE OTW nozzle, which are shown in figure 8, indicate that the lift and drag performance of this configuration satisfied the representative landing approach criteria established by the Langley Research Center for powered-lift aircraft: a lift coefficient of 4.0, a 6° glide slope, and a 15° stall margin. The momentum or thrust coefficient required for this performance corresponds to approximately 50 percent of the installed thrust.

Model discharge coefficient characteristics. - Discharge coefficient data from static model tests (ref. 3) are shown in figure 9 as a function of nozzle pressure ratio. It should be noted that the reference conditions for the dis-

charge coefficient were the nozzle entrance pressure and temperature and the cruise nozzle exit area. Takeoff area was not used because the nozzle exhaust is not completely bounded with the side doors open, and, also, the use of a cruise area reference allowed a straightforward analysis of the effective exhaust area with the side doors open. Therefore the discharge coefficient for the takeoff nozzle has values greater than unity, as indicated by the data at the top of the figure, while the cruise nozzle has more conventional values, as indicated by the data at the bottom of the figure.

The effect of wing proximity on discharge coefficient is noted for both the takeoff and cruise nozzle configurations. Installed data, which were obtained with a large plate at the nozzle exit, indicate a small back pressure effect caused by placing an obstruction in the path of the nonaxial discharge. The back pressure causes a reduction of about 2 percent for the cruise nozzle and a smaller reduction for the takeoff nozzle because the open side doors allow additional lateral spreading of the exhaust. For the installed configuration, the effective area increase between the cruise and takeoff nozzles is about 21 percent, about 1 percent higher than for the uninstalled configuration (fig. 5). Definition of this area differential was restricted to a pressure ratio of about 1.25 because of test model limitations.

Velocity coefficient characteristics. - Figure 10 presents velocity coefficients obtained in static tests of the QCSEE OTW nozzle model (ref. 3). Velocity coefficient is determined by dividing measured thrust by an ideal thrust based on the measured flow and nozzle entrance pressure and temperature. Data are again presented for both takeoff and cruise nozzles in installed and uninstalled configurations. Installed performance is as much as 5 percent lower, with the difference attributed to skin friction on the simulated wing, spanwise velocity components caused by the jet spreading, and jet impingement losses associated with turning the exhaust along the surface of the simulated wing. Apparently the difference between installed and uninstalled velocity coefficients is less for the cruise nozzle because the flow spreading is reduced substantially when the side doors are closed.

Model Cruise Drag

As stated in the INTRODUCTION, some model cruise drag information was obtained in a general technology program related to the QCSEE Project (refs. 6 and 7). A fundamental investigation of OTW propulsion and airframe interference effects was conducted by the Douglas Aircraft Company and NASA in the Lewis Research Center 8- by 6-Foot Wind Tunnel. The model shown in figure 11 was tested at Mach numbers from 0.6 to 0.8 with a series of OTW nozzles, including a model of the QCSEE OTW nozzle. Powered fan engine models were used to provide realistic propulsion effects on the airplane model.

Figure 12 shows some interference drag data from this experiment (ref. 6) compared with data from the YC-14 STOL transport program (data from Elling Tjonneland of the Boeing Aerospace Co.). Interference drag is defined as measured airplane drag with propulsion effects minus the sum of the airplane drag without a propulsion system (i.e., clean-wing drag) and the isolated nacelle

drag. Therefore it represents a drag penalty associated with the propulsion system *installation.*

Obviously the drag associated with the QCSEE nozzle is quite high, between 15 and 20 percent of the net thrust at a cruise Mach number of 0.7. To help assess this result, Boeing aerodynamicists have used YC-14 two-engine configuration data along with results of the Lewis wind tunnel tests to estimate the drag level of a four-engine airplane with YC-14 type nacelles. This hypothetical aircraft would have interference drag equivalent to about 7 percent of net thrust at a cruise Mach number of 0.7, less than half of that measured with the QCSEE nozzle. The reference nozzle, for which drag data are also shown in the figure, had a crown-line boattail angle of only 11° and was well rounded relative to the QCSEE nozzle. It was used to indicate the drag of an OTW nozzle designed with only cruise drag considerations and undoubtedly would not have the jet turning characteristics required for STOL performance. At Mach 0.7, the reference nozzle interference drag was less than 3 percent of net thrust.

Static pressure measurements and flow visualization with tuft surveys indicate that the high drag of the QCSEE nozzle installation was caused by extensive flow separation from the aft part of the boattail. Boeing experience with similar configurations shows that vortices form at the shoulders of the nacelle and cause the separation. As previously noted, the abrupt shoulders of the QCSEE nozzle resulted from the high jet turning angle requirement. Therefore it can be stated that the QCSEE nozzle design has emphasized the low speed STOL performance requirements to the detriment of cruise drag.

Because the scope of the project did not allow further experimentation, it can only be suggested, as has been done by Boeing, that it may be possible to improve cruise performance by rounding the shoulders of the nozzle and still maintain the 60° low speed jet turning performance through the use of vortex generators on the wing upper surface, as on the YC-14 airplane (ref. 8). However, the most promising suggestion may be included in the results of the preliminary flight propulsion system study (ref. 9) conducted by GE with the assistance of Boeing and American Airlines. This study indicated that the requirements for a commercial short-haul transport could be obtained with a landing approach flap setting of 40°. Therefore the jet turning requirement would also be about 40°, and this would significantly reduce the requirements for the nozzle design which resulted in the high cruise drag demonstrated for the nozzle of the QCSEE OTW experimental propulsion system.

Engine Static Test Results

Because a completely instrumented QCSEE OTW propulsion system has not yet been tested with a wing and flap mounted on a force balance, only uninstalled engine (fig. 13) static test results are presented. A combination of data from reference 10 and recently obtained Lewis Research Center test results indicates that the uninstalled engine nozzle jet exhaust angle is about 12.0° at a pressure ratio of 1.25. This is within 1° of the comparable model test result shown in figure 5, and, therefore, the engine jet turning angle with a wing and flap is assumed to be also nearly the same as measured with the model, about

60° (fig. 6). This assumption has been supported by flow visualization in recent Lewis Research Center tests with a wing and flap.

Discharge coefficient. - Engine nozzle discharge coefficients are presented in figure 14 and compared with model test results. The engine data have the predicted increasing trend with pressure ratio, but are 2 to 3 percent higher than predicted for the cruise nozzle and as much as 3 percent lower than predicted for the takeoff nozzle. Because of the lower than predicted takeoff nozzle performance and higher than predicted cruise nozzle performance, the effective area increase for the takeoff nozzle is only about 16 percent for the engine, as compared with 20 percent predicted from the model data (fig. 5). However, the predicted operation of the engine as indicated by the fan operating line was not significantly affected by the relatively small differences between predicted and measured flow performance noted for the individual takeoff and cruise configurations. The scatter in the engine test data is probably indicative of the difficulties in obtaining accurate performance measurements for low-pressure-ratio, unchoked nozzles, where the pressure differentials are small and performance is influenced by ambient wind conditions.

Velocity coefficient. - Engine nozzle velocity coefficients are presented in figure 15 and compared with model test results. Although velocity coefficient normally tends to increase with increasing pressure ratio, the scatter in both model and engine data makes it difficult to define trends for the relatively narrow range of pressure ratio. The engine data are significantly lower than the model data, about 3 to 4 percent for both the takeoff and cruise nozzle configurations. Although these differences cannot be explained with certainty, it should be recalled that the model propulsion system, which had a tip-turbine-driven fan, was significantly different from the experimental engine. Also, only limited pressure instrumentation was available in the model, and, at a nozzle pressure ratio of 1.25, a 1-percent error in pressure ratio causes about a 2-percent error in ideal velocity or velocity coefficient.

The engine nozzle velocity coefficients are also a few percent lower than representative values for round nozzles. This may be partly explainable by the somewhat tortuous flow path of the D-nozzle. It is also noteworthy that the velocity coefficients are about the same for both the takeoff and cruise nozzles, which may indicate that the flow does not spread significantly for the uninstalled nozzle with the side doors open to the takeoff position.

THRUST REVERSER PERFORMANCE

Because the QCSEE OTW propulsion system is envisioned as being installed forward and above an aircraft wing, a top-mounted thrust reverser similar to that used in the YC-14 STOL aircraft (ref. 11) is an obvious design selection. As shown by the schematic representation of the reverser flow path in figure 16, a single large deflector, or blocker door, directs the combined fan and primary streams upward and forward. A lip on the upper edge of the blocker and skirts on the sides of the blocker further direct the flow forward to increase the reverse thrust performance. This reverser design, which was based on a

Boeing (ref. 11) and NASA (ref. 12) data base, results in ingestion-free engine operation, no foreign object damage due to ground debris, increased wheel loads for additional braking capability, and optimal use of flap drag during ground roll.

Although a target type of thrust reverser is conceptually a simple device, a large number of design parameters affect the performance of the QCSEE OTW propulsion system. Reverser geometry investigated in the QCSEE program (ref. 3) included blocker axial spacing, height, and angle; lip length and angle; and side skirt geometry and angle. To obtain the objective reverse thrust performance, it was necessary to incorporate a longer lip than was used on the YC-14 and to use side skirts, which were not used on the YC-14. The values of the design parameters shown in the figure are the recommended values resulting from the model test program to be discussed next.

Model Test Results

As previously noted, the nozzle design problem was investigated with primarily cut-and-try procedures. In contrast, it was easier to investigate the thrust reverser design problem with a more typical parametric screening test (ref. 3). The results of the model static tests are obtained in a form similar to that indicated in figure 17, where the effects of blocker angle and lip length are demonstrated for fixed values of the other design parameters corresponding to the recommended configuration. Reverse thrust is referenced to takeoff thrust to allow convenient comparison with the objective. Takeoff thrust corresponds to a nozzle pressure ratio of 1.29. Reverse thrust performance is shown for a near takeoff value of pressure ratio, 1.3, and also for a pressure ratio of 1.2, approximately equal to the value specified for landing approach. These results indicated that it was not possible to obtain the objective reverse thrust level (i.e., 35 percent of takeoff thrust) with a practically configured reverser at the lower pressure ratio corresponding to the landing approach throttle setting. It was determined that a pressure ratio closer to that specified for takeoff was required to obtain the objective reverse thrust with a reverser having practical variable geometry features.

Figure 18 shows model reverse airflow performance in a format similar to that used for presentation of reverse thrust. However, in this case, the reference is forward airflow at the same pressure ratio as the reverse thrust. This reference is used to indicate the back pressure effect of the blocker, which reduces the effective exhaust area and causes a predicted reduction in fan stall margin relative to forward thrust operation (ref. 4). The reverse airflow is only about 75 percent of the forward airflow for large blocker or flow deflection angles. The effect of side skirt angle on airflow is relatively small, but the only purpose of the side skirt is to improve reverse thrust by preventing spillage around the blocker door. At a pressure ratio of 1.3, the recommended configuration with a 45° side skirt angle had 20 percent more reverse thrust than that with a 0° side skirt angle (ref. 4).

The model test program also included an investigation of exhaust reingestion effects of airflow and reverse thrust (ref. 3). A shield was placed be-

183

tween the thrust reverser and the fan engine model inlet to ensure that the thrust reverser exhaust was not ingested by the inlet. Comparison of results from this configuration with those from the basic configuration without a shield indicated no differences in airflow or reverse thrust characteristics. Therefore the model tests demonstrated reverser operational capability at static conditions which exceeds the design objective at 5.1 meters per second (10 knots).

Engine Test Results

The recommended thrust reverser configuration with the longer lip was tested with the experimental engine (ref. 10), and the results are shown in figure 19. Airflow and reverse thrust are presented as a function of pressure ratio with the same references as for the model data previously discussed. The objective thrust level was demonstrated at a pressure of about 1.25. At this operating condition, the reverse airflow was about 82 percent of the forward airflow.

A comparison of the engine (ref. 10) and model test results (refs. 3 and 4) indicates that airflow and reverse thrust data differ by only about 3 percent. Because it was not practical to simulate the leakages which exist around the engine blocker, the model blocker was sealed to the side walls of the nacelle, and the effect of leakage on engine reverser performance was predicted from estimated leakage areas and flow coefficients. However, the engine data agree best with the basic model data having no leakage correction. This may be fortuitous or it may be that leakage effects were overestimated.

Finally it should be noted that the reverser airflow performance results in a significant reduction in fan stall margin as predicted. Based on fan performance measurements (ref. 10), the stall margin in reverse is only about 5 percent, in contrast with about 17 percent for forward operation at the same pressure ratio. Although this thrust reverser performance is satisfactory for an experimental engine, some improvement would be required for a production engine. The necessary improvement in area matching for the target type of thrust reverser could be obtained by increasing the fan duct area or by adding forward opening doors in the fan duct, which would improve both thrust and airflow performance. However, these changes could result in a larger or more complex nacelle. Another promising alternative, suggested by a GE study for the NASA Ames Research Center (ref. 13), is a partial emission cascade type of thrust reverser.

CONCLUDING REMARKS

In general, the design objectives for the nozzle and thrust reverser of the QCSEE OTW propulsion system have been achieved. However, because the scope of the program was limited to those design details pertinent to the static demonstration of an experimental engine, significant further development would be required to demonstrate a nozzle and reverser for a flight system. A combina-

tion of model and engine test data have resulted in the following specific conclusions:

1. The nozzle provides excellent jet turning angles and efficiencies for flap angles up to 60° at static and low speed flight conditions. The design emphasis on jet turning performance with high flap angles has resulted in a nacelle shape with unsatisfactory cruise drag characteristics. However, a flight system study indicates that lower flap angles are practical, and, therefore, the nacelle shape can be modified to improve cruise drag.

2. The nozzle side door configuration provided the necessary area variation between takeoff and cruise operation. A back pressure effect on flow caused by installing the nozzle on a simulated wing was partially relieved by the side doors because of lateral spreading of the exhaust jet, but the spreading also resulted in a thrust reduction.

3. A top mounted target-type thrust reverser demonstrated the objective 35 percent of takeoff thrust in reverse operation, but the back pressure effect of the blocker door caused a large reduction in effective exit area. To maintain adequate fan stall margin, the effective exit area would have to be increased for a flight propulsion system.

REFERENCES

1. Armstrong, R.: YC-14 Propulsion Performance and Noise. Presented at Conference on Quiet Powered Lift Propulsion, NASA Lewis Research Center (Cleveland, Ohio), Nov. 14-15, 1978.

2. Phelps, Arthur E., III: Static and Wind-On Tests of an Upper-Surface Blown Jet Flap Nozzle Arrangement for Use on the Quiet Clean Short-Haul Experimental Engine. NASA TN D-8476, 1977.

3. Ammer, Robert C.; and Kutney, John T.: Analysis and Documentation of QCSEE Over-the-Wing Exhaust System Development. NASA CR-2792, 1977.

4. Quiet Clean Short-Haul Experimental Engine Over-the-Wing Final Design Report. (R75AEG443, General Electric Co.; NASA Contract NAS3-18021; Proj. FEDD.) NASA CR-134848, 1977.

5. Wimpress, John K.: Upper Surface Blowing Technology as Applied to the YC-14 Airplane. SAE Paper 730916, Oct. 1973.

6. Meleason, Edward T.: Effects of Nozzle Design and Power on Cruise Drag for Upper-Surface-Blowing Aircraft. Powered-Lift Aerodynamics and Acoustics. NASA SP-406, 1976, pp. 183-196.

7. Wells, O. D.; et al.: Wind Tunnel and Analytical Investigation of Over-the-Wing Propulsion/Air Frame Interferences for a Short-Haul Aircraft at Mach Numbers from 0.6 to 0.78. NASA CR-2905, 1977.

8. Skavdahl, Howard; Wang, Timothy; and Hirt, William J.: Nozzle Development for the Upper Surface-Blown Jet Flap on the YC-14 Airplane. SAE Paper 740469, Apr. 1974.

9. Howard, D. F.: QCSEE Preliminary Over-the-Wing Propulsion System Analysis Report. (R77AEG305, General Electric Co.; NASA Contract NAS3-18021; Proj. FEDD.) NASA CR-135296, 1977.

10. Quiet Clean Short-Haul Experimental Engine Over-the-Wing Propulsion System Test Report. Vol. 2: Aerodynamics and Performance. (R77AEG474-Vol. 2, General Electric Co.; NASA Contract NAS3-18021; Proj. FEDD.) NASA CR-135324, 1978.

11. Grotz, Charles A.: Development of the YC-14 Propulsion System. AIAA Paper 75-1314, Sep. 1975.

12. Falarski, Michael D.: The Aerodynamic and Acoustic Characteristics of an Over-the-Wing Target-Type Thrust Reverser Model. AIAA Paper 76-523, July 1976.

13. Ammer, Robert C.; and Sowers, Harry D.: Thrust Reverser Design Studies for an Over-the-Wing STOL Transport. (R77AEG190, General Electric Co.; NASA Contract NAS2-9254.) NASA CR-151958, 1977.

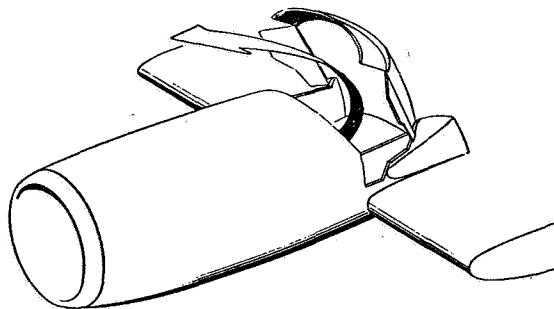# QCSEE OTW NOZZLE

DESIGN OBJECTIVES
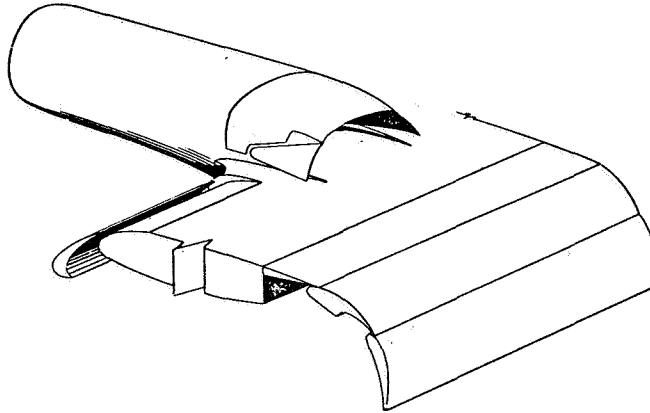
1. REPRESENTATIVE OF A 4-ENGINE AIRCRAFT INSTALLATION, BUT NOT TAILORED TO A SPECIFIC AIRCRAFT DESIGN
2. EXTERNAL FLOW LINES REPRESENTATIVE OF A 0.72 CRUISE MACH NO.
3. UPPER SURFACE FLOW ATTACHMENT FOR ALL FLAP POSITIONS
   A. APPROACH FLAP CHORD LINE ANGLE = 60^0
   B. TAKEOFF FLAP CHORD LINE ANGLE = 30^0
4. ABOUT 25% AREA VARIATION BETWEEN TAKEOFF & CRUISE OPERATION

CS-78-3263

Figure 1

QCSEE OTW THRUST REVERSER

DESIGN OBJECTIVES

1. REVERSE THRUST EQUIVALENT TO 35% OF TAKEOFF STATIC THRUST.
2. OPERATIONAL CAPABILITY DOWN TO 5.1 m/sec (10 KNOTS) WITHOUT EXCEEDING ENGINE LIMITS.

CS-78-3254

Figure 2

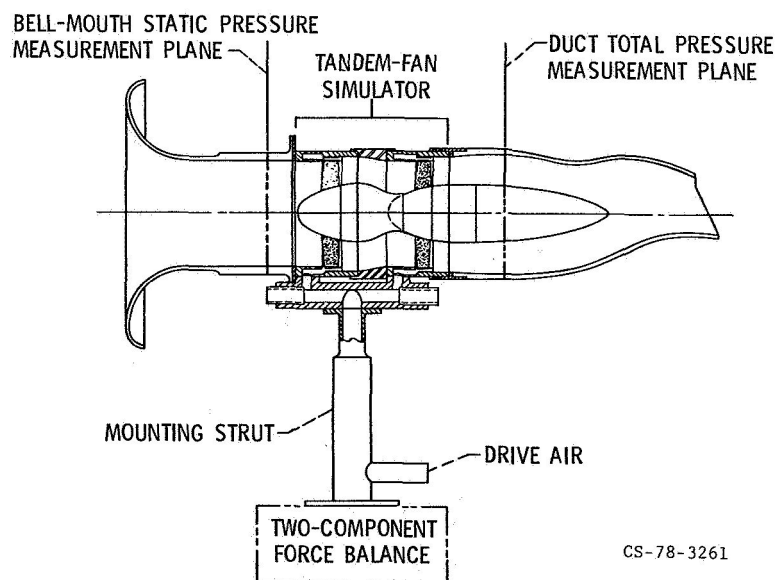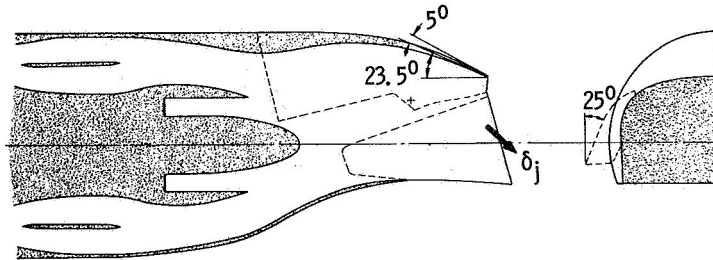# COMPARISON OF QCSEE OTW AND YC14/CF6 NOZZLES

QCSEE OTW

YC14/CF6

10	BYPASS RATIO	4
1.38	FAN PRESSURE RATIO	1.65
28.5	CROWN LINE BOAT TAIL ANGLE, deg	28.5
0.50	CRUISE EXIT AREA/NACELLE AREA	0.32
1.2	EXIT TAKEOFF AREA/CRUISE AREA	1.05
1.9	CRUISE EXIT WIDTH/HEIGHT	3.3
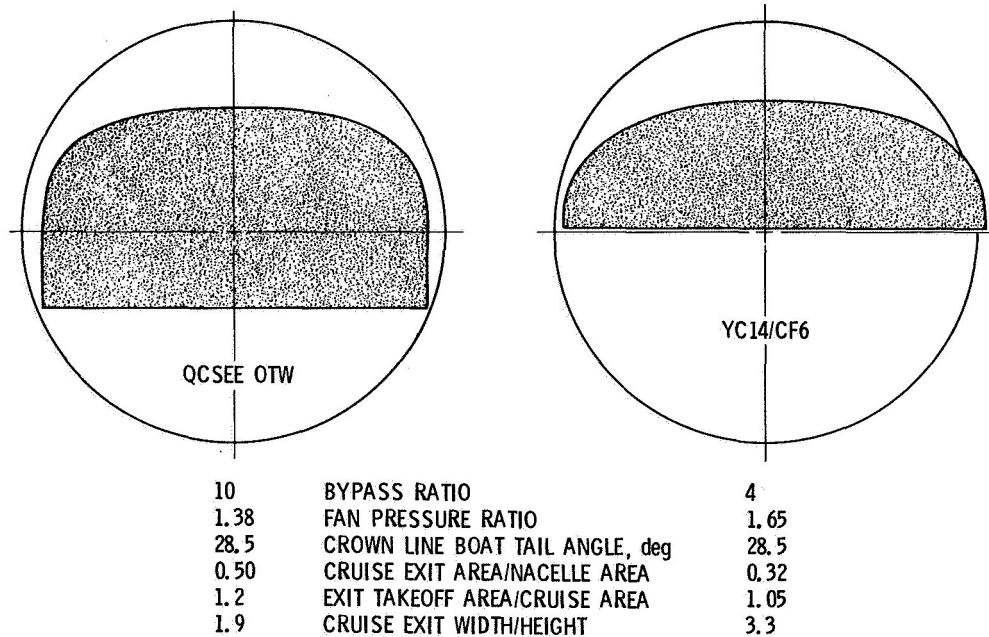
Figure 3

GE/NASA LANGLEY 14 cm (5.5 in.) FAN ENGINE MODEL

BELL-MOUTH STATIC PRESSURE
MEASUREMENT PLANE

TANDEM-FAN
SIMULATOR

DUCT TOTAL PRESSURE
MEASUREMENT PLANE

MOUNTING STRUT

DRIVE AIR

TWO-COMPONENT
FORCE BALANCE

CS-78-3261

Figure 4

188

QCSEE OTW NOZZLE FLOWPATH

UNINSTALLED MODEL PERFORMANCE AT A PRESSURE RATIO OF 1.25

EFFECTIVE TAKEOFF/CRUISE EXIT AREA	EXHAUST FLOW ANGLE, δ_j, deg	
	TAKEOFF	CRUISE
1.20	12.2	7.8

CS-78-3253

Figure 5

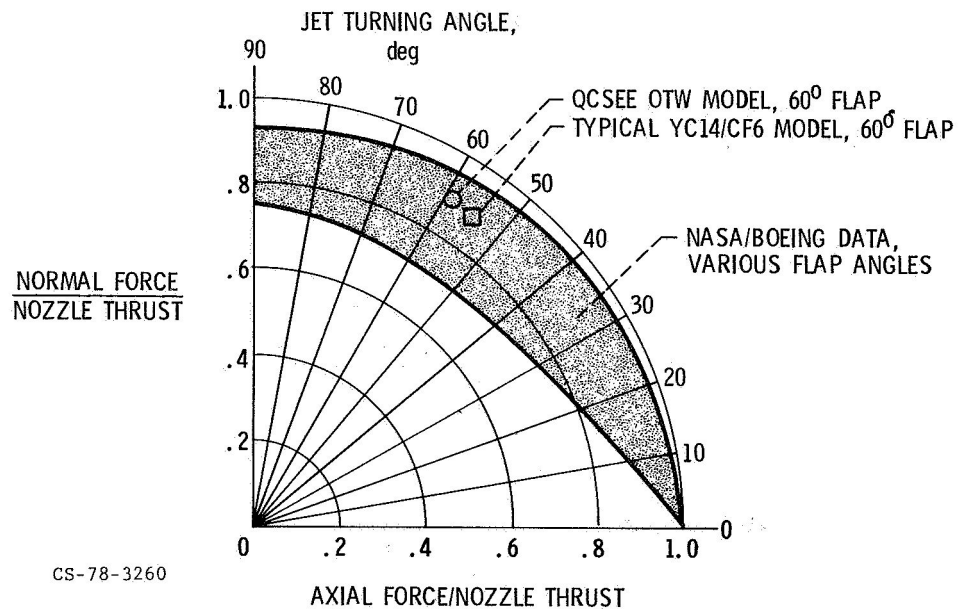# JET STATIC TURNING PERFORMANCE

CS-78-3260

Figure 6

189

QCSEE OTW LOW SPEED AERODYNAMICS MODEL
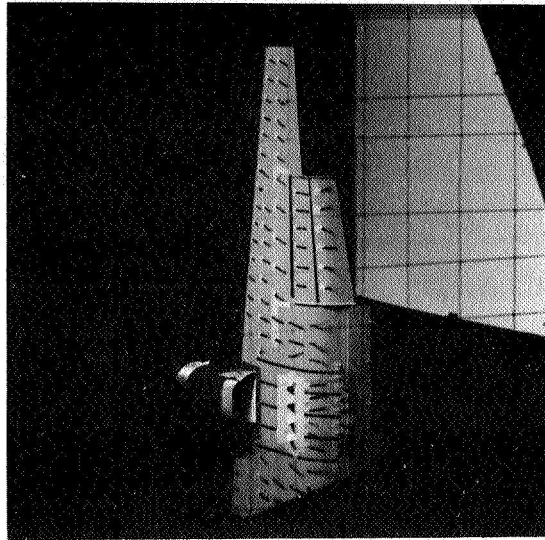
Figure 7

QCSEE OTW NOZZLE/WING PERFORMANCE
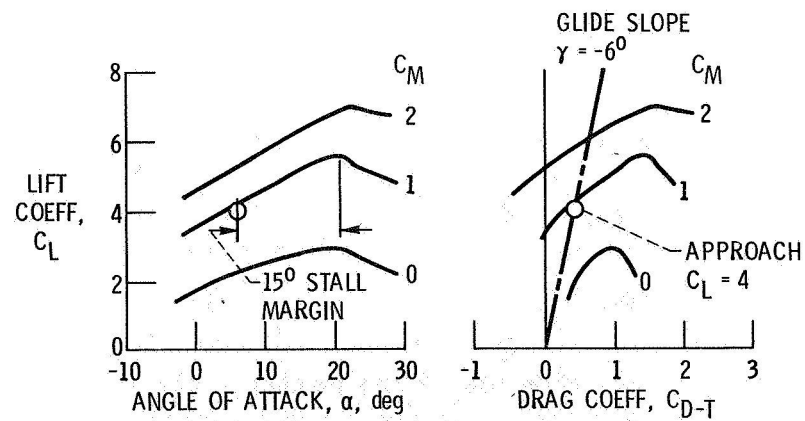### 60° FLAP ANGLE; 25° NOZZLE SIDE DOOR ANGLE;
MOMENTUM COEFF $C_M \equiv$ GROSS THRUST/qS

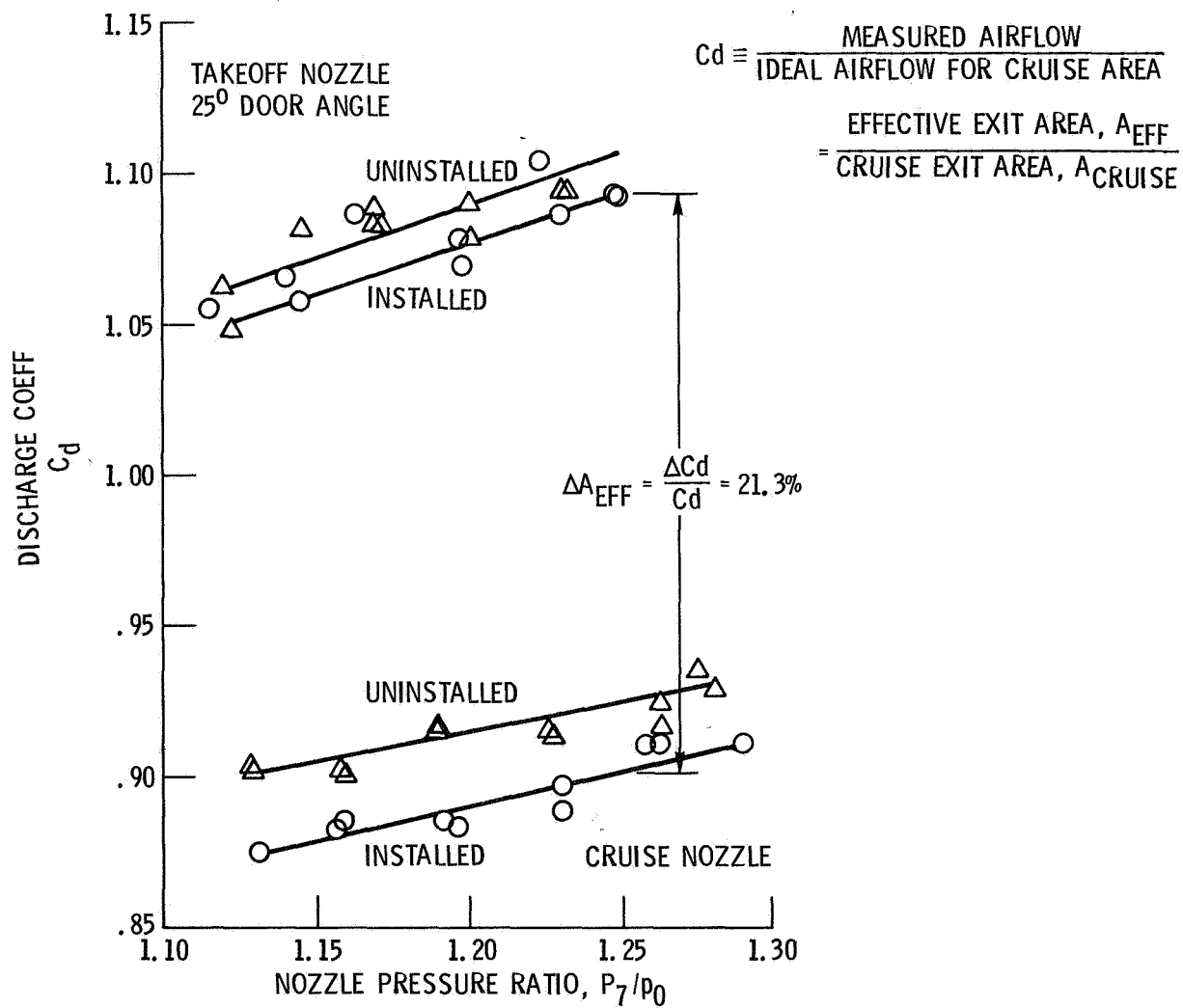

Figure 8

QCSEE OTW MODEL NOZZLE DISCHARGE COEFFICIENTS

$$Cd \equiv \frac{\text{MEASURED AIRFLOW}}{\text{IDEAL AIRFLOW FOR CRUISE AREA}}$$

$$= \frac{\text{EFFECTIVE EXIT AREA, } A_{EFF}}{\text{CRUISE EXIT AREA, } A_{CRUISE}}$$

TAKEOFF NOZZLE
25° DOOR ANGLE

UNINSTALLED

INSTALLED

$$\Delta A_{EFF} = \frac{\Delta Cd}{Cd} = 21.3\%$$

UNINSTALLED

INSTALLED   CRUISE NOZZLE

DISCHARGE COEFF C_d

NOZZLE PRESSURE RATIO, P_7/p_0

Figure 9

191

QCSEE OTW MODEL NOZZLE VELOCITY COEFFICIENTS
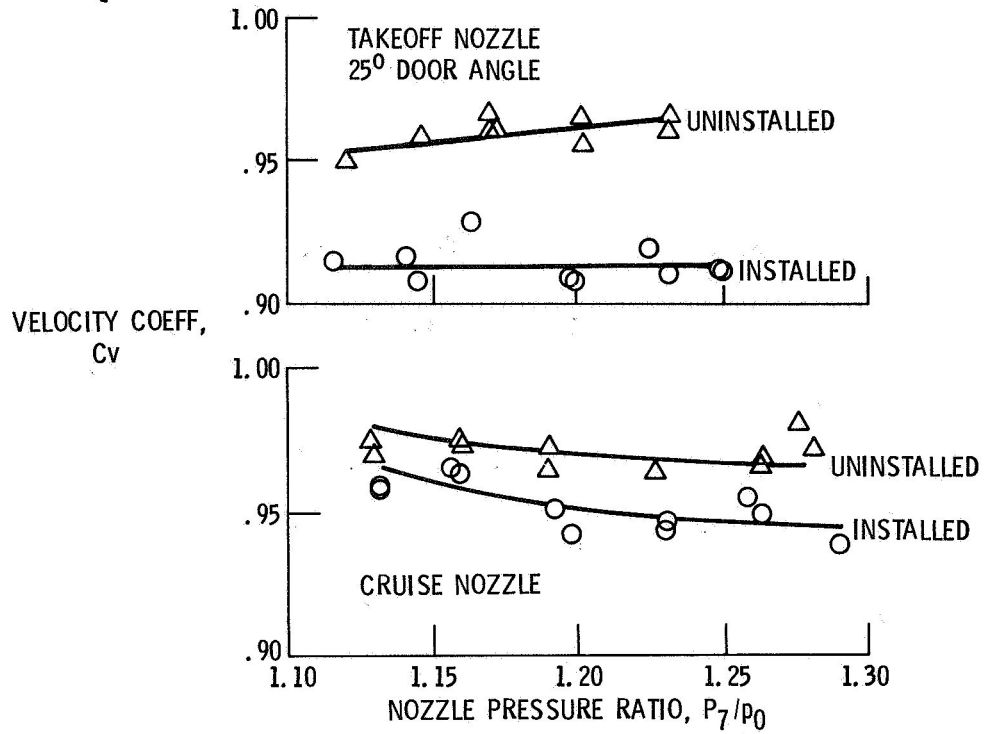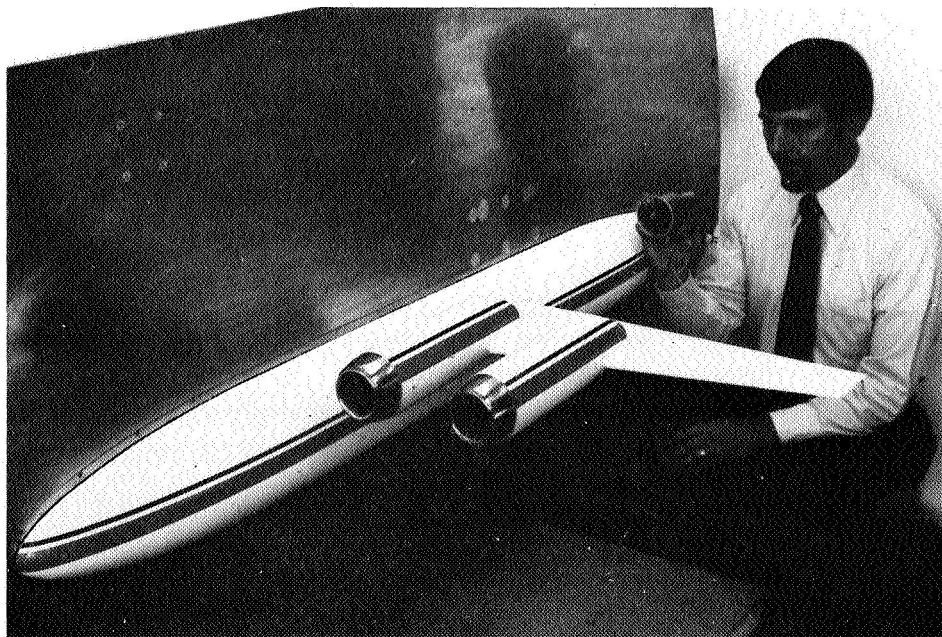

Figure 10

OTW AIRPLANE MODEL FOR CRUISE DRAG EXPERIMENT

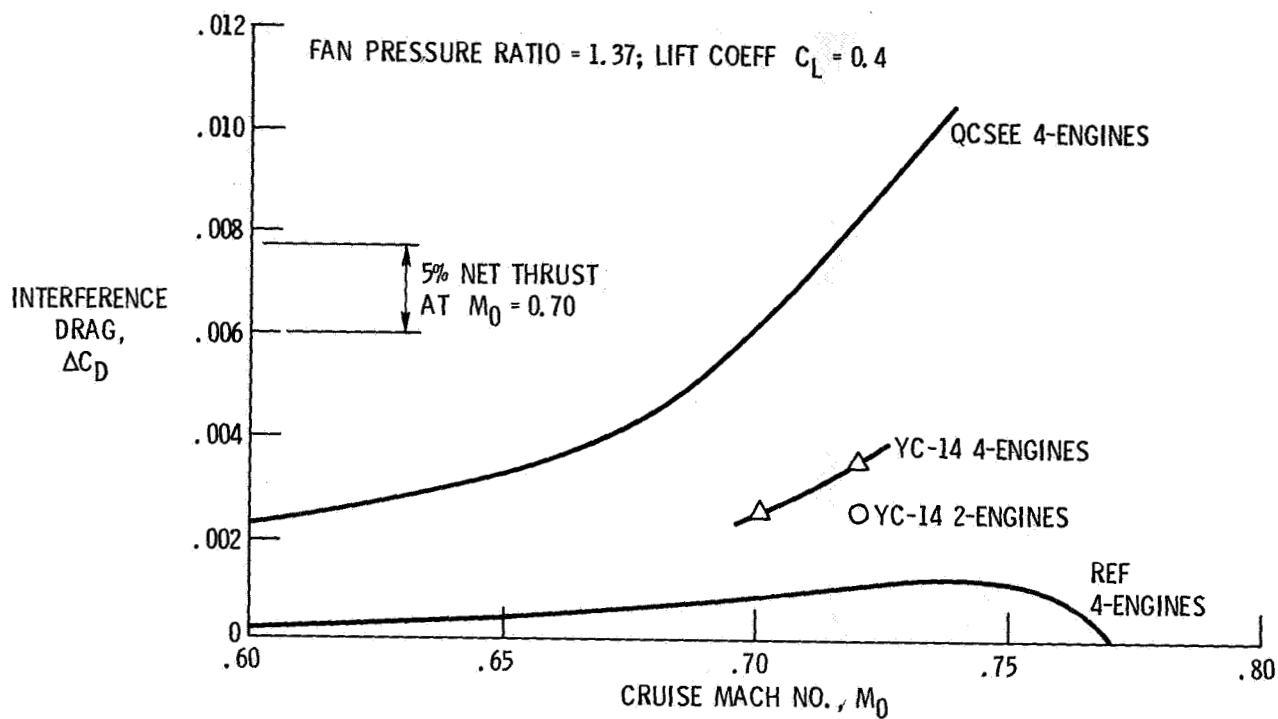Figure 11

192

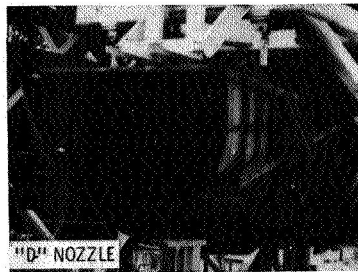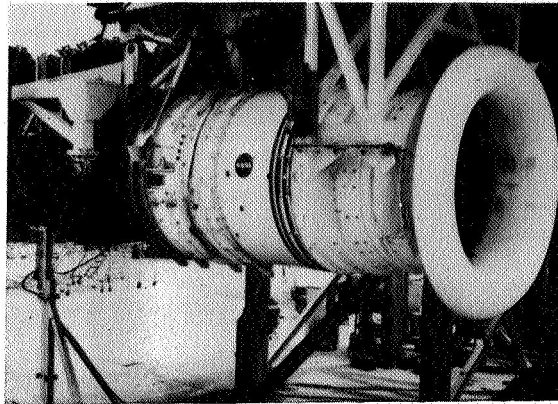# OTW NOZZLE INSTALLATION INTERFERENCE DRAG

Figure 12

CS-77-2302

Figure 13

ENGINE VS MODEL UNINSTALLED
NOZZLE DISCHARGE COEFFICIENTS
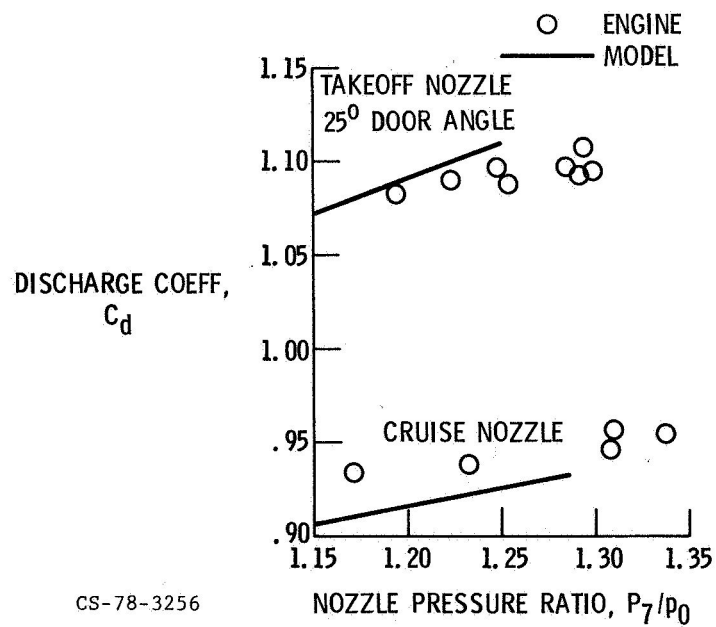
CS-78-3256

Figure 14

194
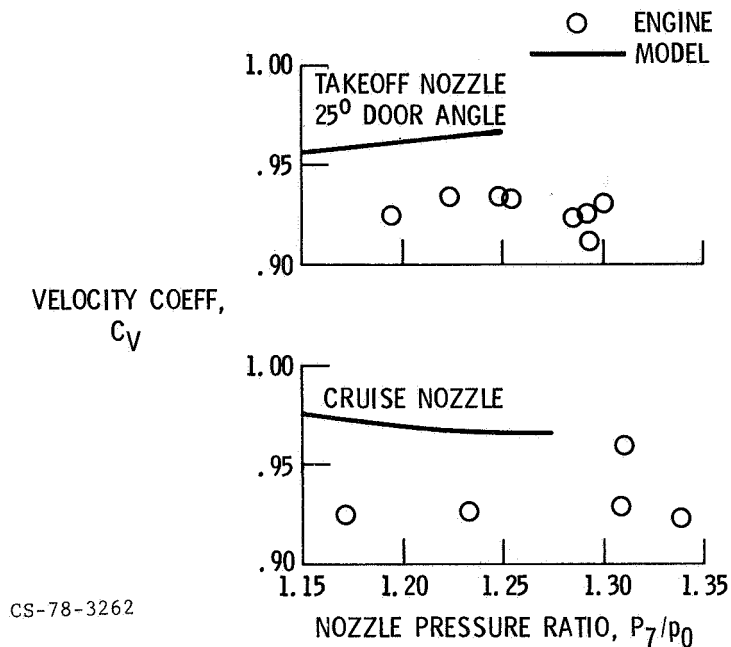
ENGINE VS MODEL UNINSTALLED NOZZLE VELOCITY COEFFICIENTS

Figure 15

QCSEE OTW THRUST REVERSER

BLOCKER

PIVOT $X_P/D_{TH} = 0.865$
SPACING $X_B/D_{TH} = 1.11$
HEIGHT $H_B/D_{TH} = 1.63$
ANGLE $\theta = 105^0$

LIP

LENGTH $L/D_{TH} = 0.4$ TO 0.6
ANGLE $\beta = 25^0$

SIDESKIRT ANGLE $\varphi = 45^0$

SECTION A-A

CS-78-3259
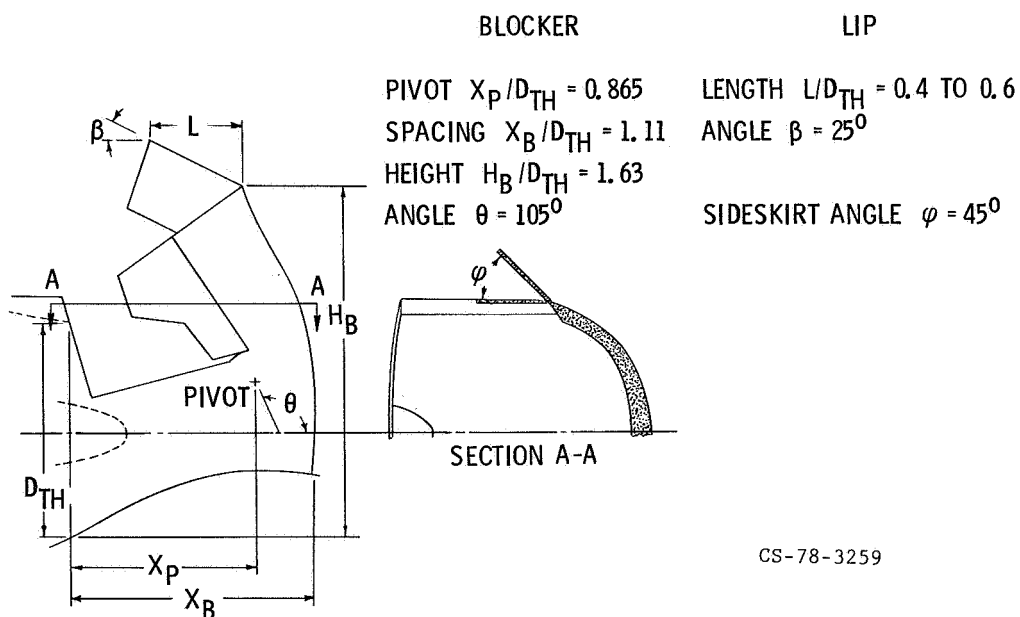
Figure 16

MODEL REVERSE THRUST PERFORMANCE

LIP ANGLE $\beta = 25^0$; PIVOT $X_P/D_{TH} = 0.865$; SIDESKIRT ANGLE $\varphi = 45^0$

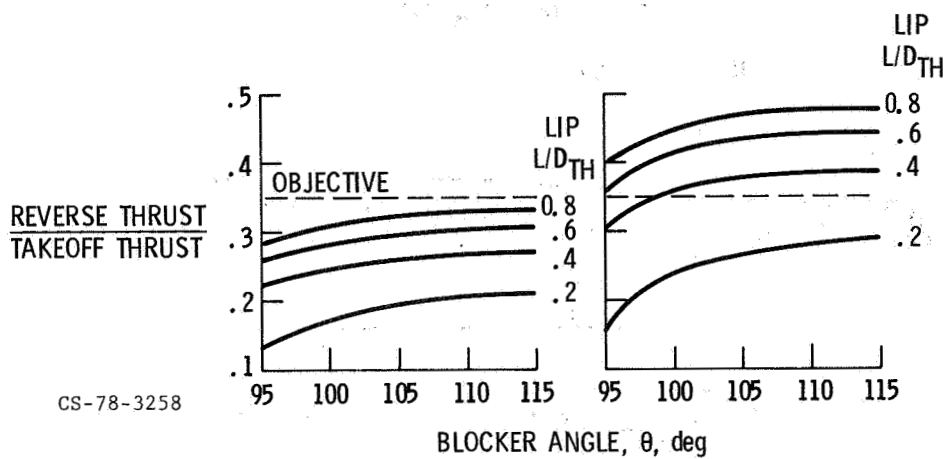PRESSURE RATIO $P_{TH}/p_0 = 1.2$ PRESSURE RATIO $P_{TH}/p_0 = 1.3$

Figure 17

MODEL REVERSE AIRFLOW PERFORMANCE

LIP ANGLE $\beta = 25^0$; PIVOT $X_P/D_{TH} = 0.865$

PRESSURE RATIO $P_{TH}/p_0 = 1.2$ PRESSURE RATIO $P_{TH}/p_0 = 1.3$

Figure 18

196
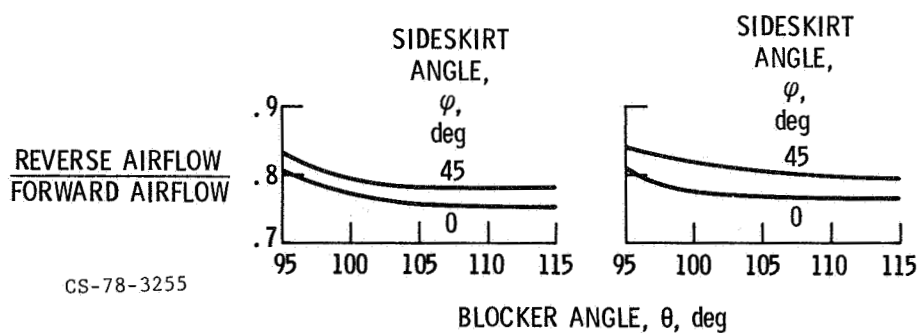
ENGINE VS MODEL THRUST REVERSER PERFORMANCE

RECOMMENDED DESIGN WITH LIP $L/D_{TH} = 0.6$

$\dfrac{\text{REVERSE THRUST}}{\text{TAKEOFF THRUST}}$

$\dfrac{\text{REVERSE AIRFLOW}}{\text{FORWARD AIRFLOW}}$

OBJECTIVE

O   ENGINE
———   MODEL WITH LEAKAGE PREDICTION
— — —   MODEL WITH NO LEAKAGE

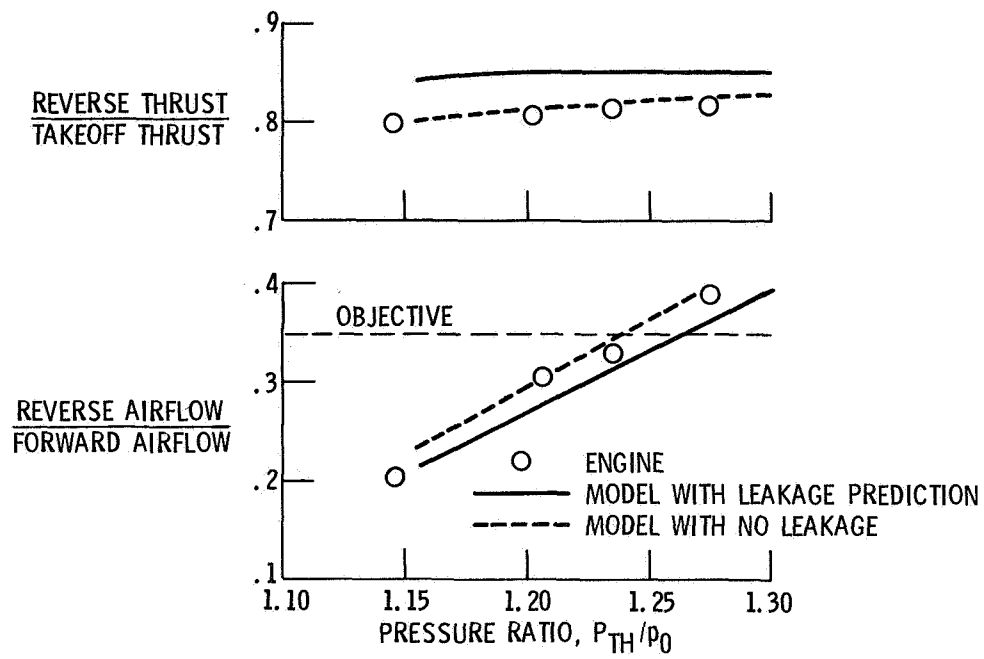PRESSURE RATIO, P_{TH}/P_0

Figure 19

197

QCSEE ACOUSTIC DESIGN*

D.L. Stimpert
General Electric Company
Cincinnati, Ohio

SUMMARY

Overall program goals for the Quiet Clean Short-haul Experimental
Engine (QCSEE) program have been discussed in earlier papers. The program
included the design, development, and static testing of two separate engine
systems, one for an under-the-wing (UTW) application and one for an over-
the-wing (OTW) application. Both engines were designed to meet stringent
noise goals and had many features incorporated specifically to reduce noise.

This paper is intended to give an overview of the general acoustic de-
sign procedures and the specific acoustic features on each engine. Since
the final design selection was based upon component and model tests, these
will also be reviewed briefly. System noise level estimates for a four-
engine powered lift aircraft powered by the QCSEE engines will be presented
and compared to the noise goals.

INTRODUCTION

A schematic showing the QCSEE noise objectives is presented in figure 1.
These objectives are for a four-engined aircraft operating in the powered-
lift mode out of a 610 m (2000 ft.) long runway. The noise levels are
those that would be heard by an observer on a 152 m (500 ft.) sideline
parallel to the runway centerline. At takeoff, the noise goal was 95 EPNdB
with the engines at 100 percent thrust and on a 12.5 degree flight path.
Under approach conditions, with the engines developing 65 percent of takeoff
thrust, and the aircraft on a 6 degree glide path, the goal was also 95
EPNdB. After touchdown on the 610 m (2000 ft.) runway, with the engines
developing reverse thrust which is 35 percent of takeoff thrust, the noise
goal was 100 PNdB on the 152 m (500 ft.) sideline. These noise objec-
tives were very challenging which can be seen more clearly by examination
of figure 2. This figure shows the relative decrease in EPNL over the
years for the older narrowbody aircraft, current widebody, next generation
widebody, and finally an Energy Efficient Engine (E^3) powered aircraft.
QCSEE powered aircraft that meet the 95 EPNdB goal are about 10 EPNdB
below the next generation aircraft.

199

These stringent noise goals meant that any noise source on the engine which had the potential for contributing to the farfield had to be evaluated. The sources which were considered are listed below:

o   Fan inlet radiated noise
o   Fan exhaust radiated noise
o   Turbine noise
o   Combustor noise
o   Jet/flap noise
o   Compressor noise
o   Gear noise
o   Treatment regenerated flow noise
o   Strut noise
o   Splitter trailing edge noise

The design procedure for each noise constituent was to estimate the level by scaling existing test data from similar fan and core engines or by using the latest analytical techniques available. These estimated levels were then extrapolated to a simulated flight condition of 61 m (200 ft.) altitude, 152 m (500 ft.) sideline. Pre-contract studies had indicated that maximum noise levels would occur with the aircraft at 61 m (200 ft.) altitude during either takeoff or approach. As an example, the predicted unsuppressed fan exhaust radiated noise spectrum for the UTW engine at takeoff is shown in figure 3. This spectrum was then noy-weighted to determine the frequencies at which suppression or source noise reduction techniques should be applied to provide the most acoustic benefit. It can be seen that the second harmonic tone requires more reduction than the blade passing frequency and that after noy-weighting, treatment should be tuned to 2500 to 3150 Hz to provide the best broadband suppression.

A similar procedure was followed for each potential noise source for each of the three operating conditions. After several iterations, levels of suppression which were required to meet the noise goals were established. Test and component programs were then conducted to verify not only that the required levels of suppression could be achieved, but also that the basic source noise (unsuppressed) levels were correct. System noise levels were updated and revised continuously as new data became available.

ENGINE ACOUSTIC FEATURES

Before discussing the component tests which led to the treatment designs, the basic acoustic features on each engine will be reviewed. These acoustic features can be divided into two main categories - those dealing with reduction of the source itself and those dealing with the reduction of noise after it has been generated.

UTW features are shown in figure 4. A low pressure ratio fan was selected primarily to keep jet/flap interaction noise as low as possible by reducing the fan bypass exit velocity. This low pressure ratio also aided in keeping exhaust radiated fan noise levels low. The fan has a subsonic tip speed of 290 m/sec (950 ft/sec) at takeoff which eliminated high noise levels from multiple pure tones associated with supersonic tip speed fans. A wide rotor-stator spacing of 1.5 rotor tip chords was selected to lower rotor stator interaction noise. Additional reduction could have been achieved with wider spacing; however, an acoustic splitter could achieve the reduction with less weight penalty than that associated with a fan frame weight increase due to wider spacing. The vane-blade ratio of 1.83 was selected based upon the analysis presented in reference 1. This vane-blade ratio minimized propagation of the UTW fan second harmonic tone which makes a major contribution to the noy-weighted spectrum.

A 'high throat Mach number (0.79) inlet was used to suppress inlet radiated fan noise at takeoff with wall treatment having a length equal to 0.74 fan diameters added to provide suppression at approach and in reverse thrust.

Fan exhaust suppression utilized inner and outer wall suppression with variable depth, variable porosity treatment sections to provide wide suppression bandwidth. Preliminary design studies indicated that wall treatment alone would not achieve sufficient suppression in the length allowable; therefore, a 1.02 m (40 in.) acoustic splitter was added to provide the required exhaust suppression. Mach number in the fan exhaust duct was limited to 0.47 to minimize strut noise, treatment regenerated noise, and splitter trailing edge noise. Treatment was added to the core inlet to suppress high frequency compressor tones. Fan frame treatment consisted of wall treatment to suppress fan blade passing frequency tones and treatment on the pressure surface of the outlet guide vanes (OGV's) to attenuate high frequency fan broadband noise.

The single-degree-of-freedom (SDOF) treatment that was specified on the UTW was an integral part of the support and load carrying structure of the composite nacelle.

The engine utilized a "stacked" treatment core suppressor which was designed to attenuate both low frequency combustor noise and high frequency turbine noise.

In order to maintain commonality, the OTW engine shown in figure 5 utilized essentially the same composite fan frame design as the UTW. With the 33 vanes and 28 fan blades, the OTW vane blade ratio is a low 1.18. This low vane-blade rato was a departure from our usual design practice of having a vane-blade ratio value near two to achieve cutoff of rotor-stator interaction noise. It was felt that the wide spacing of 1.93 rotor tip chords for the OGV/fan rotor would reduce rotor-stator interaction noise to the point where it would not be a major contributor and thus there was no need for an "overskill" by selecting a high vane-blade ratio.

Other acoustic features on the OTW are very similar to the UTW including the treated vanes, "stacked" core treatment, variable depth and variable porosity fan exhaust wall treatment, 1.02 m (40 in.) acoustic splitter, and high throat Mach number inlet. At approach and reverse thrust, the OTW inlet provides suppression with bulk absorber wall treatment. For more details into the acoustic design of both engines, the reader is referred to references 2 and 3.

FAN INLET DESIGN

Preliminary system studies conducted on both engines indicated that achieving a balanced design would require the following levels of inlet PNL suppression:

	UTW (PNdB)	OTW (PNdB)
Takeoff	12.8	13.5
Approach	6.3	10.4
Reverse Thrust	4.5	11.5

These high levels of required suppression could be achieved with a conventional inlet; however, with wall treatment only, the treated length to diameter ratio would be much greater than 1.0 and/or inlet splitters would be required. Previous experience had shown that large levels of inlet suppression could be achieved from high throat Mach number inlets. As shown in figure 6, which compares inlet reduction concepts, takeoff suppression can be achieved with a treated high throat Mach number inlet. At approach and reverse thrust, suppression is achieved with the wall tratment only since the inlet Mach number is much lower.

In order to demonstrate that the high levels of inlet suppression could be achieved, a scale model test program was conducted in the General Electric Anechoic Chamber shown in figure 7. The anechoic chamber can handle models for inlet radiated noise studies as shown in figure 7 or exhaust radiated noise as will be discussed later. The models are powered by a 1.86 megawatt (2500 horsepower) drive system. Physical dimensions of the chamber are approximately 10.7 m (35 ft.) long by 7.6 m (25 ft.) wide by 3 m (10 ft.) high with microphones located at model centerline height on a 5.2 m (17 ft.) arc.

An exact scale model of the UTW fan was used for these studies. It was 50.8 cm (20 in.) in diameter and could be manually adjusted for various blade angles including those required to demonstrate reverse thrust. Test objectives are summarized below:

Forward Thrust

o   Define unsuppressed spectrum and level
o   Define suppression due to high throat Mach number
o   Define suppression due to treated wall

Reverse Thrust

o   Define unsuppressed spectrum and level
o   Define suppression due to treated wall

Details of the test and a tabulation of the data are presented in references 4 and 5; however, a few of the important results will be discussed here. Figure 8 presents the variation in inlet noise with throat Mach number and the PNL suppression that was achieved. These results indicate that the UTW takeoff suppression requirement of 12.8 PNdB could be met at an average throat Mach number of 0.79. The suppression due to high Mach number alone was about 10 PNdB with the wall treatment adding almost 3 PNdB.

In reverse thrust, the model tests indicated, as shown in figure 9 that the objective level of suppression could be achieved; however, the unsuppressed levels were higher than expected. As will be shown later, this fact resulted in the UTW system noise estimate in reverse thrust being revised to be above the goal of 100 PNdB.

Both inlets as finally designed are shown schematically in figure 10 and are high throat Mach number inlets designed to achieve takeoff suppression at a 0.79 throat Mach number. The treated length to diameter ratio was 0.74 for both inlets. Wall treatment utilized on the inlets is shown schematically in figure 11. The UTW utilized single-degree-of freedom resonator treatment with a faceplate porosity of 10 percent and cavity depths ranging from 1.2 cm (0.5 in.) to 3.8 cm (1.5 in.). A bulk absorber type treatment was incorporated into the OTW inlet to provide wider bandwidth suppression. The bulk absorber consisted of seven compressed layers of a Kevlar material. It was a constant depth of 2.54 cm (1 in.) with porosity of 14 percent over the first half and 22 percent over the latter half. Although a scale model of the OTW fan was not tested, the inlet design was based upon General Electric experience from previous tests and consideration of the results of the UTW model tests.

FAN EXHAUST DESIGN

As was pointed out earlier in figures 4 and 5 the engine designs incorporated both source noise reduction techniques and signficant amounts of acoustic treatment to reduce exhaust radiated noise. Source noise reduction techniques and treatment configurations were evaluated on the basis of past

experience and tests (ref. 6 and 7) of a low pressure ratio, variable pitch model fan (NASA Rotor 55) in the General Electric Company Anechoic Chamber. A photograph of the model as installed in the exhaust mode is shown in figure 12. Testing evaluated such source noise reduction concepts as optimizing vane-blade ratio to minimize second harmonic tone propagation, rotor-stator spacing, and rotor-OGV treatment.

The vane-blade ratio study was conducted at two different rotor-stator spacings. As shown in figure 13, the data at 0.5 chord spacing indicates a second harmonic SPL minimum at a vane-blade ratio of 1.88. At the wider spacing of 1.5 chords the data do not show this because the rotor-stator interaction noise is masked by rotor-turbulence noise caused by turbulence generated upstream of the rotor. At the close spacing, rotor-stator noise is dominant allowing us to see the second harmonic minimum and thus verifying the analysis made by Mani in reference 1.

A series of spacing tests from 0.5 chords to 2.0 chords was conducted. The results are shown in figure 14 which is a comparison between the measured levels and the sum of predicted rotor-stator interaction noise and rotor-turbulence noise at each spacing. This was done at the optimum vane-blade ratio. Excellent agreement between predicted and measured data is evident.

Tests of treatment between the rotor and OGV indicated that 4 to 5 dB suppression could be achieved at the blade passing frequency. Accordingly, the engine fan frame was designed to incorporate rotor-OGV treatment.

The model fan in the exhaust mode had the capability to test up to four axial sections of treatment. Various combinations of faceplate porosity, treatment depths, and axial deployment were evaluated. Suppression results from one of those configurations are presented in figure 15. Note the axial variation in treatment depth and faceplate porosity. The results indicate that such an orientation achieves higher suppression above the peak tuning frequency than one would predict from summing the suppression of the individual panels. On the basis of these results, our design curves for the engines were changed to account for this higher level of suppression with variable depth, variable porosity treatment.

A schematic of the exhaust treatment design for the UTW is presented in figure 16. OTW engine exhaust treatment was very similar (see ref. 2 and 3 for more details). All the suppression material was a single-degree-of-freedom resonator type which is shown in figure 17. Fan frame treatment between the rotor and OGV was tuned to the blade passing frequency of each engine and had a faceplate porosity of 10 percent. Fan bypass wall treatment depths varied from 1.9 cm (0.75 in.) to 5.1 cm (2.0 in.) and porosities from 15 to 22 percent. Specific length of 1.02 m (40 in.) included single-degree-of-freedom treatment of 1.27 m (0.5 in.) with a porosity of 11.5 percent. Although a scale model test with treated vanes was not conducted, design studies indicated a potential for reducing high frequency broadband noise and thus the pressure surface of the OGV's was treated on the full

scale engines. The resulting suppression spectrum for the UTW aft radiated fan noise utilizing the treatment of figure 16 is shown in figure 18. Such a suppression spectrum would achieve 13.4 PNdB of aft fan noise suppression at takeoff on the UTW.

CORE SUPPRESSOR DESIGN

The QCSEE core exhaust provides a rather severe problem in acoustic suppression design. The unsuppressed source noise spectrum has both high frequency broadband turbine noise and low frequency broadband noise from the combustor. To attain any meaningful noise reduction, the suppressor must attenuate both the high and low frequency noise levels. Physical constrdints on the engine prevented sufficient amounts of thick (low frequency) and thin (high frequency) treatment from being installed in tandem to give adequate suppression. It was decided to adopt a new concept as shown in figure 19 and employ a "stacked" treatment design. In this concept the thin treatment is placed along the duct walls. Thick combustor treatment is then placed behind this turbine treatment and communicates to the duct by means of tubes passing through the turbine treatment. Figure 20 shows the treated QCSEE core plug. Note the larger diameter holes which communicate to the combustor treatment.

A model of this advancec concept was built and tested in the General Electric High Temperature Duct Facility. Results from these tests are shown in figure 21 and indicated that the stacked treatment would provide the required levels of suppression of 5.1 and 9.8 PNdB in the low and high frequency regimes. Reference 8 details more of the design philosophy and test results on the stacked treatment.

QCSEE UTW SYSTEM NOISE PREDICTIONS

Since the engine noise levels are to be measured during static testing, a procedure for determining in-flight noise levels from static data was established as a part of this contract. This procedure, given in Appendix A of reference 9, establishes the following:

o   Jet/flap noise calculation procedure
o   Extrapolation procedures
o   Correction for engine size
o   Doppler shift corrections
o   Correction for number of engine
o   Dynamic effect correction
o   In-flight clean-up angle correction
o   Relative velocity correction for jet/flap noise
o   Fuselage shielding and OTW wing shielding
o   PNL to EPNL calculation

Jet/flap noise as calculated from reference 10 was used to replace the jet noise on the static engine; however, an advanced technology allowance was assumed on jet/flap noise of 3.5 PNdB on the UTW and 2.5 PNdB on the OTW to account for anticipated reduction in jet/flap noise by the 1980's when QCSEE powered aircraft might by flying.

System noise levels for the QCSEE UTW engine shown in figure 22 are presented in figure 23 at the takeoff condition. Unsuppressed noise is dominated by the fan in both the forward and aft quadrants. The suppressed levels are balanced between fan, jet/flap, and combustor noise in the aft quadrant and dominated by jet/flap noise in the forward quadrant. The predicted EPNL for the four-engine UTW configuration at takeoff is 93.6 EPNdB compared to the goal of 95.0 EPNdB on a 152 m (5090 ft. sideline).

To obtain 65 percent of takeoff thrust at approach, the QCSEE UTW engine with its variable pitch fan may be operated over a range of fan speeds, blade pitch angles, and nozzle area combinations. For these acoustic predictions, the fan speed was held at a takeoff speed to minimize engine response time in the event of a waveoff during landing. Fan nozzle area was wide open to a lower jet velocity and hence jet/flap noise, and the blade pitch angle was closed down to give the required thrust. In such a mode of operation, unsuppressed noise in figure 24 is dominated by fan noise in both forward and aft quadrants. Suppressed, the forward quadrant is dominated by fan noise while the aft quadrant has a balanced design with fan, combustor, and jet/flap noise about the same level. Estimated EPNL for approach is 93.3 compared to our goal of 95.0 EPNdB.

In reverse thrust, shown in figure 25, the UTW noise levels are dominated by the forward quadrant fan noise both unsuppressed and suppressed. These levels based on the 50.8 cm (20 in.) model tests indicate that in reverse thrust the engine will be 103.9 PNdB on a 152 m (500 ft.) sideline or 3.9 PNdB over the goal of 100 PNdB. It would be difficult to obtain further fan inlet suppression without degrading the suppression at takeoff and approach and eroding the margin present at those conditions. This treated composite nacelle design provides the most balanced approach to meeting the three noise goals.

QCSEE OTW SYSTEM NOISE

System noise levels for the QCSEE OTW engine shown in figure 26 were also predicted. At takeoff (shown in figure 27) unsuppressed fan noise controls forward and aft quadrants. In the suppressed configuration, fan and jet/flap noise are about the same level. The resulting system EPNL is 95.4 EPNdB, only slightly above the goal of 95. Any reduction to lower the level to 95.0 EPNdB must include jet/flap noise reduction since it is a major contributor.

At approach in figure 28 fan suppression has lowered the dominant un-
suppressed fan noise to the level of jet/flap noise. These two sources,
suppressed fan and jet/flap, combine to give a predicted EPNL of 90.0 EPNdB
which is well under the goal of 95.0.

For the reverse thrust operation, the OTW engine utilized a target re-
verser which is shown deployed in figure 29. Although not discussed earlier,
General Electric has conducted tests on a 1/6 scale model of the OTW target
thrust reverser system (reference 11). On the basis of these tests it was
realized that the jet noise levels of the target reverser were much higher
than anticipated and that only a reduction in fan pressure ratio was likely
to produce a signficant reduction in reverse thrust noise. With this in
mind, the predicted OTW reverse thrust noise level in figure 30 is 106.4
PNdB or 6.4 PNdB above the goal.

CONCLUDING REMARKS

The QCSEE acoustic design was based on consideration of ten separate
noise constituents on each engine. Both engines incorporated low noise
features such as:

   o   Low pressure fans
   o   High throat Mach number inlets with treatment
   o   Bulk absorber inlet treatment
   o   Treated outlet guide vanes
   o   Vane-blade ratio selection to minimize UTW second
        harmonic tone noise
   o   "Stacked-treatment" core suppressor
   o   Low Mach number exhaust duct
   o   Acoustic splitter

The predicted noise levels and constituent suppression were based upon
various engine scale model tests and a number of laboratory flow duct
tests, most of which were performed as part of the QCSEE program.

REFERENCES

1. Mani, R., "Discrete Frequency Noise generation from an Axial Flow Fan Blade Row," Paper 69-GE-12, ASME, presented at Applied Mechanics and Fluids Engineering Conference, June 16-18, 1969.

2. Sowers, H.D., "Quiet Clean, Short-Haul, Experimental Engine (QCSEE) Under-the-Wing (UTW) Engine Acoustic Design," NASA Contract Report 135267, January 1978.

3. Sowers, H.D., "Quiet Clean, Short-Haul Experimental Engine (QCSEE) Over-the-Wing (OTW) Engine Acoustic Design," NASA Contractor Report 135268, June 1978.

4. Bilwakesh, K.R., Clemons, A., Stimpert, D.L., "Quiet Clean, Short-Haul Experimental Engine (QCSEE) Acoustic Performance of a 50.8 cm (29 in.) Diameter Variable Pitch Fan and Inlet," Volume I, NASA Contractor Report 135117, to be published.

5. Bilwakesh, K.R., Clemons, A., Stimpert, D.L., "Quiet Clean Short-Haul Experimental Engine (QCSEE) Acoustic Data," NASA Contractor Report 135118, to be published.

6. Stimpert, D.L., McFalls, R.A., "Demonstration of Short-Haul Aircraft Aft Noise Reduction Techniques on a Twenty Inch (50.8 cm) Diameter Fan," Volume I, NASA Contractor Report 134849, April 1975.

7. Stimpert, D.L., Clemons, A. "Acoustic Analysis of Aft Noise Reduction Techniques Measured o a Subsonic Tip Speed 50.8 cm (20 in.) Diameter Fan," NASA Contractor Report 134891, January 1977.

8. "Quiet Clean, Short-Haul Experimental Engine (QCSEE) Acoustic Treatment Development and Design," NASA Configuration Report 135266, to be published.

9. "Quiet Clean, Short-Haul Experimental Engine (QCSEE) Preliminary Analyses and Design Report," Volumes I and II, NASA Contractor Reports 134838 and 134839, October 1974.

10. Clark, B.J., and Dorsch, R.G., "Flap Noise Prediction Method for a Powered Lift System," AIAA Paper 73-102B, October 14, 1973.

11. Stimpert, D.L., "Quiet Clean, Short-Haul Experimental Engine (QCSEE) Acoustic and Aerodynamic Tests on a Scale Model Over-the-Wing Thrust Reverser and Forward Tnrust Nozzle," NASA Contractor Report 135254, January 18, 1978.

QCSEE Acoustic Objectives

- **4 Engines**
- **400 KN (90,000 lbs)**
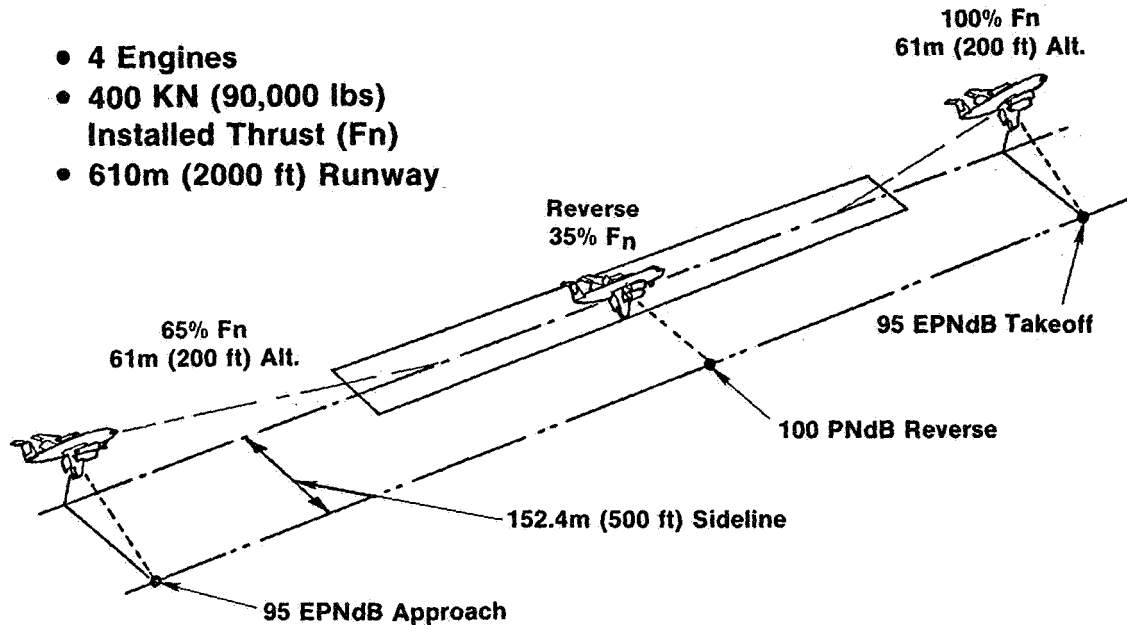 **Installed Thrust (Fn)**
- **610m (2000 ft) Runway**

100% Fn
61m (200 ft) Alt.

Reverse
35% Fn

65% Fn
61m (200 ft) Alt.

95 EPNdB Takeoff

100 PNdB Reverse

152.4m (500 ft) Sideline

95 EPNdB Approach

Figure 1

Aircraft Noise Trends

Relative
EPNL, EPNdB

Narrowbody-Turbofans

Widebody-Turbofans

E³ Aircraft

New Generation Widebody

QCSEE

+10
+5
0
-5
-10
-15

1960   1970   1980   1990
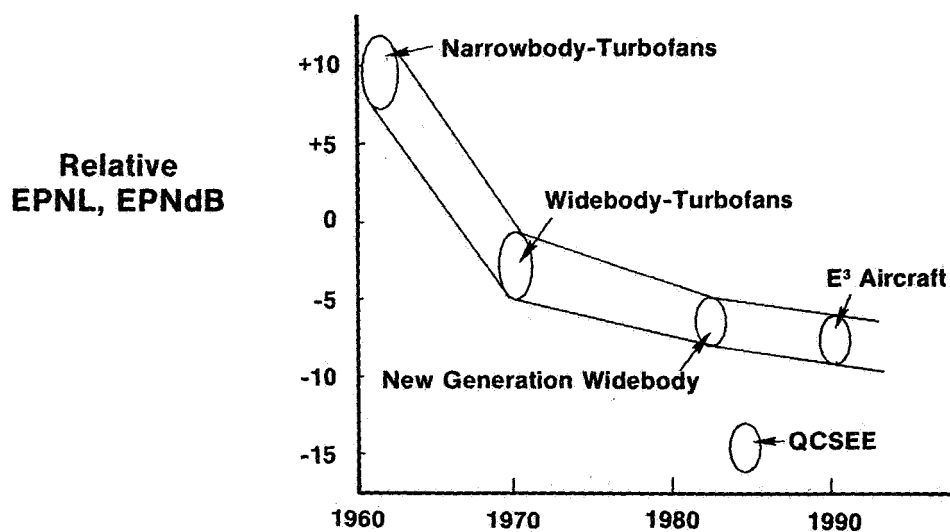
Figure 2

Unsuppressed Fan Exhaust Spectra

- **152m (500 ft) Sideline**
- **61m (200 ft) Altitude**
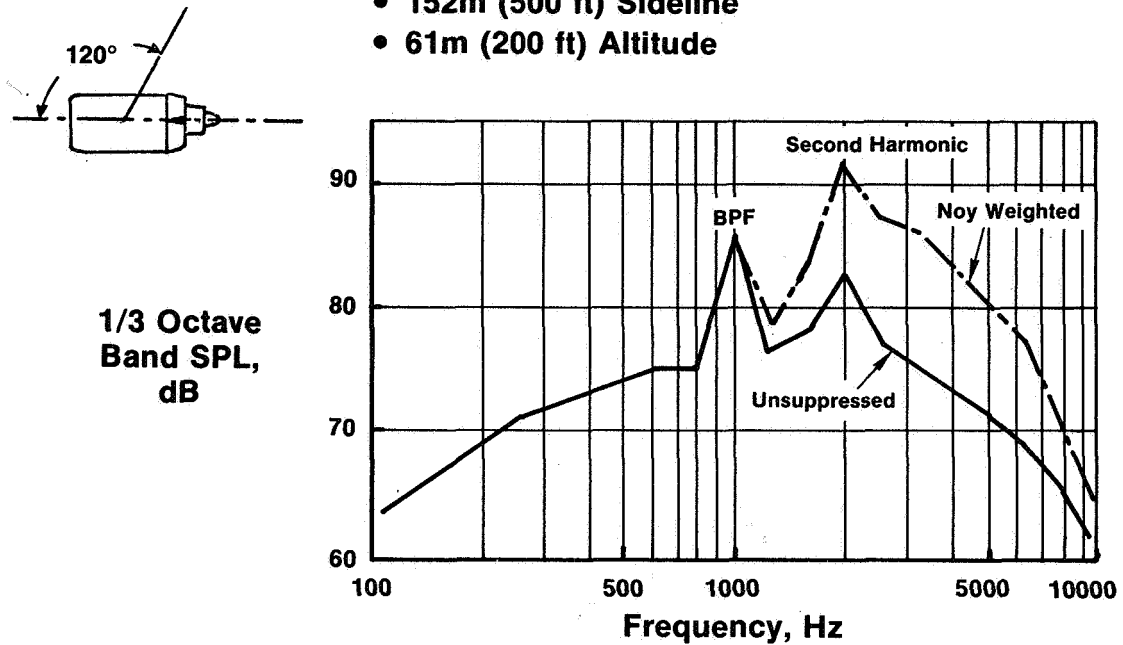
Figure 3

QCSEE UTW Engine Acoustic Features

- **p/p = 1.27**
- **Tip Speed = 290m/sec (950 ft/sec)**
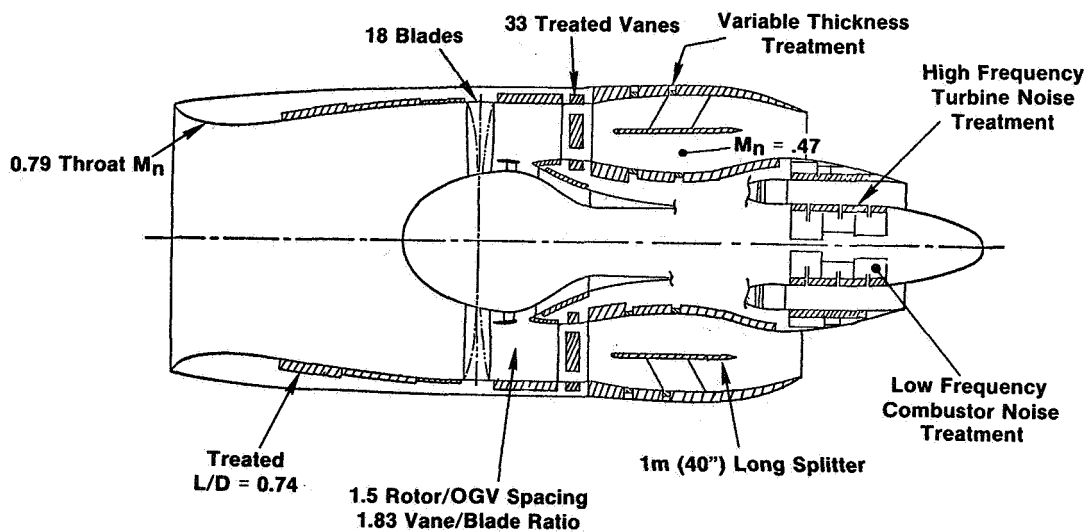
Figure 4

QCSEE OTW Engine Acoustic Features

- p/p = 1.34
- Tip Speed = 350m/sec (1150 ft/sec)

Bulk Absorber Treated L/D = 0.74

33 Treated Vanes

Variable Thickness Treatment

High Frequency Turbine Noise Treatment

M_n = .47

.79 Throat Mach No.

28 Rotor Blades

1.93 Rotor/OGV Spacing
1.18 Vane/Blade Ratio

1m (40") Long Splitter

Low Frequency Combustor Noise Treatment
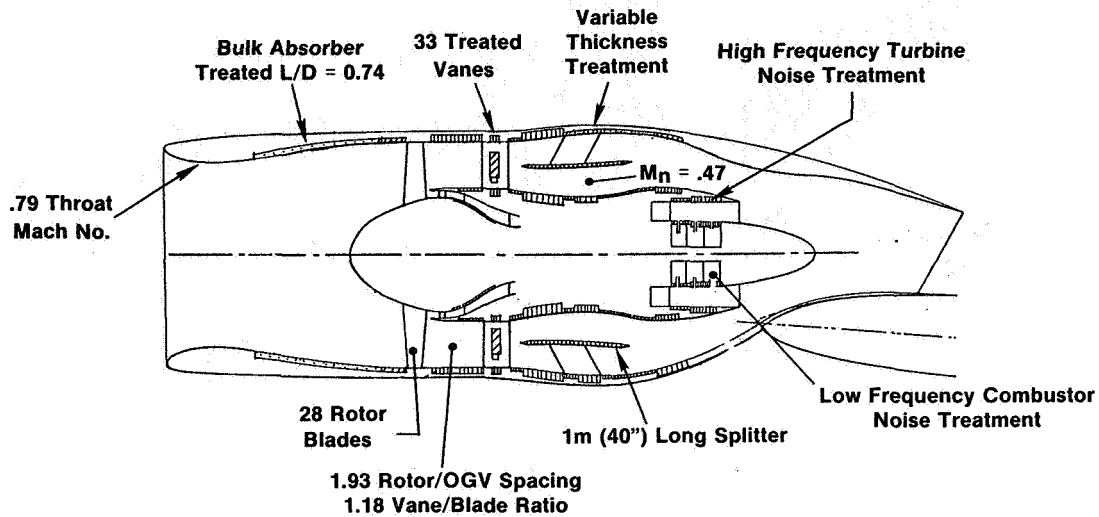
Figure 5

QCSEE Inlet Noise Reduction Concepts

- Takeoff

- Approach
- Reverse Thrust

M_T = .79

L_T

D

Mach Number Suppression

Treatment Suppression

Δ PNdB

Δ PNdB

Reverse Thrust — UTW

Increasing Mach Number

Increasing L_T/D

Figure 6

211
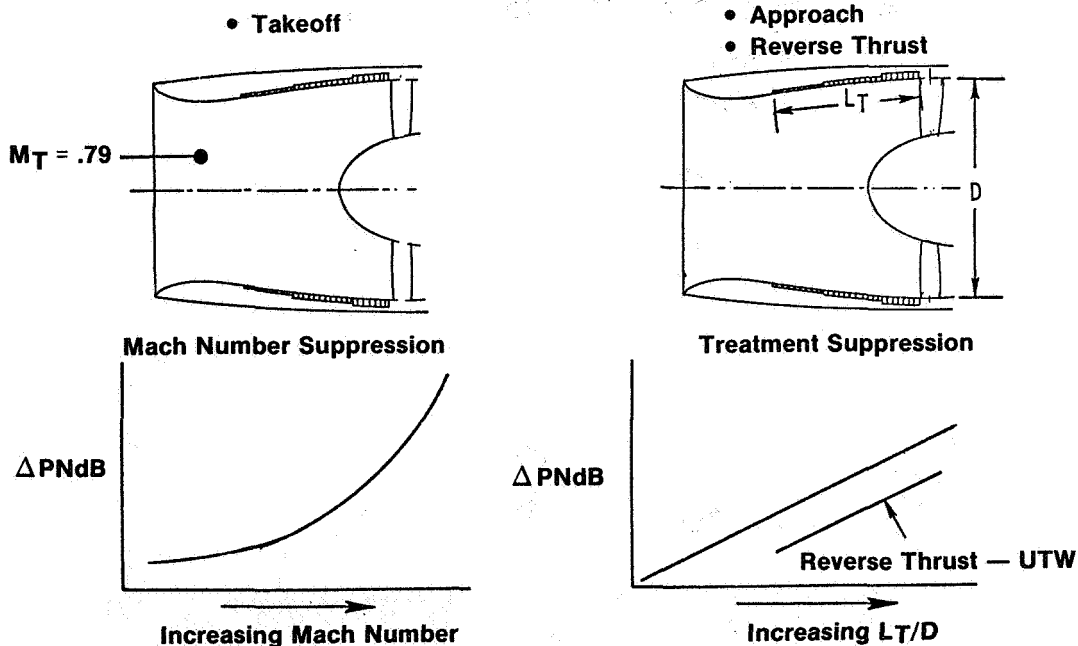
QCSEE UTW

**50.8 cm (20 in.) Diameter
Scale Model Fan**

Farfield
Microphones
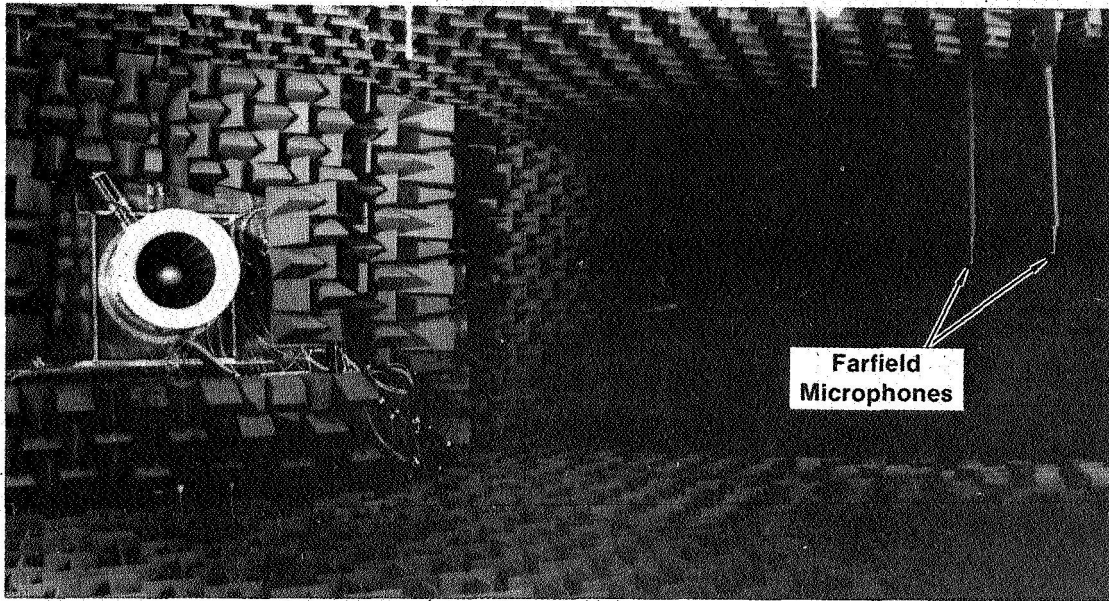
Figure 7

50.8 cm (20") Simulator Test of
High Throat Mach No. Inlet Suppression

● Baseline Bellmouth

▲ Treated High Throat
Mach No. Inlet

■ Hardwall High Throat
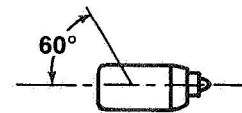Mach No. Inlet

● Scaled to Full Size
● 61m (200 ft) Sideline

60°

Perceived
Noise
Level,
PNdB

12.8 dB Suppression

0.79 M_{th}

Average Throat Mach Number, M_{th}
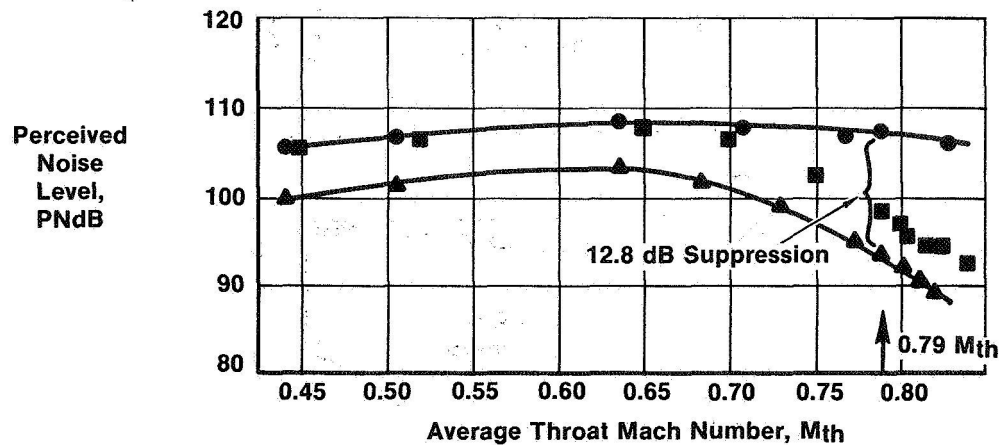
Figure 8

50.8 cm (20 in.) Simulator Test of Reverse Thrust Suppression

60°

- **High Throat Mach No. Inlets**

Perceived Noise Level, PNdB

Hardwall

Suppressed

35% of Takeoff Thrust

Percent Corrected Fan Speed
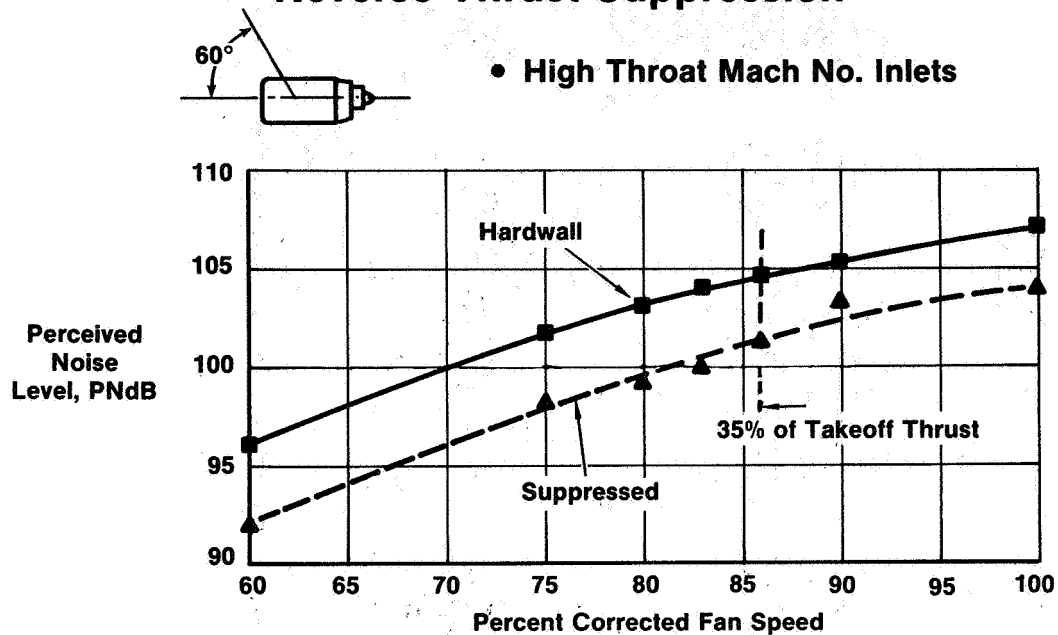
Figure 9

QCSEE Engine Inlet Acoustic Configurations

- **0.79 Design Throat Mach Number**
- **Treated L/D = 0.74**

Throat   Variable Depth SDOF Treatment

UTW

Throat   Bulk Absorber Treatment

OTW

Figure 10

213
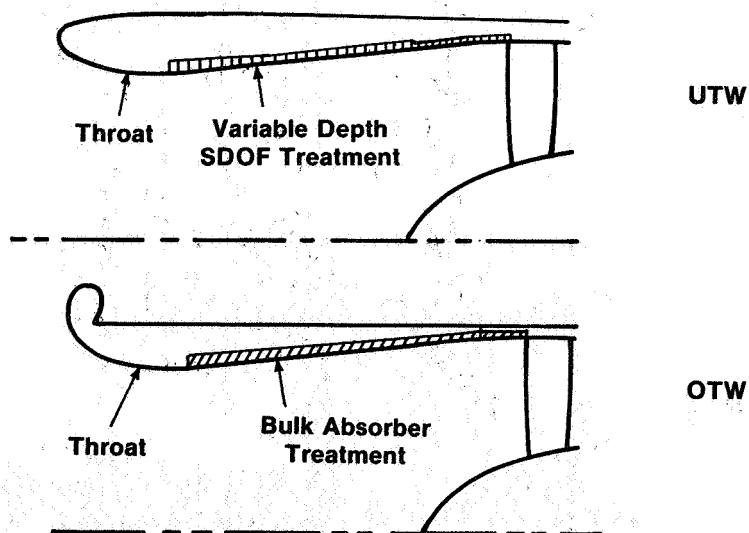
QCSEE Inlet Acoustic Treatment

Perforated Facesheet

Cavity Depth

Hexagonal Honeycomb Cell

Solid Backing Sheet

UTW (SDOF)
Facesheet Porosity _____ 10%
Cavity Depth _____ 1.2cm to 3.8cm
(0.5 in. to 1.5 in.)

Perforated Facesheet

Depth

7 Kevlar Layers

OTW (Bulk Absorber)
Facesheet Porosity _____ 14 to 22%
Depth _____ 2.5 cm (1 inch)
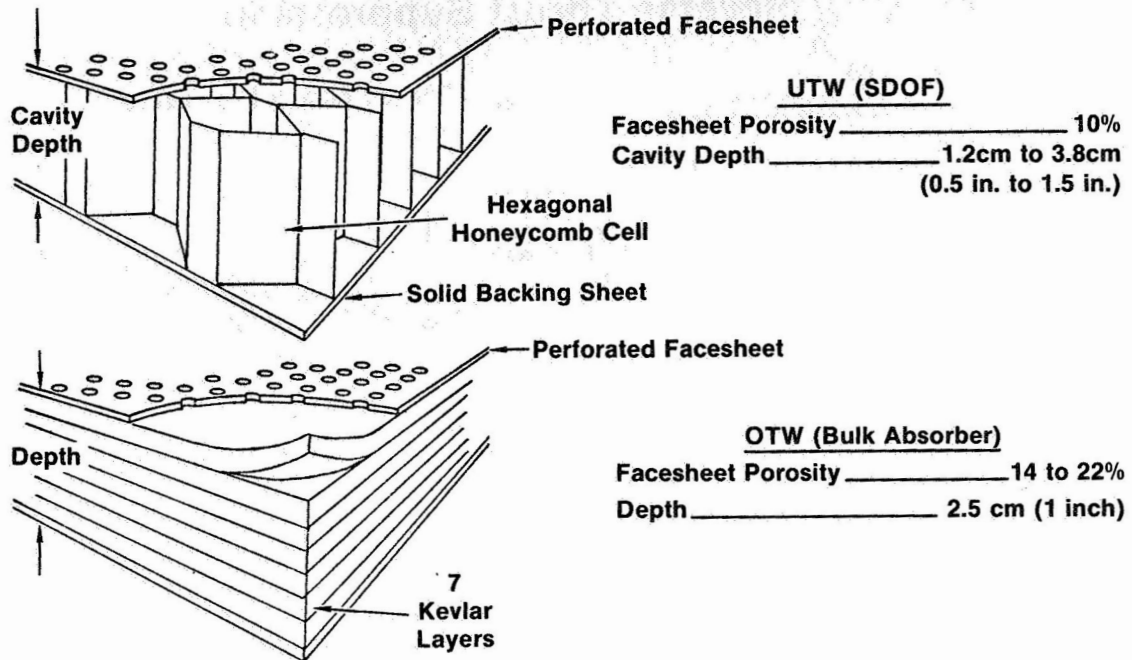
Figure 11

General Electric Company Anechoic Chamber

Exhaust Radiated Noise Model
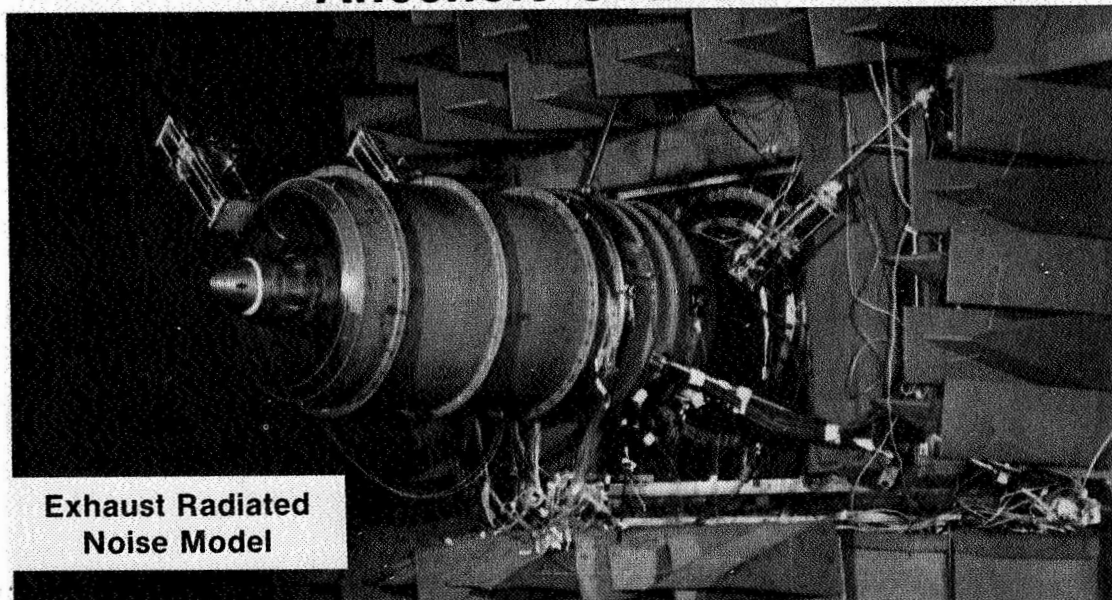
Figure 12

Effect of Vane Number on Second Harmonic SPL

- 100% Corrected Speed
- Model Data

120°

1/3 Octave
Band SPL,
dB

110

100

Optimum V/B Ratio

0.5 Chord Rotor — Stator Spacing

1.5 Chord Rotor — Stator Spacing

12   16   20   24   28   32

Number of Vanes

1.0   1.5   2.0

Vane/Blade Ratio
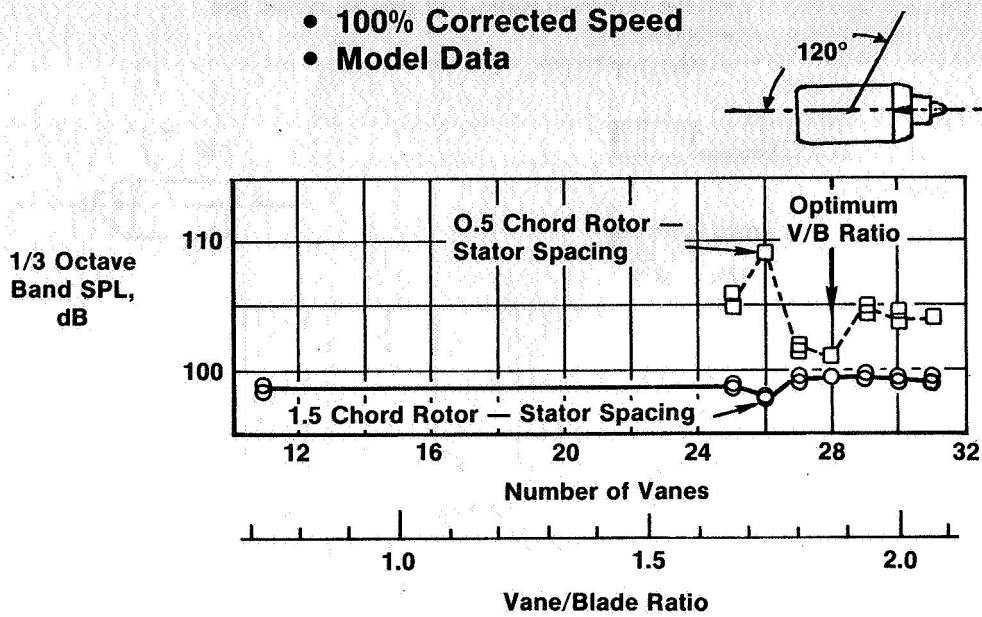
Figure 13

Summation of Rotor-Turbulence and Rotor-Stator Noise

- Low Pressure Ratio Model Fan

Sound Power
Level, dB

135

130

125

120

0   0.5   1.0   1.5   2.0

Total Predicted

Measured

Rotor-Turbulence
Noise

Rotor-Stator
Interaction Noise

Spacing, Rotor Tip Chords

Figure 14

215
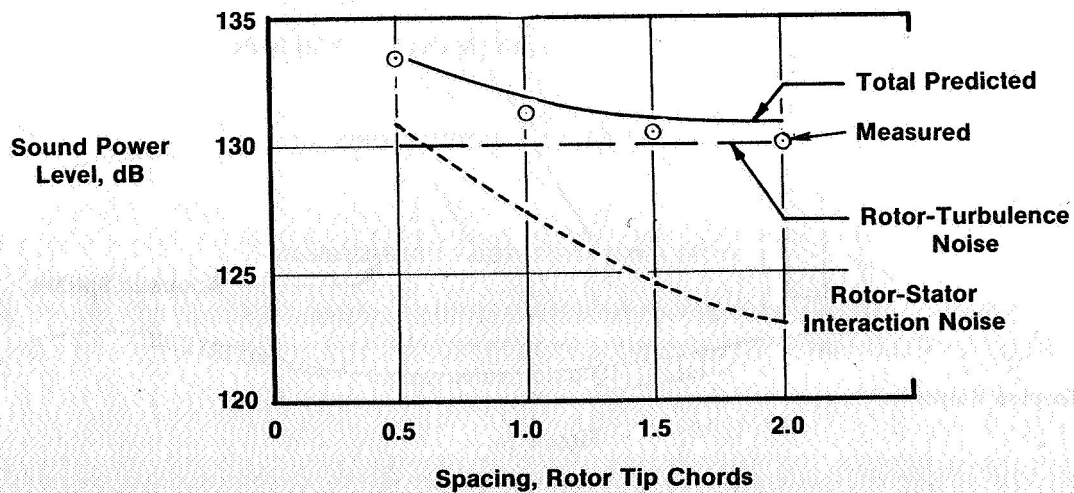
Scale Model Suppression Test Results

- Low Pressure Ratio Fan (NASA Rotor 55)
- 100% N/$\sqrt{\theta}$
- Variable Depth, Variable Porosity

Flow ➡

Porosity   12%   12%   12%   27%

120°

1/3 Octave Band
Suppression,
dB

Measured

Predicted

Frequency, Hz
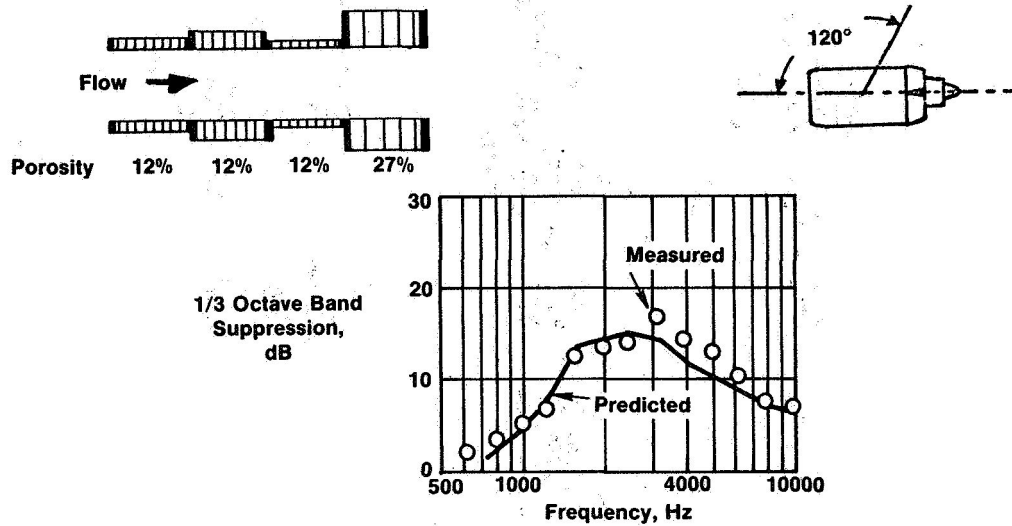
Figure 15

UTW/OTW Fan Exhaust Treatment Configuration

Variable Depth, Variable Porosity Treatment

Acoustic Splitter

Treated Vanes
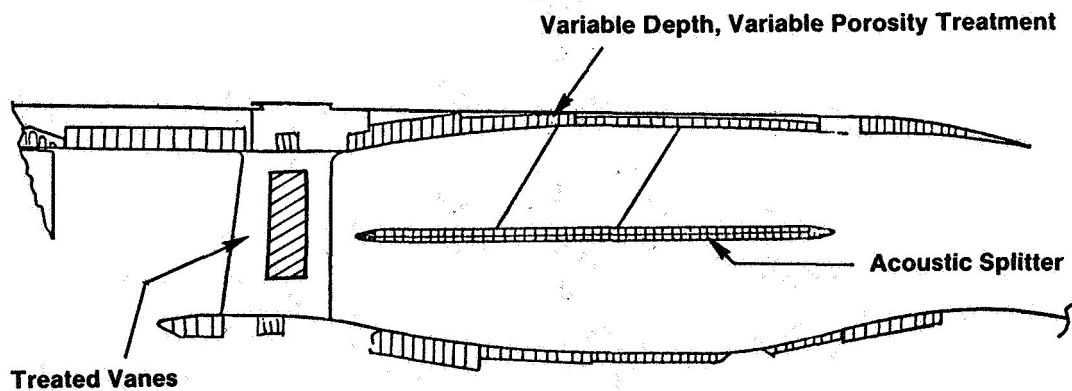
Figure 16

QCSEE Exhaust Acoustic Treatment
SDOF

Perforated Facesheet

Cavity Depth

Solid Backing Sheet

Hexagonal Honeycomb Cell
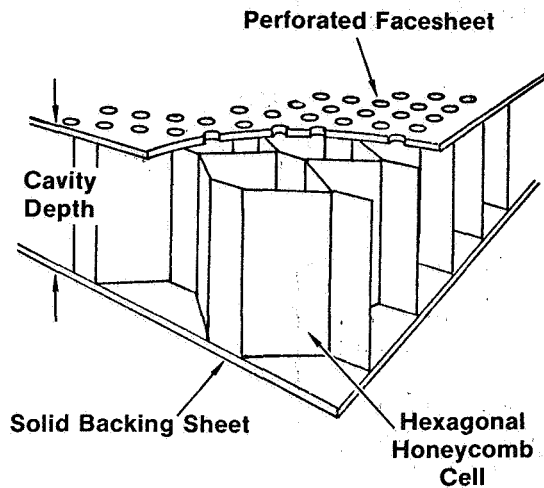
Wall Treatment

Facesheet Porosity _____ 10 to 22%
Cavity Depth _____ 1.9 cm to 5.1 cm
(0.75 to 2.0 in.)

Acoustic Splitter

Facesheet Porosity _____ 11.5%
Cavity Depth _____ 1.27 cm
(0.5 in.)

Figure 17

Predicted UTW Fan Exhaust Suppression

1/3 Octave Band Sound Pressure Level Suppression, dB

PNL Suppression
13.4 PNdB

Frequency, Hz
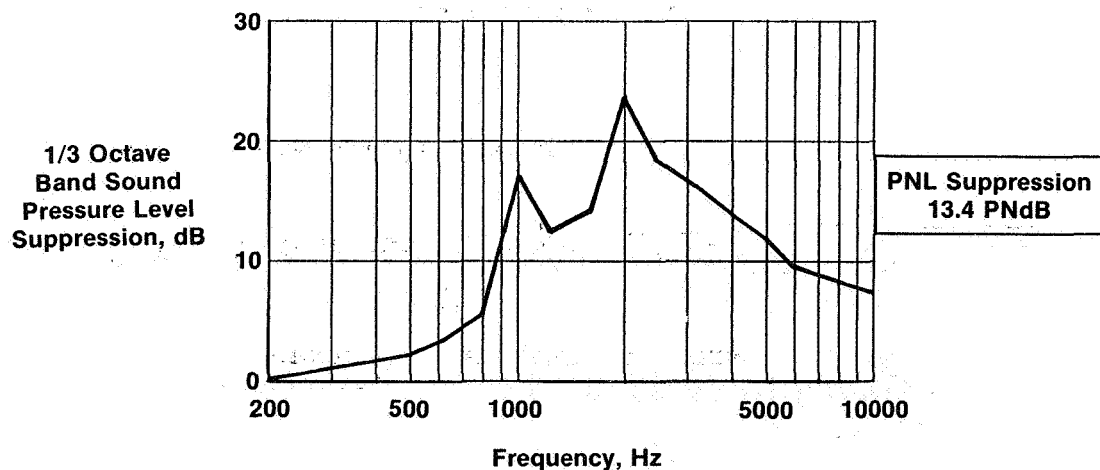
- Takeoff Power
- Max Aft Angle

Figure 18

217

Core Stacked-Treatment Suppression
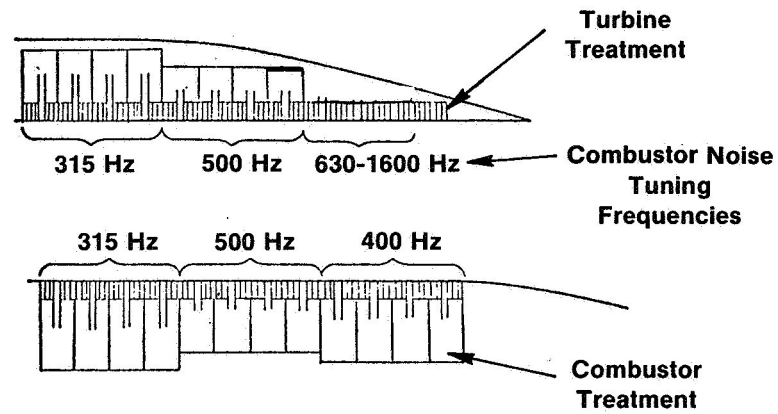
Figure 19

QCSEE Core Exhaust Nozzle
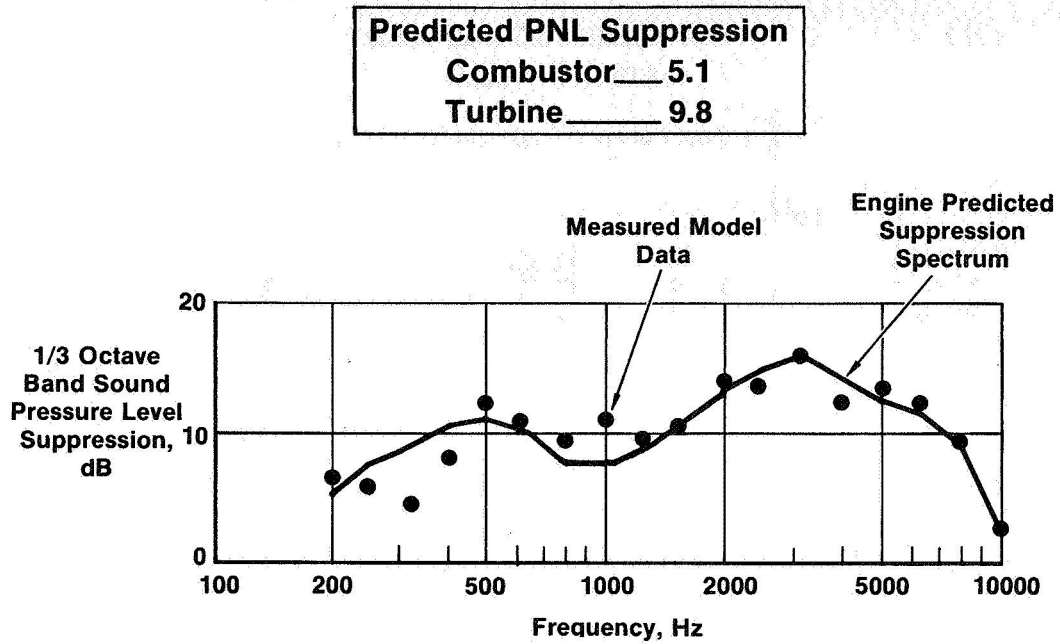

Figure 20

218

Hot Duct Model Test Data

Predicted PNL Suppression	
Combustor___	5.1
Turbine_____	9.8

Measured Model Data

Engine Predicted Suppression Spectrum

1/3 Octave Band Sound Pressure Level Suppression, dB

Frequency, Hz
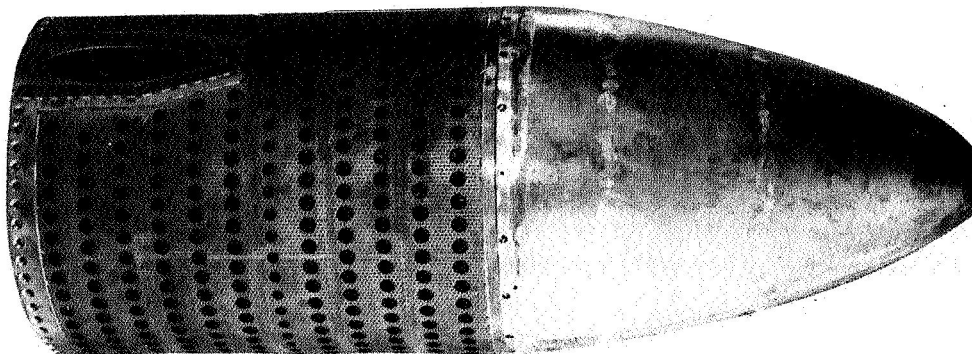
Figure 21

QCSEE UTW Engine
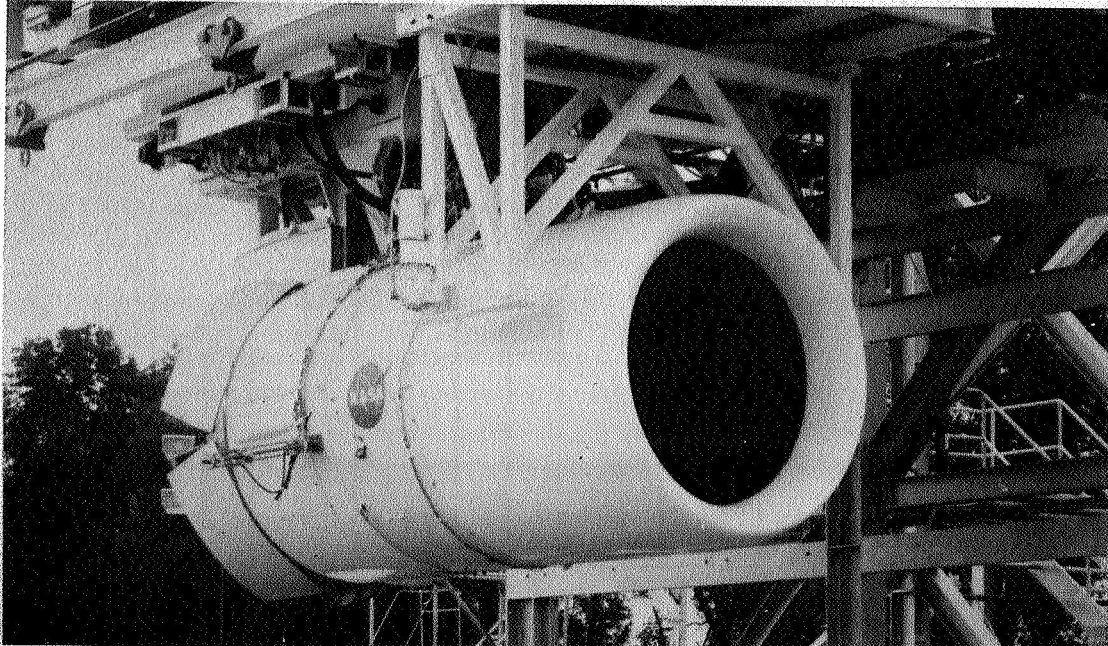
Figure 22

UTW Takeoff Noise Predictions

- Goal = 95.0 EPNdB
- EPNdB = 93.6
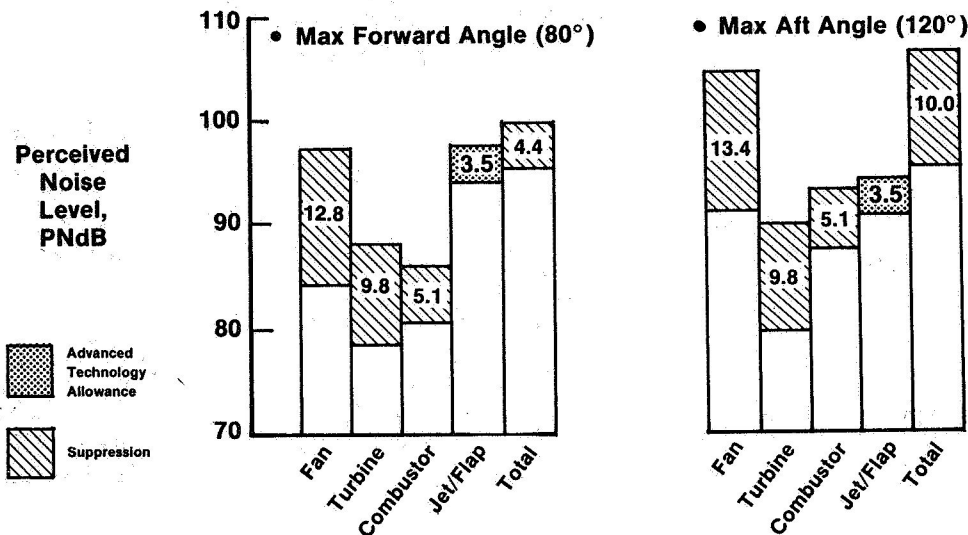
Figure 23

UTW Approach Noise Predictions
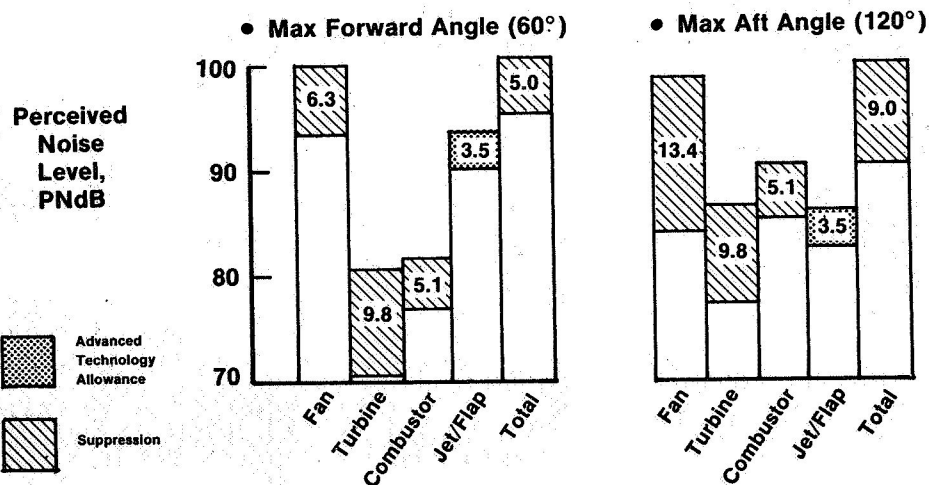
- 65% of Takeoff Thrust
- Goal = 95.0 EPNdB
- EPNdB = 93.3

Figure 24

220

UTW Reverse Thrust Noise Predictions
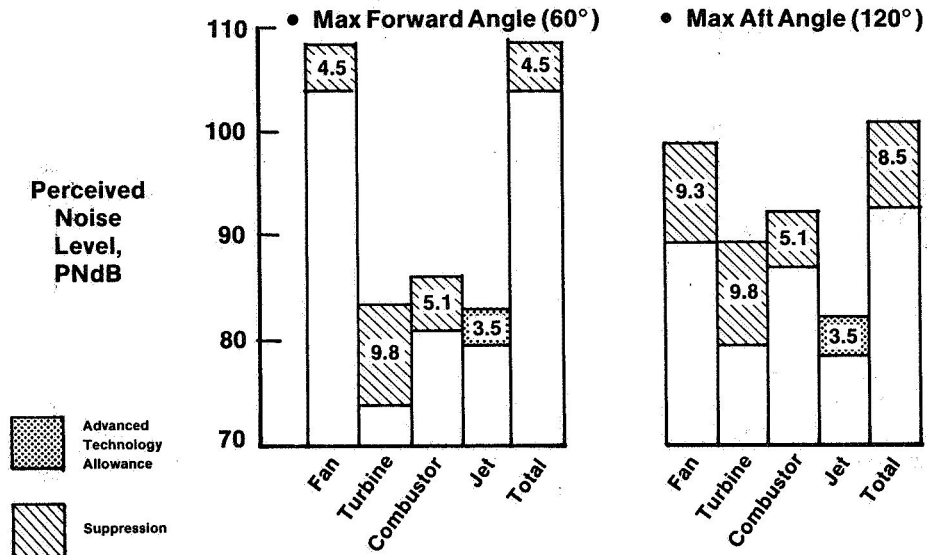
- Goal = 100 PNdB
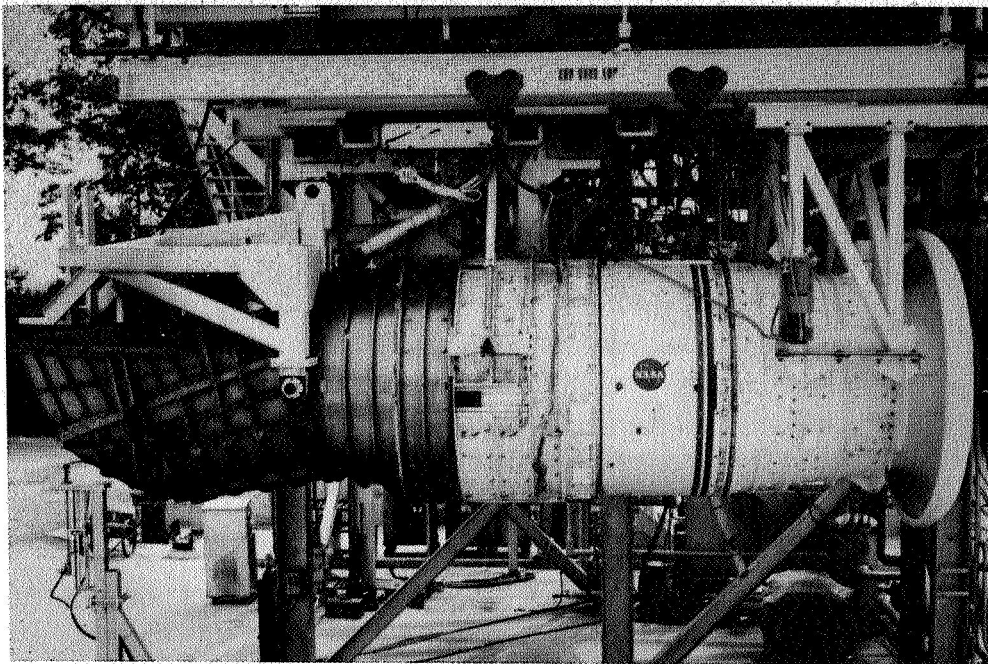- Max PNdB = 103.9

Figure 25

QCSEE OTW Engine

Figure 26

OTW Takeoff Noise Predictions
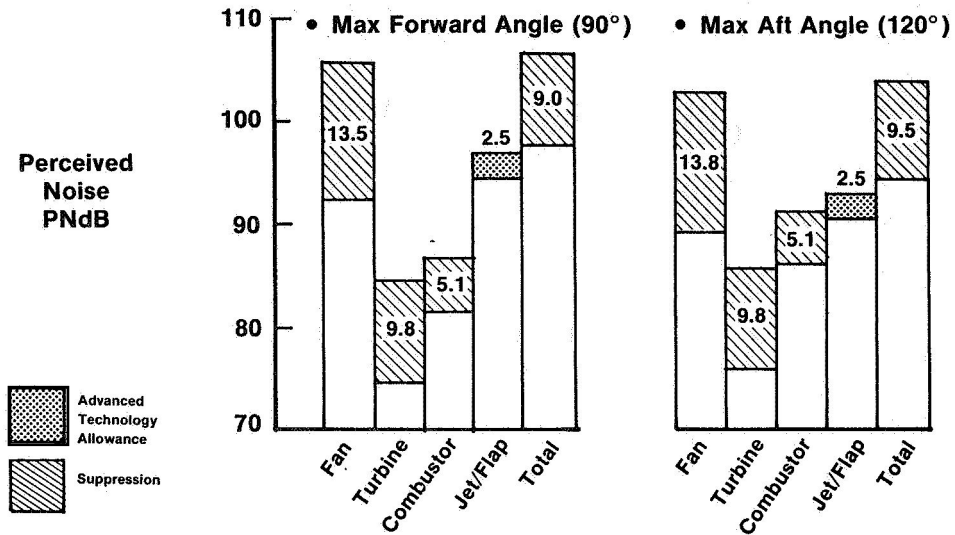
- Goal = 95.0 EPNdB
- EPNdB = 95.4

Perceived Noise PNdB

- Max Forward Angle (90°)
- Max Aft Angle (120°)

Advanced Technology Allowance

Suppression

Figure 27

OTW Approach Noise Predictions

- Goal = 95.0 EPNdB
- EPNdB = 90.0

Perceived Noise Level, PNdB

- Max Forward Angle (90°)
- Max Aft Angle (120°)

Advanced Technology Allowance
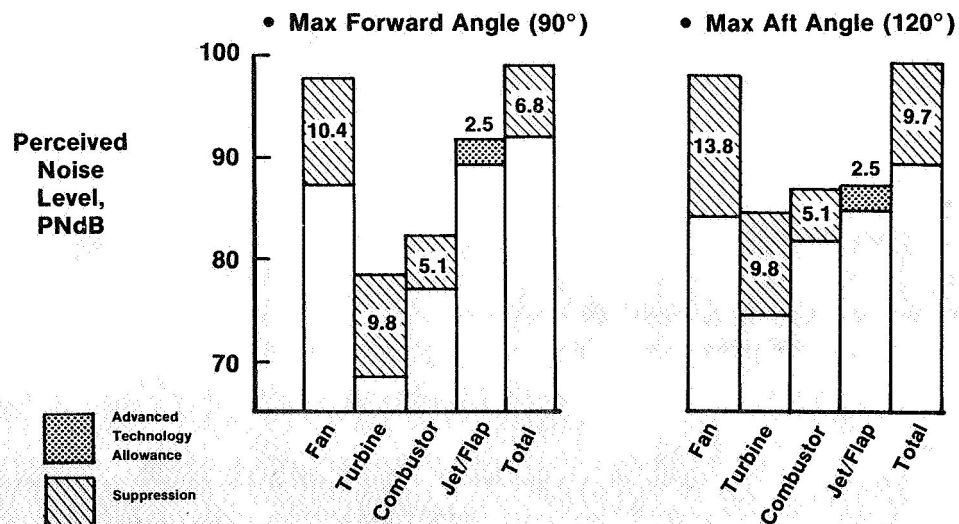
Suppression

Figure 28

QCSEE OTW Engine With Thrust Reverser Deployed
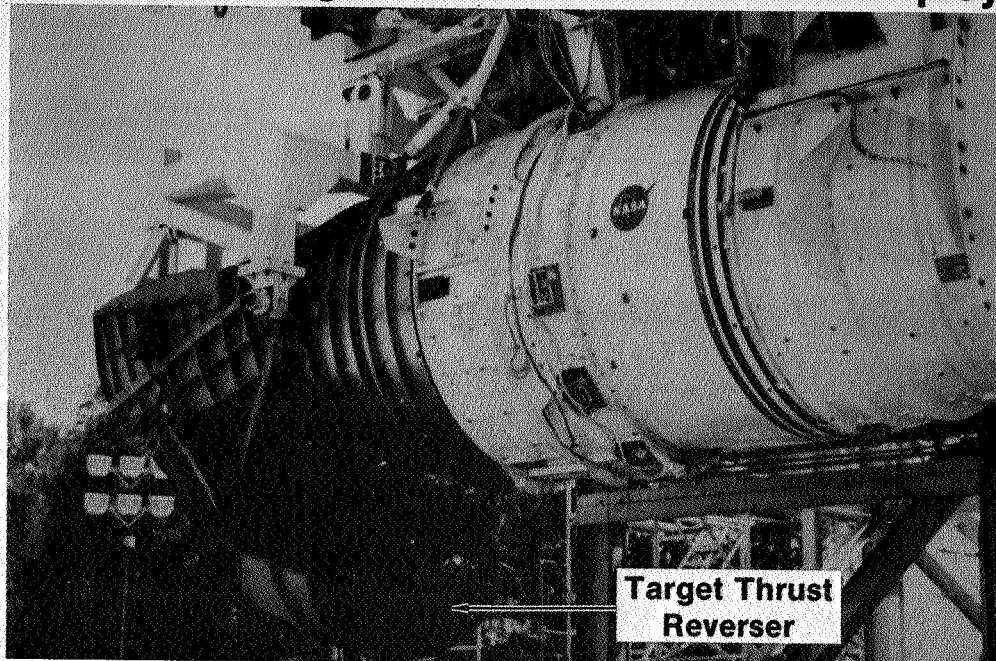

Figure 29

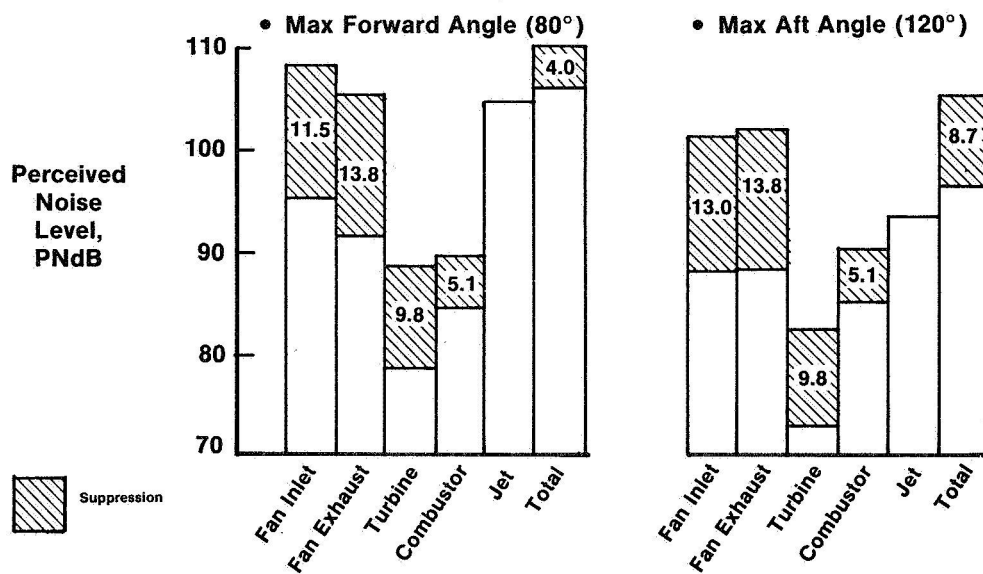# OTW Reverse Thrust Noise Predictions

- Goal = 100 PNdB
- Max PNdB = 106.4

Figure 30

QCSEE ACOUSTIC RESULTS - ENGINE ALONE[*]

E.B. Smith
General Electric Company
Cincinnati, Ohio

INTRODUCTION

The QCSEE acoustic test program has been conducted in order to measure the system noise levels of both the UTW and OTW engines and to evaluate the component technology features on both engines. Both forward and reverse thrust noise levels were measured with the engine alone, i.e. without a wing-flap system in place. Where possible the component source levels and suppression have been assessed but in some cases the noise reduction achieved by the total system will be presented.

The UTW acoustic test program was carried out with the composite nacelle mounted as shown in Figure 1 on the acoustic test pad. The engine centerline was 3.96 m (13 feet) from the ground. Since data was taken without the wing-flap system in place; the noise produced by the jet-flap interaction source had to be calculated and added to the measured engine noise level in order to calculate the aircraft system noise and compare to the program noise goals.

TEST CONFIGURATION AND MEASUREMENTS

The five test configurations shown in Figure 2 permitted the evaluation of the basic UTW engine noise levels as well as an assessment of the major noise components. The baseline configuration was untreated with the exception of the fan frame between the rotor and OGV's, treatment on the OGV's, and in the core compressor inlet. Configuration No. 2 was the same as the baseline with the exception that the vanes were taped to determine the effect of this treatment. Both of these configurations were run with an untreated bellmouth inlet, and the resulting data used to define the baseline system and fan component noise levels. The fully suppressed nacelle was run in both forward and reverse thrust. Configurations four and five were tested with the fan exhaust splitter and the core suppressor removed respectively, to determine the impact of these two suppression elements. All configurations were operated over a range of engine conditions including speed variation, blade angle setting and nozzle area.

All noise testing was done on the acoustic pad at the Peebles test facility. The ground surface shown in Figure 3 is concrete, but most of the testing was carried out with a gravel field surface. Noise measurement instrumentation locations are shown in Figure 4, and consisted of a farfield microphone arc at 46.5 m (152.4 ft) with microphones on 12.2 m (40 ft)

towers, every 10°. The acoustic directional array which was used at six angles to separate engine sources and aid in component suppression evaluation is a highly directional receiver mounted on a movable cart. Internal engine instrumentation was also used and consisted of sound separation probes and wall pressure transducers in the fan inlet and fan exhaust ducts.

UTW ENGINE TEST RESULTS

Prior to test the major noise component spectra were estimated, using calculation procedures for the jet noise, combustion noise and turbine noise, and scaling fan noise spectra from previously measured fixed pitch fan noise data. Fan pressure ratio and tip speed were the primary scaling parameters used to obtain estimates of both inlet radiated and exhaust radiated fan noise. Each of these component spectra are plotted in figure 5 and 6 at the maximum forward and aft angles of noise radiation for the takeoff power setting of the UTW engine. The heavy line on each plot is the logarithmic sum of these individual spectra and is an estimate of the measured baseline engine spectra at 46.3 m (152 feet) radius. The symbols on figure 5 and 6 are the measured data from the baseline test. In general the measured levels are on the order of 5 dB higher than expected over the entire high frequency spectrum. Since the system noise above 800 Hz is controlled by fan noise, it appears that the estimates based on the fixed-pitch fan data cannot be used to reliably predict a variable-pitch fan design, i.e. solidity, blade number, and perhaps the vane-frame design, is probably the cause of this divergence and the exact cause need to be the focus of additional investigation.

One of the potential advantages of a variable pitch fan was thought to be the capability to minimize noise, at thrust, by continuously optimizing blade incidence angle and loading over the fan speed range. Data shown in figure 7, taken at both forward and aft max angles, takeoff and approach thrusts show no tendency to identify a minimum noise point. This data represents a range of incidence angles and loading large enough to reveal any acoustic advantages which might be present. Fan source mechanisms are many and varied for the static test case. For example, one of the major noise source mechanisms statically is known to be the interaction of the rotor with inlet turbulence. This source appears to be made up of both a dipole source and a quadrapole source; one of which varies with blade loading and one independent of loading. If for this fan design the dipole, rotor-turbulence interaction source controls, then no change with blade angle would occur. In flight, however, the ingested turbulence is no longer affected by the contraction ratio of the static inlet and this rotor-turbulence interaction noise is reduced. In the flight case then, the effect of blade angle may be important.

The inlet design which has been described in the previous paper is shown in figure 8 in cross section. The treatment begins 11.2 cm (4.4 in.) downstream of the high Mach number throat and is designed to provide the

predicted 12.8 PNdB suppression at takeoff and 6.3 PNdB suppression at approach, both at the maximum forward radiation angle on a 152.4 m (500 ft) sideline.

The suppression results of this inlet design are shown in Figure 9, where the sideline PNL has been plotted as a function of throat Mach number, for the baseline test and the fully suppressed configuration. (The baseline data taken with the cylindrical inlet is plotted at equivalent fan RPM points since, of course, the inlet Mach numbers are quite low). Several sets of data with different blade angle settings makeup the fully suppressed line. The indicated suppression at a throat M_n of 0.79 is only 9 PNdB and is changing very slowly with increasing throat M_n. This trend is contrary to the scale model results and additional analysis with the directional array revealed the problem. Separating the measured spectrum into noise emanating from the inlet and noise reaching the forward quadrant but radiated from the fan exhaust, produced the dotted and dashed curves of this figure. It is obvious that the aft radiated noise which is increasing with engine speed (and M_{th}) is a "floor" to the inlet noise reduction. The indicated suppression (baseline to "inlet noise") is now seen to be 14.5 PNdB at the design Mach number.

The aft treatment design is shown in Figure 10 with the predicted system suppression values at takeoff and approach. Due to the large bypass ratio and fan diameter, the fan exhaust passage height is 50.8 cm (20 inches) The desired fan exhaust suppression required the use of a splitter in this large duct. This splitter was removable and the exhaust suppression was measured with and without the splitter in place. The measured system suppression as a function of engine thrust at the maximum aft radiation angle is plotted in Figure 11, and shows a value of 8.0 PNdB, roughly constant over the engine power setting range. The suppression spectra, for the splitter-out case shown in Figure 12 at takeoff and approach, are in good agreement with the prediction, but miss the predicted suppression by two dB in one critical band (2000 Hz). This results in PNL reduction short of the prediction by about 1.5 PNdB. With the exhaust splitter in place, peak SPL suppression of almost 15 dB was measured at the 120° far-field position and this is shown in Figure 13. In general, the suppression did not meet expectations at the 2nd harmonic frequency at approach nor at the fundamental and second harmonic frequencies at takeoff. There appears to be a flanking transmission path which prevents the full suppression from being measured and this is the subject of additional data analysis.

Taping the treatment in the vanes provided an opportunity to evaluate the suppression potential of treatment in this location. Total treated area is small, (about 0.67 m^2 (7.2 ft^2)) and because of treatment thickness limitations the design frequency was high (about 4 KHz). The measured suppression spectrum (Figure 14) in the aft quadrant shows about 2 dB over a broad frequency range which could be very beneficial to engine systems whose suppression is marginal or inadequate.

The core suppressor for the QCSEE engines was designed to suppress both high frequency, turbine generated noise and low frequency, combustor generated noise. Since both of these components are marginal in terms of contribution

to the total system noise, it was recognized in the beginning of the program that it would be extremely difficult to measure the unsuppressed and suppressed levels of these components. If the fan exhaust suppression levels were achieved, however, this core noise must be reduced to meet the system goals. The difficulty in measurement of the core suppression has been compounded by the fan source noise increase (5 dB), which results in aft fan noise levels high enough to completely mask the high frequency core suppression. In a similar fashion, low frequency jet noise masks the low frequency suppression of the combustor noise. The comparison of the measured and predicted core suppression in Figure 15, therefore, reflects the measurement difficulties just described, rather than poor performance of the core suppression. Additional engine testing is required to confirm the good suppression performance of the core suppressor indicated from the component test.

Reverse thrust noise testing of the UTW engine was done with two blade angles over a range of reverse thrust. The measured max PNL values shown in Figure 16, occurred at an angle of 70° on a 152.4 m (500 ft.) sideline and were substantially above the noise goal of 100 PNdB for 35% reverse thrust. Maximum reverse thrust achieved was 27% and at this thrust level the 152.4 m (500 foot) sideline noise is 106 PNdB. Although higher than the goal this engine-measured reverse thrust noise level is consistent with the scale model fan data and collectively provides a good data base for future reverse pitch fan noise predictions.

The UTW engine noise summary in table I shows that the aft radiated engine noise is 9 PNdB higher than the calculated jet flap component and makes a major contribution to the system EPNL at takeoff. The noise goal was exceeded by 2.2 EPNdB primarily as a result of the unexpected increase in aft fan source noise. At approach the forward radiated fan noise is slightly higher than expected due to low approach suppression but the system noise misses the goal of 95 EPNdB by only 0.7 EPNdB.

OTW ENGINE TEST RESULTS

The OTW engine was tested in an inverted mode (Figure 17) to permit the deployment of the thrust reverser. Acoustic testing was conducted with five configurations (Figure 18), starting with a baseline which was untreated except for treatment in the frame area and on the vanes. Three forward thrust configurations were used to determine system noise levels and to evaluate component suppression. The hybrid inlet was evaluated without treatment in order to determine the acceleration-suppression alone and a more moderate suppression approach was evaluated by removing the aft fan duct splitter and the core suppressor. The reverse thrust noise was measured with the fully suppressed nacelle.

The agreement of the measured inlet radiated baseline levels with the predicted spectrum was excellent as seen in Figure 19. All the major features of the dominant fan inlet noise are seen to be accurately predicted. The aft radiated noise shown in Figure 20 was correctly predicted at blade passing

frequency but SPL's at the second harmonic and above are substantially below that predicted. The only reason which appears to explain this over-prediction at high frequency is a very effective suppression characteristic for the frame and vane treatment which was not separately evaluated during the program.

The hybrid inlet for the OTW shown in Figure 21, was constructed with a bulk absorber material for the treated area. A Kelvar felt was used, covered with a perforated plate. This very effective treatment was used to improve the approach suppression with the hybrid inlet which was anticipated to give 13.5 PNdB suppression at the takeoff power setting.

The takeoff suppression spectrum shown in Figure 22, exceeded the goal slightly, reaching 14 PNdB at the maximum forward angle, and suppressing the inlet noise down to the jet noise floor up to 2500 Hz. Peak suppression at blade passing frequency was almost 20 dB. The suppression was entirely due to the acceleration effect since the untreated inlet was identical to the treated. At approach (Figure 23) the inlet suppression with the bulk absorber is improved over that achieved wth the resonator treatment, but the OTW inlet did not achieve the predicted suppression. The difficulty in this design is not the performance of the bulk absorber as a treatment, but that the requirement for a high porosity perforated face sheet in the presence of high subsonic wall Mach numbers tends to generate high frequency broadband noise, which reduces the effective suppression bandwidth. In spite of this, 7.5 PNdB of inlet suppression with only wall treatment is a good suppression performance.

The measured system exhaust suppression is shown in Figure 24 by comparing the baseline and the fully suppressed configurations. The suppressed spectrum which will be shown later, is controlled by jet noise making the measurement of aft suppression very difficult. Less than 5 PNdB of system suppression is shown here and increases to only 6 PNdB when the calculated jet noise is removed. The four shaded symbols are reduced by removing the calculated jet noise. In Figure 25 the plot of the suppressed and unsuppressed spectra shows two reasons for the low measured suppression. First, the second harmonic source level being lower than predicted leaves very little tone suppression available. Second, the suppression above 2500 Hz is effectively zero and this is the apparent result of a "floor noise source" which prevents the suppression from being detected in the farfield measurements. This floor source is apparently boundary layer noise, generated in the exhaust duct and common nozzle, from the high velocity air flow over perforated surfaces. Although the wall Mach numbers were kept as low as possible, the calculated levels from flow noise are very close to the measured spectrum levels above 2500 Hz. The lack of high frequency suppression is evident in Figure 26 in this comparison of the measured and predicted suppression spectra at takeoff. The "missing second harmonic" in the source spectra produces the discrepancy at 3150 Hz.

The OTW reverse thrust test was operated with the exhaust deflected downward and forward with impingement on the concrete pad, as shown in Figure 27. Scale model testing prior to selecting the engine test indicated that the flow-over-the-ground-plane source would not be a major

factor in the engine reverse thrust noise measurements. Of greater impor-
tance were parameters such as lip angle, lip length, and distance of blocker
from nozzle exit plane. The full scale engine design incorporated these
scale model results, to the fullest extent possible consistent with thrust
reverser performance and mechanical design. But it was expected, based on
the scale model program, that the engine levels would exceed the noise goal
by about 6 PNdB. This prediction was confirmed by the engine data shown in
Figure 28. Based on the scale model tests, lower noise levels could have
been achieved with larger nozzle-to-blocker spacing and increased reverser
lip length but these "noise improvements" could not be incorporated in the
current engine design and meet the mechanical design requirements for deploy-
ment and stowage.

In summary the calculated system levels shown in table II for the
OTW were within 2.2 EPNdB of meeting the system noise goal at takeoff and
were lower by 0.4 EPNdB than the noise goal at approach.

SUMMARY

Using the measured engine noise levels from the program and calculated
flap noise, contours have been calculated for both UTW and OTW powered
aircraft. The takeoff and approach flight paths are shown in Figure 29 for
a 66,700 kg (147,000 lb) TOGW aircraft, along with 90, 95 and 100 EPNdB
contours. In order to provide some perspective of how small these noise
contours are, the 95 EPNdB contour areas are listed in table III and compared
to similar areas of two typical narrowbody jets and a widebody aircraft. The
contour area for the widebody is one-fourth to one-tenth of the narrowbody
contour while the QCSEE powered aircraft give another step reduction of
one-tenth, producing 95 EPNdB contours of less than one-half square mile.

In summary, the noise goals for the QCSEE program were very challenging,
representing a noise reduction technology step of about 10 EPNdB. Although
much of the low noise characteristic of the engines resulted from the basic
cycle design, several unique noise reduction concepts have been demonstrated
which are applicable to many engines, and these represent an improvement
in low noise technology. The most difficult aspect of the QCSEE noise goal
was to achieve simultaneous success with the prediction and suppression
of several major noise source components. Simultaneous success was necessary
since all of these sources were contributors to the suppressed engine per-
ceived noise levels, and therefore missing even one of the component levels
jeopardized achievement of the noise goals. As a result of this aspect
of the program the following list of accomplishments can be placed in perspec-
tive.

o   Takeoff and Approach System levels for both engines were within
     2 EPNdB of the 152.4 m (500 ft) sideline goal of 95 EPNdB.

o   The baseline system noise predictions met or were lower than the
     predictions on the OTW engine. Baseline levels on the UTW engine

230

were higher than anticipated but the program has provided a large data base for understanding and predicting variable pitch fan noise.

o The hybrid inlet was successful at Takeoff power settings achieving 14 to 15 PNdB suppression at the maximum forward angle. This represents three times the suppression achieved in the past without the use of splitters or variable inlet geometry. Up to 7.5 PNdB suppression was measured at approach power which is an improvement over previous designs.

o Aft fan suppression of 2 dB was demonstrated for treated vanes. This is a significant suppression for a very modest amount of treated area.

o Aft fan duct suppression was as predicted, where flanking noise transmission paths and/or "floor noise noise sources" didn't prevent accurate measurement.

o The suppression of the unique core nozzle suppressor designed to attentuate both high frequency turbine noise and low frequency combustor noise was not completely measured due to masking of jet noise and duct flow noise.

o The reverse thrust noise produced by both the UTW reverse pitch fan and the OTW reverser was higher than predicted but again, the data available from both engine and scale model programs provide the basis for more accurate prediction models.

Finally, from the acoustic technology standpoint, in almost every case where component acoustic objectives were not completely met, the data and understanding of the limiting problems is available and will insure the improvement of similar designs in the future.

TABLE I. - UTW COMPOSITE NACELLE SYSTEM NOISE

	Forward Quadrant		Aft Quadrant	
	Engine	Jet/Flap	Engine	Jet/Flap
Takeoff				
PNL	91.7	94.6	99.0	90.0
Quadrant Total PNL	97.0		99.9	
System EPNL	97.2			
Approach				
PNL	96.7	89.8	95.6	82.7
Quadrant Total PNL	97.9		96.0	
System EPNL	95.7			

TABLE II. - OTW BOILERPLATE NACELLE SYSTEM NOISE

	Forward Quadrant		Aft Quadrant	
	Engine	Jet/Flap	Engine	Jet/Flap
Takeoff				
PNL	94.8	95.8	96.8	93.2
Quadrant Total PNL	99.0		99.1	
System EPNL	97.2			
Approach				
PNL	95.4	89.9	90.8	87.2
Quadrant Total PNL	97.1		93.1	
System EPNL	94.6			

TABLE III. - COMPARISON OF FOOTPRINT AREAS
QCSEE TO TYPICAL PRESENT DAY AIRCRAFT

Aircraft	TOGW		95 EPNL Contour Area	
	kg	(lb)	Sq km	Sq mi
707 (Jet)	146,000	(322,000)	66.5	25.66
DC-9 (Fanjet)	44,500	(98,000)	31.6	12.25
DC-10-30 (Fanjet)	252,000	(555,000)	9.4	3.57
QCSEE — UTW	66,700	(147,000)	1.0	0.38
QCSEE — OTW	66,700	(147,000)	0.8	0.32

QCSEE UTW ENGINE
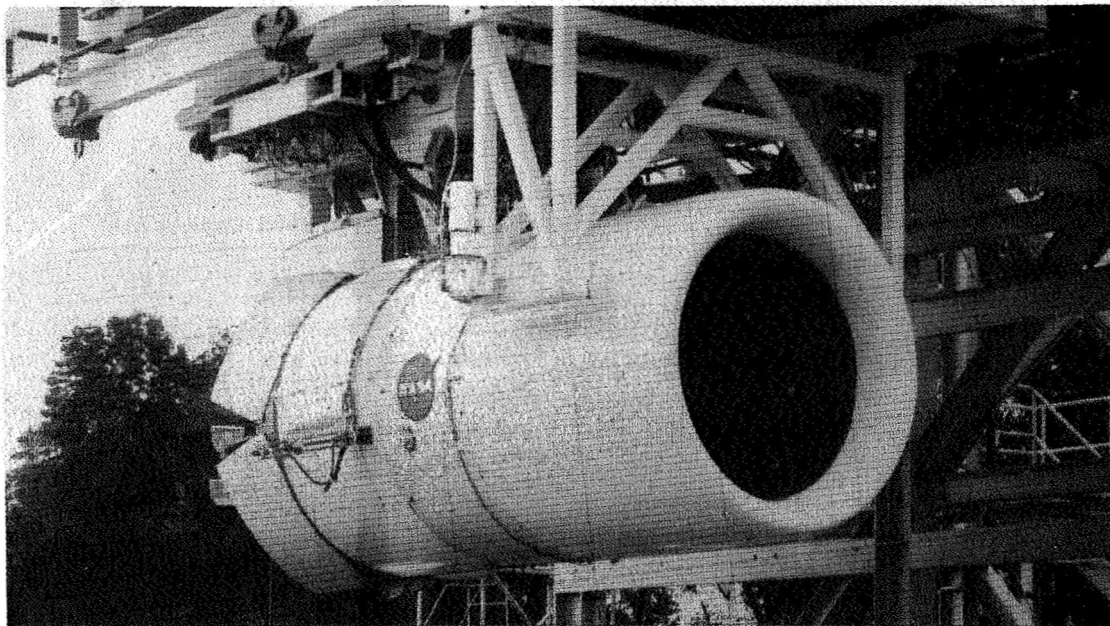
Figure 1

UTW Acoustic Test Configurations
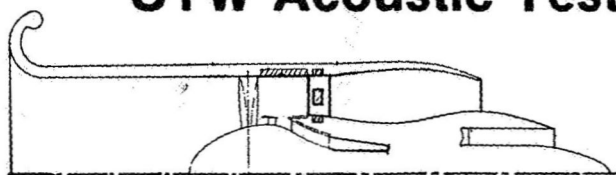
1. Baseline (Untreated Except for Treated Frame and Vane)
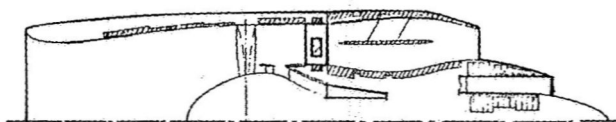
2. Baseline with Untreated Vanes
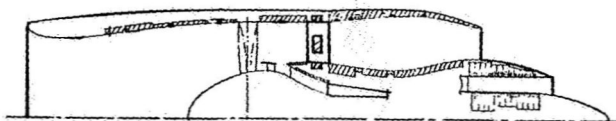
3. Fully Suppressed (Forward and Reverse Thrust)
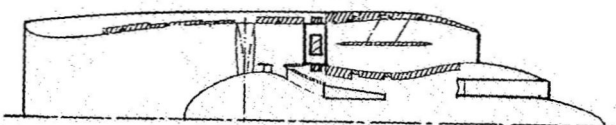
4. Without Fan Exhaust Splitter

5. Without Core Treatment
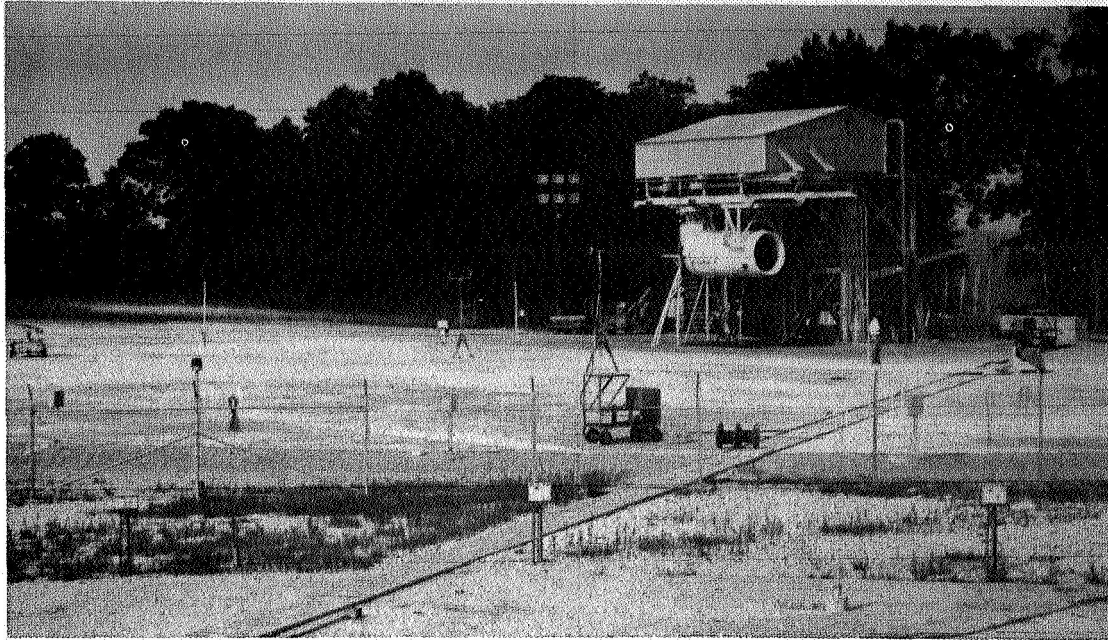
Figure 2

Acoustic Test Site

Figure 3

Sound Field Acoustic Instrumentation
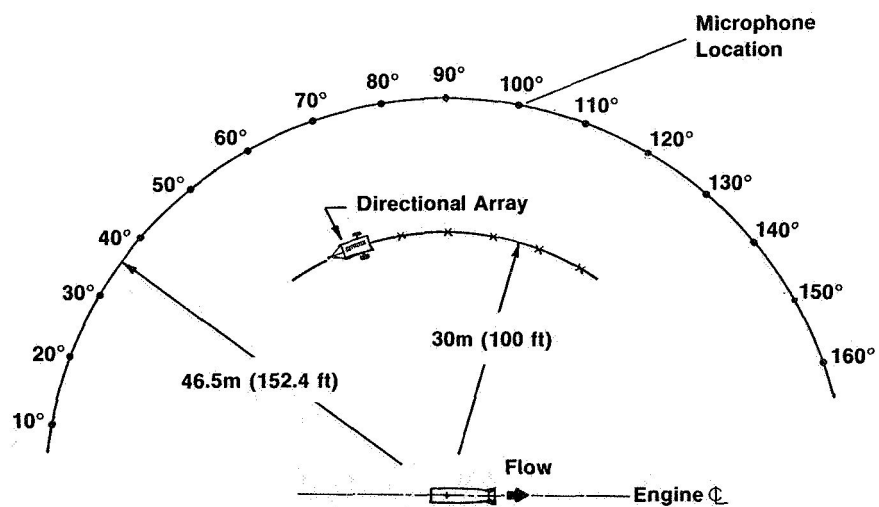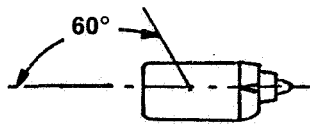## General Electric Peebles Test Facility

Figure 4

UTW Inlet Radiated Baseline Noise
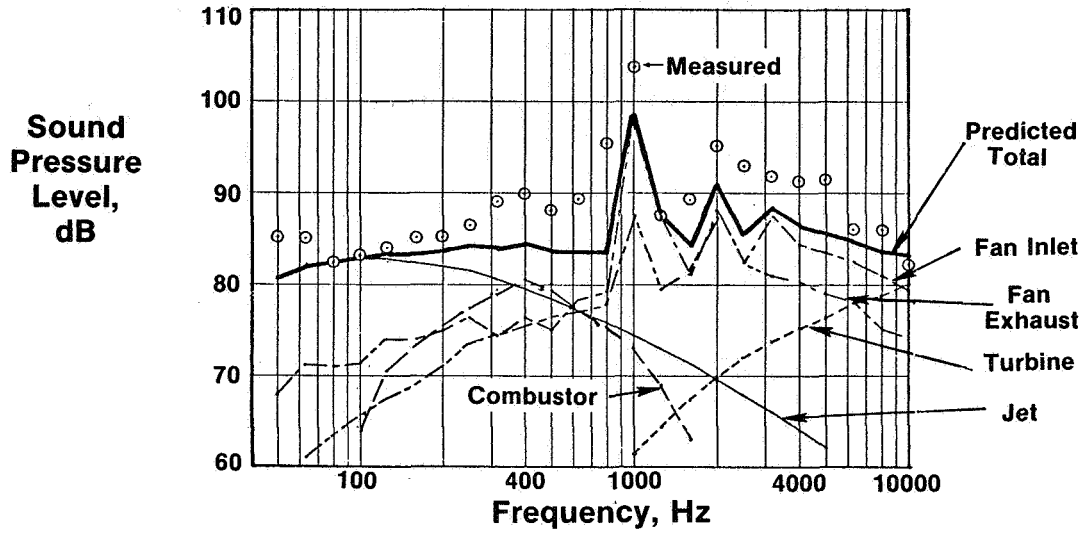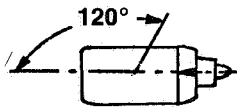
- Takeoff Power
- 46.5m (152.4 ft) Arc

Figure 5

UTW Exhaust Radiated Baseline Noise
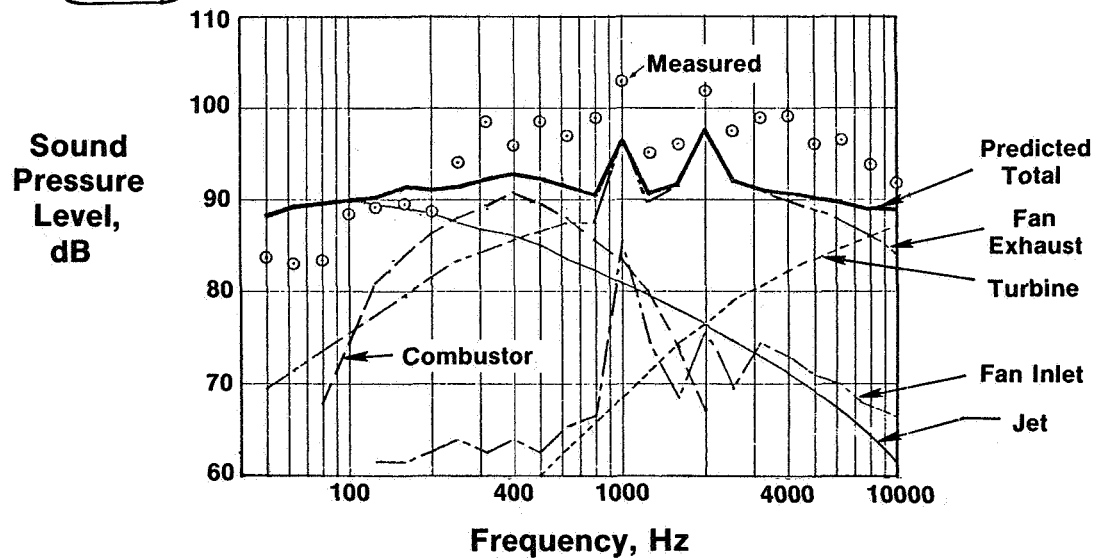
- Takeoff Power
- 46.5m (152.4 ft) Arc

Figure 6

Variation of PNL With Blade Angle
Baseline Configuration

Approach Thrust

Takeoff Thrust

%N/√θ
(80) (81) (84) (89) (95)

10 PNdB

%N/√θ
(92) (94)

60°

Perceived Noise Level,
PNdB

10 PNdB

120°

6   4   2   0   2

8   6   4

⟵ Open

⟵ Open

Blade Angle, Degrees
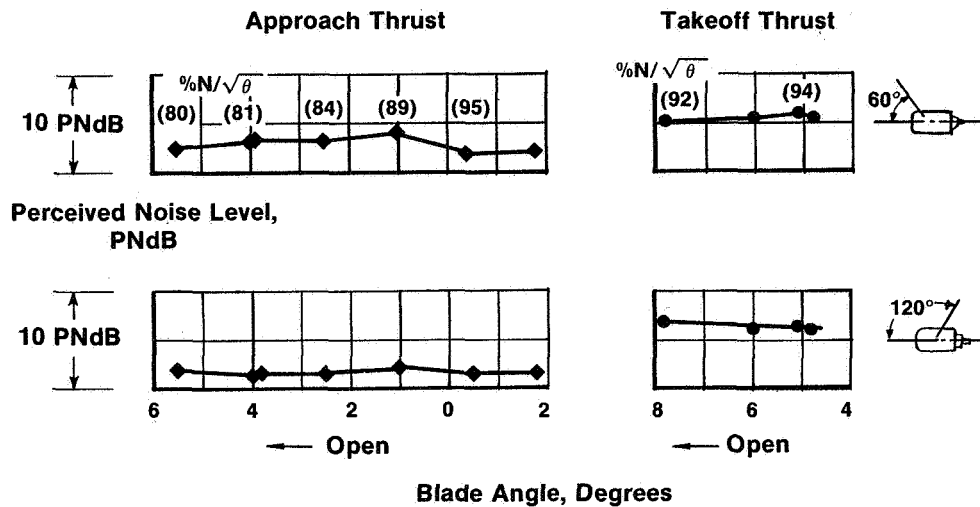
Figure 7

UTW Inlet Configuration

Throat
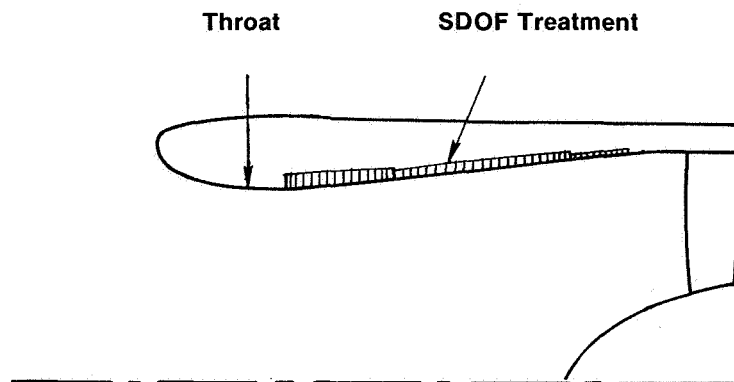
SDOF Treatment

PNL Suppression Prediction

Takeoff	**12.8 PNdB**
Approach	**6.3 PNdB**

Figure 8

Effect of Inlet Throat Mach Number on PNL

Blade Angle

X 3.3° Open
△ 4.7° Open
O 5.0° Open
□ 8.0° Open

Baseline (Hardwall Bellmouth)

Fully Suppressed High Mach Inlet

Exhaust Radiated Noise

Inlet Radiated Noise

10 PNdB

Throat Mach Number
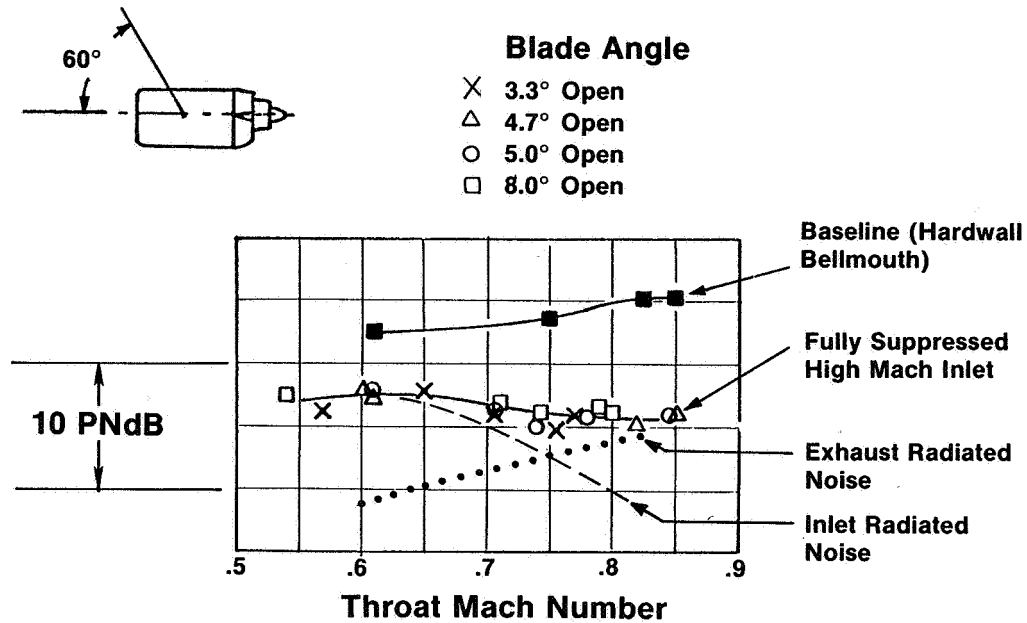
Figure 9

UTW Exhaust Treatment Configuration

- Predicted Exhaust Suppression
  Takeoff   9.2 PNdB
  Approach   9.6 PNdB
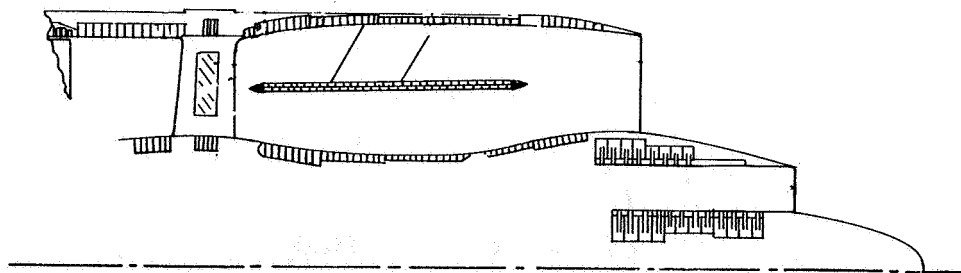
Figure 10

Exhaust Quadrant PNL Variation
With Thrust

Baseline (Frame Treatment Only)
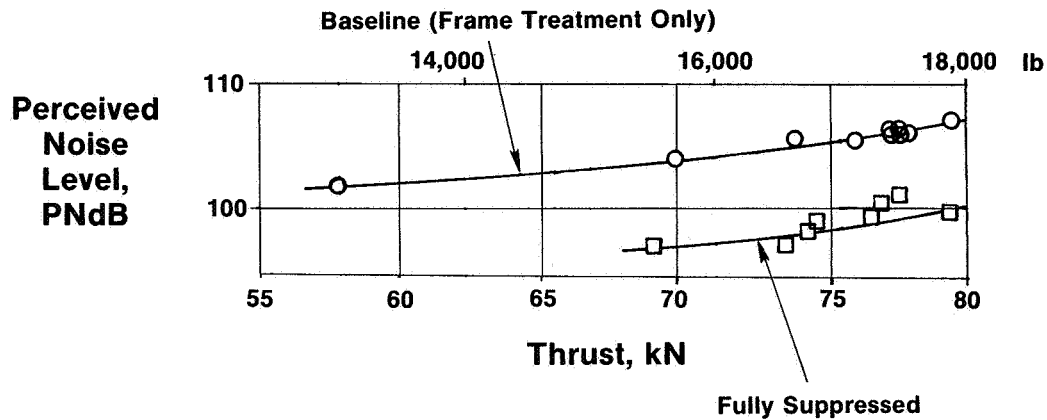
Figure 11

Exhaust Quadrant System Suppression Spectra

• Wall Treatment Only
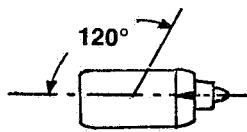
1/3 OBSPL
Suppression,
Δ dB

	Δ PNdB	
	Approach	Takeoff
Measured	4.4	4.0
Predicted	5.8	5.4

Figure 12

239
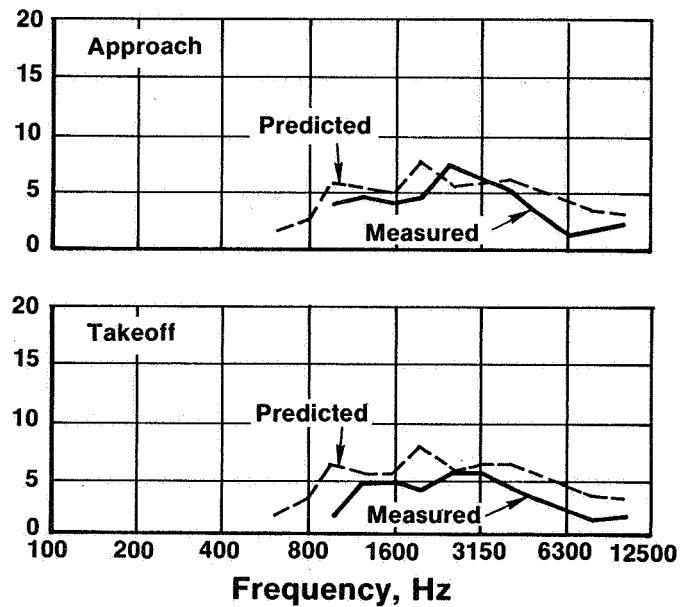
Exhaust Quadrant System Suppression Spectra

120°
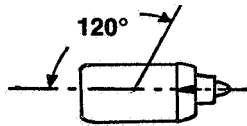
- **With Splitter**

**1/3 Octave
Band SPL
Suppression, dB**

	Δ PNdB	
	Approach	Takeoff
Measured	8.0	7.5
Predicted	9.6	9.2
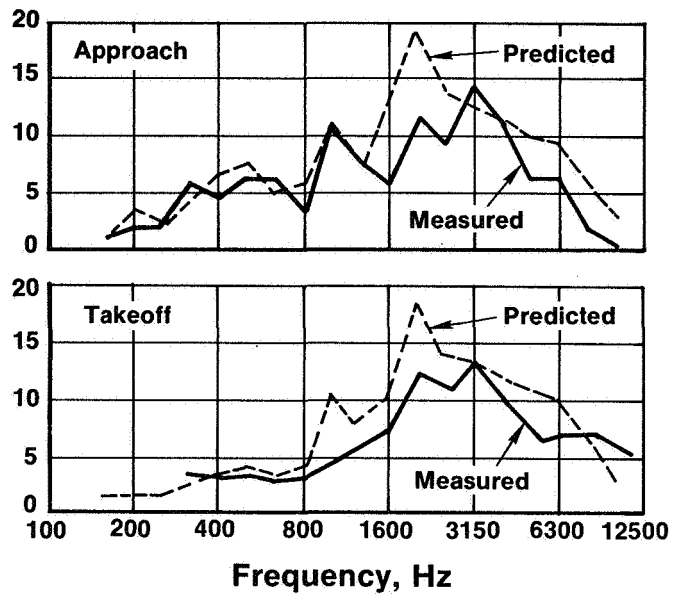
Figure 13

Treated Vane Suppression

**Vane
Treatment**

120°
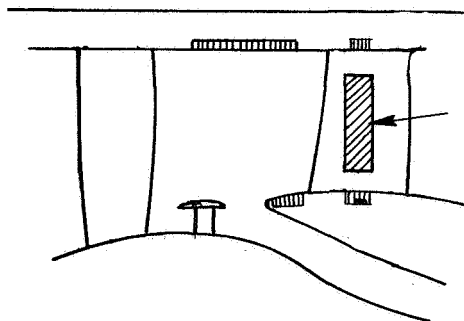
**1/3 Octave Band
Sound
Pressure
Level
Suppression,
dB**

Figure 14

240
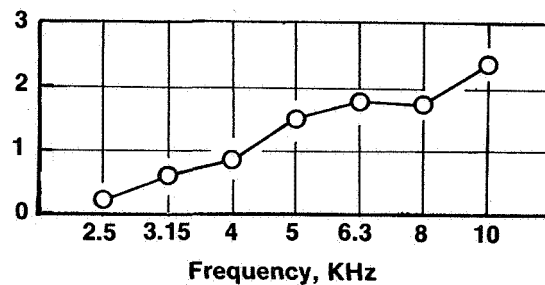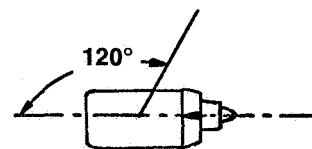
Core Suppression
From Far Field Measurements
Approach Thrust

1/3 Octave Band
SPL
Suppression,
dB

Frequency, Hz
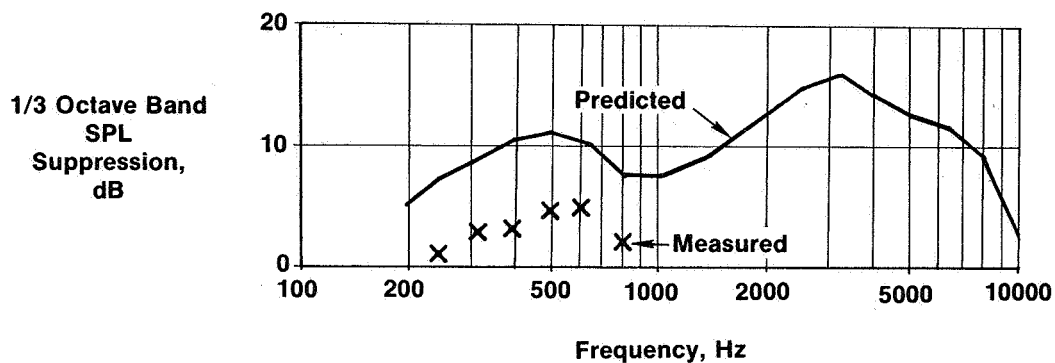
Figure 15

Variation of Peak PNL With Percent
Reverse Thrust

152m (500 ft) Sideline
Fully Suppressed

Perceived
Noise
Level,
PNdB

Blade Angle

■ 95° Open
● 100° Open

Percent of Takeoff Thrust
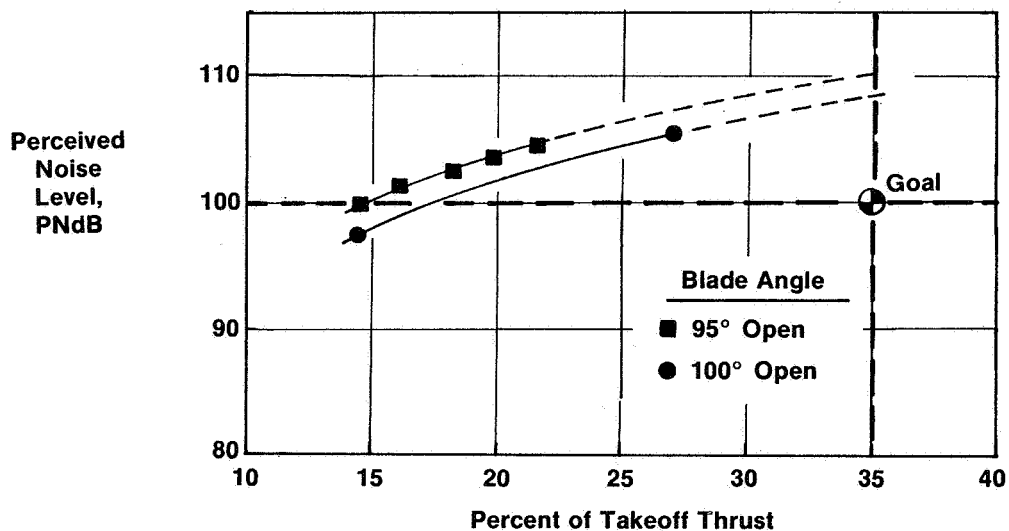
Figure 16

QCSEE OTW Engine
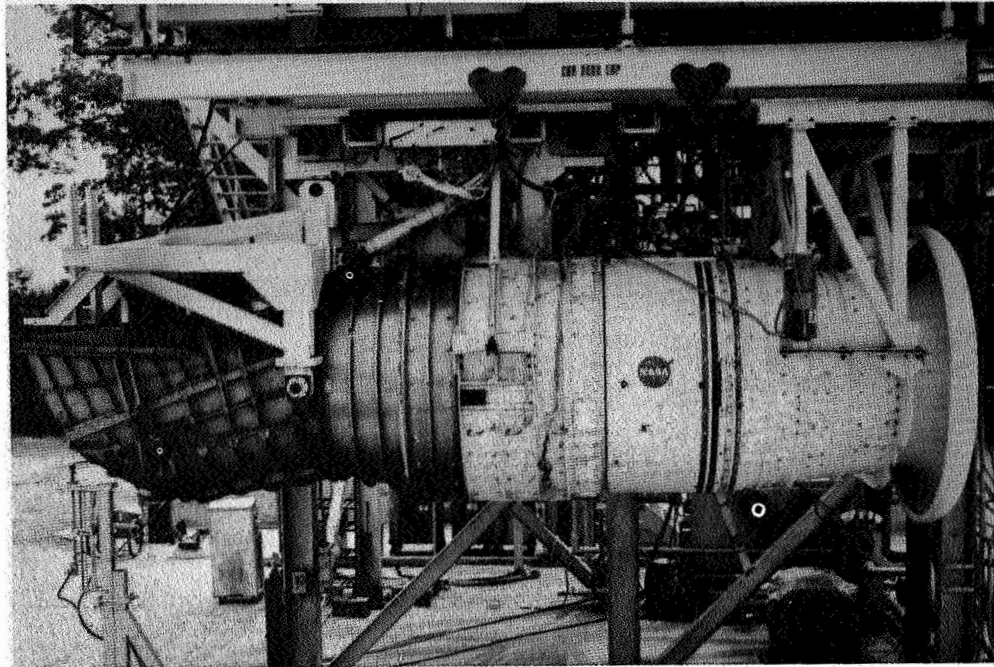
Figure 17

OTW Acoustic Test Configurations
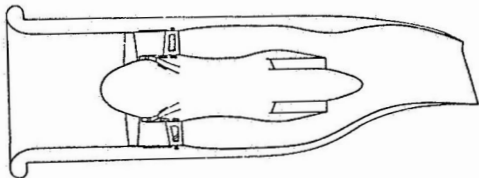
Baseline
1. **Untreated Except for Frame and Vane Treatment**
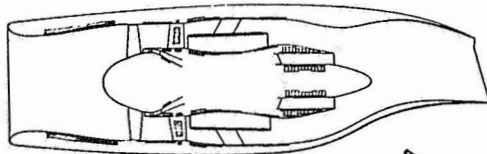
Suppressed Engine-Forward Thrust
2. **Fully Suppressed**
3. **Untreated High Mach Inlet**
4. **Untreated Core and Splitter Removed**
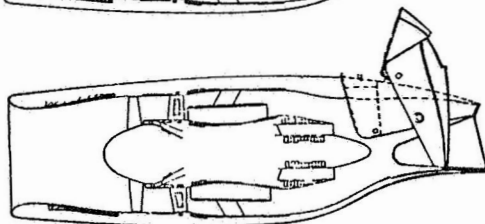
Suppressed Engine-Reverse Thrust
5. **Fully Suppressed**

Figure 18

OTW Inlet Radiated Baseline Noise

Takeoff Power
46.5m (152.4 ft) Arc
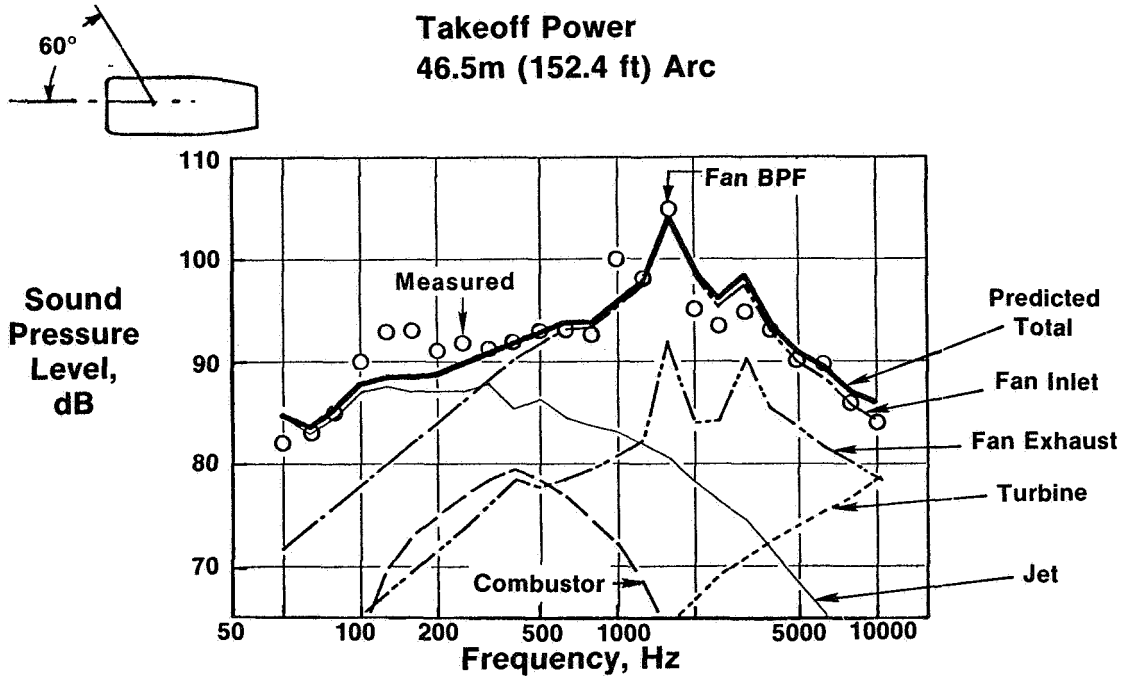
Figure 19

OTW Exhaust Radiated Baseline Noise

- ### Takeoff Power
- ### 46.5m (152.4 ft) Arc

Figure 20

243
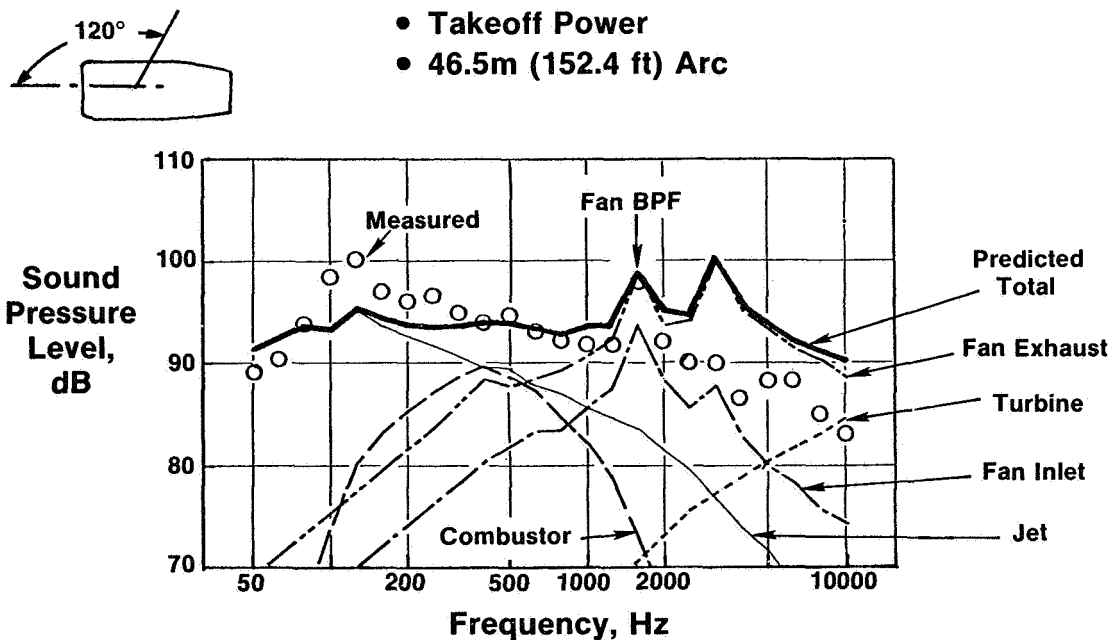
OTW Inlet Configuration

Throat

Bulk Absorber
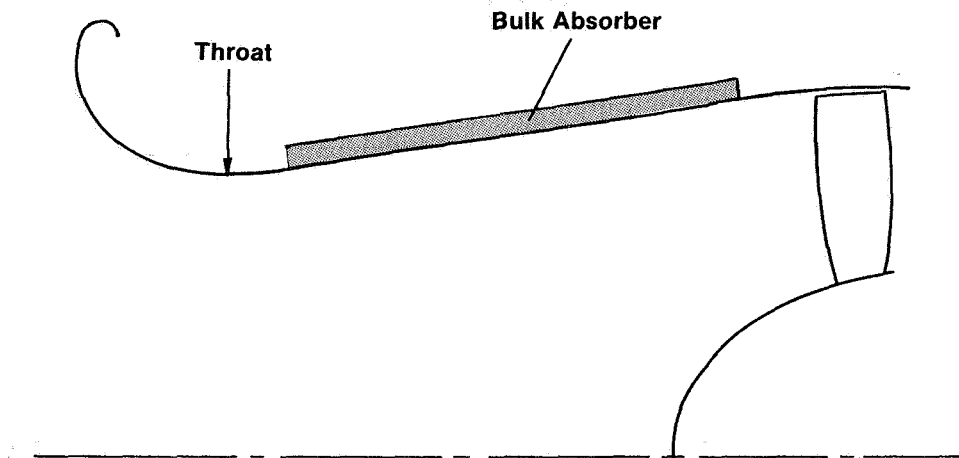
PNL Suppression Predicted

Takeoff   13.5 PNdB
Approach   10.4 PNdB

Figure 21

OTW Inlet Radiated Noise at Takeoff

152m (500 ft) Sideline

60°

○ Bellmouth
◇ Untreated High Mach Inlet
□ Treated High Mach Inlet

Sound
Pressure
Level,
dB

PNL Suppression
Predicted 13.5
Measured 14.0

Estimated Jet

Frequency, Hz
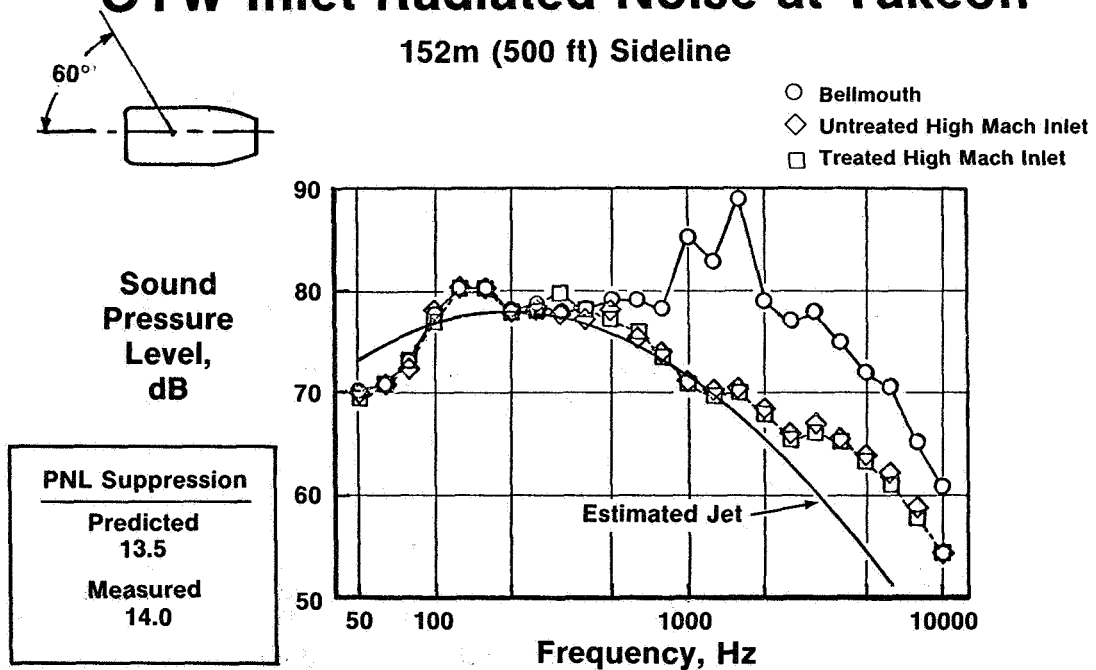
Figure 22

OTW Inlet Radiated Noise at Approach
152m (500 ft) Sideline

60°

O Bellmouth
◇ Untreated High Mach Inlet
□ Treated High Mach Inlet
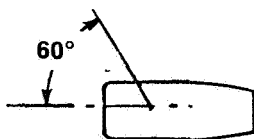
Sound
Pressure
Level,
dB

PNL Suppression	
Predicted	Measured
10.4	7.5

Estimated Jet

Frequency, Hz
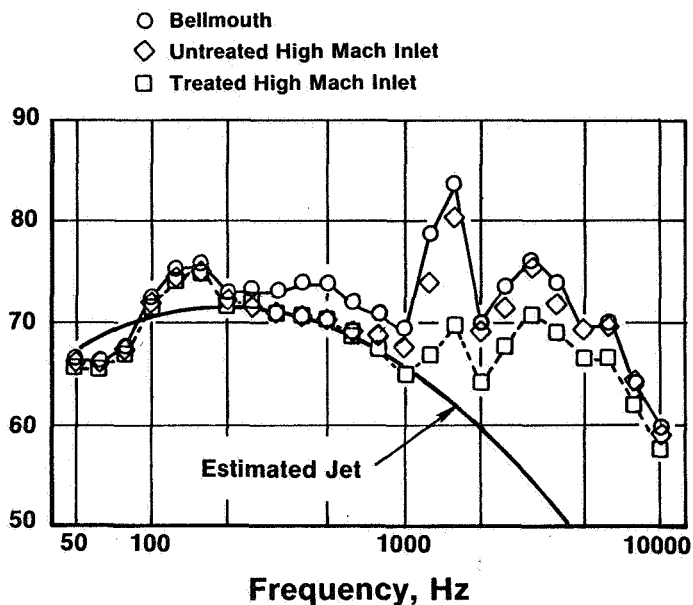
Figure 23

Measured Exhaust PNL
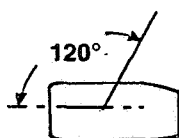
- **152m (500 ft) Sideline**
- **Flagged Symbols Corrected for Jet Noise**

120°

O Baseline
□ Fully Suppressed

Perceived
Noise
Level,
PNdB

Baseline

Fully Suppressed

Percent Corrected Fan Speed

Figure 24

245

OTW Exhaust Radiated Noise at Takeoff

Figure 25

OTW Exhaust Suppression at Takeoff
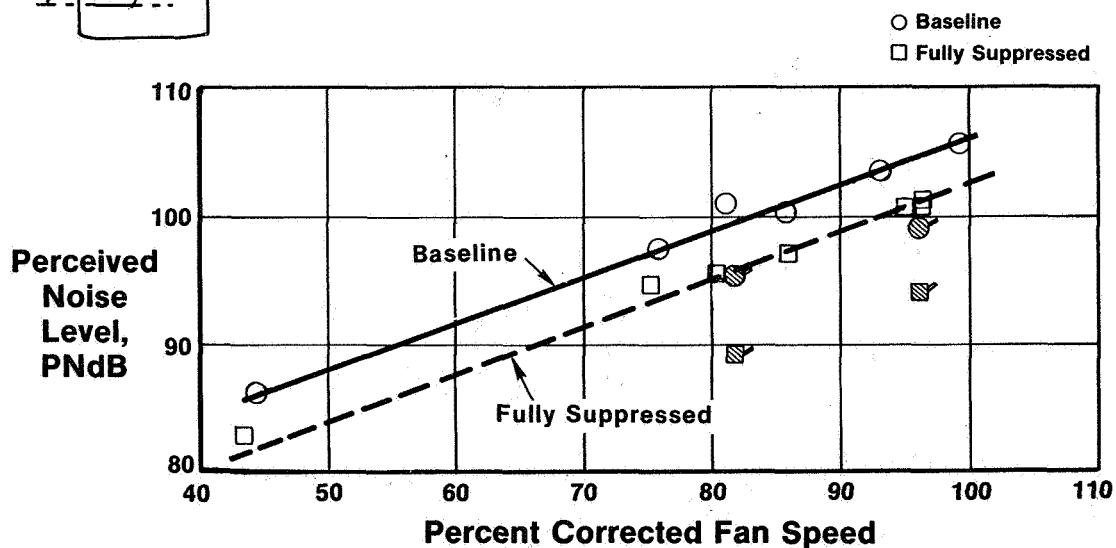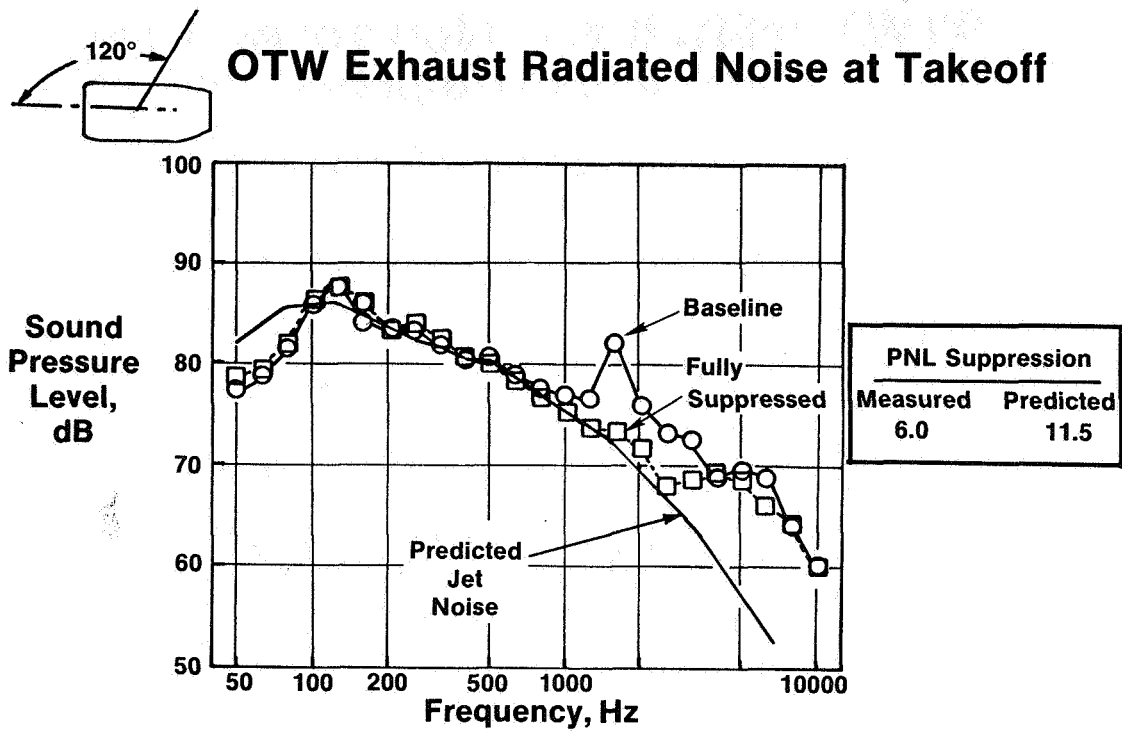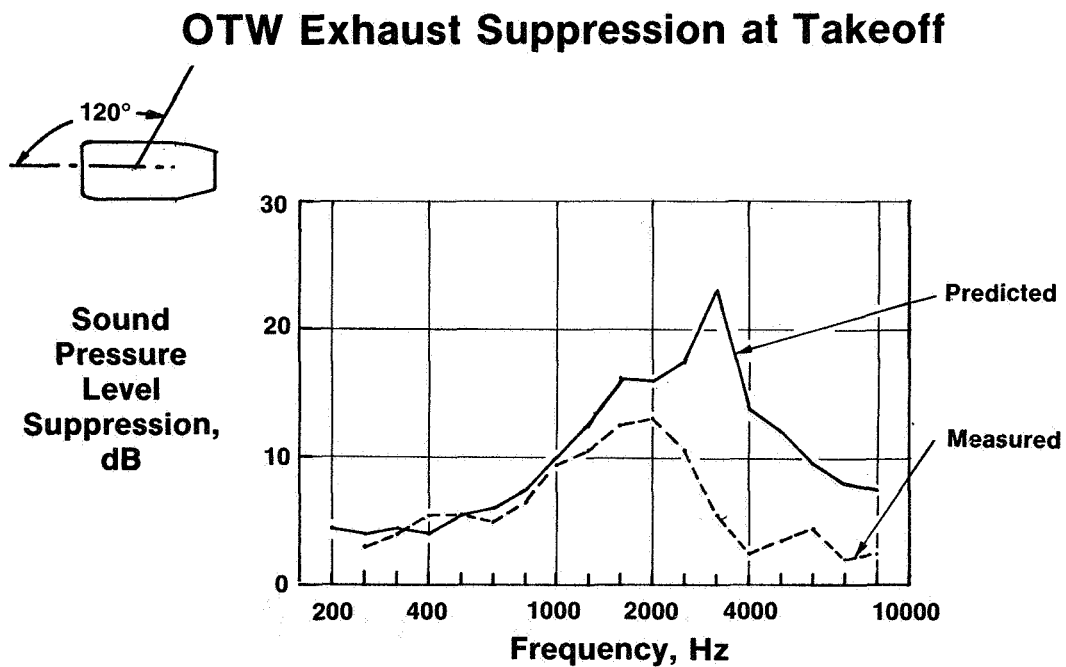
Figure 26

QCSEE OTW Engine With Thrust Reverser Deployed
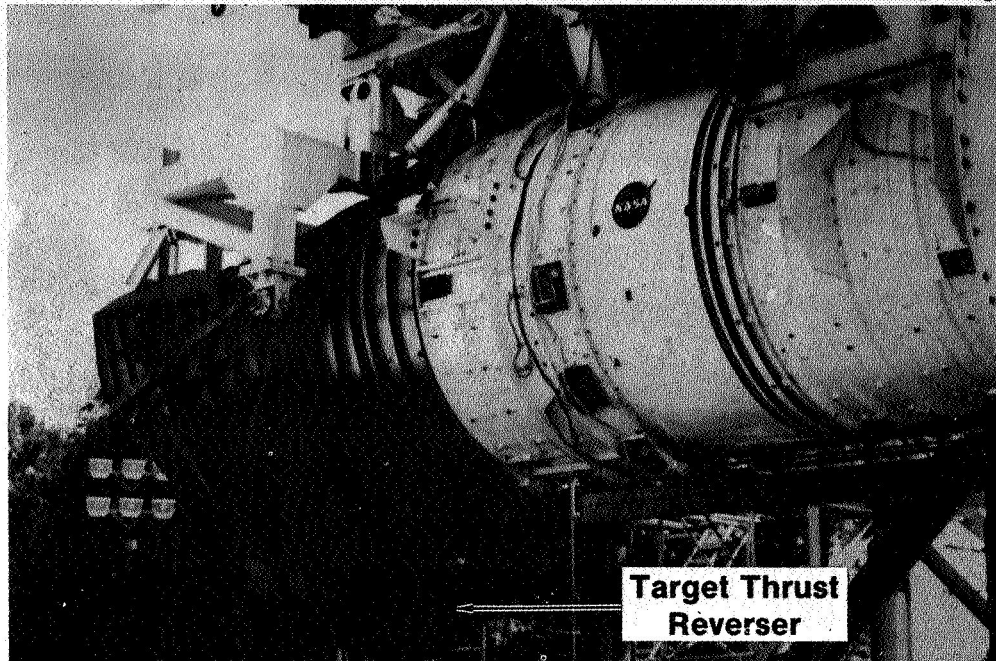
Figure 27

OTW Reverse Thrust System Noise

152m (500 ft) Sideline
Fully Suppressed
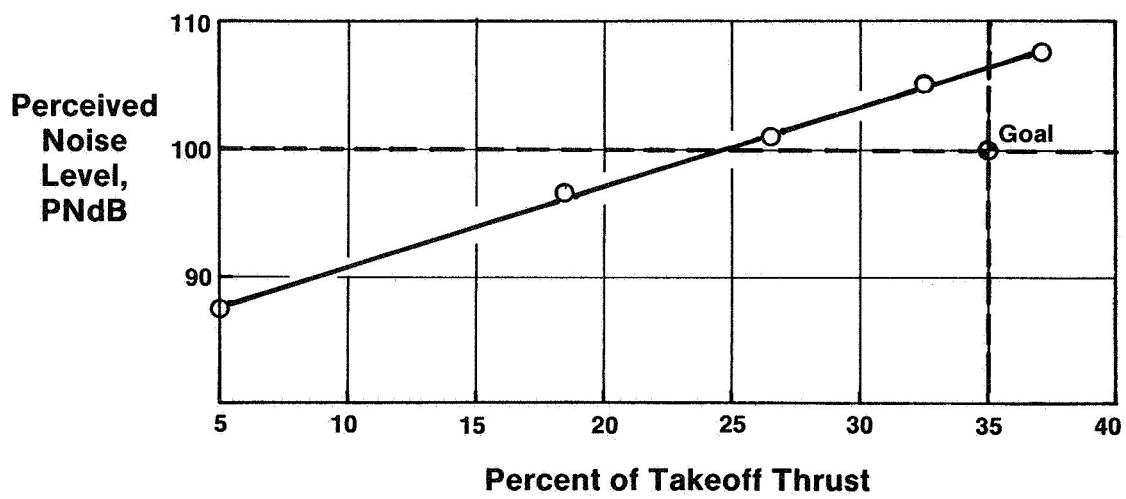
Figure 28

QCSEE Approach and Takeoff
EPNdB Contours
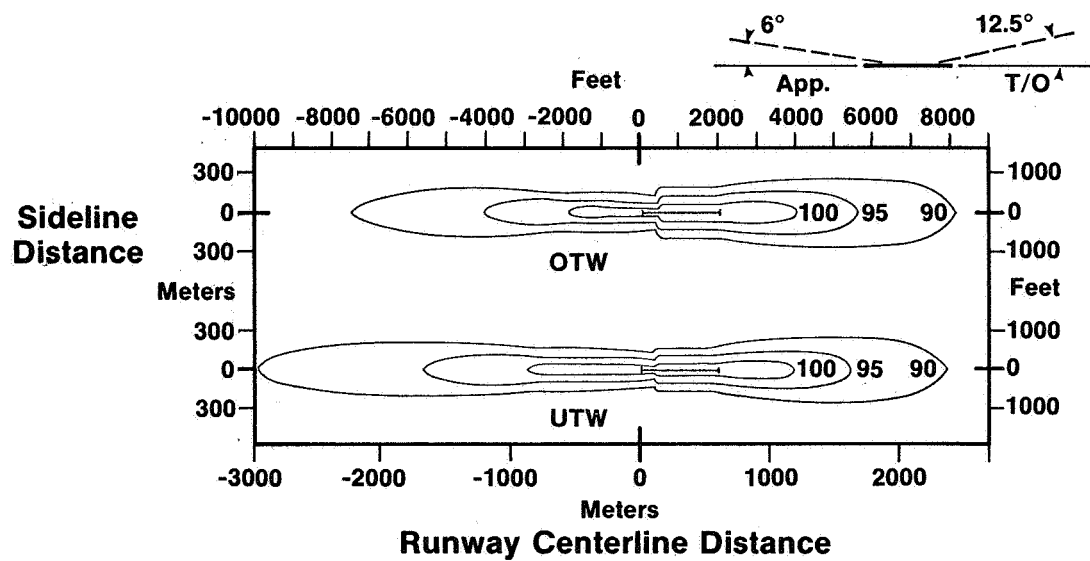
Figure 29

QCSEE ENGINE AND WING TESTS AT NASA*

Irvin J. Loeffler
NASA Lewis Research Center

SUMMARY

The QCSEE under-the-wing (UTW) and over-the-wing (OTW) engine test program includes engine and wing tests at NASA Lewis to directly measure powered-lift system noise. The OTW engine and wing tests are currently in progress; the UTW tests are scheduled. The OTW, powered-lift system, takeoff noise level of 98.4 EPNdB exceeds the 95-EPNdB noise goal; while the 94.6-EPNdB approach noise level meets the goal. The 95-EPNdB contour area goal of 1.3 km^2 (0.5 mi^2) was also achieved. Slightly lower total system levels were obtained from engine-alone tests by the General Electric Co., due primarily to slight differences between the jet-flap noise of the NASA test and the jet-flap noise specification used during the design of the engine and in the engine-alone tests. Most of the QCSEE acoustic technology is applicable to convential jet engines.

INTRODUCTION

The QCSEE takeoff and approach noise goals were established for the complete powered-lift system in flight and include jet-flap noise as well as engine noise. Jet-flap noise results from the interaction of the engine exhaust with the wing and flap surfaces in the production of powered-lift. In a UTW installation, the jet-flap noise is also known as externally blown-flap (EBF) noise. For an OTW installation, the term upper surface blowing (USB) is sometimes used.

Engine-alone acoustic tests were conducted by General Electric, as reported in the preceding paper. To obtain powered-lift system noise levels from these tests, it was necessary to mathematically add predicted jet-flap noise levels to the measured engine noise. The purpose of the engine and wing tests at NASA Lewis is to measure directly the combined engine and jet-flap noise.

OTW TEST CONFIGURATIONS

Three OTW configurations, for which tests have been completed, are illustrated in figure 1. The first configuration is the fully suppressed engine with a wing and flap system. Acoustic suppression is provided by the high-Mach-number inlet and by acoustic treatment shown by the blackened areas in the fan inlet and exhaust and engine-core flow passages.

The OTW wing surface is a Whitcomb supercritical wing design. The rela-
tive dimensions correspond to the inboard engine mounting of a four-engine air-
craft. The wing and flap system was tested with two flap-angle settings; a 30°
trailing-edge angle for 30° of flow turning at takeoff and a 75° trailing-edge
angle for 60° of flow turning at approach. The wing-and-flap length from the
engine nozzle to the flap trailing edge, measured in multiples of the engine
nozzle height, was 6.2 for the takeoff flap setting and 6.6 at approach. The
span length of the wing segment was 7.1 engine nozzle heights. This configura-
tion is the prime configuration with respect to the QCSEE program goals.

For the second configuration the splitter and core treatment are removed,
giving a partially suppressed engine with wing. The third configuration, the
partially suppressed engine alone, is the same as the second configuration, but
with the wing removed.

QCSEE TEST FACILITY

The QCSEE test facility is illustrated in figure 2. The trimetric drawing
shows the UTW engine and wing with the span in the vertical direction. The OTW
engine and wing were mounted in a similar manner, with the OTW D-shaped nozzle
turned on its side for proper alinement with the upper surface of the wing.

The primary microphone system for QCSEE measurements is the sideline noise
measurement array, in which microphones are suspended from a cable hanging be-
tween a 36.6-m (120-ft) high tower and a shorter, 18.3-m (60-ft) tower. These
microphones lie in a plane perpendicular to the engine axis. They are located
on the cable at selected positions that correspond to the angle, with respect
to an observer on the ground, of an aircraft flying at altitudes, respectively,
of 0, 30.5, 61.0, 91.4, and 121.9 m (0, 100, 200, 300, and 400 ft) on a 152.4-m
(500-ft) sideline.

A photograph of the test arena is shown in figure 3. The asphalt surface
of the sound field is painted white, except for the area immediately adjacent
to the engine, to minimize thermal gradients and ground surface turbulence.
The sideline microphones can be seen hanging from the supporting cable. One
microphone was attached to a portable boom to obtain sideline microphone data
at directions other than 90° from the engine, which is a limitation of the
fixed tower microphone system.

EXHAUST FLOW VELOCITY MEASUREMENTS

Before conducting acoustic tests external-flow measurements were made to
determine whether the engine exhaust flow was properly attached to the upper
surface of the wing-flap system. A sample of the measured velocity distribu-
tion with the takeoff flap is shown in figure 4. Velocity measurements were
made at the engine exhaust-nozzle exit plane, near midwing, and at the flap
trailing edge. The values shown in the figure are measured local velocities
divided by the mass-averaged nozzle-exit velocity. In the chordwise direction

a continuous velocity decay is evident as the flow approaches the trailing edge of the flap. The velocity contours in a plane normal to the flow evidence the higher velocity core flow. At the flap trailing edge it is quite evident that the high-velocity flow remains near the wing surface, indicating that the flow is attached at the trailing edge. Similar profiles were obtained for the approach flap measurements and for a variety of engine speeds.

ACOUSTIC TEST RESULTS

Comparison of NASA and General Electric Data

Engine-alone noise for the partially suppressed engine at takeoff conditions is presented in figure 5 as measured by NASA and by General Electric. Since engine acoustic evaluation measurements in the QCSEE program involve two quite different test facilities with quite different engine mountings, an inverted D nozzle at General Electric; and a side-mounted D nozzle at NASA; it is desirable to know whether the NASA and General Electric measurements can be directly compared. The two test arenas have only one microphone direction in common, the 30.4-m (100-ft) altitude microphone on the NASA facility, and the 12.2-m (40-ft) high, 90° microphone of the General Electric Peebles facility. The measured spectra were corrected to free-field conditions. Agreement is very good at both low and high frequencies with only minor discrepancies. The NASA perceived noise level (PNL) is 0.7 dB higher than the General Electric value. About 0.4 dB of this can be accounted for in that the engine corrected speed of 96.4 percent at NASA exceeds the engine speed of 94.6 percent at General Electric.

Engine Alone and Total System Noise

Figure 6 compares the engine-alone noise and total system noise for the partially suppressed engine. The spectra are for takeoff conditions on a 152.4-m (500-ft) sideline at an altitude of 91.4 m (300 ft). The engine-alone noise peaks at about 400 Hz. Above 800 Hz engine-alone noise is dominated by the fan-exhaust noise. With the addition of the wing and flap system, an increase in low-frequency noise, characteristic of jet-flap noise is observed. However, the fan-exhaust broadband noise above 800 Hz is reduced some 5 or 6 dB below the engine-alone levels, an indication of the effectiveness of wing shielding of sideline noise for the OTW powered-lift system.

Note also that the blade-passing frequency (BPF) tone is not completely suppressed to the broadband level in the engine-alone spectrum and remains almost equally visible in the total system spectrum indicating that engine noise is dominant in the high-frequency region.

Measured and Predicted Powered-Lift System Noise

Measured and predicted powered-lift system noise levels at takeoff are plotted in figure 7. The spectrum given by the solid triangles was obtained by combining engine-alone noise with jet-flap noise. The jet-flap noise was obtained from NASA Lewis acoustic tests of a 1/12-scale model of the QCSEE OTW D-shaped nozzle with a wing and flap system (ref. 1); the engine-alone noise was obtained from measured engine noise with adjustment for wing shielding and with jet noise removed. The combination of the two noise spectra is a prediction of the total system noise. The measured total-system noise (open triangles) shows good agreement with the predicted levels at the lower frequencies. But at higher frequencies, where there is more divergence, the data indicate the possibility of a larger wing shielding effect than the 5-dB adjustment in engine-alone noise spectrum.

Effect of Flap Angle

In figure 8 the effective perceived noise level (EPNL) is plotted as a function of the mass-averaged exhaust velocity for both the takeoff and approach flap settings. For the partially mixed flow of the QCSEE D-shaped nozzle, the powered-lift system's perceived noise level is relatively insensitive to the flap-angle setting for fixed engine operating conditions. This result is consistent with jet-flap noise test results of small-scale, single-flow, round nozzle and wing-flap systems (refs. 2 and 3).

Powered-Lift System Inflight Noise

The QCSEE OTW powered-lift-system's inflight noise levels are plotted as a function of altitude on a 152.4-m (500-ft) sideline in figure 9. The inflight noise levels are determined from the measured static noise test levels 90° from the inlet, as obtained by the sideline microphone array system. Data from ground tests of the engine and wing system are extrapolated to the inflight condition by accounting for atmospheric attenuation, extra ground attenuation, fuselage shielding, inlet cleanup, relative velocity effects, and conversion from PNL to EPNL values (see appendix A of ref. 4).

During the design phase of the contract the only available test model data for jet-flap noise were for NASA tests of circular nozzles with exhaust deflectors to insure flow attachment to the upper wing surface (ref. 2). Detailed calculations based on these data indicated that the jet-flap noise would peak at an altitude of 61 m (200 ft) and would be about 0.4 dB lower at an altitude of 91.4 m (300 ft).

Figure 9 shows that at takeoff the maximum is actually achieved near 91.4 m (300 ft). This is true for both the fully and partially suppressed engine systems. The partially suppressed engine's maximum level of 98.1 EPNdB is lower than the fully suppressed engine's 98.8 EPNdB. The difference, however, is due

252

to data scatter in jet-flap noise in the low-frequency end of the spectrum. At takeoff exhaust velocities the jet-flap noise dominates and obsured, in this case, a slight advantage for the fully suppressed engine in the high-frequency fan-noise region. Hence, instead of the lower value of 98.1, the average of the two values, 98.4 EPNdB, will be considered as the takeoff noise value. The General Electric engine-alone acoustic tests resulted in an OTW system takeoff noise level of 97.2 EPNdB (see previous paper). This is 1.2 dB below the NASA engine and wing test value. However, the jet-flap noise specification for the engine design effort and for the General Electric system noise calculation was based on circular nozzle studies by NASA, with an allowance for lower jet-flap noise with expected advances in jet-flap noise technology. Since engine-alone noise levels at NASA and General Electric are comparable, it is evident that the jet-flap noise associated with the current state-of-the-art flap is somewhat higher than the previously used specification for the takeoff condition.

At approach the maximum measured EPNL occurred at an altitude of 121.9 m (400 ft), reflecting directivity differences between the takeoff and approach conditions. At approach the relative contribution of fan exhaust noise is greater than at takeoff, and the superior suppression of the fully suppressed engine results in lower inflight noise levels than for the partially suppressed engine system. Thus, the approach noise level is 94.6 EPNdB, which, by coincidence, is the same value obtained from the General Electric engine-alone acoustic tests as presented in the previous paper.

OTW powered-lift system inflight noise is plotted against the mass-averaged engine exhaust velocity in figure 10. The lower curve shows the variation of system noise with velocity for the takeoff flap setting at an altitude of 91.4 m (300 ft) on a 152.4-m (500-ft) sideline. At the takeoff exhaust velocity the maximum system noise is about 3.4 EPNdB above the 95 EPNdB goal, as indicated earlier. At the approach condition the maximum measured inflight noise occurs at an altitude of 121.9 m (400 ft). The approach noise level of 94.6 EPNdB meets the 95 EPNdB noise goal. Both curves show a variation of EPNdB with approximately the fifth power of the exhaust velocity for the straight line approximations to the data.

QCSEE POWERED-LIFT SYSTEM NOISE STATUS

The QCSEE powered-lift system noise status is summarized in table I. From engine-alone acoustic tests with an extrapolation to powered-lift system noise levels in flight and using a NASA jet-flap noise specification, General Electric obtained values of 97.2 EPNdB at takeoff and 95.7 EPNdB at approach for the UTW system. These values are slightly above the 95 EPNdB goal for both conditions. The 95-EPNdB contour area of 1.0 km^2 (0.38 mi^2), however, does meet the goal of 1.3 km^2 (0.5 mi^2).

For the OTW system, General Electric reported values of 97.2 EPNdB at takeoff, slightly over the goal, and 94.6 EPNdB at approach, slightly below the goal. Here again, the OTW 95 EPNdB contour footprint area of 0.8 km^2 (0.32 mi^2) meets the 1.3 km^2 (0.5 mi^2) goal.

From NASA engine-and-wing tests using current jet-flap technology for the OTW engine with the D-shaped nozzle, 98.4 EPNdB at takeoff was obtained - slightly higher than the General Electric value of 97.2 EPNdB. The difference is due to jet-flap noise, which dominates the system noise level at takeoff. Any significant reduction of this level requires a flap designed for lower noise or a reduction in fan pressure ratio since jet-flap noise reduction is primarily needed.

At approach the NASA engine-and-wing test results are in agreement with the General Electric engine-alone value of 94.6 EPNdB. As for takeoff, the jet-flap noise elements are different for the NASA and General Electric test conditions, and the agreement is coincidental.

The projected 95-EPNdB noise contour footprint area of 1.3 km^2 (0.5 mi^2) also meets the 1.3 km^2 (0.5 mi^2) goal, although it is larger than the General Electric value.

The OTW powered-lift system, although designed for low noise at a sideline distance of only 152.4 m (500 ft) from the runway, is also some 7 EPNdB below the strict 1978 Stage 3 FAA limits at a 450-meter sideline, about 3 times farther from the runway.

If the takeoff and approach noise levels are averaged on a tradeoff basis similar to the FAA FAR 36 practices, the average for the two conditions is only 1.5 dB above the 95 EPNdB goal.

In summary, the QCSEE acoustic designs meet or nearly meet the powered-lift system noise goals, and provide considerably lower noise levels than the best of the current jet transports, the quiet, modern, wide-body jets. The QCSEE designs represent a significant advance in acoustic technology, most of which can also be applied to conventional jet engines.

REFERENCES

1. Olsen, W.; Burns, R.; and Groesbeck, D.: Flap Noise and Aerodynamic Results for Model QCSEE Over-the-Wing Configurations. AIAA Paper 77-23, Jan. 1977. (NASA TM X-73588, 1977.)

2. Clark, B.; Dorsch, R. G.; and Reshotko, M.: Flap Noise Prediction Method for a Powered Lift System. AIAA Paper 72-1028, Oct. 1973. (NASA TM X-71449, 1973.)

3. Dorsch, R.; Clark, B. J.; and Reshotko, M.: Interim Prediction Method for Externally Blown Flap Noise. NASA TM X-71768, 1975.

4. Quiet Clean Short-Haul Experimental Engine (QCSEE) Preliminary Analyses and Design Report, Vol. II. (R74AEG479-Vol. 2, General Electric Co.; NASA Contract NAS3-18021.) NASA CR-134839, 1974.

TABLE I. - QCSEE POWERED-LIFT SYSTEM NOISE STATUS

	500 ft SIDELINE, EPNdB		95 EPNdB NOISE CONTOUR AREA, sq mi
	TAKEOFF	APPROACH	
QCSEE GOAL	95	95	0.5
G.E. ENGINE ALONE NOISE TEST WITH NASA JET-FLAP NOISE SPEC			
UTW SYSTEM	97.2	95.7	.38
OTW SYSTEM	97.2	94.6	.32
NASA ENGINE-WING TEST WITH CURRENT JET-FLAP TECHNOLOGY			
OTW SYSTEM*	98.4	94.6	.5

*7 EPNdB BELOW NEW NOISE LIMIT AT FAA FAR 36 SIDELINE DISTANCE (FAR 1978 REV).

CS-78-3483

OTW ENGINE TEST CONFIGURATIONS

◼ ACOUSTIC TREATMENT

FULLY SUPPRESSED ENGINE WITH WING

PARTIALLY SUPPRESSED ENGINE WITH WING

PARTIALLY SUPPRESSED ENGINE ALONE

CD-12324-23

CS-78-3339
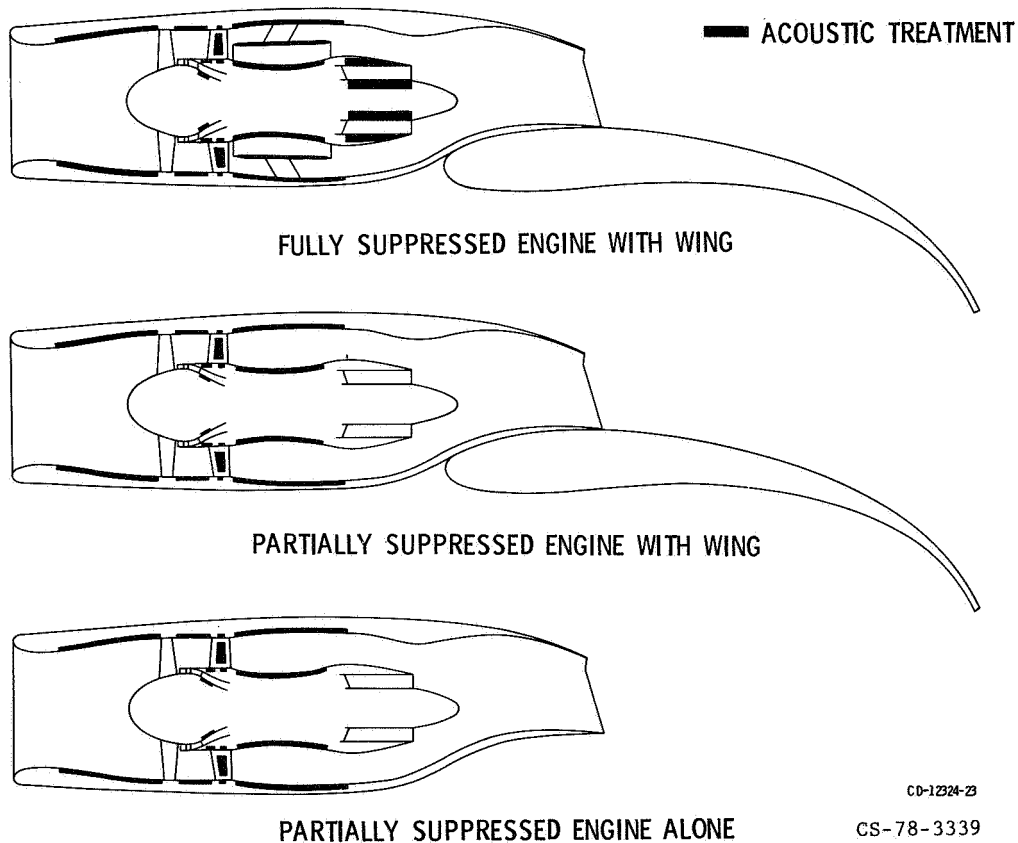
Figure 1

QCSEE TEST INSTALLATION
SHOWING MICROPHONE TOWERS
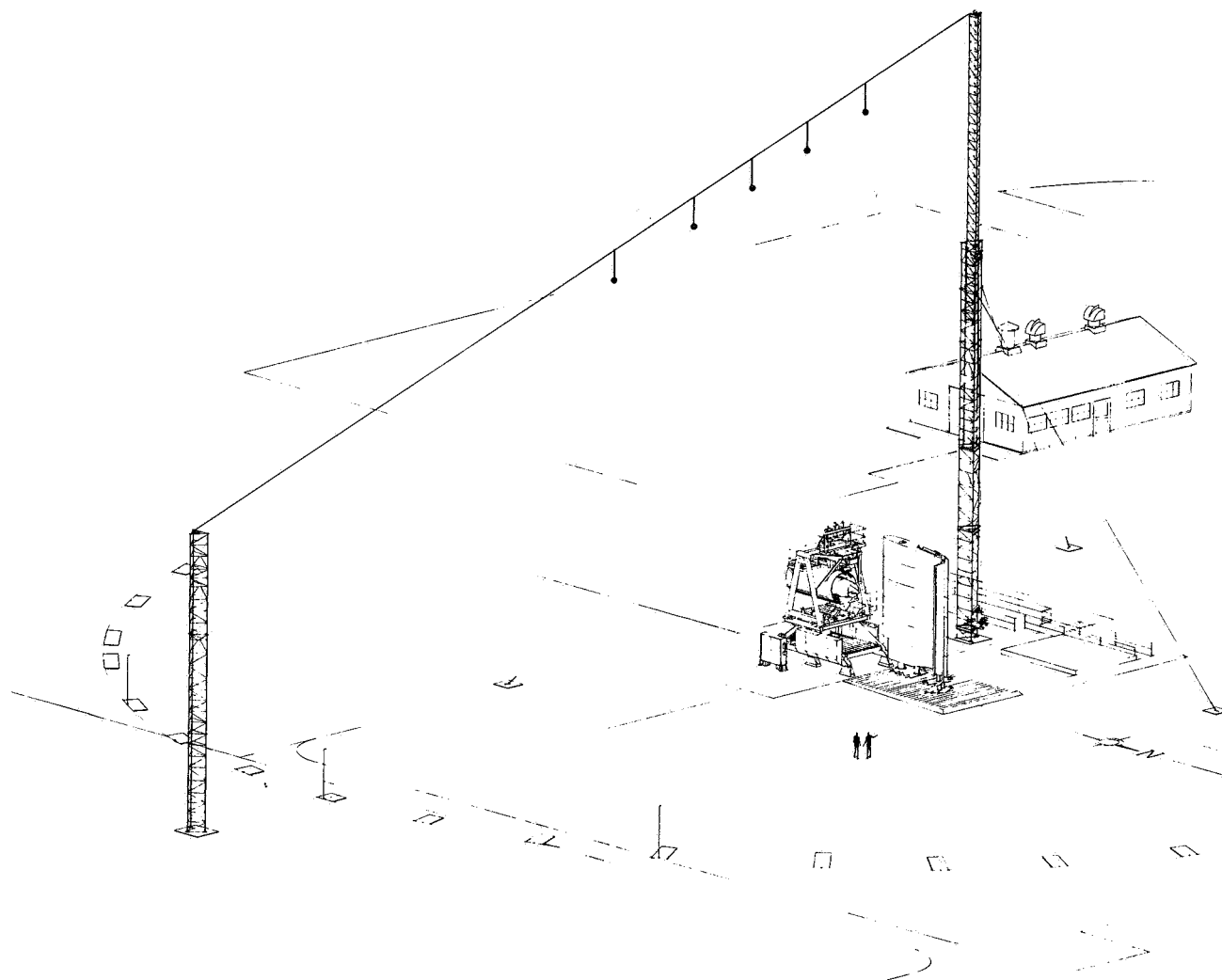
Figure 2

QCSEE TEST INSTALLATION
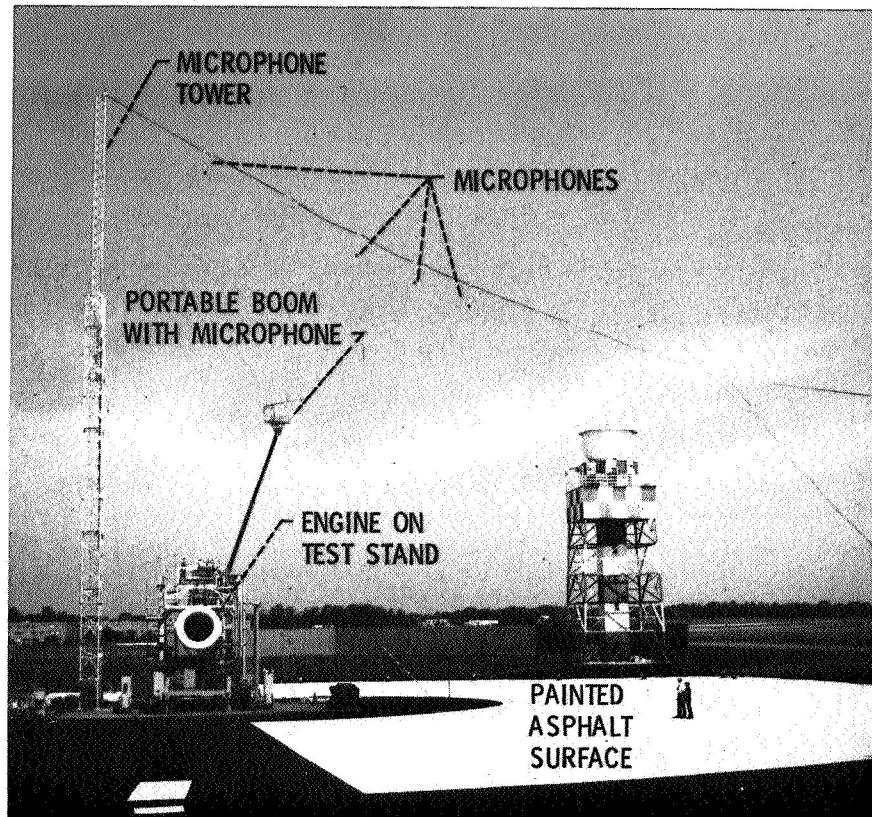
Figure 3

QCSEE OTW EXHAUST VELOCITY DISTRIBUTION

$$V = \frac{V_{LOCAL}}{V_{NOZZLE}}$$

STA

0 1

$V = 1.45$

2

1.35

3

$.95$

(a) ALONG CHORD $\cancel{\mathcal{L}}$.

STA 0

2h

h

STA 1

V

1.45

1.2

y/h

1.0

$.05$

$.5$

1.0

0   1.0

STA 3

y/h

2.0

1.0

$.95$

$.8$

V

0.05

$.2$

$.3$

$.5$

$.6$

0   1.0   2.0

x/h

CS-78-3334

(b) ALONG SPAN.
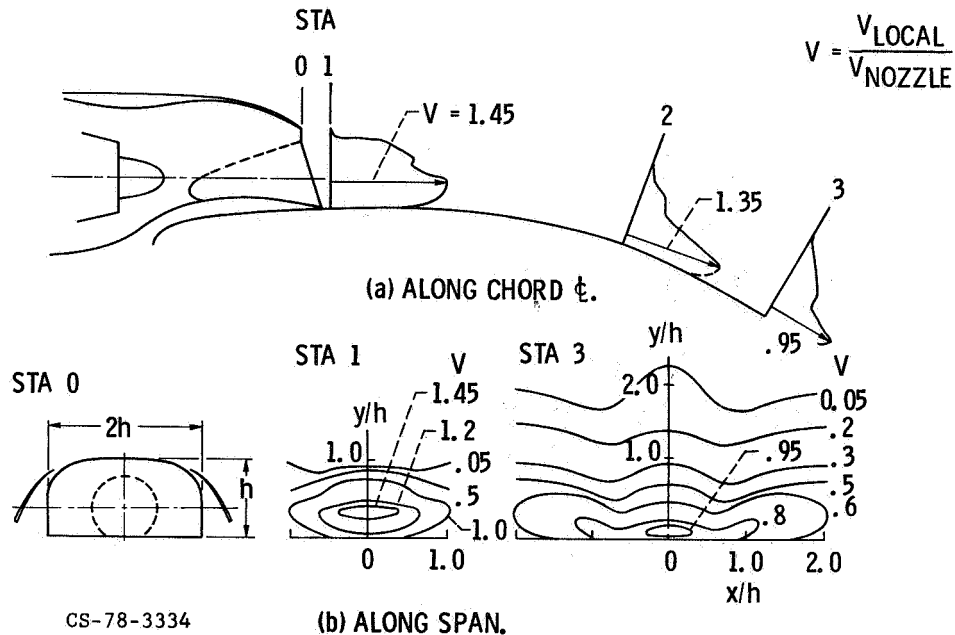
Figure 4

COMPARISON OF NASA AND GENERAL ELECTRIC ACOUSTIC DATA

PARTIALLY SUPPRESSED QCSEE OTW ENGINE; TAKEOFF SPEED;
FREE FIELD DATA ON 152 m (500 ft) SIDELINE AT 30.4 m (100 ft) ALTITUDE

1/3 O.B. SOUND PRESSURE LEVEL, dB

BPF

	% FAN SPEED	PNL, PNdB
O NASA	96.4	101.3
△ G.E.	94.6	100.6

FREQUENCY, Hz

CS-78-3332

Figure 5

258
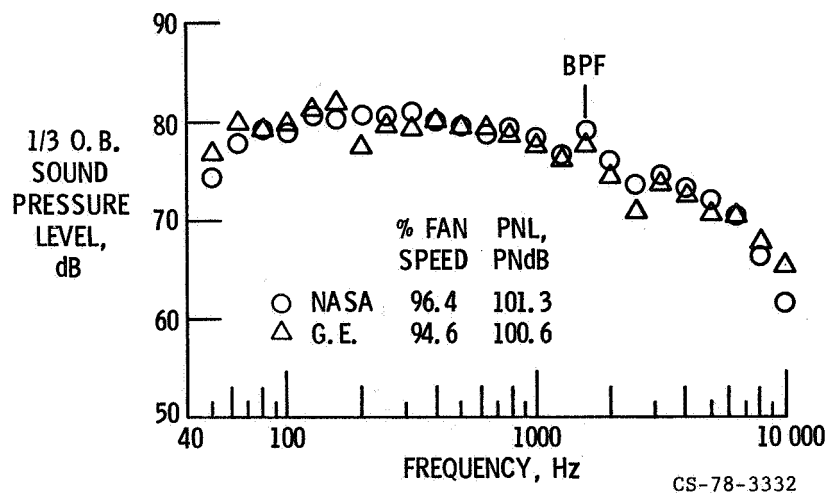
QCSEE OTW ENGINE ALONE VS POWERED LIFT SYSTEM NOISE

PARTIALLY SUPPRESSED ENGINE, TAKEOFF CONDITIONS;
152.4 m (500 ft) SIDELINE AT 91.4 m (300 ft) ALTITUDE

Figure 6

CS-78-3333
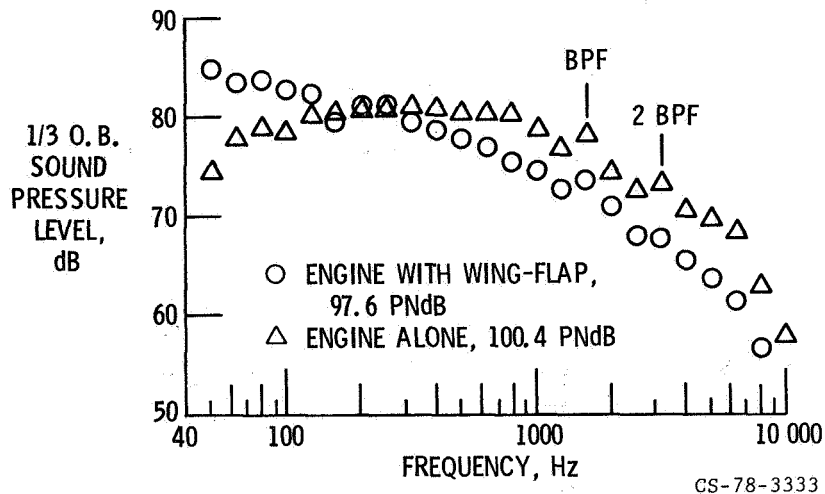
COMPARISON OF MEASURED AND PREDICTED POWERED LIFT SYSTEM NOISE

TAKEOFF CONDITIONS, PARTIALLY SUPPRESSED ENGINE,
152 m (500 ft) SIDELINE AT 91.4 m (300 ft) ALTITUDE

Figure 7

CS-78-3335
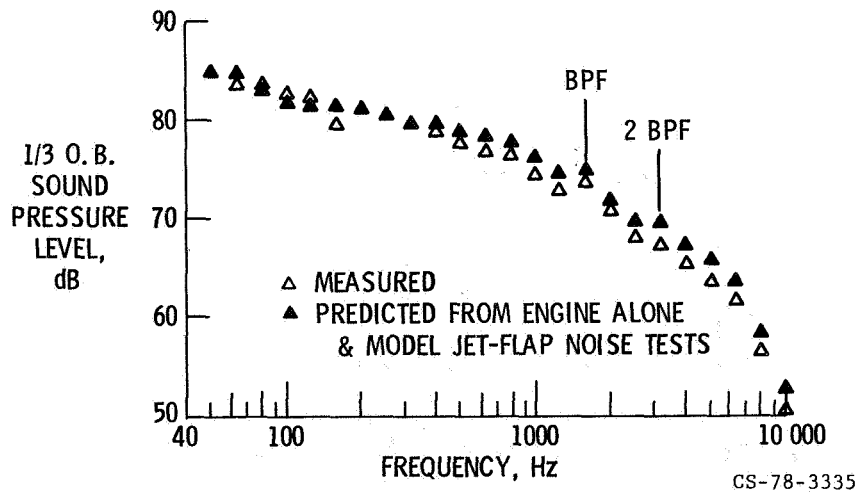
EFFECT OF FLAP ANGLE ON POWERED-LIFT SYSTEM NOISE

152.4 m (500 ft) SIDELINE AT 91.4 m (300 ft) ALTITUDE

FLAP SETTING
o 30° (TAKEOFF)
△ 60° (APPROACH)
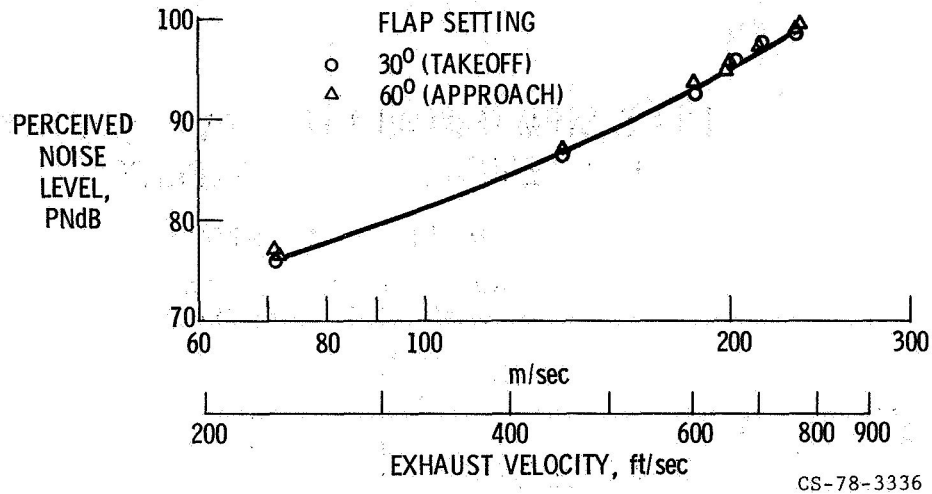
Figure 8

QCSEE OTW INFLIGHT NOISE LEVELS

152.4 m (500 ft) SIDELINE; 4 ENGINE AIRCRAFT; 400.3 KN (90 000 lb) THRUST

MODE	SUPPRES-SION	ALTITUDE m (ft)	MAX EPNdB
TAKEOFF	FULL	91.4 (300)	98.8 ⎫ 98.4
	PARTIAL	91.4 (300)	98.1 ⎭
APPROACH	FULL	122 (400)	94.6
	PARTIAL	122 (400)	95.6

o FULLY SUPP ENGINE
△ PARTIALLY SUPP ENGINE

Figure 9

260
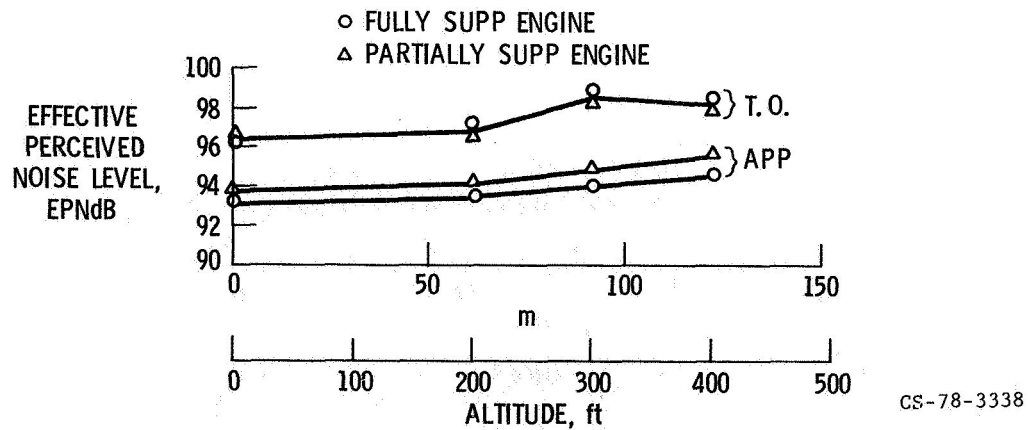
OTW POWERED-LIFT SYSTEM MAXIMUM EFFECTIVE PERCEIVED NOISE LEVEL VS ENGINE EXHAUST VELOCITY

FULLY SUPPRESSED ENGINE, 152.4 m (500 ft) SIDELINE

Figure 10

CS-78-3337

261
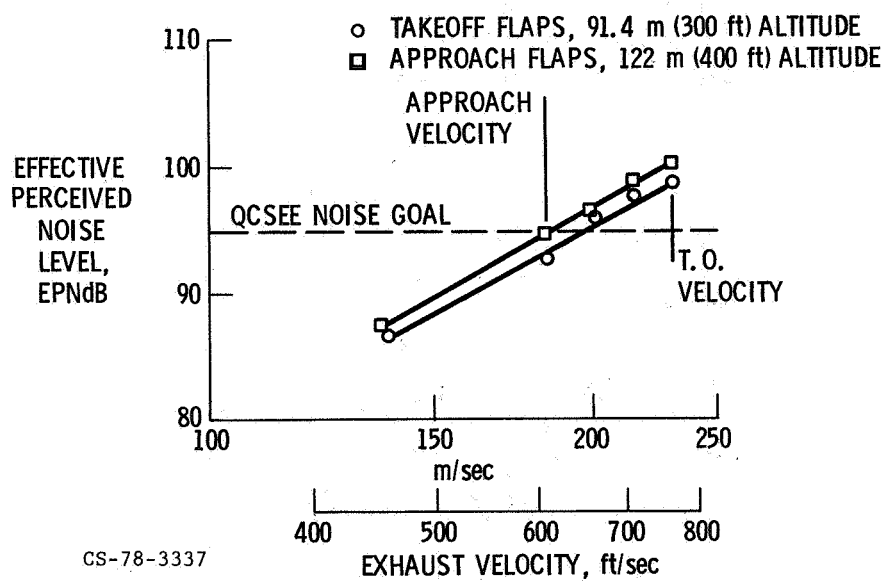
QCSEE OVERALL PERFORMANCE AND THRUST TO WEIGHT RATIO[*]

W.S. Willis
General Electric Company
Cincinnati, Ohio

INTRODUCTION

This paper will review the results of performance testing of both the UTW and OTW engines, and the results of weighing the experimental hardware. These results will be compared with the technical goals established at the start of the program, to bring into focus the benefits that can be realized by application of the QCSEE technology.

UTW PERFORMANCE TEST RESULTS

Figure 1 shows the UTW engine as it was initially tested with a bellmouth inlet for airflow calibration, and to establish uninstalled performance levels with essentially 100% ram recovery. The high throat Mach number inlet, shown in figure 2, was then used to determine installed performance with realistic induction losses.

Measured uninstalled thrust with the bellmouth inlet is shown on figure 3 as a function of airflow for operating lines established by four fan exhaust nozzle areas. Points along each operating line represent various combinations of blade angle and fan speed that can pump the indicated airflow. Thus, the curve is independent of blade angle and speed. the goal thrust level could be reached with a variety of settings of the controlled parameters.

Figure 4 shows the same parameters, thrust versus airflcw, but at a constant 97% corrected fan speed. Curved lines represent three fan blade angle settings. The sensitivity of thrust to blade angle is apparent in the three blade settings. No data points are shown, but the curve represents the best fit of all the data, cross-plotted to eliminate scatter. The goal thrust was reached at this fan speed with about 4° open blade setting over a more limited range of nozzle areas.

Typical SFC buckets are shown on figure 5, again as a function of the same three blade settings. The curve shows that at an open pitch setting of about 4° the SFC goal can be met at rated thrust. Since acoustic data did not indicate a significant difference in noise signature over a limited range of fan blade angles, the rating point was selected at 97% rather than 100% corrected speed and at the slightly opened pitch setting. Installed data

263

with the high throat Mach number inlet yielded similar results, but with thrust levels slightly reduced by the lower ram recovery of the flight design inlet.

Figure 6 shows the UTW engine with the exhaust nozzle in the flared position, acting as an inlet for reverse thrust testing. The engine was started and accelerated with the blades at the reverse setting, so no transitions were made from forward to reverse.

Figure 7 shows the reverse thrust performance with the blades set 95 and 100° open. Blade angle movement to these open angles indicates passage through aerodynamic stall rather than through flat pitch. This was the direction shown by the scale model fan test to provide the greatest reverse thrust. The open 95° position is nearer to the stall line, and produced a higher thrust per pound of airflow, but in both cases the turbine discharge temperature limit was reached before the 35% reverse thrust goal was achieved.

It was thought that the acoustic splitter might be channeling the flow in the outer annulus of the duct, and increasing the pressure loss into the core, so a run was made with the splitter removed. This did increase the reverse thrust by about 2% but again the turbine discharge limit prevented reaching the goal. Further work would be required to increase the reverse thrust capability.

Table I summarizes the UTW performance goals, and the demonstrated performance levels. The engine met both the uninstalled and installed forward thrust and SFC goals. The reverse thrust goal was not reached as noted above because operational limits were reached first; however, it did produce a potentially useful amount of reverse thrust. Aircraft studies indicated that the 27% reverse thrust that was achieved with the 100° open blade setting may be acceptable for stopping the airplane on a 914.4 m (3000 ft) runway.

OTW PERFORMANCE TEST RESULTS

Figure 8 shows the OTW engine which was also tested with both the bellmouth and boilerplate high throat Mach number inlets.

Since the "D" shaped exhaust nozzle was designed to turn the exhaust down over the wing/flap surface, and since the thrust meter was capable of reading the horizontal component only, its goals were based on an equivalent conical exhaust nozzle having a velocity coefficient of 0.995.

Measured axial thrust values are shown on Figure 9 as a function of corrected airflow. The effect of side door setting on exhaust nozzle area is apparent in the three different operating lines. Data includes both inlet configurations with fan inlet pressure being corrected to sea level. Excellent agreement is shown between the two inlets.

264

Figure 10 shows specific fuel consumption versus equivalent conical nozzle thrust for the same nozzle areas. The areas corresponding to a 11-1/2 and 25° side door settings are seen to meet the thrust goal and to better the SFC goals by about 3%. The 25° setting was selected for establishing the engine take-off rating.

The exhaust nozzle was run in the inverted position so that in the reverse configuration, the jet efflux would be directed forward and into the ground rather than into the overhead test facility and instrumentation lines. To avoid reingestion of hot exhaust gases and kicked up debris, a long reingestion shield was used as shown in figure 11. The effect of the shield on thrust meter reading was first calibrated in the forward thrust mode to establish a correction for the reverse thrust data.

Figure 12 shows the measured axial component of reverse thrust as a function of airflow for the two blocker door angles tested. While both angles exceeded the desired 35% reverse thrust, pressure loss in the turn was greater than expected. This caused a back-pressurizing of the fan and required a greater than expected fan speed. Although the 115° blocker angle produced more turning, and more reverse thrust per pound of airflow, it also produced a higher pressure loss. Both angles required 82% corrected fan speed to reach the 35% thrust goal. As discussed in the paper on nacelle aerodynamics, the turning loss could be reduced by increasing the bypass duct area and lowering the Mach number entering the turn. This would have a beneficial effect on reverse thrust noise by reducing both the jet velocity and fan speed.

The OTW engine met its uninstalled and installed forward thrust and exceeded its reverse thrust goal and SFC goal as shown in Table II.

MEASURED PROPULSION SYSTEM WEIGHT

Weight of each of the advanced components was measured during buildup of the engines. However, the UTW and OTW experimental engines contained a number of differences from ultimate flight configurations that affected system weight. These included the following items.

In the interest of reducing program cost, a number of material substitutions and fabrication shortcuts were made in the experimental hardware. An example is the use of titanium blades in place of composites in the OTW fan.

Boilerplate nacelle components were built to allow the use of interchangeable acoustic treatment and hardwall panels. The nacelle hardware was designed for use on both engines, with some compromise in flowpath and length for the OTW engine.

Both engines were heavily instrumented for experimental testing. A photograph of the UTW engine nearing completion of assembly is shown in figure 13. The weight of wires, tubes, connectors, rake mounting pads and slip ring supporting structure totalled several hundred pounds in each engine.

Finally, the engines were designed to meet noise objectives with a 609.6 m (2000 ft) runway. As a result of the airline's operational scenario and the aircraft company design studies, it was determined that a 914.4 m (3000 ft) runway would be a better compromise between ability to operate from small airports and aircraft economics. This would be reflected in a reduced take-off power setting for the flight engines, reducing noise and allowing the acoustic splitter and core exhaust nozzle treatment to be eliminated with significant weight saving.

Because of these differences between the experimental and flight engine configurations, it was necessary to modify the actual hardware weight results to reflect the equivalent weight of flight engines.

Table III shows the weight breakdown of the UTW experimental engine, and the projected weight of a UTW flight configuration. Some of the significant differences are as follows:

The F101 core was designed for a supersonic flight envelope and provided excess inlet temperature capability. The use of more titanium in the compressor and freedom to redesign the turbine frame would save weight as shown.

The fan rotor utilized a steel shaft, and the reduction gear a steel star carrier for cost saving. Substitution of titanium would save weight.

The composite fan frame included many shortcuts in fabrication technique material thicknesses, potting and sealing compounds, additional instrumentation and service lines. A detailed analysis of the measured frame weight showed that a substantial weight saving from the experimental hardware is possible, even after adding a metal sump liner to the flight frame.

Differences in the smaller components are primarily a result of using special purpose parts in place of off-the-shelf components.

Total projected weight of the flight engine is 1436 kg (3166 lb) compared to the actual weight of the experimental engine of 1693 kg (3732 lb).

Table IV shows a similar comparison of the nacelle components. The major differences here are a result of eliminating the acoustic splitter and core nozzle treatment. In addition a number of metal inserts for instrumentation rakes and struts could be eliminated. The core cowl could be made in two pieces instead of four if a larger autoclave were available. The equivalent flight weight of the composite nacelle is 466 kg (1028 lb) which, added to the engine weight, results in a total propulsion system weight of 1902 kg (4194 lb).

Table V shows the OTW engine weight breakdown. Differences between the experimental and flight weight numbers are much like those of the UTW engine with one major exception: the titanium fan blades and resulting heavier disk are reflected in a much greater saving in fan rotor weight in the flight configuration.

266

The OTW nacelle weight is shown on Table VI for the flight engine since only boilerplate components were built for this engine. The projected flight propulsion system weight is 1980 kg (4364 lb).

THRUST TO WEIGHT RATIO ASSESSMENT

Thrust to weight ratio was evaluated on both an uninstalled and an installed basis. Table VII shows both goal and projected values. The goals were set on the basis of conceptual design studies at the outset of the program. The projected numbers have been adjusted to take into account the results of actual design and testing experience. This experience has caused a small reduction in our expectations, but the absolute levels are still relatively high, and the reductions are within the scatter range of such predictions.

To place these installed values in their proper context, the experimental engine cycles were selected for acoustic and other considerations rather than to optimize weight. Large, high bypass engines generally suffer heavy installation penalties. These penalties have been largely offset by the lightweight integrated QCSEE nacelle components, with the result that both propulsion systems exhibit attractive installed thrust-to-weight characteristics that are comparable with the best of todays CTOL propulsion systems.

CONCLUSIONS

The general conclusion to be reached from the performance and weight analysis is that a short-haul propulsion system can be designed to meet stringent environmental requirements and can still have a high enough thrust-to-weight ratio to be economically competitive.

267

TABLE I. – UTW MEASURED PERFORMANCE.
SEA LEVEL STATIC, 305.5K (90° F) DAY

Forward Mode	Goal	UTW Engine
• Uninstalled Thrust kN (lb)	81.4 (18,300)	81.4 (18,300)
• Uninstalled SFC, g/sN (lb/hr/lb)	0.0096 (0.34)	0.0096 (0.34)
• Installed Thrust, kN (lb)	77.4 (17,400)	77.4 (17,400)
• Bypass Ratio	11.8	11.6
• Cycle Pressure Ratio	13.7	15.2
Reverse Mode		
• Installed Thrust, % Max Fwd.	35	27

TABLE II. – OTW MEASURED PERFORMANCE.
SEA LEVEL STATIC, 305.5 K (90° F) DAY
(Based on Equivalent Conical Nozzle, CV = 0.995)

Forward Mode	Goal	OTW Engine
Uninstalled Thrust, kN (lb)	93.4 (21,000)	93.4 (21,000)
Uninstalled SFC, g/sN (lb/hr/lb)	0.0102 (0.36)	0.0099 (0.35)
Installed Thrust, kN	90.3 (20,300)	90.3 (20,300)
Bypass Ratio	10.2	10.3
Cycle Pressure Ratio	15.5	17.2
Reverse Mode		
Installed Thrust, % Max Fwd.	35	35

TABLE III. — UTW ENGINE WEIGHT

	Experimental (kg)	(lb)	Flight (kg)	(lb)
Modified F101 Core & LPT Turbine	663	1461	622	1372
Fan Rotor	217	478	192	423
Reduction Gear	93	204	86	190
Composite Fan Frame	318	702	215	474
Brgs., Drives & Lube Components	275	607	201	444
Fuel System	32	70	20	45
Electrical System	26	58	15	33
VP Mechanism (Ball Spline)	69	152	62	137
Piping, Wiring and Misc.	36	80	22	48
Total Engine	1693	3732	1436	3166

TABLE IV. — UTW NACELLE WEIGHT

	Experimental (kg)	(lb)	Flight (kg)	(lb)
Composite Inlet	242	533	150	330
Composite Fan Duct	125	275	91	201
Composite Flare Nozzle	41	90	30	67
Composite Core Cowl	69	153	41	91
Core Exhaust Nozzle	93	206	64	142
Lube & Hydraulic System	161	354	78	172
Instrumentation (Approximately)	227	500	11	25
Total Nacelle	958	2111	466	1028
Engine			1436	3166
Propulsion System			1902	4194

TABLE V. - OTW ENGINE WEIGHT

	Experimental (kg)	(lb)	Flight (kg)	(lb)
Modified F101 Core & LP Turbine	663	1461	622	1372
Fan Rotor	364	802	173	382
Reduction Gear	90	198	83	184
Composite Fan Frame	312	687	208	459
Brgs., Drives & Lube Components	275	607	189	417
Fuel System	34	74	20	44
Electrical System	26	58	15	33
Piping, Wiring and Misc.	36	80	20	43
Total Engine	1799	3967	1331	2934

TABLE VI. - OTW NACELLE WEIGHT

	Experimental	Flight (kg)	(lb)
Composite Inlet		150	330
Composite Fan Duct		117	259
Composite Core Cowl		40	88
Core Exhaust Nozzle	Boilerplate	38	84
Aft Nacelle		113	250
"D" Nozzle/Thrust Reverser		121	266
Lube & Hydraulic System		64	140
Instrumentation		6	13
Total Nacelle		649	1430
Engine		1331	2934
Propulsion System		1980	4364

TABLE VII. – THRUST-TO-WEIGHT ASSESSMENT

	UTW		OTW	
	N/kg	lb/lb	N/kg	lb/lb
Uninstalled				
• **Goal**	60.8	(6.2)	72.6	(7.4)
• **Projected**	56.7	(5.78)	70.2	(7.16)
Installed				
• **Goal**	42.2	(4.3)	46.1	(4.7)
• **Projected**	40.7	(4.15)	45.6	(4.65)

UTW Engine with Bellmouth Inlet
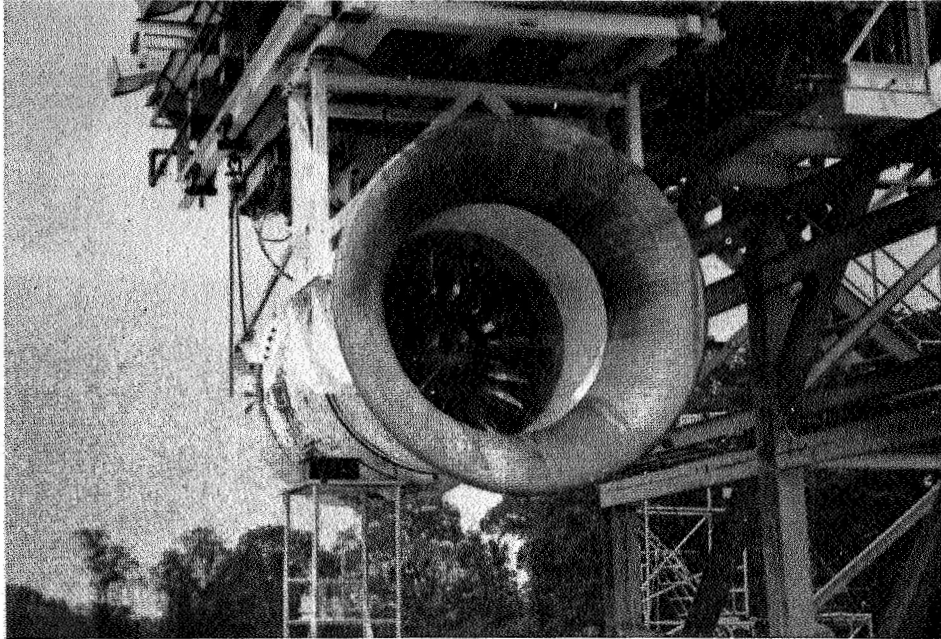
Figure 1

UTW Experimental Propulsion System Test Installation
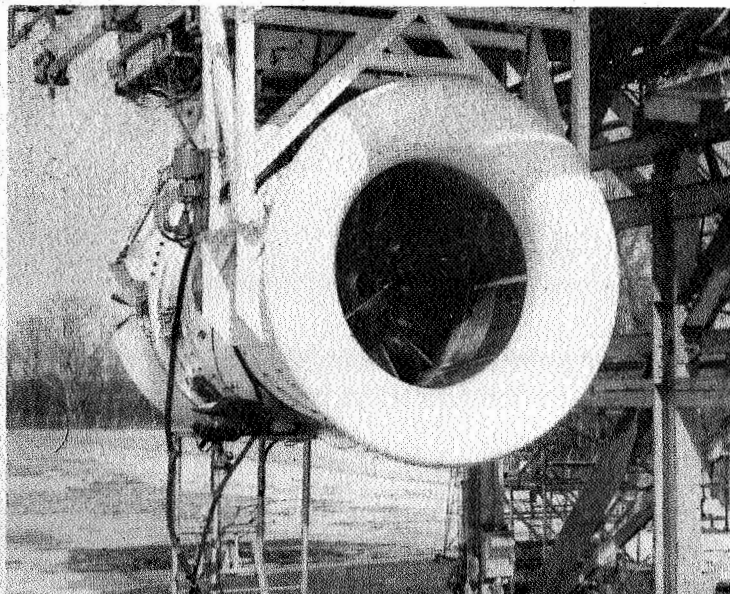
Figure 2

UTW Measured Thrust
Bellmouth Inlet
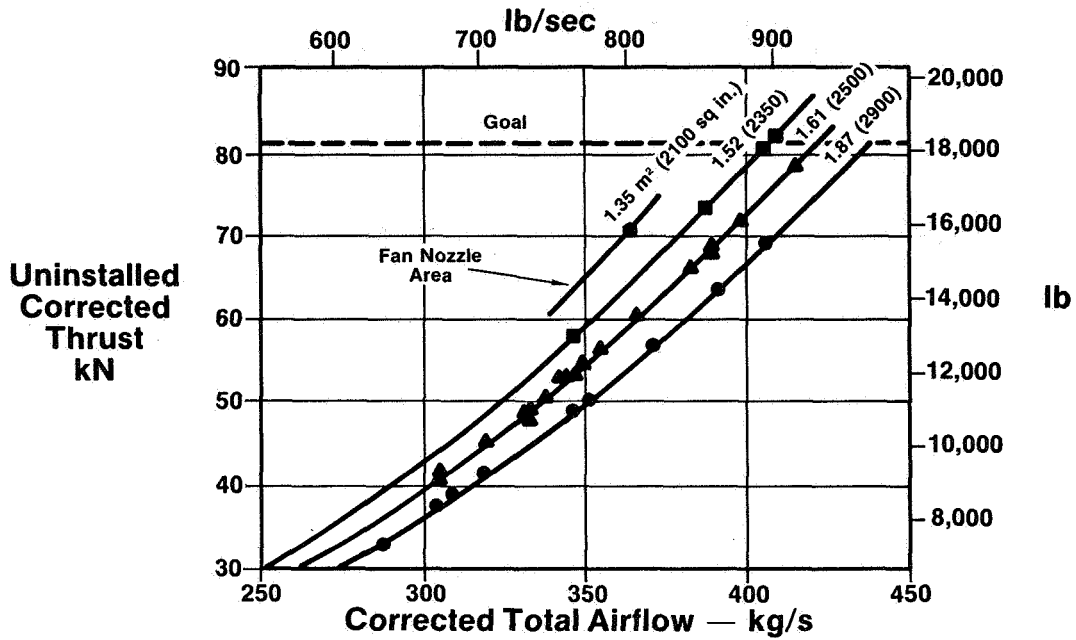
Figure 3

UTW Measured Thrust
Bellmouth Inlet

Figure 4

UTW Thrust/SFC
Bellmouth Inlet
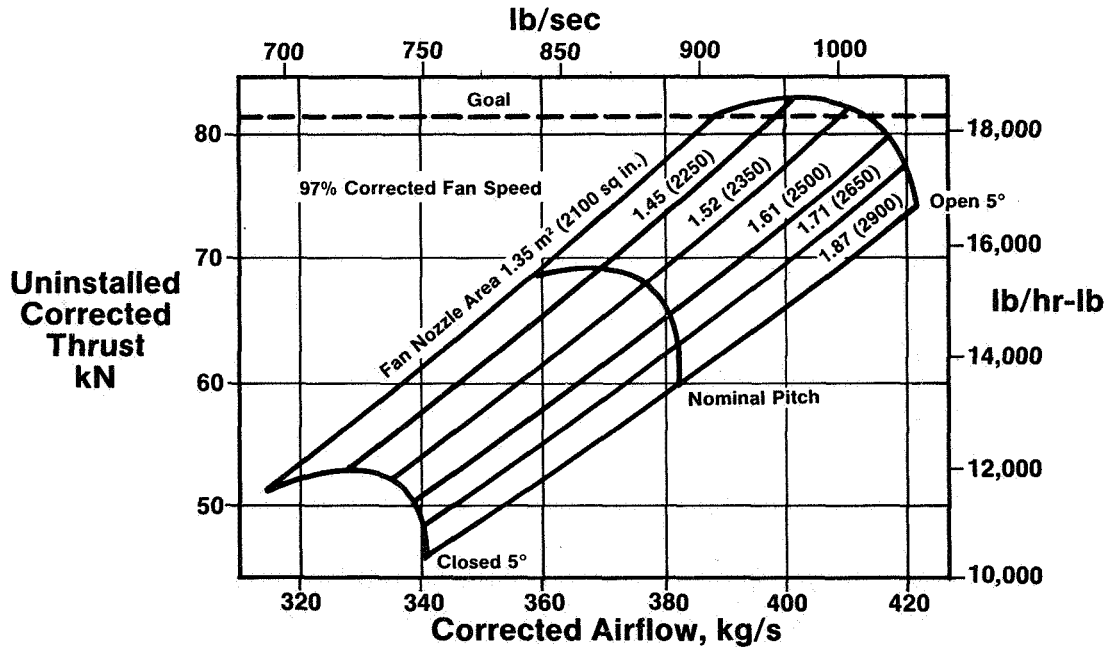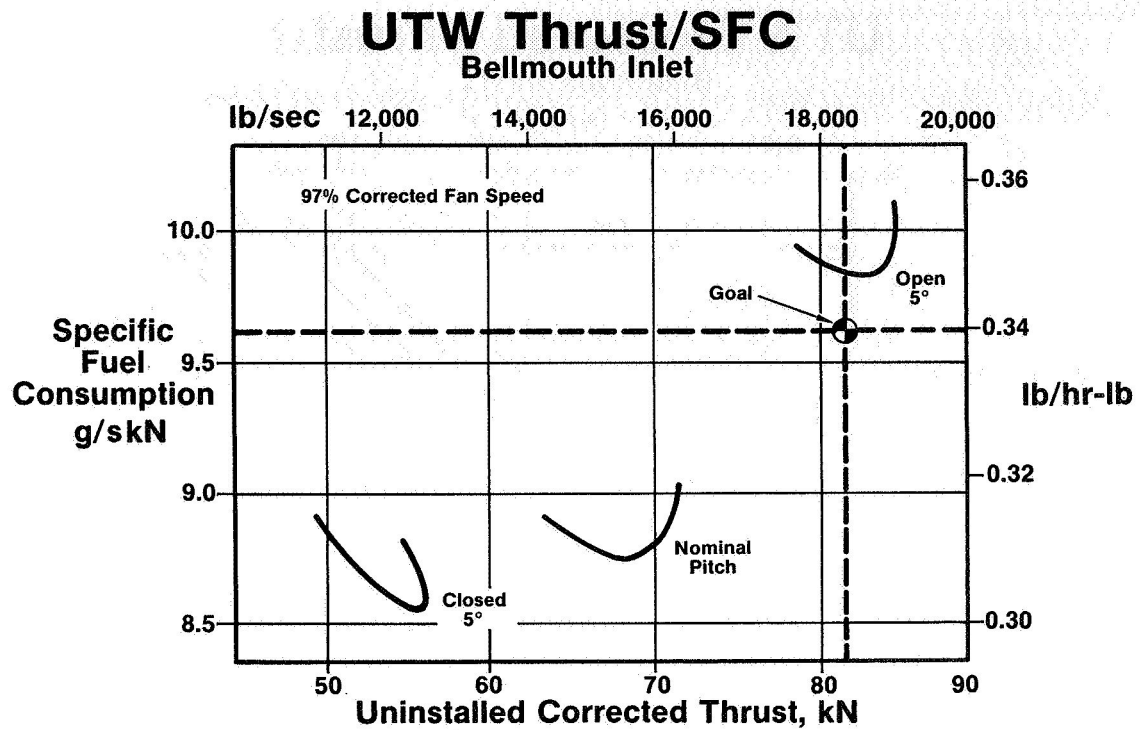
Figure 5

UTW Reverse Thrust Test
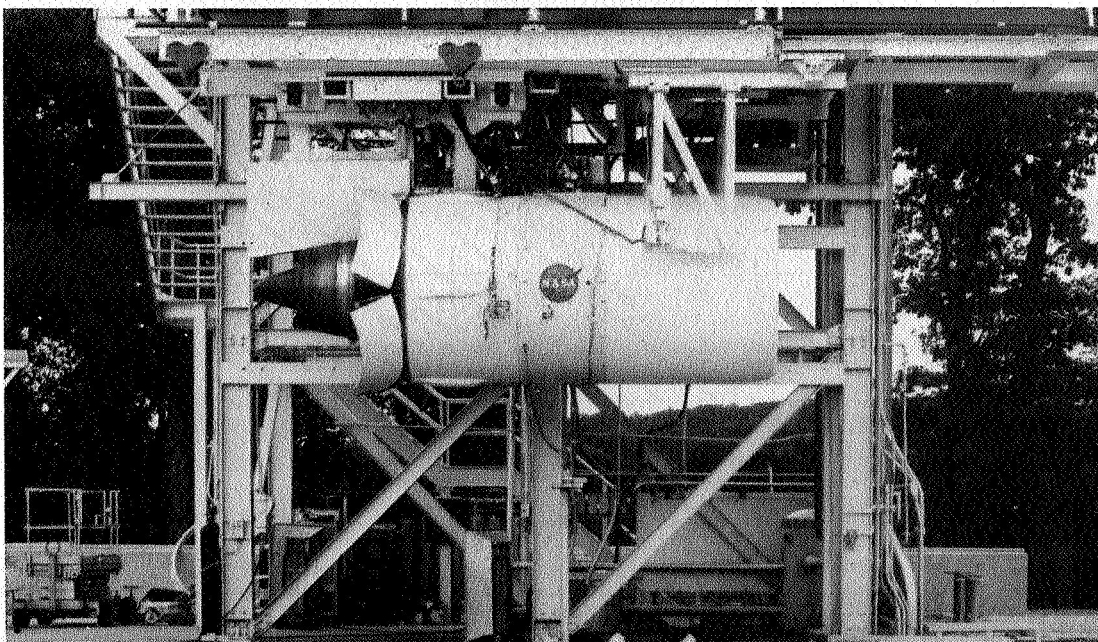
Figure 6

UTW Reverse Thrust
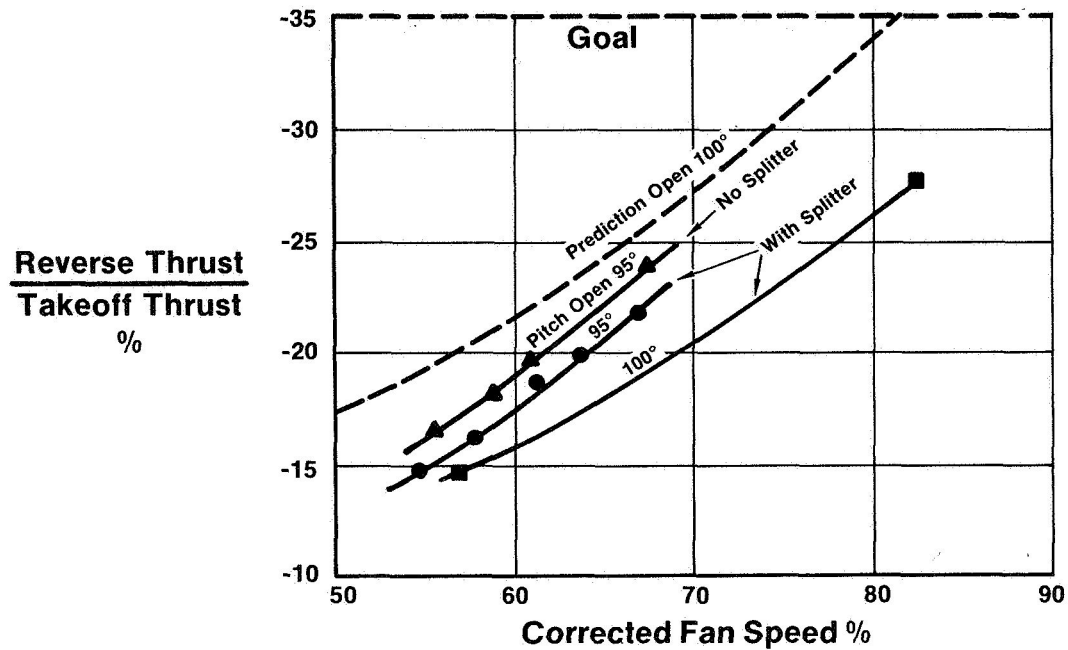
Figure 7

OTW Experimental Propulsion System Installation

CS-78-3446

Figure 8

275
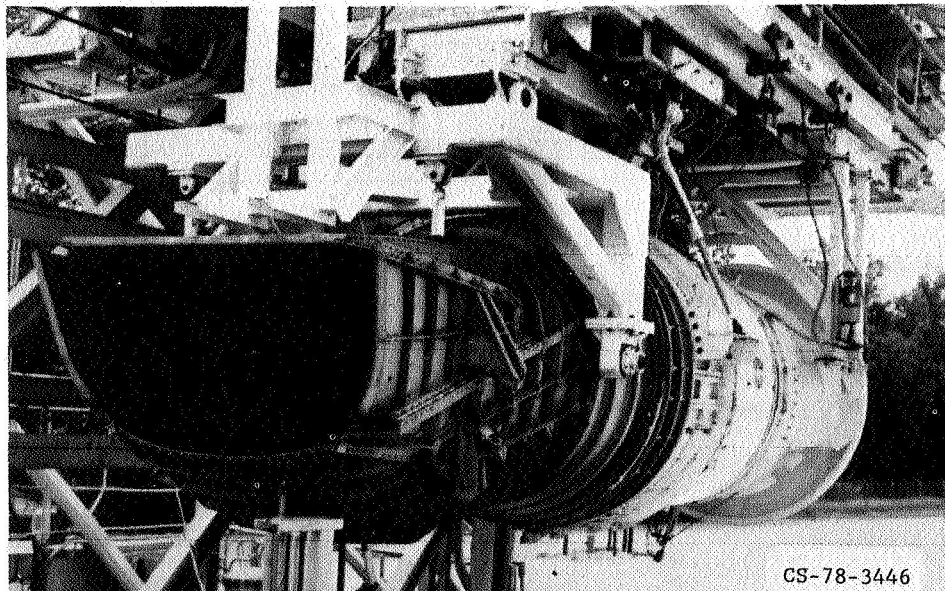
OTW Measured Axial Thrust ("D" Nozzle)
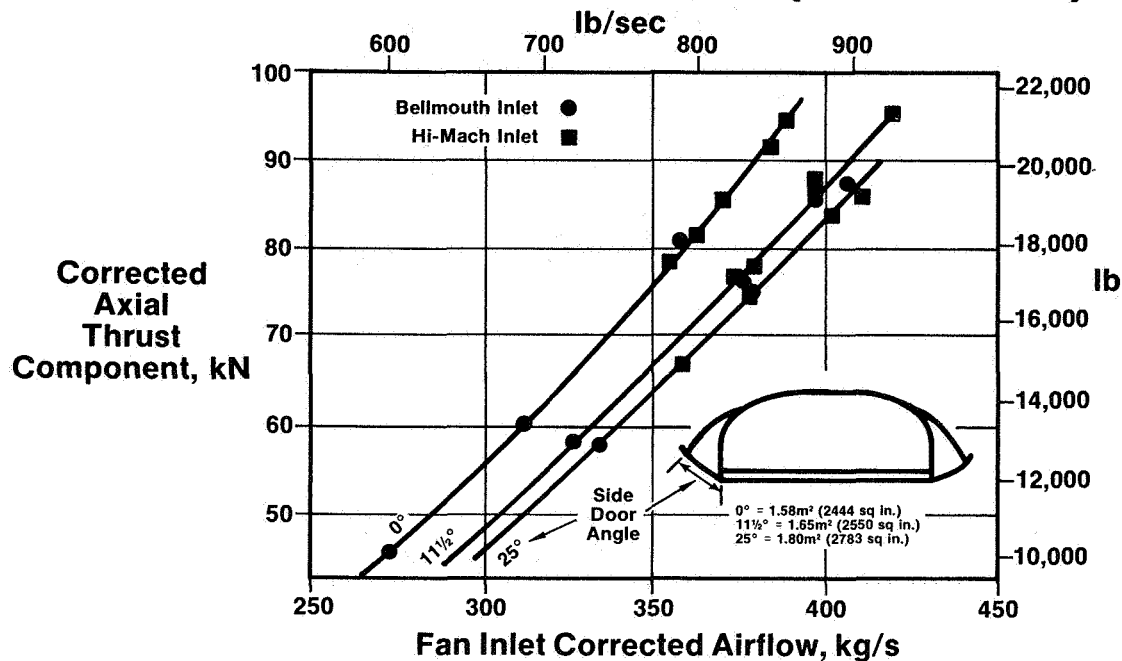
Figure 9

Uninstalled Specific Fuel Consumption vs Thrust

Figure 10

276
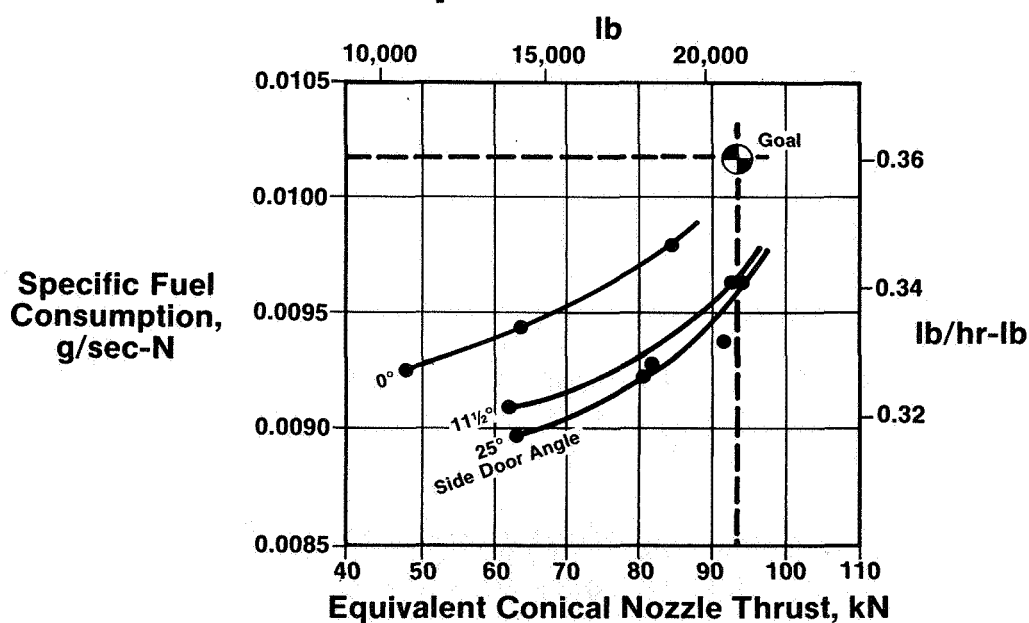
Inlet Reingestion Shield Installation
OTW Reverse Thrust Test

Figure 11

Reverse Thrust vs Airflow
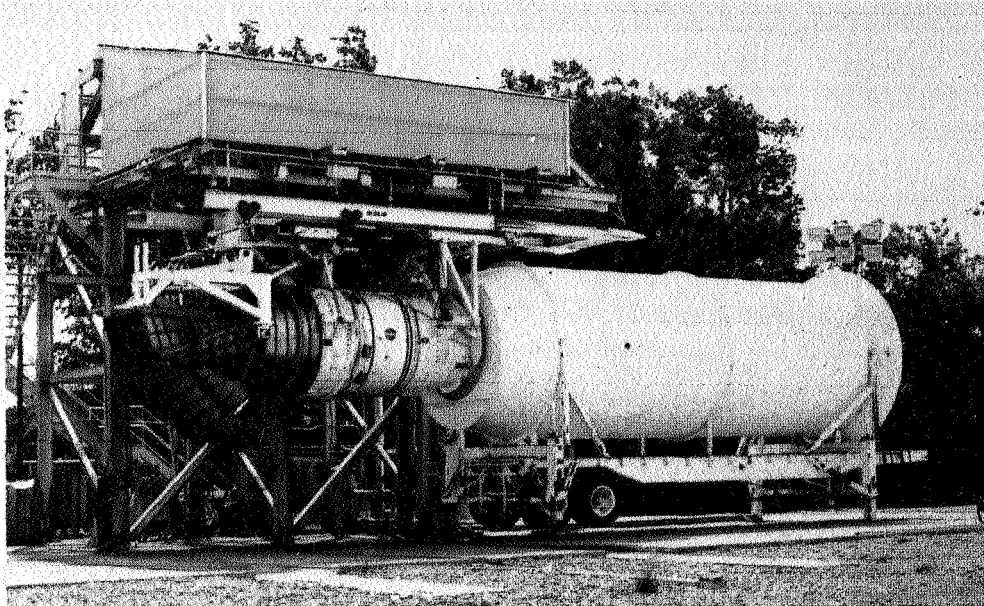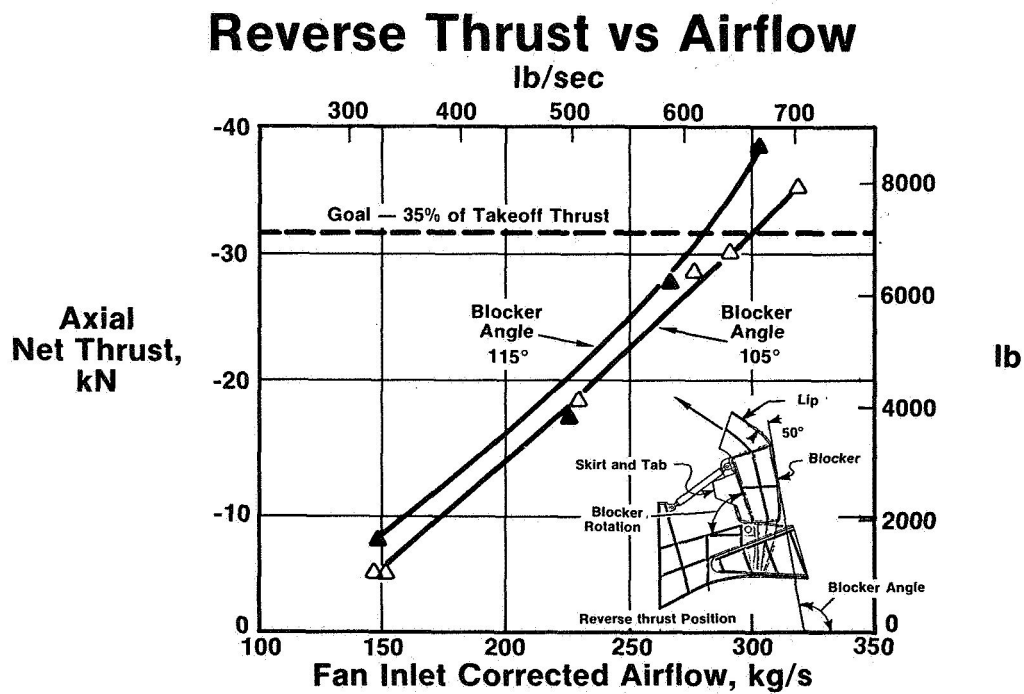
Figure 12

UTW Engine Assembly
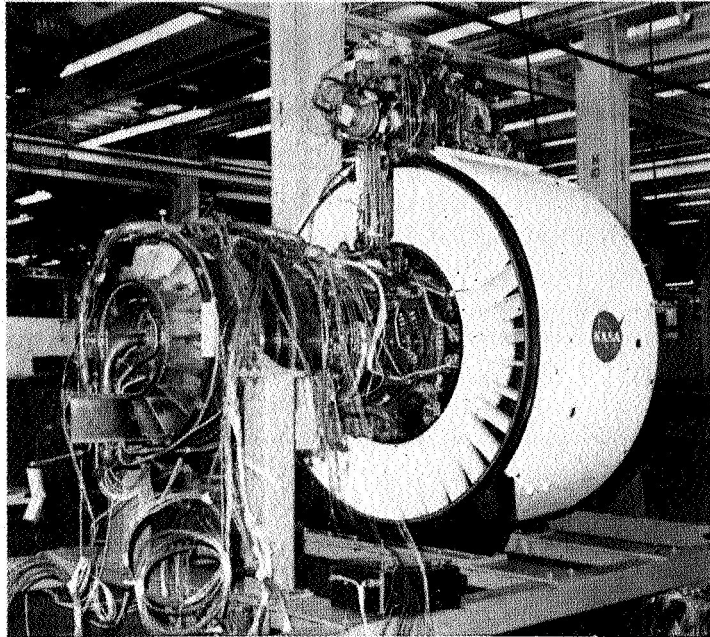
Figure 13

QCSEE PROGRAM ACCOMPLISHMENTS*

M.A. Zipkin
The General Electric Company
Cincinnati, Ohio

During these past two days more than 15 NASA, GE and other Industry speakers have given you in depth reports on the accomplishments of the QCSEE Program. It is not my purpose to either review or summarize what you have heard but rather to add a few observations from the perspective of General Electric Company Management. I would like to comment on three aspects of the program.

1. The work done/scope of technology accomplishments.

2. The utility of the program/value and applicability of the accumulated technology.

3. How it was done/the effectiveness of the Government/ Industry team.

Let us look first at the work done. The major technology accomplishments of the QCSEE Program reduced to generic terms are as follows:

1. Major reduction in noise levels.

2. Reduced levels of exhaust emissions.

3. Demonstration of variable pitch fan concept.

4. Expanded use of composite materials.

5. Test experience with main reduction gear.

6. On-engine testing of digital control.

To briefly review what the many papers have covered:

In the area of environmental concerns, the QCSEE engines demonstrated sideline noise levels far lower than the quietest commercial engines in service today QCSEE demonstrated that the 95 EPNL noise level footprint could be contained within less than one-half of a square mile, confining the nuisance area to the airport proper.

The QCSEE combustor, an extension of the NASA Experimental Clean Combustor Program is the first to meet the demanding EPA standards for exhaust emissions. Furthermore, it accomplishes its objective in an extremely short, compact design. This combustor is directly applicable to other engines where it can reduce vital concerns over air quality.

279

The variable-pitch concept was shown to be a viable means to control fan pumping characteristics, and to have potential as a thrust reverser. Both pitch actuator designs built and tested proved to be practical and can be further developed for operational use.

A major saving in system weight was demonstrated in the extensive use of composite materials in the frame and nacelle components. These components proved to be structurally sound, durable and readily repairable. The fan frame was certainly the most ambitious undertaking to date in the application of composite materials to major engine structural components. Its success should lead to a number of future applications of composites.

The QCSEE main reduction gear transmitted up to 18,000 horsepower for many hours without incident - a significant accomplishment for an aircraft lightweight gear system. Many of us had reservations about the reliability of this main reduction gear. While thousands of test hours will be required to validate gearing for operational use, this initial step has been very encouraging.

The digital control provided excellent control of all variables on both engines. This was the first time an all-electronic control system has progressed to the full-authority stage at General Electric. This engine-mounted electronic package demonstrated that it could survive and operate very well in the adverse temperature and vibration environment of the engine.

A few of the elements have been disappointing, but this is typical of any advanced development program. The composite blades are an example. While they proved adequate for the completion of the experimental program, we still do not have a design that can take bird strikes with acceptable damage.

Let us consider next the utility of the QCSEE program. Overall, the QCSEE program contained more new ideas and advanced features than any other engine project in recent memory. In each of the important technologies QCSEE has pushed the existing boundaries a measurable step forward. Most of these new elements proved highly successful, and it is inevitable that they will find their way into production engines of the future. For starters, the technology is now ready to permit the development of an environmentally acceptable, economically viable engine for short haul aircraft. Perhaps even more important, however, many elements of the QCSEE developed technology are directly applicable to other engines and can be introduced sooner with an earlier return on the investment. Elements of the QCSEE technology are already flowing into this Company's current CF6 transport engine family and its future engines such as the NASA sponsored Energy Efficient Engine (E^3). It is our expectation that as a result of the numerous reports published during the course of the program, and this conference, the QCSEE technology will get broad dissemination within U.S. Industry and will find many additional applications in your own organizations. The next paper will have more to say on the application of the QCSEE

technology, so I will defer to it on this vitally important aspect of the program.

I would like to turn now to my last point - how the work was done or the effectiveness of the Government/Industry team. It should be evident by now that we have had an effective team throughout the QCSEE program. To be effective, both parts of the team had to have perspective, objectivity and patience. As I recall this program started with a so-called 60 day plan. Consequently, the patience aspect was tested early as the engineers wanted to get moving. In retrospect, that particular activity was, as later events indicated, very beneficial. Whether a 60 day period is the appropriate time may be questioned, but the program benefitted in the long run from the effective planning base established. While there were changes made to the plan throughout the 4-1/2 years, the original plan proved to be remarkably close to the final product.

Another aspect of the QCSEE team effectiveness becomes evident when you recognize that cost estimates prepared in 1973 were subject to more than a slight aberration when viewed through the inflationary spiral of 1974 and 1975 and the ongoing inflation that is still with us. As you have observed from the material presented at this conference, the planned technology effort was nevertheless reasonably well-protected. In addition to the normal technical problems and the financial pressures of double digit inflation you may recall that the Winter of 1977-'78 provided history's worst weather ever for outdoor testing - precisely the time period allocated for the acoustic tests. Despite these hurdles, the dedication of our respective management teams, while sometimes subjected to considerable strain, prevailed and the technical goals of the program were ultimately achieved. The QCSEE program has, in my view, proven once again the wisdom of approaching new technology challenges through the mechanism of a strong Government/Industry team. The total capability of the joint effort is clearly greater than the sum of the individual efforts.

In closing, it seems appropriate to thank the members of the QCSEE team, who working together have made the program a considerable success and have made this technical conference possible. We at GE wish to thank NASA for the opportunity to have conducted the exciting QCSEE program. We wish to particularly thank the Program Managers - first Ray Rulis and subsequently Carl Ciepluch for their guidance, their confidence in our technical judgements and their patience with our shortcomings. These leaders, together with their competent staffs, were vital to achieving the objectives of the program. We, at GE have considered them our "best friends and worst critics" although not always in that order.

I would also like to thank the GE technical staff headed by Art Adamson I believe their presentations in the last two days speak eloquently of their efforts throughout the QCSEE program. The Company is proud of them and their contributions to the advancement of jet engine technology.

QCSEE PROGRAM APPLICATIONS[*]

by Carl Ciepluch
NASA Lewis Research Center

The preceding series of papers has presented an in-depth review of the QCSEE program. It is appropriate to close this review with some remarks on two subjects: the QCSEE engine performance with an improved engine core and the potential use and benefits of the QCSEE technology.

As you recall, Art Adamson, author of the first paper, pointed out that an unmodified F-101 engine core was used in the engines. Modifications to improve performance by raising the cycle-pressure ratio were not made because the technical benefits did not justify the added program costs. However, during the program an estimate was made of the improvements attainable with a more optimum cycle-pressure-ratio, advanced-technology-engine core. The results (shown in fig. 1) indicate that the specific fuel consumption (SFC) of an OTW engine with an improved core is nearly 20 percent lower than that of the OTW engine as tested. The SFC is in the 0.0532 (kg/hr)/N (0.54 (lb/hr)/lb) range, which is very attractive. Similar improvements would be obtainable for the UTW engine with an improved core.

The cycle pressure ratio of the OTW engine with an improved core was about 31 compared with 17 for the current OTW engine. The improved engine core also has component efficiencies equivalent to those anticipated for the mid 1980's. The improved core will weigh more than the current core because of the higher cycle pressure ratio. This greater weight will reduce the engine thrust-to-weight ratio but not significantly. Also, since the engine noise is controlled primarily by the jet and fan noise, the addition of an improved core will not materially affect the overall engine noise levels. Therefore, the significantly improved QCSEE OTW engine fuel consumption that can be obtained by the use of an improved engine core should not adversely affect engine weight or noise.

The engines in the QCSEE program incorporate many advanced technologies. These advanced technologies can be applied beneficially to many other future aircraft propulsion systems. Some of these applications and systems are listed in table I.

The propulsion systems for some proposed V/STOL military aircraft are strikingly similar to the UTW engine (e.g., the use of the variable pitch fan). Accordingly, the majority of the QCSEE technology is potentially applicable to the V/STOL propulsion systems.

For conventional takeoff and landing aircraft, particularly if the new energy efficient propfan propulsion systems are used, the reduction-gear technology will be beneficial. In addition, the use of lightweight composite materials should lower the operating costs of this type of aircraft. Some of the

[*]For Early Domestic Dissemination.

variable cycle features (including digital controls) and environmental technology can also be of benefit to the conventional takeoff and landing aircraft.

Future supersonic aircraft may make use of some of QCSEE's variable-cycle technology features and some of the environmental technology.

In summary, QCSEE propulsion technology is applicable to a broad range of future aircraft.

TABLE I. - POTENTIAL APPLICATION OF QCSEE ADVANCED TECHNOLOGY

TECHNOLOGY AREA	TYPE OF AIRCRAFT			
	POWERED-LIFT SHORT-HAUL	VERTICAL TAKEOFF & LANDING	CONVENTIONAL TAKEOFF & LANDING	SUPERSONIC
POWERED-LIFT ACOUSTICS & AERO	✓			
LOW PRESSURE RATIO FANS	✓	✓		
LIGHTWEIGHT REDUCTION GEARS	✓	✓	✓ (PROPFAN)	
ADVANCED COMPOSITE MATERIALS				
FRAME	✓	✓	✓	
NACELLE	✓	✓	✓	
FAN BLADES	✓	✓	✓	
VARIABLE CYCLE FEATURES				
VARIABLE PITCH FAN	✓	✓		
VARIABLE NOZZLE AREA	✓	✓		✓
VARIABLE GUIDE VANES	✓	✓	✓	✓
FUEL CONTROL	✓	✓	✓	✓
DIGITAL ELECTRONIC CONTROL	✓	✓	✓	✓
ENVIRONMENTAL IMPACT				
LOW NOISE	✓	✓	✓	✓
LOW EMISSIONS	✓	✓	✓	✓

CS-78-3309

OTW ENGINE CRUISE FUEL CONSUMPTION WITH IMPROVED ENGINE CORE

CS-78-3482

Figure 1

285
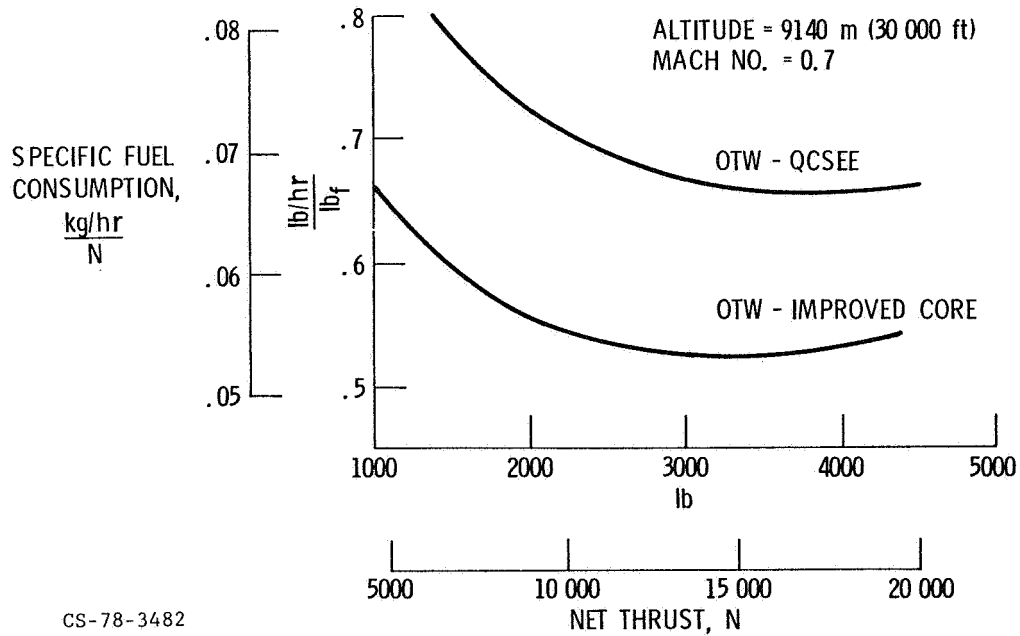
AN OVERVIEW OF THE QUIET SHORT-HAUL

RESEARCH AIRCRAFT PROGRAM

Michael D. Shovlin and John A. Cochrane
Ames Research Center

INTRODUCTION

The Quiet Short-Haul Research Aircraft (QSRA) is a new research aircraft which NASA will use as a flight facility for advanced flight experiments in terminal area operations. Because the nature and use of research aircraft by NASA are frequently misunderstood, the following discussion is presented to clarify the subsequent description of the QSRA and its use as a research facility.

NASA research aircraft are not prototypes and frequently they are not experimental aircraft. For example, the Kuiper Airborne Observatory, which is operated by Ames Research Center, is a standard Lockheed/USAF C-141 modified to carry a telescope and other airborne scientific experiments. Other research aircraft such as the X-15 series are highly experimental in nature, but are not prototypes for future aircraft. Occasionally, an aircraft built as a prototype is used as a research aircraft; examples are the Boeing "Dash Eighty," which was the 707 prototype and the USAF AMST prototypes. These aircraft were used or planned to be used by NASA for flight research after completing their prototype missions. All of these aircraft had a common denominator: as research aircraft their mission was one of data gathering, and indeed, this is usually the primary mission of NASA research aircraft. For this reason, NASA frequently views research aircraft as facilities, just as a wind tunnel or a simulator is considered a test facility.

The data resulting from the QSRA flight research program will be used by the United States aircraft industry to establish design criteria and by regulatory agencies to establish certification criteria for advanced STOL aircraft. This is important from a national point of view since aircraft exports exert an important positive influence on the U.S. balance of payments. In addition, QSRA flight data will lead to improved air transportation at reduced noise levels and with less air traffic congestion.

Another characteristics of many NASA research aircraft is lower cost than that typically associated with a prototype development. Limited budgets and fiscal responsibility dictate that research capability must be maximized relative to cost, and experience with research airplane projects has led to certain approaches developed to minimize their cost. These include:

1. Use of an existing airframe where possible
2. Use of "off-the-shelf" hardware
3. Use of goals instead of requirements

4. In-house participation where appropriate
5. Cost consciousness at all organizational levels
6. Soft tooling
7. Informal documents

The application of these concepts to the QSRA will be discussed later.

HISTORICAL BACKGROUND

NASA has conducted research with powered-lift airplanes since the 1950s. The first jet STOL research airplane developed by NASA was the Augmented Jet Flap STOL Research Airplane (ref. 1) developed in the early 1970s. This was an austere program which consisted of a modification of an existing deHavilland C-8A Buffalo, powered by two modified Rolls Royce Spey engines. It recently completed 500 hr of highly successful flight research and after a major inspection has been placed back in service for futher work. Its performance is representative of the first generation of jet STOL aircraft with an approach lift coefficient in the 3.5 to 4.0 range. Its major limitation is high levels of sideline noise.

A second, more ambitious jet STOL research airplane program, initiated in the early 1970s was the Quiet Experimental STOL airplane (QUESTOL). Three preliminary design studies and a design competition (won by Lockheed-Georgia) were completed before this project was cancelled in January 1973 due to budgetary limitations. The QUESTOL was planned as a four-engine, externally blown-flap STOL airplane, powered by four General Electric TF-34 turbofan engines.

In January 1974, a decision was made to embark on an austere jet STOL research aircraft which would feature very low sideline noise levels and "next generation" performance (approach lift coefficient of 4.5 to 5.5). Preliminary design contracts were awarded the Boeing Commercial Airplane Company and the Lockheed-Georgia Company to study an augmented jet-flap concept and a hybrid upper surface blowing concept. These studies were not competitive in the sense that they did not form the basis for the selection for the winner of the subsequent hardware competition. Each design team operated independently, and only at an industry-wide conference at the end of the study was the work of one team revealed to the other. In this way, NASA was able to obtain two independent approaches to the problem. The results of these studies were presented to industry in September 1974 (refs. 2, 3), and a request for proposal for detail design, fabrication, and test of the QSRA was issued in November 1974. Important excerpts from the initial statement of work are given in table 1. Boeing, Douglas, and Lockheed responded to the request for proposal and after a lengthy evaluation, the Boeing Commercial Airplane Company was awarded the hardware contract in March 1976.

The QSRA made its first flight on schedule—July 6, 1978. The aircraft departed Boeing Field in Seattle to go to Paine Field in Everett, Washington in order to begin its initial 17.5-hr flight-test program. Although the primary objective of this program was to demonstrate the airworthiness of the

aircraft and its systems, the last 2 to 2.5 hr were devoted to internal and external noise measurements. This initial flight test program proceeded very smoothly and was accomplished 1 month ahead of schedule, allowing the aircraft to be delivered in August instead of in September of 1978 as originally planned. Figure 1 shows the aircraft on final approach into Moffett Field, California where 9.5 hr were flown in order to verify data system operation at Ames and to provide pilot familiarization and training. After a thorough inspection of the aircraft and its engines, the second phase of the NASA flight research program was begun in November at Ames where the propulsive-lift, handling, and acoustic characteristics are being investigated, with improvement modifications as required.

MANAGEMENT APPROACH

The total funding for the QSRA was established at $29 million in January 1974. At the start of the project, a firm commitment was made to complete the project within the available funds. Since these funds had to cover costs for all studies, test, engine and airframe procurement, and proof-of-concept flight tests, an austere and innovative management approach was required. The approximate distribution of the available money is given in table 2.

Scope Versus Cost

The techniques discussed in the Introduction were all applied to the task of developing a technically meaningful project within the budgetary limitations. An important aspect of living within the budget was definition of the scope of the project, which was largely accomplished during the preliminary design studies. Within limits, a project such as QSRA can "cost what you want it to cost." This is due to the fact that many features, while highly desirable, are not essential. An example of this occurred during the preliminary design studies. An article in a trade magazine indicated that $32 million were available for the QSRA project. The first cost estimates, independently prepared by the two study contractors, were for about $30 million. A special trip was made to NASA project managers to explain the distribution of funds as shown in table 2. The second round cost estimates were about $20 million. Both estimates were legitimate; the difference was in the scope and detail of the tasks to be accomplished.

There is, however, a lower limit beyond which a technically meaningful cost cannot be implemented. Some fortunate circumstances contributed to the completion of the QSRA project within the available funds. These included: (1) the availability of a suitable airplane, the deHavilland C-8A, for modification; and (2) the availability of suitable engines which could be configured for use in the QSRA.

Airframe Acquisition

The C-8A was obtained at no cost, through appropriate government channels, from the National Center for Atmospheric Research (NCAR). The physical size and the T-tail configuration of the C-8A made it an ideal airframe for modification into an advanced STOL aircraft and prior experience with a similar modification, the Augmented Jet Flap STOL Research Aircraft (AWJSRA), further enhanced its desirability.

When the Fairchild A-10 airplane was selected as the winner of the United States Air Force AX fly-off competition, the two Northrop A-9A airplanes were transferred to NASA for a possible flight research program. A later decision not to fly the two prototype airplanes made the engines, equipment, and spares from this program available for QSRA use. Six Lycoming YF-102 engines and four accessory power packages were salvaged from the A-9A program together with many other miscellaneous components. The YF-102 engines, although relatively immature prototype engines, were almost ideal for the QSRA. They are high by-pass ratio, geared-fan engines that generate 33,410 N (7,500 lb) of thrust at low noise levels.

The use of the C-8A and the YF-102 engines was an important first step in minimizing the cost of the QSRA project, but many additional cost-reduction factors were necessary. They included: in-house participation, cooperative approach, detailed tracking of costs, and a full appreciation of the importance of cost at all organizational levels.

In-House Participation

The approach to in-house participation was to let NASA do that which NASA could do best and to let Boeing do those things which Boeing could do best. The large-scale wind-tunnel model is an excellent example of this concept. Early in the program, a large-scale, powered wind-tunnel model was identified as a project requirement. Ames Research Center has a long history of constructing large powered models for research in the Ames 40- by 80-Foot Wind Tunnel. Boeing, on the other hand, had a detailed knowledge of the details of the QSRA design. In order to take advantage of the expertise of each organization, Boeing was assigned the task of designing the model and NASA assumed responsibility for fabricating and instrumenting the model.

Another example of a NASA in-house program was the engine program. An extensive ground test program was completed by the Lewis Research Center in which both performance and acoustic data were acquired in support of the QSRA design effort. Lewis also managed the program to refurbish and update the flight engines.

Cost Consciousness

It is beyond the scope of this paper to discuss the details of QSRA management beyond the examples that have already been presented. However, no discussion of QSRA management would be complete without emphasizing the

importance of the outstanding cooperation between the Boeing project team and the NASA Project Office and the detailed tracking of costs accomplished by both these groups. The Boeing project control group tracked cost for 38 work breakdown structure elements on a weekly basis at the peak of the project. These data were provided in a timely manner to the NASA Project Office and were on display in a control room in the Boeing project area. Thus, project personnel to the lowest organizational levels were made aware of cost performance. The NASA Project Office was consulted whenever transfers were made from the Boeing management reserve. In this way, project funds were not expended to correct minor performance deficiencies that were not important to NASA, and available resources could be concentrated on important problems.

A paper planned for later publication by the QSRA project personnel will deal with this subject in depth.

IN-HOUSE PROGRAMS

Wind-Tunnel Tests

The need for accurate, large-scale, wind-tunnel testing of the specific powered-lift airplane configuration had been identified in studies previous to the QSRA contract award (ref. 4). In order to support the QSRA design effort, and to reduce costs and risk by utilizing NASA talent and facilities, an existing large-scale, wind-tunnel model was modified to be aerodynamically similar to the QSRA and tested in the Ames 40- by 80-Foot Wind Tunnel. This 0.55-scale model was used to provide aerodynamic and loads data for the QSRA design, and the control stability data for the flight simulation program.

Wind-tunnel model—The QSRA wind-tunnel model is shown mounted in the Ames 40- by 80-Foot Wind Tunnel, in figure 2. This model is powered by five JT-15D turbofan engines. Four of these engines are mounted above the wing; the fifth, mounted in the fuselage, provides boundary-layer control (BLC) air. The model has three trailing-edge flap systems. Upper-surface-blown flaps are located directly behind the engines, with double-slotted flaps outboard of these and blown ailerons at the wing tips. The entire leading edge is blown for boundary-layer control, including the area between the nacelle and fuselage. Although the leading edge flaps were fixed, the trailing-edge flap systems and spoilers could be remotely actuated during the test runs.

This model had over 600 pressure and temperature measuring points in order to provide airloads and temperature design data for the QSRA. Engine thrust levels were measured under static conditions with flaps up and correlated with fan speed. These correlation equations were used to determine thrust levels during the wind-tunnel test points. The corrected mass flows were obtained from ideal mass flows, calculated by using the average static pressure at the farthest downstream inlet measuring point and the test section total temperature and pressure. This ideal flow was corrected for pressure recovery and inlet losses by assuming a 0.98 correction factor.

Aircraft design contributions—The wind-tunnel tests of this model made
a number of important contributions to the final QSRA design. These tests
defined the airload data used in the QSRA structural design, showing that
these loads were slightly different in location and magnitude than those pre-
dicted using YC-14 data, particularly on the fuselage near the wing leading
edge. These tests also verified the mixed flow nozzle and propulsion system
simulation which was based on Langley JT-15D tests simulating the YC-14 pro-
pulsion system. The tests defined the BLC system requirements, showing that
blowing was necessary at all times along the leading edge during high angle-
of-attack operations, resulting in a redesign of the QSRA's BLC system. These
tests defined and verified the effectiveness of the control surfaces and the
effects of engine-out and other failure conditions, providing a data base for
the flight simulation. Finally, these tests defined a serious nacelle/wing
aerodynamic interference problem and provided a simple, effective, low-cost
solution for the aircraft design, by showing that several small vortex gener-
ators could eliminate the boundary-layer separation at this interface. A more
detailed summary of the test data is contained in references 5-7.

Configuration optimization—A continuing benefit of these wind-tunnel
tests is in the use of this data base and the model as a tool for further con-
figuration development and optimization. As an example, the early wind-tunnel
tests showed that although blowing was essential along the leading edge at
high angles-of-attack, only very small amounts were required to keep the flow
attached over the wing. In subsequent tests, a slotted leading-edge flap was
fabricated and tested to determine what performance penalties, if any, were
associated with removing the outboard leading edge BLC system (ref. 5).
Although performance improved slightly, there was a loss of about 4° in
angle-of-attack margin. One of the projected studies to be made with the
QSRA will be to verify in flight the effect of replacing the outboard leading
edge BLC system with a slotted flap, a change that would considerably simplify
the aircraft pneumatic system. This change will be made, however, only after
a thorough documentation of the flying characteristics of the basic configura-
tion.

Engine Ground Tests

As discussed previously, the QSRA is powered by the Lycoming YF-102
engines acquired from the A-9A aircraft program. Although these are rela-
tively immature prototype engines, they had met all of their performance goals
during the AX program, and had demonstrated operational reliability. The QSRA,
however, required a much more complex engine installation with a confluent
flow exhaust system and with a bleed air schedule requiring up to 10% of core
airflow at low power settings. These QSRA requirements were so far beyond
the existing engine performance data base that there were questions regarding
engine operation and its effect on cost and aircraft safety. In addition, the
ambitious acoustic goals of the QSRA required an extensive acoustic data base
in order to develop an adequate low-noise nacelle design within cost con-
straints. It became obvious that it was necessary to develop these data bases
in order to minimize program cost and risk, and again it was clearly an area
where NASA talent and facilities could be used most effectively.

Vertical Lift Fan Facility—The Lewis Research Center Vertical Lift Fan Facility is an outdoor engine test stand sheltered by a service building which is moved away on tracks before testing. The engine is suspended beneath the thrust measuring system, which can be pivoted around a vertical axis for operational flexibility. A frame work extending from the thrust measuring system is used to mount inlet and exhaust hardware separately from the engine. The engine centerline was 2.9 m (9.5 ft) above the ground; the facility, with the baseline confluent flow YF-102 mounted on the thrust stand, is shown in figure 3. The area beneath the engine is paved with concrete and asphalt out to the acoustic data microphones which are located on a 30-m (100 ft) radius circle over a 160° arc from the inlet centerline. The control room is located about 152 m (500 ft) from the stand and affords a good view of the engine inlet.

Propulsion design refinements—The engine ground test contributed to the final QSRA aircraft design in a number of different ways. The tests were used to define the engine base-line performance for the confluent flow configuration and to update the engine performance prediction deck. These tests defined the transient operating characteristics of the engine and the effect of BLC system failures on the engine stability and safe operation. These tests showed that the engine was unable to accelerate from low power settings under high core bleed conditions, requiring the design of a BLC control system that limits core bleed to power settings where the engine can be safely operated. New acceptance test procedures were developed as a result of these ground tests in order to ensure adequate, stable, and safe engine operation when installed in the QSRA. Finally, a special test was run to verify the design and adequate operation of the fan bleed air S-duct and its flow characteristics at the ejector inlet (ref. 8).

Acoustic design refinements—Acoustic performance is a second area where the Lewis test program made significant contributions to the QSRA design. These tests developed all of the acoustic data base for the YF-102 engine, providing a measure of the component noise levels and their directivity. The induct fan tones and their location relative to the duct walls were determined along with their mode shapes and other design data. Acoustic design simplifications eliminating splitter rings and engine spinner treatment were verified, eliminating considerable cost and performance penalties. The effect of wing shielding was determined and, finally, special techniques were developed to determine the contribution of combustor noise (ref. 9).

Flight Simulation

The Ames Flight Simulator for Advanced Aircraft (FSAA) was used to define those combinations of flight conditions, aircraft configuration, control power, and control rates that would ensure acceptable handling qualities for both normal operation and in various single or multiple failure occurrences in either propulsion or flight control systems.

FSAA—The FSAA is a six-degree-of-freedom motion simulator with very high fidelity motion and visual cues. It has two pilot stations and room for an observer in the cab. It was configured to closely approximate the flight

deck of the QSRA with similar instruments, throttles and controls. A pilot's eye view of the simulation is shown in figure 4. Experience with the FSAA has shown that realistic, accurate simulations can be made and, indeed, the pilot ratings of 2-3 for normal operation at low speed and 4-5 for a single failure were verified in flight.

Simulation design refinements—These simulations showed a need for several design changes to improve handling qualities under a variety of STOL operations and simulated failure conditions. The need for longitudinal stability augmentation and direct lift control was identified, as was a change in horizontal stabilizer incidence. A requirement was also determined for automatic retraction of the upper surface blown flaps to reduce drag during go-around. Pilot procedures and handling qualities were also defined for operations with one or more engines inoperative, and for situations where electrical power was lost, or hydraulic or boundary-layer control systems had failed. Steep curvilinear landing approach operating procedures were investigated for noise abatement.

Further details of the QSRA flight simulations, the QSRA mathematical model, and the results of these simulations are contained in references 10-12.

AIRPLANE DESCRIPTION

The general arrangement of the QSRA is shown in figure 5 and a photograph of the airplane is shown in figure 1. The fuselage is that of a deHavilland C8-A Buffalo with structural reinforcement in the aft fuselage and new fairings at the wing-body intersection. The C-8A empennage was used without structural or aerodynamic modification. SAS actuators were added to both the rudder and the elevator and a hydraulic actuator was added for power actuation of the elevator. The C-8A landing gear was modified to increase the sink rate capability of the aircraft.

The QSRA wing was designed and fabricated by Boeing with a wingspan of 22.4 m (73.5 ft), a wing area of 55.74 m^2 (600 ft^2), and a quarter chord sweep of 15°. Figure 6 shows the wing being attached to the fuselage at the Boeing Development Center in Seattle. The center section of the wing is sealed to form two integral fuel cells which contain a total of 4535.9 kg (10,000 lb) of Jet A-1 (JP-5) fuel. Fixed leading edge flaps are blown by a mixed flow boundary layer control system. The trailing edge on either side of the centerline consists of two upper surface blowing (USB) flaps, a double-slotted flap, and a drooped, blown aileron.

The flaps and ailerons are supported by external beams and linkages. In keeping with the austere nature of the program and the low-speed environment of the QSRA, these are not faired. The main landing gear is fixed and is attached to the underside of the wing between the two nacelles. The wing is attached to the fuselage by the same pin joints as those used in the original C-8A. This provided a significant cost saving but it did require the addition of 418.7 kg (923 lb) of ballast in the tail.

294

Propulsion System

The QSRA main propulsion system consists of four AVCO-Lycoming YF-102 (QSRA) engines mounted in above-the-wing nacelles (fig. 5). These prototype engines, acquired from the A-9A program, were extensively refurbished and updated in a program managed by the Lewis Research Center. The principal elements of this update include a fan containment ring, combustor case high-pressure air bleed ports, new oil coolers, and improved shafting material.

Powerplant—A cutaway view of the engine is shown in figure 7. The low-pressure spool incorporates a single-stage fan which provides bypass and core air to the engine. The core airflow is further compressed by a single-stage supercharger attached to the fan. The fan is driven by a two-stage, uncooled turbine through a single planetary reduction gear (2.3 speed ratio) located in the fan module.

The gas producer section of the engine is essentially a T-55 core with slight modifications. The high-pressure components include an axial/centrifugal compressor, a reverse-flow combustor, and a two-stage, air-cooled turbine to drive the compressor. The high-pressure compressor has seven axial stages followed by a centrifugal stage. It features variable inlet guide vanes (VIGV's) and a sixth-stage bleed band to minimize the possibility of compressor stall during transient operations.

The engine weighs 5412 N (1215 lb) and has a basic diameter of 1.077 m (42.4 in.) with an overall length of 1.621 m (63.8 in.) including the fan spinner, while the fan has a diameter of 1.024 m (40.3 in.). The engine geometry and unstalled performance are shown in figure 8.

Nacelle structure—The nacelle layout is shown in figure 9 and the major external nacelle structural components are shown in figure 10. The external nacelle is composed of two main assemblies, the structural cowl and nozzle assembly and the engine build-up assembly. The structural cowl and nozzle assembly is attached to the wing front spar, forming the structural nacelle and pylon. The engine build-up assembly is then mounted to this structure and forms the front half of the nacelle. The nose cowl is attached to the engine as shown in figure 11 and forms the inlet and outer nacelle. In addition to the nose cowl, a core cowl and the primary nozzle are installed as part of the engine buildup. Engine driven accessories are airframe-mounted in the nose cowl, resulting in this area being one of the three primary fire zones in the nacelle. Other fire zones are the core cavity and the outer fan case. Fire protection behind the nacelle is provided by an external heat shield attached to the upper surface of the wing, together with the use of heat-resistant materials in the wing flaps and trailing edge. In addition, the primary nozzle is canted upwards allowing cooling fan air to be drawn between the wing surface and the high-temperature jet in normal operation.

Exhaust nozzle—The QSRA/YF-102 exhaust system is a confluent-flow design with both primary and fan streams discharging through a common D-shaped exit nozzle having an aspect ratio of 3.5. As indicated in figure 12, the core exhaust diffuses as it passes through the primary nozzle and then mixes with

the surrounding fan stream, exiting through the D-shaped upper-surface blowing nozzle. The core nozzle is canted upward 9.4° relative to the engine center-line to minimize the heat effects on the wing and flaps.

The flow areas in the fan-duct and core-nozzle exit plane (mixing plane) are chosen to provide adequate performance without significantly affecting surge margins. The main control on surge margins and engine match, however, is provided by the final exit area of the D-nozzle, which is designed to spread the exhaust into a thin sheet, which is then turned by the Coanda effect over the USB flaps, providing lift.

The QSRA D-duct design has mixing plane areas of 0.44 m^2 (682.5 $in.^2$) and 0.156 m^2 (250 $in.^2$) for the fan and core airstreams, respectively. The D-nozzle was designed so that the exit area could be increased as much as 10%, if needed, from an effective area of 0.42 m^2 (650 $in.^2$) which was 7.5% under the assumed baseline area. Subsequent calculations showed that there would be adequate surge margins at this area, however, and that no nozzle trim would be needed. Measured results discussed in a later section showed that indeed this was the case.

Acoustic treatment—The location of the nacelle acoustic liners is shown in figure 12. These liners are located in two different nacelle areas, the fan duct and the inlet. The fan duct liners, which are located on both the structural cowl and on the core cowl, are composed of perforated aluminum face sheets bonded to an aluminum honeycomb core with solid aluminum outer backing sheets. These panels cover about 0.75 m (30 in.) of duct length and are estimated to provide about 12 PNdB of aft fan attenuation. These panels serve as an integral part of the cowl structure and are load-carrying in addition to providing sound attenuation.

The second area of the nacelle that is lined is the inlet. The inlet acoustic panels are double-layer construction with perforated aluminum face sheet and septum with aluminum honeycomb cores and a solid aluminum backing sheet. The lower acoustic panel honeycomb cores are slotted and drain holes are provided in the outer sheet to prevent water accumulation and possible freeze damage.

BLC System

A unique feature of the QSRA is the mixed-flow boundary-layer control (BLC) system for the wing leading edges and ailerons. Air for the BLC system is bled from both the fan and the engine core and mixed in an ejector. A schematic of this system is shown in figure 13.

The BLC air is distributed by cross-ducting from each engine to the oppo-site side of the wing leading edge or aileron surfaces. Interconnecting ducting and check valves are installed between the two BLC system manifolds; they are located externally under the wing outboard of the outboard nacelles. The aileron ducting is located in a cavity aft of the rear spar; however, the leading edge ducting had to be located externally behind the leading edge flaps and crosses over inside the fuselage, under the wing. As was previously

discussed, these ducts may be simplified, in a future test period, to eliminate some of the external ducts. The BLC ducting is arranged so that each engine feeds a separate part of the BLC system, as shown in table 3. This arrangement provides a degree of automatic roll compensation in the event of the loss of a critical (outboard) engine.

Key elements in the BLC system are the mixing ejector and servo-regulator valve which are located as shown in figure 14. The ejector, which is shown in the insert of figure 15, has a fixed-geometry mixing section with an elliptical center body, and 42 circumferentially distributed ejector nozzles. These convergent-divergent nozzles, with length-to-diameter ratios of 5:1, limit the high-pressure bleed to a nominal 10% of the engine core flow, and fan bleed is limited to 3% due to duct size. Figure 15 shows the effect of this ejector design on net blowing momentum of the aileron nozzles. The upper curve represents the performance of the ejector without any pressure regulation. The servo-regulator valve limits the downstream duct pressure to a preset value, however, and the regulated system follows the lower curve of figure 15, yielding a nearly constant value of blowing momentum over the entire engine thrust range. This valve regulates high-pressure flow from the compressor so that it is zero at high power settings where the fan pressure ratio is high, and about 10% of the core airflow at low power settings. Although there is a loss in engine thrust at the 10% bleed airflow, it only occurs when a low-thrust level is commanded by the pilot. At high-thrust setting, the thrust loss is less than 1% due to BLC system losses.

Flight Controls

The flight control surfaces are shown schematically in figure 16. All wing trailing edge surfaces are electrically controlled (fly-by-wire) except the ailerons. The spoilers, double-slotted flaps, and USB flaps are electrically commanded and hydraulically powered; the ailerons are mechanically controlled and hydraulically powered. Both the rudder and elevator are C-8A components which are mechanically controlled and both are hydraulically powered.

Flap system—The USB flaps are deployed to the 30° position with the pilots flap lever. A thumb switch located in the throttle handle for the No. 1 engine controls USB flap position from 30° to the full deflection of 66°. This provides the pilot with a convenient means of varying USB flap setting, during a landing approach, as a means of glide path control. Deployment of the double-slotted flaps is controlled by a separate lever on the pilot's console. The aileron droop is slaved to the double-slotted flaps. The USB flaps, the spoilers, and the double-slotted flaps are all individually actuated by digital, electronically controlled, hydraulic actuators. This allows any flap or spoiler to be actuated independently of any other by proper preprogramming. This feature provides maximum research capability for the QSRA. As initially configured, the QSRA pilot has the capability to command assymetric deployment of the double-slotted flaps to trim engine-out rolling moment.

Stability augmentation system—The QSRA has a single channel, three-axis limited authority series type stability augmentation system (SAS). The roll and yaw axes are stabilized by a simple analog system similar to the one used in the Augmented Jet Flap STOL Research Airplane. The longitudinal SAS is a rate-command, attitude-hold system. It uses a General Electric MCP-701A digital computer to provide both pitch SAS functions and to control the direct lift control system and certain other logic functions. When the direct lift control (DLC) function is selected, the spoilers are deployed to about $-13°$. An increase in thrust (thrust levers forward) causes the spoilers to retract, and a decrease in thrust causes them to extend beyond the nominal $-13°$ angle. After each excursion from the $-13°$ position, a washout circuit gradually returns the spoilers to the $-13°$ position until the throttle is once again moved. At go-around thrust levels, the DLC system is automatically disabled and the spoilers are retracted.

Additional information on the QSRA configuration and systems is contained in reference 13.

AIRCRAFT PERFORMANCE

Although a large number of ground and flight tests have been performed to determine the QSRA's operating characteristics, many of these data are still being analyzed at this writing. Therefore, many of the aircraft performance curves presented are based on predicted, wind-tunnel, or simulation results. Most of the ground test data have been analyzed, however, allowing a comparison of the predicted and measured characteristics of the propulsion and BLC systems. In addition, sufficient flight data have been checked to verify that the airplane performance is close to that predicted, and these flight results will be commented on in the presentation of the individual data curves.

Propulsion System

Most of the measurements of propulsion system characteristics were made during the Boeing ground test. The primary objectives of this ground test were: (1) to determine the component map characteristics and to verify adequate surge margins (nozzle trim); (2) to measure engine performance with and without the BLC system operating; (3) to trim and adjust the engine fuel controls for idle, takeoff power, and acceptable acceleration characteristics; and, (4) to measure flaps-up thrust and flaps-down turning. In order to meet these objectives, a large number of data points were taken and analyzed for each engine; however, it will only be possible to present a small representative sample of the data here. Four summary plots will be presented. Two deal with engine thrust relationships, one with the location of the engine operating lines on the fan map, and the fourth with the acceleration characteristics of the engines with the BLC bleed schedule.

Thrust characteristics—The relationship of the engine thrust with fan speed is shown in figure 17, which also shows the relationship between fan and core speed for these engines. This curve is based on the ground test

results of all four of the engines (the results had less than ±1% scatter). The correlation between the predicted performance is very good above 72% of the corrected core speed but very poor at lower core speeds; hence, this curve gives better results than computer deck and will be used for performance estimation in the flight test program. As measured in the ground test, the inboard engines have about 3% less installed thrust than the outboard engines which have a maximum installed thrust of 30,068 N (6,750 lb). The effect of ambient temperature at sea level on this maximum installed thrust is shown in figure 18. These takeoff data are shown for no-bleed and ECS-bleed only because the high pressure bleed is normally shut off at this power setting. One additional item to note is the restricted zone shown in figure 17. This restriction results from a resonance problem in the sun gear at a fan speed of 55.5%. Although this resonance has a very sharp peak, the restricted operating band has been set between 50 and 60% to prevent excessive excursions into this zone, particularly near the resonance peak. This band causes a basic problem in the aircraft operation by forcing the STOL flight idle setting to be at a nominal 60% which is about 5-6% higher than is desirable. AVCO-Lycoming is working on a redesign of the sun gear to eliminate this resonance problem and expects to have a solution some time in 1979.

Fan operation—Figure 19 shows test data from all four engines plotted on the YF-102 fan map. This map includes predicted operation for a range of relative nozzle areas with the base area corresponding to the untrimmed nozzles. The test data were plotted using fan pressure ratio and corrected bypass flow as primary parameters with corrected fan speed as a secondary parameter. The test data indicated good correlation with predictions up to fan speeds of 70%; at higher speeds, these data indicated a nozzle under-area condition of up to 2%. This nozzle area spread was considered good in light of the rather limited instrumentation and hence a decision was made to operate without additional nozzle trim. The upper limit for fan operation used during the A-9A program's YF-102 acceptance tests is also shown in the figure for reference.

Engine acceleration—Engine accelerations were initially conducted on all engines starting at three fan speeds—48, 53, and 60%—which encompassed the predicted STOL flight idle range. Adjustments were made, to the fuel controls of all the engines, to increase the acceleration schedule in order to increase the acceleration rate with the Boeing high-pressure bleed schedule. Figure 20 shows the thrust versus time for accelerations from 53% fan speed for all the engines with the final fuel control adjustment. All of the engines accelerate to 65% thrust in approximately the same time; however, from that point on engine No. 2 was markedly slower and took several more seconds than the other engines to come up to the 95% thrust point. This slowness is due to an interaction with the BLC system, where the valve on engine No. 2 begins to close at a higher speed and appears to close at a slower rate. This results in higher bleed rates at a given fan speed for engine No. 2 which reduces the acceleration rate at higher fan speeds. Engine No. 1 also exhibits this characteristic but to a much lesser extent than engine No. 2.

Initially, these accleration data were to be used to establish the STOL idle detent position which corresponded to a fan speed of 53%. However, due to the problems discussed in the previous section, the throttle has no flight

idle detent and normal STOL landing operation is at 60% of fan speed. Because of the geometry of the overhead throttle system, the 60% setting forms a "natural" flight idle position.

Engine stability—Stability tests were conducted on all engines to demonstrate acceptable inlet operation and acceptable surge margins with increased fuel control acceleration schedules. These tests were conducted with all bleeds off and the fuel flow increased by 5% (TEST position for compressor surge detection). To check stability under severe operating conditions a series of transients, consisting of rapid accelerations, decelerations, and Bodies, were performed on the engines. No adverse engine operation was noted and the engines operated surge-free during this entire series of tests.

One final stability test was conducted on the engine in order to check inlet and fan operation at high angles of attack. A wind machine was positioned to provide a 36 m/s (72 knot) wind at 51° to the inlet centerline which was estimated to be the most critical inlet inflow condition. Tests were run on engines Nos. 1 and 2 using the same procedures as in the previous tests and also with the engines at ground idle (low mass flow) in a crosswind, which is the worst condition for inlet separation. Again no adverse engine operation was detected.

BLC System Performance

An evaluation of the ground-test data showed that the BLC system performance was essentially as predicted with the amount of net blowing momentum better than or equal to predicted levels at both STOL idle and takeoff power. The operation of the high-pressure regulator valve was stable with the pumping performance of each ejector compatible with its system demands. The performance of the aileron system was in excellent agreement with calculated performance, both with and without the regulator valve working (fig. 15). The only deviation from this curve occurred at thrust settings above 70% where system performance was slightly higher than that predicted. The test results showed that system losses at the design point were in good agreement with predictions, the losses being 5.2 and 6.5 % of the mixing total pressure for the leading edge and aileron systems, respectively.

During the BLC system tests, the only significant problem that was encountered was the inability of the pneumatically powered section of the pressure regulator valve to remain closed during engine starts, leading to long start times and poor engine acceleration characteristics. This lack of pneumatic power was a result of lower bleed duct pressures than preducted which are believed to be caused by higher losses in the engine bleed ports and high-pressure ducting. This problem was solved by placing a motorized valve in series with the regulator valve which ensures a positive closure during low-speed engine operation.

Additional information on the engine operation and ground test can be found in references 14-16.

Flight Performance

As a part of the management approach discussed earlier in this paper, rigid performance requirements were not imposed on Boeing, the airplane prime contractor. However, ambitious performance goals were established at the start of the project and current predictions indicate that most of these will be met or exceeded. The reason for the high-performance levels is to provide the QSRA with the maximum amount of research capability. Propulsive-lift, roll acceleration, approach capability, and low community noise are technology targets that were emphasized by NASA and that were of primary importance in the development of the QSRA design. Some of the more significant performance capabilities of the QSRA are summarized in table 4.

Lift capability—One of the primary performance goals, a minimum usable approach lift coefficient (C_L) of 4.6, is expected to be exceeded by about 16% after allowance has been made for commercial flight safety margins. Figure 21 compares the lift performance of the QSRA to that of a standard medium commercial jet transport (the B-727) and to the Boeing Advanced Military STOL Transport (YC-14). The high-lift capability for the QSRA was achieved by applying propulsive-lift and leading edge BLC, as discussed previously. This four-engine configuration permits a larger span USB flap and reduces adverse yaw and roll moments with one engine inoperative, thus yielding the improvement in lift over the twin-engine YC-14. The actual flight data indicate that the QSRA performance is nearer to prediction at the higher angles of attack than to the wind-tunnel data. The reasons for this are complex, but are believed to be due to the fact that the QSRA USB performance configuration has not been truly optimized yet and performance is expected to improve as more is known about the flow over the USB portion of the wing.

Another performance area which is vital to the QSRA research mission is the roll control responsiveness of the airplane. The QSRA roll acceleration is compared to that of several other airplanes in figure 22. This high QSRA roll control effectiveness is achieved by incorporating blown ailerons, minimizing roll inertia, minimizing engine-out rolling moment, and by the assymetric use of the double-slotted flaps for trim. This roll-control power is important because much of the research flying will be done with one of the outboard (critical) engines shut down under unfavorable conditions in order to develop criteria for future STOL aircraft. This curve has not been verified in flight at this time but will be explored during the next phase of flight testing at Ames.

STOL operating envelope—The STOL operating envelope of the QSRA with all engines operating is shown in figure 23 and the envelope with the critical engine (either outboard engine) inoperative is shown in figure 24. These figures show the aerodynamic capability of the airplane. Pitch control limitations of the present configuration prevent operation at full USB flap deflection, at 100% thrust, and at low speeds. Similarly, directional control considerations limit the minimum speed with an engine out in a go-around configuration. However, future modifications to the QSRA empennage, which are presently under consideration, will make it possible to explore all corners of the envelope. The existing configuration can safely operate at a lift coefficient of 5.5 while maintaining speed, angle of attack, maneuver, and

301

go-around climb margins. When the thrust is increased to 100% in a go-around situation, the USB flaps are autmoatically retracted to the go-around setting. As shown in figure 24, this permits a climb angle of +2° (equivalent to a rate of climb of 1.22 m/s (240 ft/min)) at an approach lift coefficient of 5.5 with the critical engine inoperative. As the speed is allowed to increase, the climb angle increases to over +6°.

These operating envelopes have been partially verified in the initial Boeing flight test and also in the Ames flight test. Values of airplane drag are slightly higher than those predicted and performance at the very high flap settings (over 63°) indicates that there is some flow separation and slightly lower turning angles than were attained in wind-tunnel tests. However, as discussed earlier, it is believed that configuration optimization and a better understanding of propulsive-lift aerodynamics will allow the airplane to eventually exceed performance predictions at the highest STOL flap settings. This flow field has been explored to a minor extent (tufts) during the first series of Ames tests and will be explored in great depth in the next phase of the Ames flight research program.

Approach angle—A short-field airplane requires a steep descent capability (high approach angle) in order to minimize the required airspace in the terminal area, as well as to minimize community noise effects. The USB nozzle and flaps of the QSRA have been designed to provide exceptionally high flow turning of the engine exhaust, yielding high lift approach lift coefficients (> 5.5) which enable this aircraft to achieve very steep approaches with full safety margins. Figure 25 gives a comparison of the QSRA STOL capabilities and the descent angle and ground roll of a conventional transport aircraft landing. At the same distance from the airport, the QSRA is more than twice as high as the conventional airliner and it is able to stop on the runway before today's commercial transports complete their flare and touch down on the runway. The landing and takeoff performance of the QSRA has been verified during the initial flight test with ground roll distance of 202.4 m (664 ft) during a maximum performance takeoff and of less than 167.6 m (550 ft) during a STOL landing.

Because noise attenuates rapidly with distance, the higher approach altitude of the QSRA is a big factor in reducing community noise effects; this height can be increased even more by landing toward the center of the runway. Another technique that may reduce community noise effects, by keeping the noise completely within the airport boundaries during takeoff, is a spiral or circling approach and departure. Simulation studies have shown that the QSRA noise can be confined to the boundaries of a typical general aviation airport, and flight test has shown that the QSRA is capable of a 337.1-m (1106 ft) radius departure with a 30° bank angle with an increase in altitude of 884 m (2900 ft) after a full 360° turn.

Acoustic Performance

One of the primary goals of the QSRA program was to have a 90-EPNdB community noise impact area of no more than 2.5 km^2 (1 mile^2) for a 668,182-N (150,000 lb) commercial airplane based on QSRA technology. Figure 26 shows

how this goal compares with the noise-impact area of a current medium short-haul commercial transport (B-737, DC-9). The actual noise levels of the QSRA were measured during the final phase of the Boeing flight-test program, extrapolated, and compared to the program goals. The maximum effective perceived noise level (EPNL) measured on the 152.4-m (500 ft) sideline during takeoff was 93.5 EPNdB and the goal was 92 EPNdB; during landing it was 89 EPNdB and the goal was 90 EPNdB. As can be seen, the values are slightly higher during takeoff and slightly lower during landing. (It should be noted that these takeoff and landing noise levels are based on a 152.4-m (500 ft) sideline and hence the takeoff noise is substantially greater than that which would be measured in accordance with FAR 36.) Several major differences exist between the QSRA and any potential transport aircraft based on the QSRA technology, with the most important of these being the high drag configuration of the QSRA during takeoff, due to the absence of fairings and retractable landing gear, and the fact that the QSRA has nonretractable vortex generators and nozzle doors in the takeoff and cruise configuration. The clean transport configuration would result in a takeoff/climbout speed increase from the 90 knot QSRA speed to about 130 knots, resulting in a decrease in the takeoff sideline noise level to approximately 91.5 EPNdB. Based on this clean configuration QSRA, a 668,182-N (150,000 lb) commercial transport would have a 90 EPNdB noise impact area of 7.03 km^2 (2.8 mile^2) compared to the QSRA goal of 2.51 km^2 (1 mile^2). These noise extrapolations are preliminary results based on a limited data base and are believed to be considerably larger than the noise areas that will be achievable by a commercial transport based on the QSRA technology. This belief is based on a number of factors, discussed in the following sections, that can be eliminated in any future transport if they are isolated as significant noise sources (e.g., nonretracting vortex generators).

Data analysis—The data were analyzed by the systems and methods used in FAR-36 noise certifications, with 1/3 octive band spectra integrated over 0.5-sec periods at increments of 0.5 sec. Computer processing mated acoustic data with the airplane position as determined optically and with the flight profile data, synthesizing flyover noise time histories for the various reference flight profiles.

Far field results—The community noise level data result from measurements made with a precision of about ±1 EPNdB in the EPNL measurements and about ±2 PNdB in PNL measurements. The noise levels along the flight path are higher with the USB flaps retracted than they were with a 30° flap setting and the sideline noise levels were relatively unaffected by flap configuration. Although airframe noise was present in some measurements, it did not significantly influence the PNL and EPNL noise levels. The measured noise exceeded predictions, with the higher levels appearing to be related to a random aerodynamic noise generated by interaction of turbulence within the jet flow with the wing trailing edge. It is believed that one possible source of this noise may be the vortex generators. In addition, a large, low-frequency (200 Hz) component seems to be the result of engine installation effects.

An additional anomaly appeared in some of the data for retracted USB flap that was taken at a different time than the rest of the data. The levels of this data point appeared to be essentially the same as the 30° flap data. This lower far-field noise level was corroborated by near-field measurements

discussed in the next section. There is no reasonable explanation of this anomaly at this time but subsequent testing of the QSRA will investigate this effect.

Near-field measurements—Near-field noise measurements were made with eight microphones flush-mounted on the fuselage exterior surface and four located inside the aircraft. These measurements showed that noise levels increased uniformly with engine power levels, approximating a 40 log V_J relationship, with maximum exterior noise levels of about 150 dB. The interior noise levels with inboard engines shut down were about 10 dB less than with all engines operating, especially in locations where flow attachment and fuselage scrubbing occurred. The maximum measured interior noise levels were 118 dB in the aft cabin at high power settings. It should be noted that the fuselage interior is untreated and is not representative of the noise levels that would exist in a similar commercial transport aircraft.

Data significance—The acoustic data presented in this section are preliminary and do not represent a complete analysis or a good data base. Rather, they represent a starting point from which to build a more complete understanding of propulsive-lift aircraft noise, and to develop the required flight experiments that will provide a technology base for future transports based on QSRA program goals. As has occurred in several other areas, the QSRA acoustic configuration has not been optimized. Optimization of the configuration can be expected to reduce the noise levels from those measured in these tests. It should be noted that a reduction in measured noise level of only 2 dB will result in noise impact area reduction of approximately 60%. Additional data on the QSRA flight tests and acoustic tests are given in reference 17.

FUTURE PLANS AND EXPERIMENTS

Initial Tests and Configuration Optimization

The initial NASA flight program at Ames Research Center will last for approximately 1½ years and will be devoted to envelope documentation with configuration optimization as required. As discussed in several previous sections, small changes in the configuration or flow field can have a significant effect on propulsive-lift aircraft performance. During these initial tests, a series of experiments will be performed to define the flow field and the effect of this flow field on the QSRA powered-lift performance. For example, a number of experiments will be performed to determine the effect of vortex generator size and location on the QSRA aerodynamic performance and far-field acoustics. Aerodynamic performance will be documented and compared to a reference baseline as provided by a relatively sophisticated mathematical model of the QSRA and by the use of flow-visualization techniques such as tufts. The acoustic measurements will be cross correlated with near-field measurements in order to isolate and identify the sources of the noise, and these experiments will be augmented with small scale tests as required. In addition, alternative flight profiles will be evaluated in order to further reduce community noise impact areas.

One interesting modification under consideration is the replacement of the present blown leading edge with an unblown leading edge slat. Wind-tunnel tests described earlier showed that an unblown leading edge would degrade performance by reducing the angle-of-attack margin 4° to 5° (ref. 18). If this can be verified in flight, future designers of high-performance STOL aircraft will have a firm technical base for the selection of blown versus unblown leading edges.

Another modification planned for the QSRA is to increase the gross weight to 267,273 N (60,000 lb). This will provide a wing loading of 4795 N/m^2 (100 lb/ft^2) and give the QSRA the capability of operating over a range of wing loadings from 3117 to 4795 N/m^2 (65 to 100 lb/ft^2) to increase its research versatility.

Flight Experiments

After the initial NASA flight research program and configuration optimization, the QSRA will be made available for the flight-experiments program. In the initial sections of this paper, the concept of a research aircraft being a facility for flight research was discussed. When the QSRA enters the flight-experiments phase it will fulfill this goal and become a national facility for flight research. Research personnel within NASA are planning a program of flight experiments. Some of the experiments will be accomplished as in-house efforts; others will be done jointly with other government agencies, for example, the development of certification criteria for future STOL aircraft. In other cases, the work will be contracted, particularly when the experiment involves structural modification to the airplane or the development and installation of new equipment. The QSRA is, however, a national flight facility. As such, it is available to the aeronautical community in the same way that a NASA wind tunnel or simulator is available.

QSRA workshop—On November 29 and 30, 1978 a workshop will be held at Ames Research Center in order to provide industry, universities, and government agencies with information on the capabilities of the QSRA and to provide a mechanism by which participation in the flight experiments program can be implemented. It is hoped that this procedure will lead to broad participation by the aeronautical community in the QSRA flight research program.

Although the flight-experiments phase will not "officially" begin for several years, it is believed that many experiments, particularly, self-contained experiments, can be flown on the QSRA during the initial flight tests. In addition, some experiments, such as acoustic measurements and correlation of small-scale testing with the QSRA, can and should be done concurrently with the early flight program. For example, one series of acoustic experiments which is under consideration involves the use of Ames' quiet noise measuring airplane, the YO-3A, to make free-field acoustic measurements of the QSRA flap and inlet noise. A number of other experiments are planned in various research areas such as avionics, computer control systems, inlet flow fields, acoustics, structural vibration, and aerodynamic performance.

Flight demonstration—Another activity in the early planning stages is demonstration flights at airports in the San Francisco Bay Area for potential users of the technology. This would include airline and airport officials and technical personnel from interested aircraft manufacturers. The QSRA will not carry passengers because it is qualified only for a crew of two research pilots. However, flight demonstrations will expose potential users of this technology to the short-field capability, the maneuverability, and the low community noise levels of which the QSRA is capable. Late in the initial flight program, it is also planned that qualified pilots from other organizations will be invited to fly and evaluate the QSRA with a NASA research pilot as an "instructor-pilot." This was done successfully with the Augmented Jet Flap STOL Research Airplane and will be repeated with the QSRA.

REFERENCES

1. Quigley, Hervey C.; Innis, Robert C.; and Grossmith, Seth: A Flight Investigation of the STOL Characteristics of an Augmented Jet Flap STOL Research Aircraft. NASA TM X-62334, 1974.

2. Quiet Propulsive Lift Research Aircraft Design Study. NASA CR-137557, 1974.

3. Quiet Short Haul Research Aircraft Design Study. NASA CR-137554, 1974.

4. Cochrane, John A.; and Carros, Robert J.: Hybrid Upper Surface Blown Flap Propulsive-Lift Concept for the Quiet Short-Haul Research Aircraft. AIAA Paper 75-1220, Oct. 1975.

5. Cochrane, John A.; and Boissevain, Alfred G.: Quiet Short-Haul Research Aircraft—Current Status and Future Plans. AIAA Paper 78-1468, Aug. 1978.

6. Shovlin, Michael D.: Effects of Inlet Airframe Integration on the Inlet of a USB Four Engine STOL Airplane. AIAA Paper 78-959, July 1978.

7. Nickson, Theodore B.: Large Scale Wind Tunnel Investigation of the Quiet Short-Haul Research Aircraft (QSRA) Configuration. NASA CR-152095, 1978.

8. Gunnarson, Daniel W.; and McArdle, Jack C.: Development and Test of an Inlet and Duct to Provide Airflow for a Wing Boundary Layer Control System. AIAA Paper 78-141, Jan. 1978.

9. Reshotko, Meyer; Karchmer, Allen N.; Penko, Paul F.; and McArdle, Jack G.: Core Noise Measurements on a YF-102 Turbofan Engine. AIAA Paper 77-21, Jan. 1977.

10. Middleton, Robie; and Vincent, James H.: Quiet Short-Haul Research Aircraft Phase II Flight Simulation Math Model—Final Report. NASA CR-152197, 1978.

11. Wilcox, Darrell E.; and Quigley, Hervey C.: V/STOL Aircraft Simulation—Requirements and Capabilities at Ames Research Center. AIAA Paper 78-1515, Aug. 1978.

12. Riddle, Dennis W.: A Piloted Simulator Analysis of the Carrier Landing Capability of the Quiet Short-Haul Research Aircraft. NASA TM-58508, 1978.

13. Stevens, Fred: Configuration Definition Document of the QSRA. (Proposed NASA high number contractor report.)

14. McNeill, John M.: QSRA/YF-102 Engine Performance and Control. Boeing Document D340-10206, Boeing Commercial Airplane Company, Seattle, Washington, 1978.

15. McNeill, John M.; and Harkonen, Dennis L.: QSRA Ground Test Report Volume I—Propulsion and Fuel System Testing. Boeing Document D340-13701-1, Boeing Commercial Airplane Company, Seattle, Washington, 1978.

16. Shah, Anil D.: QSRA Ground Test Report Volume II—Systems. Boeing Document D340-13701-2, Boeing Commercial Airplane Company, Seattle, Washington, 1978.

17. Analysis of Contractor's Taxi and Flight Test of the QSRA. (Proposed NASA high number contractor report.)

18. Holtman, Donald N.; and Howard, Wes M.: Large Scale Wind Tunnel Investigation for Future Modifications to the Quiet Short-Haul Research Aircraft (QSRA) Configuration. (Proposed NASA high number contractor report.)

TABLE 1. - QSRA INITIAL GOALS AND REQUIREMENTS
(PARTIAL LIST)

Requirements

- Day, VFR operation only

- Crew of two research pilots only

- Modification of GFE C-8A Buffalo

- Use of four GFE YF-102 engines

- Hybrid upper surface blowing propulsive lift concept

Goals

- Approach lift coefficient - 4.6 (steep approach with margins)

- Approach path of -7.5° with margin for gusts, wind, etc.

- 90 EPNdB combined takeoff and landing footprint area, when scaled to 668,182 N (150,000 lb) of 2.5 km^2 (1 $mile^2$)

- Minimum duration of test mission—50 min

- Minimum wing loading at gross weight = 3117 N/m^2 (65 lb/ft^2)

- Maximum cruise speed 160 knots

- Wing/nacelle configuration representative of cruise at M = 0.74.

TABLE 2. – QSRA FUNDING DISTRIBUTION

Preliminary design studies	$ 2,000,000
Wind tunnel and engine tests	1,000,000
Engine program	2,000,000
Airplane detail design and fabrication	22,000,000
Proof-of-concept flight test	2,000,000
Total funding available	$29,000,000

TABLE 3. – BLC FLOW DISTRIBUTION

Engine position	BLC segment
1	Right aileron
2	Right leading edge
3	Left leading edge
4	Left aileron

TABLE 4.– QSRA PREDICTED PERFORMANCE

Approach lift coefficient (steep approach with margins)	5.5
Approach path with margin for wind, gusts, etc.	-7.5°
Duration of STOL test mission	102 min
Landing field length at 213,370 N (48,000 lb) $(W/S = 3836$ N/m^2 (80 lb/ft^2)) (1.67 factor over 10.7-m (35 ft) obstacle)	426.7 m (1400 ft)
Takeoff field length at 668,182 N (150,000 lb) (10.7-m (35 ft) obstacle with critical engine inoperative (CEI) at decision speed)	403.9 m (1325 ft)
Turn radius at 30° bank angle	213.4 m (700 ft)
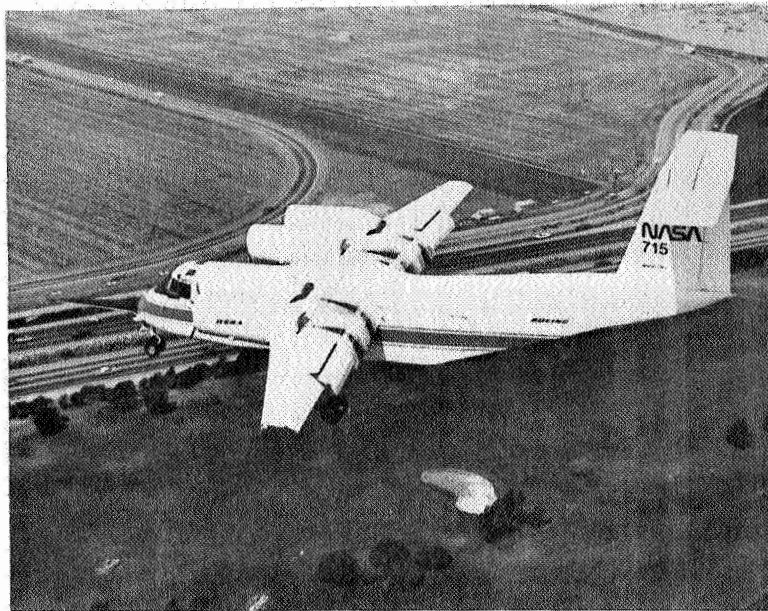
Figure 1. – The Quiet Short-Haul Research Airplane (QSRA) performing a STOL
approach prior to landing at Ames Research Center.
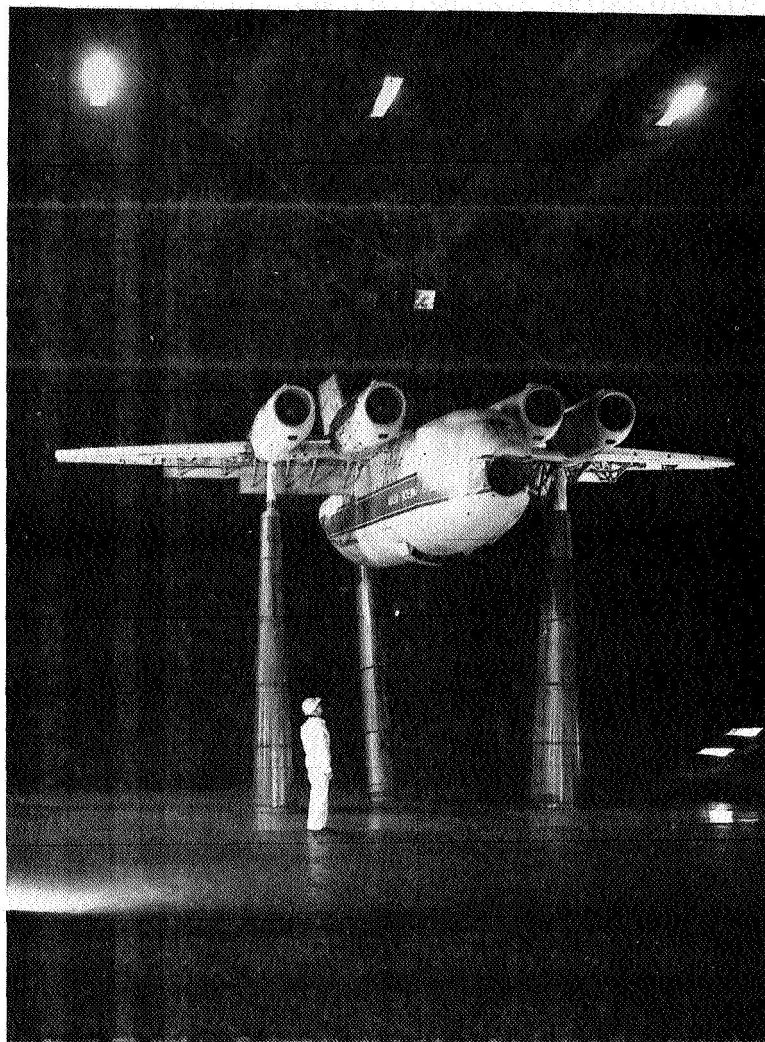
Figure 2. – The 0.55-scale QSRA model mounted in the Ames 40- by 80-Foot Wind Tunnel.
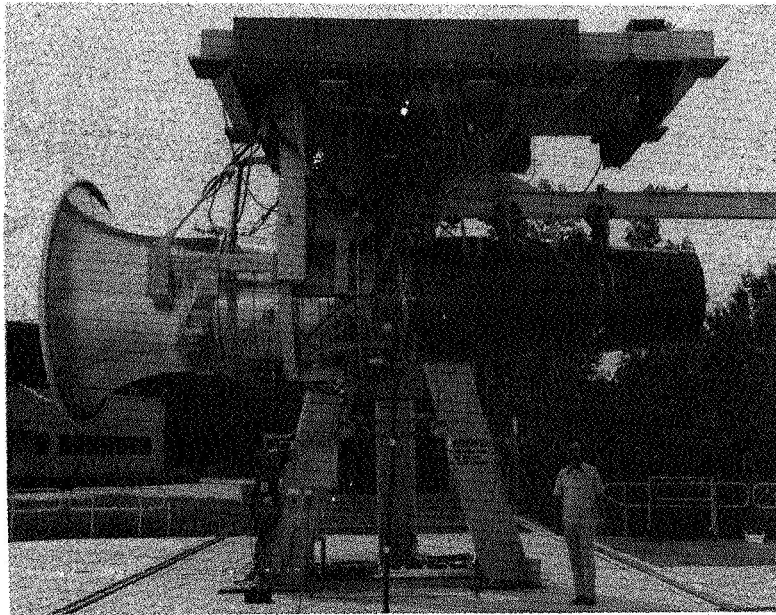
Figure 3. – The YF-102 (QSRA) engine installed in the Lewis Vertical Lift Fan
Facility in preparation for confluent flow baseline testing.

312

Figure 4. – Pilot's view from the cab of the Ames FSAA during the QSRA flight simulation.

TOGW, lb	50,000	222260 N
WING AREA, ft²	600	55.74 m²
WING LOADING, lb/ft²	83	3987.4 N/m²
ASPECT RATIO	9	
THRUST/WEIGHT	.60	

32 ft
9.75 m

27.8 ft
7.06 m

73.5 ft
22.40 m

93.25 ft
28.42 m
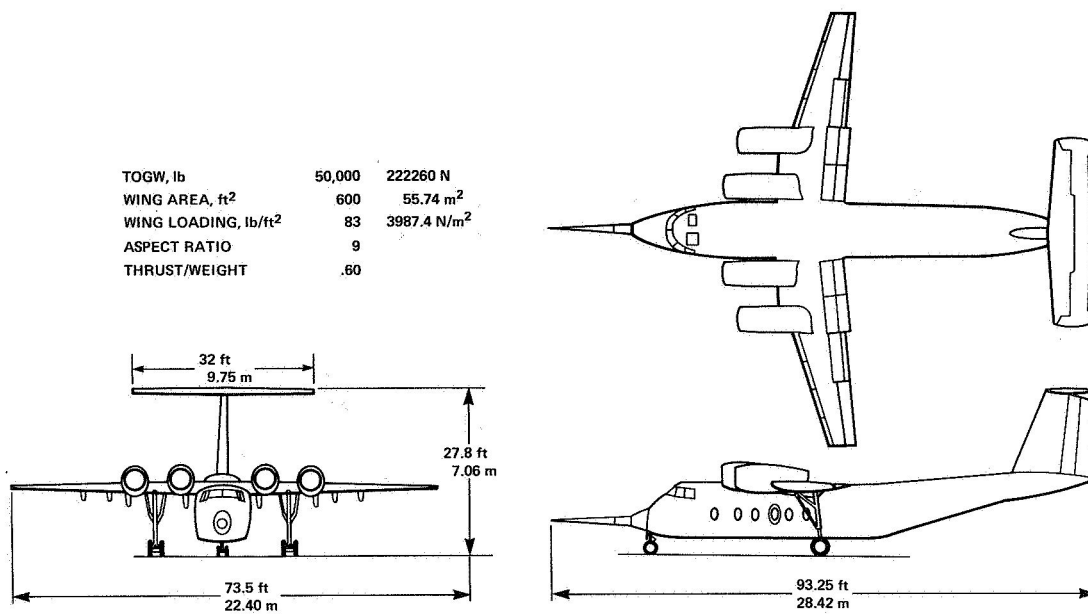
Figure 5. – The QSRA airplane layout.
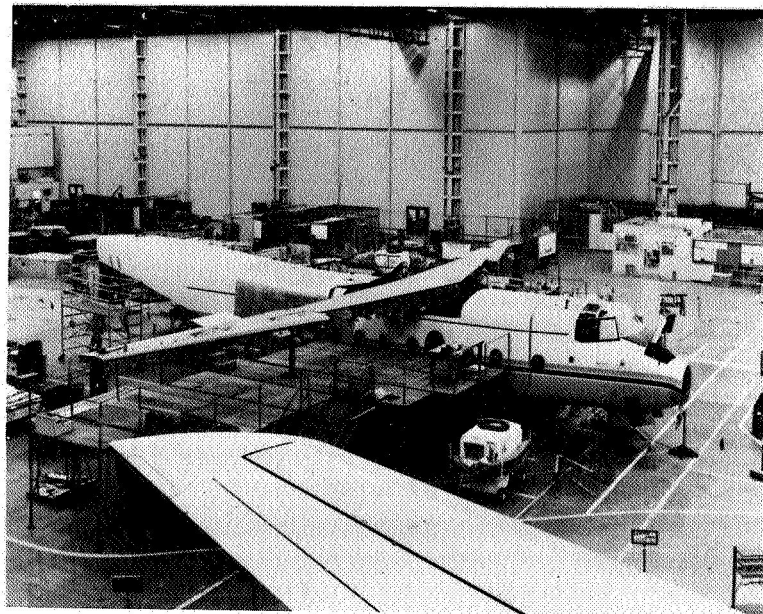
Figure 6. – The QSRA wing and fuselage under construction at the Boeing Developmental Center in Seattle, Washington.

314
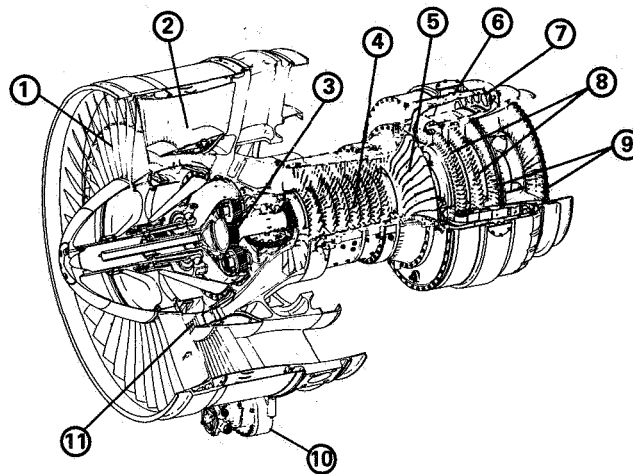
1. FAN STAGE
2. FAN STATOR
3. REDUCTION GEAR ASSEMBLY
4. CORE AXIAL COMPRESSOR
5. CORE CENTRIFUGAL COMPRESSOR

6. CUSTOMER BLEED PORTS
7. COMBUSTOR
8. GAS PRODUCER TURBINES
9. POWER TURBINES
10. ACCESSORY GEARBOX
11. SUPERCHARGER

Figure 7. - A cutaway view of the YF-102 (QSRA) engine which was built by AVCO-Lycoming Division.

56.77 in.
1.442 m

26.25 in.
0.667 m

40.3 in.
1.024 m

18.56 in.
0.471 m

N_L 7600 (FAN)
        (POWER TURBINE 17600)
N_H 19660
SFC   0.41
MGT   1665°F 907°C
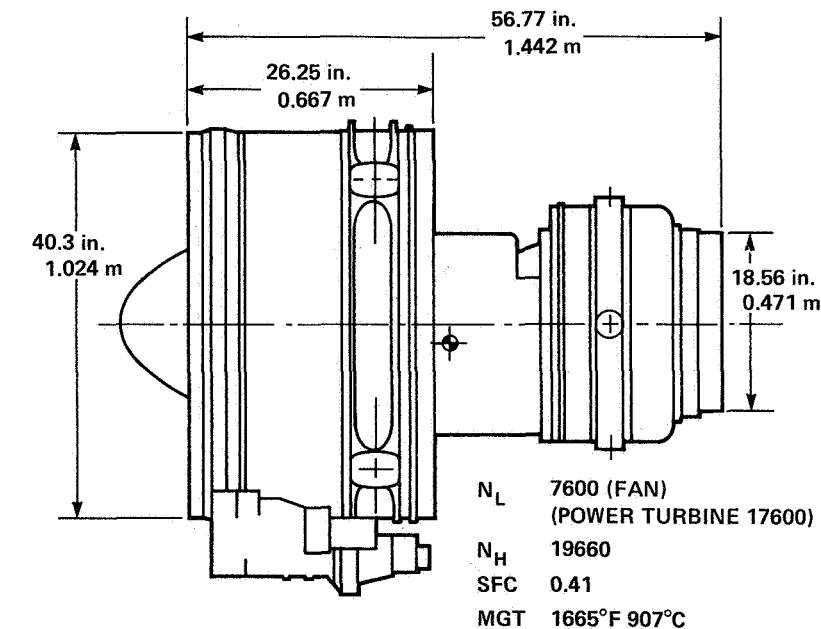
MAX. THRUST   7500 lb   33409.1 N
WEIGHT DRY   1215 lb   551.1 kg
TOTAL AIRFLOW   267 lb/sec   121.1 kg/sec
CORE AIRFLOW   37 lb/sec   16.8 kg/sec
B.P.R.   6.2

Figure 8. - YF-102 (QSRA) engine layout.
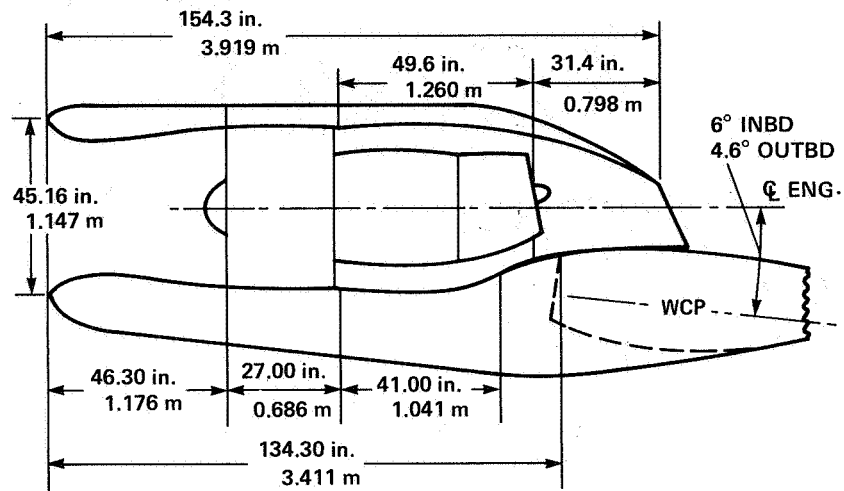
Figure 9. - The QSRA nacelle layout.
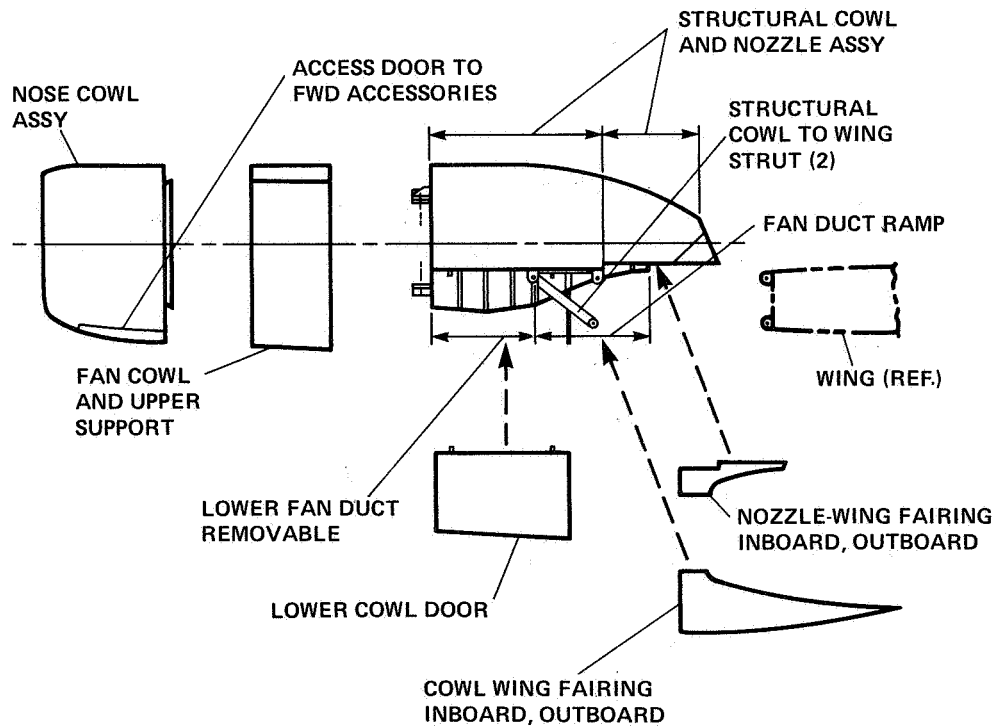
Figure 10. - View of the QSRA nacelle main structural elements.

316
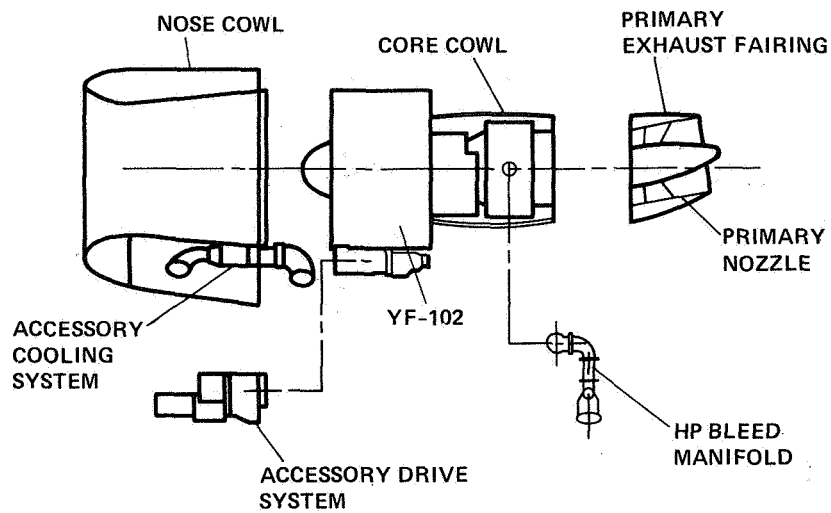
Figure 11. – The engine build up showing the YF-102 (QSRA) engine installed in an assembly consisting of the engine, core cowl, inlet, and primary nozzle.
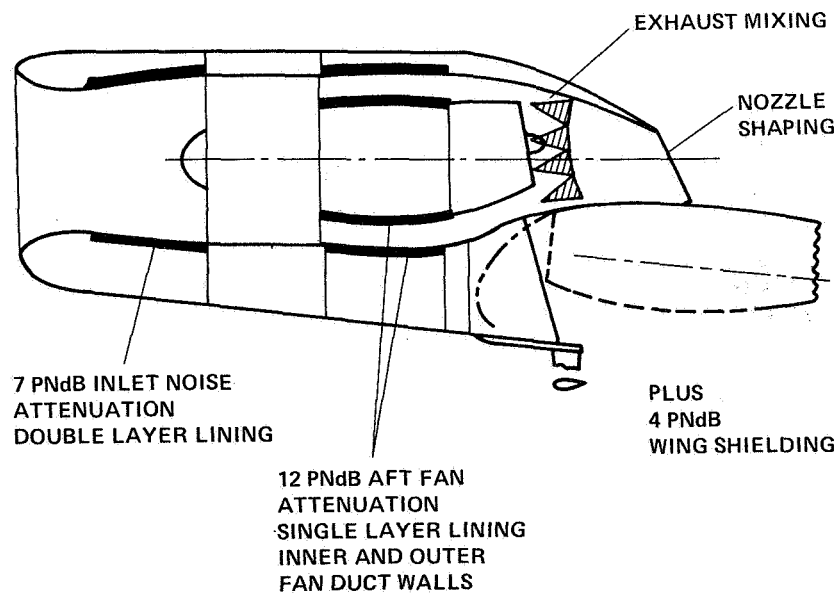
Figure 12. – Location of the acoustic lining panels in the QSRA inlet and aft fan flow passages.
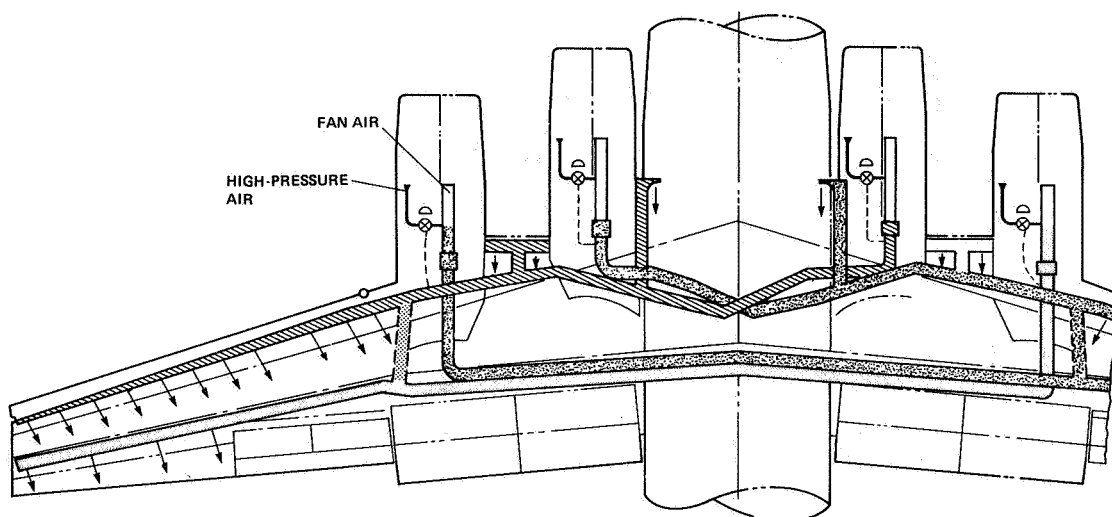
Figure 13. – The layout of the QSRA boundary-layer control (BLC) system. The two phantom line ducts only connect the leading and trailing edge systems in the event of an engine failure.
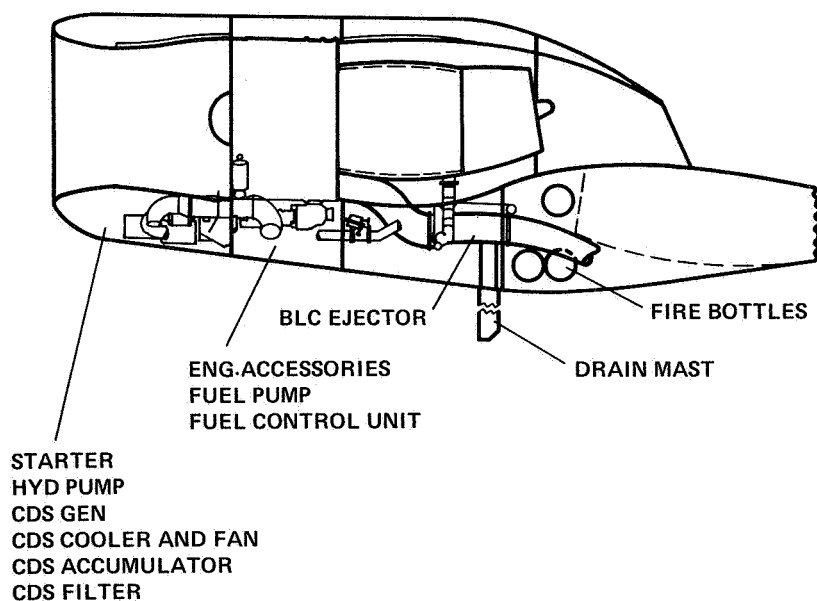
Figure 14. – Systems layout in the QSRA nacelle.

318
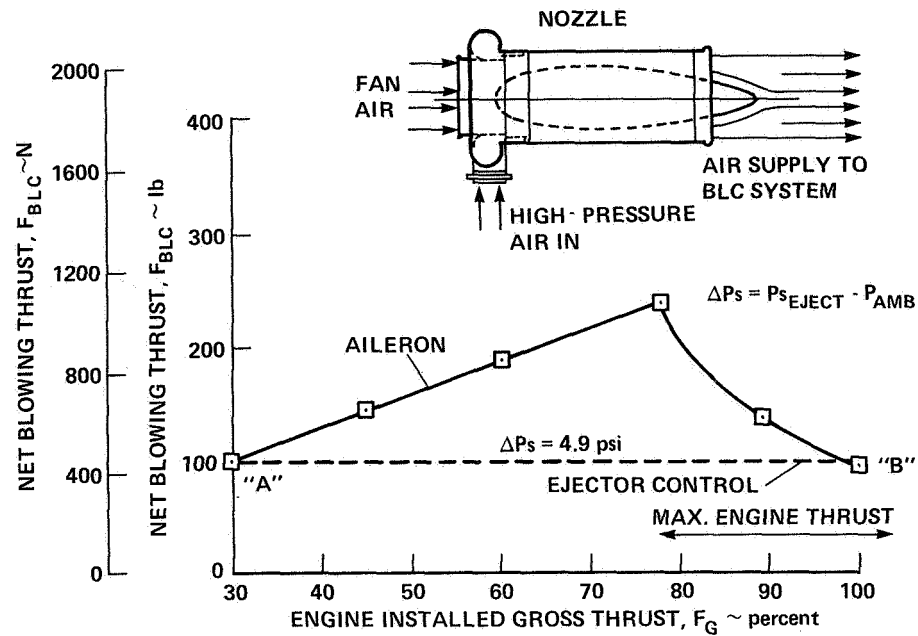
Figure 15. — The performance of the QSRA aileron BLC system shown as a function engine thrust. The BLC ejector which combines the fan and core air from the engine to provide the BLC system air flow is shown in the insert.
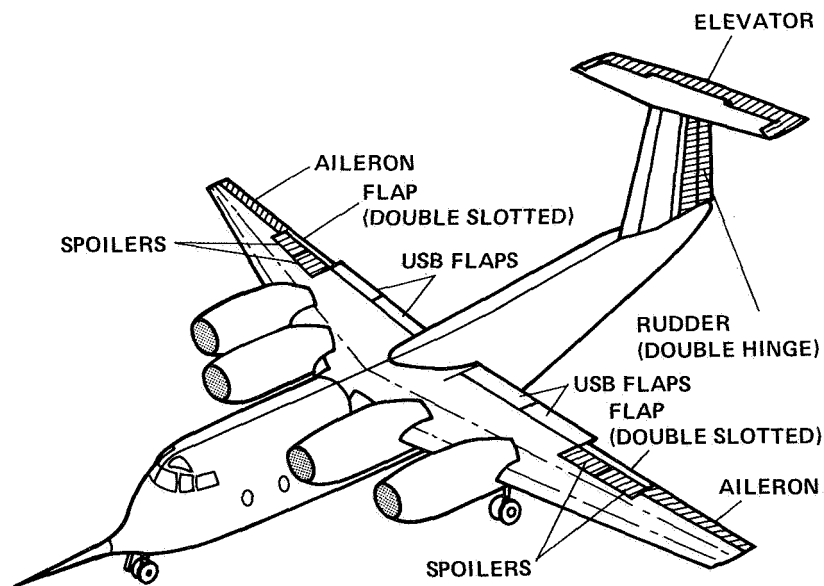

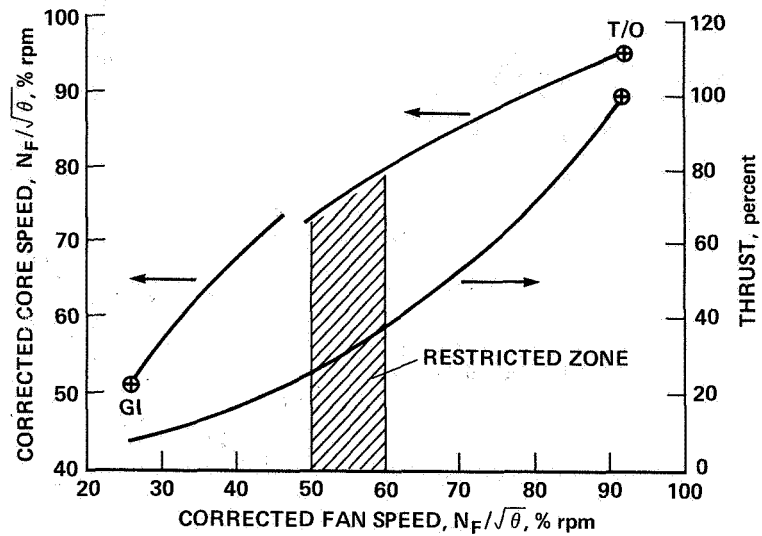Figure 16. — Location of the QSRA main flight controls.

319

Figure 17. - The relationship of the fan and core compressor speeds with each other and with engine thrust level for the YF-102 (QSRA) engine.
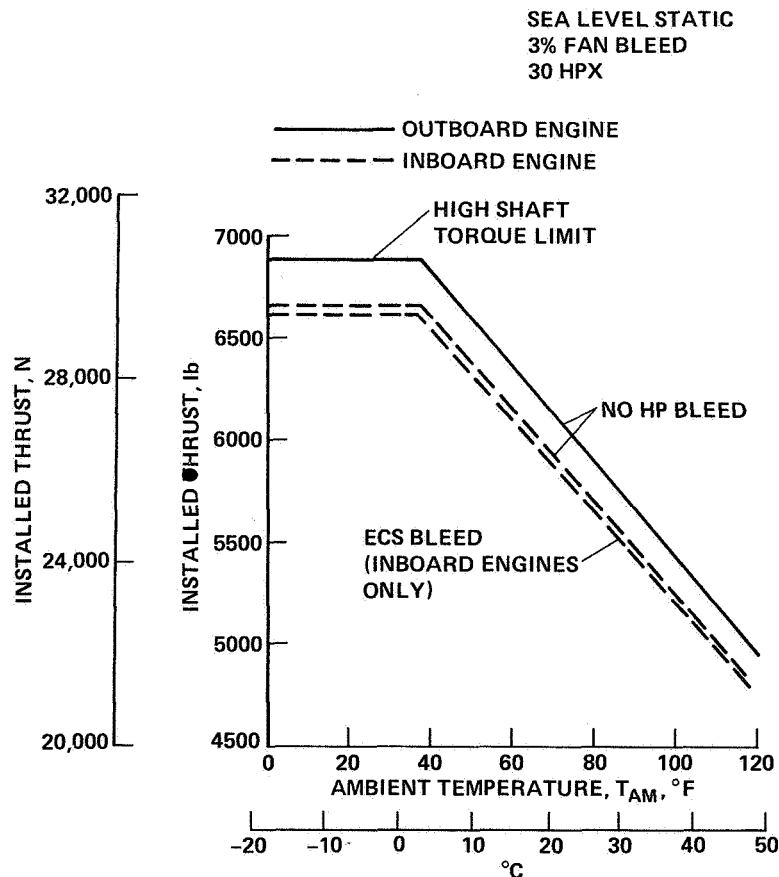

Figure 18.- The effect of ambient temperature on the YF-102 (QSRA) engine thrust. The engine is torque-limited at the lower temperatures and environment control system (ECS) bleed is only taken from the inboard engines.
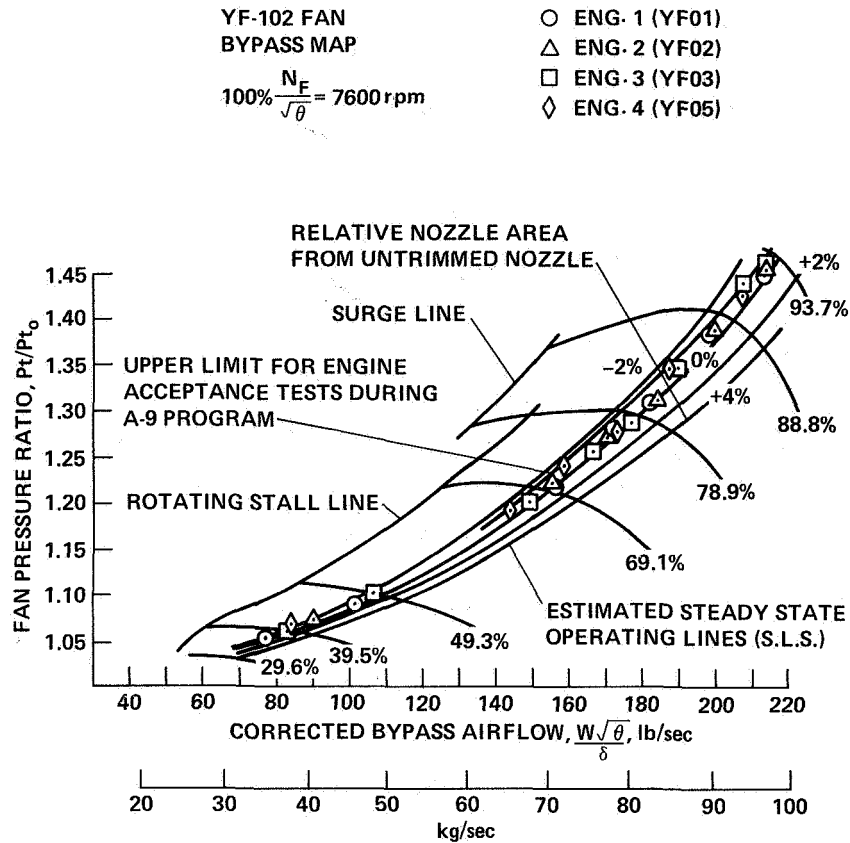
YF-102 FAN
BYPASS MAP

$100\% \dfrac{N_F}{\sqrt{\theta}} = 7600$ rpm

O ENG. 1 (YF01)
△ ENG. 2 (YF02)
□ ENG. 3 (YF03)
◇ ENG. 4 (YF05)

RELATIVE NOZZLE AREA
FROM UNTRIMMED NOZZLE

SURGE LINE

UPPER LIMIT FOR ENGINE
ACCEPTANCE TESTS DURING
A-9 PROGRAM

ROTATING STALL LINE

+2%
93.7%
-2% 0%
+4%
88.8%
78.9%
69.1%
ESTIMATED STEADY STATE
OPERATING LINES (S.L.S.)
49.3%
29.6% 39.5%

CORRECTED BYPASS AIRFLOW, $\dfrac{W\sqrt{\theta}}{\delta}$, lb/sec

kg/sec

Figure 19. – The YF-102 (QSRA) engine fan map. Results of the installed engine ground tests, which indicate that there is adequate operating margin for each engine, are shown.
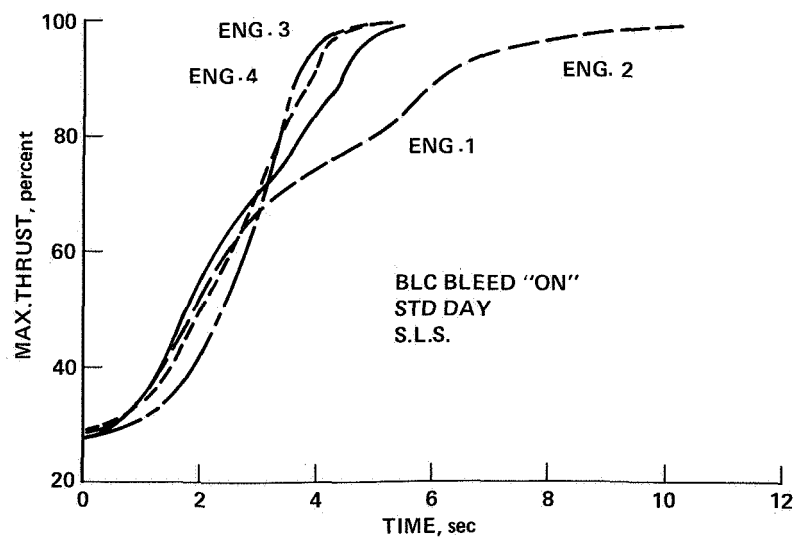

ENG. 3
ENG. 4
ENG. 2
ENG. 1

BLC BLEED "ON"
STD DAY
S.L.S.

Figure 20. – The acceleration time history for each of the QSRA engines. Note the effect of the slightly out-of-phase BLC valve operation on the acceleration of engine No. 2.
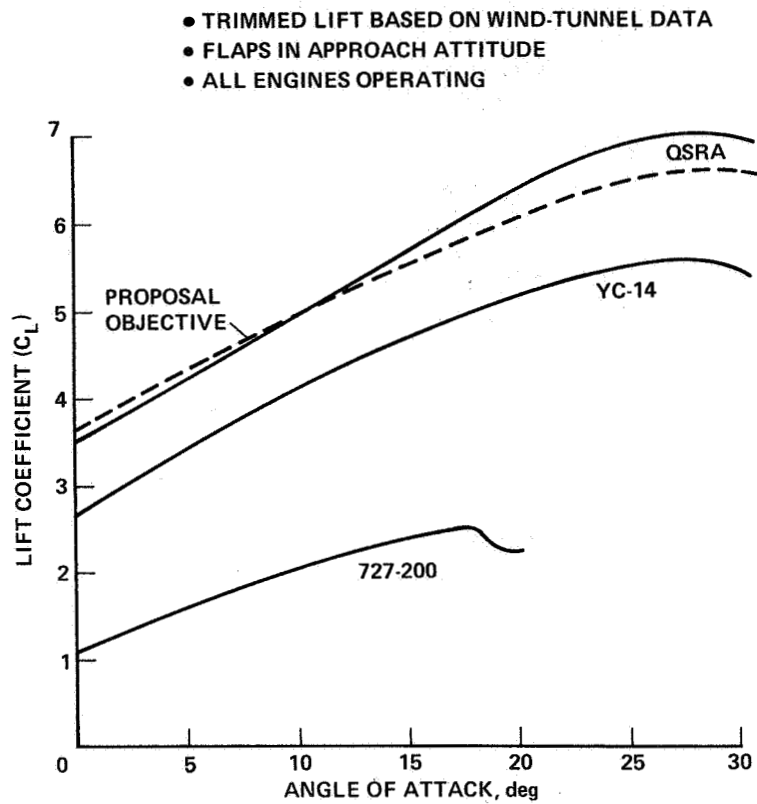
321

- TRIMMED LIFT BASED ON WIND-TUNNEL DATA
- FLAPS IN APPROACH ATTITUDE
- ALL ENGINES OPERATING

Figure 21. – Comparison of the powered-lift performance of the QSRA with a conventional transport and with an advanced STOL transport.
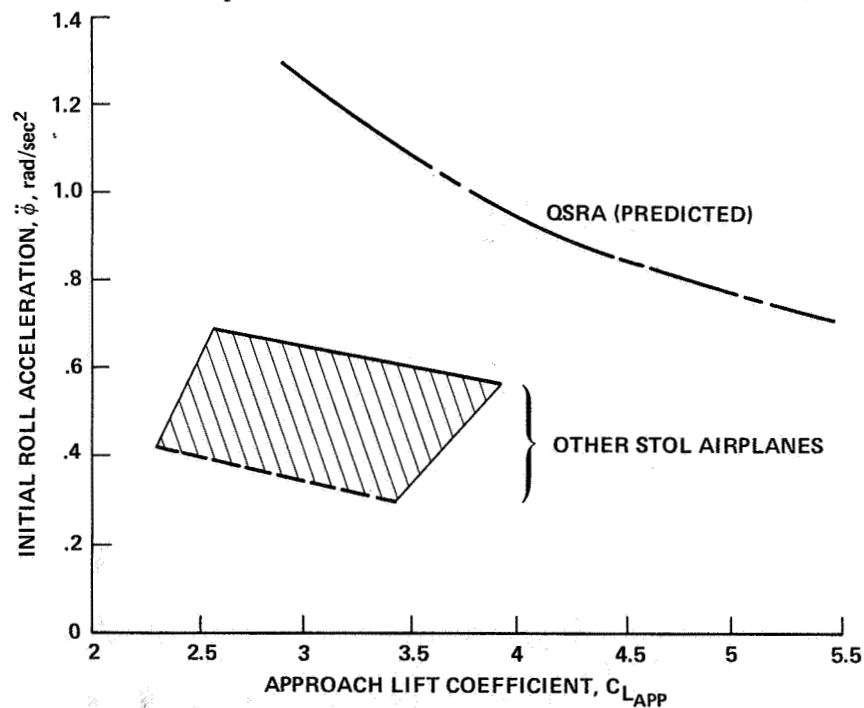

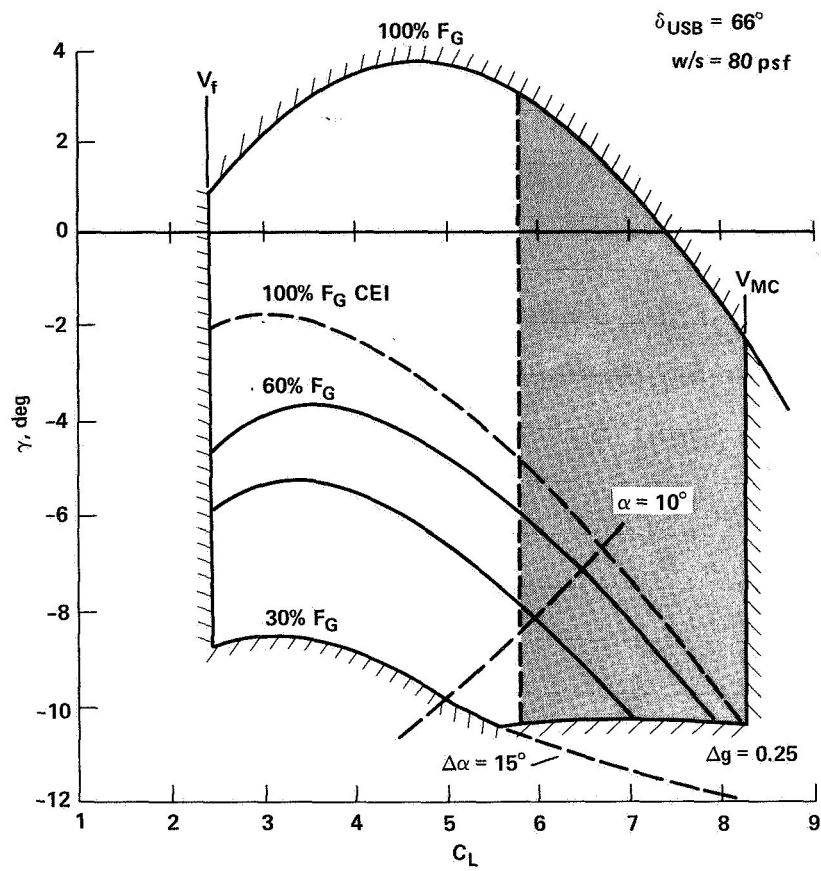Figure 22.– The predicted QSRA roll performance compared with previous STOL airplanes.

322

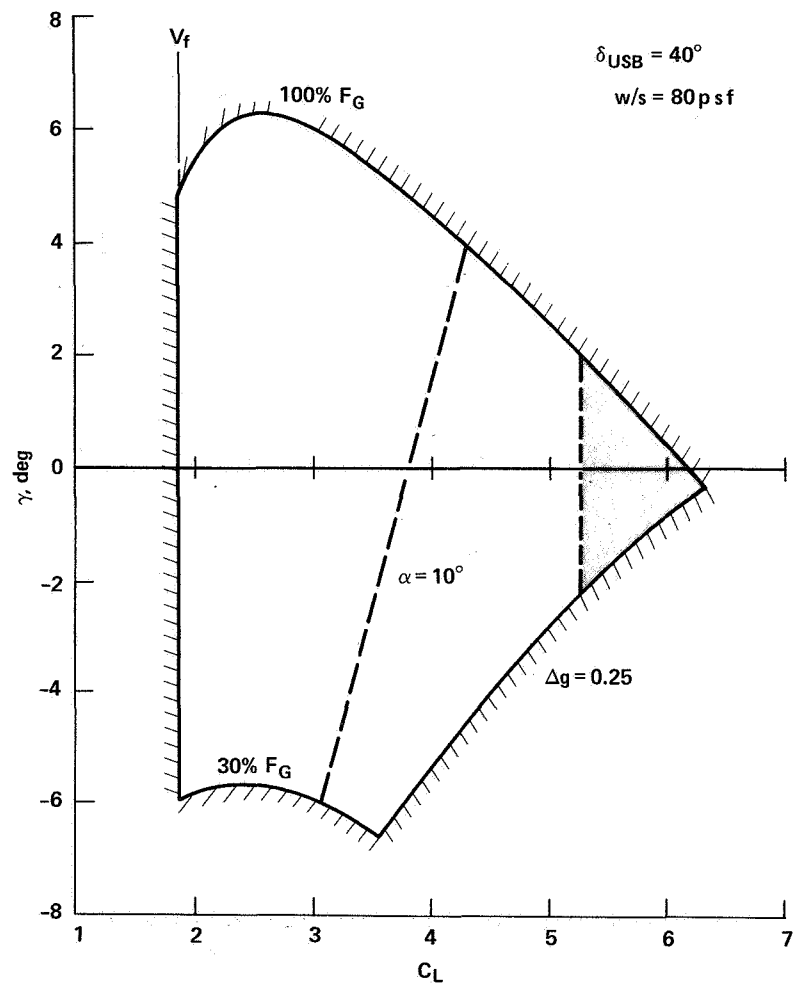Figure 23. – Approach performance of the QSRA showing flight safety margins.

Figure 24. – Performance of the QSRA after a critical (inboard) engine has failed and the QSRA is reconfigured for go-around.
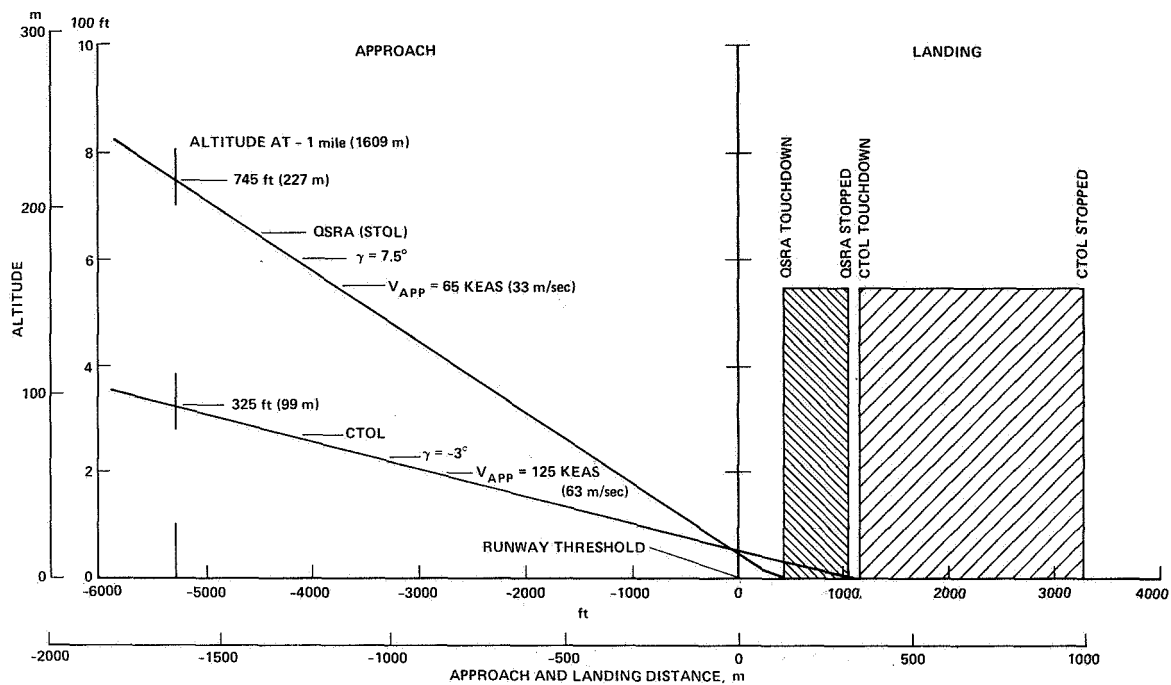
Figure 25. – The STOL landing capability of the QSRA compared to a conventional approach and landing.
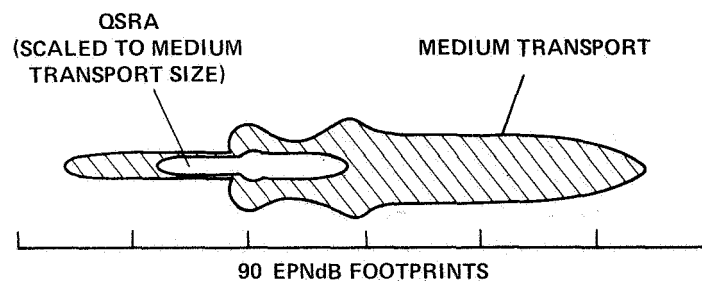

90 EPNdB FOOTPRINTS

Figure 26. – A comparison of the noise impact areas of a current medium transport aircraft and of the same size transport which meets the QSRA noise goals. There is approximately an 80 to 90 percent reduction in community noise impact.

325

USB FLAP NOISE REDUCTION THROUGH NOZZLE EXIT

VELOCITY PROFILE SHAPING

M. C. Joshi
Joint Institute for Advancement of Flight Sciences

J. C. Yu
NASA Langley Research Center

INTRODUCTION

The existence of ordered large scale structures in turbulent jets has been suggested by several experimenters based on flow visualization and measurements in an excited jet (e.g., ref. 1). Flow visualizations of the upper surface blown flap geometry as modeled by a high velocity plane jet exhausting over a flat plate (flap) have also revealed (refs. 2 and 3) the presence of large scale vortical structures in the free shear layer of the jet and in the wake downstream of the flap trailing edge (fig. 1). This structure of the wall jet flow field bears a good resemblance to that observed in plane mixing layers by Brown and Roshko (ref. 4). The disturbance seems to grow as it moves away from the nozzle exit. While the importance of the large scale structures in jet noise production is still under investigation (e.g., ref. 5), an experimental study by Yu and Tam (ref. 6) has shown the dominant part of the upper surface blown (USB) flap noise to be due to the interaction of the large scale quasi-orderly disturbance convecting in the free shear layer with the flap trailing edge. This interaction produces a coherent dipole type radiation in the direction normal to the flap plane and it also generates large scale vortical motion in the trailing edge wake (TEW) resulting in intense turbulent mixing downstream of the flap.

The recognition of the existence of such large scale disturbance and its relation to the radiated noise suggests a new approach for jet noise and USB flap noise reduction - suppress the growth of the disturbance. One such approach for jet noise reduction has been recognized by Arndt, Fuchs and Michel (ref. 7) in a study of jet noise suppressors that attempt the breaking up of the coherent structures by means like quin-axial tubes, corrugated nozzle, mesh covered nozzle and screen tube. The approach used in the present USB flap noise reduction, on the other hand, utilizes the knowledge of the growth of shear layers. The initial development of large scale disturbances is governed by the hydrodynamic stability theory for shear flows where the mean flow distribution plays an important role. A shear layer having a velocity profile with moderate velocity gradients does not support a wave disturbance propagating downstream. It has been shown experimentally by Chan and Templin (ref. 8) that a disturbance wave in a turbulent circular jet is rapidly amplified by a top hat type velocity profile. The wave reaches its maximum amplitude at St.$x/D=0.8$ (St = Strouhal numbers based on nozzle diameter, D and x = distance from nozzle exit) and decays further downstream (see figure 2). When the velocity profile at the

327

nozzle exit is modified to a bell shaped profile the disturbance is not amplified, instead it decays rapidly downstream from the nozzle exit. By modeling the source structure as a travelling instability wave that grows and decays in amplitude and has random component in its phase velocity Ffowcs Williams and Kempton (ref. 9) were able to show that the rate of change from growth to decay determines the magnitude of the radiated sound. A favorable change in the growth and decay process of the disturbance wave in the free shear layer of a jet with modified velocity profile can then be expected to result in reduced noise production. It is the objective of the present study to establish experimentally the concept of USB flap noise reduction by altering the development of the large scale disturbance in the shear layer through nozzle exit velocity profile shaping.

EXPERIMENTAL ARRANGEMENT

The model nozzle and flap used in the present study were the same as those used in the investigation of Yu and Tam (ref. 6). The nozzle exit was rectangular with dimensions 15cm x 1.5cm. The stilling chamber to nozzle exit area ratio was 22.5. The flap (flat plate) used with the nozzle had a chord length (L) 8.5 times the nozzle height (H) and a span of 61cm. The trailing edge of the plate was machined to a knife edge. Mean flow velocity profile shaping was achieved by means of three 80 mesh wire screens inserted within the upper or lower half of the nozzle height. The splitter plate that held the screens in place was 0.16cm thick and was also sharpened to a thin edge at its nozzle exit. For the 80 mesh screen (ℓ = 1/80) the distance to the nozzle exit is then greater than 200 ℓ which is considered adequate for the screen generated turbulence to decay to a low value at the nozzle exit. Two modifications of the reference top-hat velocity profile were obtained: the Γ profile with screens in the lower half of the nozzle and the L profile with screens in the upper half. The variations, as is obvious from figure 3, are named after the shape of the profile.

The thrust of the nozzle or nozzle flap combination was measured by means of a thrust stand which consisted of a large thick plate pivoted along its mid length in smooth bearings. Impingement of the jet on one half of the plate exerted a force on the load cell on which the other half of the plate was resting. This force is a measure of the thrust of the impinging jet. Velocity profiles in the jet or wall jet were obtained by traversing a total pressure tube along the height of the nozzle. This was done in the mid span plane but at several stations along the jet by means of a DISA traversing rig. The rig had a linear resolution of 0.1mm and the traverse was done at a slow rate to allow adequate averaging. Flow field visualization was done using spark shadowgraphy.

The far field noise was measured by means of B&K half-inch free field microphones. Four microphones were placed in the flyover plane (fig. 4) at a nominal distance of 3 meters from the flap trailing edge. Microphones above the flap at $\theta=+90°$ and $\theta=+45°$ will be referred to as Mic. 1 and Mic. 3 respectively, and those below the flap at $\theta=-45°$ and $\theta=-90°$ as Mic. 2 and Mic. 4. A fifth microphone was used to measure the sideline noise as shown in figure 4. All the measurements were done in an anechoic flow facility at NASA Langley Research Center. Far field noise data from all the microphones were

328

simultaneously recorded in the FM mode on an Ampex tape recorder for later analysis using a time series analysis program and/or a Spectral Dynamics SD-360 Signal Processor.

EVALUATION OF NOISE REDUCTION

In order to establish the effectiveness of a noise reduction concept a basis of evaluation must be selected. Equal total thrust is the most common basis of comparison. In the present study, however, thrust per unit exit area was chosen as the basis for the following reason. The objective of the study is to establish the effect of velocity profile shaping on the USB flap noise and the screen insert is the simplest arrangement to produce profile shaping. But the finite sectional area of the insert caused a blockage of about 15% of the total exit area. It is therefore assumed that the modified nozzle is a scaled down version of the one that should be the equivalent of the unmodified nozzle. This area factor is accounted for if a comparison is made on a constant thrust per unit area basis. This basis of comparison was also used in reference 7. If no allowance is made for the area blockage and the comparison of noise radiation is based on constant total thrust, the noise reduction would be about 2 dB lower assuming a U^6 dependence of far field noise.

Another practical aspect of the performance basis is the base drag due to the splitter plate. From the static pressure measurements of Blake (ref. 10) on struts with blunt and rounded trailing edges, it was estimated that the maximum base drag of the present splitter plate is about four percent of the total thrust. This would introduce a discrepancy of only 0.5 dB in the noise comparison, again assuming a U^6 dependence of far field noise.

FLOW FIELD DATA

Thrust measurements were made for several values of the stilling chamber total pressure for the top hat, Γ and L nozzle flap configurations in order to be able to select pressure values that give equal thrust per unit exit area. The operating points chosen correspond to thrust per unit exit area, F/A=34475, 45967, 68950 and 91931 N/m^2.

The effect of profile shaping on the wall jet flow field was examined by means of spark shadowgraphy and pitot pressure surveys. The shadowgraphs for the top-hat profile showed two major regions of large scale activity - the upper shear layer (USL) downstream of the nozzle exit and the trailing edge wake (TEW) aft of the flap trailing edge. Figures 5 and 6 show the effects of profile shaping on the large scale disturbances in the USL and the TEW respectively for a thrust setting of F/A=68950 N/M^2. As observed in figure 5(a), for the top-hat profile, the large scale structure in the USL grows in size as it moves downstream and seems to have counterclockwise vorticity. Modification of the profile to a Γ shaped profile causes the effective length of the upper potential core to become almost half that of the top-hat profile (figure 5(b)). The large scale structures in the USL still exist but their extent across and along the jet

is reduced since the upper potential core is terminated earlier and after the end of the potential core the growth of the USL is affected by the lower half jet. For the L-profile, figure 5c, large scale activity in the USL is not as clearly defined as for the top-hat and Γ profiles. The structure in the TEW shown in figure 6(a) for the top hat profile has the shape of a shed vortex with clockwise vorticity. It grows considerably within a short distance from the flap trailing edge. The large scale structure in the TEW of the Γ-profile configuration, figure 6(b), is much weaker in comparison to that for the top hat profile. For the L profile, figure 6(c), no large scale disturbance is observed in the TEW except for a roll up immediately downstream of the flap. These effects were seen at other thrust settings also. In summary, figures 5 and 6 show that velocity profile shaping alters the large scale disturbance activity both in the USL and in the TEW. While the L profile suppresses considerably the large scale structures in the USL and the TEW, the major influence of the Γ profile is in the TEW.

The total pressure profiles measured using the pitot tube were converted to mean velocity profiles by means of gasdynamic equations. These profiles for several stations along the flow are plotted in figure 7 for the top hat, Γ-profile and L profile configurations operating at F/A=91931 N/m^2. They show the differences in the development of the flow field for the three profile shapes. The set of profiles at x/H=0.42 indicate that the screen inserts are fairly successful in modifying the velocity profiles to the desired shape except for the dip due to the splitter wake. Furthermore the inserts for the Γ and L profiles produce nearly identical (but on opposite sides of the jet centerline) modifications about the top hat profile. At this station, the velocity gradient in the free shear layer is moderately low for the L profile compared to those for the Γ and top-hat profiles. This smoothing of the mean velocity distribution apparently affects the growth of the large scale disturbances as was obvious in the shadowgraphs of figure 5. Comparison of profiles at locations further downstream indicate considerable difference in the growth of the wall jet flow. Near the flap trailing edge, x/H=8.89, the L profile has a velocity distribution that is only slightly different from the top hat profile, but the Γ profile has a higher velocity gradient in the free shear layer and a thicker boundary layer that causes a lower velocity gradient near the wall. Its effect is reflected in the shadowgraph, figure 6(b), as a weakened large scale structure in the TEW of the Γ profile configuration. Since turbulence production depends on the mean velocity gradient and since considerable differences exist in the velocity profiles near the flap trailing edge, the TEW characteristics may be expected to be different for the three profile shapes.

FAR FIELD NOISE DATA

The effect of velocity profile shaping on the USB flap noise production can be seen by comparing the far field noise spectra in several directions of radiation for the three profile shapes. Figures 8 and 9 show one third octave band sound pressure level comparisons for Mic. 4 (θ=-90°) and Mic. 2 (θ=-45°) respectively, the thrust setting being F/A=68950 N/m^2. It can be seen that the modified profiles produce reduced noise levels at frequencies around and above

the spectral peak of the top-hat profile. The Γ profile, however, increased the levels at lower frequencies. Thus the L profile provided a better overall noise reduction while the Γ profile generally caused a redistribution of acoustic energy to lower frequencies. Directionally, maximum noise reduction in the flyover plane was observed at Mic. 2 ($\theta=-45°$) and this can be seen in figure 9 to be of the order of 6 dB in one third octave bands for frequencies near and greater than the peak frequency of the unmodified top hat profile. The overall noise reduction was 1.8 dB for the Γ profile and 3.6 dB for the L profile. At the position of Mic. 3 ($\theta=+45°$) the effects of profile shaping were of lower magnitude. The general trends discussed above were observed for all thrust values but the noise reduction was, in general, greater at higher thrust settings. The effect of profile shaping on sideline noise radiation (Mic. 5) was not much different from that observed in the flyover plane. The reduced levels in all directions is an indication of the reduction being in the total power produced as opposed to a redistribution in space of the radiated power.

An interesting characteristic of the radiation field is shown in figures 10(a) and 10(b) which are plots of the peak levels in the third octave spectra versus the maximum velocity near the flap trailing edge (x/H=8.89). For all the three profile shapes the variation is as near sixth power for Mic. 4 ($\theta=-90°$) and as near eighth power for Mic. 2 ($\theta=-45°$) location. This difference in the velocity power law was also observed at the corresponding positions above the flap. Brown et al (ref. 11) in a study of model upper surface blowing lift system found the velocity exponent to increase from a value of nearly 5 at $\theta=-90°$ position to about 7.5 as the $\theta=-45°$ direction was approached. It is pertinent to point out that the amount of noise reduction obtained through velocity profile shaping is not simply related to the maximum velocity at the trailing edge. The local maximum velocity at the flap trailing edge for the Γ profile is less than that for the top hat profile but the L profile configuration has values greater than or almost equal to the top hat value.

The variation in the velocity exponent observed above suggests the possibility of preferential directional radiation from certain regions of the flow field. The U^8 dependence of a quadrupole generated field and the U^6 dependence of a dipole generated field can be used to identify significant contribution to the USB flap acoustic field in a $\theta=-45°$ direction from the trailing edge wake and a dominance of a dipole type field in a $\theta=\pm90°$ directions. The study of Yu and Tam (ref. 6) has clearly identified the acoustic field to be in phase opposition across the flap in $\theta=\pm90°$ directions. This was also shown to be due to the interaction with the flap trailing edge of the large scale disturbance convecting in the upper shear layer. Becker's investigation (ref. 12) of the acoustic field in $\theta=\pm45°$ directions for a smaller USB flap model showed the trailing edge wake to be the dominant noise contributor in $\theta=-45°$ direction. However, as pointed out in reference 6, due to the proximity of the shear layer to the flap the passage of the USL large scale disturbance past the trailing edge forces the TEW into large scale oscillations. This causes the USL to be the most important flow region for the USB flap geometry. Besides radiating a dipole type field due to its interaction with the trailing edge, it produces large scale disturbance in the wake which with the high turbulent mixing becomes an efficient quadrupole radiator.

331

The nearly identical velocity power laws for the three profile shapes both at $\theta=-45°$ and $\theta=-90°$ positions imply no change in the noise production mechanisms due to profile shaping, but merely a loss of coherence or reduced strength of the sources. Greater noise reductions in $\theta=-45°$ direction compared to other directions in the flyover plane suggests that mean flow profile shaping causes considerable change in the trailing edge wake noise production. This possibility is of course supported by the shadowgraphic observations which showed the large vortical structure in the wake of the top hat configuration to weaken when the mean flow was shaped to a Γ profile and almost disappear when shaped to a L profile. The suppression of the growth of large scale disturbance in the USL by profile shaping reduces its interaction with the trailing edge and is responsible for the noise reduction observed in $\theta=\pm90°$ directions.

Based on the shadowgraphic observations, and measured velocity profiles it can be said that the L profile is effective in suppressing the growth of the large scale disturbance in the USL due to the smoother velocity distribution in the shear layer at the nozzle exit. Since the TEW is coupled to the USL, the suppression of the large scale disturbance in the USL also reduces the large scale activity in the TEW. The Γ shaping, on the other hand, increases the gradient in the USL which may aid the growth of the disturbance. But the lower mean velocity on the wall side results in a broad smooth velocity distribution near the flap trailing edge and this in turn weakens the large scale activity in the TEW. The direct effect of L shaping on the large scale disturbance in USL may be the cause of its greater noise benefit.

SUMMARY

The effect of nozzle exit velocity profile shaping on the noise production of USB flaps has been studied experimentally. The usual top-hat profile was modified to Γ shaped and L shaped profiles. The L profile produced a maximum noise reduction of 6 dB in one third octave bands around and above the peak frequency of the top hat spectrum when compared on equal thrust per exit area basis. The Γ profile, in general, resulted in a shift of the spectrum to lower frequencies and therefore lower overall noise reduction. Maximum noise reduction was observed in $\theta=-45°$ direction below the flap. The noise benefit was higher at higher thrust settings.

It is believed that profile shaping causes a modification of the growth of the large scale disturbance in the USL which reduces its interaction with the trailing edge and a consequent reduction in the dipole type noise radiation in $\theta=\pm90°$ direction. The coupling between the USL and the TEW and the dependence of turbulence production on the mean velocity gradients near the trailing edge causes the large scale activity in the TEW to weaken and this results in a reduction of the quadrupole type noise radiation in directions below the flap.

REFERENCES

1. Crow, S. C. and Champagne, F. H.: Orderly Structure in Jet Turbulence.

332

Journal of Fluid Mechanics, Volume 48, Part 3, 1971, pp. 547-591.

2. Tam, C. K. W. and Yu, J. C.: Trailing Edge Noise. Progress in Astronautics and Aeronautics, Vol. 45, 1976, AIAA, New York, pp. 259-280.

3. Patterson, G. T.; Joshi, M. C. and Maus, J. R.: Experimental Investigation of the Aeroacoustic Characteristics of Model Slot Nozzles with Straight Flaps. Progress in Astronautics and Aeronautics, Vol. 45, AIAA, New York, 1976, pp. 41-57.

4. Brown, G. L. and Roshko, A.: On Density Effects and Large Scale Structures in Turbulent Mixing Layers. Journal of Fluid Mechanics, Vol. 64, 1974, pp. 775-816.

5. Sarohia, V. and Massier, P. F.: Experimental Results of Large Scale Structures in Jet Flows and Their Relation to Jet Noise Production. AIAA Journal, Vol. 16, No. 8, August 1978, pp. 831-835.

6. Yu, J. C. and Tam, C. K. W.: An Experimental Investigation of the Trailing Edge Noise Mechanics. AIAA Paper 77-1291, 1977.

7. Arndt, R. E. A.; Fuchs, H. V. and Michel, V.: Laboratory Study of Jet-Noise Suppressors. Journal of Acoustical Society of America, Vol. 63, No. 4, April 1978, pp. 1060-1068.

8. Chan, Y. Y. and Templin, J. T.: Suppression of Spatial Waves by Distortion of Jet Velocity Profile. The Physics of Fluids, Vol. 17, No. 11, November 1974, pp. 2124-2125.

9. Ffowcs Williams, J. E. and Kempton, A. J.: The Noise from the Large Scale Structure of a Jet. Journal of Fluid Mechanics, Vol. 84, Part 4, 1978, pp. 673-694.

10. Blake, W. K.: A Statistical Description of Pressure and Velocity Fields at the Trailing Edges of a Flat Strut. Report 4241, David W. Taylor Naval Ship Research and Development Center, December 1975.

11. Brown, W. H.; Searle, N.; Blakney, D. F.; Pennock, A. P. and Gibson, J. S.: Noise Characteristics of Upper Surface Blown Configurations: Experimental Programs and Results. NASA CR-145143, October 1977.

12. Becker, R. S.: Acoustic Source Location in a Jet Blown Flap Using a Cross-Correlation Technique. Ph.D. Thesis, University of Tennessee Space Institute, March 1977.

$U_J = 194$ m/s

U.S.L.

λ

T.E.W.
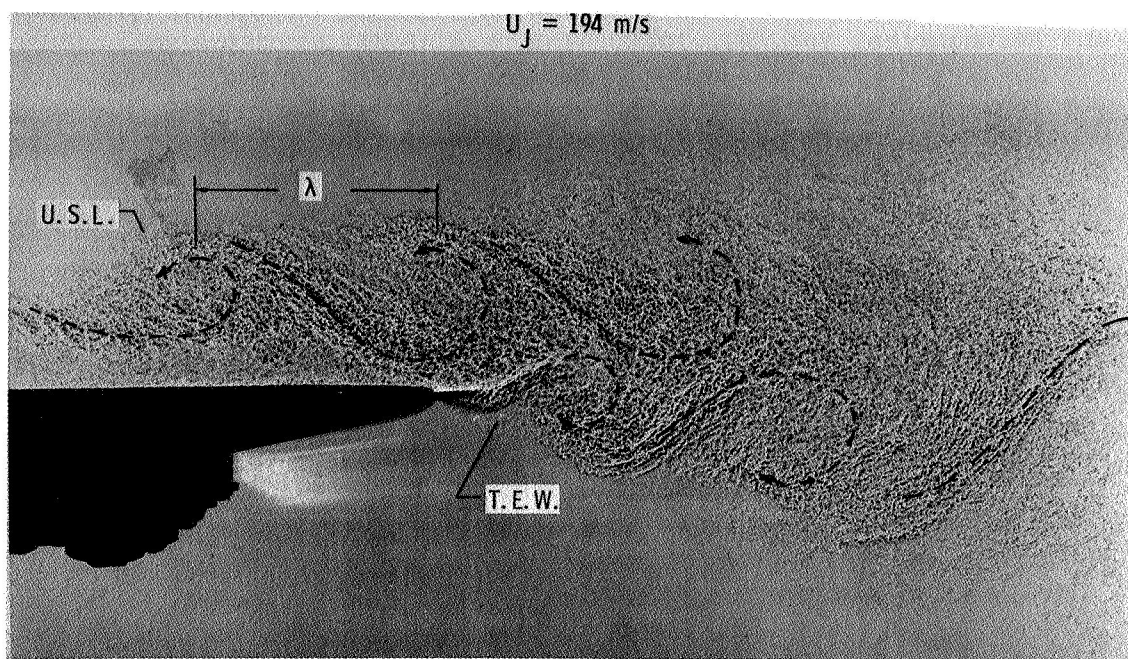
λ = SCALE OF DISTURBANCE, USL = UPPER SHEAR LAYER, TEW = TRAILING EDGE WAKE

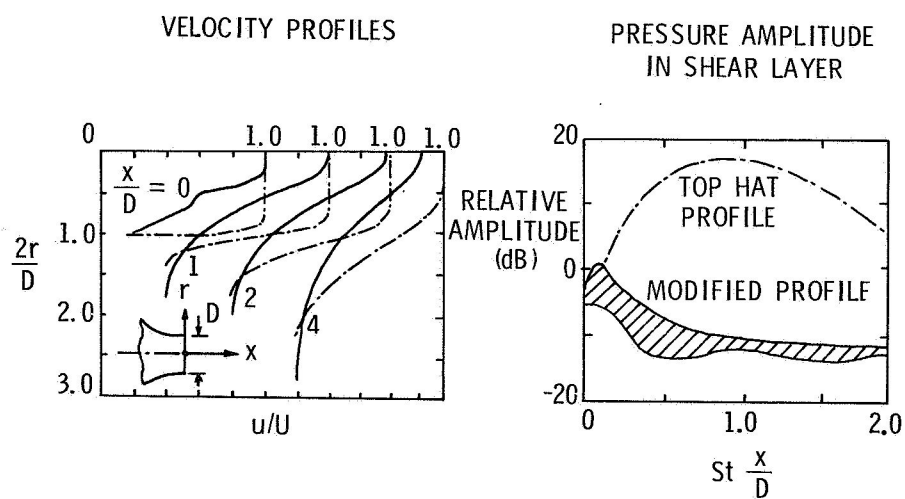FIGURE 1.- SPARK SHADOWGRAPH SHOWING FLOW FIELD NEAR FLAP
TRAILING EDGE.

VELOCITY PROFILES

PRESSURE AMPLITUDE
IN SHEAR LAYER

FIGURE 2.- SUPPRESSION OF SPATIAL WAVE IN SHEAR LAYERS
(FROM REFERENCE 8).
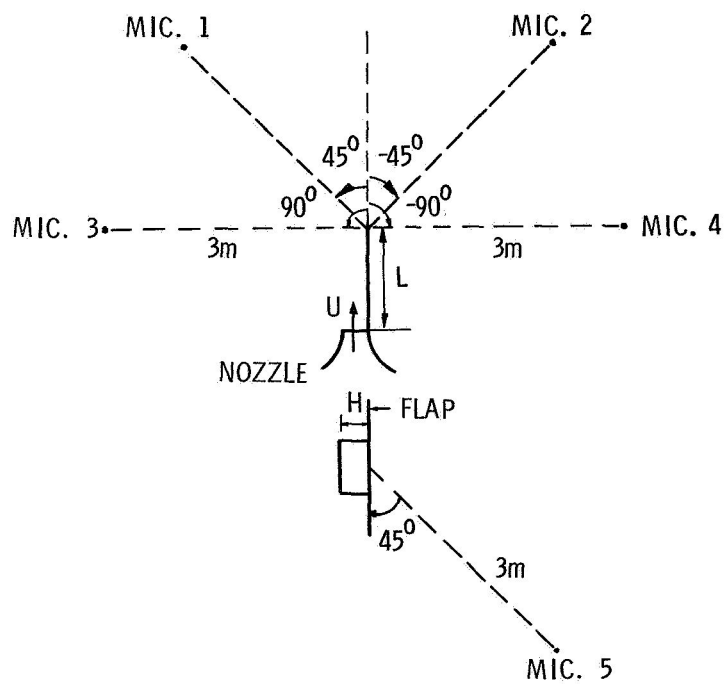
334
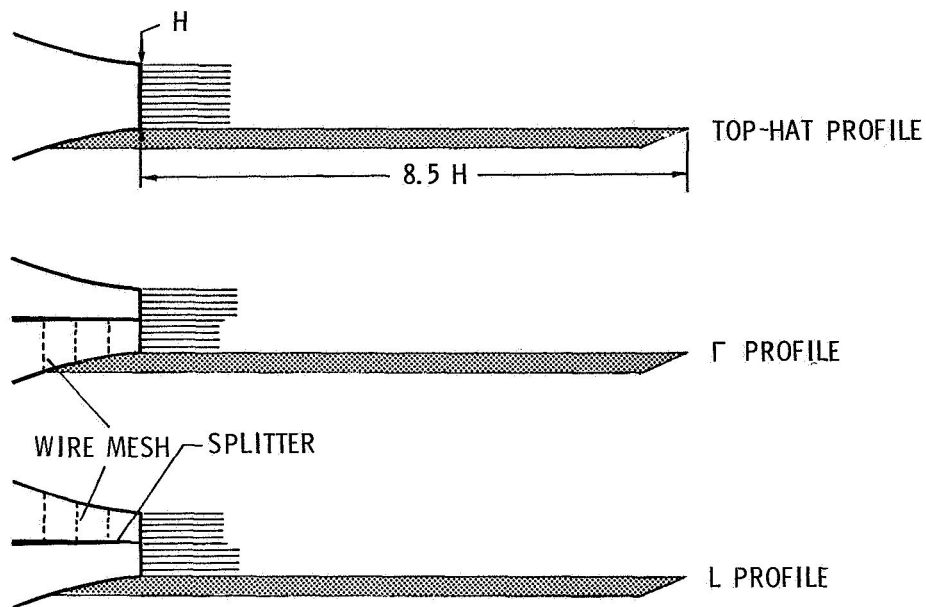
FIGURE 3. - MEAN VELOCITY PROFILES INVESTIGATED.

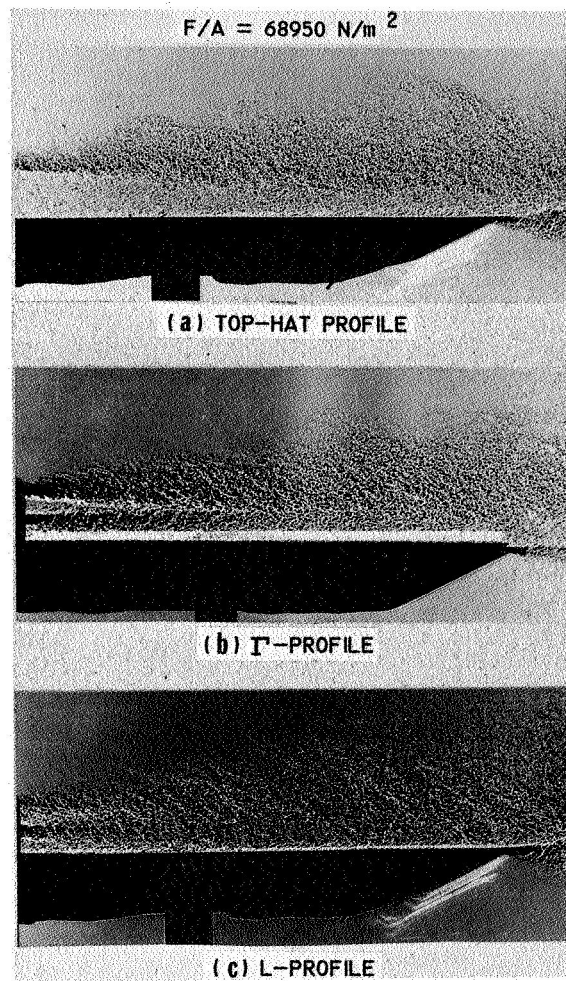FIGURE 4. - SCHEMATIC OF THE MICROPHONE ARRANGEMENT.

F/A = 68950 N/m^2

(a) TOP-HAT PROFILE

(b) Γ-PROFILE

(c) L-PROFILE

FIGURE 5. - SHADOWGRAPHS OF UPPER SHEAR LAYER.

F/A = 68950 N/m^2

(a) TOP-HAT PROFILE

(b) Γ - PROFILE
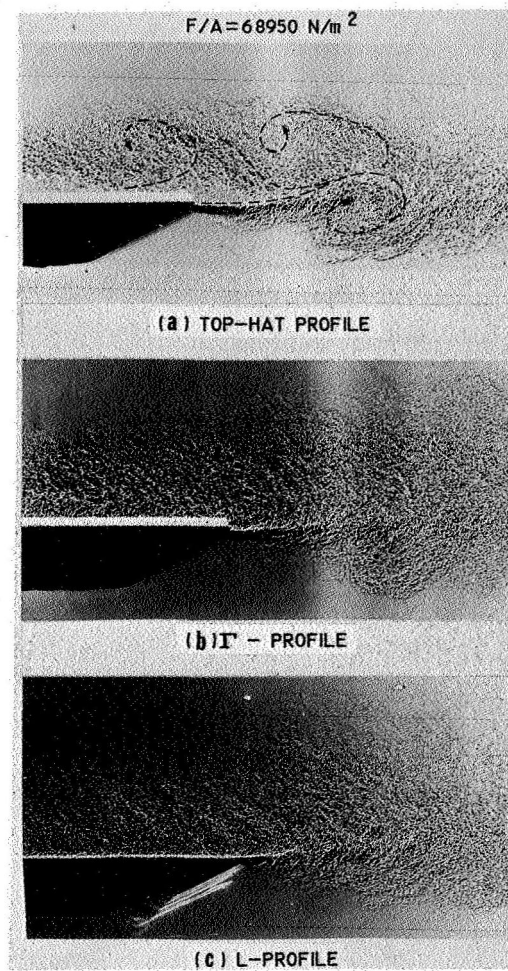
(c) L-PROFILE

FIGURE 6. - SHADOWGRAPHS OF TRAILING EDGE WAKE.

$F/A = 91931 \ N/m^2$
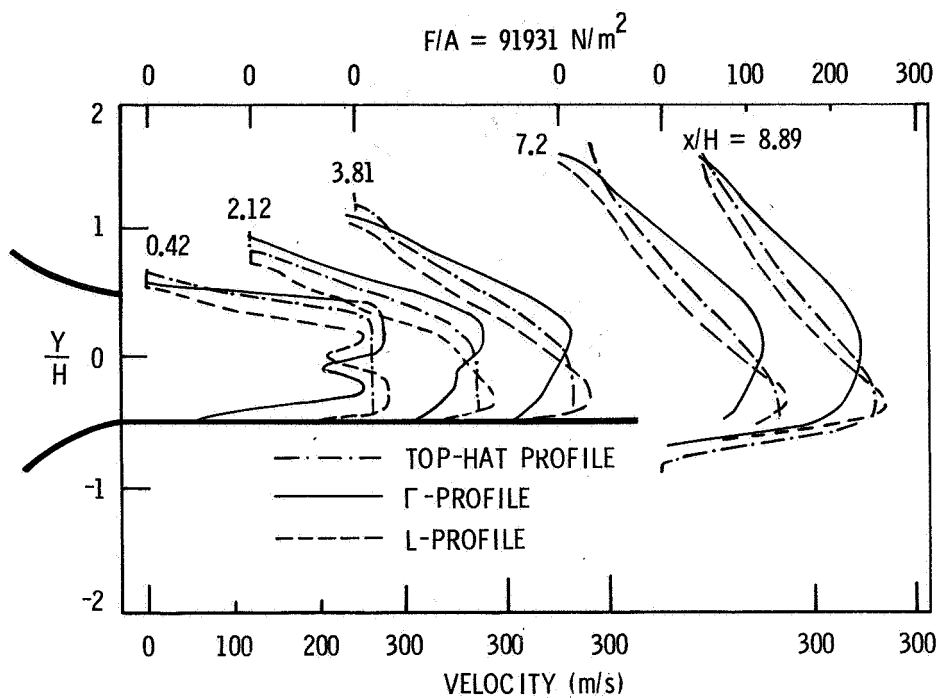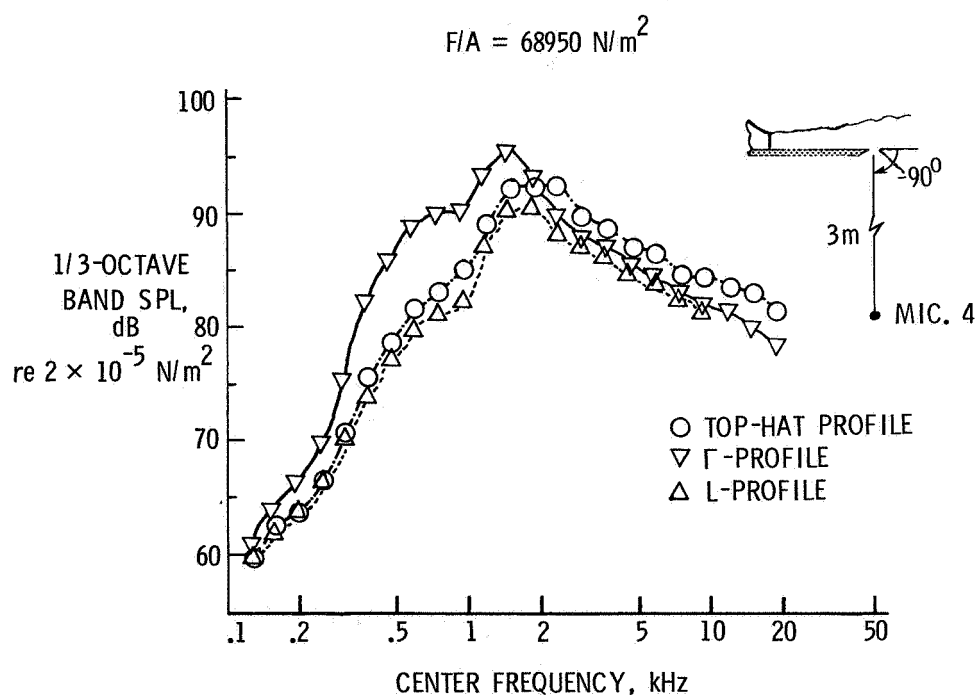
FIGURE 7. - MEAN VELOCITY PROFILES.

$F/A = 68950 \ N/m^2$

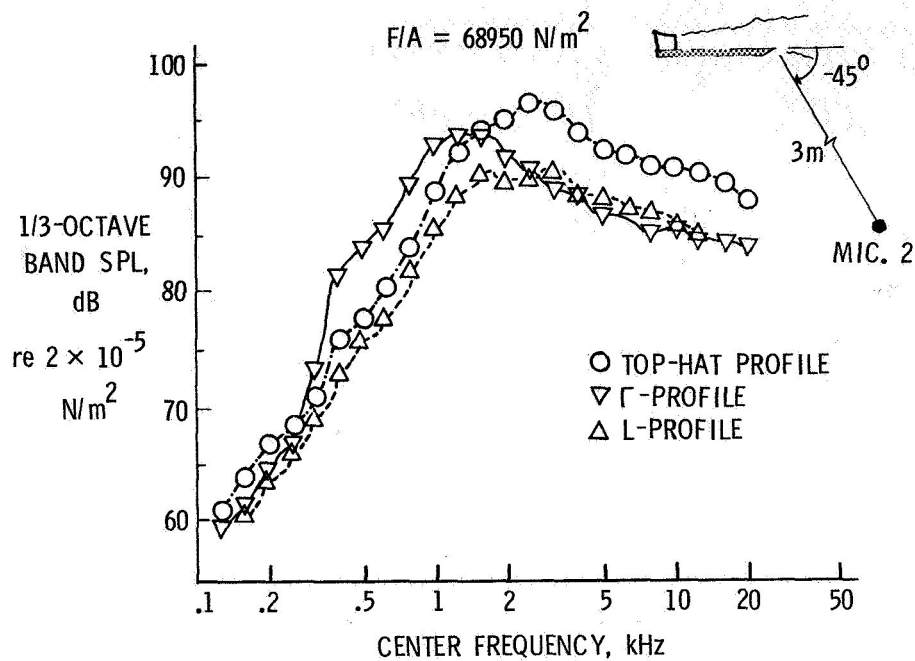FIGURE 8. - FARFIELD NOISE SPECTRUM (MIC. 4).

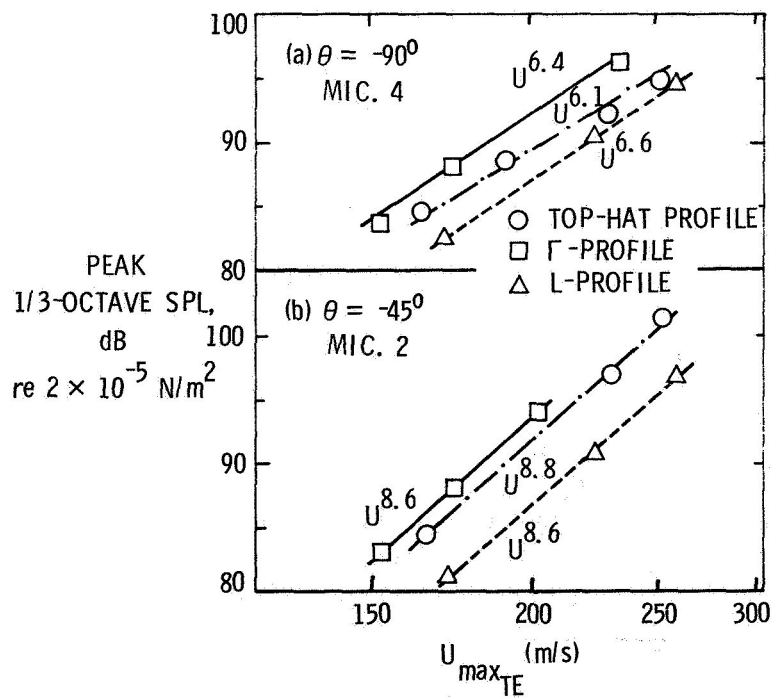FIGURE 9. - FARFIELD NOISE SPECTRUM (MIC. 2).

FIGURE 10. - VELOCITY POWER LAWS FOR MIC. 2 AND MIC. 4.

339

YC-14 PROPULSION SYSTEM PERFORMANCE, OPERATION AND COMMUNITY NOISE BASED ON FLIGHT TESTS

Robert S. Armstrong
Boeing Aerospace Company

INTRODUCTION

The Boeing Aerospace Company has been under contract to the U.S. Air Force to design and build two prototype AMST aircraft. The Boeing airplane, the YC-14, utilizes an upper surface blowing (USB) powered lift system to provide the lift augmentation necessary to meet the 2000 foot field length requirement.

The Boeing YC-14 AMST prototype is a high-wing T-tail configuration with two high bypass turbofan engines (General Electric CF6-50D) mounted over the wing, figure 1. The two prototypes are essentially identical, however ship one, foreground figure 2, was heavily instrumented for technical evaluation while ship two was oriented toward cargo handling and flight demonstrations. Propulsive lift is obtained by directing the engine exhaust flow over the upper surface blown (USB) flap, figure 3. The thrust vector is controlled by the USB flap angle; the magnitude is controlled by the throttles.

The propulsion system installation is shown in figure 4. References 1 and 2 describes the nacelle in detail. Significant features of the nacelle are as follows:

1. The engine inlet is mounted directly to the engine. It is a fixed inlet design with a large (34%) contraction ratio to reduce sensitivity to the high angles of attack required for STOL operations. Acoustic lining is provided in the inlet to reduce interior and far field noise. The inlet is canted downward 4° relative to the engine centerline and the engine is tilted downward 2½° within the nacelle. This results in a total inlet droop of 6½° relative to the wing chord plane.

2. The engine nacelle is cantilevered from the wing front spar. The lower part of the nacelle is hinged for engine accessibility as are the engine core cowl and fan cowling. Engine bleed ducts for wing leading edge boundary layer control and cabin air conditioning are located below the engine in an equipment bay.

3. The fan duct is a long duct design with the fan and primary streams discharging through a common "D" shaped exhaust nozzle. A movable door on the outboard side of the exhaust nozzle opens to spread the flow over the wing and USB flap for low speed operation and closes to reduce scrubbing and improve high speed performance.

4. The thrust reverser is top mounted and incorporates a large deflector door and small lip door to direct the flow upward and forward, thus eliminating ground interference problems while minimizing potential re-ingestion problems.

The YC-14 flight test program was conducted at Boeing Field and at Edwards Air Force Base from August 1976 to August 1977. Over 600 flight hours of testing were accomplished. All major facets of propulsion system operation and performance were investigated, including steady state and transient engine performance, in-flight starting, nacelle and engine component cooling, inlet flow environment, thrust reverser operation, and fuel system operation.

In addition, concurrent with the Air Force flight test program, a NASA funded test program, reference 3, was conducted to evaluate the USB temperature and pressure environment and the near and far field noise environment.

This paper describes the flight test results for several key elements of this powered-lift propulsion system.

IN-FLIGHT THRUST

Thrust Definitions and Method of In-Flight Measurement

In-flight thrust for purposes of airplane/propulsion system bookkeeping is defined below and described in detail in reference 4. During low speed STOL approach, the USB flaps are deployed and about one-third of the airplane lift is provided by the engine jet exhaust flow over the wing and flap surfaces. It is convenient, since lift/drag polars are so strongly influenced by jet effects, to define engine thrust at the fan/primary mixing plane upstream of the exhaust nozzle (station 16 in figure 5) and to include all jet forces aft of station 16 as part of the airplane lift and drag bookkeeping. Low speed engine thrust is determined as the product of the fan airflow at the mixing plane (W_{16}) and the ideal flow velocity ($V_{I_{16}}$) plus the product of primary flow (W_{56}) and $V_{I_{56}}$ at the mixing plane.

$$F_G = \frac{W_{16}}{g} V_{I_{16}} + \frac{W_{56}}{g} V_{I_{56}} = \text{Gross Thrust at Mixing Plane}$$

At cruise (flaps UP) conditions, the thrust/drag bookkeeping is conventional where engine thrust includes accountability for nozzle lossed and wing and fuselage jet scrubbing drag as determined from static ground testing.

Ideal engine thrust for the high speed case is defined at the fan duct pressure rake station 13 and primary nozzle rake station 55 (see figure 5). Ideal thrust is determined as the product of the flow at station 13 (W_{16_I}) and the ideal velocity ($V_{I_{13}}$), plus the product of primary flow (W_{56}) at the mixing plane and ideal velocity ($V_{I_{55}}$) at the primary nozzle pressure measurement rake station. Installed high speed net thrust is then defined as:

$$\text{Net Thrust } (F_N) = \left(\frac{W_{16_I}}{g} V_{I_{13}} + \frac{W_{56}}{g} V_{I_{55}} \right) C_{V_{IN}} - \text{Ram Drag}$$

$$\text{Ram Drag} \quad = \quad \frac{W_{2A}}{g} \, V_\infty \qquad\qquad C_{V_{IN}} = \frac{Fg_{IN} \ (\text{from ground test})}{\dfrac{W_{16_I}}{g} \, V_{I_{13}} + \dfrac{W_{56}}{g} \, V_{I_{55}}}$$

where:

W_{2A} = total airflow into the engine

$C_{V_{IN}}$ = actual gross thrust $(F_{g_{IN}})$ generated on the airplane divided by the ideal nozzle thrust at fan/primary rake stations.
(installed nozzle velocity coefficient)

In-Flight Measured Parameters

Basic engine parameters that must be determined during flight testing are as follows:

Primary and secondary airflows are calculated parameters, the remaining parameters are either direct measurements (primary and fan pressures and temperatures) or based on in-flight measurements and use of previously determined calibrations (inlet airflow, bleed flows and fuel flow).

Novel among these measurements is the method of determining the inlet airflow W_{2A}. Typically engine airflow is determined through calibration of the exhaust nozzle to establish its flow coefficient. This has proven quite satisfactory in commercial airplane practice for conventional separate flow nozzles having minimum leakage and known exit areas. This approach was not feasible in the YC-14 installation however, since the exit nozzle design shape and location does not lend itself to accurate predictions of effective area during flight conditions. However, because of the excellent flow characteristics exhibited by the inlet design chosen for the YC-14, it became an attractive alternative device for measurement of in-flight engine airflow. This measurement was achieved through calibration of static pressure ports located in the inlet; this will be discussed in more detail later.

A complicating factor in determining the in-flight engine performance is introduced by the fact that the engine primary (core) and secondary (fan) flows exhaust confluently through a single exhaust nozzle rather than through separate nozzles. It is necessary to determine primary and secondary flow rates, pressures and temperatures in order to identify ideal engine thrust. Primary nozzle flow is determined by measurement of LP turbine inlet pressure and temperature plus various internal engine measurements and correlation with engine component calibrations.

Secondary airflow, the difference between total engine flow and core flow, accounts for various bleeds and leakage. 8th and 14th stage bleed flows, used for boundary layer control (BLC) at the wing leading edge, and 10th stage bleed flows, used for air-conditioning and accessory cooling, are determined by pressure and temperature measurements in calibrated ducts.

- NOZZLE PERFORMANCE - $C_{V_{IN}}$

As shown in figure 5, the cruise nozzle (flaps UP) thrust is determined as the product of the ideal engine thrust (based on rake measurements at stations 13 and 55) and an installed nozzle velocity coefficient $C_{V_{IN}}$ from engine ground test results, reference 5. The ground test installation is shown in figure 6. The wing/flap section is flight hardware while the body section is a simulation. A six component force balance supports both engine and wing/body section to allow measurement of thrust minus scrubbing drag to determine nozzle $C_{V_{IN}}$. Full scale $C_{V_{IN}}$ is then extrapolated to flight nozzle pressure ratios using model scale test results, figure 7. $C_{V_{IN}}$ is determined for in-flight evaluation as a function of in-flight measured fan pressure ratio, $P_{T_{13}}/P_\infty$.

- INLET AIRFLOW MEASUREMENT - W_{2A}

The flight inlet was calibrated for measurement of total engine airflow as illustrated in figure 8. In-flight airflow is determined through measurement of six static pressures spaced equally around the inlet forward of the fan inlet.

The flight inlet was calibrated relative to the wall static pressures during installed engine tests at the Boeing Tulalip Ground Test Facility, reference 5. Back-to-back tests were run with the flight inlet and the G.E. Lightweight (L/W) Bellmouth, where measured engine speed $N_1/\sqrt{\theta_2}$ and engine core pressure ratio (EPR) were correlated to known L/W bellmouth flow characteristics and then to the measured static pressures in the flight inlet, reference 4. The flow characteristics of the L/W bellmouth were determined during a previous General Electric back-to-back correlation relative to their standard heavyweight bellmouth that is used for engine certification.

Flight effects on the inlet flow calibration were derived from a theoretical viscous flow analysis.

PROPULSION SYSTEM FLIGHT TESTS

Flight test results to be discussed in this paper are as follows: Engine performance in terms of thrust and specific fuel consumption at take-off, cruise and at low speed (STOL) conditions are presented relative to pre-test predictions. Performance predictions are derived from the G.E. engine performance computer deck, with installation factors determined from the engine ground rig test results. Inlet inflow angle is shown at critical inlet flight conditions. Thrust reverser and overall propulsion system operation are summarized, and finally a summary of far field noise measurements is presented.

344

Engine Performance

● TAKEOFF

Measured gross thrust and ram drag from a typical STOL takeoff are shown for each engine in figure 9. Gross thrust is shown to be 1% lower than predicted at Mach 0 and ½% higher at Mach 0.2. Ram drag based on total engine flow measured using the inlet static pressures was within ± ½% of prediction.

● CLIMB

Climb thrust and SFC are shown in figure 10 during a climb test at maximum climb thrust rating through 10,700m (35000 ft). Relative to the pre-test predictions, the average net thrust of the two engines during the climb was up by ¾% and the SFC was up by ¼%.

● CRUISE

Typical engine performance results during cruise are shown for No. 1 engine in figure 11. At cruise altitude and power conditions, net thrust was 1.6% above the level predicted by the Status Deck at a corrected fan speed of 3600 rpm. At the same conditions, SFC was higher by 0.9% than the Status Deck.

● LOW SPEED FLIGHT

The low speed performance of an airplane affects its rate of climb, takeoff gross weight and landing speed. The YC-14 uses engine bleed for environmental control (ECS) and BLC on the leading edge of the wing. The amount of BLC bleed is controlled by the flap positioning lever. A relatively large amount of engine bleed is used during STOL landing (10% of core airflow is used for BLC during a single engine landing) and engine performance is therefore strongly affected. Steady state low speed performance was not a specific item of the flight test program, however a limited amount of sufficiently steady state data was gleaned from low speed stability and control test flights. Table I summarizes the comparison of actual and predicted engine performance. The data include samples of each of the USB flap settings and bleed rate conditions. The actual gross thrust was always greater than predicted (by 0.6% for the zero bleed case and by about 3% for the maximum bleed condition).

Inlet Inflow Angle

STOL aircraft, using powered lift to achieve low landing and takeoff speeds, characteristically operate at higher angles of attack than conventional aircraft. Figure 12 shows the inlet design envelope for the YC-14. The design envelope was based on the results of complete airplane scale model wind tunnel tests using turbine powered nacelles and the arbitrary selection of a 30-knot, 90° crosswind takeoff capability. The design requirement for the inlet was that at or below the design envelope, the steady state inlet distortion should not exceed 10% where:

$$\text{Inlet Distortion} = \frac{(P_{T_{max}} - P_{T_{min}})}{P_{T_{average}}}$$

Open symbols in figure 12 are measured inflow angles during critical inlet operating conditions from flight testing. Shaded symbols denote calculated inflow angles.

● INLET INFLOW ANGLE MEASUREMENTS

Effective inlet inflow angle was measured by means of static pressures in the inlet lip. A correlation of static pressure differential across the lip with known inlet angle of attack and airspeed was performed with a 0.17 scale model inlet in the Boeing 2.74 x 2.74m (9′ x 9′) low speed wind tunnel for a wide range of inlet corrected airflow. These results were used to predict full-scale inlet inflow angle based on similar full-scale lip static pressure measurements. Figure 13 is an example of the scale model data from which the predictions are based. The example is for nominal cruise power corrected airflow; similar curves were generated for various power settings from idle to maximum power conditions.

● IN-FLIGHT TEST RESULTS

Figure 14 shows a time history of inlet angle of attack during a single-engine, flaps-60, airplane-minimum-speed excursion. In this test an airplane stall condition was appraoched with #1 engine at maximum power and #2 engine at idle. After reaching minimum allowed airspeed (V_{min}) and "pushing over" i.e., stick forward for airplane stall recovery, power on #2 engine was advanced while being reduced on #1 engine to obtain a balanced power condition. Inlet angle during approach to stall is seen to be about 10° less than wing angle of attack, α. Geometrically the inlet centerline is 6½° less than α. After the "push over" and subsequent acceleration, inlet inflow angle is indicated to be higher than wing angle. This is probably due to a combination of airplane dynamics and power effects on upwash. In any event, the inlet angles measured are well below the design envelope established for the airplane. Successful inlet operation without evidence of engine operating difficulties was demonstrated in crosswinds considerably higher than the design goal of 30 knots at a height of 15m (50 feet). A takeoff and landing were made with a direct crosswind of 36 knots gusting to 39 knots as measured at the ground wind station.

Thrust Reverser Operation

Design objectives for the thrust reverser system included:

- reverse thrust effectiveness of at least 40% in order to stop the airplane on an icy runway (u = .05) within the 396m (1300 ft) ground roll required for 610m (2000 ft) field length operation

- reingestion-free operation at full thrust down to 30 knots airspeed

- ability to back the airplane in reverse

- operate at idle power in reverse for extended periods

The first objection was essentially met during the engine ground rig tests where a reverse thrust effectiveness of 39% was measured, reference 5. Location of the engines with the inlet nineteen feet above the ground and the exhaust on top of the wing provided an advantageous positioning of the thrust reverser for the avoidance of reingestion through ground interactions and the possibility of foreign object engine damage due to ground debris. A schematic view of the thrust reverser installation is given in figure 15. The reverser utilizes a single large deflector door located just upstream of the nozzle exit plane which blocks the primary and fan streams and directs the combined flow upward and forward. A small kicker or lip door further directs the flow forward to increase the reverse thrust performance. The thrust reversers were successfully demonstrated during taxi from 110 knots to 30 knots at maximum reverse thrust (94% N_1) and at speeds below 30 knots including rearward taxi at 85% N_1 power. No evidence of reingestion or engine/reverser operating problems were encountered. Flight testing also involved operations on a semi-prepared runway. An evaluation of take-offs, landings, and taxiing in a dirt and sand environment showed essentially no ingestion into the engines. The pilots reported good visibility throughout the landing rollout, figure 16, since dust clouds caused by the main landing gear trailed behind the aircraft.

Propulsion System Operability

In general, neither the STOL airplane operating environment nor the unique, overwing engine installation presented any engine operating difficulties. In-flight starting capability, engine transient response and fan and compressor stall margins were entirely satisfactory, since they are comparable to CF6-50 experience on the 747 airplane.

Airplane Performance

- TAKEOFF

The efficient propulsive-lift system and high installed thrust-to-weight ratio of the YC-14

347

provides exceptionally short takeoff roll capability. This contributes to safer operations because of the short time on the runway. Figure 17 shows a typical STOL takeoff test result of time and distance on a semi-prepared field. Liftoff was obtained in 14 seconds at 99 knots; this exceeded predicted liftoff speed by 3 knots. Simulated engine failure tests during takeoff showed that the slight rolling tendency noted after the engine cut was easy to control.

● LANDING

Landing rolls of 183 to 244 meters (600 to 800 feet) were routinely demonstrated on the semi-prepared field using maximum reverse thrust and maximum braking. Landings were conducted using reverser thrust alone, reverse thrust and braking and braking alone. Test results are shown in Table II.

For the design case (engine-out, idle-reverse thrust), the landing distance over a 15-meter (50-foot) obstacle was 482 meters (1,580 feet), which was far better than both the predicted and required distance, figure 18.

Community Noise

● TAKEOFF-COMMUNITY NOISE

The outstanding takeoff and climb performance of the YC-14 results in low community noise on takeoff. For example, the prototype reached 503 meters (1650 feet) AGL within one mile from brake release on a hot day, 100°F, at Edwards AFB (701 meters MSL) (2300 feet MSL), exceeding the performance goal of 472 meters (1,500 feet). Community noise level was measured during flyover at nominal STOL weight and full power. After extrapolating the YC-14 noise data to FAR 36 certification conditions, it is compared in figure 19 with certification data for various commercial aircraft, 1969 FAR 36 noise rules, and with the more stringent requirements of FAR Amendment 36-7 introduced in 1977. The YC-14 is shown to meet the current takeoff community noise rules during STOL takeoff without requiring cutback procedures.

● TAKEOFF-SIDELINE NOISE

Takeoff-sideline noise measurements were extrapolated to certification conditions and are compared in figure 20 to FAR 36 rules and sideline levels for aircraft certified with high-bypass-ratio engines. Based on the extrapolated data, the YC-14 meets FAR 36-7 sideline noise rules.

● APPROACH

The YC-14 engine arrangement above and ahead of the wing is effective for low community

noise on approach since the exhaust noise and fan noise are shielded by the wing. In addition, the inlet noise is reduced by acoustic lining. Approach noise comparisons in figure 21 based on extrapolation of flight test data show that the YC-14 is much quieter (about 6 PNdB during STOL approach) than required by FAR 36-7 rules.

CONCLUSIONS

All propulsion system test objectives were met during the flight test program. The following conclusions are drawn:

1. The CF6-50 engine installation in entirely compatible with the STOL operating requirements of the YC-14 airplane.

2. Performance test results show good agreement with predictions based on engine ground testing and engine cycle analysis.

3. The YC-14 reverser installation is a reliable and effective device for routine as well as emergency use in stopping the airplane and for rearward taxi without significant reingestion.

4. Community noise analysis of the YC-14 aircraft operating in STOL mode with USB powered lift shows it will nominally meet requirements of current FAR 36 Amendment 7 noise rules for new aircraft. The overwing installation shows low fan and jet noise on approach. The takeoff noise benefits from the steep climb capability.

REFERENCES

1. Kimes, Lucas J., "YC-14 Engine Installation Features", AIAA Paper 74-972, August 12, 1974.

2. Grotz, Charles A., "Development of the YC-14 Propulsion System", AIAA Paper 75-1314, September, 1975.

3. Sussman, M. B., Reed, J. B., O'Keefe, J. V., Eldridge, W. M., et al, "USB Environment Assessment Based on YC-14 Flight Test Measurements", AIAA/NASA Ames Conference Proceedings, Paper 77-593, June 6-8, 1977.

4. Armstrong, Robert S., "YC-14 Propulsion System In-Flight Performance Methods", Boeing Document D748-0116-1, August 16, 1976.

5. Hirt, William J., "YC-14 Propulsion System Ground Rig Test", AIAA Paper 76-918, September, 1976.

Table 1.— Low Speed Performance, Nozzle Door Open

CASE NO	FLAP POSITION	BLEED 8TH %	BLEED 14TH %	10TH #/SEC	MACH NO	ALT FT	ENG NO	CORRECTED FAN SPEED	FLIGHT TEST VALUE MINUS PREDICTED / PREDICTED VALUE — GROSS THRUST	FLIGHT TEST VALUE MINUS PREDICTED / PREDICTED VALUE — NET THRUST
1	60	4.95	5*	1.54	.137	7343	1	3514	2.4%	3.0%
2	60	4.48	5.3	1.72	.153	13850	1	3522	3.4	3.4
3	60	2.0*	5.51	1.67*	.182	14245	1	2174	3.1	3.6
4	60	2.0*	4.6	1.52	.182	14245	2	2127	2.9	2.8
5	60	2.05	4.5	1.65	.153	13850	2	2963	2.4	2.7
6	45	5.2	0	2.1	.195	23041	1	3060	1.3	1.8
7	45	5*	0	2.04	.262	13012	1	3144	0.4	0.7
8	45	4.8	0	1.61	.195	23041	2	3042	1.9	2.5
9	45	5*	0	1.67*	.262	13012	2	3053	0.2	0.3
10	20	0	0	1.95	.272	13551	1	3623	0.6	0.9
11	20	0	0	1.75	.272	13551	2	3614	0.6	0.6

(48KW) (65 HP) EXTRACTED FOR ALL CONDITIONS
*NOMINAL BLEED VALUES USED

Table 2.— YC-14 Demonstrated Short Landing Distance

LANDING ROLL CONDITION MAXIMUM BRAKING	LANDING DISTANCE m FROM 15m (50') OBSTACLE	LANDING DISTANCE m LANDING ROLL	GROSS WEIGHT Kg (lb) THOUSANDS	HEAD-WIND kn
ONE ENGINE REVERSE IDLE	448 (1470)	240 (786)	71.7 (158)	15
BOTH ENGINES REVERSE IDLE	456 (1495)	231 (759)	73.5 (162.1)	10
ONE ENGINE MAX REVERSE	458 (1505)	207 (673)	69.5 (153.2)	10
BOTH ENGINES MAX REVERSE	402 (1313)	191 (628)	70.1 (154.6)	17

- WING AREA: (1,762 FT²) ← 163.7 m2
- CARGO COMPARTMENT SIZE:
- 14.3m → (47 FT) LONG
- 3.57m → (11.7 FT) WIDE
- 3.44m → (11.3 FT) HIGH (MINIMUM)
- ENGINES: CF6-50D, (48,680 LB)
  THRUST (INSTALLED) ← 216,500 KG

401.6m
(131 FT 9 IN)

39.3m
(129 FT)

14.68m
(48 FT 2 IN)

5.66m → (18 FT 7 IN)
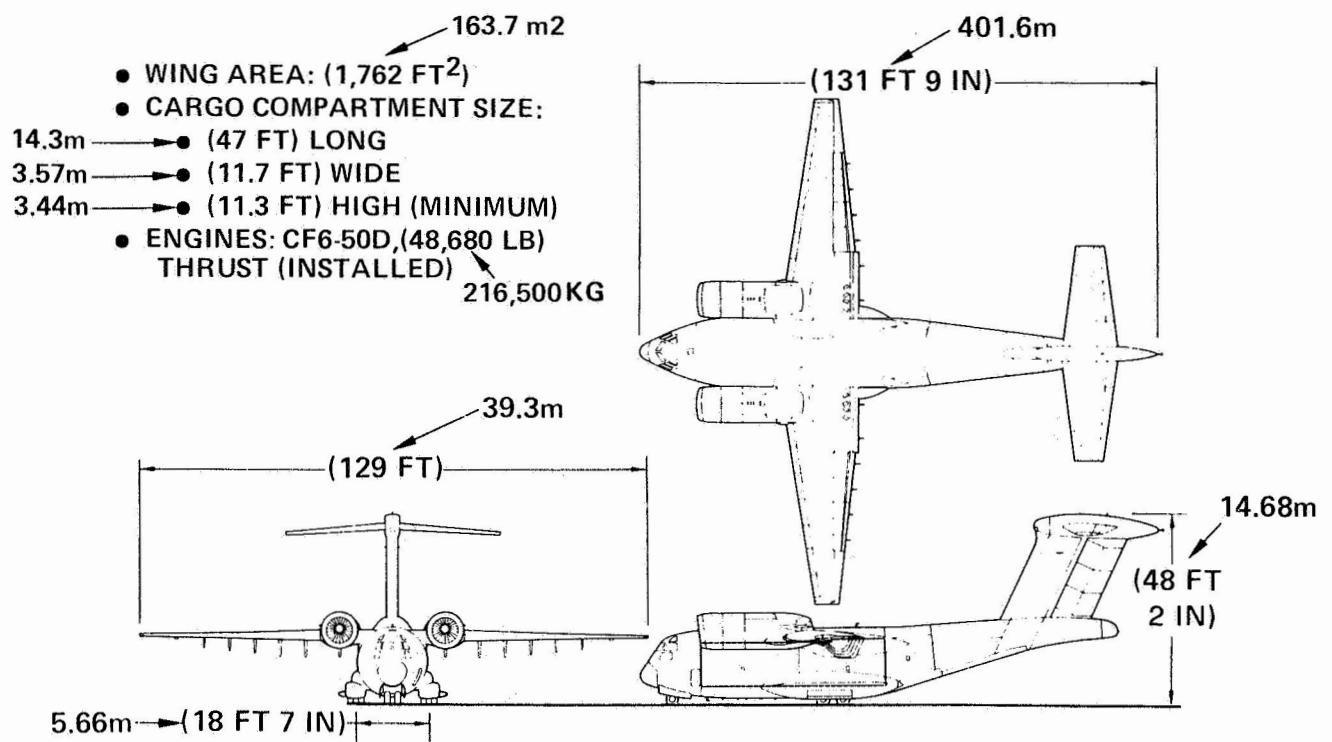
Figure 1.—YC-14 Configuration (3-View)

Figure 2.—Boeing YC-14 AMST Prototypes
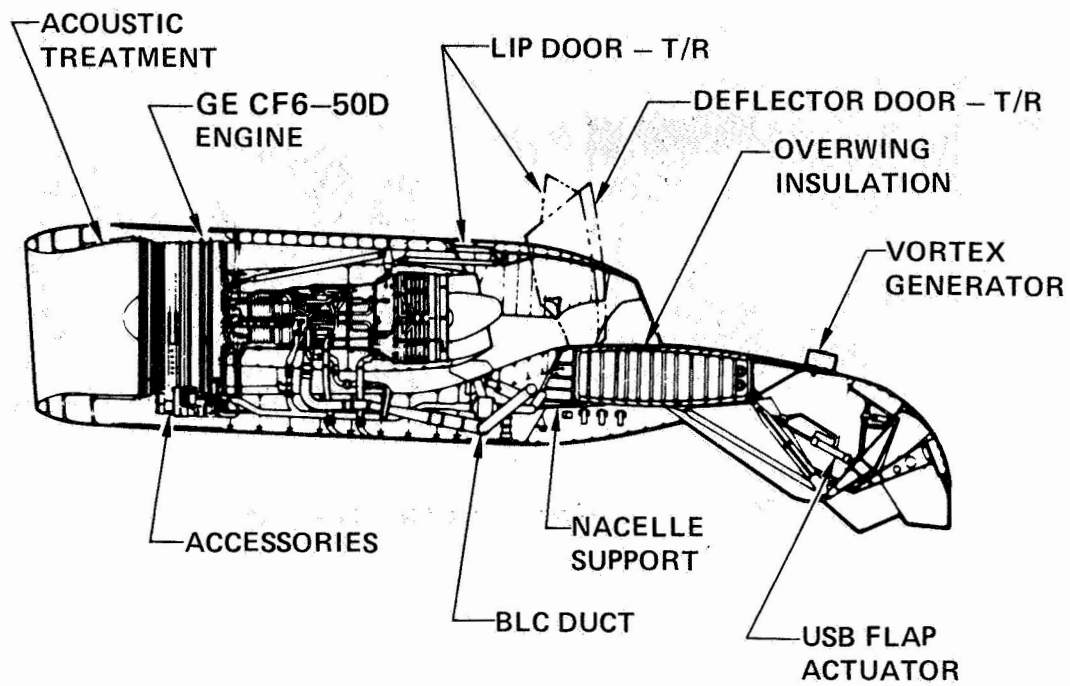
352
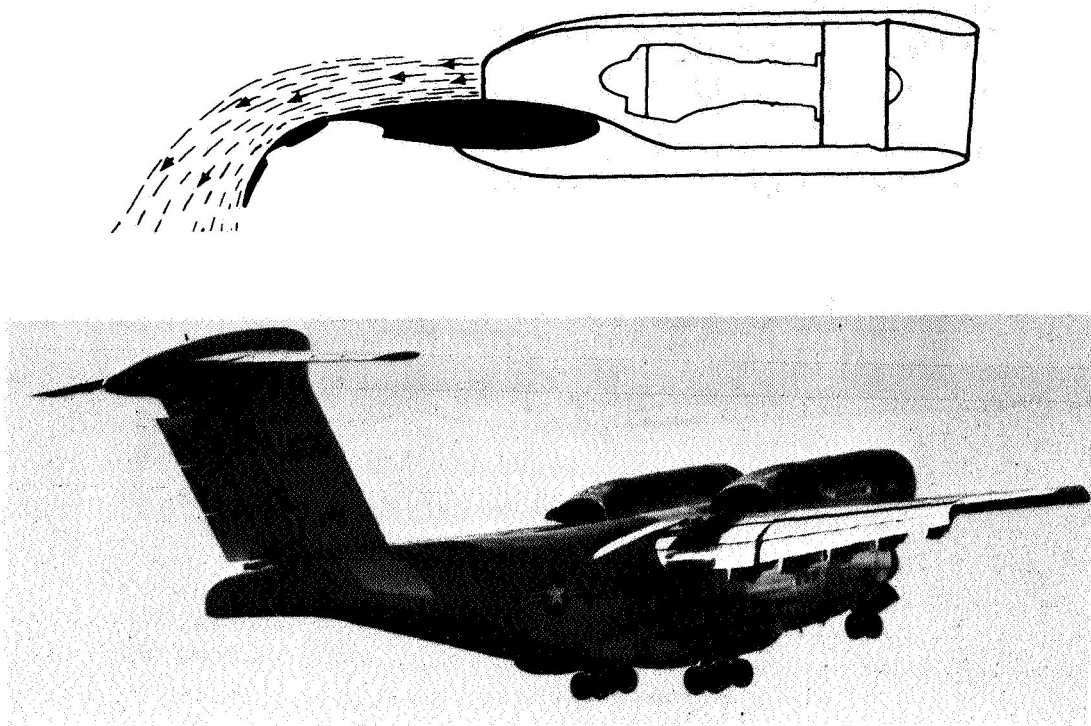
Figure 3.— Propulsive Lift Concept
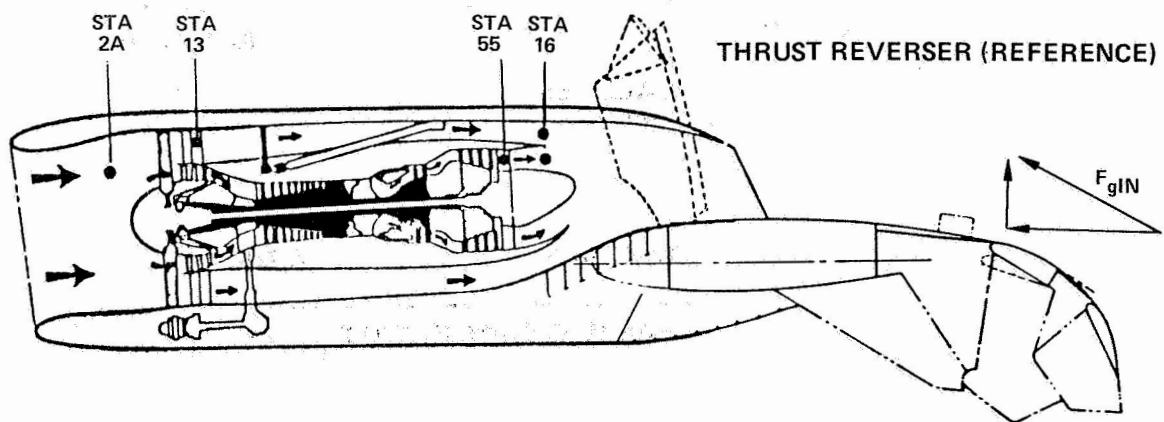
Figure 4.— Engine/Nacelle/Wing/Flap Configuration

Labels: ACOUSTIC TREATMENT; GE CF6—50D ENGINE; LIP DOOR — T/R; DEFLECTOR DOOR — T/R; OVERWING INSULATION; VORTEX GENERATOR; ACCESSORIES; NACELLE SUPPORT; BLC DUCT; USB FLAP ACTUATOR

Figure 5.— Inflight Thrust Definitions

Labels: STA 2A; STA 13; STA 55; STA 16; THRUST REVERSER (REFERENCE); F_{gIN}
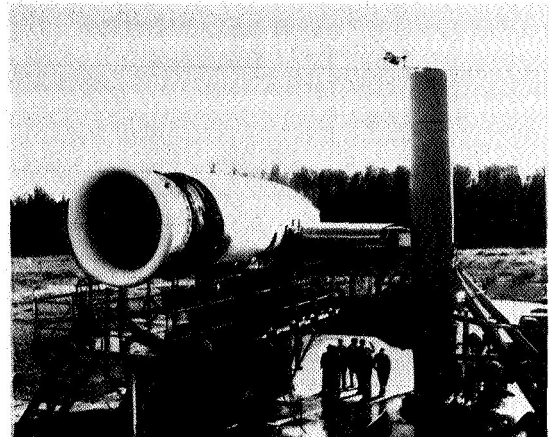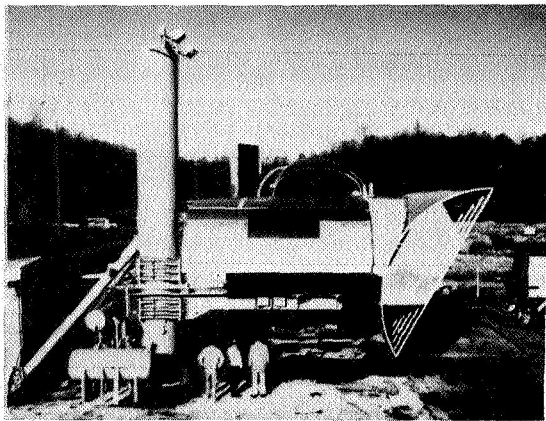
Figure 6.— Tulalip Ground Test Installation
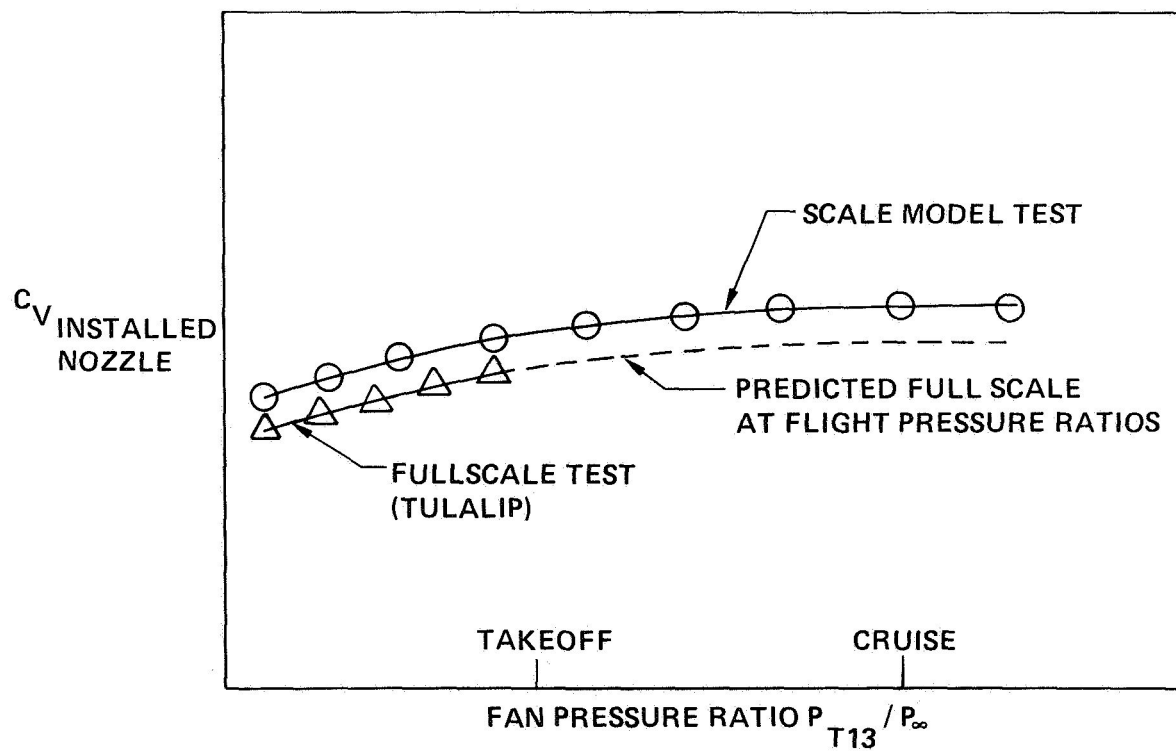
Figure 7.— High Speed Nozzle Thrust Performance
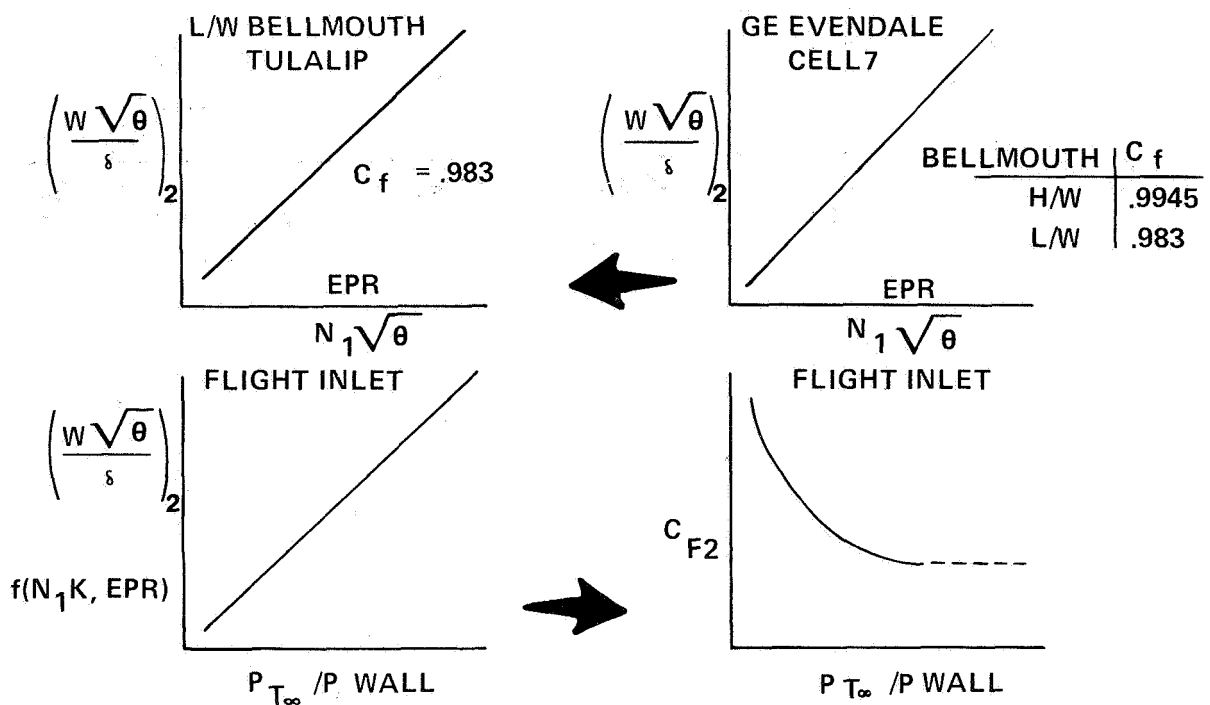
Figure 8.— Flight Inlet Airflow Calibration
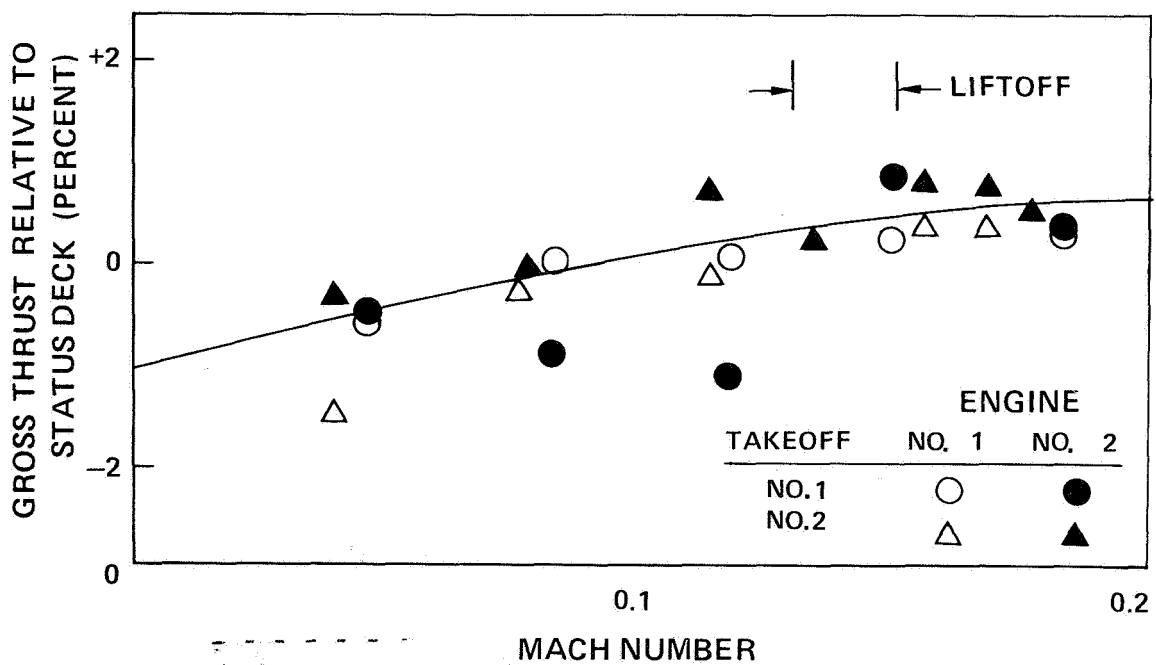
Figure 9.— STOL Takeoff Thrust
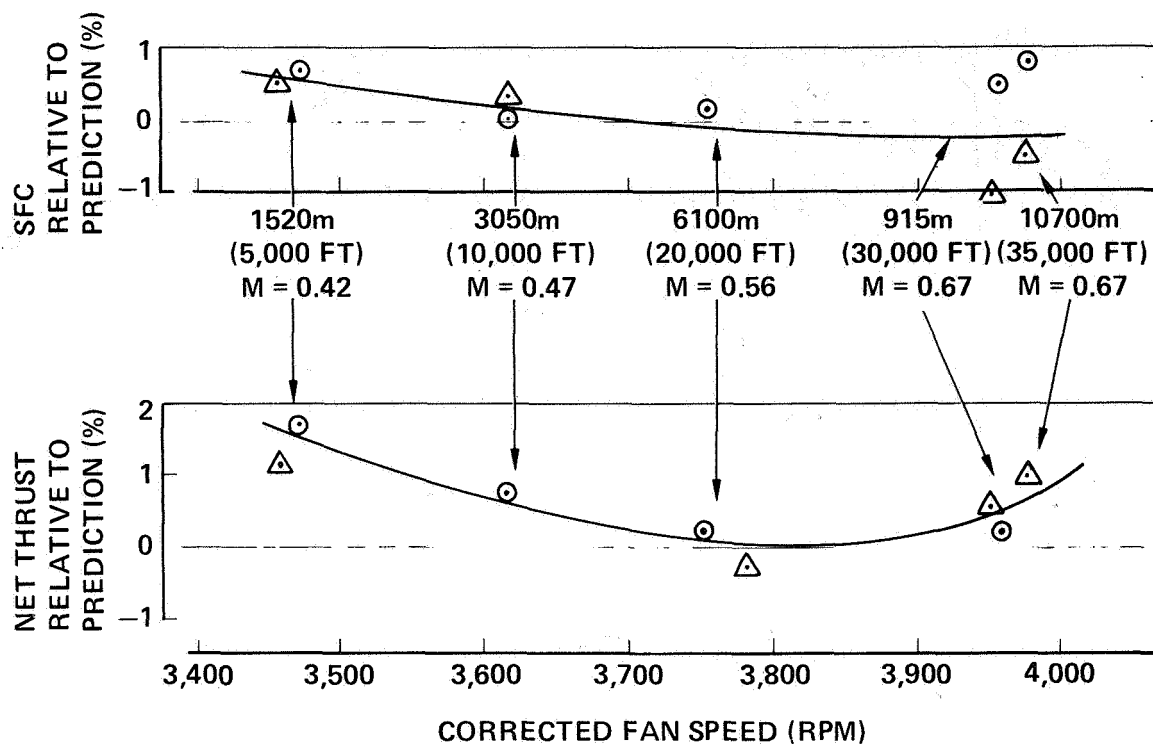
Figure 10.— Climb Thrust and SFC
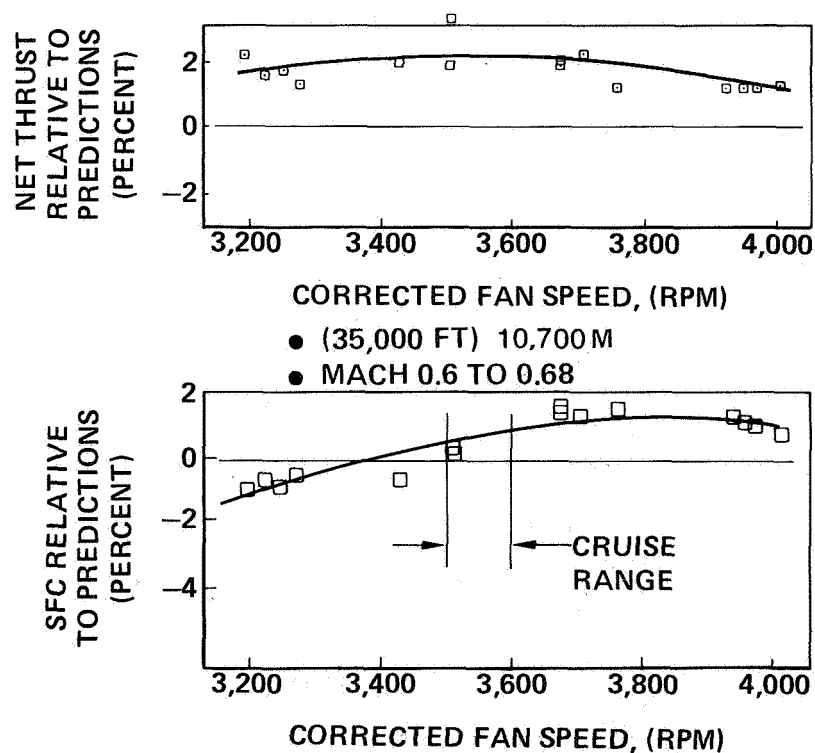
Figure 11.— Cruise Thrust and SFC

SHADED SYMBOLS DENOTE CALCULATED INFLOW ANGLES
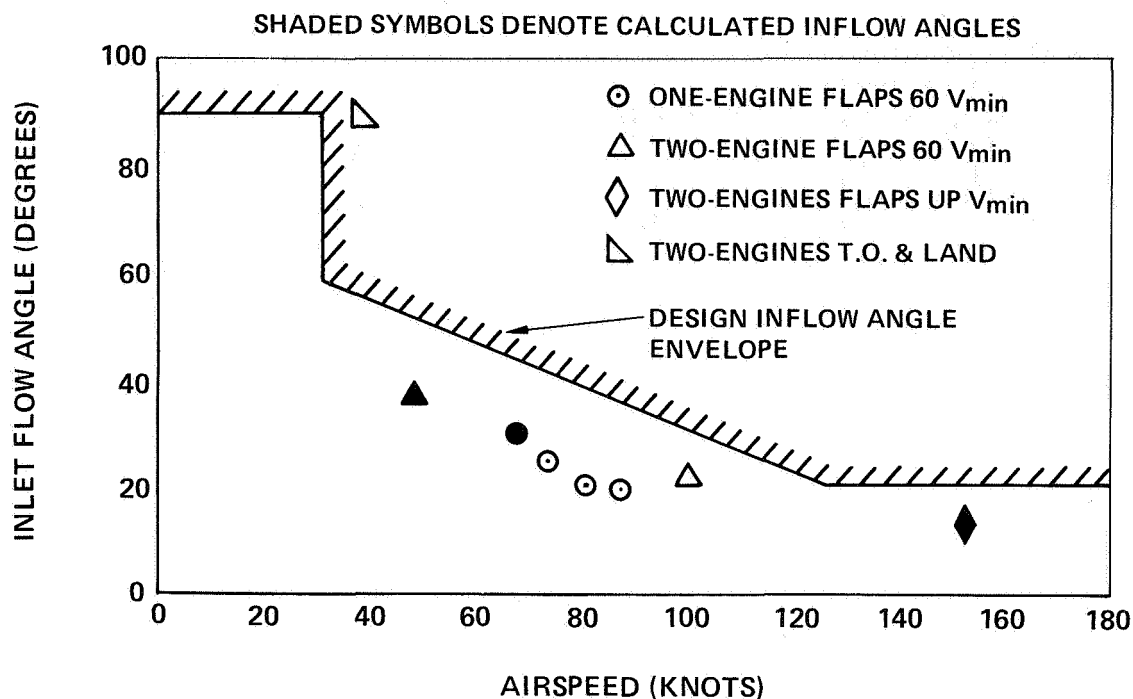
Figure 12.— *Engine Inlet Inflow Angles*

Legend:
- ⊙ ONE-ENGINE FLAPS 60 V_{min}
- △ TWO-ENGINE FLAPS 60 V_{min}
- ◇ TWO-ENGINES FLAPS UP V_{min}
- ◺ TWO-ENGINES T.O. & LAND

DESIGN INFLOW ANGLE ENVELOPE

Y-axis: INLET FLOW ANGLE (DEGREES)
X-axis: AIRSPEED (KNOTS)
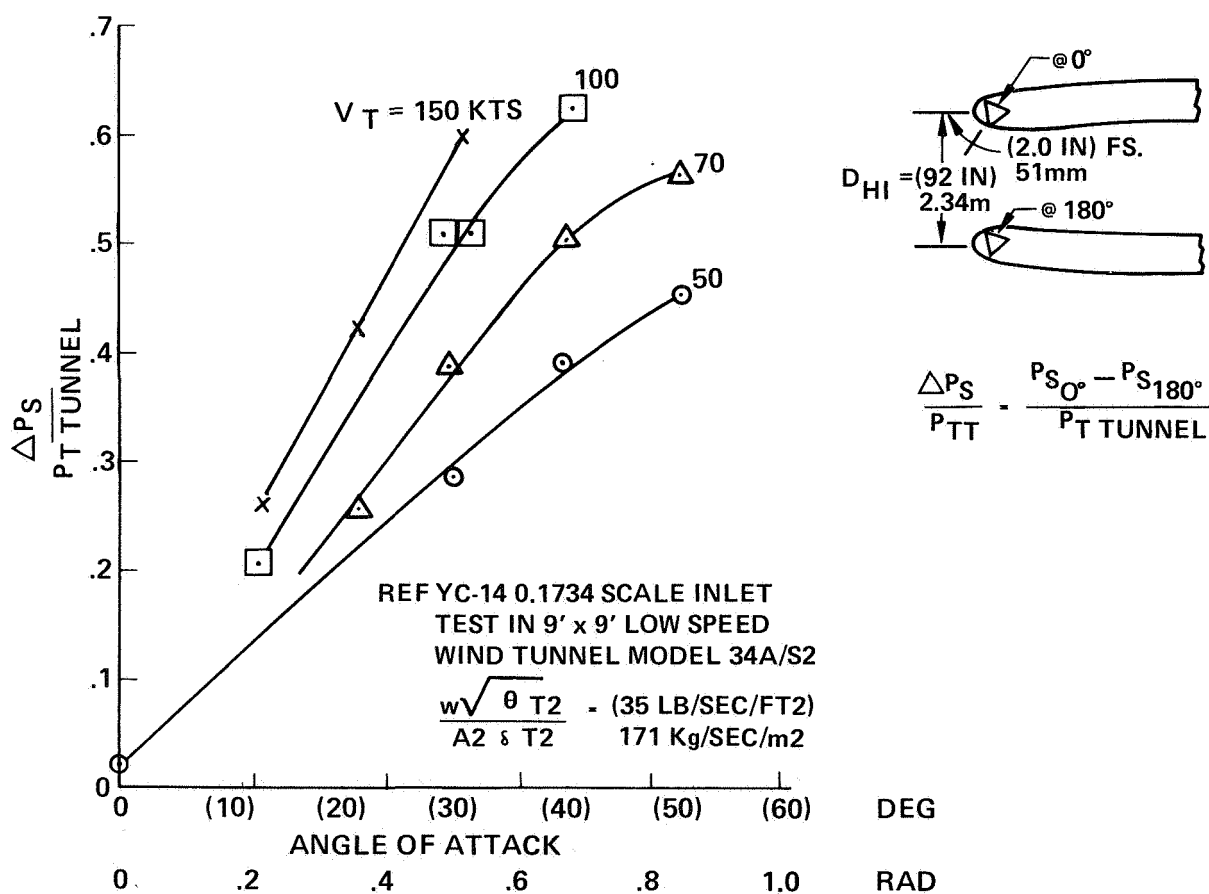
Figure 13.— *Inlet Inflow Angle Calibration*

V_T = 150 KTS

100

70

50

REF YC-14 0.1734 SCALE INLET
TEST IN 9′ x 9′ LOW SPEED
WIND TUNNEL MODEL 34A/S2

$$\frac{w\sqrt{\theta\ T2}}{A2\ \delta\ T2} = \begin{array}{l}(35\ LB/SEC/FT2)\\ 171\ Kg/SEC/m2\end{array}$$

ANGLE OF ATTACK
DEG
RAD

@ 0°

(2.0 IN) FS.
51mm

D_{HI} = (92 IN)
2.34m

@ 180°

$$\frac{\Delta P_S}{P_{TT}} = \frac{P_{S_{0°}} - P_{S_{180°}}}{P_{T\ TUNNEL}}$$

$\dfrac{\Delta P_S}{P_T\ TUNNEL}$

358
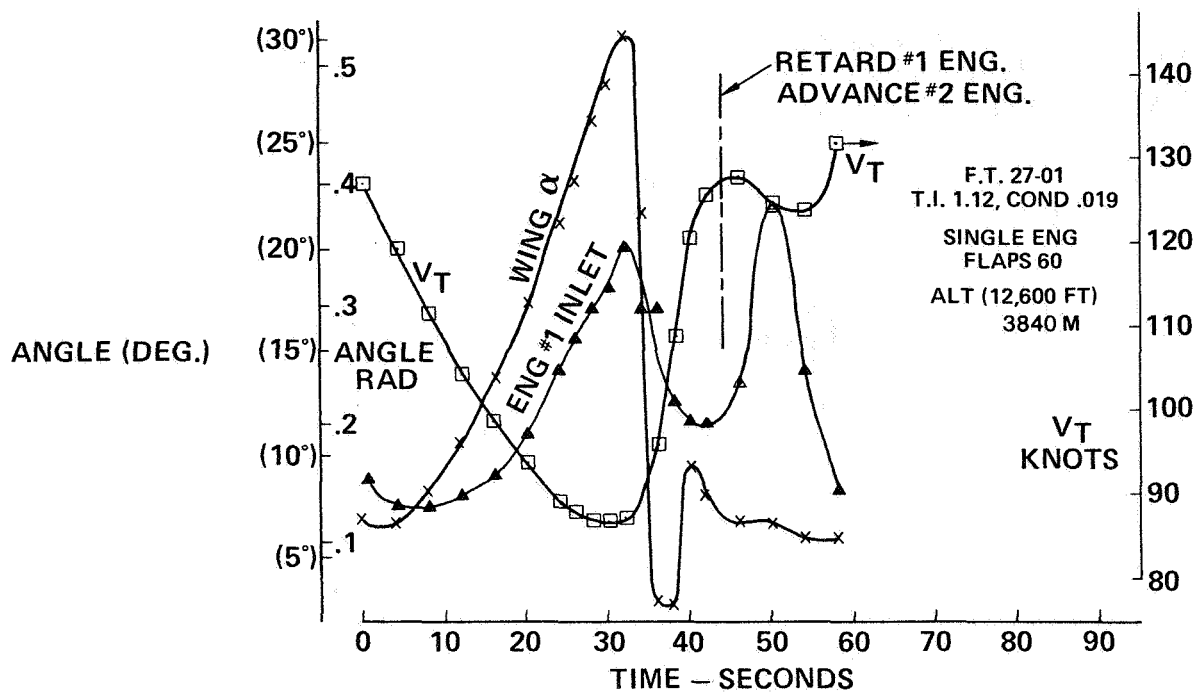
Figure 14.— Inlet Inflow Angles During V_{MIN} Excursion
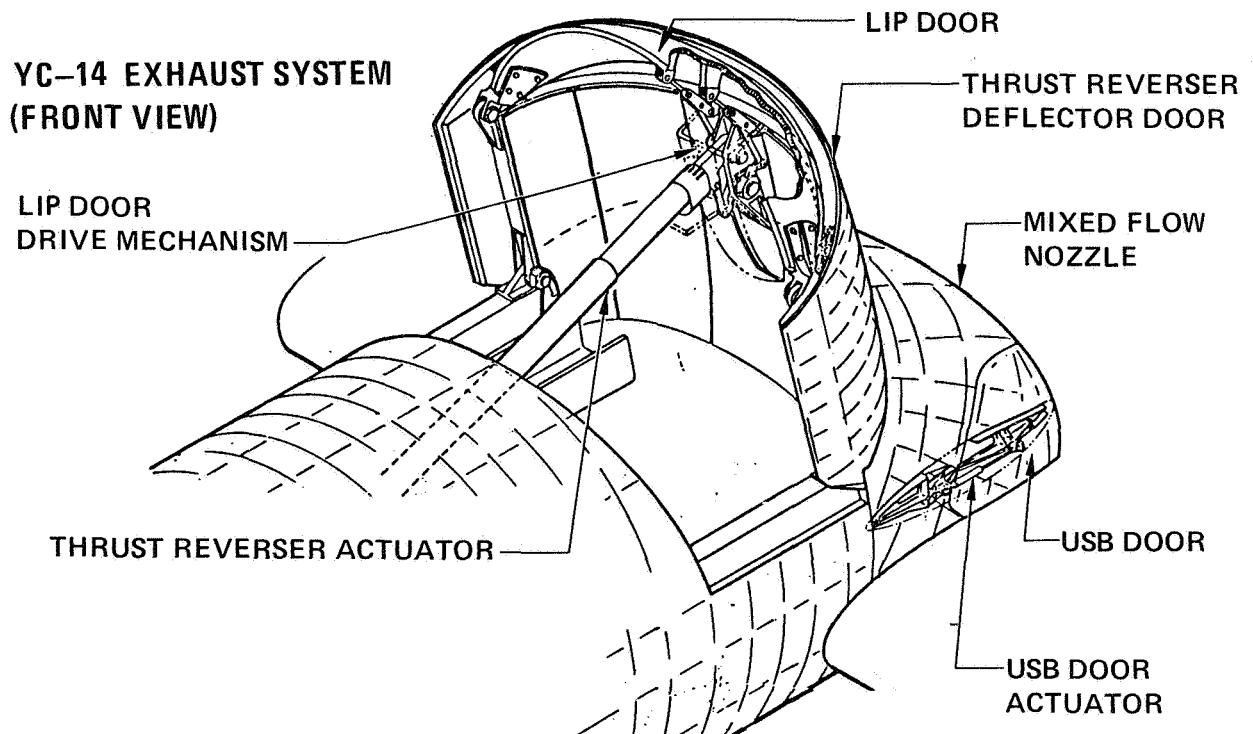
Figure 15.— Thrust Reverser Schematic

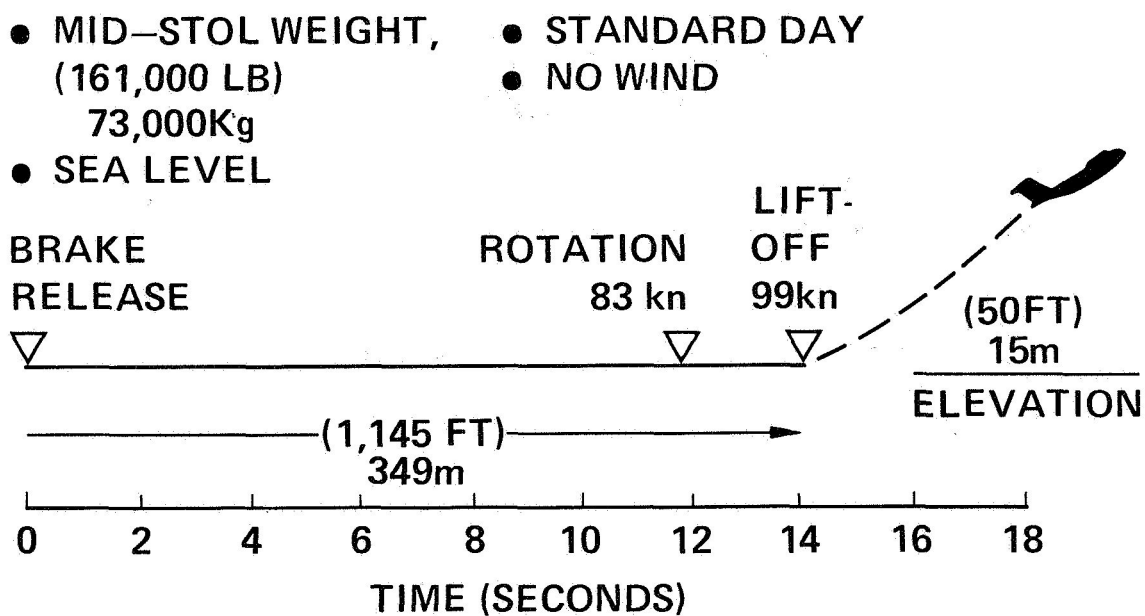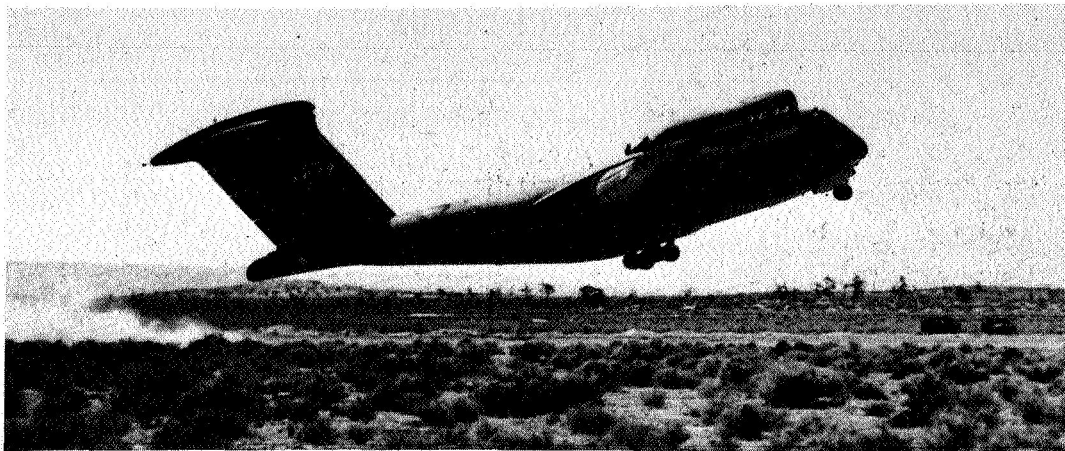*Figure 16.— Maximum Effort Stop on Semi-Prepared Field*

- MID–STOL WEIGHT, (161,000 LB) 73,000Kg
- STANDARD DAY
- NO WIND
- SEA LEVEL

BRAKE RELEASE

ROTATION 83 kn

LIFT-OFF 99kn

(50FT) 15m ELEVATION

(1,145 FT) 349m

TIME (SECONDS)

Figure 17.— Takeoff Performance on Semi-Prepared Field

361

SEMI-PREPARED RUNWAY
MID-STOL WEIGHT (161,000 LB)
 73,000 KG

SEA LEVEL
HOT DAY (103°F)
 39°C
NO WIND
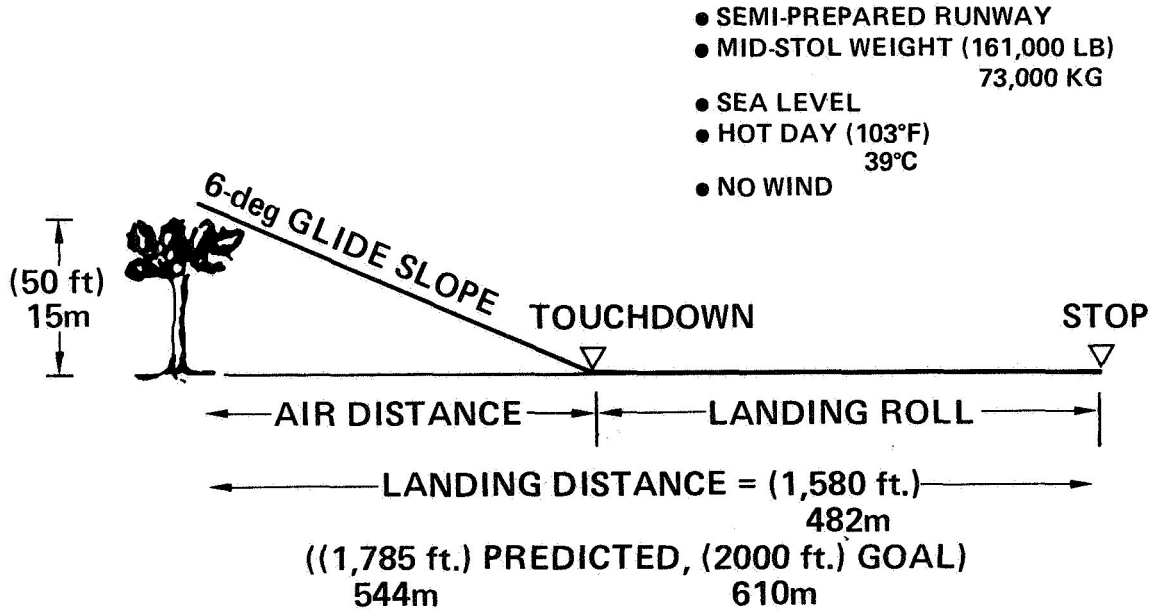
Figure 18.— Short Landing Distance on Semi-Prepared Field
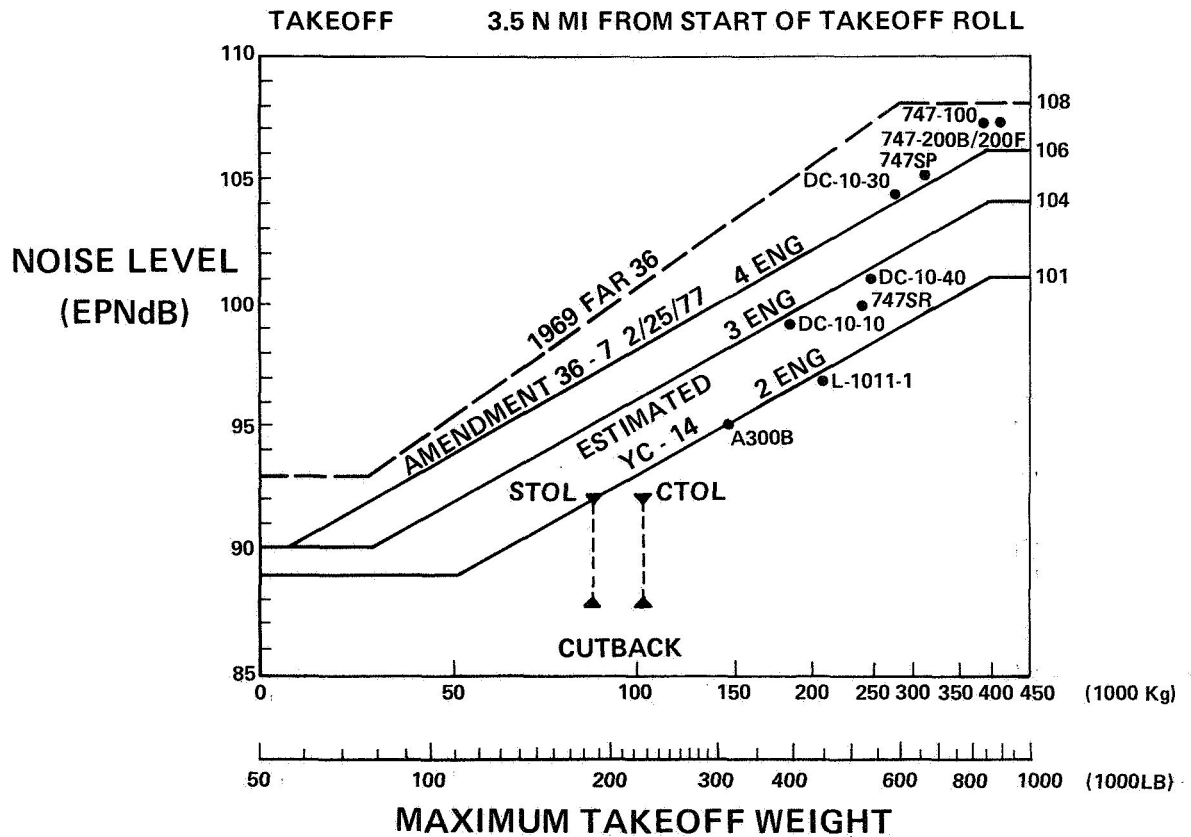
Figure 19.— YC-14 Takeoff Noise Comparison
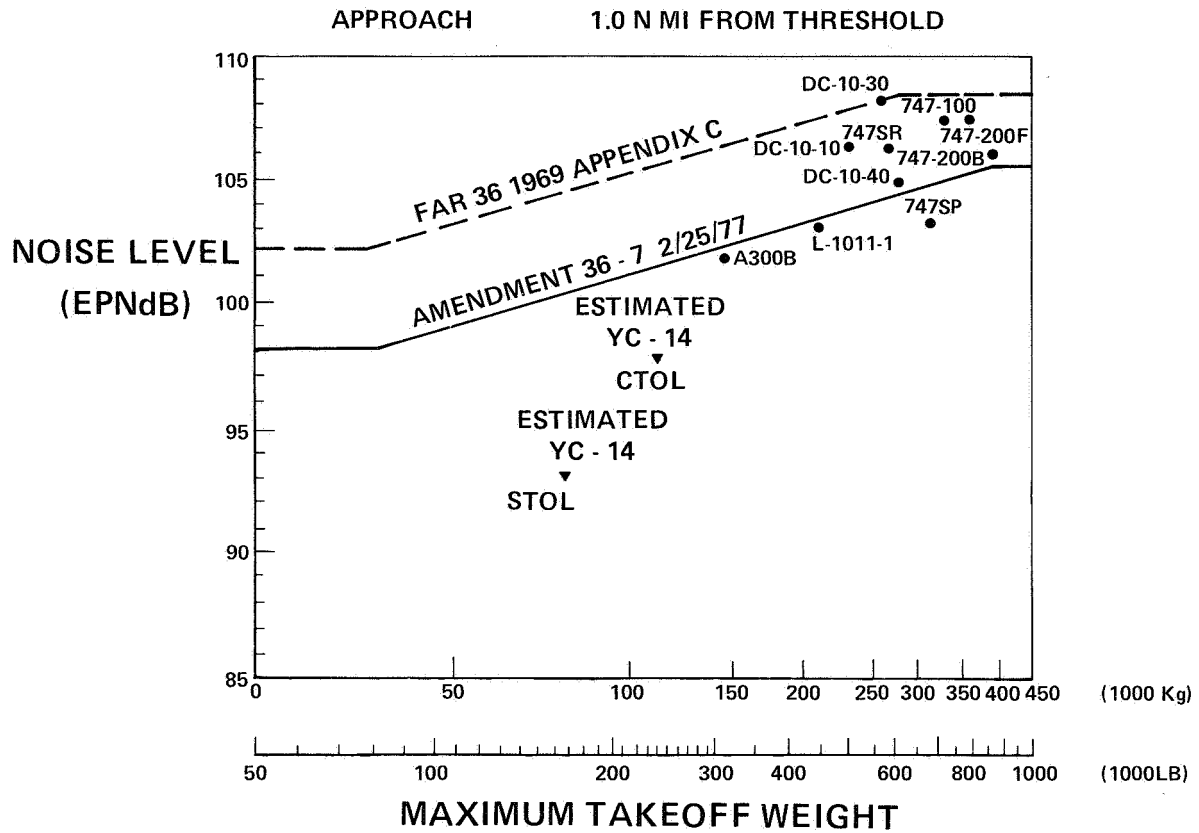
362
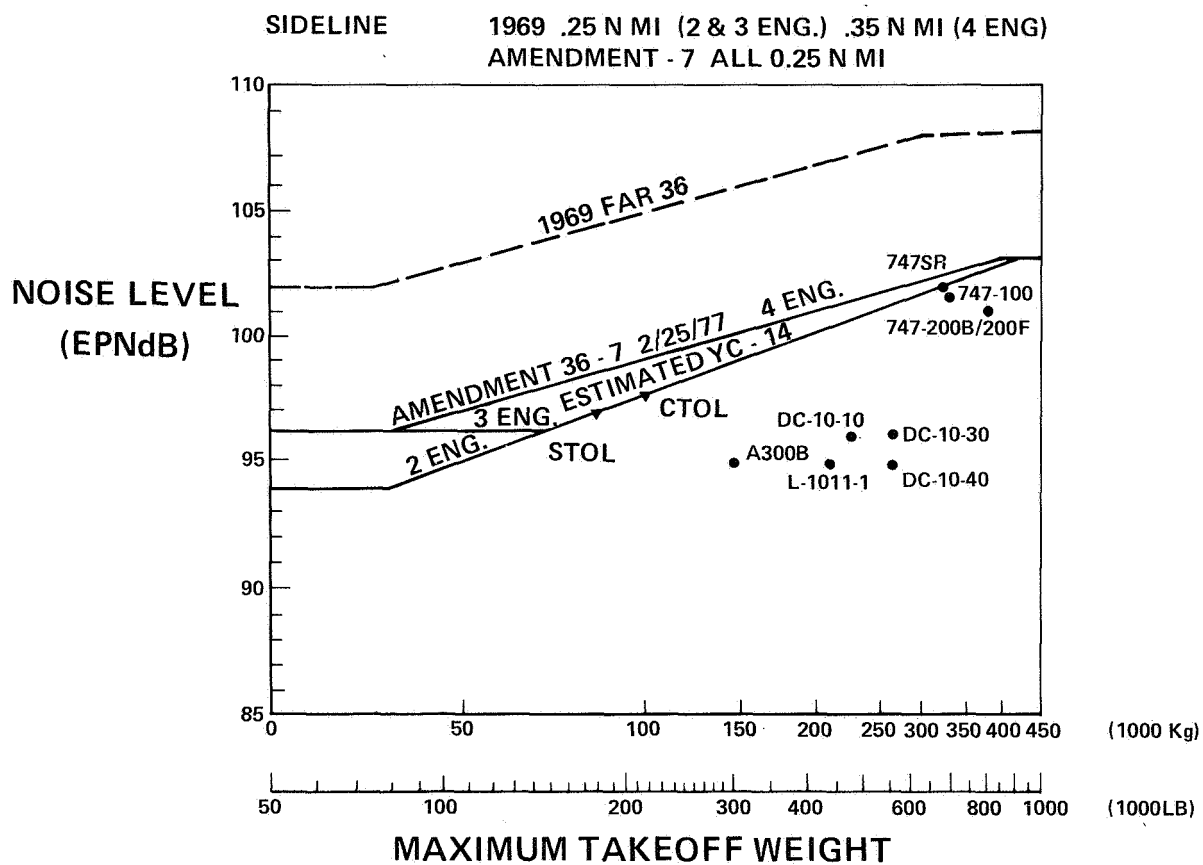
Figure 20.— YC-14 Sideline Noise Comparison

APPROACH   1.0 N MI FROM THRESHOLD

Figure 21.— Approach Noise

YC-15 PROPULSION INTEGRATION

by

KENNETH E. NORDSTROM AND CHARLES W. HARTKE

DOUGLAS AIRCRAFT COMPANY

McDonnell Douglas Corporation
Long Beach, California 90846

SUMMARY

The YC-15 Advanced Medium STOL Transport prototype was designed utilizing JT8D-17 engines to evaluate and refine the concept of producing powered lift through the use of externally blown flaps. As a result of the design of the pylon attachment to the aircraft, it was also possible to consider the adaptation of other engines to the YC-15 externally blown flap concept. Consequently, single P&WA JT8D-209 and CFM International CFM56 engines were installed on the two YC-15 aircraft for short flight test programs. These short flight test programs demonstrated the inherent flexibility of the externally blown flap propulsive lift concept to accept a wide variety of engines, from the older low-bypass engines to the most modern high-bypass engines. In addition, a contracted study effort on the feasibility of installing and flight testing a quiet, clean, short-haul experimental engine (QCSEE) on the YC-15 was performed for NASA-Lewis Research Center.

INTRODUCTION

Early in the design of the YC-15 aircraft, it was recognized that the pylon-mounted engine configuration (Figure 1) of the externally blown flap (EBF) airplane would lend itself to the installation of different engines. As a result, the pylon-wing interface was designed to take advantage of this capability. A pylon stub was designed as an integral part of the wing to carry .pylon loads into the front spar. The forward portion of the pylon, which supports the engine, was designed to mate with the pylon stub with the loads from the engine carried into the wing through four large-diameter bolts. This allowed a high degree of flexibility in the kinds of engines that could be fitted to the aircraft. Ultimately, three different types of engines, summarized in Table 1, were installed and flight-tested on the two YC-15 aircraft. The installations are shown in Figures 2 through 4.

There were two major types of problems considered in the integration of the engines with the YC-15 EBF STOL airplane, the normal considerations of a pylon/wing-mounted engine and those which were unique to the propulsive lift, STOL airplane. Of those unique to propulsive lift, the main areas of concern were engine position, flap temperatures due to exhaust impingement, wing/pylon flutter, reverser design, and inlet design.

In this paper, the main emphasis will be on those considerations unique to propulsive lift.

SYMBOLS

ALT   altitude m (ft)

ΔC_L change in lift coefficient

KEAS   knots equivalent airspeed

T_{EXH} exhaust wake temperature, °C (°F)

X   distance from nozzle exit, cm (in.)

W*/A   corrected inlet airflow, kg/sec cm^2 (lb/sec in.^{2})

a ·   angle of attack (deg)

CONVENTIONAL ENGINE-AIRFRAME INTEGRATION

With respect to the functional and physical interfaces between the engine and the aircraft, the YC-15 airplane did not present problems significantly different from any other airplane with wing-mounted engines supported from pylons. There were no pneumatic requirements beyond the normal demands for air conditioning, pressurization, ice protection, and engine starting. Electrical requirements were normal, and hydraulic requirements were only slightly in excess of normal loads due to the use of the large control surfaces associated with low-speed STOL operation. On the YC-15, hydraulic pressure was supplied from each of the four engines to four independent hydraulic systems designed so that the failure of one system would not impair aircraft operation nor affect any of the remaining systems. Cockpit instrumentation was conventional, and standard commercial design practice was used for engine fuel supply, fire detection and extinguishing systems, engine controls, electrical supply, engine starting, engine nacelle cooling, and hydraulic power supply.

The engine was supported from the pylon with conventional fore and aft engine mounts. The nacelle access doors were supported from the pylon apron and remained on the pylon when the engine was removed. The engine inlet was supported from the engine front flange. The thrust reversers on the JT8D-17-powered prototypes were supported from a track on the lower surface of the pylon to accommodate vertical loads and to reduce the moment on the engine exhaust flange. Fore and aft exhaust loads were taken out through the exhaust flange.

Although the engines used for the two single-engine retrofit programs did not employ thrust reversers, the philosophy of taking vertical loads through the pylon would have been utilized there also.

ENGINE-AIRFRAME INTEGRATION UNIQUE TO EXTERNALLY BLOWN FLAP STOL

Nacelle Position for Optimum-Powered Lift

There were a number of considerations in the placement of the engine nacelle on the YC-15 for good high-lift performance. As discussed in reference 1, the attainment of the maximum lift coefficient dictated that the engine nacelle be placed well forward and high (see Figure 5). The placement, however, was tempered by other considerations. Moving the engine forward by more than 20 percent of the wing chord would have placed the pod weight too far ahead of the wing front spar and would have required a heavier spar and pylon to handle the landing loads and flutter. Placing the engine too high represented a risk of excessive interference drag between the pod and the wing and an increase in the scrubbing drag on the lower surface of the wing during cruise. The engine

placement was also influenced by the desire to allow the largest percentage of the exhaust plume to strike the flaps, and the flaps were designed with large slots to encourage the exhaust gases to flow over their upper and lower surfaces for maximum turning. The position found to be optimum on the YC-15 was to place the exhaust nozzle exit at 10 percent of the chord ahead of the wing and 6 percent of the chord below the leading edge, as shown in Figures 6 and 7.

Lateral placement of the engines was such that aerodynamic interference between adjacent nacelles and between the inboard nacelle and fuselage was minimized. The possibility of excessive lateral and directional control forces due to an engine failure was also considered in establishing the outboard position. The inboard position was influenced by considerations of sidewash due to thrust asymmetry and the need to keep directional control requirements from becoming excessive. On the YC-15, the JT8D-17 engine pods were placed 180 cm (71 in.) apart on the 162-sq-m (1740-sq-ft) wing and 224 cm (88 in.) on the 196-sq-m (2108-sq-ft) wing (Figures 8 and 9). The fuselage clearance was 180 cm (71 in.) and 267 cm (105 in.), respectively. The spacing between the engines was compromised slightly for the JT8D-209 and CFM56 single-engine installations, shown also in Figures 8 and 9.

Flutter

The two YC-15 prototypes were designed initially with four JT8D-17 engines on a 162-sq-m (1740-sq-ft) wing, and flutter characteristics were established analytically for this configuration (Figure 10). Flight tests conducted early in the program cleared the flutter envelope to V_L and no problems were encountered. In the second phase of the prototype program, the No. 1 airplane was modified with a new wing of larger area and a CFM56 engine was installed in the No. 1 engine position (left-hand, outboard). Analysis showed that the addition of the CFM56 engine did not degrade the basic flutter characteristics; in fact, flutter was less critical because of the increased weight of the engine and nacelle. Analysis further indicated an even less critical flutter envelope if four CFM56s were used. A ground vibration test and early flight testing of this configuration cleared the flutter envelope for Phase II flight testing. At approximately the same time, a JT8D-209 engine was being installed on ship 2 in the No. 1 position, and again analysis indicated that the change would have no adverse effect on flutter characteristics. Ground vibration and flight tests cleared the flutter envelope during the initial portion of Phase II testing on that airplane. As with the CFM56 installation, the increased engine weight improved the flutter characteristics. In summary, the prototype program experience verified that the engine position requirements for good EBF STOL performance do not lead to adverse flutter characteristics.

Flap Temperatures from Exhaust Impingement

Early in the design of the YC-15 airplane it was determined that the EBF could not be constructed of aluminum due to the impingement of hot exhaust gases. In the interest of reducing weight, it was decided that the flap would be constructed of titanium, rather than a heavier material with higher-temperature capability. This dictated that the temperature of the exhaust gases impinging on the flap be kept below 316°C (600°F). Based on the results of a prior experimental program with a TF33 engine, a mixer nozzle was added to the installation of the JT8D-17 engines used on the prototype. The nozzle was required to provide just enough mixing to lower the temperature at the flap to less than 316°C, while simultaneously limiting the temperature on the lower surface of the wing to less than the 121°C (250°F) limit for aluminum.

The JT8D-17 engine is a low-bypass-ratio (1.02:1) turbofan with a long fan duct that carries the fan air to the rear of the engine where, in conventional airplanes (nonpropulsive lift), it partially mixes with the hot core stream gases before being discharged from the nozzle. However, in such designs there is no forced internal mixing and the temperature of the exhaust gases at the flap would still be too high for the titanium flap. Due to length constraints on the YC-15 which precluded the use of an internal mixer, an external daisy mixer nozzle similar to those used on the early DC-8 and B707 was designed. A 10-lobe daisy was arranged around a large plug centerbody, as shown in Figure 11. The large centerbody was chosen in order to reduce the length of the nozzle and the boat-tail angle on the nacelle. The number of daisy lobes required and the spacing between the centerbody and the bottom of the lobe were determined from testing with a TF33 engine and various mixer configurations.

Exhaust wake tests with full-scale JT8D-17 exhaust nozzle hardware confirmed that the basic temperature requirements of 316°C on the flap and 121°C on the lower wing surface had been met. Figure 12 shows the results of those tests.

The JT8D-209 engine, installed later in the program on YC-15 ship 2, is a medium-bypass-ratio (1.69:1) turbofan which also employs a long fan duct. The higher percentage of cooler fan discharge airflow and the larger fan duct diameter made it possible to design an internal forced mixer to reduce the exhaust temperature to the required level. The configuration chosen (Figure 13) was a nine-lobe daisy arranged around a moderate-sized centerbody in the core gas stream. The hot core gases flowed through the daisy lobes, while the cool fan air flowed through the valleys between the lobes. The four upper lobes were reduced in size to restrict the core gas flow and allow proportionately more fan air to be discharged in the upper portion of the nozzle. The use of a nonsymmetrical daisy was considered necessary at the time in order to reduce the temperature of the exhaust impinging on the underside of the wing. Subsequent testing proved that this was unnecessary and a symmetrical daisy could have been employed. Table 2 shows the resulting measured temperatures at the flap and wing with the JT8D-209 engine. It is apparent that the temperatures are well within the stated criteria.

The CFM56 engine, installed on YC-15 ship 1, is an advanced technology high-bypass-ratio (6.0:1) turbofan, which also required special attention due to its hot core flow. An internal forced mixer exhaust nozzle was designed similar to the configuration for the JT8D-209, except that a symmetrical 12-lobe daisy was used as shown in Figure 14. Table 2 compares the resulting measured temperatures for the CFM56 with those of the JT8D-17 and JT8D-209. Because of its higher bypass ratio, this engine produced temperatures at the flap significantly cooler than the maximum allowable. In the interest of reducing internal nozzle losses, smaller daisy lobes could have been designed by increasing the distance between the cold side of the lobe and the centerbody, thereby allowing an annulus of hot gas to exit around the bullet. This would have improved the flow characteristics in the hot and cold stream at the expense of a slightly higher mixed temperature at the flap.

Thrust Reverser Design Philosophy

One of the basic AMST design requirements was the capability to operate into short, unprepared airfields. During operation into these kinds of fields, it is highly desirable to avoid foreign object damage to the engine and the loss of visibility caused by blowing dust, and to be able to use reverse thrust all the way to a full stop and for ground maneuvering such as backing the aircraft (ref. 1). To

accomplish these objectives, two problems must be overcome: impingement of exhaust efflux onto the ground, and closed-loop ingestion of exhaust gases during reverser operation. Two features were incorporated in the thrust reverser design on the YC-15 to alleviate these problems, a directed flow thrust reverser and flow compaction.

The directed flow concept maintained pilot visibility when landing on dirt fields and reduced engine damage from foreign objects by eliminating ground impingement of exhaust gases during reverser operation. Directed flow was accomplished by blocking the lower 170 degrees of the thrust reverser and forcing the reverser efflux to exit only from the upper 190 degrees to prevent direct impingement. Additional flow up-skew was built into the lower cascade box to further ensure that the efflux did not contact the ground. The added up-skew also reduced the possibility of cross ingestion between adjacent engines.

Flow compaction featured cascades with 0-degree turning angles in the forward portion of the cascade box, as shown in Figure 15. The sheet of gas emitted by the forward cascades prevented the gases that were being turned forward by the rear cascades from attaching to the engine nacelle and forming a closed loop, causing reingestion of the hot engine exhaust and consequent engine surge. The result of this effort was a fully vectored thrust reverser system, as shown in Figure 16, with the capability to operate into semiprepared dirt strips down to zero forward speed with no loss of pilot visibility, no cross or closed-loop ingestion, and no foreign object damage.

JT8D-17/YC-15 Reverser System

The thrust reverser designed for the YC-15 is shown in Figure 17. The external daisy had the cascade boxes at its forward end and the whole assembly was supported from a track on the underside of the pylon. As the assembly translated aft, the inner surface of the daisy closed on the centerbody and shut off flow in the forward thrust direction. At the same time, the cascades were pulled out from under the nacelle access doors and the exhaust flow was reversed.

During the flight test program, it was a routine operation to maintain reverse thrust to a full stop while landing and to use the reversers for controlling taxi speeds and backing on the ground. On two occasions the airplane operated out of semiprepared fields: Graham's Ranch/Rogers Dry Lake near Edwards Air Force Base and a dirt airstrip on farmland near Yuma, Arizona, with several landings and takeoffs made without difficulty (ref. 2). In addition, though the thrust reverser system was originally designed for ground operation only, it was later decided to use it in flight in order to avoid the large trim changes associated with the use of spoilers on a supercritical wing. By restricting the power to a level consistent with allowable actuator loads and after clearing the flight envelope to ensure that no adverse airplane control reactions would be encountered, the reversers were used to make high-speed descents and level flight slowdown from high speed. Descent rates between 1829 m/min (6000 fpm) and 3048 m/min (10,000 fpm) were routinely demonstrated.

JT8D-209/CFM56 Reverser Concept

Thrust reversers were not provided as part of the exhaust systems of either the JT8D-209 or CFM56 engine installation demonstration programs on the prototype. However, the same design concept, using directed flow and flow compaction, would apply to either of those engines. The thrust reverser cascade boxes would be the same basic configuration as on the prototype but these would be fixed to the aft cowl of the nacelle and would not translate fore and aft. Flow blockage

would be provided by doors inside the exhaust nozzle, behind the mixer. Scale models of this configuration have been tested to determine reverser effectiveness and loads.

Inlet Design for STOL Operation

Based on the results of analysis and wind-tunnel testing, the EBF configuration was found to induce a high degree of circulation around the wing during STOL operation with high flap deflections. This, in turn, resulted in high angles of attack at the wing leading edge and the engine inlet face. Positioning the engine high and forward relative to the wing moved the inlet out of the highest angle-of-attack areas, but the angles were still large enough to require some modification to the inlet lip shape. On the YC-15, the engine inlet lips (Figure 18) were shaped to have a variable ratio of lip thickness (highlight radius minus inlet throat radius) to highlight radius. At the top of the inlet, this ratio was 11 percent, while on the side it was 14 percent, to allow high crosswind operation without distortion. The ratio rose to 20 percent on the bottom to handle the high upwash angles. Downstream of the lip, the inlet featured a moderate diffuser with a 3-degree half-angle, which provided good unseparated airflow to the fan front face in all operating conditions, including high angles of attack and crosswinds.

The separation boundaries shown in Figure 19 were determined for the YC-15 inlet from large-scale model tests at various flight and power conditions. At the higher airflows, the boundary represented separation due to high inlet mach numbers and shocks at high angles of attack. At lower airflows, the separation was due to adverse pressure gradients and boundary layer growth. As shown in Figure 19, the airplane operating envelope for the high-lift condition indicates that operation was always on the unseparated side of the stall boundary. Flight tests with the three different engine configurations and inlets designed with the same basic geometry demonstrated stall-free engine operation over the entire envelope of the YC-15 airplanes.

FEASIBILITY STUDY OF QCSEE ON THE YC-15

Under Contract No. NAS3-20601, a study was conducted for NASA-Lewis Research Center (ref. 3) on the feasibility of flight-testing a quiet, clean, short-haul experimental engine (QCSEE) on the YC-15 to obtain under-the-wing, blown-flap-lift, propulsion system noise data. However, an extensive study of the installation details was first conducted to establish the feasibility of the basic engine-airframe combination. From this study, the physical installation of a QCSEE pod on the YC-15, as shown in Figure 20, was determined to be straightforward due to the inherent flexibility of the four-bolt pylon stub attach point. The principle of engine position was the same as for other engines except that the low weight of the QCSEE permitted it to be placed a little farther forward of the wing. One difference in the installation, however, was that the engine accessory package was mounted above the engine in the pylon (Figure 21), which resulted in a larger pylon than would normally have been required.

An additional consideration in the design studies of a QCSEE installation was the presence of a very hot core exhaust-gas plume which was predicted to impinge on the flap during a go-around at takeoff power with the flaps in the landing position or during reverse operation on the ground. Figures 22 and 23 indicate the magnitude of the temperatures expected in the area of the lower flap during a go-around and while in reverse. Since the basic QCSEE design made it impractical to mix the exhaust to get lower temperatures, other solutions were required. As proposed in the NASA feasibility study, the solution selected for a limited flight test was to coat the rear flap with a 6.35-

mm- (1/4-inch-) thick silicone base insulating material (Figure 24) over a 305-cm (10-ft) span behind the engine. For a production installation of a QCSEE-type engine, it is probable that a permanently canted primary nozzle would be required or that some type of a deflector, actuated by flap position, or reverse thrust, or both, would have to be designed into the primary nozzle.

QCSEE Reversible Fan

The QCSEE variable pitch fan concept, in which airflow from the fan exhausts from the engine inlet during reverse operation, was also expected to pose some unique problems of integration into an EBF STOL airplane. The concept of directed reverser flow, as shown in Figures 16 and 17, would not have any real significance with this type of installation. The flight test program proposed in reference 3 was directed at exploring the problem of reverse pitch operation and suggesting potential'solutions. For ground operation, if disturbance of ground debris forward of the airplane was found to be a significant problem (Figure 25), some solution to deflect the efflux upward would be required. A deflector in the lower quadrant of the inlet was mentioned in reference 3 as one potential approach.

As discussed previously, some method of spoiling the hot primary exhaust and preventing it from impinging on the flap during reverse operation was also expected to be required. Analysis subsequent to the reference 3 study has determined that a deflection of the primary nozzle on the order of 12 degrees would be needed to reduce the flap temperature to less than 316°C. However, a fixed cant of 12 degrees built into the primary nozzle would result in a thrust penalty of approximately 2 percent at all flight conditions. The use of a movable eyelid deflector would avoid the thrust penalty, but would require an actuation system to be tied to the reverse thrust logic to operate the deflector at the proper time.

ACOUSTICS

In addition to the considerations of inlet and exhaust system design, thrust reverser operation and wing-pylon flutter, the problem of flyover noise levels on the YC-15 was also addressed. The basic YC-15 was powered by the low-bypass-ratio JT8D-17 with external mixers. This combination resulted in relatively high noise levels as measured by the Air Force during the prototype flight test program. Analysis of the JT8D-17 test data indicated that the external mixer shifted the jet noise to higher frequencies, which resulted in an increase in the aft quadrant noise. Higher bypass ratios are expected to result in significant noise reduction compared with the JT8D-17, and the shift in jet noise frequencies will not occur with the internal mixers used with the higher-bypass-ratio engines since the mixing will take place upstream of the final exhaust nozzle. In addition, the high takeoff and approach angles of an EBF STOL aircraft in combination with the low noise characteristics of a QCSEE-type engine would be expected to yield noise levels approaching 95 EPNdB on a 162-m (500-ft) sideline (ref. 3).

371

CONCLUSIONS

The requirements imposed by propulsive lift had no adverse effect on the problems of normal engine-airframe integration. Additionally, those problems which were unique to propulsive lift did not result in severe compromises or penalties to the basic propulsion system as demonstrated by the design and flight testing of off-the-shelf turbofan engines ranging in bypass ratios from 1.0 to 6.0. Even the potential problems of flap temperature and reverse thrust, identified in the QCSEE feasibility study, though not yet demonstrated, are considered readily solvable.

The YC-15 EBF STOL airplane has been proven to be readily adaptable to a variety of engines with a minimum of effort and compromise. The stub pylon interface feature (Figure 26) has been shown to offer a large degree of flexibility in accommodating engines of significantly different characteristics. The EBF has produced excellent propulsive lift over a wide range of engine bypass ratios and exhaust conditions.

REFERENCES

1. Thompson, J. D.: YC-15 Powerplant System Design and Development, AIAA Paper No. 74-973, August 1974.

2. Lane, J. P.: YC-15 Development and Test Highlights, Douglas Paper No. 6655, Douglas Aircraft Company, October 1977.

3. Thompson, J. D.: Feasibility Study of a QCSEE Flight Test Program Using the McDonnell Douglas YC-15 Aircraft, NASA CR-135390, April 1978.

TABLE 1.
TWIN SPOOL TURBOFAN ENGINES

	JT8D-17 LOW-BYPASS RATIO	JT8D-209 MEDIUM-BYPASS RATIO	CFM-56 HIGH-BYPASS RATIO
TAKEOFF THRUST — N (LB)	71,168 (16,000)	80,064 (18,000)	98,790 (22,210)
SLS FLAT RATING — °C (°F)	28.9 (84)	28.9 (84)	30 (86)
BYPASS RATIO	1.02	1.69	6.0
CORRECTED INLET FLOW — kg/SEC (LB/SEC)	146.9 (324)	213.2 (470)	355.6 (784)
TURBINE INLET TEMP — °C (°F) (HOT DAY)	1,142 (2,087)	1,010 (1,850)	1,366 (2,490)
MIXED EXHAUST TEMP — °C (°F)	387 (729)	253 (488)	149 (300)
EXHAUST VELOCITY — m/SEC (FT/SEC)	492 (1,614)	382 (1,254)	287 (941)
WEIGHT — kg (LB)	1,510 (3,330)	1,845 (4,067)	1,882 (4,150)
CRUISE PERFORMANCE			
MAX THRUST, F_N — N (LB)	22,863 (5,140)	23,797 (5,350)	25,354 (5,700)
9144 m (30,000 FT), 0.8 M_N,			
TSFC — kg/HR/N (LB/HR/LB)	0.085 (0.832)	0.075 (0.739)	0.066 (0.649)

TABLE 2.
TEMPERATURE COMPARISON

	LOWER FLAP	WING LOWER SURFACE
JT8D-17	300°C	93°C
JT8D-209	204°C	93°C
CFM56	166°C	38°C
QCSEE	616°C	27°C

SEA LEVEL STATIC TAKEOFF POWER, 21°C
FLAPS IN LANDING POSITION
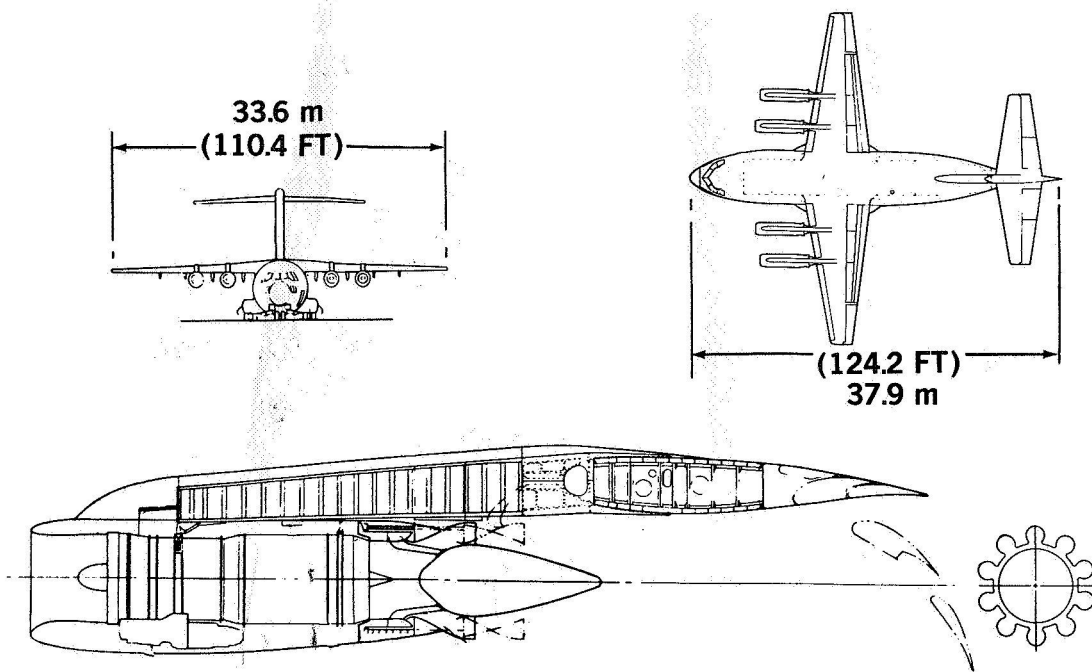
FIGURE 1. YC-15 PROPULSION SYSTEM GENERAL ARRANGEMENT

33.6 m
(110.4 FT)

(124.2 FT)
37.9 m
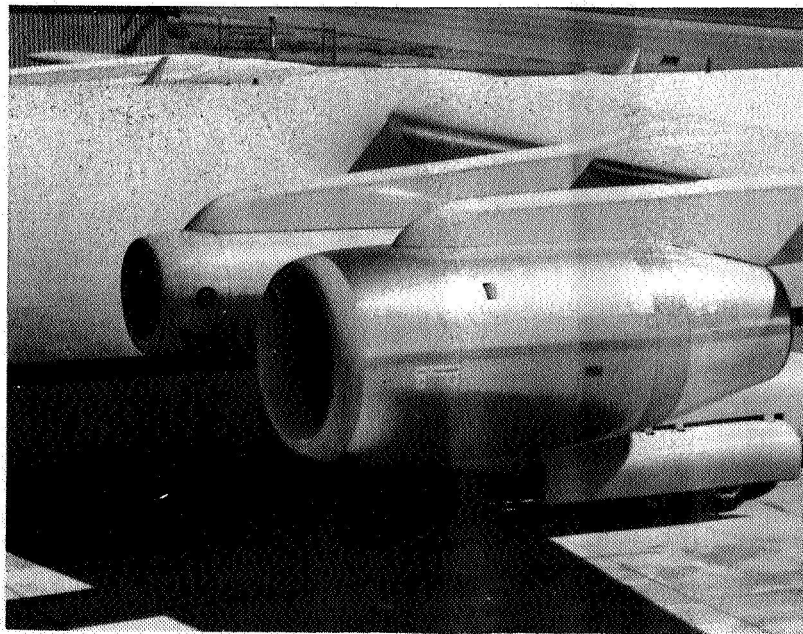
FIGURE 2. CFM56 AND JT8D-17 ON YC-15 NO. 1

374
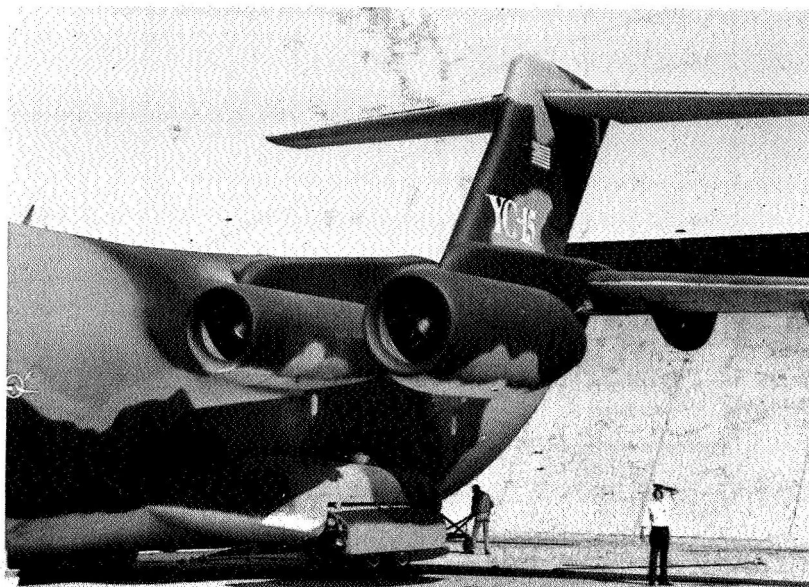
FIGURE 3. JT8D-209 AND JT8D-17 ON YC-15 NO. 2
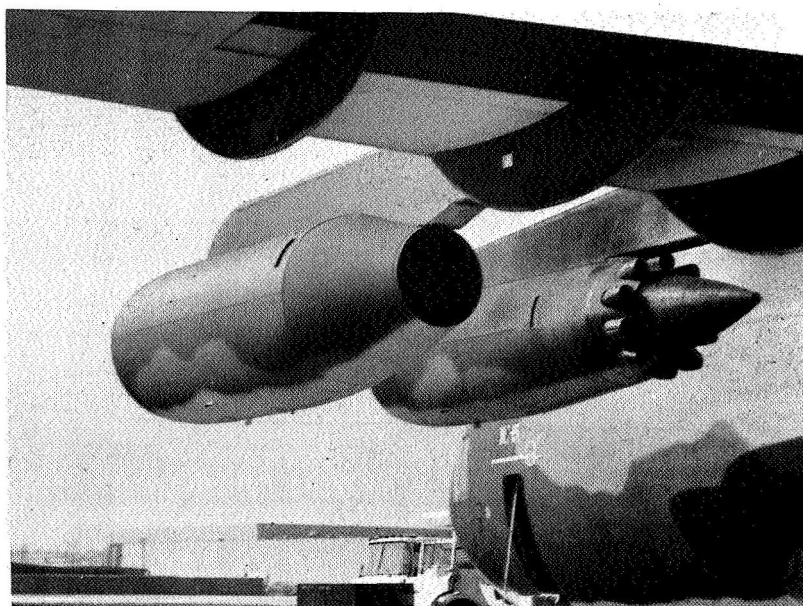
FIGURE 4. JT8D-209 AND JT8D-17 ON YC-15 NO. 2

375
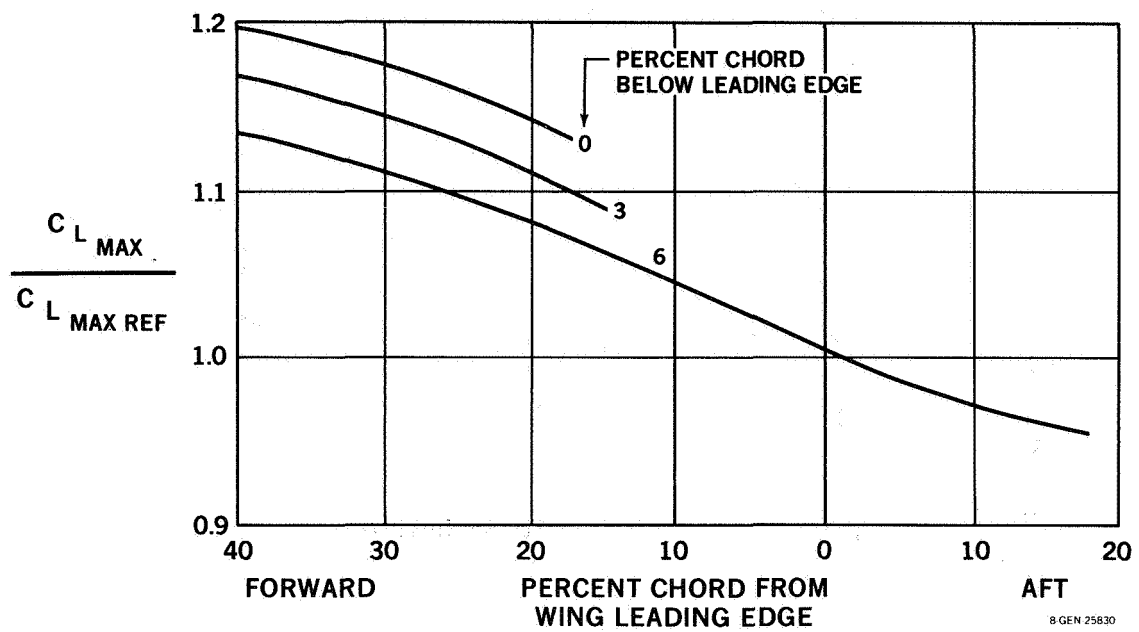
FIGURE 5. EFFECT OF EXHAUST EXIT LOCATION ON MAXIMUM LIFT
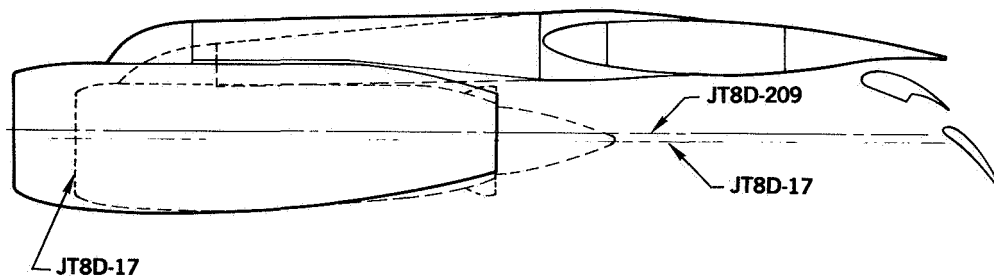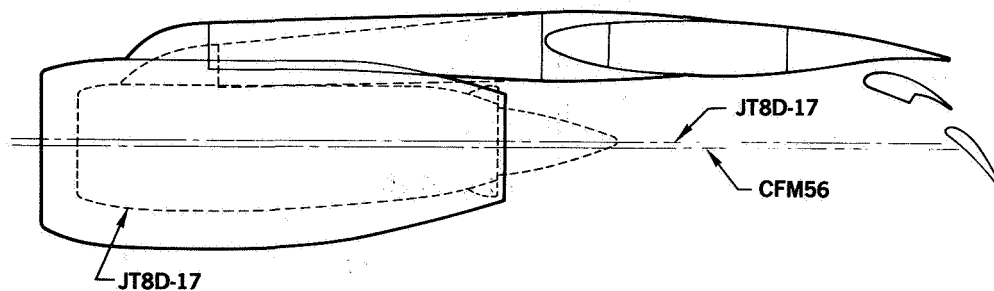

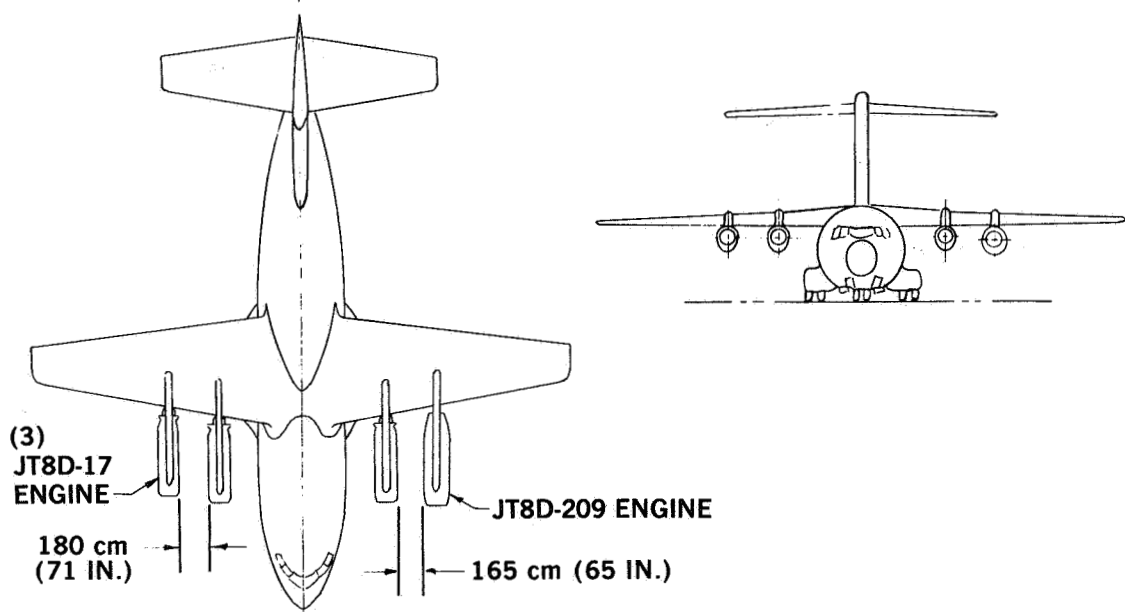FIGURE 6. JT8D-209 ENGINE AND PYLON

FIGURE 7. CFM56 ENGINE AND PYLON
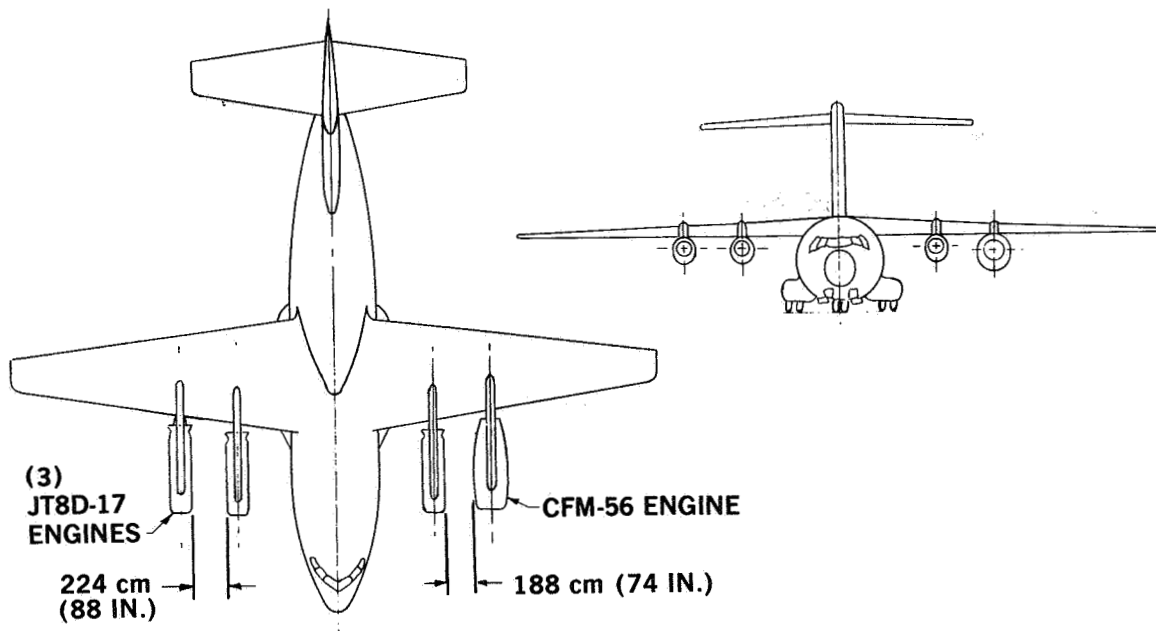
376

FIGURE 8. JT8D-209 ENGINE ON YC-15 POSITION NO. 1
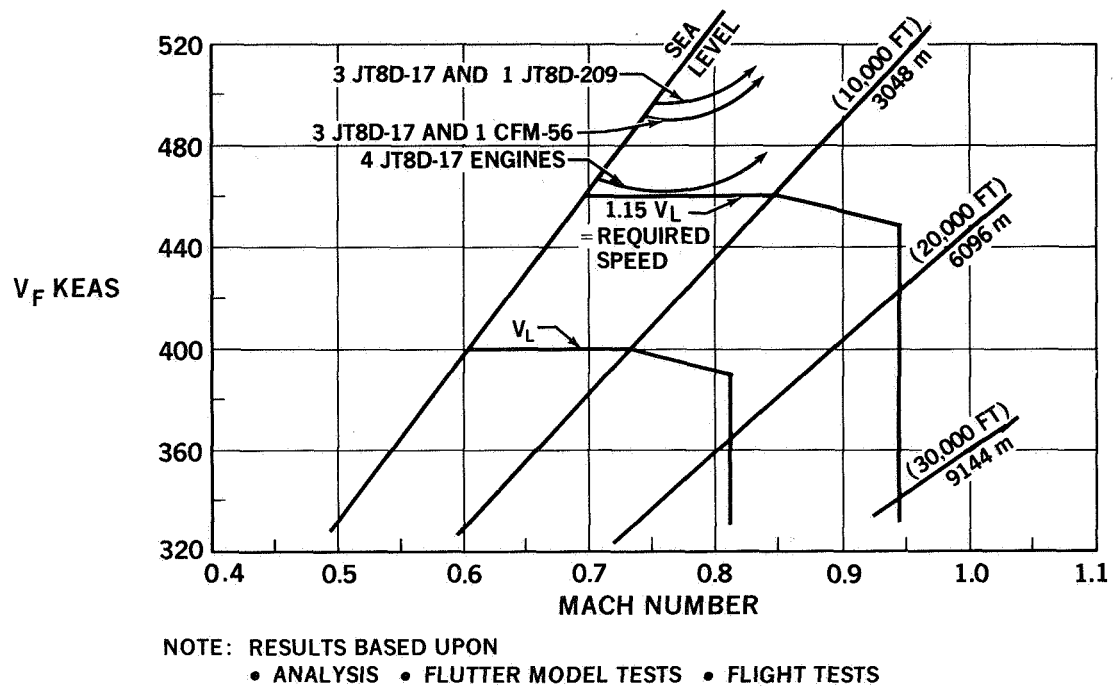

FIGURE 9. CFM56 ENGINE ON YC-15 POSITION 1

377

FIGURE 10. YC-15 FLUTTER BOUNDARIES

In the figure, the vertical axis is labeled V_F KEAS and the horizontal axis is labeled MACH NUMBER. Curve labels include "3 JT8D-17 AND 1 JT8D-209", "3 JT8D-17 AND 1 CFM-56", "4 JT8D-17 ENGINES", "1.15 V_L = REQUIRED SPEED", "V_L", "SEA LEVEL", "(10,000 FT) 3048 m", "(20,000 FT) 6096 m", "(30,000 FT) 9144 m".

NOTE: RESULTS BASED UPON
• ANALYSIS • FLUTTER MODEL TESTS • FLIGHT TESTS

4.7 cm (1.85 IN.)
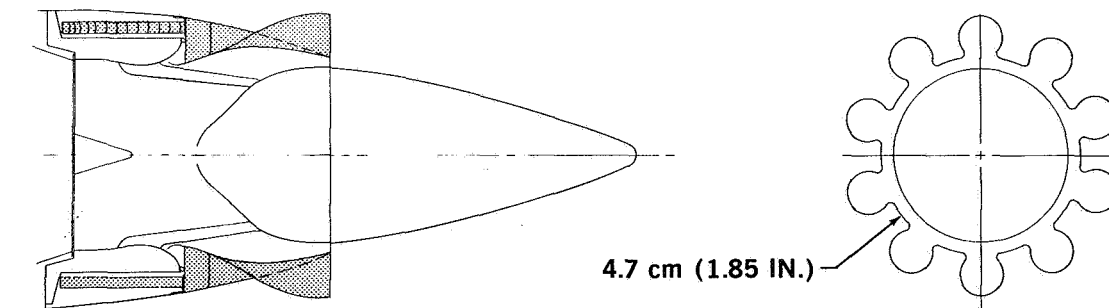
FIGURE 11. YC-15 DAISY EXHAUST NOZZLE

JT8D-17 — TAKEOFF THRUST — 21°C DAY
FREE JET
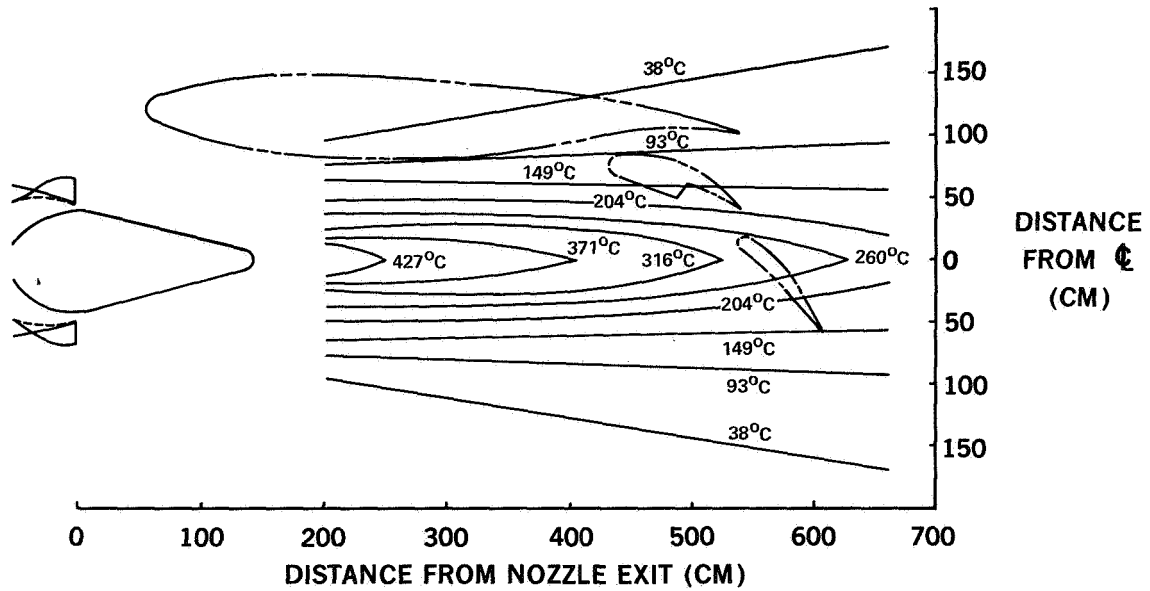
FIGURE 12. EXHAUST TEMPERATURE PROFILE
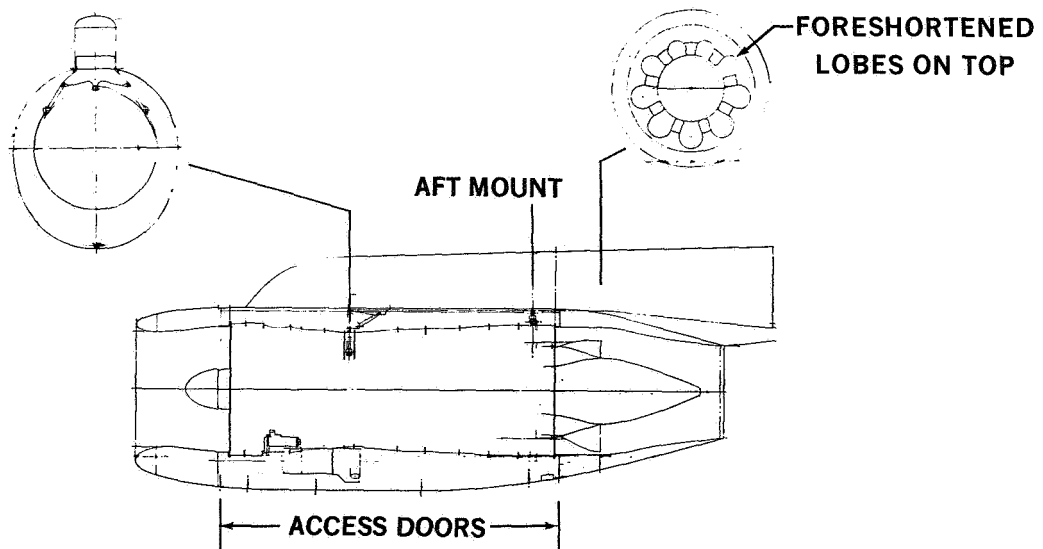
FIGURE 13. JT8D-209 ENGINE SECTION

REAR MOUNT

DAISY NOZZLE

FRONT MOUNT PLANE

ACCESS DOORS
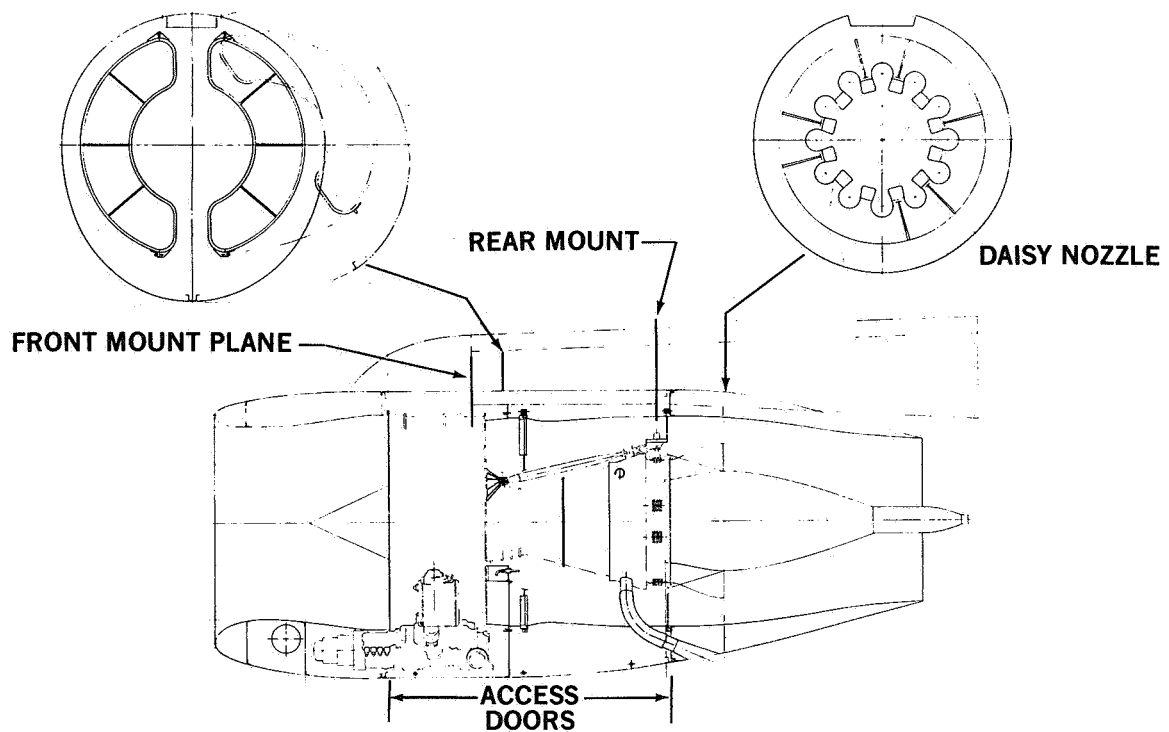
FIGURE 14. CFM56 ENGINE SECTION

REINGESTION SPEED DURING SLOWDOWN (KEAS)

UNIFORM BLADES

COMPACTED BLADES

REVERSE EFFECTIVENESS (PERCENT)
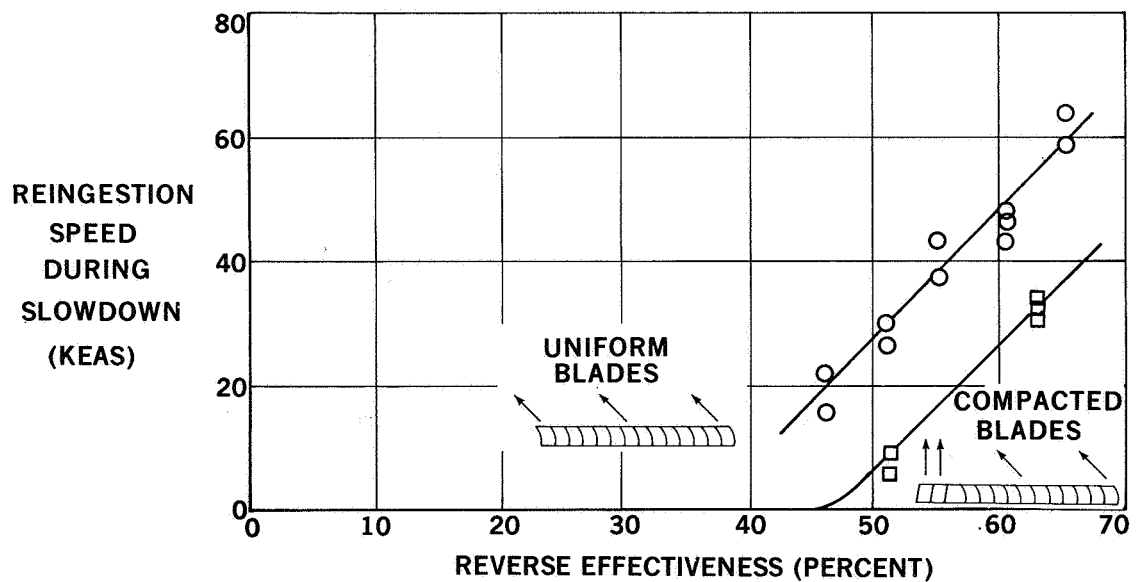
FIGURE 15. REDUCTION IN SELF-INGESTION SPEED BY CASCADE FLOW COMPACTION
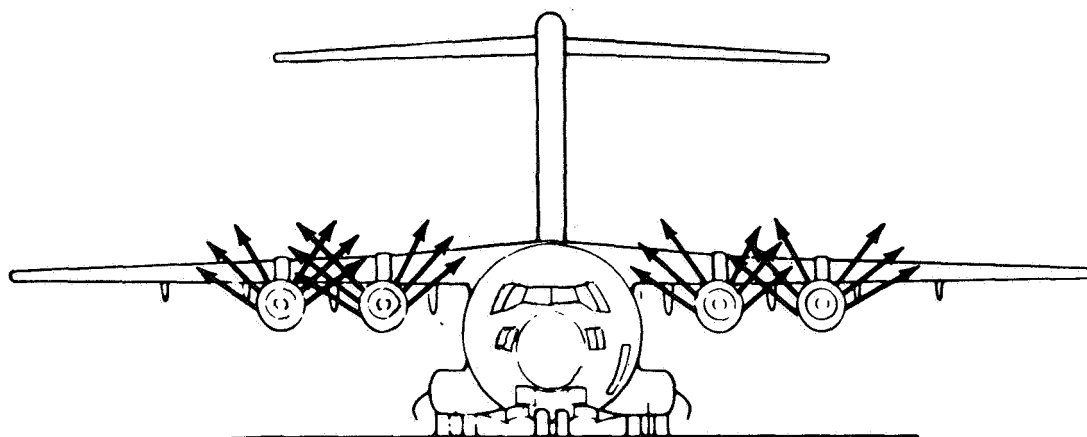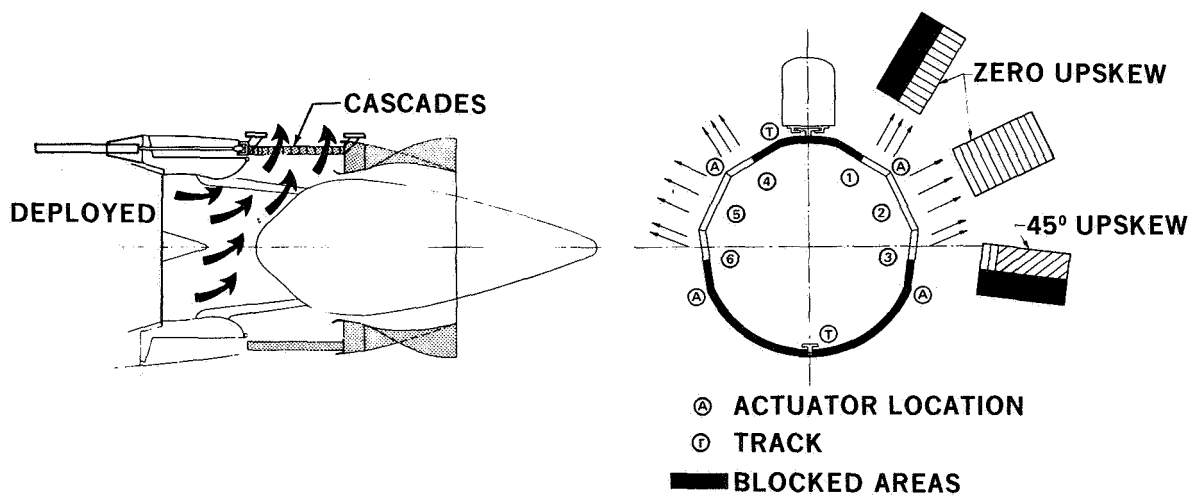
FIGURE 16. REVERSER FLOW VECTORING

CASCADES

DEPLOYED

ZERO UPSKEW

-45° UPSKEW

Ⓐ ACTUATOR LOCATION
Ⓣ TRACK
■■■BLOCKED AREAS

FIGURE 17. THRUST REVERSER/DAISY EXHAUST ASSEMBLY

381
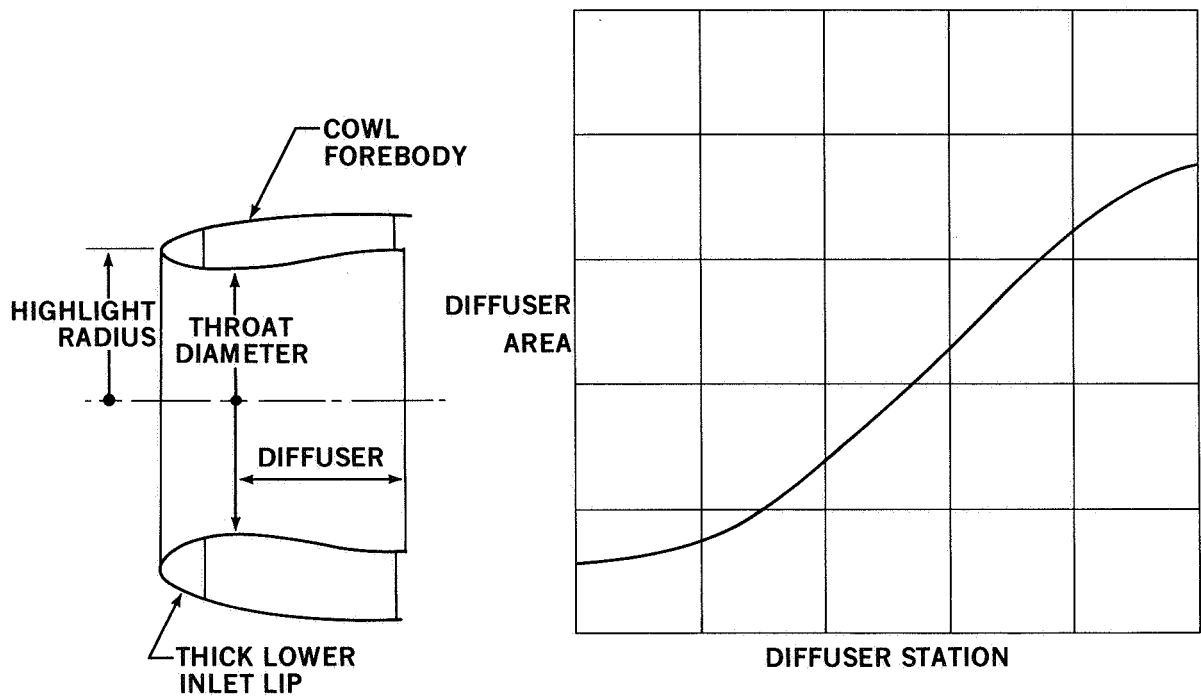
FIGURE 18. INLET GEOMETRY
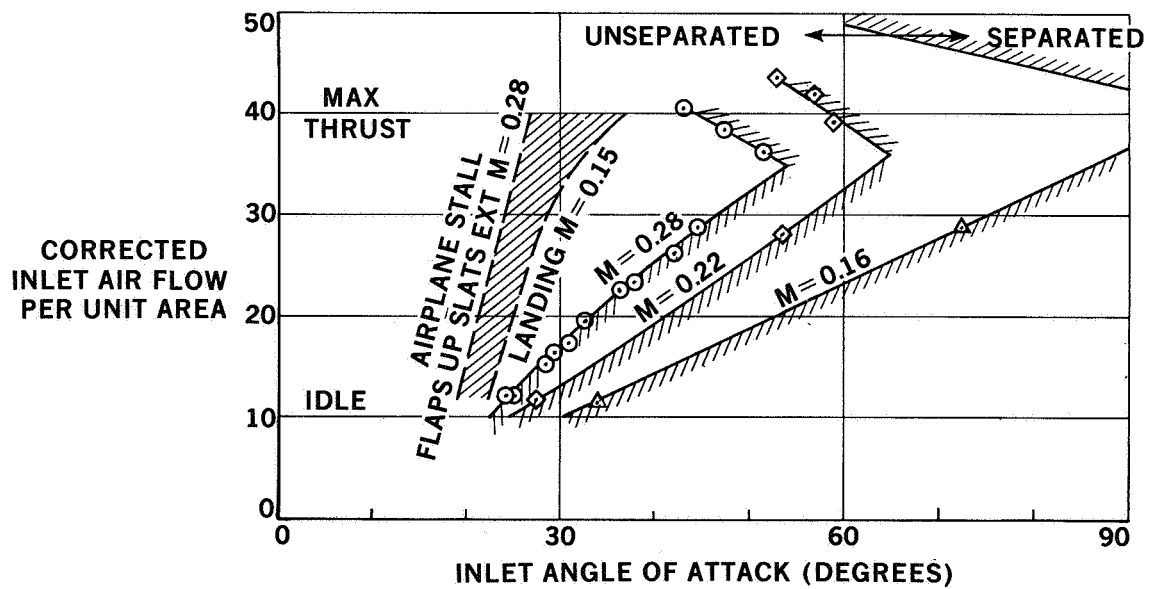
FIGURE 19. INLET SEPARATION BOUNDARIES BASED ON HIGH REYNOLDS
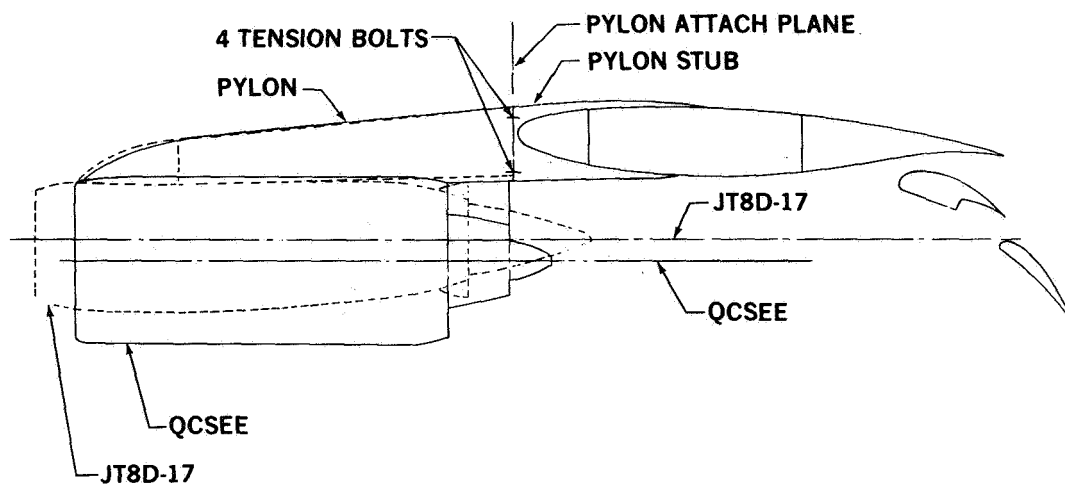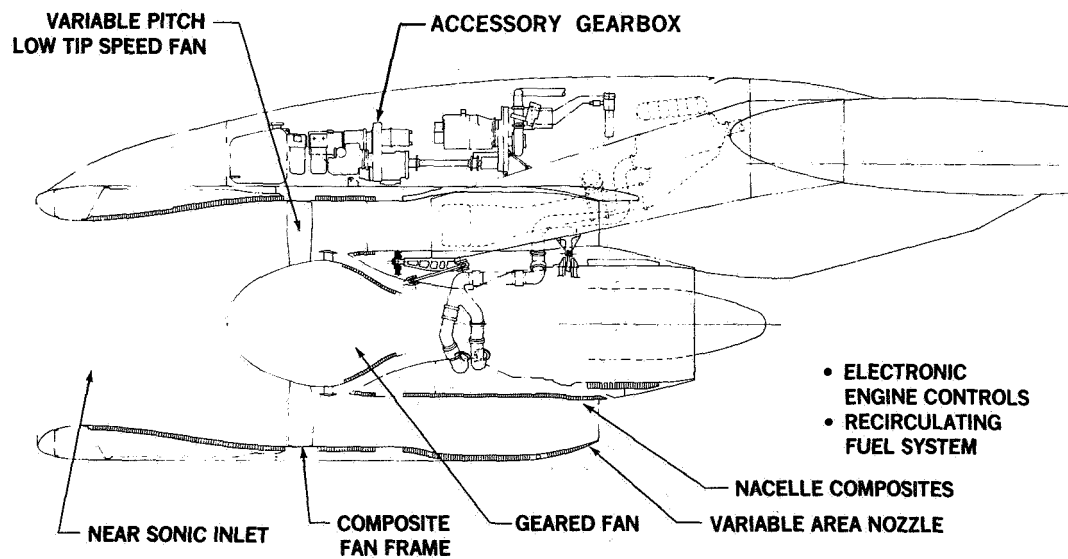NUMBER WIND-TUNNEL TEST

4 TENSION BOLTS
PYLON
PYLON ATTACH PLANE
PYLON STUB
JT8D-17
QCSEE
QCSEE
JT8D-17

FIGURE 20. QCSEE/WING RELATIONSHIP

VARIABLE PITCH LOW TIP SPEED FAN
ACCESSORY GEARBOX
- ELECTRONIC ENGINE CONTROLS
- RECIRCULATING FUEL SYSTEM
NACELLE COMPOSITES
NEAR SONIC INLET
COMPOSITE FAN FRAME
GEARED FAN
VARIABLE AREA NOZZLE

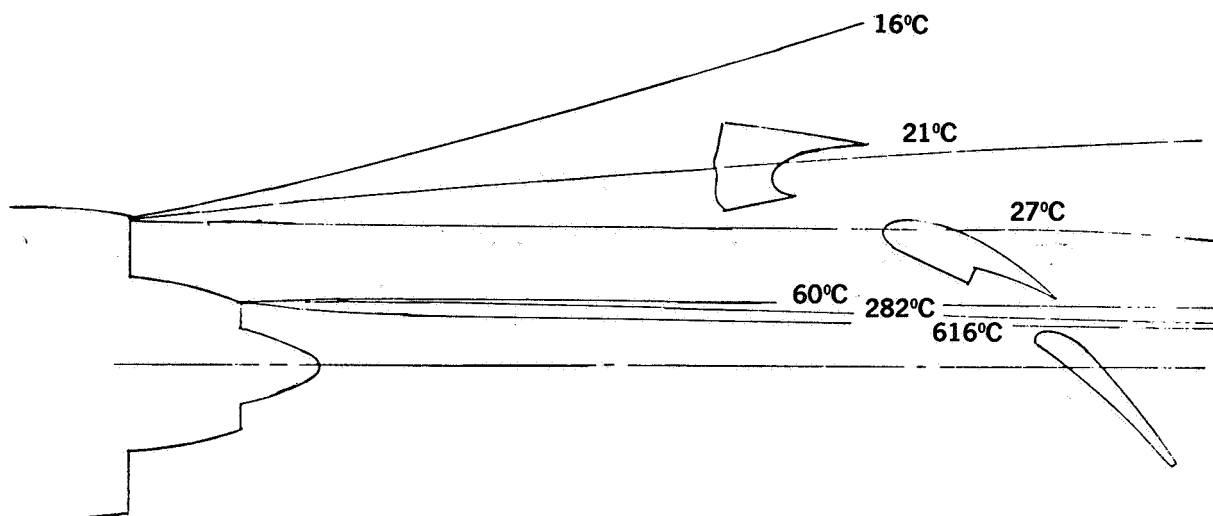FIGURE 21. QCSEE INSTALLATION

383

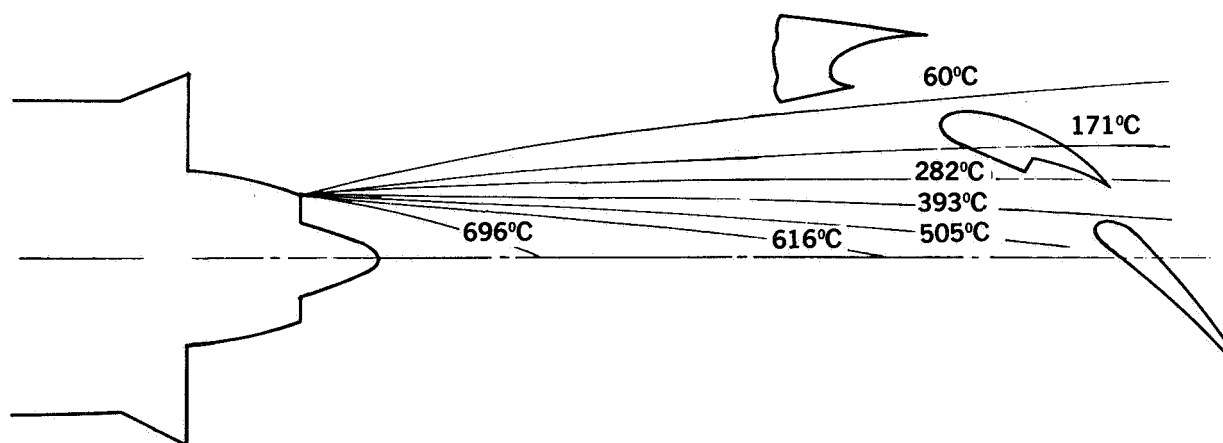FIGURE 22. FLAP HEATING — PROPULSIVE THRUST — GO-AROUND AT TAKEOFF
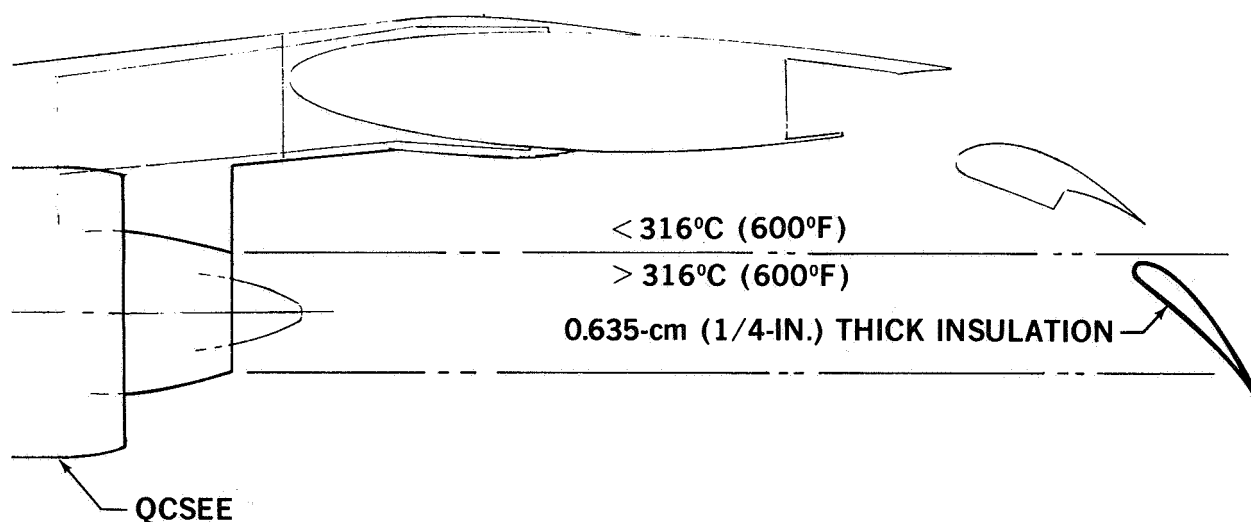POWER

FIGURE 23. FLAP HEATING — REVERSE THRUST

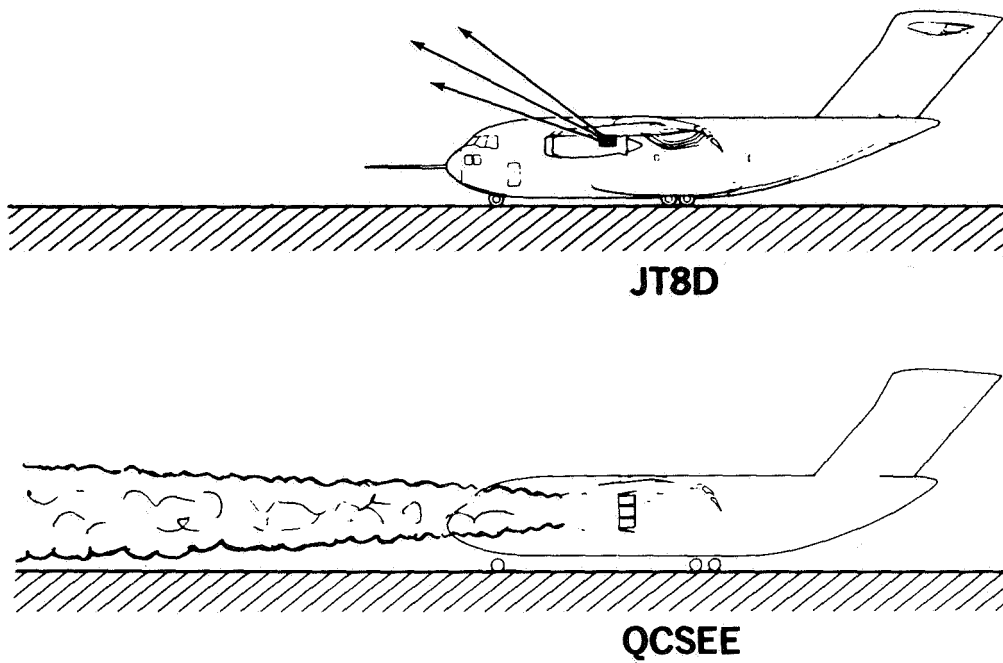FIGURE 24. THERMAL PROTECTION ON REAR FLAP
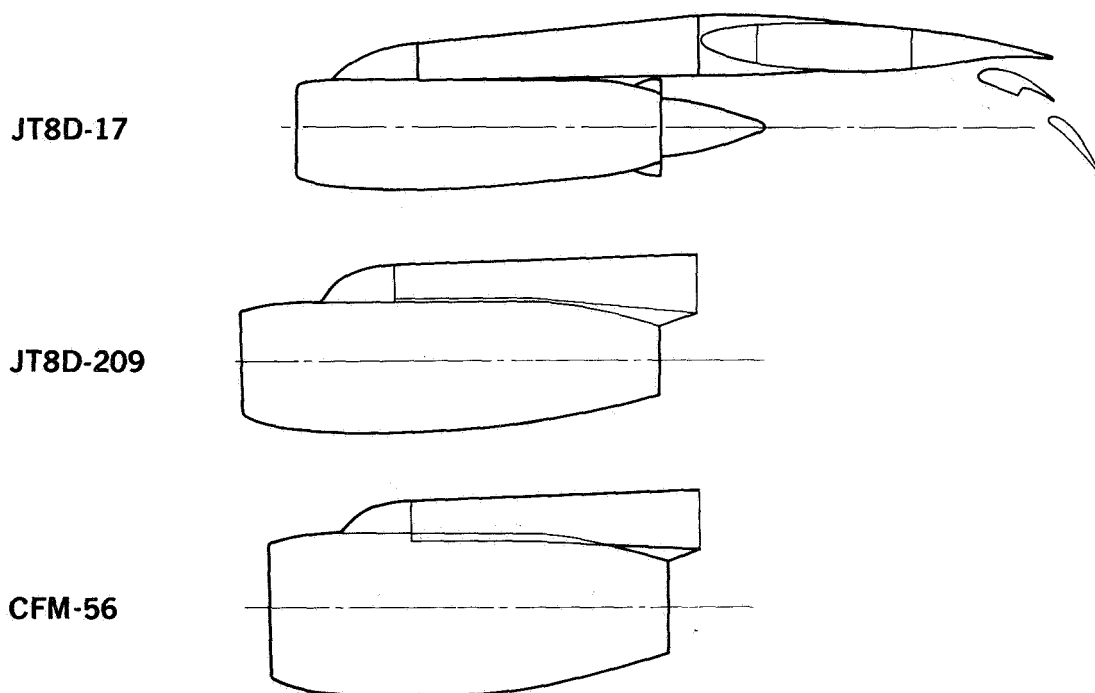
FIGURE 25. REVERSE OPERATION

FIGURE 26. YC-15 ENGINE INSTALLATION FLEXIBILITY

385

A REVIEW OF THE DESIGN AND ACOUSTIC CONSIDERATIONS
FOR THE TILT ROTOR AIRCRAFT

Martin D. Maisel,* James A. Weiberg,† and James H. Brown, Jr.*

Ames Research Center
and
Aeromechanics Laboratory
AVRADCOM   Research and Technology Laboratories

SUMMARY

Considerations of the hover and cruise mode effectiveness over a range of propulsive-lift-device hover disk loadings have resulted in recognition of the tilt rotor concept as candidate for many V/STOL applications. The NASA/Army XV-15 Tilt Rotor Research Aircraft, built to verify tilt rotor technology, is briefly described. Measured and predicted acoustic characteristics are presented for the XV-15 and tilt rotor in general. In addition, examples of potential civil and military missions are given.

INTRODUCTION

Up to the early 1960s the development of aircraft with VTOL or V/STOL capabilities focused on performance and handling qualities. As civil and military applications for VTOL aircraft (rotorcraft) increased, and as the utility of STOL aircraft became apparent in the evolving air transport system, other considerations, such as their acoustic signature, surfaced as significant factors in the design and, ultimately, the acceptability and economic success of these aircraft. This paper briefly discusses the general configuration, performance, and acoustic characteristics of one type of V/STOL aircraft, the tilt rotor, which is currently being investigated in a joint Army/NASA flight-research program.

V/STOL CONCEPT SELECTION

The efficiency of static (or hovering) propulsive lift, expressed in terms of lift capability per horsepower expended is illustrated in figure 1. The disk loading, defined as the thrust produced divided by the area of the propulsive surface (e.g., rotor disk area) is seen to be a major factor in static propulsive-lift performance. This is expressed by the momentum-energy relationship of a propulsive device which shows that moving a large quantity of air

---

*Aeromechanics Laboratory
†Ames Research Center

through a small velocity increment (as in the case of a helicopter rotor) requires less power to produce a given thrust level than moving a small quantity of air through a large velocity increment (e.g., turbofan propulsion). This allows relatively small engines to be used in large V/STOL aircraft, which pays off in reduced powerplant system weight and good hover fuel economy, as shown in figure 2 (ref. 1). Thus, for V/STOL applications where hover efficiency (duration) is important, the benefits of low disk-loading concepts must be considered since the advantages of low disk-loading more than offset the weight penalties associated with larger rotors and slow turning drive systems. Furthermore, the low axial-induced wake velocity inherently associated with low disk-loading propulsive lift may also influence concept selection if ground operations or unprepared field operations are factors (see abscissa of fig. 1).

The historical trend of the acoustic efficiency of propulsive lift devices (the audible noise energy generated by a propulsive lift system in hover divided by the total energy converted at the propulsive source) is depicted in figure 3 (from ref. 2). Although factors such as jet exhaust nozzle configuration, fan bypass pressure ratio, rotor tip speed, Mach number, blade thickness, tip shape, and number of blades greatly influence the noise level generated from any given propulsive-lift device, the general trend of this acoustic efficiency term indicates that the ability to produce lift at lower sound levels is improved at lower disk loadings.

In addition to hover capability, VTOL aircraft are required to provide desirable cruise-mode characteristics to satisfy civil or military requirements. Two important cruise-mode considerations are maximum speed and fuel efficiency which affect aircraft productivity, range, or endurance. Typically, as indicated in figure 4, the low disk-loading VTOL types that performed so well in hover are found to be extremely limited in cruise speed. The conventional helicopter encounters high oscillatory blade loads and a rapid increase in power required above 200 knots. While compound helicopters reduce the dependency on rotor lift in cruise and provide additional propulsive thrust, rotor hub drag rise and blade load limits are still serious problems above 240 knots. Of the low disk-loading concepts, the tilt rotor aircraft shows the most promise for the high cruise speeds required for intercity or executive transport and for military assault or reconnaissance applications. With the rotors tilted forward the flight characteristics and vibration levels of the tilt rotor would be similar to those of a fixed-wing turboprop aircraft. Furthermore, reducing the rotor tip speed in cruise to 70%-80% of its hover value benefits both the rotor acoustic efficiency (fig. 5) and the rotor propulsive efficiency as the large rotor would be very lightly loaded at moderate airplane-mode speeds. This variation of rotor speed also requires selective evaluation of the engine/rotor gear ratio since the specific fuel consumption of a gas turbine engine is optimum for only a narrow range of engine speeds.

XV-15 TILT ROTOR RESEARCH AIRCRAFT

Therefore, with the prospect of combining the desirable VTOL character-
istics of the helicopter and the cruise-mode characteristics of a turboprop
aircraft in one vehicle (see fig. 6), the National Aeronautics and Space
Administration (NASA) and the U. S. Army Research and Technology Laboratories
(RTL) of the U. S. Army Aviation R&D Command (AVRADCOM) jointly created the
Tilt Rotor Research Aircraft Project. The objectives of this activity include
the demonstration, through flight tests of the XV-15 research aircraft, of the
predicted performance, handling qualities, aeroelastic structural stability,
and environmental aspects of the tilt rotor. A brief description of the XV-15
follows.

The XV-15 Research Aircraft was designed to be the minimum size feasible
for investigation of the generic characteristics of, and the establishment of
meaningful design criteria for, potential tilt rotor aircraft. The aircraft
size selected for this project (fig. 7) also allows testing in the Ames 40-
by 80-Foot Wind Tunnel to collect baseline data for performance, loads, air-
craft stability and control, aeroelastic stability, and acoustics.

Design

The prominent features of the XV-15 configuration are the large diameter
rotors which are mounted on tiltable wing-tip nacelles. The wing is swept
forward slightly to provide clearance for rotor flapping in airplane-mode
flight. An H-tail configuration was selected to provide improved directional
stability around a zero yaw angle. The main landing gear retracts into pods
on the side of the fuselage located below the wing root. The nose gear
retracts into the fuselage nose section. Flight safety, achieved through
system redundancy, was an important consideration in the design of the XV-15.
In addition to propulsion system redundancies discussed below, the aircraft
is equipped with three hydraulic systems, two electrical systems, two fuel
systems, two flap drive systems, an emergency conversion system, an emergency
landing gear extension system, and an emergency egress system. The aircraft
is also equipped with multiple-axis stability and control augmentation systems,
a force-feel system, and an rpm governor system, all of which are redundant
and/or of limited authority to provide for a fail operational configuration.

Control System

The control system in hover and helicopter flight operates similar to that
of a tandem rotor helicopter (with the longitudinal and lateral axes inter-
changed). As illustrated in figure 8, fore and aft cyclic pitch provides
longitudinal control and, when differentially applied, provides yaw control.
Roll is obtained by the differential application of collective pitch. In
the airplane (cruise) flight mode, control is achieved with conventional
airplane control surfaces and engine throttle controls.

Propulsion System

The Tilt Rotor Research Aircraft propulsion system is illustrated in figure 9. Free turbine engines drive the rotors through transmissions located within the tilting nacelles. A cross-shaft system connects the transmissions in each nacelle and includes a gearbox in the center to accommodate the angular intersection of the left and right interconnect drive shaft.

Rotor— The XV-15 has two 7.62 m (25-ft) diameter, gimballed hub, three-bladed rotors. The 36 cm (14-in.) chord blades are constructed of 17-7 PH stainless steel skin bonded to a 17-7 PH stainless steel spar and aluminum honeycomb afterbody. The blade sections are NACA 64 series airfoils, 8% thick at the tip and 35% thick at the theoretical root. The blades are twisted approximately 40°. The highly twisted and cambered blades provide hover performance levels about 5% greater than that of the typical helicopter (fig. 10) and cruise propulsive efficiencies comparable to that of a turbo-prop aircraft. The rotor has cyclic and collective control through blade-pitch horns placed to provide positive pitch flap coupling ($-\delta_3$) for improved stability. Rotor speed is governor-controlled, producing tip speeds of 225 m/sec (740 ft/sec) in hover and 183 m/sec (600 ft/sec) in cruise.

Transmission and cross shafting— Power is transmitted from the engine to the rotor through a coupling gearbox and the main transmission. The main structural components of this assembly are the transmission castings and the steel spindle, which serves as the axis about which the nacelle rotates. The engine is cantilevered from its front inlet flange which attaches to the coupling gearbox casting. The nacelle cowlings are supported by the trans-mission case.

The transmissions consist of a herringbone gear train and a two-stage planetary gear assembly. The transmissions provide a reduction from an engine speed of about 24,000 rpm to a rotor shaft speed in hover of 565 rpm. High-helix-angle, fine-pitch herringbone gears in the high-speed train reduce friction loss and noise. Damping rings on the herringbone gear rims reduce "cymbal" resonant modes. The planetary systems are also low-friction, low-noise, high-contact-ratio, relatively fine-pitch gears. The planetary ring gears are loosely splined into the external cases. The interconnect drive system is driven through a spur gear set and a bevel gear set in each main transmission. Both rotors are always directly connected through the inter-connect drive train and the planetary gears. Accessories are driven off the interconnect system through a spur gear train in the main transmission. An overruning clutch is provided in the high-speed herringbone train to disengage the engine in the event of a power failure. The interconnect system is linked to the rotor side of the one-way clutch so that power to both rotors is avail-able with either engine shut down. The transmissions are rated at 1325 hp input and 1166 hp output to the mast at the hover rpm.

Engines— Two T53-L13B turboshaft engines modified to a LTC1K-4K config-uration power the Tilt Rotor Research Aircraft. The modifications provide direct drive, vertical starting, operating and stowing capability, and allow higher speeds and higher temperatures in the power turbine and gas-producer turbine sections.

390

TILT ROTOR ACOUSTICS

The principal noise sources of the tilt rotor aircraft are the wing-tip-mounted engines, transmissions, and rotors. Preliminary test results and experience with helicopters indicate that the rotors are the dominant source of external noise for hover and helicopter-mode operation of the XV-15. While this conclusion has not been empirically supported for all tilt rotor flight modes, this paper will focus on rotor-generated noise.

Unlike most helicopters, which have engines, transmissions, drive shafts, and accessories mounted in or adjacent to the fuselage, the tilt rotor's configuration allows considerable separation and isolation of these noise generators from the cabin and crew station. Therefore, for the internal noise case the discussion will also be primarily concerned with the rotor-source noise.

Near Field

The effect of the proximity of the rotor planes to the crew station and airframe is considered in this section. In hover, the crew station is located closer to the rotor tip paths than would be found on most single rotor helicopters, and similar to the distance found on tandem helicopters, such as the CH-47. Preliminary noise data taken in the XV-15 crew station during ground testing at design gross weight hover power show rotor broadband sound levels comparable to the cabin of an untreated helicopter. Without acoustic treatment this noise level requires the use of flight helmets or earphones for crew communication and comfort during sustained hover operations. Higher frequency drive system and engine pure tones were also identified in the spectrum but were found to be no greater than those found inside civilian helicopters with soundproofed interiors.

Civil missions that include considerable hover time, or where passenger acceptance is important, will require special acoustical treatment due to the low-frequency content of the acoustic signal. Since harmonics of the blade-passage frequency are expected to dominate the interior noise spectrum, advanced low-frequency attenuation methods, such as double "limp wall" (ref. 3) or "tuned-structure with damping" techniques, may be desired for maximum noise reduction.

Several differences between the conventional helicopter and the tilt rotor, which are noted below, make it difficult to confidently extend current helicopter near-field acoustic methodology or empirical data to the tilt rotor case.

	Helicopter	Tilt rotor	Effect
Rotor disk	Over fuselage	Over wings	Rotational noise, blade passage pressure impulse
Hover-induced velocity	Low	Higher	Broadband noise
Blade twist	Low (8° – 16°)	High (30° – 45°)	Spanwise blade lift distribution, tip vortex strength
Rotor configuration			
Single main rotor	Tail rotor	No tail rotor	Rotational noise
Tandem rotor	Overlap	No overlap	Impulsive noise

Near-field acoustic data will be collected during the XV-15 flight test program to determine the validity of existing analytical techniques and to provide empirical correlation factors.

In the airplane mode the configuration resembles a turboprop aircraft with the exception of the tip speed and blade spanwise loading (both lower for the tilt rotor). Studies of acoustic fatigue on the fuselage skins showed that the sound pressure levels were extremely low and no special structural consideration was required. As a result of the low tip speeds and blade loadings, the interior cabin noise levels are expected to be moderate at normal cruise velocities.

Far Field

Noise measurements of a single XV-15 rotor were first made in 1973 during hover performance tests on the Aero Populsion Laboratory whirl stand at Wright Patterson Air Force Base (ref. 4). Data from that test, corrected for two rotors, is presented in figure 11 along with XV-15 data collected during subsequent ground and hover tests, and tests in the Ames 40- by 80-Foot Wind Tunnel. The peak perceived noise level measured during XV-15 ground and hover tests correlated well with the projection to 152 m (500 ft), based on a 6 PNdB decrease per doubled distance and with atmospheric absorption at a 40% relative humidity level.

The XV-15 hover noise level is compared to the noise produced by various helicopters in figure 12. The tilt rotor data fall at the lower boundary of the helicopter noise band. It is interesting to note that the 5900-kg (13,000-lb) XV-15 was as quiet as the 1225-kg (2700-lb) Bell Jetranger used as a chase aircraft during hover tests.

The effect of tip speed on far-field hovering noise level is illustrated in figure 13. At the XV-15 design hover tip speed the noise generated at various gross weights is shown in figure 14. The trends are comparable to helicopter noise sensitivities to thrust (see fig. 12) and tip speed.

In the airplane mode, the low tip speed and low blade span loading result in an exceptionally quiet cruising aircraft. For a flyover at 305 m (1000 ft) and 370 km/hr (200 knots), a ground observer would measure noise levels no greater than 63 PNdB and would be exposed to 55 PNdB or greater for less than 8 sec. This is below the daytime level of urban residential area noise.

Community Impact

The predicted XV-15 noise level observed at a ground station located 1 n. mi. from a liftoff/touchdown point is shown in figure 15 for typical departure and approach operations in the VTOL and STOL configurations. Because of the directional characteristics of the rotor acoustic signature, the sound of the tilt rotor flying overhead will build up and fall off in a short time. The time history predictions indicate that noise levels, at the maximum STOL gross weight, will not exceed 77 PNdB for the STOL approach or 81 PNdB for the STOL departure. For VTOL operations, peak noise levels are predicted to be 75 PNdB for approach and 72 PNdB for departure. The design gross weight VTOL takeoff and landing footprint is shown in figure 16. Although the XV-15 flight- test program will investigate a variety of arrival and departure profiles, for this analytical case, steep departure and descent angles were used, consistent with maintaining best one-engine-inoperative speed for safety. During departure, the analysis assumes that the aircraft first hovers, then accelerates to 111 km/hr (60 knots) at 61 m (200 ft). Climbout is then made in the helicopter mode at climb power at a 75° pylon angle. The approach is initiated at 610-m (2000-ft) altitude with a 90° pylon angle. Descent is performed at minimum power in an autorotational mode with the pylon angle at 95°. Power is applied prior to touchdown and final descent is made in the helicopter hovering mode. The estimated 95 PNdB contour encloses about 0.21 km^2 (0.08 miles^2) of ground surface. The predicted noise footprint for the XV-15 operating at its maximum STOL gross weight of 6800 kg (15,000 lb) from an airport at an elevation of 1524 m (5000 ft) is shown in figure 17. The area exposed to 95 PNdB and above for this STOL condition is about 0.41 km^2 (0.16 miles^2).

POTENTIAL TILT ROTOR APPLICATIONS

The tilt rotor aircraft has been evaluated and compared to other V/STOL aircraft types by industry and government for various civil and military applications. While optimization and selection criteria often stress performance and economy factors, the tilt rotor aircraft sized for these applications often offers desirable noise levels as well.

Civil

A NASA sponsored study of commercial VTOL transports that utilize rotors was conducted in 1974 by the Boeing Vertol Company, Bell Helicopter, and Sikorsky (refs. 5-7). One hundred-passenger VTOL rotorcraft were sized to perform a short haul 370 km (200 n. mi.), mission with reserve capability for terminal area maneuvers and holds. Single main, tandem, and compound helicopters were compared with tilt rotor configurations. Most of these baseline designs were reconfigured to show the effect of increased or decreased noise levels at the hover condition on costs and operation factors. Figure 18 illustrates some of the results of this study.

Operating costs— The tilt rotor, operating at higher disk loadings, generated more noise in hover at a given tip speed than the helicopter or compound designs. However, for designs predicted to produce equivalent sideline noise levels in hover, the increased cruise speed and propulsive efficiency of the tilt rotor results in a significant reduction of block time and direct operating cost per seat mile compared to the helicopter. In this example, the tilt rotor's block time is about half that of the helicopter (0.75 hr compared to 1.45 hr) and the DOC is about three fourths of the helicopter's cost (approximately 2.3 cents per seat mile compared to the helicopter's 3.2 cents per seat mile in 1974 dollars). While the compound helicopter block time (0.95 hr) closely approaches the tilt rotor's capability, its DOC is comparable to that of the helicopter. In addition, some analyses indicate that the ground area exposed to 95 PNdB or greater during helicopter landings or takeoffs may be about twice as large as would be affected by the tilt rotor operations due to the helicopter rotor bang phenomenon (which could be averted by tilt rotor nacelle incidence variation).

The tilt rotor aircraft also shows considerable promise in view of the energy expended. Figure 19 shows the estimated block fuel required for the commercial VTOL mission previously discussed. A comparison of configurations that produce equivalent hovering noise levels shows that the tilt rotor requires only about two thirds of the fuel required by the helicopter designs for this mission.

The overall efficiency of a design point tilt rotor and a design point helicopter, expressed in terms of productivity ratio (payload × block speed/ empty weight) is presented in figure 20. Clearly, for the short range mission of 80 to 500 km (about 50 to 300 miles), such as oil rig resupply, the tilt rotor is superior.

Ride qualities— In addition to the benefits discussed above, the tilt rotor aircraft will offer cruise-mode ride characteristics comparable to a turboprop airliner. Edgewise-helicopter-rotor oscillatory loads will not be present and the wing will provide some engine/transmission/rotor vibration attenuation. During takeoff and landings, there will be some rotor-induced vibration, but it will be at a low level, equal to or better than that of the smoothest riding helicopter. After tilting over to the airplane cruise mode, rotor-induced vibration will be very low. Gust response of the wing will also be at a low level because high wing loadings (with their insensitivity to gusts) can be used since the wing is not sized by takeoff and landing require-

ments. Gust response of the rotor has been of some concern, but this area is expected to be researched during the XV-15 program.

Component life— The tilt rotor aircraft operates in the helicopter regime of flight a very small portion of its total operating time. The XV-15 can accelerate from a hover to airplane cruise flight in 30 sec; conversion time is 12 sec. In a civil operation approach and departure, times would be lengthened to several minutes as dictated by airport and traffic control procedures, but still, helicopter time would be only a small portion of total flight time. This means that the rotor and other components subject to vibratory and fatigue loading would have greatly extended TBO's and service lives in comparison to their counterparts on helicopters which are subject to these vibratory loads for their total flight time.

Military

Many existing military mission applications would benefit from the rapid response characteristics resulting from the combination of VTOL capability and cruise performance in the 300-knot speed range. The tilt rotor would also result in longer ranges and increased endurance for a given fuel load than are obtainable with current helicopters.

Search and rescue— One obvious mission application is search and rescue. This mission requires a rapid response and extended range capability and a loiter capability in the search area (see fig. 21). With variable pylon angles, the tilt rotor can search at the airspeeds required by the conditions. For example, for an ocean search, where the area is large and open, the airspeed would be higher than for a search over a forested area. During the rescue, extended hover out of ground effect may be necessary. The tilt rotor, with its low disk loading and low downwash velocities, would be well suited for this operation.

Reconnaissance and surveillance— Reconnaissance and surveillance missions require many of the same capabilities as the search and rescue mission, but with some additional requirements. The on-station loiter for a surveillance mission takes advantage of the same capability used during the search. In addition, this vehicle would have the low-speed agility and ability to operate in the nap-of-the-earth near enemy front lines where operations as a conventional fixed-wing aircraft could be hazardous. The absence of a tail rotor will be beneficial in reducing the noise and radar signature of the tilt rotor. Because most of the engine power is transferred to the rotor, the IR signature of the vehicle will be minimal and easily suppressible.

The limited number of vehicles required for either search and rescue or reconnaissance and surveillance by any one service places a barrier in the way of full-scale development. The Department of Defense would be required to coordinate such an effort in order to make it affordable.

Logistics and utility— The good productivity potential of the tilt rotor makes it a likely candidate for logistics missions of all three branches of the

395

U. S. military. The ability to disperse aircraft landing areas and the elim-
ination of the need for runways would give an added degree of flexibility. It
is envisioned that a light transport in the 13,500 to 22,500 kg (30,000 to
50,000-lb) class would be developed first before proceeding with larger and
heavier sizes.

Another potential application is to the utility mission (fig. 22). An
example of a variant of this type is the Marine assault (CH-46 replacement)
aircraft. This vehicle must provide a rapid response time for delivery of
first-wave troops and supplies plus a high productivity resupply capability
for subsequent waves. Efficient hover is required to allow emergency vertical
landing capability shortly after takeoff with full payload. For the important
support element of a diversified mission, the high altitude cruise-mode
efficiency of the tilt rotor aircraft enables cost-effective cargo transpor-
tation. Configurations with stoppable and stowable rotors with cruise fans
are being considered for enhanced cruise-mode capabilities for applications
of this type. Additional illustrations of potential military useage of the
tilt rotor are presented in reference 8.

CONCLUSION

Evolving military and civil V/STOL short-range missions which require
both efficient hover-mode operation and productive or cost-effective cruise
flight provide strong incentives for the development of the tilt rotor air-
craft. Compared to the helicopter, the tilt rotor offers improved ride
qualities, block time, maximum speed, and fuel economy; in addition, there is
a potential for reduced maintenance. Its hover and low-speed flight character-
istics are superior to any higher disk-loading VTOL concept. In addition, the
tilt rotor's noise signature is expected to meet terminal area criteria set
for rotorcraft and will not be a community disturbance factor during airplane-
mode operations.

REFERENCES

1. Kingston, L.; and De Tore, J.: Tilt Rotor V/STOL Aircraft Technology.
    Paper 36, Second European Rotorcraft and Powered Lift Aircraft
    Forum, Bückeburg, Federal Republic of Germany, Sept. 1976.

2. Stepnewski, W. Z.; and Schmitz, F. H.: Noise Implications for VTOL
    Developments. SAE 700286, April 1970.

3. Hopkins, J. P.; and Wharton, H. E.: Study of the Cost/Benefit Tradeoffs
    for Reducing the Energy Consumption of the Commercial Air Transportation
    System. Lockheed California Company, LR27769-2, NASA CR-137926,
    Aug. 1976.

4. Full Scale Hover Test of a 25-Foot Tilt Rotor. Bell Helicopter Company
    300-099-010, NASA CR 114626, May 1973.

5. Magee, J. P.; Clark, R.; and Alexander, H.: Conceptual Design Studies of 1985 Commercial VTOL Transports that Utilize Rotors. Boeing Vertol Company D210-10858, NASA CR 137599, Nov. 1974.

6. DeTore, J. A.; and Sambell, K. W.: Conceptual Design Study of 1985 Commercial Tilt Rotor Transports. Volume 1, VTOL Design Summary. Bell Helicopter Company Report Number D312-099-002, NASA CR 137602, Nov. 1974.

7. Kefford, N. F. K.; and Munch, C. L.: Conceptual Design Study of 1985 Commercial VTOL Transports that Utilize Rotors. Sikorsky Aircraft Division of United Aircraft Corporation, SER-50891, NASA CR 2532, Feb. 1975.

8. Brown, J. H., Jr.; and Edenborough, H. K.: Evaluation of the Tilt Rotor Concept - the XV-15's Role. AGARD Symposium on Rotorcraft Design, Paper 16, May 1977.
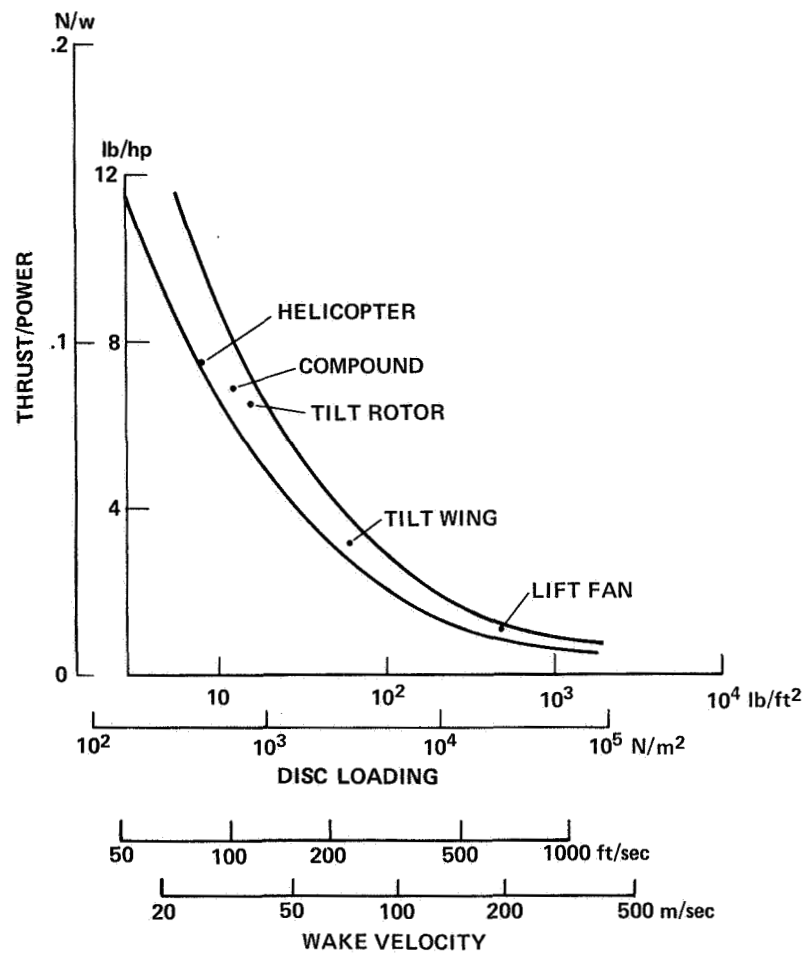
Figure 1.— Hover efficiency for various aircraft types.
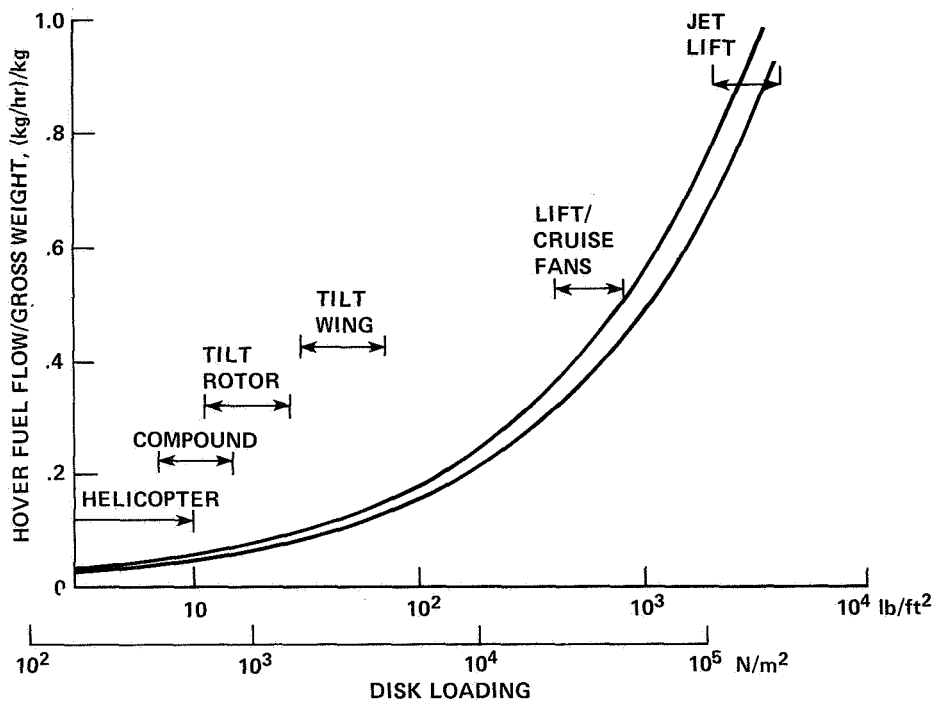
Figure 2.— Hover fuel-flow fractions of V/STOL aircraft.
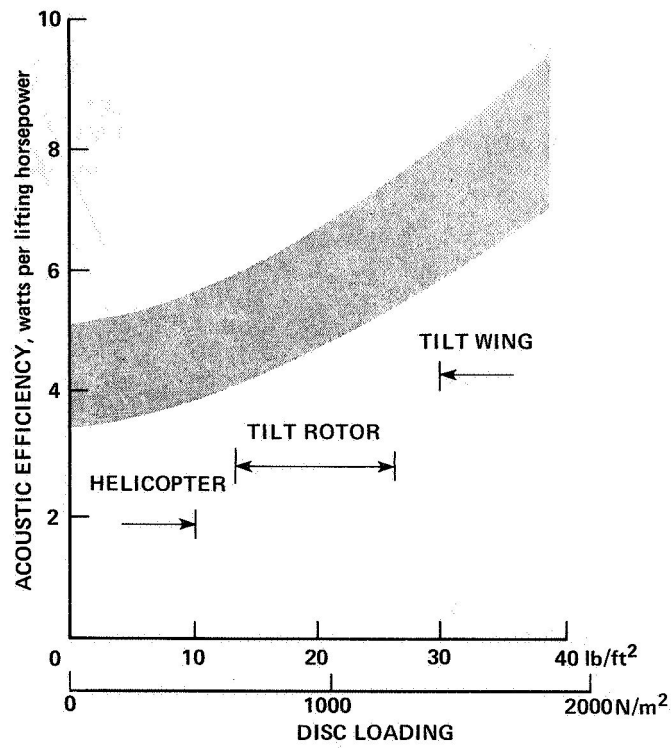
Figure 3.— Acoustic efficiency in hover vs disc loading for V/STOL and rotor-craft propeller.
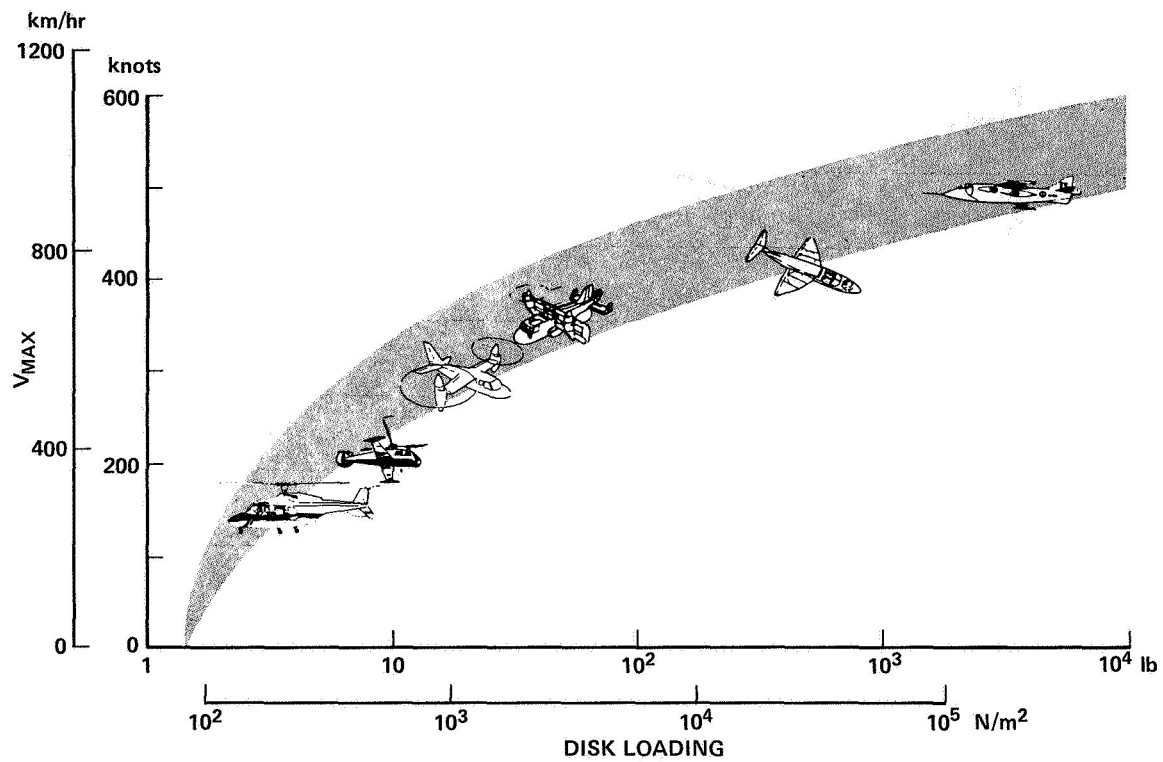
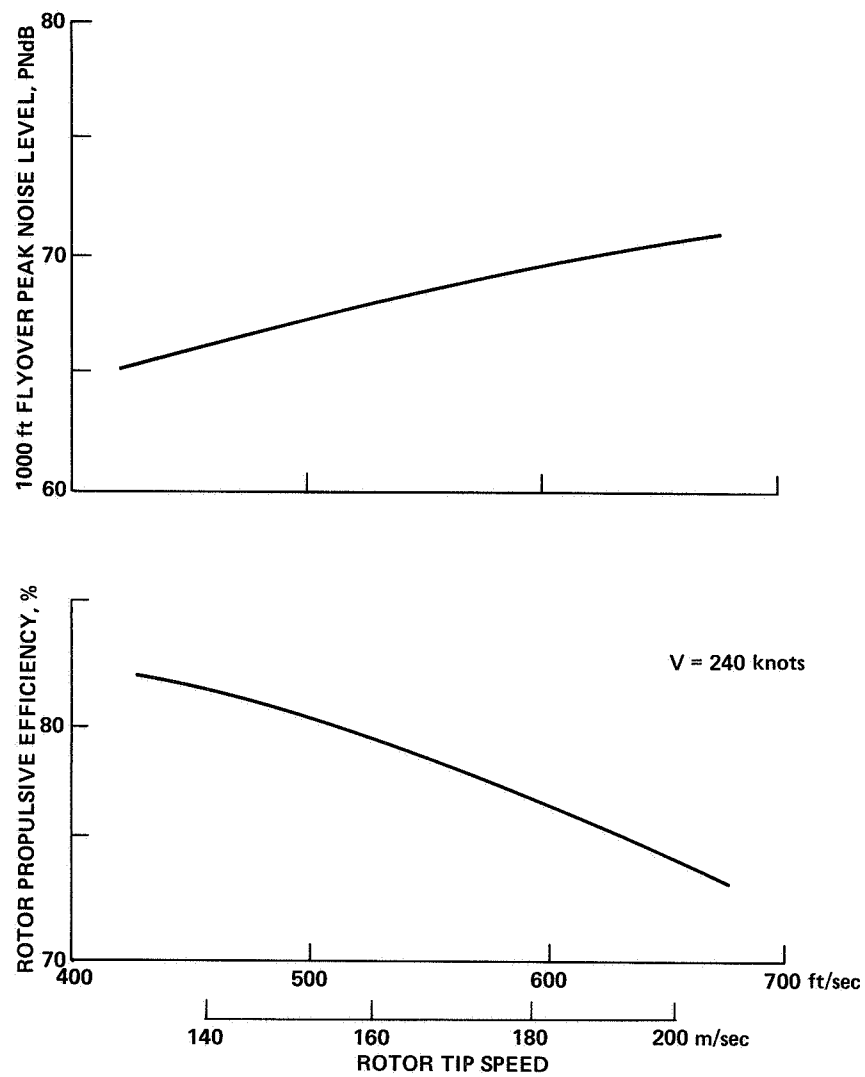Figure 4.— Cruise mode performance of subsonic VTOL aircraft.

Figure 5.— Airplane-mode rotor efficiency and noise trends with tip speed.
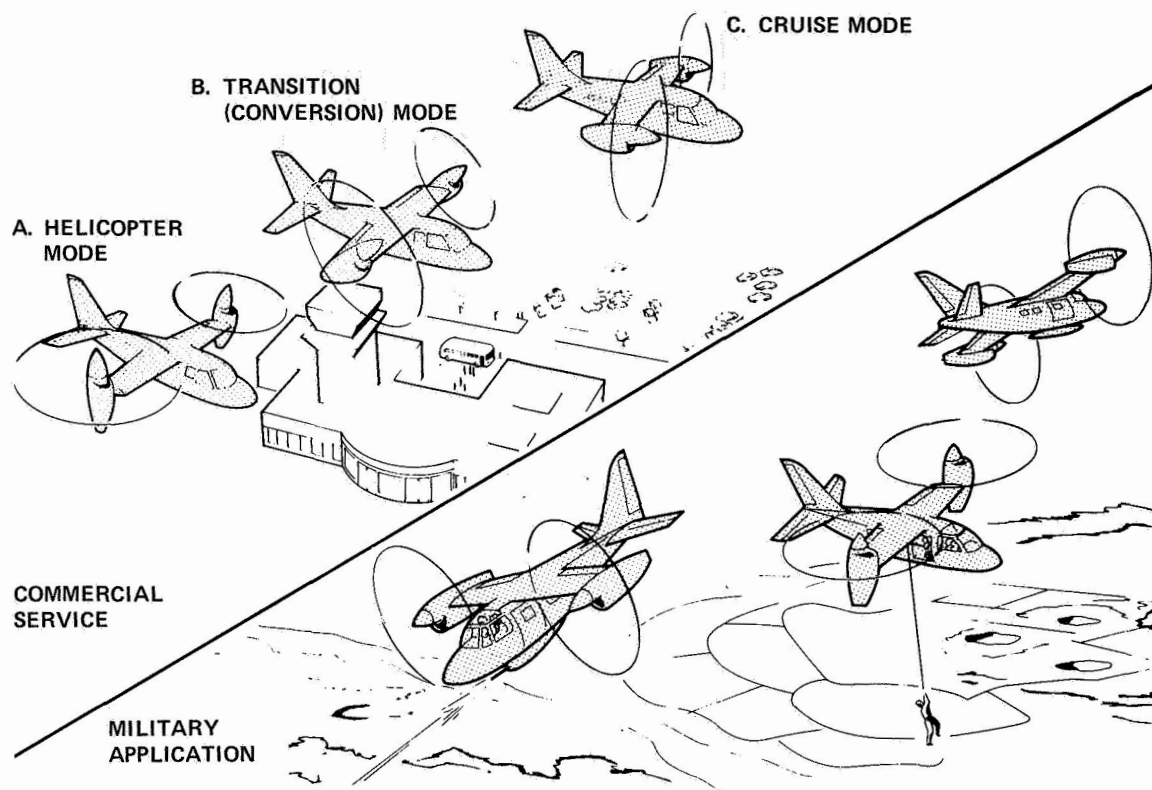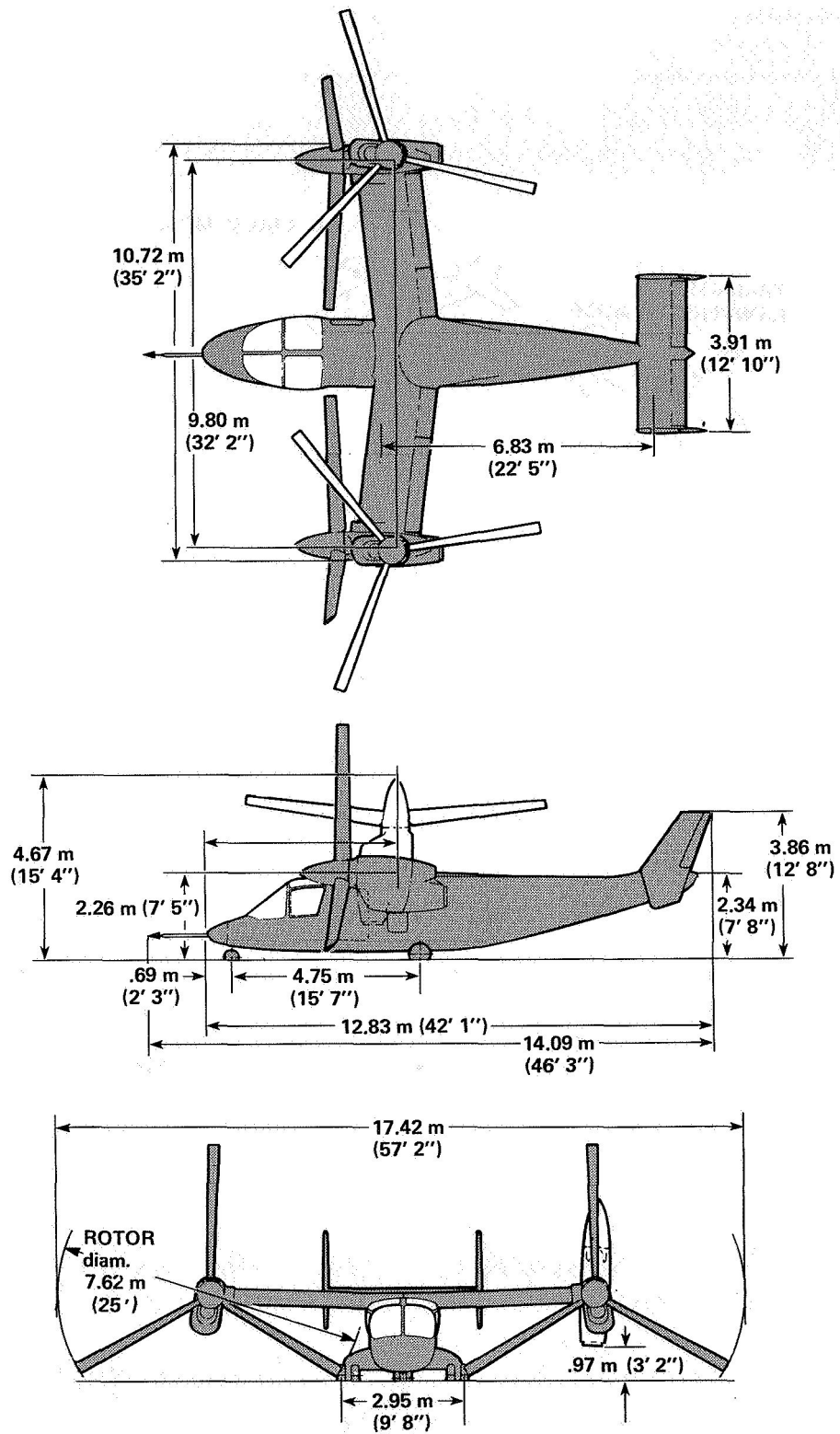
A. HELICOPTER MODE

B. TRANSITION (CONVERSION) MODE

C. CRUISE MODE

COMMERCIAL SERVICE

MILITARY APPLICATION

Figure 6.— Tilt rotor aircraft flight modes.

403

Figure 7.— XV-15 geometry.

404

VERTICAL CONTROL

ROLL CONTROL

PITCH CONTROL

YAW CONTROL
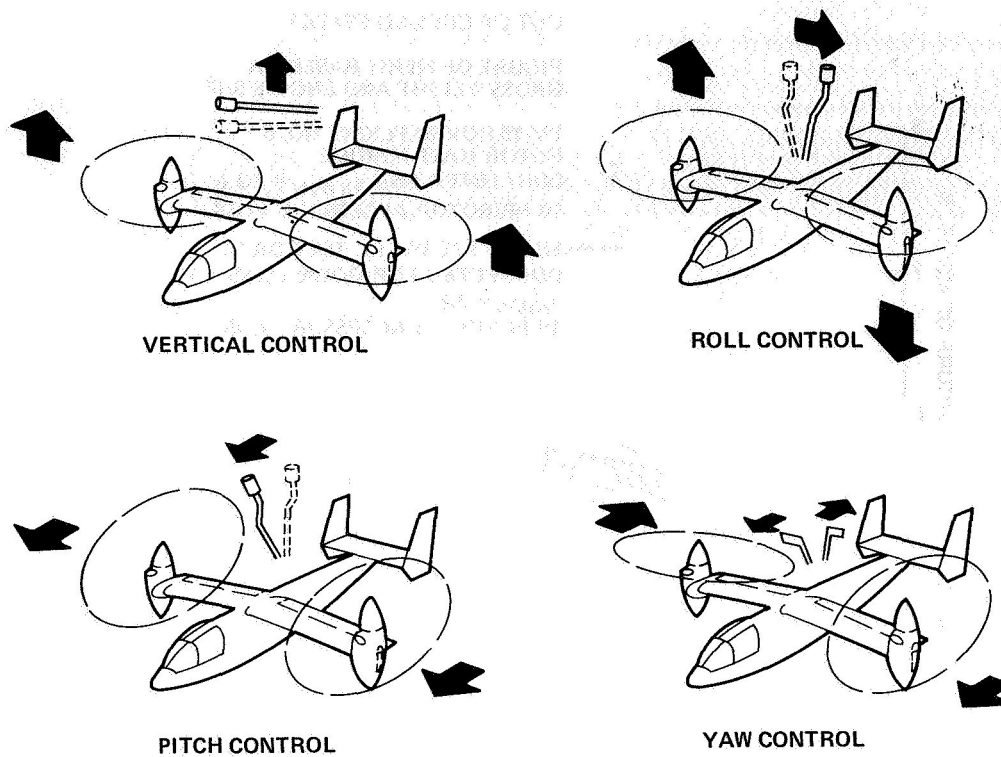
Figure 8.— XV-15 helicopter-mode control system.

ROTOR MAST

INPUT HERRINGBONE
GEAR STAGE

TWO PLANETARY
STAGES

INTERCONNECT DRIVESHAFT

CENTER GEARBOX

BEARING HANGERS

FREE TURBINE ENGINE

COUPLING GEARBOX
HERRINGBONE GEARS
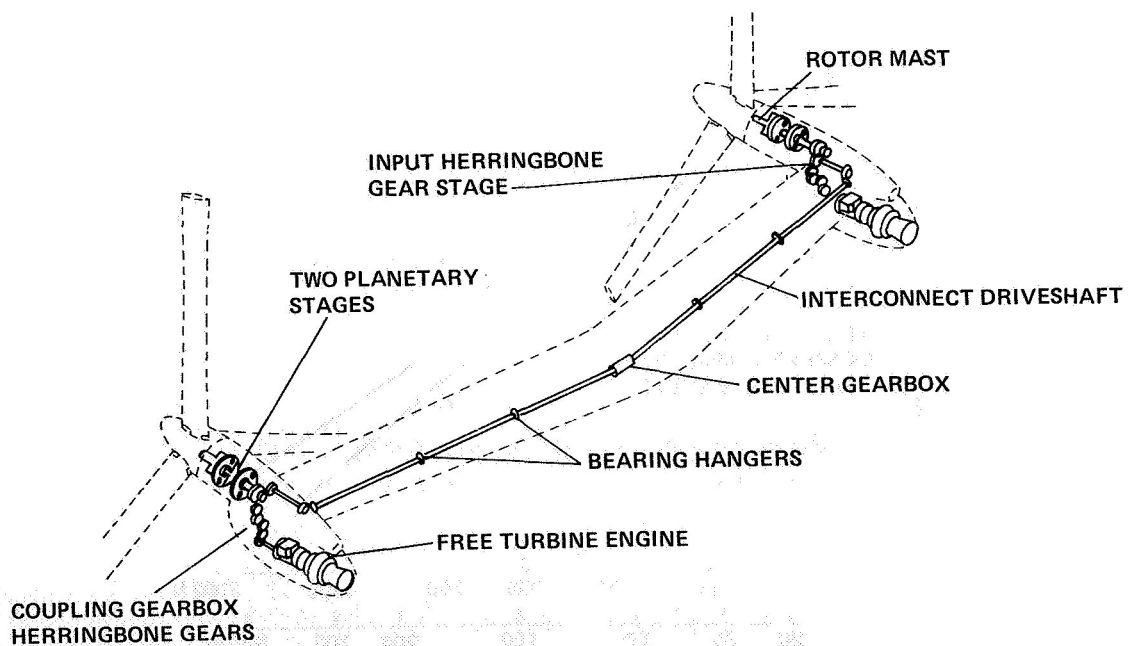
Figure 9.— XV-15 propulsion system.

OUT OF GROUND EFFECT

FIGURE OF MERIT BASED ON
GROSS WEIGHT AND ENGINE SHP

XV-15 HOVER FLIGHT NO. 5
ROTOR MAST TORQUE
CORRECTED FOR $\eta_{X\ MSN}$ = .93 &
10 HP/ROTOR ACCESSORY LOSS

WPAFB APL WHIRL TEST DATA
CORRECTED FOR DOWN LOAD = 7%
$\eta_{X\ MSN}$ = .93
10 HP/ROTOR ACCESSORY LOSS
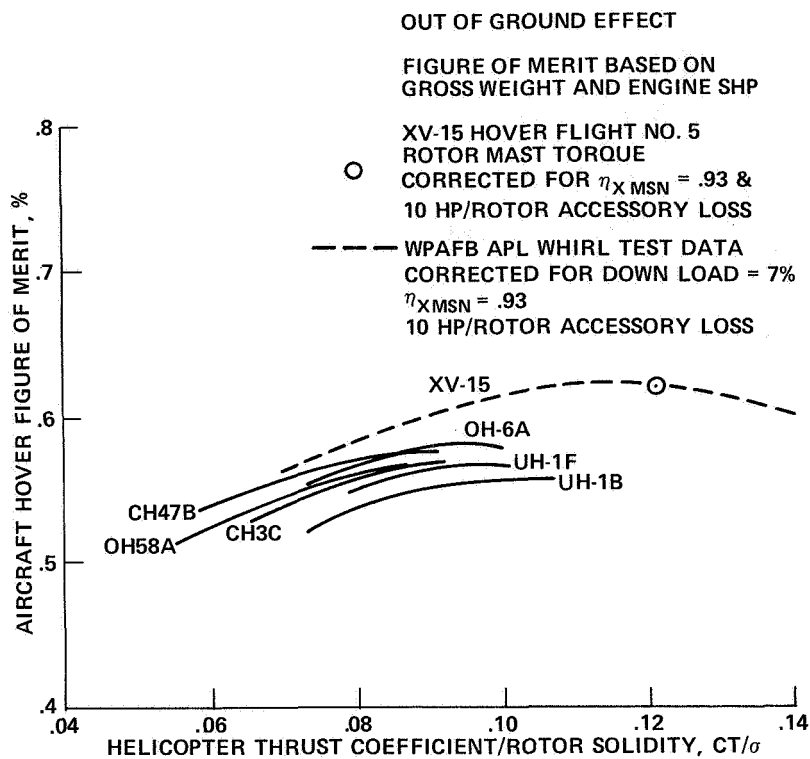
Figure 10.— Rotor hover performance.

△ GROUND/HOVER TEST
+ WHIRL STAND
✕ WIND TUNNEL

5,900 kg (13,000 lb) GROSS WEIGHT

PROJECTED NOISE: 6 PNdB
DECREASE PER DOUBLED
DISTANCE

PROJECTED NOISE WITH
ATMOSPHERIC ABSORPTION @
40% RELATIVE HUMIDITY
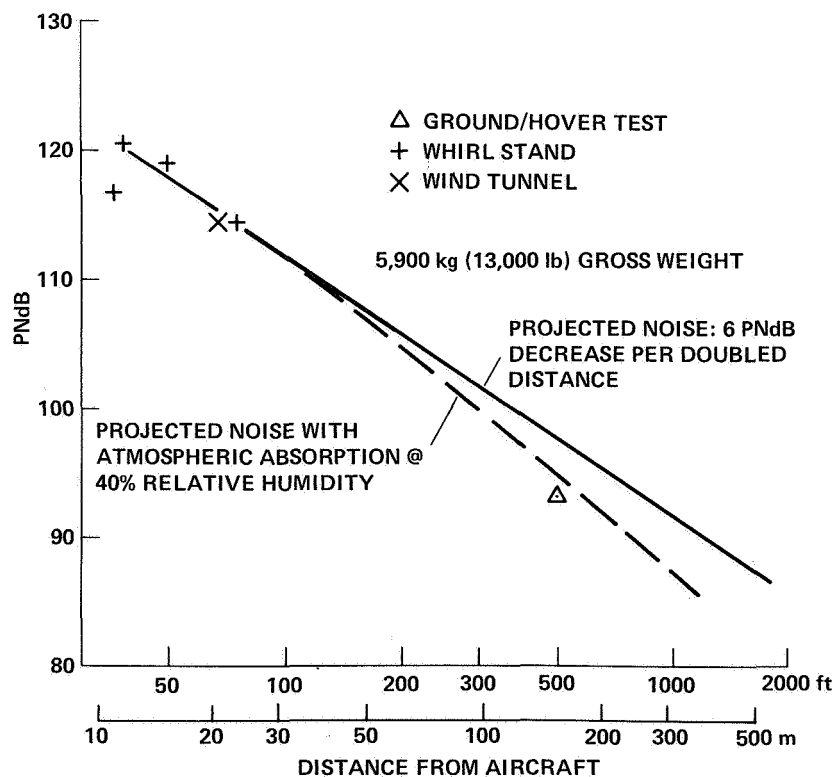
Figure 11.— Variation of XV-15 hover noise level with distance from aircraft.

406
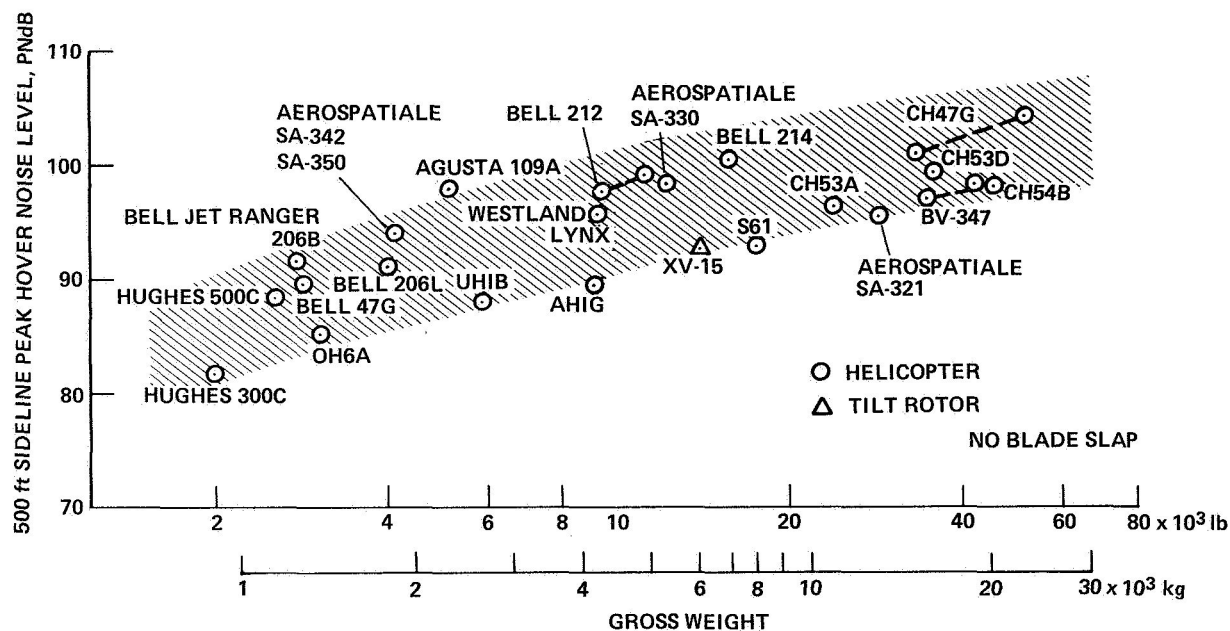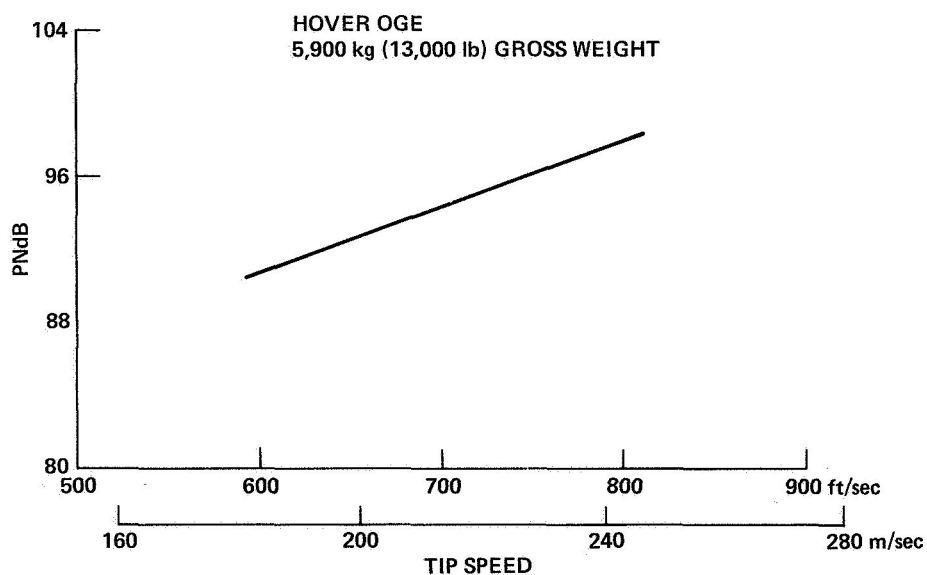
Figure 12.— Hover noise levels of rotorcraft.

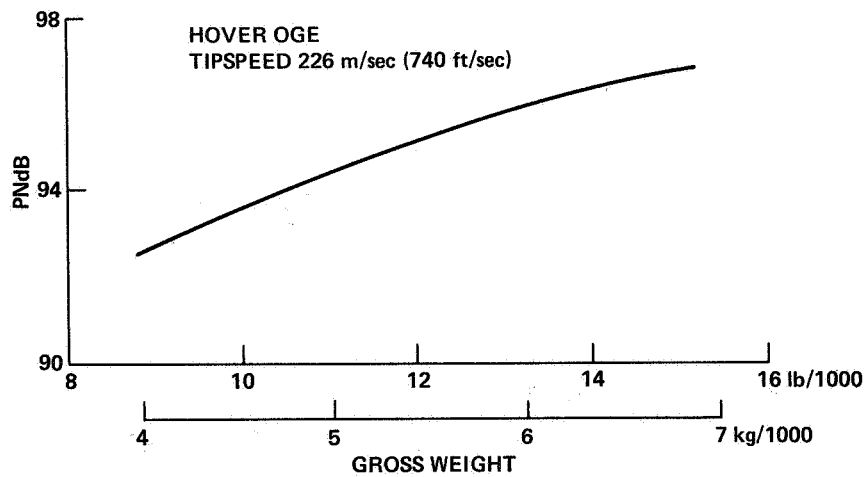Figure 13.— Effect of tip speed on XV-15 hover noise.

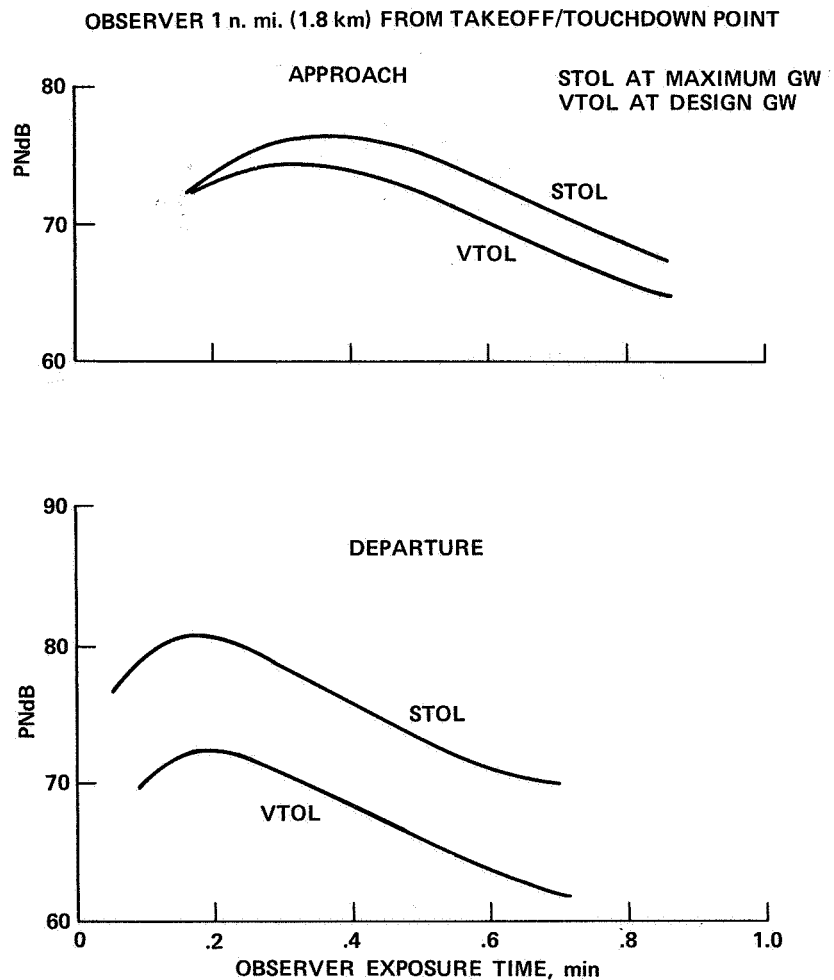Figure 14.— Effect of gross weight on XV-15 hover noise.

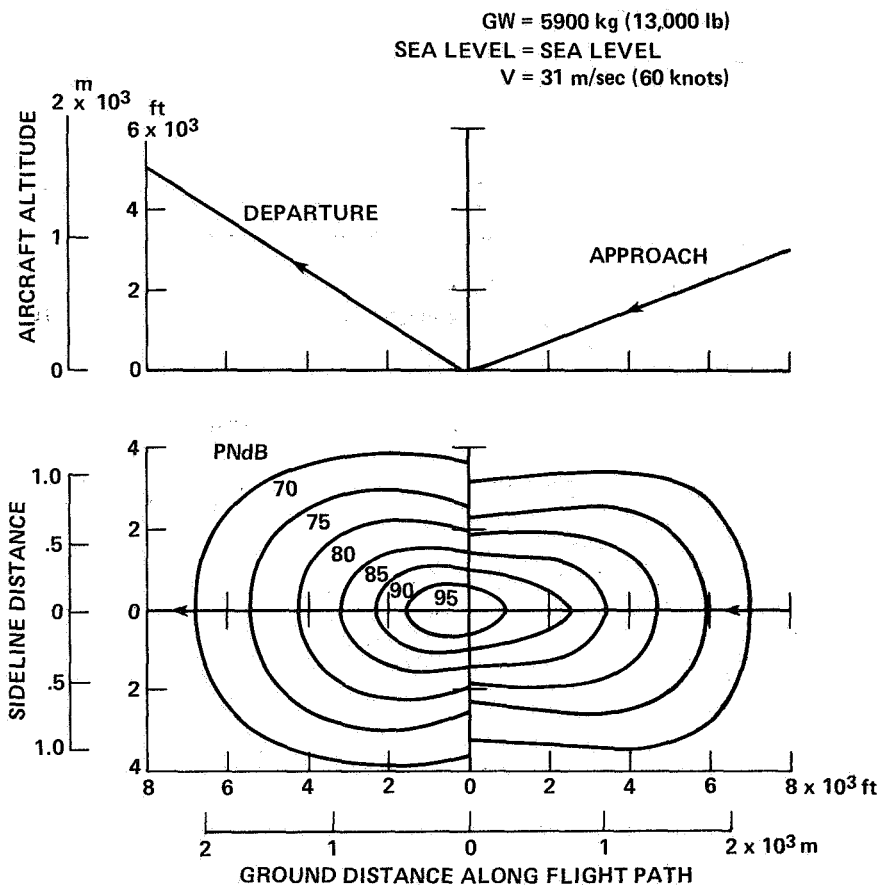Figure 15.— XV-15 noise time histories for approach/departure.

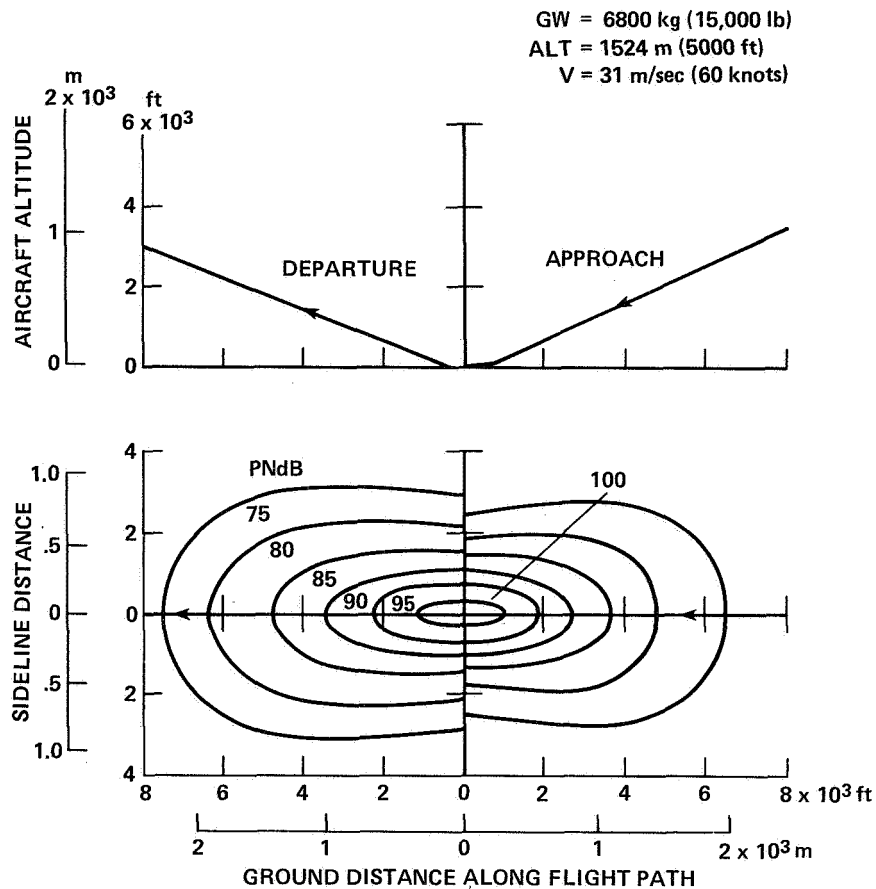Figure 16.— XV-15 VTOL takeoff and landing noise exposure footprint.

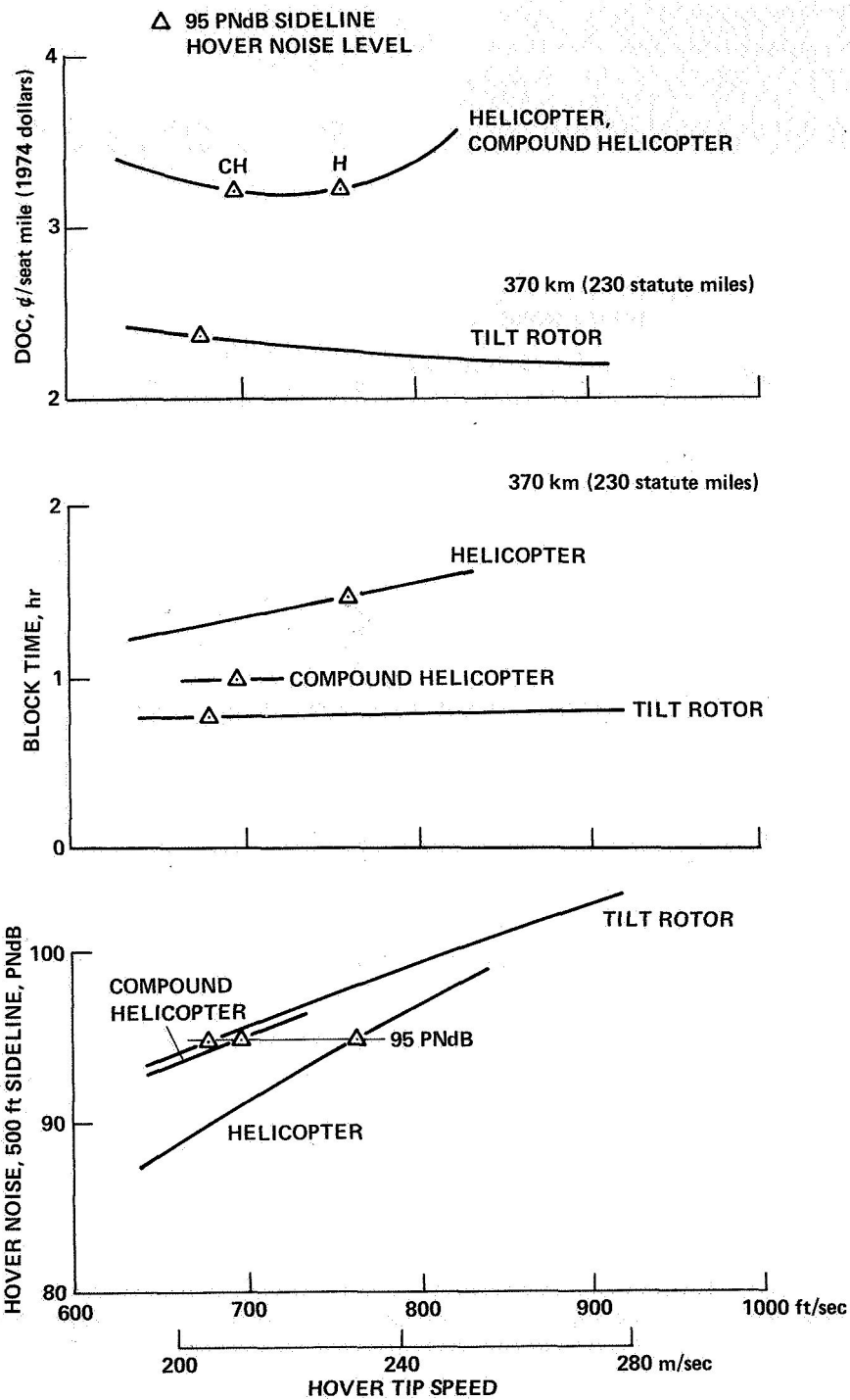Figure 17.— XV-15 STOL takeoff and landing noise exposure footprint.

Figure 18.— 100-passenger commercial VTOL transport noise and operational efficiency variation with tip speed.
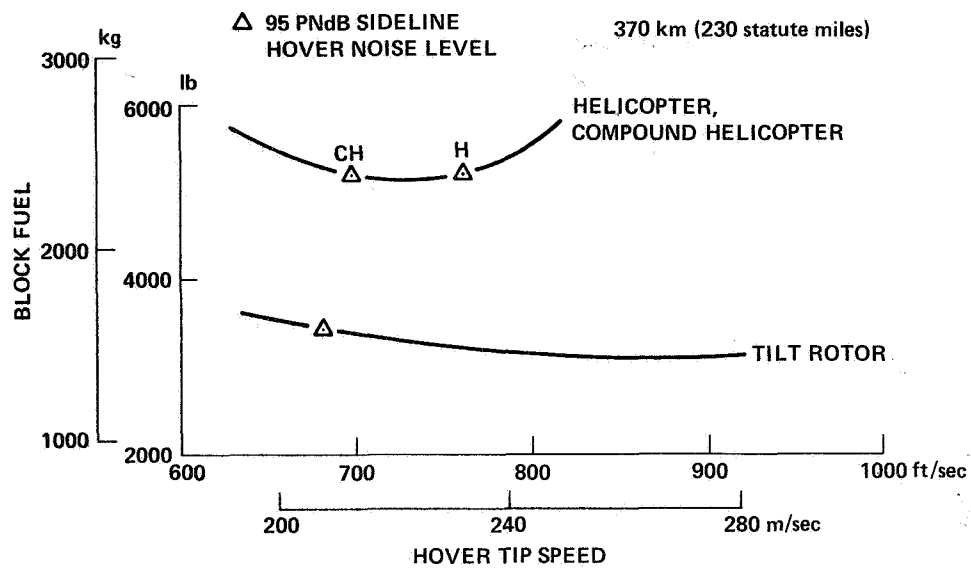
Figure 19.— Mission fuel required for 100-passenger commercial VTOL transport.

Figure 20.— 100-passenger VTOL transport productivity ratio comparison: helicopter and tilt rotor.

OUT —
556 km @ 4572 m
(300 knots @ 15,000 ft)

SEARCH —
LOITER 45 min

BACK —
472 km @ 3048 m
(260 knots @ 10,000 ft)

RESCUE —
20 min OGE HOVER

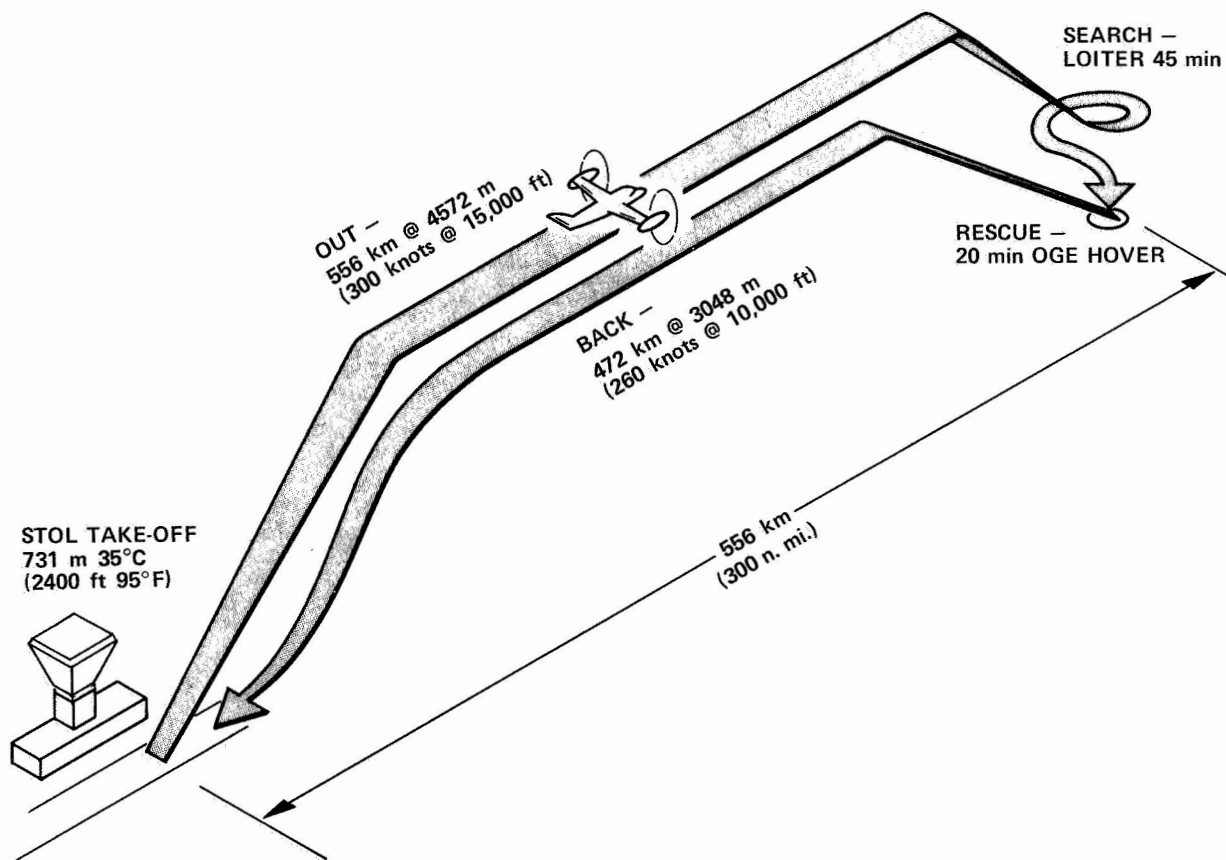STOL TAKE-OFF
731 m 35°C
(2400 ft 95°F)

556 km
(300 n. mi.)

Figure 21.— Tilt rotor 300 n. mi search and rescue mission profile.
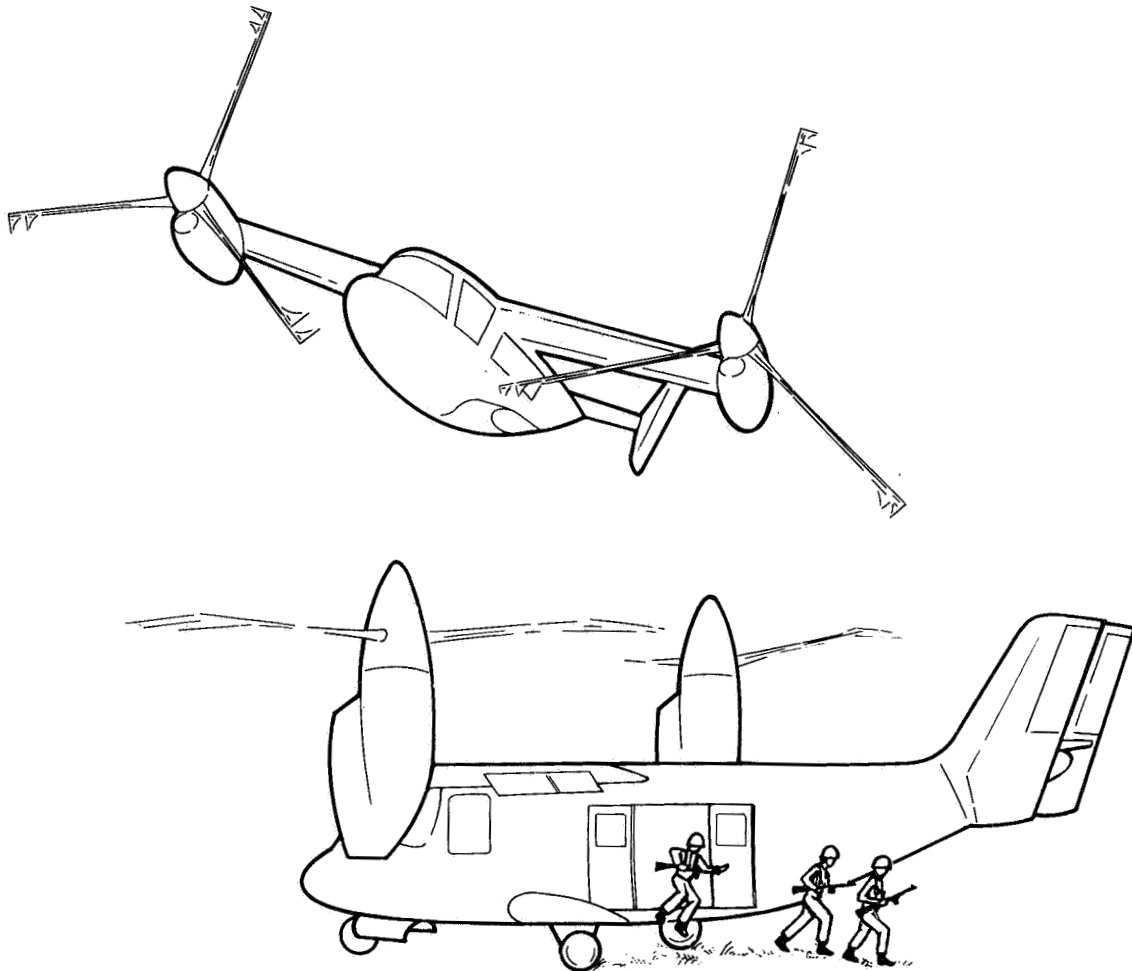
Figure 22.— Utility tilt rotor aircraft.

BIBLIOGRAPHY OF QCSEE PUBLICATIONS[1]

1974

QCSEE Preliminary Analysis and Design Report, Vol. I.   (R74AEG479-Vol-1, General Electric Co.)   NASA CR-134838, 1974.

QCSEE Preliminary Analysis and Design Report, Vol. II.   (R74AEG479-Vol-2, General Electric Co.)   NASA CR-134839, 1974.

1975

QCSEE Aerodynamic Characteristics of 30.5 cm Diameter Inlets.   (R75AEG494, General Electric Co.)   NASA CR-134866, 1975.

QCSEE Aerodynamic and Preliminary Mechanical Design of the QCSEE OTW Fan.   (R75AEG381, General Electric Co.)   NASA CR-134841, 1975.

QCSEE Clean Combustor Test Report.   (R75AEG449, General Electric Co.)   NASA CR-134916, 1975.

QCSEE Main Reduction Gears Bearing Development program.   (Curtiss-Wright Corp.)   NASA CR-134890, 1975.

QCSEE Test Results from a 14 cm Inlet for a Variable Pitch Fan Thrust Reverser.   (R75AEG387, General Electric Co.)   NASA CR-134867, 1975.

QCSEE Under-the-Wing Engine Composite Fan Blade Design.   (R75AEG278, General Electric Co.)   NASA CR-134840, 1975.

QCSEE Under-the-Wing Engine Composite Fan Blade Preliminary Design Test Report.   (R75AEG411, General Electric Co.)   NASA CR-134846, 1975.

QCSEE UTW Fan Preliminary Design.   (R75AEG213, General Electric Co.)   NASA CR-134842, 1975.

Stimpert, D. L.; and McFalls, R. A.:   Demonstration of Short Haul Aircraft Aft Noise Reduction Techniques on a 20 Inch (50.8 cm) Diameter Fan, Vol. 1.   (R75AEG252-Vol-1, General Electric Co.) NASA CR-134849, 1975.

Stimpert, D. L.:   Demonstration of Short Haul Aircraft Aft Noise Reduction Techniques on a 20 Inch (50.8 cm) Diameter Fan, Vol. II.   (R75AEG252- Vol-2, General Electric Co.)   NASA CR-134850, 1975.

---

[1] The work reported in these documents was done under NASA Contract NAS3-18021.

Stimpert, D. L.: Demonstration of Short Haul Aircraft Aft Noise Reduction Techniques on a 20 Inch (50.8 cm) Diameter Fan, Vol. III. (R75AEG252-Vol-3, General Electric Co.) NASA CR-134851, 1975.

1976

Howard, D. F.: QCSEE Preliminary Under-the-Wing Flight Propulsion System Analysis Report. (R75AEG349, General Electric Co.) NASA CR-134868, 1976.

QCSEE Aerodynamic and Mechanical Design of the QCSEE Over-the-Wing Fan. (General Electric Co.) NASA CR-134915, 1976.

QCSEE Hamilton Standard Cam/Harmonic Variable Pitch Fan Actuation System Detailed Design Report. (HSER-7001, Hamilton Standard.) NASA CR-134852, 1976.

QCSEE Whirl Test of Cam/Harmonic Pitch Actuation System. (HSER-7002, Hamilton Standard.) NASA CR-135140, 1976.

QCSEE Under-the-Wing Boilerplate Nacelle and Core Exhaust Nozzle Design Report. (R76AEG222, General Electric Co.) NASA CR-135008, 1976.

1977

Defeo, A.; and Kulina, M.: QCSEE Main Reduction Gears Detailed Design. (CW-WR-77-024, Curtiss-Wright Corp.) NASA CR-134872, 1977.

Griffin, R. G.; Aerodynamic and Aeromechanical Performance of a 50.8 cm (20 in.) Diameter 1.34 Pressure Ratio Variable Pitch Fan with Core Flow. (R75AEG445, General Electric Co.) NASA CR-135017, 1977.

Howard, D. F.: QCSEE Preliminary Over-the-Wing Flight Propulsion System Analysis Report. (R77AEG305, General Electric Co.) NASA CR-135296, 1977.

Misel, O. W.: QCSEE Main Reduction Gears Test Program Final Report. (CW-WR-77-008, Curtiss-Wright Corp.) NASA CR-134669, 1977.

QCSEE Aerodynamic and Mechanical Design of the QCSEE Under-the-Wing Fan. (R75AEG484, General Electric Co.) NASA CR-135009, 1977.

QCSEE Over the Wing. (R75AEG443, General Electric Co.) NASA CR-134848, 1977.

QCSEE Over-the-Wing Boilerplate Nacelle Design Report. (R77AEG300, General Electric Co.) NASA CR-135168, 1977.

QCSEE Over-the-Wing Digital Control Design Report. (77AEG663, General Electric Co.) NASA CR-135337, 1977.

QCSEE Under the Wing (UTW). (General Electric Co.) NASA CR-134847, 1977.

QCSEE Under-the-Wing Engine Boilerplate Nacelle Test Report. Vol. I - Summary. (R77AEG212-1-Vol-1, General Electric Co.) NASA CR-135249, 1977.

QCSEE Under-the-Wing Engine Boilerplate Nacelle Test Report, Vol. II - Aerodynamics and Performance. (R77AEG212-2-Vol-2, General Electric Co.) NASA CR-135250, 1977.

QCSEE Under-the-Wing Engine Boilerplate Nacelle Test Report, Vol. III - Mechanical Performance. (R77AEG212-3-Vol-3, General Electric Co.) NASA CR-135251, 1977.

QCSEE Under-the-Wing Engine Simulation Results (R75AEG444, General Electric Co.) NASA CR-135914, 1977.

Ravenhall, R.; Salemme, C. T.; and Stabrylla, R. G.: QCSEE Under-the-Wing Engine Composite Fan Blade Final Design Test Report. (R77AEG177, General Electric Co.) NASA CR-135046, 1977.

Sowers, H. D.; and Coward, W. E.: QCSEE Core Engine Noise Measurements. (R75AEG511, General Electric Co.) NASA CR-135160, 1977.

Stimpert, D. L.; and Clemons, A.: Acoustic Analysis of Aft Noise Reduction Techniques Measured on a Subsonic Tip Speed 50.8 cm (20 inch) Diameter Fan. (R75AEG368, General Electric Co.) NASA CR-134891, 1977.

Stotler, C. L., Jr.; and Bowden, J. H.: QCSEE Composite Fan Frame Subsystem Test Report. (R76AEG233, General Electric Co.) NASA CR-135010, 1977.

Stotler, C. L., Jr.; Johnston, E. A.; and Freeman, D. S.: QCSEE Under-the-Wing Composite Nacelle Subsystem Test Report. (R76AEG420, General Electric Co.) NASA CR-135075, 1977.

1978

Acoustic Performance of a 50.8 cm (20 inch) Diameter Variable Pitch Fan and Inlet, Vol. I. NASA CR-135117, 1978.

Acoustic Performance of a 50.8 cm (20 inch) Diameter Variable Pitch Fan and Inlet, Vol. II. NASA CR-135118, 1978.

Acoustic Treatment Development and Design. NASA CR-135266, 1978.

Johnston, E. A.: QCSEE Under-the-Wing Composite Nacelle Design Report. (R77AEG588, General Electric Co.) NASA CR-135352, 1978.

Mitchell, S. C.: QCSEE Composite Frame Design (R77AEG439, General Electric Co.) NASA CR-135278, 1978.

419

QCSEE Ball Spline Pitch Change Mechanism Design Report. (R77AEG327, General Electric Co.) NASA CR-134873, 1978.

QCSEE Ball Spline Pitch Change Mechanism Whirligig Test Report. (R77AEG394, General Electric Co.) NASA CR-135354, 1978.

QCSEE OTW Propulsion System Test Report, Vol. I - Summary. (R77AEG473-Vol-1, General Electric Co.) NASA CR-135323, 1978.

QCSEE OTW Propulsion System Test Report, Vol. II - Aerodynamics and Performance. (R77AEG474-Vol-2, General Electric Co.) NASA CR-135324, 1978.

QCSEE OTW Propulsion System Test Report, Vol. III - Mechanical Performance. (R77AEG475-Vol-3, General Electric Co.) NASA CR-135325, 1978.

QCSEE Over-the-Wing Engine and Control Simulation Results. (R76AEG218, General Electric Co.) NASA CR-135049, 1978.

QCSEE Under-the-Wing Engine Control System Design Report. (R75AEG483, General Electric Co.) NASA CR-134920, 1978.

Ruggles, C. L.: QCSEE Under-the-Wing Graphite PMR Cowl Development. (R78AEG-206, General Electric Co.) NASA CR-135279, 1978.

Sowers, H. D.; and Coward, W. E.: QCSEE Over-the-Wing (OTW) Engine Acoustic Design (R76AEG228, General Electric Co.) NASA CR-135268, 1978.

Sowers, H. D.; and Coward, W. E.: QCSEE Under-the-Wing (UTW) Engine Acoustic Design. (R76AEG195, General Electric Co.) NASA CR-135267, 1978.

Stimpert, D. L.: QCSEE Acoustic and Aerodynamic Tests on a Scale Model Over-the-Wing Thrust Reverser and Forward Thrust Nozzle. (R75AEG504, General Electric Co.) NASA CR-135254, 1978.

To be published

QCSEE Clean Combustor Development Report.

QCSEE Final Report. NASA CR-159473.

QCSEE OTW Propulsion System Test Report, Vol. IV - Acoustic Performance. NASA CR-135326.

QCSEE UTW Engine Composite Nacelle Test Report, Vol. I - Aerodynamic and Mechanical Performance. NASA CR-159471.

QCSEE UTW Engine Composite Nacelle Test Report, Vol. II - Acoustic Performance. NASA CR-159472.

1. Report No. NASA CP-2077	2. Government Accession No.	3. Recipient's Catalog No.
4. Title and Subtitle QUIET, POWERED-LIFT PROPULSION		5. Report Date February 1979
		6. Performing Organization Code
7. Author(s)		8. Performing Organization Report No. E-9906
		10. Work Unit No.
9. Performing Organization Name and Address National Aeronautics and Space Administration Lewis Research Center Cleveland, Ohio 44135		11. Contract or Grant No.
		13. Type of Report and Period Covered Conference Publication
12. Sponsoring Agency Name and Address National Aeronautics and Space Administration Washington, D.C. 20546		14. Sponsoring Agency Code

15. Supplementary Notes

16. Abstract

A 2-day conference was held at the NASA Lewis Research Center, November 14-15, 1978, to provide leaders from government, industry, and universities with the latest results of NASA programs being conducted to explore and demonstrate new technologies in quiet, powered-lift propulsion systems. Topics discussed included results from the Quiet, Clean, Short-Haul Experimental Engine (QCSEE) program and progress reports on the Quiet, Short-Haul, Research Aircraft (QSRA) and Tilt-Rotor Research Aircraft programs. In addition to these NASA programs, the Air Force AMST YC 14 and YC 15 programs were reviewed.

17. Key Words (Suggested by Author(s)) Aerodynamics; Aircraft propulsion and power; Composite materials; Acoustics; Environment pollution	18. Distribution Statement Foreign distribution excluded. Available from NASA Industrial Applications Centers		
19. Security Classif. (of this report) Unclassified	20. Security Classif. (of this page) Unclassified	21. No. of Pages 427	22. Price

NATIONAL AERONAUTICS AND SPACE ADMINISTRATION
WASHINGTON, D.C. 20546

OFFICIAL BUSINESS
PENALTY FOR PRIVATE USE $300

SPECIAL FOURTH-CLASS RATE
BOOK

POSTMASTER :   If Undeliverable (Section 158
Postal Manual) Do Not Return